NASA CR
ASRL TR 1

FINITE-STRAIN LARGE-DEFLECTION ELASTIC-VISCOPLASTIC FINITE-ELEMENT TRANSIENT RESPONSE ANALYSIS OF STRUCTURES

José J.A. Rodal
Emmett A. Witmer

July 1979

Aeroelastic and Structures Research Laboratory
Department of Aeronautics and Astronautics
Massachusetts Institute of Technology
Cambridge, Massachusetts 02139

Prepared for
[illegible] SAFETY RESEARCH AND DATA INSTITUTE
LEWIS RESEARCH CENTER
NATIONAL AERONAUTICS AND SPACE ADMINISTRATION

FOREWORD

This research was carried out by the Aeroelastic and Structures Research Laboratory, Department of Aeronautics and Astronautics, Massachusetts Institute of Technology, Cambridge, Massachusetts under NASA Grant No. NGR 22-009-339 from the Lewis Research Center, National Aeronautics and Space Administration, Cleveland, Ohio as part of the NASA Rotor Burst Protection Program. Dr. Arthur G. Holms and Mr. Solomon Weiss of NASA-LeRC served as technical monitors. The valuable advice and cooperation from these individuals is acknowledged most gratefully.

The authors are also indebted to their colleagues for stimulating discussion, advice, and assistance in this effort: Dr. Robert L. Spilker, Dr. Denny Meredith, Mr. Thomas R. Stagliano, Mrs. Susan E. French, Dr. John W. Leech, and Mr. Fred Merlis. The computations were carried out at the Information Processing Center of MIT.

The use of SI units (NASA Policy Directions NPD 2220.4, September 14, 1970) was waived for the present document in accordance with provisions of paragraph 5d of that Directive by the authority of the Director of the Lewis Research Center.

This report was submitted to NASA-Lewis for pre-publication review in August 1979. The authors wish to thank Dr. M.S. Hirschbein and Dr. C.C. Chamis of NASA-Lewis for their thoughtful review and for constructive suggestions on this report. Subsequently, the authors carried out necessary report revisions which were completed in July 1980. Report reproduction followed immediately thereafter.

CONTENTS

CONTENTS CONTINUED

CONTENTS CONTINUED

CONTENTS CONTINUED

CONTENTS CONTINUED

CONTENTS CONTINUED

LIST OF ILLUSTRATIONS

LIST OF ILLUSTRATIONS (Continued)

LIST OF ILLUSTRATIONS (Continued

LIST OF ILLUSTRATIONS (Continued)

LIST OF ILLUSTRATIONS (Concluded)

LIST OF TABLES

LIST OF SYMBOLS

Symbol	Definition	Page
a	Determinant of the reference surface metric tensor in the reference configuration	176
$a_{\alpha\beta}$	Metric tensor covariant components of the reference surface in the reference configuration	176
$a^{\alpha\beta}$	Same as above but contravariant components	176
$\bar{a}_{\alpha}$	Covariant base vectors of the reference surface in the reference configuration	175
$\bar{a}^{\alpha}$	Same as above but contravariant	176
A	Cross-sectional area in the present configuration	90
dA	Differential element of area in the present configuration	51
A	Determinant of the reference surface metric tensor in the present configuration	176
A_o	Cross-sectional area in the reference configuration	91
dA_o	Differential element of area in the reference configuration	51
$A_{o\bar{t}}$	Boundary surface area in the reference configuration with prescribed surface traction $\bar{t}$	232
A_s	Weighting factor of sublayer s in the mechanical-sublayer model of plasticity	117,123
$A_{\alpha\beta}$	Metric tensor covariant components of the reference surface in the present configuration	176
$A^{\alpha\beta}$	Same as above but contravariant components	176
$\bar{A}_{\alpha}$	Covariant base vectors of the reference surface in the present configuration	176
$\bar{A}^{\alpha}$	Same as above but contravariant	176

Symbol	Definition	Page
b	Determinant of the second fundamental tensor of the reference surface in the reference configuration	178
$b_{\alpha\beta}$	Covariant components of the second fundamental tensor of the reference surface in the reference configuration	178
b^{α}_{β}	Same as above but mixed components	178
B	Determinant of the second fundamental tensor of the reference surface in the present configuration	178
$B_{\alpha\beta}$	Covariant components of the second fundamental tensor of the reference surface in the present configuration	178
B^{α}_{β}	Same as above but mixed components	178
c		184
C		183
$\overset{=}{C}$	Cauchy-Green Deformation Tensor	36
C_{ij}	Covariant components of the Cauchy-Green Deformation Tensor in convected coordinates in the reference configuration	38,198
C^{i}_{j}	Same as above but mixed components	38
$\overset{o}{C}{}^{2}_{2}$	Mixed component of the Cauchy-Green Deformation Tensor at the reference axis in the reference configuration	140
$\overset{o}{C}_{ij}$	Covariant components of the Cauchy-Green Deformation Tensor at the reference surface in the reference configuration	204
$(C^{-1})^{ij}$	Contravariant components of the inverse of the Cauchy-Green Deformation Tensor in convected coordinates in the reference configuration	199

Symbol	Definition	Page
$({}^{o}C^{-1})^{ij}$	Contravariant components of the inverse of the Cauchy-Green Deformation Tensor at the reference surface in the reference configuration	204
d	Material strain-rate constant (viscosity coefficient)	122
${}^{s}d$	Material strain-rate constant (viscosity coefficient) of sublayer s in the mechanical-sublayer model of viscoplasticity	119
$\overset{=}{D}$	Rate of Deformation Tensor (also called stretching)	44
D^{I}_{J}	Mixed components of the Rate of Deformation Tensor in convected coordinates in the present configuration	45
${}^{s}\overset{=}{D}{}^{p}$	Plastic part of the Rate of Deformation Tensor, pertaining to sublayer s of the mechanical-sublayer model of plasticity	118
${}^{s}\overset{=}{D}{}^{e}$	"Elastic" part of the Rate of Deformation Tensor, pertaining to sublayer s of the mechanical-sublayer model of plasticity	117
$\overset{=}{D}{}^{D}$	Deviatoric part of the Rate of Deformation Tensor	119
D_{u}	Uniaxial component of the Rate of Deformation Tensor	89,125
$\overset{=}{e}$	Almansi Strain Tensor, also called Eulerian Strain Tensor	40
E	Young's (elastic) modulus	124
E_{u}	Axial relative elongation, also called engineering or nominal strain	87
E^{T}_{s}	Tangent modulus associated with sublayer s of the mechanical-sublayer model of piecewise-linear plasticity	124

Symbol	Definition	Page
$\overline{\overline{\overline{\overline{E}}}}$	Fourth-order "Elastic" (Stiffness) Tensor	122
${}^{n}\overline{\overline{\overline{\overline{E}}}}$	Fourth-order "Elastic" (Stiffness) Tensor pertaining to sublayer n of the mechanical-sublayer model of piecewise-linear plasticity	117
E^{IJ}_{KL}	Mixed components of the fourth-order "Elastic" (Stiffness) Tensor in convected coordinates in the present configuration	206
$\{f\}$	Individual finite element generalized load vector expressed in local coordinates accounting for externally-applied distributed or concentrated loads and body forces	243
$\{f^*\}$	Same as above but expressed in terms of global reference coordinates	244
$\{F\}$	Same as above but pertaining to the complete (global) finite element structure: the sum of the individual finite element contributions	246
$\{F^{NL}_q\}$	Global pseudo-load vector arising from the nonlinear terms in the strain-displacement relations in the conventional formulation of the equations of motion	247
$\{F^{L}_p\}$	Global pseudo-load vector due to plastic strains, and associated with the linear terms of the strain-displacement relations in the conventional formulation of the equations of motion	247
$\{F^{NL}_p\}$	Same as above, but associated with the nonlinear terms of the strain-displacement relations	247
$\{F^{NL}\}$	Global pseudo-load vector representing internal forces arising from (small and finite) elastic-	

Symbol	Definition	Page
	plastic strains as well as all (linear and non-linear) terms of the strain-displacement relations, in the modified unconventional formulation of the equations of motion	269
$\underline{\underline{F}}$	Deformation Gradient Tensor	30
g	Determinant of the fundamental metric tensor in the reference configuration	27,179
g_{ij}	Covariant components of the fundamental metric tensor in the reference configuration	27
g^{ij}	Same as above but contravariant components	27
$\bar{g}_i$	Covariant base vectors of the body-fixed (convected) coordinate system in the reference configuration	26
$\bar{g}^i$	Same as above but contravariant	26
G	Determinant of the fundamental metric tensor in the present configuration	27
G_{IJ}	Covariant components of the fundamental metric tensor in the present configuration	27
G^{IJ}	Same as above but contravariant components	27
$\bar{G}_I$	Covariant base vectors of the body-fixed (convected) coordinate system in the present configuration	27
$\bar{G}^I$	Same as above but contravariant	27
h	Mean curvature of the reference surface in the reference configuration	178
$[h]$	Individual finite element pseudo-stiffness matrix expressed in local coordinates arising from elastic-plastic strains as well as the nonlinear terms of the strain-displacement relations, in the unconventional form of the equations of motion	243

Symbol	Definition	Page
$[h^*]$	Same as above but expressed in terms of global reference coordinates	244
$\bar{\bar{H}}$	Logarithmic strain tensor, also associated with the name of Hencky	42
H^I_J	Mixed components of the logarithmic strain tensor $\bar{\bar{H}}$, in the body-fixed convected coordinate system in the present configuration	41
${}^s(H^I_J)^e$	Same as above but pertaining to the elastic component of the strain of the s sublayer in the mechanical-sublayer model of plasticity	167
${}^s(H^I_J)^p$	Same as above but pertaining to the plastic component of the strain of the s sublayer in the mechanical-sublayer model of plasticity	167
$\{i\}$	Individual finite element pseudo-load vector expressed in local coordinates, representing all of the internal forces arising from elastic as well as plastic strains and the linear as well as the nonlinear terms of the strain-displacement relations in the unconventional form of the equations of motion	244
$\{i^*\}$	Same as above but expressed in terms of global reference coordinates	244
$\{I\}$	Same as above but pertaining to the complete (global) finite-element structure: the sum of the individual finite element contributions	245
I_2^D	Second invariant of the deviatoric rate-of-deformation tensor	128
${}^sI_2^p$	Second invariant of the plastic part of the rate-of-deformation tensor of sublayer s of the mechanical-sublayer model of viscoplasticity	128

Symbol	Definition	Page
J_2	Second invariant of the deviatoric stress tensor	104
${}^sJ_2$	Second invariant of the deviatoric Kirchhoff stress tensor of sublayer s of the mechanical-sublayer model of viscoplasticity	128
k	Gaussian curvature of the reference surface in the reference configuration	178
[k]	Individual finite element constant stiffness matrix expressed in local coordinates arising from linear elastic effects in the conventional form of the equations of motion	247
$[k^*]$	Same as above but expressed in terms of global reference coordinates	247
[K]	Same as above but pertaining to the complete (global) finite-element structure: the sum of the individual finite-element contributions	247
$[k^T]$	Individual finite element tangent (variable) stiffness matrix arising from elastic as well as plastic strains and the linear as well as the nonlinear terms of the strain-displacement relations in the tangent stiffness form of the equations of motion	251
$[K^T]$	Same as above but pertaining to the complete (global) finite-element structure: the sum of the individual finite-element contributions	250
K	Gaussian curvature of the reference surface in the present configuration	178
${}^sk_o$	Yield stress in pure shear, under static conditions of sublayer s in the mechanical-sublayer model of plasticity	128

Symbol	Definition	Page
ℓ	Axial length in the present configuration	81
$\dot{\ell}$	Material rate of ℓ	81
ℓ_o	Axial length in the reference (original or undeformed) configuration	81
m	Mass	53
[m]	Individual finite-element mass matrix expressed in local coordinates, arising from inertial effects in the equations of motion	242
$[m^*]$	Same as above but expressed in terms of global reference coordinates	244
[M]	Same as above but pertaining to the complete (global) finite-element structure: the sum of the individual finite-element contributions	245
$\bar{n}$	Unit normal base vector to the reference <u>axis</u> in the reference configuration	137
$\bar{n}$	Unit normal base vector to the reference <u>surface</u> in the reference configuration	174
$\bar{N}$	Unit normal base vector to the reference <u>axis</u> in the present configuration	137
$\bar{N}$	Unit normal base vector to the reference <u>surface</u> in the present configuration	175
$\lfloor N_i \rfloor$	Assumed interpolation vector function for assumed displacement u_i	236
p	Material constant in strain-rate power law	122
${}^s p$	Same as above but pertaining to sublayer s of the mechanical-sublayer model of viscoplasticity	119

Symbol	Definition	Page
$\{p\}$	Individual finite-element pseudo-load vector expressed in local coordinates, representing internal forces arising from elastic as well as plastic strains and linear as well as nonlinear terms of the strain-displacement relations in the unconventional form of the equations of motion	243
$\{p^*\}$	Same as above but expressed in terms of global reference coordinates	244
$\{q\}$	Vector of nodal generalized displacements defined in terms of the local coordinate system of each finite element	236
$\{q^*\}$	Vector of independent global generalized displacements defined in terms of global reference coordinates for the structural system as a whole	243
$\{\dot{q}^*\}$	Material rate of $\{q^*\}$; the vector of independent global generalized velocities	265
$\{\ddot{q}^*\}$	Material rate of $\{\dot{q}^*\}$; the vector of independent global generalized accelerations	243
$\bar{r}$	Position vector from the origin of the fixed-in-space (inertial) system to the material point under consideration, in the reference configuration	26
$\bar{r}_o$	Position vector from the origin of the fixed-in-space (inertial) system to the curved beam <u>reference axis</u>, in the reference configuration	137
$\bar{r}_o$	Position vector from the origin of the fixed-in-space (inertial) system to the shell <u>reference surface</u>, in the reference configuration	174
$\bar{R}$	Position vector from the origin of the fixed-in space (inertial) system to the material point under consideration, in the present configuration	26

Symbol	Definition	Page
$\bar{R}_o$	Position vector from the origin of the fixed-in-space (inertial) system to the curved beam reference axis, in the present configuration	137
$\bar{R}_o$	Position vector from the origin of the fixed-in-space (inertial) system to the shell reference surface, in the present configuration	175
ds	Differential line element in the reference configuration	37
dS	Differential line element in the present configuration	37
s	Deformed arc length	146,149
$\bar{\bar{S}}$	Second Piola-Kirchhoff stress	54
$\dot{\bar{\bar{S}}}$	Material rate of the Second Piola-Kirchhoff stress	117
S^{ij}	Contravariant components of the Second Piola-Kirchhoff stress, in the body-fixed (convected) coordinate system in the reference configuration	54
$\dot{S}^{ij}$	Material rate of S^{ij}	75
t	Time	24
t_o	Reference or initial time	24
u	Displacement component of the displacement vector of the reference surface of the plate or shell, in one of the body-fixed convected coordinates that defines the reference surface	189
$\bar{u}$	Displacement vector	28
$\bar{u}_o$	Displacement vector of the reference axis of the curved beam	139
$\bar{u}_o$	Displacement vector of the reference surface of plate or shell	175

Symbol	Definition	Page
$\bar{\bar{U}}$	Right Stretch Tensor	36
${}^{o}U^{2}_{2}$	Mixed component of the right stretch tensor at the reference axis	140
U	Internal energy	76,231
δU	Virtual work of the internal stresses	231
${}^{s}\dot{U}^{p}$	Plastic power per unit mass of sublayer s in the mechanical-sublayer model of viscoplasticity	170
$\bar{v}$	Velocity vector of material points of a moving continuum (material time derivative of the displacement vector)	29
v	Displacement component of the displacement vector of the reference axis, in the body-fixed convected coordinate that defines the reference axis of the curved beam	139
v	Displacement component of the displacement vector of the reference surface of the plate or shell, in one of the body-fixed convected coordinates that defines the reference surface	189
$\bar{\bar{V}}$	Left stretch tensor	36
V	Volume in the present configuration	53
V_o	Volume in the reference (initial or undeformed) configuration	53
w	Displacement component of the displacement vector of the reference axis, in the body-fixed convected coordinate perpendicular to the reference axis of the curved beam	139
w	Displacement component of the displacement vector of the reference surface of the plate or shell, in	

Symbol	Definition	Page
	the body-fixed convected coordinate perpendicular to the reference surface	185
δW	Virtual work done by the external forces (body forces and surface tractions)	231
x	Material (Lagrangian) rectangular Cartesian coordinate defining the reference surface of the plate	189
x_i	Material (Lagrangian) coordinates belonging to the fixed-in-space (inertial) rectangular Cartesian coordinate system defining the position of the points of the continuum in the reference configuration	25
X_I	Spatial (Eulerian) coordinates belonging to the fixed-in-space (inertial) rectangular Cartesian coordinate system defining the present position of the points of the continuum	25
y	Material (Lagrangian) rectangular Cartesian coordinate defining the reference surface of the plate	189
α	Parameter in the strain-displacement relations for curved beams related to changes in the thickness or in the lateral dimensions due to finite membrane strains	165
α	Expression appearing in the bending strain part of the strain-displacement relations for plates	193
β	Parameter in the strain-displacement relations for curved beams related to changes in the thickness or in the lateral dimensions due to finite membrane strains	165
β	Expression appearing in the bending strain part of the strain-displacement relations for plates	193

Symbol	Definition	Page
$\bar{\bar{\gamma}}$	Green (Lagrangian) strain tensor	38
$\dot{\bar{\bar{\gamma}}}$	Material rate of the Green (Lagrangian) strain tensor	46
γ_{ij}	Covariant components of the Green (Lagrangian) strain tensor in the body-fixed convected coordinate system in the reference configuration	39
$\dot{\gamma}_{ij}$	Material rate of γ_{ij}	46
$\overset{o}{\gamma}{}_2^2$	Mixed component of the Green (Lagrangian) strain tensor at the body-fixed reference axis of the curved beam in the reference configuration	140
$\overset{o}{\gamma}_{\alpha\beta}$	Covariant components of the Green (Lagrangian) strain tensor at the body-fixed reference surface of the plate or shell, in the reference configuration	188
${}^s\dot{\bar{\bar{\gamma}}}{}^e$	"Elastic" part of the material rate of the Green (Lagrangian) strain of sublayer s of the mechanical-sublayer model of viscoplasticity	208
${}^s\dot{\bar{\bar{\gamma}}}{}^p$	Plastic part of the material rate of the Green (Lagrangian) strain of sublayer s of the mechanical-sublayer model of viscoplasticity	208
$\overset{*}{\varepsilon}_u$	Uniaxial logarithmic (natural, true, or Hencky) strain	88
$\dot{\overset{*}{\varepsilon}}_u$	Material rate of $\overset{*}{\varepsilon}_u$	89
${}^s\overset{*}{\varepsilon}_u$	Coordinate "s" of the uniaxial logarithmic strain $\overset{*}{\varepsilon}_u$ in the piecewise-linear approximation of the static stress-strain curve for the mechanical-sublayer model of plasticity	123

Symbol	Definition	Page
ζ^o	Lagrangian, material, or embedded coordinate that measures the distance along an outwardly-directed normal to the reference axis of the curved beam, in the reference configuration of the body-fixed system	136
ζ^o	Lagrangian, material, or embedded coordinate that measures the distance along an outwardly-directed normal to the reference surface of the plate or shell, in the reference configuration of the body-fixed system	174
η	Lagrangian, material, or embedded coordinate that defines the (curvilinear) reference axis of the curved beam, in the reference configuration of the body-fixed system	136
η	Expression appearing in the bending part of the strain-displacement relations for plates	193
θ	Rotation angle of a material point at the reference axis of the curved beam	145
λ	Parameter associated with the thickness change of the curved beam because of finite strains	137
λ^*	Parameter associated with the thickness change of the curved beam because of finite strains	137
λ_o	Parameter associated with the thickness change of the curved beam because of finite <u>membrane</u> strains	158
λ	Parameter associated with the thickness change of the plate or shell because of finite strains	175
λ_o	Parameter associated with the thickness change of the plate or shell because of finite <u>membrane</u> strains	184

Symbol	Definition	Page
$\dot{\lambda}$	Scalar factor of proportionality (not a material constant) in plasticity	105
${}^{s}\dot{\lambda}$	Scalar factor of proportionality (not a material constant) corresponding to sublayer s in the mechanical-sublayer model of viscoplasticity	118,121
${}^{s}\dot{\lambda}^{*}$	———————————————	216
μ	Parameter in the strain-displacement relations for curved beams associated with changes in the thickness or lateral dimensions because of finite membrane strains	165
μ	Expression appearing in the bending part of the strain-displacement relations for plates	193
ν	(Elastic) Poisson's ratio	127,206
ξ^{i}	Lagrangian, material, or embedded curvilinear coordinates which identify the material points of the medium, in the body-fixed system	25
ξ^{α}	Lagrangian, material, or embedded curvilinear coordinates which define the reference surface of the plate or shell in the body-fixed system	174
ρ	Mass density of the material in the present configuration	53
ρ_o	Mass density of the material in the reference (initial or undeformed) configuration	53
$\bar{\bar{\sigma}}$	Cauchy stress tensor, also called Eulerian stress tensor	52
σ_E	Uniaxial engineering stress, also called nominal or 1st Piola-Kirchhoff stress	95
σ_T	Uniaxial "true" stress, also called Cauchy stress	91

Symbol	Definition	Page
$\overset{=}{\tau}$	Kirchhoff stress tensor	52
${}^{s}\overset{=}{\tau}$	Same as above, but pertaining to sublayer s of the mechanical-sublayer model of viscoplasticity	117
$\overset{\circ}{\overset{=}{\tau}}$	Co-rotational (Zaremba-Jaumann) rate of the Kirchhoff stress	74
${}^{s}\overset{\circ}{\overset{=}{\tau}}$	Same as above, but pertaining to sublayer s of the mechanical-sublayer model of viscoplasticity	117
${}^{s}\overset{=}{\tau}{}^{D}$	Deviatoric part of ${}^{s}\overset{=}{\tau}$	118
${}^{s}\tau^{I}{}_{J}$	Mixed components of ${}^{s}\overset{=}{\tau}$ in the present configuration of the body-fixed convected coordinate system	201
${}^{s}\overset{\circ}{\tau}{}^{I}{}_{J}$	Mixed components of ${}^{s}\overset{\circ}{\overset{=}{\tau}}$ in the present configuration of the body-fixed convected coordinate system	205
τ_{u}	Uniaxial Kirchhoff stress	92
${}^{s}\tau_{u}^{Y}$	Rate-dependent uniaxial yield stress of sublayer s in the mechanical-sublayer model of viscoplasticity	119,125
${}^{s}\tau_{u_{o}}^{Y}$	Static (rate-independent) uniaxial yield stress of sublayer s in the mechanical-sublayer model of plasticity	119,124,127
${}^{s}\tau_{u_{o}}$	Coordinate "s" in the piecewise-linear approximation of the static stress-strain curve for the mechanical-sublayer model of plasticity	123
Φ	Yield surface (boundary in stress space which defines the elastic domain in the theory of plasticity)	103

Symbol	Definition	Page
${}^{s}\phi$	Yield surface in Kirchhoff stress space of the s sublayer in the mechanical sublayer model of viscoplasticity	118
χ	Displacement gradient for curved beams	140
ψ	Displacement gradient for curved beams	140

The terminology "mechanical-sublayer model of plasticity" and "mechanical-sublayer model of viscoplasticity" has been used interchangingly according to whether the quantity in question was considered as rate independent or rate dependent, respectively.

Definition of the Table 1 Symbols Used in This Report

$\bar{\bar{D}}$	Rate-of-Deformation tensor, also called stretching	44
D^{I}_{J}	Mixed components of $\bar{\bar{D}}$ in the body-fixed convected coordinate system in the present configuration	45
$\hat{D}_{IJ}$	Rectangular Cartesian components of $\bar{\bar{D}}$ in the fixed-in-space (inertial) coordinate system in the present configuration	45
$\bar{\bar{\gamma}}$	Green strain tensor, also called Lagrangian strain tensor	38
γ^{i}_{j}	Mixed components of $\bar{\bar{\gamma}}$ in the body-fixed convected coordinate system in the reference configuration	39
$\hat{\gamma}_{ij}$	Rectangular Cartesian components of $\bar{\bar{\gamma}}$ in the fixed-in-space (inertial) coordinate system in the reference configuration	39
$\bar{\bar{e}}$	Almansi strain tensor, also called Eulerian strain tensor	40

Symbol	Definition	Page
e^I_J	Mixed components of $\bar{\bar{e}}$ in the body-fixed convected coordinate system in the present configuration	41
$\hat{e}_{IJ}$	Rectangular Cartesian components of $\bar{\bar{e}}$ in the fixed-in-space (inertial) coordinate system in the present configuration	40
$\bar{T}$	Traction vector	51
$\bar{\bar{\sigma}}$	Cauchy stress tensor, also called Eulerian stress tensor	52
σ^I_J	Mixed components of $\bar{\bar{\sigma}}$ in the body-fixed convected coordinate system in the present configuration	52
$\hat{\sigma}_{IJ}$	Rectangular Cartesian components of $\bar{\bar{\sigma}}$ in the fixed-in-space (inertial) coordinate system in the present configuration	52
$\bar{\bar{\tau}}$	Kirchhoff stress tensor	53
τ^I_J	Mixed components of $\bar{\bar{\tau}}$ in the body-fixed convected coordinate system in the present configuration	54
$\hat{\tau}_{IJ}$	Rectangular Cartesian components of $\bar{\bar{\tau}}$ in the fixed-in space (inertial) coordinate system in the present configuration	54
$\bar{\bar{S}}$	Second Piola-Kirchhoff stress tensor	54
S^i_j	Mixed components of $\bar{\bar{S}}$ in the body-fixed convected coordinate system in the reference configuration	56
$\hat{S}_{ij}$	Rectangular Cartesian components of $\bar{\bar{S}}$ in the fixed-in-space (inertial) coordinate system in the reference configuration	56
$\bar{\bar{T}}$	First Piola-Kirchhoff stress tensor, also called nominal stress	57

Symbol	Definition	Page
$T^{i.}_{.J}$	Mixed components of the double tensor $\bar{\bar{T}}$ in the body-fixed convected coordinate system in the reference and present configurations	57
$\hat{T}_{iJ}$	Rectangular Cartesian components of the double tensor $\bar{\bar{T}}$ in the fixed-in-space (inertial) coordinate system in the reference and present configurations	57

SUMMARY

The object of the investigation reported herein was to develop a method of analysis for thin structures (beams, rings, plates, and shells) that incorporates finite strain, elastic-plastic, strain-hardening, time-dependent material behavior implemented with respect to a fixed reference configuration (total Lagrangian formulation) and is consistently valid for finite strains and finite rotations.

The theory is formulated systematically in a body-fixed system of convected coordinates with materially-embedded vectors that deform in common with the continuum. Tensors are considered as linear vector functions, and use is made of the dyadic representation (instead of simply considering tensors as a collection of components) because these concise tools are helpful to clarify the physical laws under which materials deform. The kinematics of a deformable continuum is treated in detail, carefully defining precisely all quantities necessary for the analysis.

The finite strain plasticity theory of Hill is extended to include very complex material behavior (like the Bauschinger effect and strain rate dependence) by means of the "mechanical sublayer method". This plasticity theory is referred to quantities associated with a fixed reference configuration by means of proper transformations.

Strain-displacement equations for beams, rings, plates, and shells, valid for finite strains and rotations and including thinning effects are derived.

A new constant stiffness formulation of the finite element equations of motion is developed. This new formulation is more efficient computationally and better conditioned numerically than the conventional pseudo-force formulation. Furthermore, this new formulation is valid for finite strain behavior of any kind of material, while the conventional pseudo-force formulation is valid only for small-strain elastic-plastic materials.

The predictions of the finite element computer programs that incorporate the finite-strain elastic-plastic time dependent theory developed are compared with experimental data conducted at the MIT-ASRL and the Picatinny Arsenal. These include impulsive loading of beams, rings, and plates, and impact tests of steel spheres against aluminum beams and plates.

The results from the finite-strain analysis are compared with the results from the small-strain theory of plasticity to ascertain the range of validity of small-strain theory for the present kind of problems.

It is shown that, for the problems investigated, the finite-strain theory developed in this report gives much better predictions and agreement with experiment than does the traditional small-strain theory, and at practically no additional cost. This represents a very significant advance in the capability for the reliable prediction of nonlinear transient structural responses, including the reliable prediction of strains large enough to produce ductile-metal rupture.

SECTION 1

INTRODUCTION

1.1 Background

Concern for the ability of structures to withstand extreme loadings associated with accident conditions is receiving increased attention from engineers. To determine the degree of safety associated with the ability of their designs to sustain damage and absorb energy, engineers must now study the dynamic large-deflection elastic-plastic responses of structures subjected to those impact and transient loads which may occur in an accident. For instance, aircraft and aircraft engine designers are now studying the responses of turbojet engine containment structures which may be subjected to impact by engine rotor fragments following the potential failure of high-energy rotating engine parts (caused by the ingestion of birds or other foreign objects, low cycle and high cycle fatigue, etc.).

The power industry is concerned with components and equipment of conventional and nuclear powerplants which may be subjected to impact from a wide variety of "internally generated" missiles such as rotor blades, rotor disk segments, pipe or valve segments, etc. or to "externally-generated" missiles such as tornado-propelled pipes, rods, planks, utility poles, and automobiles, or to impact by aircraft or other such vehicles. Naval vehicles, such as submarines, must be designed to undergo significant transient undersea environmental loadings. Nonlinear transient response analysis is also employed in studies of offshore drilling platforms, response of buildings to seismic loadings, energy-absorbing capacity of automobiles, aircraft crashworthiness design and assessment, etc.

The loadings and/or fragment sizes, masses, geometries, and especially the attendant impact velocities for these "threats" are in an analysis domain quite different from those of "military missiles or loadings". Therefore, the extensive impact, penetration, perforation, and response data which have been collected for the military in experiments on various metallic, reinforced concrete, or other target materials, cannot serve as a basis for structural design against the cited civilian threats.

Although many structures may be designed to withstand severe loads by increasing their bulk, the addition of excessive weight may introduce severe economic penalties or degradation in performance for many applications. For efficient minimum weight design, it is then necessary to take better advantage of the energy-absorbing capacities of materials by permitting them to undergo large plastic strains and deformations. The complex and nonlinear character of such structural problems, however, makes it impossible to develop a classical analytical solution, and attention has been directed at approximate methods. The computer has provided a practical means of obtaining meaningful predictions for these types of complex problems, and corresponding numerical analysis procedures have been developed and expanded.

In order to provide detailed transient response data of the high resolution and accuracy required for a definitive assessment of the various predictive methods, a variety of impulsive loading and impact experiments has been conducted at the MIT-ASRL, including impact tests of steel spheres against or impulse loading of aluminum beams [1]* and aluminum panels [2]. The missiles and targets introduced in these experiments pose well-defined impact configurations and conditions for which transient strain, permanent strain, and permanent deflection data of high quality have been obtained. These test conditions have included impulse loading or impact velocities sufficient to produce responses of various severities up to and including threshold rupture conditions; often finite strains well beyond the "small strain range" were observed.

To date, an accurate and rational accounting of theoretical transient structural response prediction methods capable of incorporating the effects of large strains and deformations in metallic structures subjected to impact or impulse loading has not been demonstrated. No comparisons between small strain theory predictions and finite strain theory results

*Numbers in brackets [ ] denote references given in the reference list.

have been found in the literature to ascertain the range of validity of small strain theory.

The comparisons of predictions vs. experiments in the literature usually involve only displacements. With one exception [3], no comparisons have been found which show strain results vs. experimental measurements for strains that are outside the "small strain" range. It is to be noted that displacement results are a much poorer basis of establishing the validity of a finite element formulation than the use of direct strain comparisons. Strains involve derivation of displacements and, hence, are a much finer measure of accuracy of numerical methods. Furthermore, the strains themselves are usually of primary interest and significance. Since the stress-strain curves for many structural materials are usually very flat in the plastic range, a small error in the strain will produce a smaller error in the stress; whereas, a small error in the stress will produce a much larger error in the strain. For this reason, strain-based criteria for necking and fracture are more "sensitive" and more reliable than are stress-based corresponding criteria.

It is evident that finite strains are present in impulsively-loaded or impacted ductile metal structures deformed to the threshold of rupture. For example, the steel-sphere impacted and explosively-loaded beams and panels reported in Refs. 1 and 2 suffered large strains. Some of them slightly exceeded the rupture threshold, while other specimens experienced large strains but did not rupture. In addition, static uniaxial tensile, compressive, and cyclic loading tests have been conducted at the MIT-ASRL on the same aluminum material employed in the beam, plate, and shell large strain elastic-plastic transient response experiments. These tests revealed that the 6061-T651 aluminum material used for the impulsively-loaded and steel-sphere impacted beam and plate specimens fractures at strains that cannot be considered "small". The 6061-T651 aluminum test coupons that were machined parallel to the plate-stock roll direction (or longitudinal, "L", specimens) fractured in static uniaxial tests at relative elongations $E_u \doteq 0.8$, where $E_u = \frac{\ell_f}{\ell_o} - 1$, $\ell_f(\ell_o)$ being the final (initial) gage length. Large permanent strains (recorded using mechanically lightly-scribed marks) in the impulsively-loaded and steel sphere impacted plates reached $E_u \approx 0.3$ for the specimens that were at the rupture threshold.

Recognizing that finite strain effects are present in these problems, reliable predictions demand that such effects be included rationally and properly in the analysis.

Various formulations have been employed to treat nonlinear static and/or dynamic problems involving large rotations, large strains, and path-independent or path-dependent material nonlinearities; see for example, the articles of Bathe et al. [4], Nemat-Nasser [5], and Stricklin and Haisler [6]. All of these formulations use either three-dimensional continuum equations (most of them restricted to plane strain, plane stress, or axisymmetric solids) or the membrane theory of plates and shells (restricted to very thin shells). Furthermore, only isotropic and/or kinematic hardening rules are present in these finite-strain elastic-plastic formulations, and it seems that none of the computer implementations of these formulations employ a (total Lagrangian) <u>fixed</u> reference configuration for the analysis of finite-strain plasticity.

Of course, the strain-displacement equations which are valid for finite strains and large displacements of a three-dimensional continuum[a] have been known for more than a century [7, page 270] being due to Cauchy [8,9,10 and 11, for example] who fully elaborated the theory of small strain, obtaining it by specialization from his general theory of finite strain. The history of the membrane theory of plates and shells goes back to the eighteenth century [12]. However, the equations for large strains of thin bodies involving both membrane and bending effects are more difficult to derive and are not found in explicit form at least in the readily accessible engineering literature. Koiter [13, page 2]

---

a: And, consequently, the even simpler strain-displacement equations of a three-dimensional continuum under the simplifying assumptions of plane strain, plane stress, or axisymmetry are also well known.

recognizes that the strain-displacement relations for large deflections[a] of shells are "extremely complicated". It is the presence of second derivatives and the larger number of terms in curved beams, plates, and shells that restricts the extensive literature in finite strain analysis to the equations of three-dimensional continua and their simplified versions, or to membrane theory. The only method of analysis of transient, large-deflection, finite-strain, elastic-plastic response of structures utilizing shell theory (including both membrane and bending effects) seems to be the PETROS [14-21] series of codes developed in the period 1960-1975.

There are many fundamental differences between the formulations used in the present study and that of the earlier work of PETROS. The present equations are solved by the spatial finite-element method while PETROS is a spatial finite-difference computer code. Also, all of the equations in the present analysis are cast in the referential description[b] of motion taking a fixed (independent of time) placement[c] as reference, while PETROS uses essentially the present[d] placement as the reference. Also, these two analyses differ in the type and implementation of finite strain plasticity theory used.

---

a: Koiter defines "large deflections" as being characterized by the absence of restrictions as to the magnitude of the displacements, which is different from the engineering definition of "large deflections" -- usually understood as deflections larger than the thickness of the thin body but smaller than its spanwise dimensions.

b: Still called the Lagrangian description of motion, especially by hydrodynamicists, although it was first introduced by Euler.

c: The choice of this reference placement is arbitrary, it can be any configuration that the body has or might occupy, but usually one chooses the original, undeformed configuration. Truesdell [22, page 79] writes about the referential description: "Some form of it is always used in classical elasticity theory, and the best studies of the foundations of classical hydrodynamics from Euler's day to the present have employed it almost without fail".

d: Truesdell calls it the "relative" description [22, page 89] and it should not be confused with the spatial description of motion, known as "Eulerian" by hydrodynamicists.

Better choices of stress and stress rate are made in the present analysis. In the past two decades the number of publications concerned with finite strain plasticity has grown tremendously and significant advances have been made in the field of constitutive equations. The present study provides a more systematic and consistent presentation, formulation, and implementation of the concepts involved than has been found in the technical literature. On the other hand, the following useful features of PETROS: (1) the strain-rate dependent mechanical-sublayer-model for time-dependent plasticity (the present analysis, however, does not include relaxation effects and is restricted to isothermal conditions) and (2) a body-fixed system of convected (intrinsic) coordinates, are employed in the present analysis.

1.2 Purpose of the Present Study

The present work extends to the realm of finite strain the work done by the MIT-ASRL on developing finite difference methods [14-21] and finite-element methods [23-31] of structural analysis to predict large-displacement, elastic-plastic transient response. The object is to develop a finite element analysis for thin structures (beams, rings, plates, and shells) that incorporates finite-strain, elastic-plastic, time-dependent material behavior implemented with respect to a fixed reference configuration, and is valid for finite strains and rotations. The results obtained from this analysis are compared with experimental data as well as with results obtained from "small strain" large-displacement analysis in order to ascertain the range of validity of the "small strain" approximation.

1.3 Synopsis of the Present Study

Section 2 contains the concepts that are necessary for the development of a general finite strain theory for thin bodies with path-dependent and time-dependent material nonlinearities. The theory is systematically formulated in a body-fixed system of convected coordinates with materially-embedded vectors that deform in common with the continuum. A parallel development is presented in the traditional fixed-in-space system of constant vectors employed in the large majority of books in continuum mechanics. After a very brief refresher of tensor analysis, the kinematics of a deformable continuum are treated in some detail, defining deformation and strain tensors and their rates, as well as stress tensors and the different stress rates that are obtained according to different observers.

Many pitfalls in the analyses of various investigations are indicated. A very important point that has been consistently neglected by many analysts and computer programs is to indicate precisely in what form the constitutive properties have to be input. Most investigators after an elaborate treatment of a general theory in tensor notation, leave undefined the constitutive equations to be measured in the laboratory. In Subsection 2.5 the homogeneous uniaxial irrotational deformation of a continuum is treated, with at least two purposes in mind: (1) to give a clear physical understanding of the quantities involved in the analysis (which is not possible to obtain through the tensor index notation) and (2) since the most common material test is the uniaxial test, to identify precisely what are the quantities that one should measure in the laboratory (as well as how to express these data to conform with the constitutive equations used in the theoretical material model).

The general form of the constitutive equations employed in the analysis is presented in Section 3.

In Sections 4 and 5, the previous developments of Sections 2 and 3 are utilized to derive consistent strain-displacement equations and constitutive equations which are valid for finite strains and rotations of thin bodies. Some of these equations seem to be original (have not been found in the literature by the authors).

Discussed in proper perspective in Section 6 are the different forms of analysis currently utilized to analyze transient response problems with material and geometric nonlinearities, as well as several different timewise finite difference operators used to integrate the transient response equations. Also, the form of analysis utilized in the computer program and the solution of the governing equations are discussed.

In Section 7 the predictions of the finite element computer programs that incorporate the finite-strain elastic-plastic time-dependent theory developed in the previous sections are compared with experimental data for cases of impulsive loading as well as impact loading that produced transient nonlinear structural responses. It is shown that for the problems investigated, the finite strain theory developed in this report gives much better predictions than the traditional small strain theory -- and at no additional cost. These problems contain the nonlinear path-dependent and time-dependent response characteristics typically experienced by ductile metal structures when full advantage is taken of their energy absorbing capacities.

The entire study is summarized and pertinent conclusions are drawn in Section 8.

Finally, those readers who are interested in the principal results obtained and a discussion of those results (without the developmental details) need read only Sections 7 and 8.

SECTION 2

GENERAL FORMULATION

2.1 Introduction

In this section the concepts, equations, and relationships necessary for the numerical analysis of the transient structural responses of thin bodies with nonlinear time-dependent and path-dependent material behavior as well as with finite strains and rotations, are presented systematically and consistently. Use is made of the general approach to continuum mechanics that has been responsible for the significant advances in continuum mechanics in the last three de ;des. References that have influenced this write-up are: Truesdell et al. [7,22,32-40], Sedov et al. [41-49], Malvern [50], Jaunzemis [51], Leigh [52], Eringen [53-54], Biot [55], Green et al. [56-58], Prager [59], and Fung [60].

Tensors are considered as linear vector functions, and use is made of the dyadic representation (instead of simply considering tensors as a collection of components) because these concise tools are helpful to clarify the physical laws under which materials deform.

The brief refresher on tensor calculus, Subsection 2.3, follows Malvern [50]. Other more extensive references on this subject are the classic works of Schouten [61], Eisenhart [62], McConnell [63], and Synge and Schild [64], as well as the books of Sokolnikoff [65] and Willmore [66]. Designed especially for students of continuum mechanics are the monograph of Ericksen [67], the modern treatment of tensor analysis by Bowen and Wang [68], and the clear and lucid presentation by Sedov [41,42 and 45].

When considering finite deformations, it is essential to distinguish between a present configuration and a reference configuration which for many purposes one identifies as the original configuration. The concept of finite strain admits infinitely many definitions, but only a handful of these are useful for the solution of general problems. In the formulation of rate-type constitutive equations, the concepts of stress, stress rate, and strain rate, which admit infinitely many defintions as well, have to be defined properly. It turns out that the strain, stress, strain rate, and stress rate measures which a physically-valid theory of finite deformation of an elastic-plastic continuum uses are not (unfortunately) the same measures which are convenient for the numerical computation of the problem, and that both of these measures (the measures that the physically-valid theory and the numerical solution uses) are not the same as the quantities that one usually measures in a laboratory. Hence, it is of great importance to define all of these quantities in a consistent and rational way, and to define the relationships that transform one set of quantities into another. If this is not done properly and consistently in every area of analysis (the physical formulation, the numerical analysis of the problem, and the experimental measurements of the quantities that are necessary for the solution of the problem), then the results are not going to be fruitful.

Since the theory and analysis used in the present work is of considerable generality, a great many definitions are necessary. The work of laying down the foundations of this analysis has been exhaustive and time consuming. Unfortunately, many of the results present in Section 2 are scattered in a number of references, some of them of difficult access, and other results are just not present in any work.

2.2 Notation

Scalars (zero order tensors) are identified simply by letters; for example, the volume V, the mass density ρ, and the mass m.

Vectors (first order tensors) are identified by letters with an overbar: the displacement vector $\bar{u}$, the velocity vector $\bar{v}$, and the position vector $\bar{R}$.

Second order tensors are identified by letters with double overbars; for example, the Cauchy stress tensor $\bar{\bar{\sigma}}$, the Green (Lagrangian) strain tensor $\bar{\bar{\gamma}}$, and the spin tensor $\bar{\bar{W}}$.

The scalar components of tensors are denoted by attaching indices to a kernel letter without overbars. This kernel letter is the same letter used to denote the tensor quantity. These indices are lower case letters when the tensor is expressed in terms of the base vectors of the curvilinear coordinate system of the reference (undeformed or initial) configuration. They are capital letters when the tensor is expressed in terms of the base vectors of the curvilinear coordinate system of the present (deformed or current) configuration. Since the base vectors of a rectangular Cartesian system are constants (with respect to space and time), the base vectors of the Cartesian systems of the reference and present configuration are the same. Hence, it is an arbitrary choice to assign either lower case or capital letters to the indices of a tensor component in a Cartesian system. Usually this choice is done according to the most frequently used curvilinear representation of the tensor.

When the components of tensors are referred to a rectangular Cartesian coordinate system, they are identified by a circumflex sign "^" (a "hat") on top of the kernel letter. Components of tensors referred to a curvilinear coordinate system do not have the circumflex sign (they do not wear hats).

For example $\bar{\bar{A}}$ is a second order tensor; A_{ij} are its components* in a curvilinear coordinate system related to the reference configuration, A_{IJ} are its components* in a curvilinear coordinate system related to the present configuration; and $\hat{A}_{ij}$ are its components in a rectangular Cartesian coordinate system.

In order to help the reader, Table 1 relates the notation utilized in this review with the notation utilized in some treatises of Continuum Mechanics. The number in parenthesis indicates the page in which the quantity is defined or first appears.

2.3 Review of Tensor Analysis

2.3.1 Vectors

In an n-dimensional vector space any set of n linearly independent vectors $\bar{b}_1, \bar{b}_2, \ldots \bar{b}_n$ is called a basis. Any $\bar{v}$ in the space can be expressed as a unique linear combination of the n base vectors of the basis:

*These components are the so-called covariant components.

$$\bar{v} = \sum_{k=1}^{n} v^k \bar{b}_k \equiv v^k \bar{b}_k = v^1 \bar{b}_1 + v^2 \bar{b}_2 + \ldots\ldots + v^{(n)} \bar{b}_{(n)} \tag{2.1}$$

The coefficients v^k are called the contravariant components i.e., with superscript k of the vector $\bar{v}$ with respect to the basis $\bar{b}_k$. Note that the base vectors $\bar{b}_k$ need not be unit vectors, and they need not be orthogonal.

If the Euclidean vector space is referred to a basis, then

$$\bar{u} = u^r \bar{b}_r \qquad \bar{v} = v^s \bar{b}_s \tag{2.2}$$

and then

$$\bar{u}\cdot\bar{v} = u^r v^s \bar{b}_r \cdot \bar{b}_s \tag{2.3}$$

where $\bar{u}.\bar{v}$ is the dot or scalar product of the vectors $\bar{u}$ and $\bar{v}$.

Let

$$g_{rs} \equiv \bar{b}_r \cdot \bar{b}_s \tag{2.4}$$

then it follows from Eq. 2.3 that

$$\bar{u}\cdot\bar{v} = u^r v^s g_{rs} \tag{2.5}$$

Note that g_{rs} is symmetric; that is,

$$g_{rs} = g_{sr} \tag{2.6}$$

since the dot product of two vectors is commutative:

$$\bar{b}_r \cdot \bar{b}_s = \bar{b}_s \cdot \bar{b}_r \tag{2.7}$$

Dual (or reciprocal) base vectors $\bar{b}^q$ ($q = 1,2, \ldots n$) are defined for each given set $\bar{b}_p$ ($p = 1,2, \ldots n$) of base vectors in Euclidean vector space as the set of vectors satisfying

$$\bar{b}_p \cdot \bar{b}^q = \delta_p^q \tag{2.8}$$

where the Kronecker delta δ^r_s is defined by $\delta^r_s = \begin{cases} 1 \text{ if } r=s \\ 0 \text{ if } r\neq s \end{cases}$

For the important case of ordinary vectors with n = 3 one can express the dual base vectors $\bar{b}^k$ in terms of the original basis $\bar{b}_k$ by using the cross product $(\bar{u} \times \bar{v})$ as follows:

$$\bar{b}^1 = \frac{\bar{b}_2 \times \bar{b}_3}{\bar{b}_1 \cdot (\bar{b}_2 \times \bar{b}_3)} \quad \bar{b}^2 = \frac{\bar{b}_3 \times \bar{b}_1}{\bar{b}_1 \cdot (\bar{b}_2 \times \bar{b}_3)} \quad \bar{b}^3 = \frac{\bar{b}_1 \times \bar{b}_2}{\bar{b}_1 \cdot (\bar{b}_2 \times \bar{b}_3)} \tag{2.9}$$

If the given basis is orthonormal (composed of mutually orthogonal unit vectors), then $\bar{b}_1 \cdot (\bar{b}_2 \times \bar{b}_3) = 1$ (for a right-handed system) and the dual basis is identical to the given basis. When the base vectors of the given basis are mutually orthogonal but not orthonormal, then the magnitude of each of the dual base vectors is then the reciprocal of the corresponding base vector in the given basis:

$$|\bar{b}^K| = \frac{1}{|\bar{b}_K|} \qquad \text{where} \qquad |\bar{b}_K| = \sqrt{\bar{b}_K \cdot \bar{b}_K} \tag{2.10}$$

<u>Covariant components</u> v_k (i.e. subscript k) of the vector $\bar{v}$ <u>with respect to the basis $\bar{b}^k$</u> are defined as

$$\bar{V} = V_K \bar{b}^K = V^K \bar{b}_K \tag{2.11}$$

Note that

$$V_p = \bar{V} \cdot \bar{b}_p \tag{2.12}$$

$$V^q = \bar{V} \cdot \bar{b}^q \tag{2.13}$$

The fundamental-tensor components g_{ij}, g^{ij}, $g^{i\cdot}_{\cdot j}$, $g^{\cdot i}_{j \cdot}$ are defined as follows:

$$g_{ij} \equiv \bar{b}_i \cdot \bar{b}_j \quad g^{ij} \equiv \bar{b}^i \cdot \bar{b}^j \quad g^{i\cdot}_{\cdot j} \equiv \bar{b}^i \cdot \bar{b}_j \quad g^{\cdot j}_{i \cdot} \equiv \bar{b}_i \cdot \bar{b}^j \tag{2.14}$$

Observe that the following relations are satisfied:

$$g_{ij} = g_{ji} \qquad g^{ij} = g^{ji} \qquad g^{i\cdot}_{\cdot j} = g^{\cdot i}_{j\cdot} = \delta^i_j \tag{2.15}$$

Therefore, one can express the contravariant components v^i and the covariant components v_i of a vector $\bar{v}$ in terms of the reciprocal components and the fundamental-tensor components, as follows:

$$\begin{aligned}
v_i &= \bar{v}\cdot\bar{b}_i = v^j\,\bar{b}_j\cdot\bar{b}_i = v^j g_{ij} \\
v^i &= \bar{v}\cdot\bar{b}^i = v_j\,\bar{b}^j\cdot\bar{b}^i = v_j\,g^{ij} \\
v^i &= \bar{v}\cdot\bar{b}^i = v^j\,\bar{b}_j\cdot\bar{b}^i = v^j g_{j\cdot}^{\cdot i} = v^j\,\delta^i_j \\
v_i &= \bar{v}\cdot\bar{b}_i = v_j\,\bar{b}^j\cdot\bar{b}_i = v_j\,g^{j}_{\cdot i} = v_j\,\delta^j_i
\end{aligned} \tag{2.16}$$

Evidently the various sets of quantities g_{ij}, g^{ij}, $g^{i\cdot}_{\cdot j}$ and $g^{\cdot i}_{j\cdot}$ have the property that when they are used as the coefficients of a linear transformation operating on the covariant or contravariant components of a vector, they yield as a result of the operation the components <u>of the same vector</u> (covariant or contravariant components, depending on which set is used). These quantities are therefore components of the <u>unit</u> (second-order) <u>tensor</u> $\bar{\bar{1}}$ such that

$$\bar{v} = \bar{v}\cdot\bar{\bar{1}} = \bar{\bar{1}}\cdot\bar{v} \tag{2.17}$$

The unit tensor $\bar{\bar{1}}$ is also called the <u>fundamental tensor</u> or the <u>metric tensor</u>* of the space. The g_{ij} are its covariant components, g^{ij} its contravariant components, and $g^{i\cdot}_{\cdot j} = g^{\cdot i}_{j\cdot} = \delta^i_j$ its mixed components. The process of raising or lowering indices can also be performed on the base vectors themselves:

$$\bar{b}^j = g^{ji}\,\bar{b}_i \qquad \bar{b}_j = g_{ji}\,\bar{b}^i \tag{2.18}$$

---

*They are called the metric tensors, because all essential metric properties of space are completely determined by these tensors, and their derivatives.

The matrices $[g^{ij}]$ and $[g_{ij}]$ are inverse to each other:

$$[g^{ij}] = [g_{ij}]^{-1} \tag{2.19}$$

By definition, the determinants of these matrices are

$$g \equiv \det [g_{ij}] \qquad \frac{1}{g} = \det [g^{ij}]$$

2.3.2 Tensors

2.3.2.1 Linear Vector Functions

A second order tensor $\bar{\bar{T}}$ is a linear vector function associating with each argument vector another vector, e.g.,

$$\bar{u} = \bar{\bar{T}} \cdot \bar{v} \tag{2.20}$$

For any given basis $\bar{b}_1, \bar{b}_2, \ldots \bar{b}_n$ either of the two vectors may be represented by either covariant or contravariant components v_j or v^j and u_i or u^i. There are, thus, four possible sets of n^2 coefficients for the four different linear transformations

$$u_i = T_{ij} v^j \qquad u_i = T_{i\cdot}^{\cdot j} v_j \qquad u^i = T^{ij} v_j \qquad u^i = T_{\cdot j}^{i\cdot} v^j \tag{2.21}$$

involving, respectively, the

covariant components T_{ij}

contravariant components T^{ij}

or mixed components $T_{\cdot j}^{i\cdot}$ or $T_{i\cdot}^{\cdot j}$

Since in general $T_{\cdot j}^{i\cdot} \neq T_{j\cdot}^{\cdot i}$, it is necessary to observe carefully the order of the indices.

One can also express these tensor components as the dot products of the base vectors and the second order tensor, using Eqs. 2.12 and 2.13, as follows. Observe that since $u_i = \bar{b}_i . \bar{u}$ and $v_j = \bar{b}_j . \bar{v}$, then

$$T_{ik} = \bar{b}_i \cdot \overline{\overline{T}} \cdot \bar{b}_k \qquad T^{ik} = \bar{b}^i \cdot \overline{\overline{T}} \cdot \bar{b}^k$$

$$T_{i\cdot}^{\cdot k} = \bar{b}_i \cdot \overline{\overline{T}} \cdot \bar{b}^k \qquad T^{i\cdot}_{\cdot k} = \bar{b}^i \cdot \overline{\overline{T}} \cdot \bar{b}_k \tag{2.22}$$

A symmetric tensor $\overline{\overline{T}}$ is defined as one that is operationally identical to its transpose $\overline{\overline{T}}^T$, so that if $\overline{\overline{T}}$ is symmetric:

$$\overline{\overline{T}} = \overline{\overline{T}}^T$$

$$\overline{\overline{T}} \cdot \bar{v} = \bar{v} \cdot \overline{\overline{T}} \qquad \text{for any vector } \bar{v} \tag{2.23}$$

Also, its components obey:

$$T_{ij} = T_{ji} \qquad T^{ij} = T^{ji} \qquad T^{i\cdot}_{\cdot j} = T_{j\cdot}^{\cdot i} \tag{2.24}$$

It is convenient to write the mixed components of a symmetric tensor $\overline{\overline{T}}$ as:

$$T^i_j \equiv T^{i\cdot}_{\cdot j} = T_{j\cdot}^{\cdot i} \tag{2.25}$$

But note, that, in general (even for symmetric and antisymmetric tensors)

$$T^i_j \neq T^j_i \tag{2.26}$$

For a symmetric tensor, the matrix of covariant or contravariant components is symmetric while the mixed component matrices are not in general symmetric, because the third equation relates elements of the two different matrices of mixed components instead of symmetrically placed elements of the same matrix. To make this point clear, and for convenient reference, these matrices* are, for n = 3:

*The symbol || || is standard notation for matrices in books on tensor analysis (for example, see Refs. 7,22,40,41,42, and 61).

$$T_{ij} = \begin{Vmatrix} T_{11} & T_{12} & T_{13} \\ T_{21} & T_{22} & T_{23} \\ T_{31} & T_{32} & T_{33} \end{Vmatrix} \underset{\bar{\bar{T}} = \bar{\bar{T}}^{T}}{\overset{=}{if}} \begin{Vmatrix} T_{11} & T_{12} & T_{13} \\ T_{12} & T_{22} & T_{23} \\ T_{13} & T_{23} & T_{33} \end{Vmatrix} \tag{2.27}$$

$$T^{ij} = \begin{Vmatrix} T^{11} & T^{12} & T^{13} \\ T^{21} & T^{22} & T^{23} \\ T^{31} & T^{32} & T^{33} \end{Vmatrix} \underset{\bar{\bar{T}} = \bar{\bar{T}}^{T}}{\overset{=}{if}} \begin{Vmatrix} T^{11} & T^{12} & T^{13} \\ T^{12} & T^{22} & T^{23} \\ T^{13} & T^{23} & T^{33} \end{Vmatrix} \tag{2.28}$$

$$T^{i\cdot}_{\cdot j} = \begin{Vmatrix} T^{1\cdot}_{\cdot 1} & T^{1\cdot}_{\cdot 2} & T^{1\cdot}_{\cdot 3} \\ T^{2\cdot}_{\cdot 1} & T^{2\cdot}_{\cdot 2} & T^{2\cdot}_{\cdot 3} \\ T^{3\cdot}_{\cdot 1} & T^{3\cdot}_{\cdot 2} & T^{3\cdot}_{\cdot 3} \end{Vmatrix} \tag{2.29}$$

$$T_{i\cdot}^{\cdot j} \quad \begin{Vmatrix} T_{1\cdot}^{\cdot 1} & T_{1\cdot}^{\cdot 2} & T_{1\cdot}^{\cdot 3} \\ T_{2\cdot}^{\cdot 1} & T_{2\cdot}^{\cdot 2} & T_{2\cdot}^{\cdot 3} \\ T_{3\cdot}^{\cdot 1} & T_{3\cdot}^{\cdot 2} & T_{3\cdot}^{\cdot 3} \end{Vmatrix} \tag{2.30}$$

$T^{i}_{\cdot j} = T_{j\cdot}^{\cdot i}$ if $\bar{\bar{T}}$ is symmetric, implies for n = 3:

$$\begin{Vmatrix} T^{1\cdot}_{\cdot 1} & T^{1\cdot}_{\cdot 2} & T^{1\cdot}_{\cdot 3} \\ T^{2\cdot}_{\cdot 1} & T^{2\cdot}_{\cdot 2} & T^{2\cdot}_{\cdot 3} \\ T^{3\cdot}_{\cdot 1} & T^{3\cdot}_{\cdot 2} & T^{3\cdot}_{\cdot 3} \end{Vmatrix} = \begin{Vmatrix} T_{1\cdot}^{\cdot 1} & T_{2\cdot}^{\cdot 1} & T_{3\cdot}^{\cdot 1} \\ T_{1\cdot}^{\cdot 2} & T_{2\cdot}^{\cdot 2} & T_{3\cdot}^{\cdot 2} \\ T_{1\cdot}^{\cdot 3} & T_{2\cdot}^{\cdot 3} & T_{3\cdot}^{\cdot 3} \end{Vmatrix} \tag{2.31}$$

or $$\left\| T^{i\cdot}{}_{\cdot j} \right\| = \left\| T_{i\cdot}{}^{\cdot j} \right\|^{T} \qquad \left\| T^{i\cdot}{}_{\cdot j} \right\| \neq \left\| T^{i\cdot}{}_{\cdot j} \right\|^{T}$$

In effect, independently of its position, whether up or down, the first index of an element of the matrix denotes the number of the row, and the second the number of the column corresponding to that element.

As Sedov points out [41], the operations of addition, of multiplication by a number, and of scalar multiplication of tensors of the second rank correspond to analogous operations on matrices; hence, the use of methods and results of matrix calculus facilitates the development of the theory of tensor functions.

The <u>operational product</u> ($\overline{\overline{T}}.\overline{\overline{S}}$ or $\overline{\overline{T}}\,\overline{\overline{S}}$) of two second order tensors ($\overline{\overline{T}}$ and $\overline{\overline{S}}$) produces a second order tensor ($\overline{\overline{P}}$) such that

$$\overline{\overline{P}} = \overline{\overline{T}} \cdot \overline{\overline{S}} \tag{2.32}$$

Also,

$$\overline{\overline{P}} \cdot \overline{v} = (\overline{\overline{T}} \cdot \overline{\overline{S}}) \cdot \overline{v} = \overline{\overline{T}} \cdot (\overline{\overline{S}} \cdot \overline{v}) \tag{2.33}$$

Its components are given by

$$P_{ij} = T_{i\cdot}{}^{\cdot k} S_{kj} = T_{ik} S^{k\cdot}{}_{\cdot j} \tag{2.34}$$

$$P^{ij} = T^{i\cdot}{}_{\cdot k} S^{kj} = T^{ik} S_{k\cdot}{}^{\cdot j} \tag{2.35}$$

$$P^{i\cdot}{}_{\cdot j} = T^{i\cdot}{}_{\cdot k} S^{k\cdot}{}_{\cdot j} \tag{2.36}$$

$$P_{i\cdot}{}^{\cdot j} = T_{i\cdot}{}^{\cdot k} S_{k\cdot}{}^{\cdot j} \tag{2.37}$$

Two <u>scalar products</u> (i.e., $\overline{\overline{T}}:\overline{\overline{S}}$ and $\overline{\overline{T}}\cdot\cdot\overline{\overline{S}}$) of two second order tensors can be defined. The <u>scalar</u> product $\overline{\overline{T}}:\overline{\overline{S}}$ is produced by a double contraction of the outer product as follows:

$$\overline{\overline{T}} : \overline{\overline{S}} \equiv T^{ij} S_{ij} = T_{ij} S^{ij} = T^{i\cdot}{}_{\cdot j} S_{i\cdot}{}^{\cdot j} = T_{i\cdot}{}^{\cdot j} S^{i\cdot}{}_{\cdot j} \tag{2.38}$$

Note that the two first suffixes are the same, while the two second indices are the same.

The scalar product $\bar{\bar{T}} \cdot \bar{\bar{S}}$ is defined as follows:

$$\bar{\bar{T}} \cdot\cdot \bar{\bar{S}} = T^{ij} S_{ji} = T_{ij} S^{ji} = T^{i}_{\cdot j} S^{j}_{\cdot i} = T_{i}^{\cdot j} S_{j}^{\cdot i} \tag{2.39}$$

Note that the two inside indices are equal and the two outside indices are equal. In general $\bar{\bar{T}} : \bar{\bar{S}} \neq \bar{\bar{T}} \cdot\cdot \bar{\bar{S}}$, but if either one of the two tensors symmetric then $\bar{\bar{T}} : \bar{\bar{S}} = \bar{\bar{T}} \cdot\cdot \bar{\bar{S}}$.

2.3.2.2 Dyadic Representation of a Tensor

The open product or tensor product $\bar{a}\bar{b}$ of two vectors $\bar{a}$ and $\bar{b}$ is called a dyad. A linear combination of such dyads is called a dyadic. Higher-order open products are called polyads and linear combinations of polyads are called polyadics (all polyads in a polyadic must be of the same order). All usual multiplicative rules of elementary algebra hold for polyads, except that open multiplication is not commutative, that is, in general

$$\bar{a}\bar{b} \neq \bar{b}\bar{a} \tag{2.40}$$

Also, the single dot product of two dyads is not commutative:

$$\bar{a}\bar{b} \cdot \bar{c}\bar{d} \neq \bar{c}\bar{d} \cdot \bar{a}\bar{b} \tag{2.41}$$

The scalar product (or double dot product) of two dyads denoted by $\bar{a}\bar{b}:\bar{c}\bar{d}$ is defined as the scalar obtained by multiplying together the two scalar products $\bar{a}.\bar{c}$ and $\bar{b}.\bar{d}$. Note that the first vector of the first dyad multiplies the first vector of the second dyad, and the second vector of the first dyad multiplies the second vector of the second dyad. The scalar product is commutative:

$$\begin{aligned} \bar{a}\bar{b} : \bar{c}\bar{d} &= (\bar{a} \cdot \bar{c})(\bar{b} \cdot \bar{d}) = (\bar{c} \cdot \bar{a})(\bar{d} \cdot \bar{b}) \\ &= \bar{c}\bar{d} : \bar{a}\bar{b} \end{aligned} \tag{2.42}$$

The double dot notation with the two dots on the same level denotes the product obtained by multiplying the two outside vectors together and the two inside vectors together:

$$\bar{a}\bar{b} \cdot\cdot \bar{c}\bar{d} = (\bar{a}\cdot\bar{d})(\bar{b}\cdot\bar{c}) \tag{2.43}$$

Every second order tensor can be represented as a dyadic, a linear combination of the n^2 dyads formed from n linearly independent base vectors of the n-dimensional vector space on which the tensor is defined. For example, in three dimensions ($n = 3$, $n^2 = 9$) with base vectors $\bar{b}_1$, $\bar{b}_2$, $\bar{b}_3$, one may write any second order tensor $\bar{\bar{T}}$ as:

$$\begin{aligned}\bar{\bar{T}} = {} & T^{11}\bar{b}_1\bar{b}_1 + T^{12}\bar{b}_1\bar{b}_2 + T^{13}\bar{b}_1\bar{b}_3 \\ & + T^{21}\bar{b}_2\bar{b}_1 + T^{22}\bar{b}_2\bar{b}_2 + T^{23}\bar{b}_2\bar{b}_3 \\ & + T^{31}\bar{b}_3\bar{b}_1 + T^{32}\bar{b}_3\bar{b}_2 + T^{33}\bar{b}_3\bar{b}_3\end{aligned} \tag{2.44}$$

or

$$\bar{\bar{T}} = T^{rs}\bar{b}_r\bar{b}_s \tag{2.45}$$

where the T^{rs} are the contravariant components of the tensor with respect to the basis $\bar{b}_r\bar{b}_s$. In Euclidean vector space, by introducing the dual basis $\bar{b}^k$, one obtains additional representations for $\bar{\bar{T}}$:

$$\bar{\bar{T}} = T^{rs}\bar{b}_r\bar{b}_s = T_{rs}\bar{b}^r\bar{b}^s = T^{r\cdot}_{\cdot s}\bar{b}_r\bar{b}^s = T_{r\cdot}^{\cdot s}\bar{b}^r\bar{b}_s \tag{2.46}$$

The convention of upper and lower indices does not guarantee a unique tensor for a given set of components, since, for example, in general

$$T^{r\cdot}_{\cdot s}\bar{b}_r\bar{b}^s \neq T^{r\cdot}_{\cdot s}\bar{b}^s\bar{b}_r \tag{2.47}$$

For definitiveness, the convention that the first index on the tensor component goes with the first vector of the dyad is adopted as, for example:

$$\overline{\overline{\overline{T}}} = T^{r\cdot}_{\cdot s}\,\bar{b}_r\,\bar{b}^s \neq T^{r\cdot}_{\cdot s}\,\bar{b}^s\,\bar{b}_r \qquad (2.48)$$

The polyadic representation of a tensor makes it much simpler to develop the theory of operations on tensors, particularly in the theory of differentiation of tensors with respect to coordinates or scalar parameters when the vectors of the bases are variable, and especially when a given tensor has to be considered simultaneously in different bases moving with respect to one another.

2.3.2.3 Covariant Differentiation of a Tensor

The set of partial derivatives (with respect to the coordinates) of a covariant vector, in general, is not a tensor.

The covariant derivatives of a tensor component are defined in such a way that they are tensor components which reduce to the usual partial derivatives in rectangular Cartesian coordinates. The covariant derivative appears naturally when the partial derivative of a vector is taken, and in the process certain non-tensor, three-index quantities, called Christoffel Symbols arise naturally when partial derivatives of the base vectors are taken; since the base vectors are functions of position, they cannot be treated as constants in differentiation. The derivative of the covariant and contravariant base can be shown to be:

$$\frac{\partial \bar{g}_m}{\partial \xi^n} = \left\{ {s \atop m\ \ n} \right\} \bar{g}_s \qquad (2.49)$$

$$\frac{\partial \bar{g}^m}{\partial \xi^n} = -\left\{ {m \atop n\ \ s} \right\} \bar{g}^s \qquad (2.50)$$

where the (nontensor) three index quantities called Christoffel symbols of the second kind are

$$\left\{ {s \atop m\ \ n} \right\} \equiv \frac{1}{2} g^{rs} \left(\frac{\partial g_{nr}}{\partial \xi^m} + \frac{\partial g_{rm}}{\partial \xi^n} - \frac{\partial g_{mn}}{\partial \xi^r} \right) \qquad (2.51)$$

If the coordinate system is Cartesian, i.e. the base vectors are constants, then the Christoffel symbols of the second kind are identically zero:

$$\left\{ {k \atop i\ \ j} \right\} = 0 \qquad \text{for a Cartesian coordinate system.}$$

Therefore, the covariant derivative (denoted by $a_{i,j}$) of a covariant vector component a_i is:

$$\bar{a} = a_i \bar{g}^i \tag{2.52}$$

$$\frac{\partial \bar{a}}{\partial \xi^j} = \frac{\partial a_i}{\partial \xi^j} \bar{g}^i + a_k \frac{\partial \bar{g}^k}{\partial \xi^j} = \frac{\partial a_i}{\partial \xi^j} \bar{g}^i - a_k \left\{ {k \atop j\ \ i} \right\} \bar{g}^i$$

$$= \left(\frac{\partial a_i}{\partial \xi^j} - a_k \left\{ {k \atop i\ \ j} \right\} \right) \bar{g}^i \equiv a_{i,j} \bar{g}^i$$

$$\boxed{a_{i,j} \equiv \frac{\partial a_i}{\partial \xi^j} - a_k \left\{ {k \atop i\ \ j} \right\}} \tag{2.53}$$

Similarly, the covariant derivative (denoted by $a^i{}_{,j}$) of a contravariant vector component a^i is:

$$\bar{a} = a^i \bar{g}_i \tag{2.54}$$

$$\frac{\partial \bar{a}}{\partial \xi^j} = \frac{\partial a^i}{\partial \xi^j} \bar{g}_i + a^k \frac{\partial \bar{g}_k}{\partial \xi^j} = \frac{\partial a^i}{\partial \xi^j} \bar{g}_i + a^k \left\{ {i \atop k\ \ j} \right\} \bar{g}_i$$

$$= \left(\frac{\partial a^i}{\partial \xi^j} + a^k \left\{ {i \atop k\ \ j} \right\} \right) \bar{g}_i \equiv a^i{}_{,j} \bar{g}_i$$

$$\boxed{a^i{}_{,j} = \frac{\partial a^i}{\partial \xi^j} + a^k \left\{ {i \atop k\ \ j} \right\}} \tag{2.55}$$

Furthermore,

$$\frac{\partial \bar{g}_m}{\partial \xi_n} = \frac{\partial \bar{g}_m}{\partial \xi^i} \frac{\partial \xi^i}{\partial \xi_n} = \frac{\partial \bar{g}_m}{\partial \xi^i} g^{ni} = g^{ni} \left\{ {s \atop n\ \ i} \right\} \bar{g}_s \tag{2.56}$$

and

$$\frac{\partial \bar{g}^m}{\partial \xi_n} = - g^{ni} \left\{ {m \atop s \;\; i} \right\} \bar{g}^s \tag{2.57}$$

since

$$d\xi^i = g^{ni} d\xi_n$$

Covariant derivatives of higher order tensor components appear quite naturally when the partial derivative of the polyadic is taken. For example, if

$$\bar{\bar{\bar{T}}} = T^{rs} \bar{g}_r \bar{g}_s = T_{rs} \bar{g}^r \bar{g}^s = T^{r\cdot}_{\cdot s} \bar{g}_r \bar{g}^s = T_{r\cdot}^{\cdot s} \bar{g}^r \bar{g}_s \tag{2.58}$$

then

$$\begin{aligned} \frac{\partial \bar{\bar{\bar{T}}}}{\partial \xi^p} &= \frac{\partial T^{rs}}{\partial \xi^p} \bar{g}_r \bar{g}_s + T^{ks} \frac{\partial \bar{g}_k}{\partial \xi^p} \bar{g}_s + T^{rk} \bar{g}_r \frac{\partial \bar{g}_k}{\partial \xi^p} \\ &= \frac{\partial T^{rs}}{\partial \xi^p} \bar{g}_r \bar{g}_s + T^{ks} \left\{ {r \atop k \;\; p} \right\} \bar{g}_r \bar{g}_s + T^{rk} \left\{ {s \atop k \;\; p} \right\} \bar{g}_r \bar{g}_s \\ &= T^{rs}_{\;\;,p} \bar{g}_r \bar{g}_s = \left(\frac{\partial T^{rs}}{\partial \xi^p} + T^{ks} \left\{ {r \atop k \;\; p} \right\} + T^{rk} \left\{ {s \atop k \;\; p} \right\} \right) \bar{g}_r \bar{g}_s \end{aligned} \tag{2.59}$$

hence,

$$\boxed{T^{rs}_{\;\;,p} = \frac{\partial T^{rs}}{\partial \xi^p} + T^{ks} \left\{ {r \atop k \;\; p} \right\} + T^{rk} \left\{ {s \atop k \;\; p} \right\}} \tag{2.60}$$

Similarly,

$$\boxed{T_{rs,p} = \frac{\partial T_{rs}}{\partial \xi^p} - T_{ks} \left\{ {k \atop r \;\; p} \right\} - T_{rk} \left\{ {k \atop s \;\; p} \right\}} \tag{2.61}$$

$$\boxed{T^{r\cdot}_{\cdot s,p} = \frac{\partial T^{r\cdot}_{\cdot s}}{\partial \xi^p} + T^{k\cdot}_{\cdot s} \left\{ {r \atop k \;\; p} \right\} - T^{r\cdot}_{\cdot k} \left\{ {k \atop s \;\; p} \right\}} \tag{2.62}$$

where,

$$\frac{\partial \overline{\overline{T}}}{\partial \xi^p} = T^{rs}{}_{,p}\, \bar{g}_r \bar{g}_s = T_{rs,p}\, \bar{g}^r \bar{g}^s = T^{r}{}_{\cdot s,p}\, \bar{g}_r \bar{g}^s \qquad (2.63)$$

2.4 Kinematics of a Deformable Medium

Motion is always determined with respect to some reference coordinate system. A correspondence between numbers and spatial points is established with the aid of a coordinate system. A continuous medium represents a continuous accumulation of material points. By definition, knowledge of the motion of a continuous medium implies knowledge of the motion of all material points. For this purpose, one must treat individually distinct material points.

In kinematics, a continuous medium may be conceived of as an abstract geometrical object, and not merely a material body. For instance, it may sometimes be agreed to represent by points in a plane the prices of some products and to study the motion of prices in economics by the methods of the kinematics of continuous media.

Besides the concept of laws of motion and coordinate systems, one must still introduce for the description of the motion of continuous media certain other concepts, in particular, that of velocities of particles of a continuum medium. Strain tensors are fundamental characteristics which arise in the deformation of bodies, and they enter into the basic equations which describe the motion of continua. Strain tensors compare two states of a medium, while the rate-of-deformation tensor is a characteristic of the medium at a given instant of time.

2.4.1 General Description

Lower case letters are used for quantities that identify the points of the medium at some reference instant of time t_o. Capital letters are used for quantities that correspond to the points of the medium at the current time t.

Consider arbitrary displacements of a continuum. Let the position of the points of the continuum be defined in a rectangular <u>Cartesian system</u> of spatial (Eulerian) coordinates $X_I = X_1, X_2, X_3$ and the reference position of the points of the continuum by the referential (also called Lagrangian or material) coordinates $x_i \equiv X_i = x_1, x_2, x_3$ (here, for example, it is convenient to adopt $x_i \equiv X_i$ so as to differentiate between x_1 and X_1). This system of Cartesian coordinates is <u>fixed-in-space</u>, or inertial, and it has orthonormal base vectors: $\bar{i}_I = \bar{i}^I = \bar{i}_i = \bar{i}^i$.

Also, it will be convenient to use the <u>convected body-fixed</u> (also called intrinsic) system of (Lagrangian, material or embedded) curvilinear coordinates ξ^i which moves with the points of the medium, has base vectors $\bar{g}_i$ in the reference configuration and base vectors $\bar{G}_I \equiv \dot{\bar{g}}_I$ in the deformed configuration. These two systems can be displayed conveniently as follows; for a three-dimensional Euclidean space:

<u>Fixed-in-Space</u> (Inertial) <u>System</u>	Rectangular Cartesian Coordinates	Reference Configuration ($t = t_o$)	x_1, x_2, x_3
		Present Configuration ($t = t$)	X_1, X_2, X_3
	Base Vectors	$\bar{i}_1$, $\bar{i}_2$, $\bar{i}_3$	
<u>Body-Fixed</u> (Convected, Intrinsic, or Embedded) <u>System</u>	Curvilinear Coordinates	ξ^1, ξ^2, ξ^3	
	Base Vectors	Reference Configuration ($t = t_o$)	$\bar{g}_1$, $\bar{g}_2$, $\bar{g}_3$
		Present Configuration ($t = t$)	$\bar{G}_1$, $\bar{G}_2$, $\bar{G}_3$

Note that the (Lagrangian) coordinates ξ^i are "frozen" into the medium, and they deform with it so that a given material point is always identified with its material coordinate ξ^i. When motion is considered, all three bases ($\bar{i}_i$, $\bar{g}_i$, and $\bar{G}_I$) can coincide at some instant of time, but the rate of change of these bases with respect to the motion of a fixed point of the medium will be different.

Position vectors $\bar{r}$ and $\bar{R}$ (see Fig. 1) from the origin of the Cartesian system X_I to the undeformed curvilinear system ξ^i with base vectors $\bar{g}_i$ and to the deformed curvilinear system ξ^i with base vectors $\bar{G}_I$, respectively, are defined as

$$\bar{r} = x_i \bar{i}_i \qquad \bar{R} = X_I \bar{i}_i$$

$$d\bar{r} = dx_i \bar{i}_i = d\xi^i \bar{g}_i = d\xi_i \bar{g}^i \tag{2.64}$$

$$d\bar{R} = dX_I \bar{i}_i = d\xi^i \bar{G}_I = d\xi_i \bar{G}^I$$

Observe that, for <u>any</u> time t,

$$\bar{g}_I = \bar{G}_I \qquad \bar{g}_i = \bar{G}_i \qquad \bar{g}_i \neq \bar{G}_I \qquad x_i \neq X_I$$
$$x_i = X_i \qquad x_i = X_i \qquad \bar{i}_I = \bar{i}_i \qquad \xi^i = \xi^I \tag{2.65}$$

and that

$$\bar{g}_i = \bar{G}_I \; (t = t_0) \qquad x_i = X_I \; (t = t_0)$$

The base vectors of the undeformed and deformed configuration, in the convected system can be expressed as:

$$\bar{g}_i = \frac{\partial \bar{r}}{\partial \xi^i} = \frac{\partial x_j}{\partial \xi^i} \bar{i}_j \qquad \bar{G}_I = \frac{\partial \bar{R}}{\partial \xi^i} = \frac{\partial X_J}{\partial \xi^i} \bar{i}_j \tag{2.66}$$

The metric tensor components in the undeformed and the deformed configuration are

$$g_{ij} = \bar{g}_i \cdot \bar{g}_j \qquad G_{IJ} = \bar{G}_I \cdot \bar{G}_J \tag{2.67}$$

The determinants of those matrices are defined as

$$g \equiv \det[g_{ij}] \qquad G \equiv \det[G_{IJ}] \tag{2.68}$$

The reciprocal base vectors are

$$\bar{g}^i = \frac{\partial \bar{r}}{\partial \xi_i} = \frac{\partial x_j}{\partial \xi_i}\bar{\iota}_j \qquad \bar{G}^I = \frac{\partial \bar{R}}{\partial \xi_i} = \frac{\partial X_J}{\partial \xi_i}\bar{\iota}_j \tag{2.69}$$

$$\bar{g}^1 = \frac{\bar{g}_2 \times \bar{g}_3}{\sqrt{g}} \qquad \bar{g}^2 = \frac{\bar{g}_3 \times \bar{g}_1}{\sqrt{g}} \qquad \bar{g}^3 = \frac{\bar{g}_1 \times \bar{g}_2}{\sqrt{g}} \tag{2.70}$$

$$\bar{G}^1 = \frac{\bar{G}_2 \times \bar{G}_3}{\sqrt{G}} \qquad \bar{G}^2 = \frac{\bar{G}_3 \times \bar{G}_1}{\sqrt{G}} \qquad \bar{G}^3 = \frac{\bar{G}_1 \times \bar{G}_2}{\sqrt{G}} \tag{2.71}$$

The contravariant components of the metric tensor are:

$$g^{ij} = \bar{g}^i \cdot \bar{g}^j \qquad G^{IJ} = \bar{G}^I \cdot \bar{G}^J \tag{2.72}$$

Also, the following relationships are satisfied:

$$[g^{ij}] = [g_{ij}]^{-1} \qquad [G^{IJ}] = [G_{IJ}]^{-1} \tag{2.73}$$

$$\frac{1}{g} = \det[g^{ij}] \qquad \frac{1}{G} = \det[G^{IJ}] \tag{2.74}$$

2.4.1.1 Double Tensors

Let M be a material point identified by $\bar{r} = x_i \bar{i}_i$ in its original position and $\bar{R} = X_I \bar{I}_i$ in its final position in Euclidean space. The quantities $T^{k\ldots m\ K\ldots M}_{p\ldots q\ P\ldots Q}$ constitute a double tensor* if they obey the transformation law for a tensor of type $T^{K\ldots M}_{P\ldots Q}$ when the X_I coordinates are transformed, and for a tensor $T^{k\ldots m}_{p\ldots q}$ when the x_i coordinates are transformed. As a special case, it follows that the components of a double tensor of the type $T^{K\ldots M}_{P\ldots Q}$ transform as scalars under x_i transformations. In other words, ordinary tensor fields are included as a special kind of double fields.

2.4.1.2 The Unit (Metric) Tensor

The unit second order (metric) tensor $\bar{\bar{I}}$ can be expressed as:

$$\begin{aligned}\bar{\bar{I}} &= g_{ij}\bar{g}^i\bar{g}^j = g^{ij}\bar{g}_i\bar{g}_j = \delta^i_j\bar{g}_i\bar{g}^j = \delta^j_i\bar{g}^i\bar{g}_j \\ &= \delta^i_j\bar{i}_i\bar{i}_j = G_{IJ}\bar{G}^I\bar{G}^J = G^{IJ}\bar{G}_I\bar{G}_J = \delta^I_J\bar{G}_I\bar{G}^J = \delta^J_I\bar{G}^I\bar{G}_J\end{aligned} \tag{2.75}$$

Observe that the mixed components are the same in any coordinate system.

2.4.1.3 The Displacement Vector

A displacement vector $\bar{u}$ can be defined as the vector difference between the position vector $\bar{R}$ defining the present location of a material point and the position vector $\bar{r}$ defining the reference (undeformed) location of that same material point:

$$\bar{u} = \bar{R} - \bar{r} \tag{2.76}$$

with components

$$\bar{u} = u_i\bar{g}^i = u^i\bar{g}_i = U_I\bar{G}^I = U^I\bar{G}_I = \hat{u}_i\bar{i}_i \tag{2.77}$$

Observe that

$$\hat{u}_i = X_I - x_i \tag{2.78}$$

*When the indices of a kernel letter do not all belong to the same space, the quantity is called a connecting quantity [61].

2.4.1.4 The Velocity Vector

The velocity vector $\bar{v}$ of material points of a moving continuum is defined by the material time derivative* (time derivative holding the material coordinates constant) of the displacement vector $\bar{u}$:

$$\bar{V} \equiv \dot{\bar{u}} = \left.\frac{\partial \bar{u}}{\partial t}\right|_{\xi^i = \text{CONST}} = (\dot{\bar{R} - \bar{r}}) = \dot{\bar{R}} = \frac{\partial X_I}{\partial t}\bar{\iota}_i = \dot{\hat{u}}_i \bar{\iota}_i \tag{2.79}$$

$$= \dot{u}_i \bar{g}^i = \dot{u}^i \bar{g}_i = \left.\frac{\partial \hat{u}_i}{\partial t}\right|_{X_i = \text{CONST}} \bar{\iota}_i = \left.\frac{\partial u_i}{\partial t}\right|_{\xi^i = \text{CONST}} \bar{g}^i = \left.\frac{\partial u^i}{\partial t}\right|_{\xi^i = \text{CONST}} \bar{g}_i$$

Notice that

$$\dot{\bar{r}} = \dot{\bar{g}}_i = \dot{\bar{g}}^i = \bar{0} \qquad\qquad \dot{g}_{ij} = \dot{g}^{ij} = 0 \tag{2.80}$$

This velocity vector $\bar{v}$ has components:

$$\bar{V} = v_i \bar{g}^i = v^i \bar{g}_i = \hat{v}_I \bar{\iota}_i = V_I \bar{G}^I = V^I \bar{G}_I \tag{2.81}$$

$$\hat{v}_I = \dot{\hat{u}}_i = \dot{X}_I \qquad\qquad v_i = \dot{u}_i \qquad\quad v^i = \dot{u}^i \tag{2.82}$$

By differentiating with respect to time t keeping ξ^i = constant, one obtains the time derivative of the deformed base vectors from Eqs. 2.64, 2.66, 2.79, and 2.53-2.55:

$$\boxed{\dot{\bar{G}}_I = \frac{\partial \dot{\bar{R}}}{\partial \xi^i} = \frac{\partial \bar{V}}{\partial \xi^i} = V^J_{\ ,I}\bar{G}_J = V_{J,I}\bar{G}^J} \tag{2.83}$$

From differentiation of the scalar product $\bar{G}^I \cdot \bar{G}_J = \delta^I_J$, the derivatives of the contravariant base vectors are found to be:

$$\dot{\bar{G}}^I \cdot \bar{G}_J + \bar{G}^I \cdot \dot{\bar{G}}_J = \dot{\delta}^I_J = 0$$

*This derivative with respect to time is symbolized in this work by a dot on top of the quantity being differentiated. The symbol $\frac{D}{Dt}$ is also often used in hydrodynamics texts for the material time derivative.

$$\dot{\bar{G}}^I \cdot \bar{G}_J = -\bar{G}^I \cdot \dot{\bar{G}}_J = -\bar{G}^I \cdot (V^K_{,J} \bar{G}_K) = -V^K_{,J} \delta^I_K$$

$$\dot{\bar{G}}^I \cdot \bar{G}_J = -V^I_{,J} \tag{2.84}$$

$$\boxed{\dot{\bar{G}}^I = -V^I_{,J} \bar{G}^J = -V^{I,J} \bar{G}_J}$$

2.4.2 Deformation and Strain Tensors

2.4.2.1 The Deformation Gradient Tensor

The deformation gradient tensor $\bar{\bar{F}}$ is the simplest to define in terms of the deformation equations and it includes more information about the motion than do the strain tensors.

The deformation gradient tensor is denoted by $\bar{\bar{F}}$, and its transpose by $\bar{\bar{F}}^T$. The deformation-gradient $\bar{\bar{F}}$ is defined as the tensor whose rectangular Cartesian components are the partial derivatives $\frac{\partial X_I}{\partial x_j}$ and which operates on an arbitrary infinitesimal material vector $d\bar{r}$ at $\bar{r}$ to associate with it a vector $d\bar{R}$ at $\bar{R}$ as follows:

$$d\bar{R} = \bar{\bar{F}} \cdot d\bar{r} = d\bar{r} \cdot \bar{\bar{F}}^T \tag{2.85}$$

Also,

$$\bar{G}_I = \bar{\bar{F}} \cdot \bar{g}_i = \bar{g}_i \cdot \bar{\bar{F}}^T$$

$$\boxed{\bar{\bar{F}} = \bar{G}_I \bar{g}^i} \tag{2.86}$$

Evidently $\bar{\bar{F}}$ measures <u>rotation</u> as well as <u>deformation</u> since a vector $\bar{g}_i$ deforms and rotates to become $\bar{G}_I$. Because the deformation gradient $\bar{\bar{F}}$ includes the rotation as well as the deformation, constitutive equations employing it will have to be constructed so that they will not predict a stress arising from pure rigid body rotation.

The deformation gradient tensor $\bar{\bar{F}}$ operates on the vectors $d\bar{r}$ and $\bar{g}_i$, associated with the <u>reference configuration</u>, to produce the vectors $d\bar{R}$ and $\bar{G}_I$, respectively, which are associated with the <u>present configuration</u>. Therefore, $\bar{\bar{F}}$ is a <u>double tensor</u> (previously defined in Subsection 2.4). Components of this double tensor are:

$$\begin{aligned}\bar{\bar{F}} &= \hat{F}_{Ij}\,\bar{\iota}_i\bar{\iota}_j = F^{Ij}\bar{G}_I\bar{g}_j = F_{Ij}\bar{G}^I\bar{g}^j = F^{I}{}_{\cdot j}\bar{G}_I\bar{g}^j \\ &= F_I{}^{\cdot j}\bar{G}^I\bar{g}_j = F^{ij}\bar{g}_i\bar{g}_j = F_{ij}\bar{g}^i\bar{g}^j = F^{i}{}_{\cdot j}\bar{g}_i\bar{g}^j = F_i{}^{\cdot j}\bar{g}^i\bar{g}_j\end{aligned} \tag{2.87}$$

From Eqs. 2.85, 2.64, and 2.87, one can obtain expressions for the components of $\bar{\bar{F}}$, as follows:

$$d\bar{R} = \bar{\bar{F}}\cdot d\bar{r} = dX_I\,\bar{\iota}_i = (\hat{F}_{Ij}\bar{\iota}_i\bar{\iota}_j)\cdot(dx_k\bar{\iota}_k) = \hat{F}_{Ij}\,dx_j\,\bar{\iota}_i \tag{2.88}$$

Hence,

$$\boxed{\hat{F}_{Ij} = \frac{\partial X_I}{\partial x_j}} \tag{2.88a}$$

From Eq. 2.78, one can express the components of $\bar{\bar{F}}$ in a rectangular Cartesian fixed-in-space frame in terms of the displacement vector:

$$X_I = x_i + \hat{u}_i \tag{2.89}$$

Hence,

$$\boxed{\hat{F}_{Ij} = \delta_{ij} + \frac{\partial \hat{u}_i}{\partial x_j}} \tag{2.90}$$

One can also express $\bar{\bar{F}}$ in terms of components in the convected system, by employing Eq. 2.86 as follows:

$$\bar{G}_J = \bar{\bar{F}} \cdot \bar{g}_j = \left(F^{I\cdot}_{\cdot k} \bar{G}_I \bar{g}^k\right) \cdot \bar{g}_j = F^{I\cdot}_{\cdot j} \bar{G}_I \tag{2.91}$$

Hence,

$$\boxed{F^{I\cdot}_{\cdot j} = \delta^i_j} \tag{2.92}$$

Therefore:

$$F^{Ij} = g^{ij} \tag{2.93}$$

$$F_{Ij} = G_{IJ} \tag{2.94}$$

$$\boxed{F_{I\cdot}^{\cdot j} = G_{IK}\, g^{kj}} \tag{2.95}$$

Also, $\bar{\bar{F}}$ can be expressed in terms of components of the displacement vector in a convected system, as follows:

$$\bar{G}_J = \bar{\bar{F}} \cdot \bar{g}_j = \left(F^{i\cdot}_{\cdot k}\, \bar{g}_i \bar{g}^k\right) \cdot \bar{g}_j = F^{i\cdot}_{\cdot j}\, \bar{g}_i \tag{2.96}$$

From Eqs. 2.76, 2.77, 2.69, 2.52, 2.53, 2.54, and 2.55, one obtains:

$$\frac{\partial \bar{u}}{\partial \xi^j} = \frac{\partial \bar{R}}{\partial \xi^j} - \frac{\partial \bar{r}}{\partial \xi^j} = \bar{G}_J - \bar{g}_j = u^i_{,j}\, \bar{g}_i = u_{i,j}\, \bar{g}^i \tag{2.97}$$

Then

$$\bar{G}_J = \bar{g}_j + u^i_{,j}\, \bar{g}_i = \left(\delta^i_j + u^i_{,j}\right) \bar{g}_i \tag{2.98}$$

Then

$$\left(\delta^i_j + u^i_{,j}\right) \bar{g}_i = F^{i\cdot}_{\cdot j}\, \bar{g}_i \tag{2.99}$$

Therefore,

$$\boxed{F^{i}_{\cdot j} = \delta^{i}_{j} + u^{i}_{,j}} \tag{2.100}$$

Hence,

$$F_{ij} = g_{ik}(\delta^{k}_{j} + u^{k}_{,j}) = g_{ij} + u_{i,j} \tag{2.101}$$

$$F^{ij} = g^{jk}(\delta^{i}_{k} + u^{i}_{,k}) = g^{ij} + u^{i,j} \tag{2.102}$$

$$F_{i}^{\cdot j} = g_{il}\, g^{kj}(\delta^{l}_{k} + u^{l}_{,k}) = \delta^{j}_{i} + u_{i,}{}^{j} \tag{2.103}$$

2.4.2.2 The Spatial Deformation Gradient Tensor

The spatial deformation gradient tensor $\bar{\bar{F}}^{-1}$ is the inverse of the deformation gradient tensor $\bar{\bar{F}}$. It operates on the quantities associated with the present configuration ($d\bar{R}$ and $\bar{G}_I$) to produce the quantities associated with the reference configuration ($d\bar{r}$ and $\bar{g}_i$), as follows:

$$d\bar{r} = \bar{\bar{F}}^{-1} \cdot d\bar{R} = d\bar{R} \cdot (\bar{\bar{F}}^{-1})^{T} \tag{2.104}$$

$$\bar{g}_i = \bar{\bar{F}}^{-1} \cdot \bar{G}_I = \bar{G}_I \cdot (\bar{\bar{F}}^{-1})^{T} \tag{2.105}$$

$$\boxed{\bar{\bar{F}}^{-1} = \bar{g}_i \bar{G}^{I}}$$

Components of the spatial deformation gradient tensor $\bar{\bar{F}}^{-1}$ are:

$$\begin{aligned}
\bar{\bar{F}}^{-1} &= (\hat{F}^{-1})_{iJ}\,\bar{i}_i \bar{i}_j = (F^{-1})^{iJ}\,\bar{g}_i \bar{G}_J = (F^{-1})_{iJ}\,\bar{g}^{i} \bar{G}^{J} \\
&= (F^{-1})^{i}_{\cdot J}\,\bar{g}_i \bar{G}^{J} = (F^{-1})_{i}^{\cdot J}\,\bar{g}^{i} \bar{G}_J = (F^{-1})^{IJ}\,\bar{G}_I \bar{G}_J \\
&= (F^{-1})_{IJ}\,\bar{G}^{I} \bar{G}^{J} = (F^{-1})^{I}_{\cdot J}\,\bar{G}_I \bar{G}^{J} = (F^{-1})_{I}^{\cdot J}\,\bar{G}^{I} \bar{G}_J
\end{aligned} \tag{2.106}$$

Utilizing Eqs. 2.104, 2.105, 2.64, and 2.106, one can obtain expressions for these components, as follows:

$$d\bar{r} = \bar{\bar{F}}^{-1} \cdot d\bar{R} = dx_i \bar{i}_i = \left[(\hat{F}^{-1})_{iJ} \bar{i}_i \bar{i}_j \right] \cdot dX_K \bar{i}_k = (\hat{F}^{-1})_{iJ} dX_J \bar{i}_i$$

Hence,

$$\boxed{(\hat{F}^{-1})_{iJ} = \frac{\partial x_i}{\partial X_J}} \tag{2.107}$$

Also, from Eq. 2.78:

$$x_i = X_I - \hat{u}_i \tag{2.108}$$

Hence,

$$\boxed{(\hat{F}^{-1})_{iJ} = \delta_{ij} - \frac{\partial \hat{u}_i}{\partial X_J}} \tag{2.109}$$

From Eqs. 2.105 and 2.106:

$$\bar{g}_j = \bar{\bar{F}}^{-1} \cdot \bar{G}_J = \left[(F^{-1})^{i\cdot}_{\cdot K} \bar{g}_i \bar{G}^K \right] \cdot \bar{G}_J = (F^{-1})^{i\cdot}_{\cdot J} \bar{g}_i$$

Hence,

$$\boxed{(F^{-1})^{i\cdot}_{\cdot J} = \delta^i_j} \tag{2.110}$$

Therefore,

$$(F \quad)^{iJ} = G^{IJ} \tag{2.111}$$

$$(F^{-1})_{iJ} = g_{ij} \tag{2.112}$$

$$\boxed{(F^{-1})_{i\,\cdot}^{\cdot\,J} = g_{ik}\, G^{KJ}} \tag{2.113}$$

Again, from Eqs. 2.105 and 2.106:

$$\bar{g}_j = \bar{\bar{F}}^{-1}\cdot\bar{G}_J = \left[(F^{-1})^{I\,\cdot}_{\cdot\,K}\,\bar{G}_I\bar{G}^K\right]\cdot\bar{G}_J = (F^{-1})^{I\,\cdot}_{\cdot\,J}\,\bar{G}_I \tag{2.114}$$

From Eqs. 2.76, 2.77, 2.66 and 2.52-2.55, one obtains:

$$\frac{\partial\bar{u}}{\partial\xi^j} = \frac{\partial\bar{R}}{\partial\xi^j} - \frac{\partial\bar{r}}{\partial\xi^j} = \bar{G}_J - \bar{g}_j = U^I_{\ ,J}\,\bar{G}_I = U_{I,J}\,\bar{G}^J \tag{2.115}$$

Then

$$\bar{g}_j = \bar{G}_J - U^I_{\ ,J}\,\bar{G}_I = (\delta^i_j - U^I_{\ ,J})\bar{G}_I \tag{2.116}$$

Then

$$(\delta^i_j - U^I_{\ ,J})\bar{G}_I = (F^{-1})^{I\,\cdot}_{\cdot\,J}\,\bar{G}_I \tag{2.117}$$

Therefore

$$\boxed{(F^{-1})^{I\,\cdot}_{\cdot\,J} = \delta^i_j - U^I_{\ ,J}} \tag{2.118}$$

Hence,

$$(F^{-1})_{IJ} = G_{IK}(\delta^k_j - U^K_{\ ,J}) = G_{IJ} - U_{I,J} \tag{2.119}$$

$$(F^{-1})^{IJ} = G^{JK}(\delta^i_k - U^I_{\ ,K}) = G^{IJ} - U^{I}{}_{,}{}^{J} \tag{2.120}$$

$$(F^{-1})_{I\,\cdot}^{\cdot\,J} = G_{IL}G^{KJ}(\delta^l_k - U^L_{\ ,K}) = \delta^j_i - U_{I,}{}^{J} \tag{2.121}$$

2.4.2.3 Rotation, Stretch, and Strain Tensors

The polar decomposition theorem* indicates that any invertible linear transformation $\bar{\bar{F}}$ has two unique multiplicative decompositions

$$\boxed{\bar{\bar{F}} = \bar{\bar{R}} \cdot \bar{\bar{U}} = \bar{\bar{V}} \cdot \bar{\bar{R}}} \qquad (2.122)$$

in which $\bar{\bar{R}}$ is orthogonal ($\bar{\bar{R}} \cdot \bar{\bar{R}}^T = \bar{\bar{I}}$) and $\bar{\bar{U}}$ and $\bar{\bar{V}}$ are symmetric ($\bar{\bar{U}} = \bar{\bar{U}}^T$, $\bar{\bar{V}} = \bar{\bar{V}}^T$) and positive definite. $\bar{\bar{R}}$ is called the rotation tensor, $\bar{\bar{U}}$ is the right stretch tensor, and $\bar{\bar{V}}$ is the left stretch tensor of the deformation.

One may consider the deformation of an infinitesimal volume element at $\bar{r}$ to consist of the successive application of:

(1) A stretch by the operator $\bar{\bar{U}}$, and

(2) a rigid body rotation by the operator $\bar{\bar{R}}$.

Alternatively, the same deformation can be produced by the successive application of:

(1) A rigid body rotation by $\bar{\bar{R}}$, and

(2) a stretch by $\bar{\bar{V}}$.

It can be shown that the following relations are valid:

$$\bar{\bar{U}}^2 \equiv \bar{\bar{U}} \cdot \bar{\bar{U}} = \bar{\bar{F}}^T \cdot \bar{\bar{F}} \qquad \bar{\bar{V}}^2 \equiv \bar{\bar{V}} \cdot \bar{\bar{V}} = \bar{\bar{F}} \cdot \bar{\bar{F}}^T \qquad (2.123)$$

Cauchy-Green Deformation Tensors

The square of the right stretch tensor

$$\boxed{\bar{\bar{C}} \equiv \bar{\bar{U}}^2 = \bar{\bar{U}} \cdot \bar{\bar{U}} = \bar{\bar{F}}^T \cdot \bar{\bar{F}}} \qquad (2.124)$$

is called the right Cauchy-Green deformation tensor. The square of the left stretch tensor

---

*See, for example, Section 83 of P.R. Halmos (Ref. 69) and Section 43 of J.L. Ericksen (Ref. 67).

$$\boxed{\bar{\bar{B}} \equiv \bar{\bar{V}}^{\cdot 2} = \bar{\bar{V}} \cdot \bar{\bar{V}} = \bar{\bar{F}} \cdot \bar{\bar{F}}^T} \tag{2.125}$$

is called the <u>left Cauchy-Green</u> tensor of deformation. It can be easily shown that

$$\bar{\bar{B}} = \bar{\bar{R}} \cdot \bar{\bar{C}} \cdot \bar{\bar{R}}^T \tag{2.126}$$

The right Cauchy-Green deformation tensor $\bar{\bar{C}}$ is associated with the reference configuration, and it gives the new squared length $(dS)^2$ of the differential line element $d\bar{R}$ into which the given differential element $d\bar{r}$ is deformed:

$$(dS)^2 \equiv d\bar{R} \cdot d\bar{R} = (d\bar{r} \cdot \bar{\bar{F}}^T) \cdot (\bar{\bar{F}} \cdot d\bar{r}) = d\bar{r} \cdot (\bar{\bar{F}}^T \cdot \bar{\bar{F}}) \cdot d\bar{r} = d\bar{r} \cdot \bar{\bar{C}} \cdot d\bar{r} \tag{2.127}$$

The inverse of the left Cauchy-Green deformation tensor $\bar{\bar{B}}$, denoted by $\bar{\bar{B}}^{-1}$ gives the initial squared length $(ds)^2$ of a deformed differential line element $d\bar{R}$

$$\begin{aligned}(ds)^2 &\equiv d\bar{r} \cdot d\bar{r} = (d\bar{R} \cdot (\bar{\bar{F}}^{-1})^T) \cdot (\bar{\bar{F}}^{-1} \cdot d\bar{R}) = d\bar{R} \cdot (\bar{\bar{F}} \cdot \bar{\bar{F}}^T)^{-1} \cdot d\bar{R} \\ &= d\bar{R} \cdot \bar{\bar{B}}^{-1} \cdot d\bar{R}\end{aligned} \tag{2.128}$$

The right Cauchy-Green deformation tensor has components

$$\bar{\bar{C}} = \hat{C}_{ij}\,\bar{i}_i \bar{i}_j = C^{ij}\,\bar{g}_i \bar{g}_j = C_{ij}\,\bar{g}^i \bar{g}^j = C^i_j\,\bar{g}_i \bar{g}^j \tag{2.129}$$

and from Eqs. 2.124, 2.88, 2.90-2.95 and 2.100-2.103, one can express $\bar{\bar{C}}$ in terms of the displacement vector components, as follows:

$$\begin{aligned}\hat{C}_{ij} &= (\hat{F}_{iK})^T \hat{F}_{Kj} = \hat{F}_{Ki} \hat{F}_{Kj} = \frac{\partial X_K}{\partial x_i} \frac{\partial X_K}{\partial x_j} \\ &= \left(\delta_{ik} + \frac{\partial \hat{u}_k}{\partial x_i}\right)\left(\delta_{kj} + \frac{\partial \hat{u}_k}{\partial x_j}\right) = \delta_{ij} + \frac{\partial \hat{u}_i}{\partial x_j} + \frac{\partial \hat{u}_j}{\partial x_i} + \frac{\partial \hat{u}_k}{\partial x_i}\frac{\partial \hat{u}_k}{\partial x_j}\end{aligned} \tag{2.130}$$

$$C_{ij} = (F_{\cdot i}^{\ \ k})^T F^{k\cdot}_{\ \cdot j} = F_{ki} F^{k\cdot}_{\ \cdot j} = G_{IJ} = (g_{ij} + u_{k,i})(\delta^k_j + u^k_{,j})$$

$$= g_{ij} + u_{i,j} + u_{j,i} + u^k_{,j} u_{k,i} \tag{2.131}$$

$$C^i_j = (F^{i\cdot}_{\ \cdot k})^T F^{k\cdot}_{\ \cdot j} = F_k^{\cdot i} F^{k\cdot}_{\ \cdot j} = g^{ik} G_{KJ}$$

$$= (\delta^i_k + u_{k,}^{\ \ i})(\delta^k_j + u^k_{,j}) = \delta^i_j + u^i_{,j} + u_{j,}^{\ \ i} + u_{k,}^{\ \ i} u^k_{,j} \tag{2.132}$$

$$C^{ij} = (F^{i\cdot}_{\ \cdot k})^T F^{kj} = F_k^{\cdot i} F^{kj} = g^{il} g^{jk} G_{LK}$$

$$= (\delta^i_k + u_{k,}^{\ \ i})(g^{kj} + u^{k,j}) = g^{ij} + u^{i,j} + u^{j,i} + u^{k,j} u_{k,}^{\ \ i} \tag{2.133}$$

Notice, that although $\bar{\bar{C}} \neq \bar{\bar{F}}$, from Eqs. 2.95, 2.132, 2.94, and 2.131, the following components are equal:

$$C^i_j = F_J^{\cdot i} \tag{2.134}$$

$$C_{ij} = F_{Ij} \tag{2.135}$$

<u>The Green Strain Tensor</u>

The Green* strain tensor $\bar{\bar{\gamma}}$ is defined as follows:

$$\boxed{\bar{\bar{\gamma}} = \frac{1}{2}(\bar{\bar{C}} - \bar{\bar{1}})} \tag{2.136}$$

*According to Truesdell (Ref. 15, page 266), this strain measure was introduced by Green in 1841, and by St. Venant in 1844; since its components are usually referred to a fixed reference configuration, it goes by the name of "Lagrangian strain" in the older engineering literature.

From Eq. 2.124, it is easily shown that equivalent expressions are:

$$\bar{\bar{\gamma}} = \frac{1}{2}\left(\bar{\bar{U}}^2 - \bar{\bar{I}}\right) = \frac{1}{2}\left(\bar{\bar{F}}^T \cdot \bar{\bar{F}} - \bar{\bar{I}}\right) \tag{2.137}$$

This strain measure gives the <u>change</u> in the <u>squared length</u> of the material vector $d\bar{r}$ as follows from Eqs. 2.127 and 2.128:

$$(dS)^2 - (ds)^2 = d\bar{R} \cdot d\bar{R} - d\bar{r} \cdot d\bar{r} \tag{2.138}$$

Expressing this in terms of the material vector $d\bar{r}$, one obtains from Eq. 2.127:

$$(dS)^2 - (ds)^2 = d\bar{r} \cdot \bar{\bar{C}} \cdot d\bar{r} - d\bar{r} \cdot \bar{\bar{I}} \cdot d\bar{r} = d\bar{r} \cdot \left(\bar{\bar{C}} - \bar{\bar{I}}\right) \cdot d\bar{r} \tag{2.139}$$

Defining $\bar{\bar{\gamma}} \equiv \frac{1}{2}\,(\bar{\bar{C}} - \bar{\bar{I}})$, one obtains

$$\boxed{\frac{(dS)^2 - (ds)^2}{2} = d\bar{r} \cdot \bar{\bar{\gamma}} \cdot d\bar{r}} \tag{2.140}$$

Components of the Green strain tensor $\bar{\bar{\gamma}}$ are:

$$\bar{\bar{\gamma}} = \hat{\gamma}_{ij}\,\bar{i}_i \bar{i}_j = \gamma_{ij}\,\bar{g}^i \bar{g}^j = \gamma^{ij}\,\bar{g}_i \bar{g}_j = \gamma^i_j\,\bar{g}_i \bar{g}^j \tag{2.141}$$

These components can be expressed in terms of the displacement vector components, from Eqs. 2.136 and 2.130-2.133, obtaining:

$$\hat{\gamma}_{ij} = \frac{1}{2}\left(\hat{C}_{ij} - \delta_{ij}\right) = \frac{1}{2}\left(\frac{\partial X_K}{\partial x_i}\frac{\partial X_K}{\partial x_j} - \delta_{ij}\right) = \left(\frac{\partial \hat{u}_i}{\partial x_j} + \frac{\partial \hat{u}_j}{\partial x_i} + \frac{\partial \hat{u}_k}{\partial x_i}\frac{\partial \hat{u}_k}{\partial x_j}\right)\Big/2 \tag{2.142a}$$

$$\gamma_{ij} = \frac{1}{2}\left(C_{ij} - g_{ij}\right) = \frac{1}{2}\left(G_{IJ} - g_{ij}\right) = \left(u_{i,j} + u_{j,i} + u^k{}_{,j}\,u_{k,i}\right)/2 \tag{2.142b}$$

$$\gamma^i_j = \frac{1}{2}\left(C^i_j - \delta^i_j\right) = \frac{1}{2}\left(g^{ik} G_{KJ} - \delta^i_j\right) = \left(u^i{}_{,j} + u_{j,}{}^i + u^k{}_{,j}\,u_{k,}{}^i\right)/2 \tag{2.142c}$$

$$\gamma^{ij} = \frac{1}{2}\left(C^{ij} - g^{ij}\right) = \frac{1}{2}\left(g^{il} g^{jk} G_{LK} - g^{ij}\right) = \left(u^{i,j} + u^{j,i} + u^{k,j}\,u_{k,}{}^i\right)/2 \tag{2.142d}$$

The Almansi Strain Tensor

The Almansi* strain tensor $\bar{\bar{e}}$ is defined as follows:

$$\boxed{\bar{\bar{e}} = \frac{1}{2}\left(\bar{\bar{1}} - \bar{\bar{B}}^{-1}\right)} \tag{2.143}$$

Equivalent expressions for the Almansi strain $\bar{\bar{e}}$ are obtained from the definition of the left Cauchy-Green deformation tensor $\bar{\bar{B}}$, Eq. 2.125:

$$\bar{\bar{e}} = \frac{1}{2}\left(\bar{\bar{1}} - \left(\bar{\bar{V}}^{2}\right)^{-1}\right) = \frac{1}{2}\left(\bar{\bar{1}} - \left(\bar{\bar{F}}^{-1}\right)^{T} \cdot \bar{\bar{F}}^{-1}\right) \tag{2.144}$$

The Almansi strain also gives the <u>change</u> in the <u>squared length</u> of the material vector $d\bar{r}$ as follows, from Eqs. 2.138, and 2.128:

$$(dS)^2 - (ds)^2 = d\bar{R}\cdot\bar{\bar{1}}\cdot d\bar{R} - d\bar{R}\cdot\bar{\bar{B}}^{-1}\cdot d\bar{R} = d\bar{R}\cdot\left(\bar{\bar{1}} - \bar{\bar{B}}^{-1}\right)\cdot d\bar{R} \tag{2.145}$$

Defining $\bar{\bar{e}} = \frac{1}{2}\left(\bar{\bar{1}} - \bar{\bar{B}}^{-1}\right)$, one obtains:

$$\boxed{\frac{(dS)^2 - (ds)^2}{2} = d\bar{R}\cdot\bar{\bar{e}}\cdot d\bar{R}} \tag{2.146}$$

Components of the Almansi (Eulerian) strain tensor $\bar{\bar{e}}$ are:

$$\bar{\bar{e}} = \hat{e}_{IJ}\,\bar{i}_i\bar{i}_j = e_{IJ}\,\bar{G}^I\bar{G}^J = e^{IJ}\,\bar{G}_I\bar{G}_J = e^I_J\,\bar{G}_I\bar{G}^J \tag{2.147}$$

where

$$\hat{e}_{IJ} = \frac{1}{2}\left(\delta_{ij} - \frac{\partial x_k}{\partial X_I}\frac{\partial x_k}{\partial X_J}\right) \tag{2.148}$$

$$e_{IJ} = \frac{1}{2}\left(G_{IJ} - g_{ij}\right) \tag{2.149}$$

---

*According to Truesdell (Ref. 15, page 266), this strain measure was introduced by Almansi in 1911 and Hamel in 1912; since its components are usually referred to the present configuration, it goes by the name "Eulerian strain" in the older engineering literature.

$$e^I_J = \frac{1}{2}\left(\delta^i_j - G^{IK} g_{kj}\right) \qquad (2.150)$$

$$e^{IJ} = \frac{1}{2}\left(G^{IJ} - G^{IL} G^{JK} g_{lk}\right) \qquad (2.151)$$

Observe that the covariant components of the Green $\bar{\bar{\gamma}}$ and Almansi $\bar{\bar{e}}$ strain tensors with respect to the reference base vectors $\bar{g}^i$ and to the present base vectors $\bar{G}^I$, respectively, are the same:

$$\gamma_{ij} = e_{IJ}$$

Therefore, from Eqs. 2.140, 2.64, and 2.141:

$$\frac{(dS)^2 - (ds)^2}{2} = d\bar{r} \cdot \bar{\bar{\gamma}} \cdot d\bar{r} = d\xi^i \bar{g}_i \cdot \bar{\bar{\gamma}} \cdot \bar{g}_j d\xi^j$$

$$= d\xi^i \bar{g}_i \cdot \left(\gamma_{ij} \bar{g}^i \bar{g}^j\right) \cdot \bar{g}_j d\xi^j$$

or

$$\boxed{\frac{(dS)^2 - (ds)^2}{2} = \gamma_{ij} d\xi^i d\xi^j} \qquad (2.152)$$

Also, from Eqs. 2.145, 2.64, and 2.146:

$$\frac{(dS)^2 - (ds)^2}{2} = d\bar{R} \cdot \bar{\bar{e}} \cdot d\bar{R} = d\xi^i \bar{G}_I \cdot \bar{\bar{e}} \cdot \bar{G}_J d\xi^j$$

$$= d\xi^i \bar{G}_I \cdot \left(e_{IJ} \bar{G}^I \bar{G}^J\right) \cdot \bar{G}_J d\xi^j$$

$$\boxed{\frac{(dS)^2 - (ds)^2}{2} = e_{IJ} d\xi^i d\xi^j} \qquad (2.153)$$

Of, course, although $\gamma_{ij} = e_{IJ}$, these are different tensors, and this equality does not hold in the absolute tensor notation:

$$\bar{\bar{\gamma}} \neq \bar{\bar{e}}$$

Other Strain Measures

Since in Euclidean space distances are measured by a quadratic form, the Cauchy-Green deformation tensors, and the Green and Almansi strain tensors are by far the most popular strain measures. However, as Weissenberg [70] has observed, <u>any</u>* measure sufficient to determine the directions of the principal axes of strain and the magnitudes of the principal elongations may be employed and is fully general.

Other strain measures of interest in the present analysis are the elongation tensors $\overline{\overline{\tilde{E}}}$ (associated with the name of Biot [71, page 118]) and $\overline{\overline{E}}$ (associated with the name of Swainger [72]) as well as the logarithmic strain tensors $\overline{\overline{\tilde{H}}}$ and $\overline{\overline{H}}$ (associated with the name of Hencky [73]). These strain tensors are defined as follows:

$$\overline{\overline{\tilde{E}}} = \overline{\overline{U}} - \overline{\overline{1}} = \sqrt{\overline{\overline{C}}} - \overline{\overline{1}} = \sqrt{\overline{\overline{F}}^{T}\cdot\overline{\overline{F}}} - \overline{\overline{1}} = \sqrt{\overline{\overline{1}}+2\overline{\overline{\gamma}}} - \overline{\overline{1}} \tag{2.154}$$

$$\overline{\overline{E}} = \overline{\overline{1}} - (\overline{\overline{V}})^{-1} = \overline{\overline{1}} - \sqrt{\overline{\overline{B}}^{-1}} = \overline{\overline{1}} - \sqrt{\overline{\overline{1}} - 2\overline{\overline{e}}} \tag{2.155}$$

$$\overline{\overline{\tilde{H}}} = \ln \overline{\overline{U}} = \frac{1}{2}\ln \overline{\overline{C}} = \frac{1}{2}\ln(\overline{\overline{F}}^{T}\cdot\overline{\overline{F}}) = \frac{1}{2}\ln(\overline{\overline{1}}+2\overline{\overline{\gamma}}) \tag{2.156}$$

$$\overline{\overline{H}} = \ln \overline{\overline{V}} = \frac{1}{2}\ln \overline{\overline{B}} = -\frac{1}{2}\ln(\overline{\overline{1}} - 2\overline{\overline{e}}) \tag{2.157}$$

with components

$$\overline{\overline{\tilde{E}}} = \hat{\tilde{E}}_{ij}\,\bar{i}_i\bar{i}_j = \tilde{E}_{ij}\,\bar{g}^i\bar{g}^j = \tilde{E}^{ij}\,\bar{g}_i\bar{g}_j = \tilde{E}^{\,i}_{j}\,\bar{g}_i\bar{g}^j \tag{2.158}$$

$$\overline{\overline{E}} = \hat{E}_{IJ}\,\bar{i}_i\bar{i}_j = E_{IJ}\,\bar{G}^I\bar{G}^J = E^{IJ}\,\bar{G}_I\bar{G}_J = E^{I}_{J}\,\bar{G}_I\bar{G}^J \tag{2.159}$$

---

*As a matter of fact, it is possible to describe strain correctly by measures which are not tensors; Truesdell points out (Ref. 15, page 269): "but there can hardly be any advantage, and attempts of this kind have usually led to confusion if not disaster".

$$\tilde{\bar{\bar{H}}} = \hat{\tilde{H}}_{ij}\,\bar{i}_i\bar{i}_j = \tilde{H}_{ij}\,\bar{g}^i\bar{g}^j = \tilde{H}^{ij}\,\bar{g}_i\bar{g}_j = \tilde{H}^i_j\,\bar{g}_i\bar{g}^j \tag{2.160}$$

$$\bar{\bar{H}} = \hat{H}_{IJ}\,\bar{i}_i\bar{i}_j = H_{IJ}\,\bar{G}^I\bar{G}^J = H^{IJ}\,\bar{G}_I\bar{G}_J = H^I_J\,\bar{G}_I\bar{G}^J \tag{2.161}$$

Relations between Strain Tensors

The tensors $\bar{\bar{U}}$, $\bar{\bar{C}}$, $\bar{\bar{\gamma}}$, $\tilde{\bar{\bar{E}}}$, and $\tilde{\bar{\bar{H}}}$ all have the same principal axes of strain at $\bar{r}$, in the reference shape at $t = t_0$. The tensors $\bar{\bar{V}}$, $\bar{\bar{B}}$, $\bar{\bar{e}}$, $\bar{\bar{E}}$ and $\bar{\bar{H}}$ all have the same principal axes of strain at $\bar{R}$, in the present shape at $t = t$. The rotation tensor $\bar{\bar{R}}$ carries principal axes of strain at $\bar{r}$ into principal axes of strain at $\bar{R}$.

The tensors $\bar{\bar{U}}$ and $\bar{\bar{V}}$ have the same principal values. These principal values, called the principal stretches λ_α, are the ratios of the deformed line elements dS_α in the principal directions $\bar{b}_\alpha$ to the undeformed line elements ds_α in the same principal directions: $\lambda_\alpha = \dfrac{dS_\alpha}{ds_\alpha}$.

The tensors $\bar{\bar{C}}$ and $\bar{\bar{B}}$ have the same principal values $(\lambda_\alpha)^2$, and these principal values are equal to the squares of the principal stretches λ_α. The principal values γ_α of the strain tensor $\bar{\bar{\gamma}}$ are related to the principal stretches by: $\gamma_\alpha = \frac{1}{2}\,((\lambda_\alpha)^2 - 1)$, while the principal values e_α of the strain tensor $\bar{\bar{e}}$ are $e_\alpha = \frac{1}{2}\,(1 - (\lambda_\alpha)^{-2})$. The principal values $\tilde{E}_\alpha$ of the elongation tensor $\tilde{\bar{\bar{E}}}$ are related to the principal stretches by $\tilde{E}_\alpha = \lambda_\alpha - 1$, while the principal values E_α of the elongation tensor $\bar{\bar{E}}$ are $E_\alpha = 1 - (\lambda_\alpha)^{-1}$. The principal values $\tilde{H}_\alpha$ and H_α of the tensors $\tilde{\bar{\bar{H}}}$ and $\bar{\bar{H}}$ are equal; that is, $\tilde{H}_\alpha = H_\alpha$, and are related to the principal stretches by $\tilde{H}_\alpha = H_\alpha = \ln \lambda_\alpha$. The mixed components of the tensor $\tilde{\bar{\bar{H}}}$ and the tensor $\bar{\bar{H}}$ in the reference base and the present base respectively, are equal:

$$\tilde{H}^i_j = H^I_J \tag{2.162}$$

If the axes of deformation are fixed and several deformations are carried out successively, each principal component of the tensors $\bar{\bar{H}}$ and $\tilde{\bar{\bar{H}}}$ in the resultant deformation is equal to the sum of the corresponding principal components for the several successive deformations. For the tensors $\bar{\bar{U}}$, $\bar{\bar{C}}$, $\bar{\bar{\gamma}}$, $\bar{\bar{E}}$, and $\bar{\bar{V}}$, $\bar{\bar{B}}$, $\bar{\bar{e}}$, $\bar{\bar{E}}$ this property does not exist. The components of the tensors $\bar{\bar{U}}$, $\bar{\bar{V}}$, $\bar{\bar{E}}$, $\bar{\bar{E}}$, $\bar{\bar{H}}$, $\bar{\bar{H}}$ are complicated irrational or transcendental functions of the components of $\bar{\bar{F}}$, and hence in the solution of problems it is usually better to use components of $\bar{\bar{\gamma}}$, $\bar{\bar{C}}$ and $\bar{\bar{e}}$, $\bar{\bar{B}}$ (since they are polynomials in the components of $\bar{\bar{F}}$) rather than $\bar{\bar{U}}$, $\bar{\bar{E}}$, $\bar{\bar{H}}$ and $\bar{\bar{V}}$, $\bar{\bar{E}}$ and $\bar{\bar{H}}$ as measures of strain.

2.4.3 Deformation Rate Tensors

2.4.3.1 The Rate-of-Deformation Tensor

The rate-of-deformation tensor $\bar{\bar{D}}$ (also called stretching) is the rate of change of the stretch $\bar{\bar{U}}$ or $\bar{\bar{V}}$ at $\bar{R}$ in the shape at time $t + \varepsilon$ with respect to that at time t, in the limit as $\varepsilon \to 0$ [22]:

$$\bar{\bar{D}} \equiv \dot{\bar{\bar{U}}}_t(t) = \dot{\bar{\bar{V}}}_t(t) \tag{2.163}$$

where, in this notation the subscript t denotes that the present (time t) configuration has been chosen as the reference configuration. Also, in this notation [22]:

$$\dot{\bar{\bar{U}}}_t(t) \equiv \left.\frac{\partial \bar{\bar{U}}_t(\tau)}{\partial \tau}\right|_{\tau=t} \tag{2.164}$$

If a fixed reference configuration is used, then

$$d\bar{R}\cdot\bar{\bar{D}}\cdot d\bar{R} = \frac{1}{2}\frac{d}{dt}\left[(dS)^2\right] = \frac{1}{2}\frac{d}{dt}\left[d\bar{R}\cdot d\bar{R}\right] \tag{2.165}$$

$$\boxed{d\bar{R}\cdot\bar{\bar{D}}\cdot d\bar{R} = \frac{1}{2}\left(d\bar{R}\cdot d\bar{v} + d\bar{v}\cdot d\bar{R}\right)}$$

Also, it can be shown that

$$\bar{\bar{D}} = \frac{1}{2}\bar{\bar{R}}\cdot\left(\dot{\bar{\bar{U}}}\cdot\bar{\bar{U}}^{-1} + \bar{\bar{U}}^{-1}\cdot\dot{\bar{\bar{U}}}\right)\cdot\bar{\bar{R}}^{T} \tag{2.166}$$

Components of $\bar{\bar{D}}$ are:

$$\bar{\bar{D}} = \hat{D}_{IJ}\, \bar{i}_i \bar{i}_j = D_{IJ}\, \bar{G}^I \bar{G}^J = D^{IJ}\, \bar{G}_I \bar{G}_J = D^I_J\, \bar{G}_I \bar{G}^J \quad (2.167)$$

Since $\bar{\bar{U}}_t$ is symmetric, so is $\bar{\bar{D}}$, being its derivative with respect to a parameter:

$$\bar{\bar{D}} = \bar{\bar{D}}^T \qquad D_{IJ} = D_{JI} \qquad D^{IJ} = D^{JI} \qquad D^{I\cdot}_{\cdot J} = D_{J\cdot}^{\cdot I} = D^I_J \quad (2.168)$$

Recalling that the velocity vector $\bar{v} = \dot{\bar{u}} = \dot{\bar{R}}$ can be expressed as

$$\bar{V} = \hat{V}_I\, \bar{i}_i = V^I \bar{G}_I = V_I \bar{G}^I \quad (2.169)$$

Then:

$$\hat{D}_{IJ} = \frac{1}{2}\left(\frac{\partial \hat{V}_I}{\partial X_J} + \frac{\partial \hat{V}_J}{\partial X_I}\right) \quad (2.170)$$

$$D_{IJ} = \frac{1}{2}\dot{G}_{IJ} = \frac{1}{2}\frac{d}{dt}\left(\bar{G}_I \cdot \bar{G}_J\right) = \frac{1}{2}\left(\dot{\bar{G}}_I \cdot \bar{G}_J + \bar{G}_I \cdot \dot{\bar{G}}_J\right) \quad (2.171)$$

$$= \frac{1}{2}\left(V_{I,J} + V_{J,I}\right) \quad (2.172)$$

$$D^{IJ} = -\frac{1}{2}\dot{G}^{IJ} = \frac{1}{2} G^{IL} G^{JK} \dot{G}_{KL} = \frac{1}{2}\left(V^{I}{}_{,}{}^{J} + V^{J}{}_{,}{}^{I}\right) \quad (2.173)$$

$$D^I_J = \frac{1}{2} G^{IK} \dot{G}_{KJ} = \frac{1}{2}\left(V^I{}_{,J} + V_J{}_{,}{}^I\right) \quad (2.174)$$

2.4.3.2 Relations between Strain Rate Tensors

Observe that the covariant components D_{IJ} of the rate-of-deformation tensor $\bar{\bar{D}}$ in convected coordinates are equal to the material rate of the covariant components γ_{ij} of the Green (Lagrangian) strain tensor $\bar{\bar{\gamma}}$ and also are equal to the material rate of the covariant components e_{IJ} of the Almansi (Eulerian) strain tensor $\bar{\bar{e}}$:

$$D_{IJ} = \frac{1}{2}\dot{G}_{IJ} = \frac{1}{2}\dot{C}_{ij} = \dot{\gamma}_{ij} = \dot{e}_{IJ} \qquad (2.175)$$

But, this does not at all imply that the rate-of-deformation tensor is equal to the material rates of the Green and Almansi strain tensors. In fact, the rectangular Cartesian components are different:

$$\hat{D}_{IJ} \neq \dot{\hat{\gamma}}_{ij} \neq \dot{\hat{e}}_{IJ} \qquad (2.176)$$

and the convected mixed components are different:

$$\dot{\gamma}^{i}_{j} = g^{ik}\dot{\gamma}_{kj} = g^{ik}G_{KL}D^{L}_{J} = C^{i}_{l}D^{L}_{J} = (\delta^{i}_{l} + 2\gamma^{i}_{l})D^{L}_{J} \qquad (2.177)$$

$$\dot{e}^{I}_{J} = \dot{(G^{IK}e_{KL})} = \dot{G}^{IK}e_{KJ} + G^{IK}\dot{e}_{KJ} = -2D^{IK}e_{KJ} + D^{I}_{J} \qquad (2.178)$$

$$= -2D^{I}_{L}G^{LK}e_{KJ} + D^{I}_{J} = D^{I}_{J} - 2D^{I}_{L}e^{L}_{J} = D^{I}_{L}(\delta^{l}_{j} - 2e^{L}_{J})$$

Then,

$$D^{I}_{J} \neq \dot{\gamma}^{i}_{j} \neq \dot{e}^{I}_{J} \qquad (2.179)$$

Also,

$$D^{IJ} \neq \dot{\gamma}^{ij} \neq \dot{e}^{IJ} \qquad (2.180)$$

The material rate of the Green strain tensor can be expressed as

$$d\bar{R}\cdot\bar{\bar{D}}\cdot d\bar{R} = \frac{1}{2}\dot{[(dS)^2]} = d\bar{r}\cdot\dot{\bar{\bar{\gamma}}}\cdot d\bar{r} = (d\bar{r}\cdot\bar{\bar{F}}^{T})\cdot\bar{\bar{D}}\cdot(\bar{\bar{F}}\cdot d\bar{r}) \qquad (2.181)$$

or $$\boxed{\dot{\bar{\bar{\gamma}}} = \bar{\bar{F}}^{T}\cdot\bar{\bar{D}}\cdot\bar{\bar{F}} = \bar{\bar{U}}\cdot\bar{\bar{R}}^{T}\cdot\bar{\bar{D}}\cdot\bar{\bar{R}}\cdot\bar{\bar{U}}}$$

$$\bar{\bar{D}} = (\bar{\bar{F}}^{-1})^{T}\cdot\dot{\bar{\bar{\gamma}}}\cdot(\bar{\bar{F}}^{-1}) = \bar{\bar{R}}\cdot\bar{\bar{U}}^{-1}\cdot\dot{\bar{\bar{\gamma}}}\cdot\bar{\bar{U}}^{-1}\cdot\bar{\bar{R}}^{T} \qquad (2.182)$$

with components

$$\dot{\bar{\bar{\gamma}}} = \dot{\gamma}_{ij}\,\bar{g}^i\bar{g}^j = \dot{\gamma}^{ij}\,\bar{g}_i\bar{g}_j = \dot{\gamma}^{i}_{j}\,\bar{g}_i\bar{g}^j = \dot{\hat{\gamma}}_{ij}\,\bar{i}_i\bar{i}_j \qquad (2.183)$$

The relation between the mixed components of the deformation rate in the present configuration D^I_J and the rate of the Green strain tensor (either $\dot{\gamma}_{ij}$ or $\dot{\gamma}^i_j$) will be of importance in the formulation of the constitutive equations for the fixed reference configuration. This relation can be obtained as follows since, from Eq. 2.175:

$$\frac{1}{2}\dot{C}_{kj} = \dot{\gamma}_{kj} = D_{KJ} \qquad (2.184)$$

$$\frac{1}{2} g_{kl}\dot{C}^l_j = g_{kl}\dot{\gamma}^l_j = G_{KI} D^I_J \qquad (2.185)$$

$$\frac{1}{2}\dot{C}^l_j = \dot{\gamma}^l_j = g^{kl} G_{KI} D^I_J = C^l_i D^I_J = (\delta^l_i + 2\gamma^l_i) D^I_J \qquad (2.186)$$

$$\dot{\gamma}^i_j = C^i_k D^K_J = (\delta^i_k + 2\gamma^i_k) D^K_J \qquad (2.187)$$

$$\boxed{D^I_J = (C^{-1})^i_l\,\dot{\gamma}^l_j = (C^{-1})^{il}\,\dot{\gamma}_{lj}} \qquad (2.188)$$

The rate of the Almansi (Eulerian) strain tensor admits many interpretations, since this strain tensor is referred to the current (deformed) configuration. For example, the rate observed by an observer that remains fixed-in-space, denoted by $\overset{\square}{\bar{\bar{e}}}$, constitutes a tensor with components

$$\overset{\square}{\bar{\bar{e}}} = \overset{\square}{e}_{IJ}\,\bar{G}^I\bar{G}^J = \overset{\square}{e}^{IJ}\,\bar{G}_I\bar{G}_J = \overset{\square}{e}^I_J\,\bar{G}_I\bar{G}^J = \overset{\square}{\hat{e}}_{IJ}\,\bar{i}_i\bar{i}_j \qquad (2.189)$$

Since $\frac{d}{dt}(\bar{i}_i) = 0$, it follows that

$$\boxed{\overset{\square}{\hat{e}}_{IJ} = \dot{\hat{e}}_{IJ}} \tag{2.190}$$

$$\overset{\square}{\bar{\bar{e}}} = \overset{\square}{e}_{IJ}\bar{G}^I\bar{G}^J = \frac{d}{dt}\left(e_{IJ}\bar{G}^I\bar{G}^J\right) = \dot{e}_{IJ}\bar{G}^I\bar{G}^J + e_{IJ}\dot{\bar{G}}^I\bar{G}^J$$

$$+ e_{IJ}\bar{G}^I\dot{\bar{G}}^J = \dot{e}_{IJ}\bar{G}^I\bar{G}^J + e_{IJ}\left(-V^I_{,K}\bar{G}^K\right)\bar{G}^J + e_{IJ}\bar{G}^I\left(-V^J_{,K}\bar{G}^K\right)$$

$$= \dot{e}_{IJ}\bar{G}^I\bar{G}^J - e_{KJ}V^K_{,I}\bar{G}^I\bar{G}^J - e_{IK}V^K_{,J}\bar{G}^I\bar{G}^J \tag{2.191}$$

$$\boxed{\overset{\square}{e}_{IJ} \equiv \dot{e}_{IJ} - e_{IK}V^K_{,J} - V^K_{,I}\,e_{KJ}}$$

$$\overset{\square}{\bar{\bar{e}}} = \overset{\square}{e}{}^I_J\,\bar{G}_I\bar{G}^J = \frac{d}{dt}\left(e^I_{\cdot J}\bar{G}_I\bar{G}^J\right) = \dot{e}^I_{\cdot J}\bar{G}_I\bar{G}^J + e^I_{\cdot J}\dot{\bar{G}}_I\bar{G}^J + e^I_{\cdot J}\bar{G}_I\dot{\bar{G}}^J$$

$$= \dot{e}^I_{\cdot J}\bar{G}_I\bar{G}^J + e^I_J\left(V^K_{,I}\bar{G}_K\right)\bar{G}^J + e^I_J\bar{G}_I\left(-V^J_{,K}\bar{G}^K\right)$$

$$= \dot{e}^I_{\cdot J}\bar{G}_I\bar{G}^J + e^K_J V^I_{,K}\bar{G}_I\bar{G}^J - e^I_K V^K_{,J}\bar{G}_I\bar{G}^J$$

$$\boxed{\overset{\square}{e}{}^I_J \equiv \dot{e}^I_{\cdot J} - e^I_K V^K_{,J} + V^I_{,K}\,e^K_J} \tag{2.192}$$

Another rate is the change observed by an observer that rotates and deforms with the medium: the "convected rate". However, <u>different</u> tensors are obtained from convected differentiation of different representations (contravariant, covariant, and mixed) of the <u>same</u> tensor. For example, the components obtained by differentiation of the covariant (convected) components e_{IJ}:

$$\overset{\triangle}{e}_{IJ} \equiv \dot{e}_{IJ} \qquad \overset{\triangle}{e}{}^I_J = G^{IK}\dot{e}_{KJ} \qquad \overset{\triangle}{e}{}^{IJ} = G^{IL}G^{JK}\dot{e}_{LK} \tag{2.193}$$

and the components obtained by differentiation of the mixed (convected) components $e^{I}_{\cdot J}$

$$\overset{\triangleright}{e}{}^{I}_{\cdot J} = \dot{e}^{I}_{\cdot J} \qquad \overset{\triangleright}{e}_{IJ} = G_{IK}\,\dot{e}^{K}_{\cdot J} \qquad \overset{\triangleright}{e}{}^{IJ} = G^{KJ}\,\dot{e}^{I}_{\cdot K} \tag{2.194}$$

are not components of one and the same tensor:

$$\overset{\triangle}{e}_{IJ} \neq \overset{\triangleright}{e}_{\cdot J} \qquad \overset{\triangle}{e}{}^{I}_{J} \neq \overset{\triangleright}{e}{}^{I}_{\cdot J} \qquad \overset{\triangle}{e}{}^{IJ} \neq \overset{\triangleright}{e}{}^{IJ} \tag{2.195}$$

2.4.3.3 Spin Tensor

The spin tensor, $\bar{\bar{W}}$ (also called vorticity tensor) is the ultimate rate of change of the rotation $\bar{\bar{R}}$ at $\bar{R}$ from the present shape to one the body had just before or will have just afterward:

$$\bar{\bar{\bar{W}}} \equiv \dot{\bar{\bar{\bar{R}}}}_t\,(t) \tag{2.196}$$

Motions in which $\bar{\bar{W}} = \bar{\bar{0}}$* are called irrotational. They form the main subject of study in classical hydrodynamics.

If a fixed reference configuration is used, more complicated formulae ensue:

$$\bar{\bar{\bar{W}}} = \dot{\bar{\bar{\bar{R}}}}\cdot\bar{\bar{\bar{R}}}^T + \frac{1}{2}\bar{\bar{\bar{R}}}\cdot\left(\dot{\bar{\bar{\bar{U}}}}\cdot\bar{\bar{\bar{U}}}^{-1} - \bar{\bar{\bar{U}}}^{-1}\cdot\dot{\bar{\bar{\bar{U}}}}\right)\cdot\bar{\bar{\bar{R}}}^T \tag{2.197}$$

Components of $\bar{\bar{W}}$ are:

$$\bar{\bar{\bar{W}}} = \hat{W}_{IJ}\,\bar{i}_i\,\bar{i}_j = W_{IJ}\,\bar{G}^I\bar{G}^J = W^{IJ}\,\bar{G}_I\bar{G}_J = W^{I}_{\cdot J}\,\bar{G}_I\bar{G}^J = W_{I\cdot}^{\cdot J}\,\bar{G}^I\bar{G}_J \tag{2.198}$$

$$\begin{gathered}\hat{W}_{IJ} = \frac{1}{2}\left(\frac{\partial\hat{V}_I}{\partial X_J} - \frac{\partial\hat{V}_J}{\partial X_I}\right) \qquad W_{IJ} = \frac{1}{2}\left(V_{I,J} - V_{J,I}\right)\\ W^{I}_{\cdot J} = \frac{1}{2}\left(V^{I}_{,J} - V_{J,}{}^{I}\right) \qquad W_{I\cdot}^{\cdot J} = \frac{1}{2}\left(V_{I,}{}^{J} - V^{J}_{,I}\right)\\ W^{IJ} = \frac{1}{2}\left(V^{I}{}_{,}{}^{J} - V^{J}{}_{,}{}^{I}\right)\end{gathered} \tag{2.199}$$

---

*Where $\bar{\bar{0}}$ is defined as the tensor which obeys $\bar{\bar{A}}\cdot\bar{\bar{0}} = \bar{\bar{0}}$ for any tensor $\bar{\bar{A}}$.

Differentiating the relation $\bar{\bar{R}}_t(\tau)\cdot\bar{\bar{R}}_t(\tau)^T = \bar{\bar{1}}$ with respect to τ, and setting $\tau = t$, one finds that $\bar{\bar{W}}$ is skew:

$$\bar{\bar{W}} + \bar{\bar{W}}^T = \bar{\bar{0}} \tag{2.200}$$

2.4.3.4 The Spatial Velocity Gradient Tensor

The spatial velocity gradient tensor $\bar{\bar{L}}$ is the ultimate rate of change of the deformation gradient tensor $\bar{\bar{F}}$ at $\bar{R}$ from the present shape to one the body had just before or will have just afterward:

$$\bar{\bar{L}} \equiv \dot{\bar{\bar{F}}}_t(t) \tag{2.201}$$

For a fixed reference configuration:

$$\boxed{\bar{\bar{L}} \equiv \dot{\bar{\bar{F}}}\cdot\bar{\bar{F}}^{-1}} \tag{2.202}$$

Also,*

$$\bar{\bar{L}} = \text{Grad}\,\dot{\bar{R}} = \text{Grad}\,\bar{v} \tag{2.203}$$

which justifies the name spatial velocity gradient.

Also, differentiating the polar decomposition

$$\bar{\bar{F}}_t(\tau) = \bar{\bar{R}}_t(\tau)\cdot\bar{\bar{U}}_t(\tau) = \bar{\bar{V}}_t(\tau)\cdot\bar{\bar{R}}_t(\tau) \tag{2.204}$$

with respect to τ, and then setting $\tau = t$, one finds that

$$\bar{\bar{L}} = \bar{\bar{D}} + \bar{\bar{W}} \tag{2.205}$$

This result shows that $\bar{\bar{D}}$ and $\bar{\bar{W}}$ are the symmetric and skew parts of the velocity gradient:

---

*Henceforth, Grad shall denote the gradient operator with respect to the spatial coordinates X_I, while grad shall denote the gradient operator with respect to the referential (material) coordinates x_i.

$$\boxed{\bar{\bar{D}} = \frac{1}{2}\left(\bar{\bar{L}} + \bar{\bar{L}}^T\right)} \quad \boxed{\bar{\bar{W}} = \frac{1}{2}\left(\bar{\bar{L}} - \bar{\bar{L}}^T\right)} \qquad (2.206)$$

It also expresses the fundamental Euler-Cauchy-Stokes decomposition of the instantaneous motion at $\bar{R}$ and t into the sum of a pure stretching ($\bar{\bar{D}}$) along the mutually orthogonal axes and a rigid spin ($\bar{\bar{W}}$) of those axes. Components of $\bar{\bar{L}}$ are:

$$\bar{\bar{L}} = \hat{L}_{IJ}\,\bar{\iota}_i\bar{\iota}_j = L_{IJ}\,\bar{G}^I\bar{G}^J = L^{IJ}\,\bar{G}_I\bar{G}_J = L^{I}_{\cdot J}\,\bar{G}_I\bar{G}^J \qquad (2.207)$$

$$\hat{L}_{IJ} = \frac{\partial \hat{V}_I}{\partial X_J} \qquad L_{IJ} = V_{I,J} \qquad L^{IJ} = V^{I}{}_{,}{}^{J} \qquad L^{I}_{\cdot J} = V^{I}{}_{,J} \qquad (2.208)$$

2.5 Stress Tensors

At a typical material point M, consider a differential element of area dA in the present configuration, and a differential element of area dA_o in the reference configuration. The orientations of these differential elements of area are defined by their unit normal vectors $\bar{N}$ (for dA) and $\bar{n}$ (for dA_o).

The force transmitted across the differential element of area dA at the material point M is $d\bar{P}$, and the corresponding traction vector is $\bar{T} = \frac{d\bar{P}}{dA}$. Also, it is convenient to define a fictitious force $d\bar{\tilde{P}} = (\bar{\bar{F}})^{-1}.d\bar{P}$, or $d\bar{\tilde{P}}.\bar{G}_I = d\bar{P}.\bar{g}_i$, a traction vector measured with respect to the undeformed area $\bar{t} = \frac{d\bar{P}}{dA_o}$, and a fictitious traction vector $d\bar{\tilde{t}} = \frac{d\bar{\tilde{P}}}{dA_o}$. These vectors have components:

$$\bar{N} = \hat{N}_I\bar{\iota}_i = N^I\bar{G}_I = N_I\bar{G}^I \qquad \bar{n} = \hat{n}_i\bar{\iota}_i = n^i\bar{g}_i = n_i\bar{g}^i \qquad d\bar{P} = \bar{\bar{F}}\cdot d\bar{\tilde{P}}$$

$$d\bar{P} = d\hat{P}_I\bar{\iota}_i = dP^I\bar{G}_I = dP_I\bar{G}^I \qquad d\bar{\tilde{P}} = d\hat{\tilde{P}}_i\bar{\iota}_i = d\tilde{P}^i\bar{g}_i = d\tilde{P}_i\bar{g}^i \qquad (2.209)$$

$$\bar{T} \equiv \frac{d\bar{P}}{dA} = \hat{T}_I\bar{\iota}_i = T^I\bar{G}_I = T_I\bar{G}^I$$

$$\bar{t} \equiv \frac{d\bar{P}}{dA_o} = \hat{t}_I\bar{\iota}_i = t^I\bar{G}_I = t_I\bar{G}^I \qquad \bar{\tilde{t}} \equiv \frac{d\bar{\tilde{P}}}{dA_o} = \hat{\tilde{t}}_i\bar{\iota}_i = \tilde{t}^i\bar{g}_i = \tilde{t}_i\bar{g}^i$$

2.5.1 The Cauchy Stress Tensor

The Cauchy stress tensor, $\bar{\bar{\sigma}}$ (sometimes called Eulerian stress in the engineering literature) is defined as

$$\boxed{\bar{T} = \bar{N} \cdot \bar{\bar{\sigma}}} \tag{2.210}$$

Components of this symmetric tensor* are

$$\bar{\bar{\sigma}} = \hat{\sigma}_{IJ} \bar{\iota}_i \bar{\iota}_j = \sigma^{IJ} \bar{G}_I \bar{G}_J = \sigma_{IJ} \bar{G}^I \bar{G}^J = \sigma^I_J \bar{G}_I \bar{G}^J \tag{2.211}$$

The first subscript on a component of $\bar{\bar{\sigma}}$ identifies the plane on which it acts, while the second subscript identifies the direction of that component. The definition can be expressed, in component form as:

$$\hat{T}_I = \hat{\sigma}_{IJ} \hat{N}_J \tag{2.212}$$

$$T^I = \sigma^{IJ} N_J = \sigma^I_J N^J \tag{2.213}$$

$$T_I = \sigma_{IJ} N^J = \sigma^J_I N_J \tag{2.214}$$

or

$$\bar{T} = \hat{\sigma}_{IJ} \hat{N}_I \bar{\iota}_j = \sigma^{IJ} N_I \bar{G}_J = \sigma^I_J N_I \bar{G}^J \tag{2.215}$$

2.5.2 The Kirchhoff Stress Tensor

The Kirchhoff stress tensor $\bar{\bar{\tau}}$, can be defined conveniently in terms of the Cauchy stress tensor as:

---

*It is not a law of mechanics that the Cauchy stress tensor is symmetric. Truesdell (32, page 14) points out that it has been known for a century that the presence of couples, acting whether from within the material like body forces or upon contiguous portions of material like stresses, is sufficient to render the stress tensor unsymmetric. These couple stresses may arise from inhomogeneity of strain. Some presentations of the continuum theory of dislocations in finite strain make use of couple stresses (polar medium). However, for the present purposes, the couple stresses are ignored and attention is restricted to the nonpolar case.

$$\boxed{\overline{\overline{\tau}} \equiv \frac{\rho_o}{\rho}\overline{\overline{\sigma}}} \qquad (2.216)$$

or, equivalently:

$$\boxed{\overline{\overline{T}} = \frac{\rho}{\rho_o}\overline{\overline{N}}\cdot\overline{\overline{\tau}}} \qquad (2.217)$$

where ρ_o is the mass density of the material in the reference configuration at $t = t_o$, defined by:

$$\rho_o \equiv \frac{dm}{dV_o} \qquad (2.218)$$

where m is the mass and V_o the volume in the reference configuration.

The mass density ρ of the material in the present configuration at $t = t$ is defined by:

$$\rho \equiv \frac{dm}{dV} \qquad (2.219)$$

Here, again, m is the mass, and V the volume in the present configuration. Observe that once a fixed reference configuration is chosen, ρ_o is a constant for a material point, while ρ is a function of time. The equation (2.219) for the mass-density expresses a relation between the body and such shapes as it may assume. To each shape of the body one may apply Eqs. 2.218 and 2.219 to obtain the same mass for the same part of the body:

$$m = \int \rho_o\, dV_o = \int \rho\, dV \qquad (2.220)$$

If one writes J for the absolute value of the Jacobian determinant, then a theorem of integral calculus* shows that

$$\int \rho_o\, dV_o = \int \rho\, J\, dV_o \qquad (2.221)$$

*For example, Theorems 3-13 and 3-14 of [74] and Theorem 8.26 of [75].

or

$$J \equiv \left|\det \bar{\bar{F}}\right| = \frac{\rho_0}{\rho} = \frac{dV}{dV_0} = \sqrt{\frac{G}{g}} \tag{2.222}$$

Therefore, one can also express the Kirchhoff stress $\bar{\bar{\tau}}$ as:

$$\bar{\bar{\tau}} = \frac{dV}{dV_0}\bar{\bar{\sigma}} = J\bar{\bar{\sigma}} = \left|\det \bar{\bar{F}}\right|\bar{\bar{\sigma}} = \sqrt{\frac{G}{g}}\,\bar{\bar{\sigma}} \tag{2.223}$$

Since the Cauchy stress tensor $\bar{\bar{\sigma}}$ is symmetric, the Kirchhoff stress tensor is also symmetric. Components of this tensor are:

$$\bar{\bar{\tau}} = \hat{\tau}_{IJ}\,\bar{i}_i\bar{i}_j = \tau^{IJ}\bar{G}_I\bar{G}_J = \tau_{IJ}\bar{G}^I\bar{G}^J = \tau^I_J\,\bar{G}_I\bar{G}^J \tag{2.224}$$

The Kirchhoff stress tensor can be defined also from:

$$d\bar{P} = \hat{\tau}_{IJ}(\hat{n}_i\,dA_0)\,\bar{i}_j = \tau^{IJ}(n_i\,dA_0)\bar{G}_J = \tau^I_J\,(n_i\,dA_0)\bar{G}^J \tag{2.225}$$

since from Nanson's relation (page 169 of [50])

$$N_I\,dA = \frac{\rho_0}{\rho}\,n_i\,dA_0 = J\,n_i\,dA_0 = \sqrt{\frac{G}{g}}\,n_i\,dA_0 \tag{2.226}$$

Hence,

$$\bar{t} = \frac{d\bar{P}}{dA_0} = \hat{\tau}_{IJ}\,\hat{n}_i\,\bar{i}_j = \tau^{IJ}n_i\,\bar{G}_J = \tau^I_J\,n_i\,\bar{G}^J \tag{2.227}$$

$$t^J = n_i\,\tau^{IJ} \qquad t_J = n_i\,\tau^I_J \qquad \hat{t}_J = \hat{n}_i\,\hat{\tau}_{IJ} \tag{2.228}$$

2.5.3 The Second Piola-Kirchhoff Stress Tensor

The Second Piola-Kirchhoff stress tensor $\bar{\bar{S}}$ is defined as:

$$\boxed{\bar{\tilde{t}} = \bar{n}\cdot\bar{\bar{S}}} \tag{2.229}$$

where $\bar{\tilde{t}}$ is a pseudo-traction vector relating a fictitious differential force $d\bar{\tilde{P}}$ to the original area dA_o as $\bar{\tilde{t}} = \dfrac{d\bar{\tilde{P}}}{dA_o}$. This pseudo-traction vector is defined by the same relation that relates the differential of the position vector to the deformed configuration $d\bar{R}$ to the differential of the position vector to the undeformed configuration $d\bar{r}$. From Eqs. 2.85 and 2.86:

$$\text{as} \quad d\bar{R} = \bar{\bar{F}} \cdot d\bar{r} \quad \text{and} \quad \bar{G}_I = \bar{\bar{F}} \cdot \bar{g}_i \tag{2.230}$$

$$\text{then} \quad d\bar{P} = \bar{\bar{F}} \cdot d\bar{\tilde{P}} \quad \text{and} \quad \bar{t} = \bar{\bar{F}} \cdot \bar{\tilde{t}} \tag{2.231}$$

$$\text{or} \quad d\bar{\tilde{P}} = \bar{\bar{F}}^{-1} \cdot d\bar{P} \quad \text{and} \quad \bar{\tilde{t}} = \bar{\bar{F}}^{-1} \cdot \bar{t} \tag{2.232}$$

Observe that these relations imply

$$d\bar{P} \cdot \bar{g}_i = d\bar{\tilde{P}} \cdot \bar{G}_I \qquad \bar{t} \cdot \bar{g}_i = \bar{\tilde{t}} \cdot \bar{G}_I \tag{2.233}$$

Writing these expressions in component form:

$$dP^I \bar{G}_I = \bar{\bar{F}} \cdot d\tilde{P}^i \bar{g}_i = d\tilde{P}^i \bar{\bar{F}} \cdot \bar{g}_i = d\tilde{P}^i \bar{G}_I \tag{2.234}$$

$$t^I \bar{G}_I = \bar{\bar{F}} \cdot \tilde{t}^i \bar{g}_i = \tilde{t}^i \bar{\bar{F}} \cdot \bar{g}_i = \tilde{t}^i \bar{G}_I \tag{2.235}$$

Hence

$$dP^I = d\tilde{P}^i \qquad t^I = \tilde{t}^i \tag{2.236}$$

But

$$dP_I \neq d\tilde{P}_i \qquad t_I \neq \tilde{t}_i \tag{2.237}$$

and, of course

$$d\overline{P} \neq d\overline{\tilde{P}} \qquad \bar{t} \neq \bar{\tilde{t}} \tag{2.238}$$

The second Piola-Kirchhoff stress is a symmetric tensor if the Cauchy stress tensor is symmetric.

Expressing the Second Piola-Kirchhoff stress tensor $\overline{\overline{S}}$ in component form:

$$\overline{\overline{S}} = \hat{S}_{ij}\,\bar{i}_i\bar{i}_j = S^{ij}\bar{g}_i\bar{g}_j = S_{ij}\,\bar{g}^i\bar{g}^j = S^i_j\,\bar{g}_i\bar{g}^j \tag{2.239}$$

Its definition (Eq. 2.229) can also be expressed in component form as

$$\bar{\tilde{t}} = n_i S^{ij}\bar{g}_j = n_i\, S^i_j\,\bar{g}^j = \hat{n}_i\,\hat{S}_{ij}\,\bar{i}_j \tag{2.240}$$

$$\tilde{t}^j = n_i S^{ij} \qquad \tilde{t}_j = n_i S^i_j \qquad \hat{\tilde{t}}_j = \hat{n}_i\,\hat{S}_{ij} \tag{2.241}$$

$$d\overline{\tilde{P}} = S^{ij}(n_i dA_o)\bar{g}_j = S^i_j\,(n_i dA_o)\bar{g}^j = \hat{S}_{ij}(\hat{n}_i dA_o)\bar{i}_j \tag{2.242}$$

Observe, from Eqs. 2.236, 2.241, and 2.228 that

$$\tilde{t}^j = t^J \tag{2.243}$$

Then,

$$n_i S^{ij} = n_i \tau^{IJ} \tag{2.244}$$

Hence,

$$\boxed{S^{ij} = \tau^{IJ}} \tag{2.245}$$

The contravariant components S^{ij} (with respect to the reference basis $\bar{g}_i$) of the Second Piola-Kirchhoff stress tensor $\overline{\overline{S}}$ and the contravariant components τ^{IJ} (with respect to the present basis $\bar{G}_I$) of the Kirchhoff stress tensor $\overline{\overline{T}}$ are equal. However, this does not at all imply that the Kirchhoff stress and the Second Piola-Kirchhoff stress are equal.

2.5.4 The First Piola-Kirchhoff Stress Tensor

The First Piola-Kirchhoff stress tensor $\overline{\overline{T}}$ (also called nominal stress) is a double tensor* defined as:

$$\boxed{\bar{t} = \bar{n} \cdot \overline{\overline{\overline{T}}}} \tag{2.246}$$

Observe that the double tensor $\overline{\overline{T}}$ operates on the unit vector $\bar{n}$, associated with the reference configuration, to produce the traction vector $\bar{t}$ associated with the present configuration. The First Piola-Kirchhoff stress tensor is, in general, an unsymmetric tensor. Components of this stress tensor are:

$$\overline{\overline{\overline{T}}} = \hat{T}_{iJ}\bar{\iota}_i\bar{\iota}_j = T^{iJ}\bar{g}_i\bar{G}_J = T^{i\cdot}_{\cdot J}\,\bar{g}_i\bar{G}^J = T_{iJ}\,\bar{g}^i\bar{G}^J = T_i^{\cdot J}\,\bar{g}^i\bar{G}_J \tag{2.247}$$

$$= T_{ij}\,\bar{g}^i\bar{g}^j = T^{ij}\,\bar{g}_i\bar{g}_j = T^{i\cdot}_{\cdot j}\,\bar{g}_i\bar{g}^j = T_i^{\cdot j}\,\bar{g}^i\bar{g}_j$$

Truesdell and Noll [40] define the First Piola-Kirchhoff stress as the transpose of this definition (Eq. 2.246) and denote it with the symbol $\mathbf{T}_R$, employing the following components:

$$\mathbf{T}_R = \overline{\overline{\overline{T}}}^T = T_R^{Ji}\,\bar{G}_J\bar{g}_i = T_R{}^{J}{}_{\cdot i}\,\bar{G}_J\bar{g}^i = T_{RJi}\,\bar{G}^J\bar{g}^i \tag{2.248}$$

in their analysis.

The definition of the First Piola-Kirchhoff stress tensor $\overline{\overline{T}}$, is, in component form

$$\bar{t} = n_i\,T^{iJ}\bar{G}_J = n_i\,T^{i\cdot}_{\cdot J}\bar{G}^J = \hat{n}_i\,\hat{T}_{iJ}\,\bar{\iota}_j \tag{2.249}$$

or

$$d\bar{P} = T^{iJ}(n_i dA_o)\bar{G}_J = T^{i\cdot}_{\cdot J}(n_i dA_o)\bar{G}^J = \hat{T}_{iJ}(\hat{n}_i dA_o)\bar{\iota}_j \tag{2.250}$$

---

*See Subsection 2.4 for a definition of a double tensor.

$$t^{J} = n_i T^{iJ} \qquad t_{J} = n_i T^{i\cdot}_{\cdot J} \qquad \hat{t}_{\cdot J} = \hat{n}_i \hat{T}_{iJ} \tag{2.251}$$

Observe that the mixed components of the Kirchhoff stress tensor with respect to the present basis $\bar{G}_I$, and the following mixed components of the First Piola-Kirchhoff stress with respect to the reference and present configuration basis, are equal:

$$\boxed{\tau^{I}_{J} = T^{i\cdot}_{\cdot J}} \tag{2.252}$$

Also, the following contravariant components of the Kirchhoff, First Piola-Kirchhoff, and Second Piola-Kirchhoff stress tensor are equal:

$$\boxed{\tau^{IJ} = T^{iJ} = S^{ij}} \tag{2.253}$$

2.5.5 Relations between Stress Tensors

The following relationships between the stress tensors can be shown to hold:

$$\bar{\bar{\tau}} = \frac{\rho_0}{\rho}\bar{\bar{\sigma}} \tag{2.254}$$

$$\bar{\bar{S}} = \frac{\rho_0}{\rho}\bar{\bar{F}}^{-1}\cdot\bar{\bar{\sigma}}\cdot(\bar{\bar{F}}^{-1})^T = \frac{\rho_0}{\rho}\bar{\bar{U}}^{-1}\cdot\bar{\bar{R}}^T\cdot\bar{\bar{\sigma}}\cdot\bar{\bar{R}}\cdot\bar{\bar{U}}^{-1} \tag{2.255}$$

$$\bar{\bar{T}} = \frac{\rho_0}{\rho}\bar{\bar{F}}^{-1}\cdot\bar{\bar{\sigma}} = \frac{\rho_0}{\rho}\bar{\bar{U}}^{-1}\cdot\bar{\bar{R}}^T\cdot\bar{\bar{\sigma}} \tag{2.256}$$

$$\bar{\bar{\sigma}} = \frac{\rho}{\rho_0}\bar{\bar{\tau}} \tag{2.257}$$

$$\bar{\bar{S}} = \bar{\bar{F}}^{-1}\cdot\bar{\bar{\tau}}\cdot(\bar{\bar{F}}^{-1})^T = \bar{\bar{U}}^{-1}\cdot\bar{\bar{R}}^T\cdot\bar{\bar{\tau}}\cdot\bar{\bar{R}}\cdot\bar{\bar{U}}^{-1} \tag{2.258}$$

$$\bar{\bar{T}} = \bar{\bar{F}}^{-1}\cdot\bar{\bar{\tau}} = \bar{\bar{U}}^{-1}\cdot\bar{\bar{R}}^T\cdot\bar{\bar{\tau}} \tag{2.259}$$

$$\bar{\bar{\sigma}} = \frac{\rho}{\rho_0}\,\bar{\bar{F}}\cdot\bar{\bar{S}}\cdot\bar{\bar{F}}^T = \frac{\rho}{\rho_0}\,\bar{\bar{R}}\cdot\bar{\bar{U}}\cdot\bar{\bar{S}}\cdot\bar{\bar{U}}\cdot\bar{\bar{R}}^T \tag{2.260}$$

$$\bar{\bar{\tau}} = \bar{\bar{F}}\cdot\bar{\bar{S}}\cdot\bar{\bar{F}}^T = \bar{\bar{R}}\cdot\bar{\bar{U}}\cdot\bar{\bar{S}}\cdot\bar{\bar{U}}\cdot\bar{\bar{R}}^T \tag{2.261}$$

$$\bar{\bar{T}} = \bar{\bar{S}}\cdot\bar{\bar{F}}^T = \bar{\bar{S}}\cdot\bar{\bar{U}}\cdot\bar{\bar{R}}^T \tag{2.262}$$

$$\bar{\bar{\sigma}} = \frac{\rho}{\rho_0}\,\bar{\bar{F}}\cdot\bar{\bar{T}} = \frac{\rho}{\rho_0}\,\bar{\bar{R}}\cdot\bar{\bar{U}}\cdot\bar{\bar{T}} \tag{2.263}$$

$$\bar{\bar{\tau}} = \bar{\bar{F}}\cdot\bar{\bar{T}} = \bar{\bar{R}}\cdot\bar{\bar{U}}\cdot\bar{\bar{T}} \tag{2.264}$$

$$\bar{\bar{S}} = \bar{\bar{T}}\cdot(\bar{\bar{F}}^{-1})^T = \bar{\bar{T}}\cdot\bar{\bar{U}}^{-1}\cdot\bar{\bar{R}}^T \tag{2.265}$$

The relation between the mixed components of the Kirchhoff stress in the present configuration, in the body-fixed convected coordinate system, τ^I_k, and the components of the Second Piola-Kirchhoff stress (S^{ij} or S^i_j) will be of importance in the formulation of the constitutive relations in the fixed reference configuration used in this work. This relationship will be needed in later parts of the analysis.

Since the contravariant components of the Kirchhoff stress tensor component in the present configuration and the Second Piola-Kirchhoff stress tensor component in the reference configuration are equal:

$$\tau^{IJ} = S^{ij} \tag{2.266}$$

it follows that

$$\tau^I_K\, G^{KJ} = S^i_\ell\, g^{\ell j} \tag{2.267}$$

$$\tau^I_K = S^i_\ell \, g^{\ell j} G_{JK} = S^i_\ell C^\ell_k = S^i_\ell(\delta^\ell_k + 2\gamma^\ell_k) \tag{2.268}$$

Hence, the mixed components are related by:

$$\tau^I_K = C^\ell_k S^i_\ell = (\delta^\ell_k + 2\gamma^\ell_k) S^i_\ell \tag{2.269}$$

or

$$\boxed{\tau^I_K = C_{k\ell} S^{\ell i} = (g_{k\ell} + 2\gamma_{k\ell}) S^{\ell i}} \tag{2.270}$$

2.6 Stress Rates and Rates of Second Order Tensors in General

The time derivative of tensor fields, such as stress, that are associated with the present configuration, admits infinitely many definitions, depending upon the observer used to compute such time derivatives. For use in constitutive equations, it is convenient that the following conditions [76] should be satisfied:

1. The Leibniz rule of differentiation of a product.

2. The time derivative should be a tensor quantity of the same type as the original tensor; in particular, if the original tensor is symmetric, its time derivative should also be symmetric.

3. The derivative should be defined uniquely; i.e., starting from one definition, the same tensor should be obtained by differentiation of various representations of the same original tensor.

4. Vanishing of the time derivative of a tensor should induce vanishing of the time derivative of its arbitrary invariant.

5. The time derivative of the tensor should vanish when the material point of a continuum with its environment performs

a rigid body motion and the tensor does not vary in time intrinsically with respect to the material point.

Since the first time derivative of a tensor (defined in this fashion) constitutes a new tensor field, second and higher time derivatives can be defined by considering this field. It, therefore, suffices to analyze in detail the definition of the first time derivative.

Three different types of observers will be considered: (1) an observer that stays fixed in an inertial frame, (2) an observer that rotates and moves with the body, and (3) observers that move, rotate, and deform (in different fashions) with the body.

The time derivative, defined from the viewpoint of an observer remaining at rest in space will be called the "fixed-observer rate". The time derivative, defined from the viewpoint of an observer that moves with the particle, participating in its rotational motion, will be called the "co-rotational rate".

The time derivative, defined from the viewpoint of an observer that moves with the particle, participating in its rotatory motion, and deforming in common with the continuum, will be called the "convected rate" (there exists more than one type of this derivative, according to what one defines as "deforming in common" with the continuum).

2.6.1 Rates of the Unit Tensor

It is intuitive that a good definition of the time rate of a tensor would make the rate of the unit tensor $\overset{\square}{\bar{\bar{1}}}$ vanish. It seems appropriate, therefore, to investigate what time rates satisfy this condition.

(a) Fixed-Observer Rate

It will be shown that the fixed-observer rate, denoted by $(\overset{\square}{\ })$, of the unit (metric) tensor vanishes:

$$\overset{\square}{\bar{\bar{1}}} \equiv \frac{d}{dt}\left(\bar{\bar{1}}\right) = \bar{\bar{0}} \qquad (2.271)$$

In the fixed-in-space Cartesian representation:

$$\overset{\square}{\bar{\bar{I}}} = \frac{d}{dt}\left(\delta_{ij}\,\bar{\iota}_i\bar{\iota}_j\right) = \bar{\bar{0}} \tag{2.272}$$

since

$$\frac{d}{dt}\left(\bar{\iota}_i\right) = \bar{0} \quad \text{and} \quad \frac{d}{dt}\left(\delta_{ij}\right) = 0 \tag{2.273}$$

In the convected system, with the <u>reference</u> configuration metric g_{ij}:

$$\overset{\square}{\bar{\bar{I}}} = \frac{d}{dt}\left(g_{ij}\,\bar{g}^i\bar{g}^j\right) = \dot{g}_{ij}\,\bar{g}^i\bar{g}^j + g_{ij}\,\dot{\bar{g}}^i\bar{g}^j + g_{ij}\,\bar{g}^i\dot{\bar{g}}^j = \bar{\bar{0}} \tag{2.274}$$

and similarly for

$$\overset{\square}{\bar{\bar{I}}} = \frac{d}{dt}\left(g^{ij}\,\bar{g}_i\bar{g}_j\right) = \frac{d}{dt}\left(\delta^i_j\,\bar{g}_i\bar{g}^j\right) = \bar{\bar{0}} \tag{2.275}$$

In the convected system, with the <u>present</u> configuration metric G_{IJ}, this result is not trivial, since:

$$\dot{G}_{IJ} \neq 0 \qquad \dot{G}^{IJ} \neq 0 \qquad \dot{\bar{G}}_I \neq \bar{0} \qquad \dot{\bar{G}}^I \neq \bar{0}$$

Employing Eq. 2.84, one finds:

$$\begin{aligned}
\overset{\square}{\bar{\bar{I}}} &= \frac{d}{dt}\left(G_{IJ}\,\bar{G}^I\bar{G}^J\right) = \dot{G}_{IJ}\,\bar{G}^I\bar{G}^J + G_{IJ}\,\dot{\bar{G}}^I\bar{G}^J + G_{IJ}\,\bar{G}^I\dot{\bar{G}}^J \\
&= \dot{G}_{IJ}\,\bar{G}^I\bar{G}^J + G_{IJ}\left(-V^I_{,K}\,\bar{G}^K\right)\bar{G}^J + G_{IJ}\,\bar{G}^I\left(-V^J_{,K}\,\bar{G}^K\right) \\
&= \dot{G}_{IJ}\,\bar{G}^I\bar{G}^J - G_{KJ}V^K_{,I}\,\bar{G}^I\bar{G}^J - G_{IK}V^K_{,J}\,\bar{G}^I\bar{G}^J \\
&= \left(\dot{G}_{IJ} - G_{IK}V^K_{,J} - V^K_{,I}G_{KJ}\right)\bar{G}^I\bar{G}^J = \overset{\square}{G}_{IJ}\,\bar{G}^I\bar{G}^J
\end{aligned} \tag{2.276}$$

$$\overset{\square}{G}_{IJ} = \dot{G}_{IJ} - G_{IK}V^K_{,J} - V^K_{,I}G_{KJ} \tag{2.277}$$

But, from Eq. 2.172

$$\dot{G}_{IJ} = V_{I,J} + V_{J,I} \tag{2.278}$$

c-2

Hence

$$\overset{\square}{G}_{IJ} = 0 \qquad\qquad \overset{\square}{\bar{\bar{I}}} = \bar{\bar{0}} \tag{2.279}$$

Also, for the mixed components:

$$\begin{aligned}
\overset{\square}{\bar{\bar{I}}} &= \frac{d}{dt}\left(\delta^I_J \bar{G}_I \bar{G}^J\right) = \dot{\delta}^I_J \bar{G}_I \bar{G}^J + \delta^I_J \dot{\bar{G}}_I \bar{G}^J + \delta^I_J \bar{G}_I \dot{\bar{G}}^J \\
&= \delta^I_J \left(V^K{}_{,I} \bar{G}_K\right)\bar{G}^J + \delta^I_J \bar{G}_I \left(-V^J{}_{,K} \bar{G}^K\right) \\
&= \delta^K_J V^I{}_{,K} \bar{G}_I \bar{G}^J - \delta^I_K V^K{}_{,J} \bar{G}_I \bar{G}^J \\
&= \left(V^I{}_{,J} - V^I{}_{,J}\right)\bar{G}_I \bar{G}^J = \overset{\square}{G}{}^I_J \bar{G}_I \bar{G}^J = \bar{\bar{0}}
\end{aligned} \tag{2.280}$$

For the contravariant components:

$$\begin{aligned}
\overset{\square}{\bar{\bar{I}}} &= \frac{d}{dt}\left(G^{IJ} \bar{G}_I \bar{G}_J\right) = \dot{G}^{IJ} \bar{G}_I \bar{G}_J + G^{IJ} \dot{\bar{G}}_I \bar{G}_J + G^{IJ} \bar{G}_I \dot{\bar{G}}_J \\
&= \dot{G}^{IJ} \bar{G}_I \bar{G}_J + G^{IJ}\left(V^K{}_{,I} \bar{G}_K\right)\bar{G}_J + G^{IJ} \bar{G}_I \left(V^K{}_{,J} \bar{G}_K\right) \\
&= \dot{G}^{IJ} \bar{G}_I \bar{G}_J + G^{KJ} V^I{}_{,K} \bar{G}_I \bar{G}_J + G^{IK} V^J{}_{,K} \bar{G}_I \bar{G}_J \\
&= \left(\dot{G}^{IJ} + G^{IK} V^J{}_{,K} + V^I{}_{,K} G^{KJ}\right)\bar{G}_I \bar{G}_J = \overset{\square}{G}{}^{IJ} \bar{G}_I \bar{G}_J \\
\overset{\square}{G}{}^{IJ} &= \dot{G}^{IJ} + V^{I}{}_{,}{}^{J} + V^{J}{}_{,}{}^{I}
\end{aligned} \tag{2.281}$$

But, from Eq. 2.173

$$\dot{G}^{IJ} = -\left(V^{I}{}_{,}{}^{J} + V^{J}{}_{,}{}^{I}\right) \tag{2.282}$$

Hence,

$$\overset{\square}{G}{}^{IJ} = 0 \qquad\qquad \overset{\square}{\bar{\bar{I}}} = \bar{\bar{0}} \tag{2.283}$$

(b) Convected Rates

The convected rate is the time derivative of the convected components of the tensor. For example, for the unit tensor:

$$\overset{\Delta}{\bar{\bar{1}}} = \dot{G}_{IJ}\, \bar{G}^{I}\, \bar{G}^{J} \equiv \overset{\Delta}{G}_{IJ}\, \bar{G}^{I}\, \bar{G}^{J} \tag{2.284}$$

Hence, employing Eq. 2.172:

$$\overset{\Delta}{G}_{IJ} \equiv \dot{G}_{IJ} = 2 D_{IJ} \tag{2.285}$$

$$\boxed{\overset{\Delta}{\bar{\bar{1}}} = 2\bar{\bar{D}}} \tag{2.286}$$

Another convected rate, denoted by $(\overset{\nabla}{\ })$, can be obtained from the material rate of the contravariant components, as follows:

$$\overset{\nabla}{\bar{\bar{1}}} = \dot{G}^{IJ}\, \bar{G}_{I}\, \bar{G}_{J} \equiv \overset{\nabla}{G}^{IJ}\, \bar{G}_{I}\, \bar{G}^{J} \tag{2.287}$$

From Eq. 2.173:

$$\overset{\nabla}{G}^{IJ} \equiv \dot{G}^{IJ} = -2 D^{IJ} \tag{2.288}$$

Therefore,

$$\boxed{\overset{\nabla}{\bar{\bar{1}}} = -2\bar{\bar{D}}} \tag{2.289}$$

Two other convected rates, denoted by $(\overset{\triangleleft}{\ })$ and $(\overset{\triangleright}{\ })$ can be obtained from the material rate of the mixed components:

$$\overset{\triangleright}{\bar{\bar{1}}} \equiv \dot{\delta}^{I}_{J}\, \bar{G}_{I}\, \bar{G}^{J} = \overset{\triangleright}{G}^{I}{}_{\cdot J}\, \bar{G}_{I}\, \bar{G}^{J} \tag{2.290a}$$

Hence

$$\overset{\triangleright}{G}^{I}{}_{\cdot J} \equiv \dot{\delta}^{I}_{J} = 0 \tag{2.290b}$$

Therefore

$$\boxed{\overset{\triangleright}{\bar{\bar{1}}} = \bar{\bar{0}}} \tag{2.290c}$$

$$\overset{\triangleleft}{\bar{\bar{1}}} \equiv \dot{\delta}^{I}_{J}\, \bar{G}^{J} \bar{G}_{I} = \overset{\triangleleft}{G}{}_{J\cdot}^{\cdot I}\, \bar{G}^{J} \bar{G}_{I} \tag{2.291a}$$

Hence

$$\overset{\triangleleft}{G}{}_{J\cdot}^{\cdot I} \equiv \dot{\delta}^{I}_{J} = 0 \tag{2.291b}$$

Therefore

$$\boxed{\overset{\triangleleft}{\bar{\bar{1}}} = \bar{\bar{0}}} \tag{2.291c}$$

which shows that only the "mixed" convected rates ($\overset{\triangleleft}{}$) and ($\overset{\triangleright}{}$) of the unit (metric) tensor do vanish; while the contravariant ($\overset{\nabla}{}$) and covariant convected ($\overset{\Delta}{}$) rates of the unit (metric) tensor do <u>not</u> vanish.

(c) <u>Co-Rotational Rate</u>

The co-rotational rate can be obtained from the additive decomposition of the velocity gradients, Eq. 2.205:

$$L^{I}_{\cdot J} = V^{I}_{,J} = D^{I}_{J} + W^{I}_{\cdot J} \tag{2.292}$$

The expression for the fixed-observer rate (Eq. 2.277) in convected coordinates can be expressed as:

$$\underbrace{\overset{\square}{G}_{IJ}}_{\substack{\text{Fixed}\\ \text{Observer}\\ \text{Rate}}} = \underbrace{\dot{G}_{IJ}}_{\substack{\text{Convected}\\ \text{Rate}}} - G_{IK}\Big(\underbrace{D^{I}_{J}}_{\substack{\text{Deformation}\\ \text{Rate}}} + \underbrace{W^{I}_{\cdot J}}_{\text{Spin}}\Big) - \Big(\underbrace{D^{K}_{I}}_{\substack{\text{Deformation}\\ \text{Rate}}} + \underbrace{W^{K}_{\cdot I}}_{\text{Spin}}\Big) G_{KJ} \tag{2.293}$$

Therefore, the co-rotational rate (the rate observed by an observer that rotates but does not deform with the body) should be

$$\underbrace{\overset{\circ}{G}_{IJ}}_{\text{Co-Rotational}} = \underbrace{\dot{G}_{IJ}}_{\text{Convected}} - G_{IK}\underbrace{D^K_J}_{\text{Deformation}} - \underbrace{D^K_I}_{\text{Deformation}} G_{KJ} \tag{2.294a}$$

$$\overset{\circ}{G}_{IJ} = \dot{G}_{IJ} - D_{IJ} - D_{IJ} = \dot{G}_{IJ} - 2D_{IJ} \tag{2.294b}$$

Hence, from Eq. 2.172:

$$\overset{\circ}{G}_{IJ} = 0 \tag{2.294c}$$

Similarly:

$$\begin{aligned}\overset{\circ}{G}{}^{IJ} &= \dot{G}^{IJ} + G^{IK}D^J_K + D^I_K G^{KJ} \\ &= \dot{G}^{IJ} + D^{IJ} + D^{IJ} = \dot{G}^{IJ} + 2D^{IJ}\end{aligned} \tag{2.295a}$$

Hence, from Eq. 2.173:

$$\overset{\circ}{G}{}^{IJ} = 0 \tag{2.295b}$$

Therefore,

$$\boxed{\overset{\circ}{\overline{\overline{1}}} = \overline{\overline{0}}} \tag{2.295c}$$

The co-rotational rate of the unit (metric) tensor does vanish.

2.6.2 Rates of the Cauchy Stress Tensor

2.6.2.1 Fixed-Observer Rate

The fixed-observer rate of the Cauchy stress tensor in Cartesian coordinates is simply:

$$\overset{\square}{\overline{\overline{\sigma}}} = \frac{d}{dt}\left(\hat{\sigma}_{IJ}\,\overline{i}_i\,\overline{i}_j\right) = \dot{\hat{\sigma}}_{IJ}\,\overline{i}_i\,\overline{i}_j \qquad \boxed{\overset{\square}{\hat{\sigma}}_{IJ} = \dot{\hat{\sigma}}_{IJ}} \tag{2.296}$$

The fixed-observer rate of the Cauchy stress tensor in convected curvilinear coordinates, is obtained by taking into account the time rate of the base vectors.

Contravariant Components:

$$\overset{\Box}{\bar{\bar{\sigma}}} = \frac{d}{dt}\left(\sigma^{IJ}\bar{G}_I\bar{G}_J\right) = \dot{\sigma}^{IJ}\bar{G}_I\bar{G}_J + \sigma^{IJ}\dot{\bar{G}}_I\bar{G}_J + \sigma^{IJ}\bar{G}_I\dot{\bar{G}}_J \tag{2.297}$$

$$= \dot{\sigma}^{IJ}\bar{G}_I\bar{G}_J + \sigma^{IJ}(V^K_{,I}\bar{G}_K)\bar{G}_J + \sigma^{IJ}\bar{G}_I(V^K_{,J}\bar{G}_K)$$

$$= \dot{\sigma}^{IJ}\bar{G}_I\bar{G}_J + \sigma^{KJ}V^I_{,K}\bar{G}_I\bar{G}_J + \sigma^{IK}V^J_{,K}\bar{G}_I\bar{G}_J$$

$$= \left(\dot{\sigma}^{IJ} + V^I_{,K}\sigma^{KJ} + V^J_{,K}\sigma^{IK}\right)\bar{G}_I\bar{G}_J = \overset{\Box}{\sigma}{}^{IJ}\bar{G}_I\bar{G}_J \tag{2.298}$$

$$\boxed{\overset{\Box}{\sigma}{}^{IJ} = \dot{\sigma}^{IJ} + V^I_{,K}\sigma^{KJ} + \sigma^{IK}V^J_{,K}}$$

Mixed Components:

$$\overset{\Box}{\bar{\bar{\sigma}}} = \frac{d}{dt}\left(\sigma^I_J\bar{G}_I\bar{G}^J\right) = \dot{\sigma}^{I}{}_{\cdot J}\bar{G}_I\bar{G}^J + \sigma^I_J\dot{\bar{G}}_I\bar{G}^J + \sigma^I_J\bar{G}_I\dot{\bar{G}}^J$$

$$= \dot{\sigma}^{I}{}_{\cdot J}\bar{G}_I\bar{G}^J + \sigma^I_J(V^K_{,I}\bar{G}_K)\bar{G}^J + \sigma^I_J\bar{G}_I(-V^J_{,K}\bar{G}^K)$$

$$= \dot{\sigma}^{I}{}_{\cdot J}\bar{G}_I\bar{G}^J + \sigma^K_J V^I_{,K}\bar{G}_I\bar{G}^J - \sigma^I_K V^K_{,J}\bar{G}_I\bar{G}^J$$

$$= \left(\dot{\sigma}^{I}{}_{\cdot J} + V^I_{,K}\sigma^K_J - \sigma^I_K V^K_{,J}\right)\bar{G}_I\bar{G}^J = \overset{\Box}{\sigma}{}^I_J\bar{G}_I\bar{G}^J$$

$$\boxed{\overset{\Box}{\sigma}{}^I_J = \dot{\sigma}^{I}{}_{\cdot J} + V^I_{,K}\sigma^K_J - \sigma^I_K V^K_{,J}} \tag{2.299}$$

Covariant Components:

$$\overset{\Box}{\bar{\bar{\sigma}}} = \frac{d}{dt}\left(\sigma_{IJ}\bar{G}^I\bar{G}^J\right) = \dot{\sigma}_{IJ}\bar{G}^I\bar{G}^J + \sigma_{IJ}\dot{\bar{G}}^I\bar{G}^J + \sigma_{IJ}\bar{G}^I\dot{\bar{G}}^J$$

$$= \dot{\sigma}_{IJ}\overline{G}^I\overline{G}^J + \sigma_{IJ}(-V^I_{,K}\overline{G}^K)\overline{G}^J + \sigma_{IJ}\overline{G}^I(-V^J_{,K}\overline{G}^K)$$

$$= \dot{\sigma}_{IJ}\overline{G}^I\overline{G}^J - \sigma_{KJ}V^K_{,I}\overline{G}^I\overline{G}^J - \sigma_{IK}V^K_{,J}\overline{G}^I\overline{G}^J$$

$$= (\dot{\sigma}_{IJ} - V^K_{,I}\sigma_{KJ} - \sigma_{IK}V^K_{,J})\overline{G}^I\overline{G}^J = \overset{\square}{\sigma}_{IJ}\overline{G}^I\overline{G}^J$$

$$\boxed{\overset{\square}{\sigma}_{IJ} \equiv \dot{\sigma}_{IJ} - V^K_{,I}\sigma_{KJ} - \sigma_{IK}V^K_{,J}} \qquad (2.300)$$

2.6.2.2 Convected Rates

The time derivative of the contravariant components of the Cauchy stress tensor in convected coordinates, was named the "convected rate" by Oldroyd [77]. This is one of four different tensors that can be obtained by time differentiation of the four components (covariant, contravariant, and the two mixed components) of the Cauchy stress in convected coordinates.

This "Oldroyd" rate will be identified here as ($^\nabla$). Therefore, in convected coordinates:

$$\overset{\nabla}{\overline{\overline{\sigma}}} \equiv \left(\frac{d}{dt}\sigma^{IJ}\right)\overline{G}_I\overline{G}_J = \dot{\sigma}^{IJ}\overline{G}_I\overline{G}_J = \overset{\nabla}{\sigma}^{IJ}\overline{G}_I\overline{G}_J$$

$$\boxed{\overset{\nabla}{\sigma}^{IJ} \equiv \dot{\sigma}^{IJ}} \qquad (2.301)$$

Oldroyd [77] shows, . .t in Cartesian coordinates:

$$\overset{\nabla}{\overline{\overline{\sigma}}} = \overset{\nabla}{\hat{\sigma}}_{IJ}\,\overline{i}_i\,\overline{i}_j$$

$$\boxed{\overset{\nabla}{\hat{\sigma}}_{IJ} \equiv \dot{\hat{\sigma}}_{IJ} - \hat{V}_{I,K}\hat{\sigma}_{JK} - \hat{V}_{J,K}\hat{\sigma}_{IK}} \qquad (2.302)$$

Another convected rate can be obtained from time differentiation of the covariant components of the Cauchy stress in convected coordinates. This stress rate, identified by ($^\Delta$) was analyzed by Cotter and Rivlin [78]. In convected coordinates:

$$\overset{\triangle}{\overline{\overline{\sigma}}} \equiv \left(\frac{d}{dt}\sigma_{IJ}\right)\overline{G}^I\overline{G}^J = \dot{\sigma}_{IJ}\overline{G}^I\overline{G}^J \equiv \overset{\triangle}{\sigma}_{IJ}\overline{G}^I\overline{G}^J \tag{2.303}$$

$$\boxed{\overset{\triangle}{\sigma}_{IJ} \equiv \dot{\sigma}_{IJ}}$$

Cotter and Rivlin [78] show that in Cartesian coordinates:

$$\overset{\triangle}{\overline{\overline{\sigma}}} = \overset{\triangle}{\hat{\sigma}}_{IJ}\,\overline{i}_i\,\overline{i}_j$$

(2.304)

$$\boxed{\overset{\triangle}{\hat{\sigma}}_{IJ} \equiv \dot{\hat{\sigma}}_{IJ} + \hat{V}_{K,I}\,\hat{\sigma}_{KJ} + \hat{V}_{K,J}\,\hat{\sigma}_{I,K}}$$

Other convected rates can be defined by time differentiation of the mixed components of the Cauchy stress in convected coordinates, as shown by Masur [79 and 80]:

$$\overset{\triangleright}{\overline{\overline{\sigma}}} \equiv \left(\frac{d}{dt}\sigma^{I}_{\cdot J}\right)\overline{G}_I\overline{G}^J = \dot{\sigma}^{I}_{\cdot J}\overline{G}_I\overline{G}^J \equiv \overset{\triangleright}{\sigma}{}^{I}_{\cdot J}\overline{G}_I\overline{G}^J$$

$$\boxed{\overset{\triangleright}{\sigma}{}^{I}_{\cdot J} \equiv \dot{\sigma}^{I}_{\cdot J}} \tag{2.305}$$

$$\overset{\triangleright}{\overline{\overline{\sigma}}} = \overset{\triangleright}{\hat{\sigma}}_{IJ}\,\overline{i}_i\,\overline{i}_j$$

$$\boxed{\overset{\triangleright}{\hat{\sigma}}_{IJ} \equiv \dot{\hat{\sigma}}_{IJ} - \hat{V}_{I,K}\,\hat{\sigma}_{KJ} + \hat{V}_{K,J}\,\hat{\sigma}_{IK}} \tag{2.306}$$

$$\overset{\triangleleft}{\overline{\overline{\sigma}}} = \left(\frac{d}{dt}\sigma_{J}^{\cdot I}\right)\overline{G}^J\overline{G}_I = \dot{\sigma}_{J}^{\cdot I}\overline{G}^J\overline{G}_I \equiv \overset{\triangleleft}{\sigma}{}_{J}^{\cdot I}\overline{G}^J\overline{G}_I$$

$$\boxed{\overset{\triangleleft}{\sigma}{}_{J}^{\cdot I} \equiv \dot{\sigma}_{J}^{\cdot I}} \tag{2.307}$$

$$\overset{\triangleleft}{\overline{\overline{\sigma}}} = \overset{\triangleleft}{\hat{\sigma}}_{IJ}\,\overline{i}_i\,\overline{i}_j$$

$$\boxed{\overset{\triangleleft}{\hat{\sigma}}_{IJ} \equiv \dot{\hat{\sigma}}_{IJ} + \hat{V}_{K,I}\,\hat{\sigma}_{KJ} - \hat{V}_{J,K}\,\hat{\sigma}_{IK}} \qquad (2.308)$$

2.6.2.3 Co-Rotational Rate

The co-rotational stress rate here denoted by $(\overset{\circ}{\ })$, in the convected coordinate system can be obtained from the fixed-observer rate in convected coordinates by replacing the velocity gradients $V^I{}_{,J} = D^I_J + W^{I\cdot}_{\cdot J}$ by D^I_J (thereby eliminating the subtraction of the spin tensor $W^{I\cdot}_{\cdot J}$ from the convected rate). Hence, in convected coordinates:

$$\overset{\circ}{\overline{\overline{\sigma}}} = \overset{\circ}{\sigma}{}^{IJ}\,\overline{G}_I\overline{G}_J = \overset{\circ}{\sigma}{}^I_J\,\overline{G}_I\overline{G}^J = \overset{\circ}{\sigma}_{IJ}\,\overline{G}^I\overline{G}^J = \overset{\circ}{\hat{\sigma}}_{IJ}\,\overline{i}_i\,\overline{i}_j \qquad (2.309)$$

$$\overset{\circ}{\sigma}{}^{IJ} = \dot{\sigma}^{IJ} + D^I_K\,\sigma^{KJ} + \sigma^{IK}D^J_K \qquad (2.310)$$

$$\overset{\circ}{\sigma}{}^I_{\cdot J} = \dot{\sigma}^{I\cdot}_{\cdot J} + D^I_K\sigma^K_J - \sigma^I_K\,D^K_J \qquad (2.311)$$

$$\overset{\circ}{\sigma}_{IJ} = \dot{\sigma}_{IJ} - D^K_I\,\sigma_{KJ} - \sigma_{IK}\,D^K_J \qquad (2.312)$$

$$\overset{\circ}{\hat{\sigma}}_{IJ} = \dot{\hat{\sigma}}_{IJ} - \hat{W}_{IK}\,\hat{\sigma}_{KJ} - \hat{W}_{JK}\,\hat{\sigma}_{IK} \qquad (2.313)$$

The co-rotational stress rate in Cartesian coordinates was first introduced by Zaremba [81], and later on by Jaumann [82]. Noll [83] and Thomas [84] rediscovered this result. The co-rotational frame is referred to as "kinematically preferred co-ordinate system" by Thomas [85] and the co-rotational stress rate is denoted as the "Jaumann stress rate" by Prager [86].

An alternative way to obtain the co-rotational rate is from the average of the convected rates of the mixed components, as shown by Masur [79,80]:

$$\overset{\circ}{\bar{\bar{\sigma}}} = \frac{1}{2}\left(\overset{\triangleright}{\bar{\bar{\sigma}}} + \overset{\triangleleft}{\bar{\bar{\sigma}}}\right) = \frac{1}{2}\left(\dot{\hat{\sigma}}_{IJ} - \hat{V}_{I,K}\hat{\sigma}_{KJ} + \hat{V}_{KJ}\hat{\sigma}_{IK} + \dot{\hat{\sigma}}_{IJ} + \hat{V}_{K,I}\hat{\sigma}_{KJ} - \hat{V}_{J,K}\hat{\sigma}_{IK}\right)\bar{\imath}_i\bar{\imath}_j \quad (2.314)$$

$$\overset{\circ}{\hat{\sigma}}_{IJ} = \dot{\hat{\sigma}}_{IJ} - \hat{W}_{IK}\hat{\sigma}_{KJ} - \hat{W}_{JK}\hat{\sigma}_{IK} = \dot{\hat{\sigma}}_{IJ} + \hat{\sigma}_{IK}\hat{W}_{KJ} - \hat{W}_{IK}\hat{\sigma}_{KJ} \quad (2.315)$$

2.6.3 Rates of a Second Order Tensor

Recapitulating, a second order tensor $\bar{\bar{\Omega}}$ having components:

$$\bar{\bar{\Omega}} = \hat{\Omega}_{IJ}\bar{\imath}_i\bar{\imath}_j = \Omega^{IJ}\bar{G}_I\bar{G}_J = \Omega^{I}_{\cdot J}\bar{G}_I\bar{G}^J = \Omega_{IJ}\bar{G}^I\bar{G}^J \quad (2.316)$$

has the following rates.

2.6.3.1 FIXED-OBSERVER RATE $\overset{\square}{\bar{\bar{\Omega}}}$

$$\overset{\square}{\hat{\Omega}}_{IJ} = \dot{\hat{\Omega}}_{IJ} \quad (2.317)$$

$$\overset{\square}{\Omega}{}^{IJ} = \dot{\Omega}^{IJ} + V^{I}{}_{,K}\Omega^{KJ} + \Omega^{IK}V^{J}{}_{,K} \quad (2.318)$$

$$\overset{\square}{\Omega}_{IJ} = \dot{\Omega}_{IJ} - V^{K}{}_{,I}\Omega_{KJ} - \Omega_{IK}V^{K}{}_{,J} \quad (2.319)$$

$$\overset{\square}{\Omega}{}^{I}{}_{\cdot J} = \dot{\Omega}^{I}{}_{\cdot J} + V^{I}{}_{,K}\Omega^{K}{}_{\cdot J} - \Omega^{I}{}_{\cdot K}V^{K}{}_{,J} \quad (2.320)$$

$$\overset{\square}{\Omega}{}_{J}{}^{\cdot I} = \dot{\Omega}_{J}{}^{\cdot I} - V^{K}{}_{,J}\Omega_{K}{}^{\cdot I} + \Omega_{J}{}^{\cdot K}V^{I}{}_{,K} \quad (2.321)$$

2.6.3.2 CO-ROTATIONAL RATE $\overset{\circ}{\bar{\bar{\Omega}}}$

$$\overset{\circ}{\hat{\Omega}}_{IJ} = \dot{\hat{\Omega}}_{IJ} - \hat{W}_{IK}\hat{\Omega}_{KJ} + \hat{\Omega}_{IK}\hat{W}_{KJ} \quad (2.322)$$

$$\overset{\circ}{\Omega}{}^{IJ} = \dot{\Omega}{}^{IJ} + D^{I}_{K}\,\Omega^{KJ} + \Omega^{IK}\,D^{J}_{K} \tag{2.323}$$

$$\overset{\circ}{\Omega}{}^{I}{}_{\cdot J} = \dot{\Omega}{}^{I}{}_{\cdot J} + D^{I}_{K}\,\Omega^{K}{}_{\cdot J} - \Omega^{I}{}_{\cdot K}\,D^{K}_{J} \tag{2.324}$$

$$\overset{\circ}{\Omega}{}_{J}{}^{\cdot I} = \dot{\Omega}{}_{J}{}^{\cdot I} - D^{K}_{J}\,\Omega_{K}{}^{\cdot I} + \Omega_{J}{}^{\cdot K}\,D^{I}_{K} \tag{2.325}$$

$$\overset{\circ}{\Omega}{}_{IJ} = \dot{\Omega}{}_{IJ} - D^{K}_{I}\,\Omega_{KJ} - \Omega_{IK}\,D^{K}_{J} \tag{2.326}$$

2.6.3.3 CONVECTED RATES $\overset{\nabla}{\Omega}, \overset{\Delta}{\Omega}, \overset{\triangleleft}{\Omega}, \overset{\triangleright}{\Omega}$

$$\overset{\nabla}{\Omega}{}^{IJ} = \dot{\Omega}{}^{IJ} \tag{2.327}$$

$$\overset{\nabla}{\hat{\Omega}}{}_{IJ} = \dot{\hat{\Omega}}{}_{IJ} - \hat{V}_{I,K}\,\hat{\Omega}_{KJ} - \hat{V}_{J,K}\,\hat{\Omega}_{IK} \tag{2.328}$$

$$\overset{\Delta}{\Omega}{}_{IJ} = \dot{\Omega}{}_{IJ} \tag{2.329}$$

$$\overset{\Delta}{\hat{\Omega}}{}_{IJ} = \dot{\hat{\Omega}}{}_{IJ} + \hat{V}_{K,I}\,\hat{\Omega}_{KJ} + \hat{V}_{K,J}\,\hat{\Omega}_{IK} \tag{2.330}$$

$$\overset{\triangleright}{\Omega}{}^{I}{}_{\cdot J} = \dot{\Omega}{}^{I}{}_{\cdot J} \tag{2.331}$$

$$\overset{\triangleright}{\hat{\Omega}}{}_{IJ} = \dot{\hat{\Omega}}{}_{IJ} - \hat{V}_{I,K}\,\hat{\Omega}_{KJ} + \hat{V}_{K,J}\,\hat{\Omega}_{IK} \tag{2.332}$$

$$\overset{\triangleleft}{\Omega}{}_{J}{}^{\cdot I} = \dot{\Omega}{}_{J}{}^{\cdot I} \tag{2.333}$$

$$\overset{\triangleleft}{\hat{\Omega}}{}_{IJ} = \dot{\hat{\Omega}}{}_{IJ} + \hat{V}_{K,I}\,\hat{\Omega}_{KJ} - \hat{V}_{J,K}\,\hat{\Omega}_{IK} \tag{2.334}$$

2.6.3.4 Relations between Rates of Second Order Tensors

The following relations between the various rates of a second order tensor $\bar{\bar{\Omega}}$ can be shown to hold:

$$\overset{\circ}{\bar{\bar{\Omega}}} = \overset{\square}{\bar{\bar{\Omega}}} - \bar{\bar{W}} \cdot \bar{\bar{\Omega}} + \bar{\bar{\Omega}} \cdot \bar{\bar{W}} \tag{2.335}$$

$$\overset{\triangle}{\bar{\bar{\Omega}}} = \overset{\square}{\bar{\bar{\Omega}}} + \bar{\bar{L}}^T \cdot \bar{\bar{\Omega}} + \bar{\bar{\Omega}} \cdot \bar{\bar{L}} \tag{2.336}$$

$$\overset{\triangledown}{\bar{\bar{\Omega}}} = \overset{\square}{\bar{\bar{\Omega}}} - \bar{\bar{L}} \cdot \bar{\bar{\Omega}} - \bar{\bar{\Omega}} \cdot \bar{\bar{L}}^T \tag{2.337}$$

$$\overset{\triangleright}{\bar{\bar{\Omega}}} = \overset{\square}{\bar{\bar{\Omega}}} - \bar{\bar{L}} \cdot \bar{\bar{\Omega}} + \bar{\bar{\Omega}} \cdot \bar{\bar{L}} \tag{2.338}$$

$$\overset{\triangleleft}{\bar{\bar{\Omega}}} = \overset{\square}{\bar{\bar{\Omega}}} + \bar{\bar{L}}^T \cdot \bar{\bar{\Omega}} - \bar{\bar{\Omega}} \cdot \bar{\bar{L}}^T \tag{2.339}$$

$$\overset{\triangle}{\bar{\bar{\Omega}}} = \overset{\circ}{\bar{\bar{\Omega}}} + \bar{\bar{D}} \cdot \bar{\bar{\Omega}} + \bar{\bar{\Omega}} \cdot \bar{\bar{D}} \tag{2.340}$$

$$\overset{\triangledown}{\bar{\bar{\Omega}}} = \overset{\circ}{\bar{\bar{\Omega}}} - \bar{\bar{D}} \cdot \bar{\bar{\Omega}} - \bar{\bar{\Omega}} \cdot \bar{\bar{D}} \tag{2.341}$$

$$\overset{\triangleright}{\bar{\bar{\Omega}}} = \overset{\circ}{\bar{\bar{\Omega}}} - \bar{\bar{D}} \cdot \bar{\bar{\Omega}} + \bar{\bar{\Omega}} \cdot \bar{\bar{D}} \tag{2.342}$$

$$\overset{\triangleleft}{\bar{\bar{\Omega}}} = \overset{\circ}{\bar{\bar{\Omega}}} + \bar{\bar{D}} \cdot \bar{\bar{\Omega}} - \bar{\bar{\Omega}} \cdot \bar{\bar{D}} \tag{2.343}$$

$$\overset{\circ}{\bar{\bar{\Omega}}} = \frac{1}{2}\left(\overset{\triangleright}{\bar{\bar{\Omega}}} + \overset{\triangleleft}{\bar{\bar{\Omega}}}\right) = \frac{1}{2}\left(\overset{\triangle}{\bar{\bar{\Omega}}} + \overset{\triangledown}{\bar{\bar{\Omega}}}\right) \tag{2.344}$$

Note: (1) The fixed-in-space observer rate, denoted by $(\overset{\square}{\ })$, does not satisfy condition 5. For example, the fixed observer rate of the Cauchy stress tensor does not vanish when the body performs a rigid body motion and the body remains unstressed.

(2) The convected rates identified by $(\overset{\triangledown}{\ })$ and $(\overset{\triangle}{\ })$ do not satisfy conditions 1 and 4.

(3) The convected rates identified by ($\triangleleft$) and ($\triangleright$) produce unsymmetric tensors even when the tensor being differentiated was originally symmetric.

(4) The co-rotational (Zaremba-Jaumann) rate satisfies all five conditions; Truesdell and Toupin [15, p. 242], Prager [86], and Guo Zhong-heng [76] expressed opinions in its favor. Lehmann [87] interpreted the co-rotational rate as covariant differentiation with respect to time, by introducing time as the fourth coordinate in an appropriate manner. Before Lehmann, Thomas [88, p. 83] had already introduced the name "covariant time derivative" for the co-rotational rate.

2.6.4 Co-Rotational Rate of the Kirchhoff Stress Tensor

The co-rotational rate $\overset{\circ}{\bar{\bar{\tau}}}$ of the Kirchhoff stress $\bar{\bar{\tau}}$ with components $\overset{\circ}{\tau}{}^{IJ}$ in the present vector bases, is

$$\overset{\circ}{\bar{\bar{\tau}}} = \overset{\circ}{\tau}{}^{IJ}\,\bar{G}_I\bar{G}_J = \overset{\circ}{\tau}{}^{I}_{J}\,\bar{G}_I\bar{G}^J = \overset{\circ}{\tau}_{IJ}\,\bar{G}^I\bar{G}^J = \overset{\circ}{\tau}_{ij}\,\bar{i}_i\bar{i}_j \tag{2.345}$$

Cartesian Components:

$$\overset{\circ}{\hat{\tau}}_{IJ} = \dot{\hat{\tau}}_{IJ} - \hat{W}_{IK}\,\hat{\tau}_{KJ} + \hat{\tau}_{IK}\,\hat{W}_{KJ} \tag{2.346}$$

Contravariant Components:

$$\overset{\circ}{\tau}{}^{IJ} = \dot{\tau}^{IJ} + D^I_K\,\tau^{KJ} + \tau^{IK}\,D^J_K \tag{2.347}$$

Mixed Components:

$$\overset{\circ}{\tau}{}^{I}_{J} = \dot{\tau}^{I}_{\cdot J} + D^I_K\,\tau^K_J - \tau^I_K\,D^K_J \tag{2.348}$$

Covariant Components:

$$\overset{\circ}{\tau}_{IJ} = \dot{\tau}_{IJ} - D^K_I\,\tau_{KJ} - \tau_{IK}\,D^K_J \tag{2.349}$$

2.6.4.1 Co-Rotational Rate of the Kirchhoff Stress Expressed in Terms of the Second Piola-Kirchhoff Stress and the Green Strain for a Convected Coordinate System

This relation is useful in an analysis formulated in terms of a reference configuration. The following expressions are used (see Eqs. 2.140, 2.175, 2.188, 2.266, and 2.270):

$$\dot{\tau}^{IJ} = \dot{S}^{ij} \qquad C^{i}_{j} = g^{ik} G_{KJ} = \delta^{i}_{j} + 2\gamma^{i}_{j}$$

$$\tau^{IJ} = S^{ij} = g^{kj} S^{i}_{k} \qquad \dot{\gamma}^{i}_{j} = g^{ik}\dot{\gamma}_{kj} = \frac{1}{2} g^{ik}\dot{G}_{KJ} = \frac{1}{2}\dot{C}^{i}_{j}$$

$$G_{IK} = C_{ik} = g_{ik} + 2\gamma_{ik} \qquad D_{IJ} = \dot{\gamma}_{ij} = \frac{1}{2}\dot{C}_{ij} \qquad (C^{-1})^{ik} = G^{IK}$$

From these equations, and Eq. 2.347, one obtains:

Contravariant Components:

$$\overset{\circ}{\tau}^{IJ} = \dot{\tau}^{IJ} + G^{IL} D_{LK} \tau^{KJ} + \tau^{IK} D_{KL} G^{LJ}$$

$$\overset{\circ}{\tau}^{IJ} = \dot{S}^{ij} + \dot{\gamma}_{lk}\left[G^{IL} S^{kj} + S^{ik} G^{LJ}\right]$$

$$\boxed{\overset{\circ}{\tau}^{IJ} = \dot{S}^{ij} + S^{km}\dot{\gamma}_{ml}\left[\delta^{i}_{k}(C^{-1})^{lj} + (C^{-1})^{il}\delta^{j}_{k}\right]} \qquad (2.350)$$

Mixed Components:

One can obtain these components from any of the following relations:

$$\overset{\circ}{\tau}^{I}_{J} = \overset{\circ}{\tau}^{IN} G_{NJ} \qquad \overset{\circ}{\tau}^{I}_{J} = \frac{1}{2}\left[G_{KJ}\overset{\circ}{\tau}^{IK} + G^{KI}\overset{\circ}{\tau}_{JK}\right]$$

$$\overset{\circ}{\tau}^{I}_{J} = \frac{1}{2}\left[\overset{\circ}{\tau}^{I}{}_{\cdot J} + G^{IK} G_{JL}\,\overset{\circ}{\tau}_{K}{}^{\cdot L}\right] \qquad (2.351)$$

Employing the first of these relations, one obtains:

$$\overset{\circ}{\tau}{}^{I}_{J} = \dot{S}^{in} G_{NJ} + S^{kn} \dot{\gamma}_{\ell k} [G^{IL} G_{NJ} + \delta^{i}_{n} \delta^{\ell}_{j}]$$

$$= \dot{S}^{i}_{m} g^{mn} G_{NJ} + S^{k}_{m} g^{mn} \dot{\gamma}^{m}_{\ell} g_{km} G^{IL} G_{NJ} + S^{ik} \dot{\gamma}_{\ell k} \delta^{\ell}_{j}$$

$$= \dot{S}^{i}_{m} (\delta^{m}_{j} + 2\gamma^{m}_{j}) + S^{k}_{m} \dot{\gamma}^{m}_{\ell} G^{LI} G_{KJ} + S^{i}_{m} g^{mk} \dot{\gamma}^{m}_{j} g_{mk}$$

$$= \dot{S}^{i}_{m} (\delta^{m}_{j} + 2\gamma^{m}_{j}) + S^{k}_{m} \dot{\gamma}^{m}_{\ell} G^{LI} G_{KJ} + S^{i}_{m} \dot{\gamma}^{m}_{j}$$

$$= \dot{S}^{i}_{m} (\delta^{m}_{j} + 2\gamma^{m}_{j}) + S^{k}_{m} \dot{\gamma}^{m}_{\ell} [\delta^{i}_{k} \delta^{\ell}_{j} + G^{LI} G_{KJ}]$$

$$= \dot{S}^{im} (g_{mj} + 2\gamma_{mj}) + S^{km} \dot{\gamma}_{m\ell} [\delta^{i}_{k} \delta^{\ell}_{j} + G^{LI} G_{KJ}]$$

$$\boxed{\overset{\circ}{\tau}{}^{I}_{J} = \dot{S}^{i}_{m} C^{m}_{j} + S^{k}_{m} \dot{\gamma}^{m}_{\ell} \, [\delta^{i}_{k} \delta^{\ell}_{j} + (C^{-1})^{\ell i} C_{kj}]} \tag{2.352}$$

$$\boxed{\overset{\circ}{\tau}{}^{I}_{J} = \dot{S}^{im} C_{mj} + S^{km} \dot{\gamma}_{m\ell} \, [\delta^{i}_{k} \delta^{\ell}_{j} + (C^{-1})^{\ell i} C_{kj}]} \tag{2.353}$$

2.7 Energy Equation

The internal energy integral U over the present volume V can be expressed as a function of the Cauchy stress $\bar{\bar{\sigma}}$ and the rate-of-deformation tensor $\bar{\bar{D}}$:

$$U = \int_V \int_t \bar{\bar{\sigma}} : \bar{\bar{D}} \, dt \, dV \tag{2.345}$$

One may write U in terms of the following components in the Cartesian and in the convected coordinate system:

$$U = \int_V \int_t \hat{\sigma}_{IJ} \hat{D}_{IJ} \, dt \, dV = \int_V \int_t \sigma^{IJ} D_{IJ} \, dt \, dV$$

$$= \int_V \int_t \sigma_{IJ} D^{IJ} \, dt \, dV = \int_V \int_t \sigma^{I}_{J} D^{J}_{I} \, dt \, dV \tag{2.355}$$

The energy integral U over the volume V_o in the reference configuration at $t = t_o$, can be easily obtained from Eqs. 2.223 and 2.355 as:

$$\mathcal{U} = \int_t \int_{V_o} \bar{\bar{\sigma}} : \bar{\bar{D}} \frac{\rho_o}{\rho} dV_o dt = \int_t \int_{V_o} \bar{\bar{\tau}} : \bar{\bar{D}} \, dV_o dt \tag{2.356}$$

where, as in Eqs. 2.218 and 2.219:

$$\rho_o = \frac{dm}{dV_o} \qquad\qquad \rho = \frac{dm}{dV}$$

Hence, the energy per unit mass $\bar{U}$ is:

$$\bar{\mathcal{U}} \equiv \frac{d\mathcal{U}}{dm} = \frac{d\mathcal{U}}{dV_o}\frac{dV_o}{dm} = \frac{1}{\rho_o(\bar{r},t_o)} \frac{d\mathcal{U}}{dV_o}$$

$$= \frac{1}{\rho_o(\bar{r},t_o)} \int_t \bar{\bar{\tau}} : \bar{\bar{D}} \, dt \tag{2.357}$$

$$\bar{\mathcal{U}} \equiv \frac{d\mathcal{U}}{dm} = \frac{d\mathcal{U}}{dV}\frac{dV}{dm} = \frac{1}{\rho(\bar{R},t)} \frac{d\mathcal{U}}{dV}$$

$$= \frac{1}{\rho(\bar{R},t)} \int_t \bar{\bar{\sigma}} : \bar{\bar{D}} \, dt \tag{2.358}$$

or

$$\boxed{\bar{\bar{\tau}} : \bar{\bar{D}} = \rho_o(\bar{r},t_o)\,\dot{\bar{\mathcal{U}}}} \tag{2.359}$$

$$\boxed{\bar{\bar{\sigma}} : \bar{\bar{D}} = \rho(\bar{R},t)\,\dot{\bar{\mathcal{U}}}} \tag{2.360}$$

These equations express the important fact (for constitutive equations based on thermodynamics principles) that the scalar product $\bar{\bar{\tau}}:\bar{\bar{D}}$ is simply related by a <u>constant</u> (ρ_o) to the power per unit mass $\dot{\bar{U}}$, while the scalar product $\bar{\bar{\sigma}}:\bar{\bar{D}}$ is related by a <u>variable</u> (ρ, which depends on the deformation history) to the power per unit mass $\dot{\bar{U}}$.

It can be shown that equivalent expressions for the internal energy U are:

$$\mathcal{U} = \int_t \int_V \bar{\bar{\sigma}} : \bar{\bar{D}} \, dV \, dt = \int_t \int_{V_0} \bar{\bar{\tau}} : \bar{\bar{D}} \, dV_0 \, dt = \int_t \int_{V_0} \bar{\bar{S}} : \dot{\bar{\bar{\gamma}}} \, dV_0 \, dt$$

$$= \int_t \int_{V_0} \frac{1}{2} \bar{\bar{S}} : \dot{\bar{\bar{C}}} \, dV_0 \, dt = \int_t \int_{V_0} (\bar{\bar{T}})^T : \dot{\bar{\bar{F}}} \, dV_0 \, dt = \int_t \int_{V_0} \bar{\bar{T}} \cdot\cdot \, \dot{\bar{\bar{F}}} \, dV_0 \, dt \qquad (2.361)$$

Therefore, $\bar{\bar{\sigma}}$ and $\bar{\bar{D}}$ are conjugate variables for the internal strain power per unit present volume V; $\bar{\bar{S}}$ and $\dot{\bar{\bar{\gamma}}}$, $\bar{\bar{S}}$ and $\dot{\bar{\bar{C}}}$, $\bar{\bar{T}}$ and $\dot{\bar{\bar{F}}}$, and $\bar{\bar{\tau}}$ and $\bar{\bar{D}}$ are conjugate variables for the internal strain power per unit reference volume V_o.

For the conjugate variables $\bar{\bar{\tau}}$ and $\bar{\bar{D}}$, the energy expression in terms of the components in the Cartesian and in the convected coordinate system in the present configuration read:

$$\mathcal{U} = \int_t \int_{V_0} \hat{\tau}_{IJ} \hat{D}_{IJ} \, dV_0 \, dt = \int_t \int_{V_0} \tau^{IJ} D_{IJ} \, dV_0 \, dt$$

$$= \int_t \int_{V_0} \tau_{IJ} D^{IJ} \, dV_0 \, dt = \int_t \int_{V_0} \tau^{I}_{J} D^{J}_{I} \, dV_0 \, dt \qquad (2.362)$$

For the conjugate variables $\bar{\bar{S}}$ and $\dot{\bar{\bar{\gamma}}} = 1/2 \, \dot{\bar{\bar{C}}}$, the energy expression in terms of the components in the Cartesian and in the convected coordinate system in the reference configuration read:

$$\mathcal{U} = \int_t \int_{V_0} \hat{S}_{ij} \dot{\hat{\gamma}}_{ij} \, dV_0 \, dt = \int_{V_0} \int_{\hat{\gamma}_{ij}} \hat{S}_{ij} \, d\hat{\gamma}_{ij} \, dV_0$$

$$= \int_t \int_{V_0} S^{ij} \dot{\gamma}_{ij} \, dV_0 \, dt = \int_{V_0} \int_{\gamma_{ij}} S^{ij} \, d\gamma_{ij} \, dV_0$$

$$= \int_t \int_{V_0} S^{i}_{j} \dot{\gamma}^{j}_{i} \, dV_0 \, dt = \int_{V_0} \int_{\gamma^{j}_{i}} S^{i}_{j} \, d\gamma^{j}_{i} \, dV_0 \qquad (2.363)$$

$$= \int_t \int_{V_0} S_{ij} \dot{\gamma}^{ij} \, dV_0 \, dt = \int_{V_0} \int_{\gamma^{ij}} S_{ij} \, d\gamma^{ij} \, dV_0$$

For the conjugate variables $\bar{\bar{T}}$ and $\dot{\bar{\bar{F}}}$ the energy expression in terms of the components in the Cartesian and in the undeformed convected coordinate system read:

$$\mathcal{U} = \int_t \int_{V_0} \hat{T}_{iJ} \dot{\hat{F}}_{Ji} \, dV_0 dt = \int_{V_0} \int_{\hat{F}_{Ji}} \hat{T}_{iJ} \, d\hat{F}_{Ji} \, dV_0$$

$$= \int_t \int_{V_0} T_{ij} \dot{F}^{ji} \, dV_0 dt = \int_{V_0} \int_{F^{ji}} T_{ij} \, dF^{ji} \, dV_0 \tag{2.364}$$

$$= \int_t \int_{V_0} T^{ij} \dot{F}_{ji} \, dV_0 dt = \int_{V_0} \int_{F_{ji}} T^{ij} \, dF_{ji} \, dV_0$$

$$= \int_t \int_{V_0} T^{i}_{\cdot j} \dot{F}^{j}_{\cdot i} \, dV_0 dt = \int_t \int_{V_0} T_{i}^{\cdot j} \dot{F}_{j}^{\cdot i} \, dV_0 dt$$

Observe that since $D_{IJ} = \dot{\gamma}_{ij} = \dot{e}_{IJ}$, equivalent expressions are:

$$\mathcal{U} = \int_t \int_V \sigma^{IJ} \dot{\gamma}_{ij} \, dV dt = \int_V \int_{\gamma_{ij}} \sigma^{IJ} d\gamma_{ij} \, dV$$

$$= \int_t \int_V \sigma^{IJ} \dot{e}_{IJ} \, dV dt = \int_V \int_{e_{IJ}} \sigma^{IJ} de_{IJ} \, dV \tag{2.365}$$

However, note that $\bar{\bar{\sigma}}$ and $\dot{\bar{\bar{\gamma}}}$, and $\bar{\bar{\sigma}}$ and $\dot{\bar{\bar{e}}}$ are not conjugate variables, since, for example:

$$\mathcal{U} \neq \int_t \int_V \sigma^{I}_{J} \dot{\gamma}^{j}_{i} \, dV dt \qquad \mathcal{U} \neq \int_t \int_V \sigma^{I}_{J} \dot{e}^{J}_{I} \, dV dt$$

$$\mathcal{U} \neq \int_t \int_V \hat{\sigma}_{IJ} \dot{\hat{\gamma}}_{ij} \, dV dt \qquad \mathcal{U} \neq \int_t \int_V \hat{\sigma}_{IJ} \dot{\hat{e}}_{IJ} \, dV dt \tag{2.366}$$

This seemingly simple distinction has been the cause of confusion by many authors.

Observe, that since

$$\tau^{IJ} = S^{ij} = T^{iJ}$$

and

$$D_{IJ} = \dot{\gamma}_{ij} = \dot{e}_{IJ}$$

then, equivalent expressions are

$$\begin{aligned}
U &= \int_t \int_{V_o} \tau^{IJ} \dot{\gamma}_{ij} \, dV_o \, dt = \int_{V_o} \int_{\gamma_{ij}} \tau^{IJ} \, d\gamma_{ij} \, dV_o \\
&= \int_t \int_{V_o} \tau^{IJ} \dot{e}_{IJ} \, dV_o \, dt = \int_{V_o} \int_{e_{IJ}} \tau^{IJ} \, de_{IJ} \, dV_o \\
&= \int_t \int_{V_o} S^{ij} D_{IJ} \, dV_o \, dt = \int_t \int_{V_o} T^{iJ} D_{IJ} \, dV_o \, dt \\
&= \int_t \int_{V_o} S^{ij} \dot{e}_{IJ} \, dV_o \, dt = \int_{V_o} \int_{e_{IJ}} S^{ij} \, de_{IJ} \, dV_o \\
&= \int_t \int_{V_o} T^{iJ} \dot{e}_{IJ} \, dV_o \, dt = \int_{V_o} \int_{e_{IJ}} T^{iJ} \, de_{IJ} \, dV_o \\
&= \int_t \int_{V_o} T^{iJ} \dot{\gamma}_{ij} \, dV_o \, dt = \int_{V_o} \int_{\gamma_{ij}} T^{iJ} \, d\gamma_{ij} \, dV_o
\end{aligned} \tag{2.367}$$

However, here again, $\bar{\bar{\tau}}$ and $\dot{\bar{\bar{\gamma}}}$, $\bar{\bar{\tau}}$ and $\dot{\bar{\bar{e}}}$, $\bar{\bar{S}}$ and $\bar{\bar{D}}$, $\bar{\bar{T}}$ and $\bar{\bar{D}}$, $\bar{\bar{S}}$ and $\dot{\bar{\bar{e}}}$, $\bar{\bar{T}}$ and $\dot{\bar{\bar{e}}}$ and $\bar{\bar{T}}$ and $\dot{\bar{\bar{\gamma}}}$ are <u>not</u> conjugate variables.

2.8 Specialization: Homogeneous Uniaxial Irrotational Deformation

The uniaxial tensile test is a common and simple way to characterize the stress-strain relation for a given material. Since the tensor components used in the constitutive relation will have to be related to this uniaxial test, and also to gain a physical understanding of the quantities involved in the analysis, it is both useful and instructive to express the tensor quantities previously discussed in terms of the uniaxial tension test variables. A homogeneous, uniaxial, irrotational deformation will be considered. Then, it is evident that the curvilinear convected coordinate ξ^1 is equal to the Lagrangian Cartesian coordinate x_1 for a bar with no initial curvature:

$$\xi^1 = x_1 \tag{2.368}$$

Observe that ξ^1 and x_1 are not functions of time (they remain the same for a given material particle).

If the original length of the bar is ℓ_o, and its present length is ℓ, then the Eulerian Cartesian coordinate X_1 is

$$X_1(x_1,t) = \frac{\ell(t)}{\ell_o} x_1 \tag{2.369}$$

If the unit vector directed along the axis of deformation is $\bar{i}_1$, then

$$\bar{g}_1 = \bar{g}^1 = \bar{i}_1 \tag{2.370}$$

and

$$g_{11} = g^{11} = 1 \tag{2.371}$$

The deformed base vectors are:

$$\bar{G}_1 = \frac{\ell}{\ell_o}\bar{i}_1 \qquad \bar{G}^1 = \frac{\ell_o}{\ell}\bar{i}_1 \tag{2.372}$$

and the metric of the deformed configuration:

$$G_{11} = \frac{\ell^2}{\ell_o^2} \qquad G^{11} = \frac{\ell_o^2}{\ell^2} \tag{2.373}$$

so that the unit second order tensor is:

$$\begin{aligned} \bar{\bar{I}} &= 1\,\bar{i}_1\bar{i}_1 = 1\,\bar{g}_1\bar{g}_1 = 1\,\bar{g}^1\bar{g}^1 = 1\,\bar{g}_1\bar{g}^1 = 1\,\bar{g}^1\bar{g}_1 \\ &= \frac{\ell^2}{\ell_o^2}\bar{G}^1\bar{G}^1 = \frac{\ell_o^2}{\ell^2}\bar{G}_1\bar{G}_1 = 1\,\bar{G}_1\bar{G}^1 = 1\,\bar{G}^1\bar{G}_1 \end{aligned} \tag{2.374}$$

The position vectors are:

$$\bar{r} = \hat{r}_1\bar{i}_1 = x_1\bar{i}_1 = r^1\bar{g}_1 = r_1\bar{g}^1 \qquad \hat{r}_1 = r^1 = r_1 = x_1$$

$$\overline{R} = \hat{R}_1 \bar{i}_1 = X_1 \bar{i}_1 = R^1 \overline{G}_1 = R_1 \overline{G}^1 \tag{2.375}$$

$$\hat{R} = X_1 = \frac{l}{l_0} x_1 \qquad R^1 = x_1 \qquad R_1 = \frac{l^2}{l_0^2} x_1$$

The displacement vector is:

$$\bar{u} = \overline{R} - \bar{r} = \hat{u}_1 \bar{i}_1 = u^1 \bar{g}_1 = u_1 \bar{g}^1 = U^1 \overline{G}_1 = U_1 \overline{G}^1$$

$$\hat{u}_1 = \hat{R}_1 - \hat{r}_1 = X_1 - x_1 = \left(\frac{l}{l_0} - 1\right) x_1$$

$$u^1 = u_1 = \hat{u}_1 = \left(\frac{l}{l_0} - 1\right) x_1$$

$$\bar{u} = R^1 \overline{G}_1 - r^1 \bar{g}_1 = x_1 \overline{G}_1 - x_1 \bar{i}_1 = x_1 \overline{G}_1 - \frac{l_0}{l} x_1 \overline{G}_1 = \left(1 - \frac{l_0}{l}\right) x_1 \overline{G}_1 \tag{2.376}$$

$$U^1 = \left(1 - \frac{l_0}{l}\right) x_1 \qquad U_1 = \frac{l^2}{l_0^2}\left(1 - \frac{l_0^2}{l^2}\right) x_1$$

The velocity vector is:

$$\overline{V} = \left.\frac{\partial \bar{u}}{\partial t}\right|_{\xi^1 = x_1 = \text{CONST.}} = \hat{v}_1 \bar{i}_1 = v^1 \bar{g}_1 = v_1 \bar{g}^1 = V^1 \overline{G}_1 = V_1 \overline{G}^1$$

$$\hat{v}_1 = \left.\frac{\partial X_1}{\partial t}\right|_{x_1 = \text{CONST.}} = \frac{\dot{l}}{l_0} x_1$$

$$v^1 = v_1 = \hat{v}_1 = \frac{\dot{l}}{l_0} x_1$$

$$\overline{V} = \frac{\dot{l}}{l_0} x_1 \bar{i}_1 = V^1 \overline{G}_1 = V_1 \overline{G}^1 = V^1 \frac{l}{l_0} \bar{i}_1 = V_1 \frac{l_0}{l} \bar{i}_1 \tag{2.377}$$

$$V^1 = \frac{\dot{l}}{l} x_1 \qquad V_1 = \frac{l^2}{l_0^2} \frac{\dot{l}}{l} x_1$$

The time rates of the deformed base vectors are:

$$\frac{d\bar{G}_1}{dt} = \frac{\partial V^1}{\partial x_1}\bar{G}_1 = \frac{\dot{l}}{l}\bar{G}_1 = \frac{\dot{l}}{l_o}\bar{i}_1 \tag{2.378}$$

$$\frac{d\bar{G}^1}{dt} = -\frac{\partial V^1}{\partial x_1}\bar{G}^1 = -\frac{\dot{l}}{l}\bar{G}^1 = -\frac{\dot{l}}{l}\frac{l_o}{l}\bar{i}_1 \tag{2.379}$$

2.8.1 Deformation and Strain Tensors

The components of the deformation gradient tensor $\bar{\bar{F}}$ are:

Cartesian Component:

$$\hat{F}_{11} = \frac{\partial X_1}{\partial x_1} = \frac{l}{l_o} \tag{2.380}$$

Double Tensor Components:

$$\begin{aligned} F^{I}{}_{\cdot j} &= \delta^{i}_{j} & \qquad F^{1}{}_{\cdot 1} &= 1 \\ F^{Ij} &= F^{I}{}_{\cdot k}\, g^{kj} & F^{11} &= 1 \\ F_{Ij} &= F^{K}{}_{\cdot j}\, G_{KJ} & F_{11} &= \frac{l^2}{l_o^2} \\ F_{I}{}^{\cdot j} &= F^{K}{}_{\cdot l}\, G_{KI}\, g^{lj} & F_{1}{}^{\cdot 1} &= \frac{l^2}{l_o^2} \end{aligned} \tag{2.381}$$

Components in the Convected Coordinate System in the Reference Configuration are:

$$F^{i}{}_{\cdot k} = \delta^{i}_{k} + u^{i}{}_{,k}$$

$$F^{1}{}_{\cdot 1} = 1 + \frac{\partial u^1}{\partial x_1} = 1 + \left(\frac{l}{l_o} - 1\right)$$

$$F^{1}{}_{\cdot 1} = F^{11} = F_{11} = F_{1}{}^{\cdot 1} = \frac{l}{l_o} \tag{2.382}$$

The components of the spatial deformation gradient tensor $\bar{\bar{F}}^{-1}$ are:

Cartesian Component:

$$\left(\hat{F}^{-1}\right)_{11} = \frac{\partial x_1}{\partial X_1} = \frac{l_0}{l} \tag{2.383}$$

Double Tensor Components:

$$\left(F^{-1}\right)^{i\,\cdot}_{\cdot\,K} = \delta^{i}_{k} \qquad \left(F^{-1}\right)^{1\,\cdot}_{\cdot\,1} = 1$$

$$\left(F^{-1}\right)^{iL} = \left(F^{-1}\right)^{i\,\cdot}_{\cdot\,K} G^{KL} \qquad \left(F^{-1}\right)^{11} = \frac{l_0^2}{l^2}$$

$$\left(F^{-1}\right)_{j\,\cdot}^{\,\cdot\,L} = \left(F^{-1}\right)^{iL} g_{ij} \qquad \left(F^{-1}\right)_{1\,\cdot}^{\,\cdot\,1} = \frac{l_0^2}{l^2}$$

$$\left(F^{-1}\right)_{jK} = \left(F^{-1}\right)^{i\,\cdot}_{\cdot\,K} g_{ij} \qquad \left(F^{-1}\right)_{11} = 1 \tag{2.384}$$

Components in the Convected Coordinate System in the Present Configuration:

$$\left(F^{-1}\right)^{I\,\cdot}_{\cdot\,K} = \delta^{I}_{K} - U^{I}_{\;,K} \qquad \left(F^{-1}\right)^{1\,\cdot}_{\cdot\,1} = 1 - \frac{\partial U^1}{\partial X_1} = 1 - \left(\frac{l - l_0}{l}\right) = \frac{l_0}{l}$$

$$\left(F^{-1}\right)^{IL} = \left(F^{-1}\right)^{I\,\cdot}_{\cdot\,K} G^{KL} \qquad \left(F^{-1}\right)^{11} = \frac{l_0^2}{l^2}\,\frac{l_0}{l} = \frac{l_0^3}{l^3}$$

$$\left(F^{-1}\right)_{JK} = \left(F^{-1}\right)^{I\,\cdot}_{\cdot\,K} G_{IJ} \qquad \left(F^{-1}\right)_{11} = \frac{l^2}{l_0^2}\,\frac{l_0}{l} = \frac{l}{l_0}$$

$$\left(F^{-1}\right)_{J\,\cdot}^{\,\cdot\,L} = \left(F^{-1}\right)_{JK} G^{KL} \qquad \left(F^{-1}\right)_{1\,\cdot}^{\,\cdot\,1} = \frac{l_0^2}{l^2}\,\frac{l}{l_0} = \frac{l_0}{l} \tag{2.385}$$

Since an irrotational deformation is being considered, then the orthogonal rotation tensor is the unit tensor:

$$\bar{\bar{R}} = \bar{\bar{1}} \tag{2.386}$$

And for this special case, the right and left stretch tensors $\bar{\bar{U}}$ and $\bar{\bar{V}}$ become both equal to the deformation gradient tensor $\bar{\bar{F}}$:

$$\bar{\bar{U}} = \bar{\bar{V}} = \bar{\bar{F}} \tag{2.387}$$

Components of the right stretch tensor in the Cartesian system and in the reference configuration of the convected coordinate system are:

$$\hat{U}_{11} = U^{11} = U^1_1 = U_{11} = \frac{l}{l_o} \tag{2.388}$$

Components of the left stretch tensor in the Cartesian system and in the present configuration of the convected coordinate system are:

$$\hat{V}_{11} = V^1_1 = \frac{l}{l_o} \qquad V^{11} = \frac{l_o}{l} \qquad V_{11} = \frac{l^3}{l_o^3} \tag{2.389}$$

Observe that the value of the stretch tensors is equal to unity for no deformation, and the possible range is

$$0 < \hat{U}_{11} = U^1_1 = \hat{V}_{11} = V^1_1 < +\infty \tag{2.390}$$

The right Cauchy-Green deformation tensor $\bar{\bar{C}} = \bar{\bar{U}}^2$ has the following components in the Cartesian system and in the convected coordinate system in the reference configuration:

$$\hat{C}_{11} = C^1_1 = C^{11} = C_{11} = G_{11} = \frac{l^2}{l_o^2} \tag{2.391}$$

The left Cauchy-Green deformation tensor $\bar{\bar{B}} = \bar{\bar{V}}^2$ has the following components in the Cartesian system and in the convected coordinate system in the present configuration:

$$\hat{B}_{11} = B^1_1 = \frac{l^2}{l_o^2} \qquad B^{11} = 1 \qquad B_{11} = \frac{l^4}{l_o^4} \tag{2.392}$$

Observe that the value of the deformation tensors is equal to unity for no deformation and that the possible range of values is:

$$0 < \hat{C}_{11} = C^1_1 = \hat{B}_{11} = B^1_1 < +\infty \tag{2.393}$$

The Green (Lagrangian) strain tensor $\bar{\bar{\gamma}}$ is defined as

$$\bar{\bar{\gamma}} = \frac{1}{2}\left(\bar{\bar{C}} - \bar{\bar{1}}\right) \tag{2.394}$$

Therefore, it has the following components in the Cartesian and in the convected coordinate system in the reference configuration:

$$\gamma_u \equiv \hat{\gamma}_{11} = \gamma_1^1 = \gamma^{11} = \gamma_{11} = \frac{1}{2}\left(\frac{l^2}{l_0^2} - 1\right) \tag{2.395}$$

The value of this strain tensor reduces to zero for no deformation, and the possible range is:

$$-\frac{1}{2} < \hat{\gamma}_{11} = \gamma_1^1 < +\infty \tag{2.396}$$

The Almansi (Eulerian) strain tensor $\bar{\bar{e}}$ is defined as

$$\bar{\bar{e}} = \frac{1}{2}\left(\bar{\bar{1}} - \bar{\bar{B}}^{-1}\right) \tag{2.397}$$

Therefore, it has the following components in the Cartesian and in the convected coordinate system in the present configuration:

$$\begin{aligned} \hat{e}_{11} &= e_1^1 = \frac{1}{2}\left(1 - \frac{l_0^2}{l^2}\right) \\ e_{11} &= \frac{1}{2}\left(\frac{l^2}{l_0^2} - 1\right) = \gamma_{11} \\ e^{11} &= \frac{1}{2}\,\frac{l_0^2}{l^2}\left(1 - \frac{l_0^2}{l^2}\right) \end{aligned} \tag{2.398}$$

The value of this strain tensor also reduces to zero for no deformation, and it has a possible range:

$$-\infty < \hat{e}_{11} = e_1^1 < +\frac{1}{2} \tag{2.399}$$

The elongation strain tensor $\bar{\bar{E}}$ is defined as

$$\bar{\bar{E}} = \bar{\bar{U}} - \bar{\bar{1}} \tag{2.400}$$

Therefore, it has the following components in the Cartesian and in the convected coordinate system in the reference configuration:

$$E_u \equiv \hat{\tilde{E}}_{11} = \tilde{E}^1_1 = \tilde{E}^{11} = \tilde{E}_{11} = \frac{l}{l_o} - 1 \tag{2.401}$$

Observe that this uniaxial component is exactly equal to the so-called "engineering strain" by the engineering literature that is measured in uniaxial tensile tests. This strain tensor also reduces to zero for no deformation and it has the following possible range of values:

$$-1 < E_u < +\infty \tag{2.402}$$

The elongation strain tensor $\bar{\bar{E}}$ is defined as:

$$\bar{\bar{E}} = \bar{\bar{1}} - \bar{\bar{V}}^{-1} \tag{2.403}$$

Therefore, it has the following components in the Cartesian and in the convected coordinate system in the present configuration:

$$\hat{E}_{11} = E^1_1 = 1 - \frac{l_o}{l}$$

$$E^{11} = \frac{l_o^2}{l^2}\left(1 - \frac{l_o}{l}\right) \qquad E_{11} = \frac{l^2}{l_o^2}\left(1 - \frac{l_o}{l}\right) \tag{2.404}$$

This strain tensor also reduces to zero for no deformation and it has the following possible range of values:

$$-\infty < \hat{E}_{11} = E^1_1 < + \frac{1}{2} \tag{2.405}$$

The logarithmic strain tensor $\bar{\bar{H}}$ is defined as:

$$\bar{\bar{\tilde{H}}} = \ln \bar{\bar{U}} \tag{2.406}$$

Therefore, it has the following components in the Cartesian and in the convected coordinate system in the reference configuration:

$$\hat{\tilde{H}}_{11} = \tilde{H}^{1}_{1} = \tilde{H}^{11} = \tilde{H}_{11} = \ln\left(\frac{l}{l_o}\right) \tag{2.407}$$

The logarithmic strain tensor $\bar{\bar{H}}$ is defined as:

$$\bar{\bar{H}} = \ln \bar{\bar{V}} \tag{2.408}$$

Therefore, it has the following components in the Cartesian and in the convected coordinate system in the present configuration:

$$\hat{H}_{11} = H^{1}_{1} = \ln\left(\frac{l}{l_o}\right)$$

$$H^{11} = \frac{l_o^2}{l^2} \ln\left(\frac{l}{l_o}\right) \qquad H_{11} = \frac{l^2}{l_o^2} \ln\left(\frac{l}{l_o}\right) \tag{2.409}$$

These strain tensors also reduce t zero for no deformation and they have the following possible range of values:

$$\varepsilon^*_u = \hat{\tilde{H}}_{11} = \tilde{H}^{1}_{1} = \hat{H}_{11} = H^{1}_{1}$$

$$\varepsilon^*_u (l = l_o) = 0 \tag{2.410}$$

$$-\infty < \varepsilon^*_u < +\infty$$

Observe that this strain tensor, unlike the other strain tensors, has a symmetric range in tension ($\varepsilon^*_u > 0$) and compression ($\varepsilon^*_u < 0$). Also, this strain tensor is called the "natural strain" or "true strain" in uniaxial tension tests by the engineering literature.

2.8.2 Deformation Rate Tensors

The rate-of-deformation tensor $\bar{\bar{D}}$ has Cartesian components

$$\hat{D}_{11} = \frac{\partial \hat{v}_1}{\partial X_1} = \frac{\partial\left(\frac{\dot{l}}{l_o} x_1\right)}{\partial x_1} \frac{\partial x_1}{\partial X_1} = \frac{\dot{l}}{l_o}\frac{l_o}{l} = \frac{\dot{l}}{l} \tag{2.411}$$

and components in the convected coordinate system in the present configuration:

$$D_{11} = \frac{1}{2}\frac{d}{dt}\left(\frac{\ell^2}{\ell_0^2}\right) = \frac{\ell^2}{\ell_0^2}\frac{\dot{\ell}}{\ell}$$

$$D_1^1 = \frac{\dot{\ell}}{\ell}$$

$$D^{11} = \frac{\ell_0^2}{\ell^2}\frac{\dot{\ell}}{\ell} \qquad (2.412)$$

Observe that the material rate of the logarithmic strain component ε_u^* is equal to the mixed components of the rate-of-deformation tensor

$$D_u \equiv \dot{\varepsilon}_u^* \equiv \frac{d}{dt}\left(\ln\frac{\ell}{\ell_0}\right) = \frac{\dot{\ell}}{\ell} = D_1^1 = \hat{D}_{11} \qquad (2.413)$$

The material rate of the Green strain tensor has the following components in the Cartesian and in the convected coordinate system in the reference configuration:

$$\dot{\gamma}_u \equiv \dot{\hat{\gamma}}_{11} = \dot{\gamma}_1^1 = \dot{\gamma}_{11} = \dot{\gamma}^{11} = \frac{\ell^2}{\ell_0^2}\frac{\dot{\ell}}{\ell} \qquad (2.414)$$

The material rate of the Almansi strain tensor components in Cartesian and in the convected coordinate system in the present configuration are:

$$\dot{\hat{e}}_{11} = \dot{e}^{1}{}_{\cdot 1} = \dot{e}_{1}{}^{\cdot 1} = \frac{\ell_0^2}{\ell^2}\frac{\dot{\ell}}{\ell}$$

$$\dot{e}_{11} = \frac{\ell^2}{\ell_0^2}\frac{\dot{\ell}}{\ell} \qquad \dot{e}^{11} = \frac{\ell_0^2}{\ell^2}\left(-1+2\frac{\ell_0^2}{\ell^2}\right)\frac{\dot{\ell}}{\ell} \qquad (2.415)$$

Observe that these convected rates are not components of one and the same tensor. However, the fixed-observer rate of the Almansi strain tensor components are components of one and the same tensor. For example, the components of the fixed-observer rate of the Almansi strain tensor in the deformed coordinate system are:

$$\overset{\square}{e}_{11} = \frac{\dot{\ell}}{\ell} \qquad \overset{\square}{e}{}_1^1 = \frac{\ell_0^2}{\ell^2}\frac{\dot{\ell}}{\ell} \qquad \overset{\square}{e}{}^{11} = \frac{\ell_0^4}{\ell^4}\frac{\dot{\ell}}{\ell} \qquad (2.416)$$

Relationships between the components of the rate-of-deformation tensor and the material rate of the Green strain tensor can be easily obtained for the uniaxial case; for example,

$$\dot{\gamma}_{11} = D_{11} \qquad \dot{\gamma}^1_1 = \frac{\ell^2}{\ell_o^2} D^1_1 = (1+2\gamma^1_1) D^1_1$$

$$D^1_1 = \frac{\dot{\gamma}^1_1}{(1+2\gamma^1_1)} \tag{2.417}$$

2.8.3 Stress Tensors

The unit normal vectors to the deformed and undeformed areas are one and the same unit vector directed along the bar axis, since the deformation is uniaxial and irrotational. Therefore,

$$\bar{N} = \bar{n} = \bar{\imath}_1 = \bar{g}_1 = \bar{g}^1.$$

$$\hat{N}_1 = 1 \qquad N^1 = \frac{\ell_o}{\ell} \qquad N_1 = \frac{\ell}{\ell_o} \tag{2.418}$$

$$\hat{n}_1 = n_1 = n^1 = 1$$

The force transmitted across the cross-sectional area of the bar is $d\bar{P}$

$$d\bar{P} = d\hat{P}_1 \bar{\imath}_1 = dP^1 \bar{G}_1 = dP_1 \bar{G}^1$$

$$d\hat{P}_1 = dP$$

$$dP^1 = \frac{\ell_o}{\ell} dP \qquad dP_1 = \frac{\ell}{\ell_o} dP \tag{2.419}$$

The fictitious force $d\tilde{\bar{P}} = (\bar{\bar{F}})^{-1} \cdot d\bar{P}$ has components:

$$d\hat{\tilde{P}}_1 = d\tilde{P}^1 = d\tilde{P}_1 = \frac{\ell_o}{\ell} dP \tag{2.420}$$

Also, the corresponding traction vector components are:

$$\hat{T}_1 = \frac{P}{A} \qquad T^1 = \frac{P}{A}\frac{\ell_o}{\ell} \qquad T_1 = \frac{P}{A}\frac{\ell}{\ell_o}$$

$$\hat{t}_1 = \frac{P}{A_o} \qquad t^1 = \frac{l_o}{l}\frac{P}{A_o} \qquad t_1 = \frac{l}{l_o}\frac{P}{A_o}$$

$$\hat{\tilde{t}}_1 = \tilde{t}^1 = \tilde{t}_1 = \frac{l_o}{l}\frac{P}{A_o} \tag{2.421}$$

The Cauchy stress tensor $\bar{\bar{\sigma}}$ is defined as:

$$\bar{T} = \bar{N} \cdot \bar{\bar{\sigma}} \tag{2.422}$$

Therefore, its Cartesian components are:

$$\frac{P}{A}\bar{i}_1 = \bar{i}_1 \cdot (\hat{\sigma}_{11}\bar{i}_1\bar{i}_1)$$

$$\hat{\sigma}_{11} = \frac{P}{A} \tag{2.423}$$

which can also be expressed in terms of the ref^rence area by the law of mass conservation:

$$\rho_o V_o = \rho V \qquad \rho_o A_o l_o = \rho A l$$

$$\frac{1}{A} = \frac{1}{A_o}\frac{l}{l_o}\frac{\rho}{\rho_o} \tag{2.424}$$

Hence,*

$$\boxed{\sigma_T \equiv \hat{\sigma}_{11} = \frac{P}{A} = \frac{\rho}{\rho_o}\frac{P}{A_o}\frac{l}{l_o}} \tag{2.425}$$

The components of the Cauchy stress tensor in the convected coordinate system in the present configuration are obtained as:

---

* The components $\hat{\sigma}_{11} = \sigma_1^1 = \frac{P}{A}$ are called "true stress" by the engineering literature.

$$\frac{P}{A}\frac{l_o}{l}\bar{G}_1 = \frac{l_o}{l}\bar{G}_1\cdot(\sigma_1^1\,\bar{G}^1\bar{G}_1) \tag{2.426}$$

Therefore,*

$$\boxed{\sigma_1^1 = \frac{P}{A} = \frac{\rho}{\rho_o}\frac{P}{A_o}\frac{l}{l_o}}$$

$$\boxed{\sigma^{11} = \frac{l_o^2}{l^2}\frac{P}{A} = \frac{\rho}{\rho_o}\frac{P}{A_o}\frac{l_o}{l}}$$

$$\boxed{\sigma_{11} = \frac{l^2}{l_o^2}\frac{P}{A} = \frac{\rho}{\rho_o}\frac{P}{A_o}\frac{l^3}{l_o^3}} \tag{2.427}$$

The Kirchhoff stress tensor is defined as

$$\bar{\bar{\tau}} = \frac{\rho_o}{\rho}\bar{\bar{\sigma}} \tag{2.428}$$

Therefore, it has the following components in the Cartesian and in the convected coordinate system in the present configuration:

$$\boxed{\hat{\tau}_{11} = \tau_1^1 = \frac{\rho_o}{\rho}\frac{P}{A} = \frac{P}{A_o}\frac{l}{l_o}} \tag{2.429}$$

$$\boxed{\tau^{11} = \frac{\rho_o}{\rho}\frac{P}{A}\frac{l_o^2}{l^2} = \frac{P}{A_o}\frac{l_o}{l}} \tag{2.430}$$

$$\boxed{\tau_{11} = \frac{\rho_o}{\rho}\frac{P}{A}\frac{l^2}{l_o^2} = \frac{P}{A_o}\frac{l^3}{l_o^3}} \tag{2.431}$$

Observe that the uniaxial component

$$\tau_u \equiv \tau_1^1 = \hat{\tau}_{11} = \frac{P}{A_o}\frac{l}{l_o} \tag{2.432}$$

---

*See the footnote on the previous page.

is the stress actually computed in most uniaxial tension tests and is also inaccurately labeled as "true stress", since it is usually assumed to be equal to the "true stress" because $\rho \approx \rho_o$ is satisfied almost identically for most metals in the plastic region.

The second Piola-Kirchhoff stress tensor is defined as

$$\bar{\tilde{t}} = \bar{n} \cdot \bar{\bar{S}} \tag{2.433}$$

Therefore, its Cartesian components are:

$$\frac{P}{A_o} \frac{l_o}{l} \bar{i}_1 = \bar{i}_1 \cdot (\hat{S}_{11} \bar{i}_1 \bar{i}_1)$$

$$\boxed{\hat{S}_{11} = \frac{P}{A_o} \frac{l_o}{l} = \frac{\rho_o}{\rho} \frac{P}{A} \frac{l_o^2}{l^2}} \tag{2.434}$$

The components in the convected coordinate system in the reference configuration are:

$$\frac{P}{A_o} \frac{l_o}{l} \bar{g}_1 = \bar{g}_1 \cdot (S_1^1 \bar{g}^1 \bar{g}_1)$$

$$\boxed{S_1^1 = S^{11} = S_{11} = \frac{P}{A_o} \frac{l_o}{l} = \frac{\rho_o}{\rho} \frac{P}{A} \frac{l_o^2}{l^2}} \tag{2.435}$$

Observe that the relation $\tau^{11} = S^{11}$ between the contravariant components of the Kirchhoff and the Second-Piola Kirchhoff stress tensors is satisfied.

The first Piola-Kirchhoff stress tensor $\bar{\bar{T}}$ is defined as:

$$\bar{t} = \bar{n} \cdot \bar{\bar{\bar{T}}} \tag{2.436}$$

Therefore, its Cartesian components are:

$$\frac{P}{A_o} \bar{i}_1 = \bar{i}_1 \cdot (\hat{T}_{11} \bar{i}_1 \bar{i}_1)$$

$$\boxed{\hat{T}_{11} = \frac{P}{A_o} = \frac{\rho_o}{\rho} \frac{P}{A} \frac{l_o}{l}} \tag{2.437}$$

The components of the double tensor $\bar{\bar{T}}$ referred to the convected coordinate system in the reference and present configuration are T^{iJ}, T_{iJ}, $T^{i\cdot}_{\cdot J}$ and $T_{i}^{\cdot J}$ and are obtained as

$$\frac{P}{A_0}\frac{l_0}{l}\bar{G}_1 = \bar{g}_1 \cdot (T_{1\cdot}^{\cdot 1}\,\bar{g}^1 \bar{G}_1)$$

$$\boxed{T_{1\cdot}^{\cdot 1} = \frac{P}{A_0}\frac{l_0}{l} = \frac{\rho_0}{\rho}\frac{P}{A}\frac{l_0^2}{l^2}} \tag{2.438}$$

$$\frac{P}{A_0}\frac{l}{l_0}\bar{G}^1 = \bar{g}^1 \cdot (T^{1\cdot}_{\cdot 1}\,\bar{g}_1 \bar{G}^1)$$

$$\boxed{T^{1\cdot}_{\cdot 1} = \frac{P}{A_0}\frac{l}{l_0} = \frac{\rho_0}{\rho}\frac{P}{A}} \tag{2.439}$$

$$\frac{P}{A_0}\frac{l_0}{l}\bar{G}_1 = \bar{g}^1 \cdot (T^{11}\,\bar{g}_1 \bar{G}_1)$$

$$\boxed{T^{11} = \frac{P}{A_0}\frac{l_0}{l} = \frac{\rho_0}{\rho}\frac{P}{A}\frac{l_0^2}{l^2}} \tag{2.440}$$

$$\frac{P}{A_0}\frac{l}{l_0}\bar{G}^1 = \bar{g}_1 \cdot (T_{11}\,\bar{g}^1 \bar{G}^1)$$

$$\boxed{T_{11} = \frac{P}{A_0}\frac{l}{l_0} = \frac{\rho_0}{\rho}\frac{P}{A}} \tag{2.441}$$

Observe that the relations $T_1^1 = T^{1\cdot}_{\cdot 1}$ and $T^{11} = T^{11}$ between the components of the Kirchhoff and the first Piola-Kirchhoff stress tensor are satisfied.

The components of the first Piola-Kirchhoff stress tensor referred to the reference configuration of the convected coordinate system are:

$$\frac{P}{A_0}\bar{g}_1 = \bar{g}_1 \cdot (T_{1\cdot}^{\cdot 1}\,\bar{g}^1 \bar{g}_1)$$

$$\boxed{T_{1\cdot}^{\cdot 1} = T^{1\cdot}_{\cdot 1} = T^{11} = T_{11} = \frac{P}{A_0} = \frac{\rho_0}{\rho}\frac{P}{A}\frac{l_0}{l}} \tag{2.442}$$

Defining

$$\sigma_E \equiv \hat{T}_{11} = T^{1}{}_{\cdot 1} = \frac{P}{A_0} \qquad (2.443)$$

This is the so-called "engineering stress" in the engineering literature and it is the easiest one to compute in uniaxial tests since it is just the load applied to the specimen divided by the original cross-sectional area A_o of the specimen.

The relationship between the components of the Kirchhoff and the second Piola-Kirchhoff stress tensors can be simply obtained:

$$\tau^{11} = S^{11}$$
$$\tau^{1}_{1} = S^{1}_{1}\left(1 + 2\gamma^{1}_{1}\right) \qquad (2.444)$$

2.8.4 Stress Rates

Since an irrotational uniaxial deformation is considered,

$$\bar{\bar{R}} = \bar{\bar{1}} \qquad \bar{\bar{W}} = \bar{\bar{0}} \qquad \bar{\bar{D}} = \bar{\bar{L}} = \bar{\bar{L}}^T \qquad (2.445)$$

Hence, from Eq. 2.335

$$\overset{\square}{\bar{\bar{\Omega}}} = \overset{\circ}{\bar{\bar{\Omega}}} \qquad (2.446)$$

For this particular kind of deformation, the <u>fixed-observer rate and the co-rotational rates of a second order tensor $\bar{\bar{\Omega}}$ are equal</u>.

The co-rotational rate of the components of the Cauchy stress tensor in Cartesian coordinates is:

$$\boxed{\overset{\circ}{\hat{\sigma}}_{11} = \dot{\hat{\sigma}}_{11} = \frac{d}{dt}\left(\frac{P}{A}\right)} \qquad (2.447)$$

The co-rotational rate of the components of the Cauchy stress tensor in convected coordinates is:

$$\overset{\circ}{\sigma}{}^{1}_{\cdot 1} = \dot{\sigma}^{1}_{\cdot 1} + D^{1}_{1}\sigma^{1}_{1} - \sigma^{1}_{1}D^{1}_{1} = \dot{\sigma}^{1}_{\cdot 1} = \frac{d}{dt}\left(\frac{P}{A}\right)$$

$$\overset{\circ}{\sigma}{}^{11} = \dot{\sigma}^{11} + D^{1}_{1}\sigma^{11} + \sigma^{11}D^{1}_{1} = \dot{\sigma}^{11} + 2D^{1}_{1}\sigma^{11}$$

$$= \frac{d}{dt}\left(\frac{P}{A}\frac{l_o^2}{l^2}\right) + 2\frac{\dot{l}}{l}\left(\frac{P}{A}\frac{l_o^2}{l^2}\right) = \frac{l_o^2}{l^2}\frac{d}{dt}\left(\frac{P}{A}\right) - 2\frac{P}{A_o}\frac{l_o^2\dot{l}}{l^2 l} + 2\frac{P}{A}\frac{l_o^2}{l^2}\frac{\dot{l}}{l}$$

$$\overset{\circ}{\sigma}{}^{11} = \frac{l_o^2}{l^2}\frac{d}{dt}\left(\frac{P}{A}\right) \qquad (2.448)$$

$$\overset{\circ}{\sigma}_{11} = \dot{\sigma}_{11} - D^{1}_{1}\sigma_{11} - \sigma_{11}D^{1}_{1} = \dot{\sigma}_{11} - 2D^{1}_{1}\sigma_{11}$$

$$= \frac{d}{dt}\left(\frac{P}{A}\frac{l^2}{l_o^2}\right) - 2\frac{\dot{l}}{l}\left(\frac{P}{A}\frac{l^2}{l_o^2}\right) = \frac{l^2}{l_o^2}\frac{d}{dt}\left(\frac{P}{A}\right) + 2\frac{P}{A}\frac{l^2}{l_o^2}\frac{\dot{l}}{l} - 2\frac{P}{A}\frac{l^2}{l_o^2}\frac{\dot{l}}{l}$$

$$\overset{\circ}{\sigma}_{11} = \frac{l^2}{l_o^2}\frac{d}{dt}\left(\frac{P}{A}\right) \qquad (2.449)$$

The convected rates of the components of the Cauchy stress tensor in the convected coordinate system in the present configuration are:

$$\overset{\triangledown}{\sigma}{}^{11} = \dot{\sigma}^{11} = \frac{d}{dt}\left(\frac{P}{A}\frac{l_o^2}{l^2}\right) = \frac{l_o^2}{l^2}\frac{d}{dt}\left(\frac{P}{A}\right) - 2\frac{P}{A}\frac{l_o^2}{l^2}\frac{\dot{l}}{l} \qquad (2.450)$$

$$\overset{\vartriangle}{\sigma}_{11} = \dot{\sigma}_{11} = \frac{d}{dt}\left(\frac{P}{A}\frac{l^2}{l_o^2}\right) = \frac{l^2}{l_o^2}\frac{d}{dt}\left(\frac{P}{A}\right) + 2\frac{P}{A}\frac{l^2}{l_o^2}\frac{\dot{l}}{l} \qquad (2.451)$$

$$\overset{\triangleright}{\sigma}{}^{1}_{\cdot 1} = \overset{\triangleleft}{\sigma}{}_{1}^{\cdot 1} = \dot{\sigma}^{1}_{\cdot 1} = \dot{\sigma}_{1}^{\cdot 1} = \frac{d}{dt}\left(\frac{P}{A}\right) \qquad (2.452)$$

Evidently these are not components of one and the same tensor. The co-rotational and convected rates of the Kirchhoff stress components referred to the convected coordinate system in the present configuration can be similarly obtained:

$$\overset{\circ}{\tau}{}^{1}_{1} = \overset{\triangleright}{\tau}{}^{1}{}_{\cdot 1} = \overset{\triangleleft}{\tau}{}_{1}{}^{\cdot 1} = \dot{\tau}{}^{1}{}_{\cdot 1} = \dot{\tau}{}_{1}{}^{\cdot 1} = \overset{\circ}{\hat{\tau}}_{11} = \dot{\hat{\tau}}_{11} = \frac{d}{dt}\left(\frac{P}{A_o}\frac{\ell}{\ell_o}\right) \tag{2.453}$$

$$\overset{\circ}{\tau}{}^{11} = \frac{\ell_o^2}{\ell^2}\frac{d}{dt}\left(\frac{P}{A_o}\frac{\ell}{\ell_o}\right) \tag{2.454}$$

$$\overset{\circ}{\tau}_{11} = \frac{\ell^2}{\ell_o^2}\frac{d}{dt}\left(\frac{P}{A_o}\frac{\ell}{\ell_o}\right) \tag{2.455}$$

$$\overset{\nabla}{\tau}{}^{11} = \dot{\tau}{}^{11} = \frac{\ell_o^2}{\ell^2}\frac{d}{dt}\left(\frac{P}{A_o}\frac{\ell}{\ell_o}\right) - 2\left(\frac{P}{A_o}\frac{\ell}{\ell_o}\right)\frac{\ell_o^2}{\ell^2}\frac{\dot{\ell}}{\ell} \tag{2.456}$$

$$\overset{\Delta}{\tau}_{11} = \dot{\tau}_{11} = \frac{\ell^2}{\ell_o^2}\frac{d}{dt}\left(\frac{P}{A_o}\frac{\ell}{\ell_o}\right) + 2\left(\frac{P}{A_o}\frac{\ell}{\ell_o}\right)\frac{\ell^2}{\ell_o^2}\frac{\dot{\ell}}{\ell} \tag{2.457}$$

The relationship between the co-rotational rate of the Kirchhoff stress tensor mixed components in the convected coordinate system in the present configuration and the Second Piola-Kirchhoff stress tensor mixed components material rate can be easily obtained from Eq. 2.269:

$$\boxed{\overset{\circ}{\tau}{}^{1}_{1} = \dot{S}^{1}_{1}\left(1+2\gamma^{1}_{1}\right) + 2\,S^{1}_{1}\dot{\gamma}^{1}_{1} = \dot{S}^{1}_{1}C^{1}_{1} + S^{1}_{1}\dot{C}^{1}_{1}}$$

Or, for this uniaxial, irrotational motion condition:

$$\overset{\circ}{\tau}{}^{1}_{1} = \dot{\tau}{}^{1}_{1} = \frac{d}{dt}\left(\frac{P}{A_o}\frac{\ell}{\ell_o}\right) \qquad S^{1}_{1} = \frac{P}{A_o}\frac{\ell_o}{\ell}$$
$$\gamma^{1}_{1} = \frac{1}{2}\left(\frac{\ell^2}{\ell_o^2} - 1\right) \qquad \dot{\gamma}^{1}_{1} = \frac{\ell^2}{\ell_o^2}\frac{\dot{\ell}}{\ell} \tag{2.458}$$

Hence,

$$\overset{\circ}{\tau}{}^1_1 = \frac{d}{dt}\left(S^1_1 \frac{\ell^2}{\ell_0^2}\right) = \dot{S}^1_1 \frac{\ell^2}{\ell_0^2} + 2 S^1_1 \frac{\ell^2}{\ell_0^2}\frac{\dot{\ell}}{\ell} \tag{2.459}$$

Therefore,

$$\overset{\circ}{\tau}{}^1_1 = \dot{S}^1_1 \left(1 + 2\gamma^1_1\right) + 2 S^1_1 \dot{\gamma}^1_1 \tag{2.460}$$

2.8.5 Energy Equation

As previously noted in Subsection 2.7, the energy integral over the present volume V can be expressed as a function of the Cauchy stress $\bar{\bar{\sigma}}$ and the rate-of-deformation tensor $\bar{\bar{D}}$ as in Eqs. 2.354 and 2.355. In this uniaxial case, one obtains:

$$\begin{aligned} U &= \int_t \int_V \hat{\sigma}_{11} \hat{D}_{11}\, dV dt = \int_t \int_V \sigma^{11} D_{11}\, dV dt \\ &= \int_t \int_V \sigma_{11} D^{11}\, dV dt = \int_t \int_V \sigma^1_1 D^1_1\, dV dt \end{aligned} \tag{2.461}$$

Notice that, from Eqs. 2.411, 2.412 and 2.413:

$$\hat{D}_{11}\, dt = D^1_1\, dt = \dot{\varepsilon}^*_u\, dt = \frac{1}{\ell}\frac{d\ell}{dt} dt = \frac{d\ell}{\ell} = d\varepsilon^*_u \tag{2.462}$$

Also, from Eqs. 2.425 and 2.427:

$$\hat{\sigma}_{11} = \sigma^1_1 = \frac{P}{A} \qquad \sigma^{11} = \frac{P}{A}\frac{\ell_0^2}{\ell^2} \qquad \sigma_{11} = \frac{P}{A}\frac{\ell^2}{\ell_0^2} \tag{2.463}$$

Therefore, Eq. 2.461 becomes:

$$\begin{aligned} U &= \int_V \int_{\ell_0}^{\ell} \left(\frac{P}{A}\right)\left(\frac{d\ell}{\ell}\right) dV = \int_V \int_{\ell_0}^{\ell} \left(\frac{P}{A}\frac{\ell_0^2}{\ell^2}\right)\left(\frac{\ell^2}{\ell_0^2}\frac{d\ell}{\ell}\right) dV \\ &= \int_V \int_{\ell_0}^{\ell} \left(\frac{P}{A}\frac{\ell^2}{\ell_0^2}\right)\left(\frac{\ell_0^2}{\ell^2}\frac{d\ell}{\ell}\right) dV = \int_V \int_{\ell_0}^{\ell} \left(\frac{P}{A}\right)\left(\frac{d\ell}{\ell}\right) dV = \int_V \int_{\ell_0}^{\ell} P\, d\ell\, \frac{dV}{V} \end{aligned} \tag{2.464}$$

which shows that the area under the "true stress" ($\sigma_T \equiv \sigma_1^1 = \frac{P}{A}$) and the logarithmic strain ($\epsilon_u^* = \ln (\frac{\ell}{\ell_o})$) is the energy per unit present volume of the material.

As pointed out in Subsection 2.7, the energy per unit reference volume of the material, can be easily obtained from the Jacobian determinant of the deformation, from Eq. 2.356:

$$\mathcal{U} = \int_t \int_{V_o} \bar{\bar{\tau}} : \bar{\bar{D}} \, dV_o dt \tag{2.465}$$

For the uniaxial case:

$$\mathcal{U} = \int_{V_o} \int_{\ell_o}^{\ell} \left(\frac{P}{A_o} \frac{\ell}{\ell_o}\right)\left(\frac{d\ell}{\ell}\right) dV_o = \int_{V_o} \int_{\ell_o}^{\ell} \left(\frac{P}{A_o} \frac{\ell_o}{\ell}\right)\left(\frac{\ell^2}{\ell_o^2} \frac{d\ell}{\ell}\right) dV_o$$

$$= \int_{V_o} \int_{\ell_o}^{\ell} \left(\frac{P}{A_o} \frac{\ell^3}{\ell_o^3}\right)\left(\frac{\ell_o^2}{\ell^2} \frac{d\ell}{\ell}\right) dV_o = \int_{V_o} \int_{\ell_o}^{\ell} \left(\frac{P}{A_o} \frac{\ell}{\ell_o}\right)\left(\frac{d\ell}{\ell}\right) dV_o = \int_{V_o} \int_{\ell_o}^{\ell} P d\ell \, \frac{dV_o}{V_o} \tag{2.466}$$

which shows that the area under the Kirchhoff stress ($\tau_u = \tau_1^1 = \frac{P}{A_o} \frac{\ell}{\ell_o}$) and logarithmic strain ($\epsilon_u^* = \ln (\frac{\ell}{\ell_o})$) is the energy per unit reference volume of the material.

The area under the Kirchhoff stress and the logarithmic strain is simply proportional to the <u>energy per unit mass of the material</u>, the proportionality factor being the mass density ρ_o per unit reference volume V_o, which does not depend on the deformation history.

The energy per unit reference volume of the material can also be expressed as a function of the second Piola-Kirchhoff stress tensor $\bar{\bar{S}}$ and the Green strain tensor $\bar{\bar{\gamma}}$ or the right Cauchy-Green deformation tensor $\bar{\bar{C}}$:

$$\mathcal{U} = \int_t \int_{V_o} \bar{\bar{S}} : \dot{\bar{\bar{\gamma}}} \, dV_o dt = \int_t \int_{V_o} \frac{1}{2} \bar{\bar{S}} : \dot{\bar{\bar{C}}} \, dV_o dt \tag{2.467}$$

For the uniaxial case:

$$\hat{S}_{11} = S^1_1 = S^{11} = S_{11} = \frac{P}{A_o}\frac{\ell_o}{\ell}$$

$$\dot{\hat{\gamma}}_{11} = \dot{\gamma}^1_1 = \dot{\gamma}^{11} = \dot{\gamma}_{11} = \frac{\ell^2}{\ell_o^2}\frac{\dot{\ell}}{\ell}$$

Hence,

$$\mathcal{U} = \int_{V_o}\int_{\ell_o}^{\ell}\left(\frac{P}{A_o}\frac{\ell_o}{\ell}\right)\left(\frac{\ell^2}{\ell_o^2}\frac{d\ell}{\ell}\right)dV_o = \int_{V_o}\int_{\ell_o}^{\ell} P\,d\ell\,\frac{dV_o}{V_o} \qquad (2.468)$$

which shows that the area under the second Piola-Kirchhoff stress ($\hat{S}_{11} = S^1_1 = \frac{P}{A_o}\frac{\ell_o}{\ell}$) and the Green strain ($\hat{\gamma}_{11} = \gamma^1_1 = \frac{1}{2}\left(\frac{\ell^2}{\ell_o^2} - 1\right)$) is equal to the energy per unit reference volume of the material, proportional to the energy per unit mass of the material.

Another expression for the energy per unit reference volume of the material relates the conjugate variables: the first Piola-Kirchhoff stress tensor $\overline{\overline{T}}$ and the rate of the deformation gradient tensor $\dot{\overline{\overline{F}}}$:

$$\mathcal{U} = \int_t \int_{V_o} \overline{\overline{T}} \cdot\cdot\, \dot{\overline{\overline{F}}}\, dV_o\, dt \qquad (2.469)$$

For the uniaxial case (convected coordinate components in the reference configuration):

$$\hat{T}_{11} = T^{1\cdot}_{\cdot 1} = T_1^{\cdot 1} = T^{11} = T_{11} = \frac{P}{A_o} \equiv \sigma_E \quad \text{("engineering stress")}$$

$$\dot{\hat{F}}_{11} = \dot{F}^{1\cdot}_{\cdot 1} = \dot{F}_1^{\cdot 1} = \dot{F}^{11} = \dot{F}_{11} = \frac{\dot{\ell}}{\ell_o} = \dot{E}_u$$

where

$$E_u = \tilde{E}^1_1 = \hat{\tilde{E}}_{11} = \frac{\ell - \ell_o}{\ell_o} \qquad \text{("engineering strain")}$$

Hence,

$$\mathcal{U} = \int_{V_o}\int_{\ell_o}^{\ell}\left(\frac{P}{A_o}\right)\frac{d\ell}{\ell_o}\,dV_o = \int_{V_o}\int_{\ell_o}^{\ell} P\,d\ell\,\frac{dV_o}{V_o} \qquad (2.470)$$

which shows that the area under the first Piola-Kirchhoff stress (or "engineering stress" $\sigma_E = \frac{P}{A_o}$) and the "engineering strain" ($E_u = \tilde{E}^1_1 = \frac{\ell}{\ell_o} - 1$) is equal to the energy per unit reference volume of the material.

SECTION 3

CONSTITUTIVE EQUATIONS

3.1 Introduction

In Section 2, the equations necessary for the precise treatment of constitutive equations were presented. In the present section, the finite-strain plasticity theory used in the present analysis is examined and displayed in the spirit of modern continuum mechanics.

3.2 Review of Small-Strain Plasticity Theory

3.2.1 Review of Principal Concepts

There are two types of plasticity theories, termed "flow" and "deformation". The deformation theory of plasticity assumes that, as in elasticity, there exists a one-to-one correspondence between stress and strain. The flow (also termed "rate-type") theory of plasticity states that there is a functional relation between the stress rate and the strain rate. Since these theories are conceived for small-strain conditions, the stress, strain, stress rate, and strain rate measures are left undefined for any strains that are not "small". Only for proportional loading where the stress ratio remains constant, and for a certain restricted range of loading paths other than proportional loading (through the assumption of the possibility of a singularity in the yield surface) does the deformation theory agree with the flow theory.

The behavior of an elastic-plastic material can be characterized by the following two ingredients. First, one assumes the existence of a boundary (yielding surface) in stress space which defines the elastic domain; within the boundary the continuum deforms elastically. The onset of plastic flow (irreversible deformation in a thermodynamic sense) is possible only at the boundary, and no meaning is associated with the region that is beyond the boundary. Second, one employs a flow rule which describes the behavior of the material after yielding has started; this rule gives the relation of plastic flow (strain rate) to the stress and the loading history.

Another basic assumption in the theory of an elastic-plastic continuum is the introduction of a plastic strain tensor. The plastic strain, γ_{ij}^{p}, is assumed to have the same invariance properties as does the strain tensor, γ_{ij}. The quantity γ_{ij}^{p} is related to γ_{ij} by an elastic strain tensor γ_{ij}^{e}, in the form:

$$\gamma_{ij} = \gamma_{ij}^{e} + \gamma_{ij}^{p} \tag{3.1}$$

The stress, S^{ij}, is related to the elastic strain $\gamma_{k\ell}^{e}$ by the components $E^{ijk\ell}$ of the fourth order elastic modulus tensor:

$$S^{ij} = E^{ijk\ell}\gamma_{k\ell}^{e} = E^{ijk\ell}\left(\gamma_{k\ell} - \gamma_{k\ell}^{p}\right) \tag{3.2}$$

and

$$E^{ijk\ell} = E^{jik\ell} = E^{ij\ell k} = E^{k\ell ij} \tag{3.3}$$

When the material is elastically isotropic, the $E^{ijk\ell}$ can be expressed as:

$$E^{ijk\ell} = \mu\left[g^{ik}g^{j\ell} + g^{i\ell}g^{jk}\right] + \lambda g^{ij}g^{k\ell} \tag{3.4}$$

where μ, λ are the Lamé constants.

The yield surface, Φ, is assumed to be expressible in terms of certain variables and may be expressed as:

$$\Phi\left(S^{ij}, K_{o}\right) = 0 \tag{3.5}$$

for <u>perfect plasticity</u> behavior, where K_{o} is a constant. For strain hardening behavior:

$$\Phi\left(S^{ij}, \gamma_{ij}^{p}, K\right) = 0 \tag{3.6}$$

where S^{ij} is the stress tensor (also undefined for finite strains) and K is a hardening parameter which depends on the strain history.

Various yield criteria have been proposed for the prediction of the onset of plastic flow. Among them is the Mises-Hencky yield criterion [89] which usually fits experimental observations better than the Tresca criterion [89], for instance, for polycrystalline metals and yet is mathematically simple. The Mises-Hencky rules will be discussed and adopted in the present analysis. The Mises-Hencky yield criterion may be interpreted as "yielding begins whenever the distortion energy per unit mass equals the distortion energy per unit mass at yield in simple tension". Thus hydrostatic pressure, for an elastically isotropic material in tension or compression does not affect the yielding, plastic flow, and resultant hardening. Stated otherwise, no plastic work is done by the hydrostatic component of the applied stress. This implies that there is no plastic (or irreversible) change in volume. Thus,

$$\dot{\gamma}^{p}_{ii} = 0 \tag{3.7}$$

For an initially-isotropic material, the Mises-Hencky yield function can be written in the form:

$$\Phi = J_2 - \frac{1}{3}(\sigma_0)^2 = 0 \tag{3.8}$$

where

$$J_2 = \frac{1}{2}\overset{D}{S}{}^{i}_{j}\,\overset{D}{S}{}^{j}_{i} = \frac{1}{2}\left[S^{i}_{j}S^{j}_{i} - \frac{1}{3}(S^{k}_{k})^2\right] \tag{3.9}$$

$\overset{D}{S}{}^{i}_{j} = S^{i}_{j} - \frac{1}{3}S^{k}_{k}\,\delta^{i}_{j}$ is the deviatoric stress

σ_0 is the yield stress in the uniaxial stress-strain state

This represents a hypersurface in nine-dimensional stress space. Any point on this surface represents a point at which yield can begin.

Considering the <u>elastic-perfectly-plastic</u> solid,[+] if the conditions (a) $\Phi < 0$ or (b) $\Phi = 0$ and $\dot{\Phi} < 0$, are satisfied, the state change can only be elastic; any plastic deformation (which may have been incurred earlier) remains unchanged. Thus,

$$\dot{\gamma}^{p}_{ij} = 0 \text{ when } \begin{cases} \Phi < 0 & \text{(elastic deformation)} \\ \Phi = 0 \quad \dot{\Phi} < 0 & \text{(unloading)} \end{cases} \tag{3.10}$$

It is postulated that the plastic strain rate $\dot{\gamma}^{p}_{ij}$ is linearly related to the

[+]With no strain-rate sensitivity.

gradient of Φ in stress space, $\partial\Phi/\partial s^{ij}$, as follows:

$$\dot{\gamma}^{P}_{ij} = \dot{\lambda}\frac{\partial\Phi}{\partial s^{ij}} \quad \text{when} \quad \Phi = 0 \quad \text{and} \quad \dot{\Phi} = 0 \quad \text{(loading)} \tag{3.11}$$

This is a consequence of Drucker's [90] stability postulate+; it implies that the plastic strain-rate vector $\dot{\gamma}^{p}_{ij}$ ($\dot{\gamma}^{p}_{ij}$ can be expressed as a vector in a strain-rate space with the <u>principal</u> strain-rate components as <u>axes</u>) is <u>normal</u> to the loading surface Φ (since $\frac{\partial\Phi}{\partial s^{ij}}$ is the normal to the loading surface Φ in stress space with <u>principal</u> stress components as axes, and the principal axes of strain rate and stress are assumed to coincide). Here $\dot{\lambda}$ is a scalar factor of proportionality; it is not a material constant, but varies with the deformation. The relation for the plastic strain rate $\dot{\gamma}^{p}_{ij}$ is independent of time as written, since it is dimensionally homogeneous in time.

Considering the <u>elastic-plastic (strain hardening)</u> solid, the state change is elastic if

$$\dot{\gamma}^{P}_{ij} = 0 \quad \text{when} \begin{cases} \Phi < 0 & \text{(elastic deformation)} \\ \Phi = 0 \quad \text{and} \quad \dot{\Phi} = 0 & \text{(neutral loading)} \\ \Phi = 0 \quad \text{and} \quad \dot{\Phi} < 0 & \text{(unloading)} \end{cases} \tag{3.12}$$

It is postulated that the plastic strain rate $\dot{\gamma}^{p}_{ij}$ is linearly related to the gradient of Φ in stress space, as follows:

$$\dot{\gamma}^{P}_{ij} = \dot{\lambda}\frac{\partial\Phi}{\partial s^{ij}} \quad \text{when} \quad \Phi = 0 \quad \text{and} \quad \dot{\Phi} > 0 \quad \text{(loading)}$$

where the factor of proportionality $\dot{\lambda}$ can be expressed as:

$$\dot{\lambda} = G\,\dot{\Phi} \tag{3.13}$$

+The work done by a set of external forces acting on a body must be positive during the application and positive or zero over a complete cycle of application and removal. For perfect plasticity, this is modified to require that the plastic work of the external agency is zero instead of positive.

$$\dot{\gamma}_{ij}^{p} = G\,\dot{\Phi}\,\frac{\partial \Phi}{\partial S^{ij}} \tag{3.14}$$

The factor G (as well as Φ) can be any scalar function of stress, strain, and strain history.

Notice that for $\dot{\Phi} = 0$ then $\dot{\gamma}_{ij}^{p} = 0$, which is consistent with the previous expression for neutral loading.

The factor G is not supposed to be a function of the stress rate. This assumption, suggested by Hill (page 34 of [89]), is based on the consideration that in a crystal grain, a plastic strain rate is produced by a combination of shears along certain slip directions, depending on the orientation of the grain and its external constraint. For the operation of such a glide-system, a certain state of stress is needed and hence, as a statistical average over all grains, a definite macroscopic stress exists. The stress rate enters only in determining the magnitude of the strain rate.

For the material to exhibit strain-hardening behavior, it implies that the yield surface will change in case of continued straining beyond the initial yield. The change of the yield surface (or loading surface) that characterizes the strain hardening (or work hardening) behavior of the material depends on the loading history.

There are several hardening rules available to describe the subsequent loading function. Among them are "isotropic hardening" and "kinematic hardening".

Isotropic hardening assumes that during subsequent yielding from a plastic state, the yield surface will expand uniformly with respect to the origin in stress space but will retain the same shape and orientation as it had initially. It does not take into account the Bauschinger effect [89]. Mathematically, the subsequent yield function for an isotropic hardening material can be put in the form:

$$\Phi = \Phi\left(S^{ij}, \gamma_{ij}^{p}, K\right)$$

and

$$K = K\left(W^{p} = \int_{0}^{\gamma_{ij}^{p}} S^{ij}\, d\gamma_{ij}^{p}\right) \quad \text{or} \quad K = K\left(\sqrt{\tfrac{2}{3}} \int_{0}^{\gamma_{ij}^{p}} \sqrt{d\gamma_{ij}^{p}\, d\gamma_{ij}^{p}}\right) \tag{3.15}$$

where W^{p} is the plastic work expended and the upper limit of the integral refers to the plastic strain at the current condition or time.

To account for the Bauschinger effect, Prager [91] introduced the "kinematic hardening rule" which postulates that during subsequent plastic flow, the yield surface translates (as a rigid body) in stress space and that it will retain the same size, shape, and orientation that it had initially. Mathematically, this can be expressed as

$$\Phi = \Phi\left(S^{ij} - \alpha^{ij}\right) = 0 \tag{3.16}$$

where $\alpha^{ij} = \alpha^{ij}(\gamma^{p}_{ij})$ represents the translation of the referenced origin in stress space of the yield surface and depends on the degree of hardening. Prager proposed that the direction of translation be normal to the yield surface:

$$\dot{\alpha}^{ij} = c \cdot \dot{\gamma}^{p}_{ij} \tag{3.17}$$

where c is a constant.

Ziegler [92] modified Prager's rule by suggesting that

$$\dot{\alpha}^{ij} = \dot{\mu}\left(S^{ij} - \alpha^{ij}\right) \tag{3.18}$$

where $\dot{\mu} > 0$. Geometrically, this means that the direction of motion of the center of the initial yield surface agrees with the radius vector that joins the instantaneous center α^{ij} with the stress point S^{ij}.

These kinematic hardening rules considerably over-estimate the Bauschinger effect, and therefore in general practice do not represent an improvement over the isotropic hardening rule, as observed by Almroth [93] and by Hunsaker et al.[94]. One exception is the case when a <u>bilinear</u> stress-strain curve provides a satisfactory approximation, as observed, for example, by Almroth [93] and by Iwan [95]. However, few materials have a hysteresis loop that is truly bilinear.

A combination of kinematic and isotropic hardening, that translates in accordance with Ziegler's rule, and whose hardening modulus and yield surface size at any point in the deformation history are assumed to be functions only of the plastic work has met with some success. It can be expressed mathematically as:

$$\begin{gathered} \phi\left(S^{ij} - \alpha^{ij}\right) = K\left(\sqrt{\tfrac{2}{3}} \int_0^{\gamma^{p}_{ij}} \sqrt{d\gamma^{p}_{ij}\, d\gamma^{p}_{ij}}\right) \\ \Phi\left[\left(S^{ij} - \alpha^{ij}\right), K\right] = 0 \end{gathered} \tag{3.19}$$

and translates according to

$$\dot{\alpha}^{ij} = \dot{\mu}\,(S^{ij} - \alpha^{ij}) \tag{3.20}$$

where $\dot{\mu} > 0$. This combined isotropic-kinematic hardening rule is usually used with a linear strain-hardening assumption.

Another hardening rule is the "mechanical sublayer model" of White [96] and Besseling [97]. In this model, the material at any point is conceived of as consisting of components, each component behaving as an elastic, perfectly-plastic medium, having common strain, but appropriately different yield stresses. If the components have the same elastic modulus, the yield stress of the composite will be the same as that of the weakest of its components. However, since the other components can take additional load, the composite will exhibit strain hardening with a piecewise linear stress-strain curve. In contrast to kinematic hardening, the mechanical sublayer model gives a hardening modulus at the outset of reversed yield which equals the hardening modulus at initial yield. This agrees well with experiments. Plastic anisotropy develops automatically in the model during loading in the plastic range. Use of only one sublayer results in the application of ideal plasticity; that is, elastic perfectly-plastic behavior. The use of two sublayers of which one has an infinite yield limit (in practice large but finite), results in the application of kinematic hardening with a bilinear stress-strain curve.

Mroz [98] introduced the concept of a "field of work-hardening moduli". A number of surfaces in stress space are introduced, and associated with each surface is the value of the work hardening modulus of the corresponding point in the uniaxial stress-strain curve of the material. On loading, all of the surfaces are shifted in stress space according to the rules of kinematic hardening. The hardening modulus obtained from the Mroz model depends on how many of the moduli are currently active. The results obtained by the use of the Mroz model are almost identical to those obtained by the use of the mechanical sublayer model [94]. While both models are practically identical for proportional loading, for nonproportional loading they differ in the following: under the Mroz [94] model the yield surfaces are not allowed to intersect, while under the mechanical-sublayer model the surfaces will intersect and corners will be created [97].

3.2.2 The Mechanical-Sublayer Model

Since the mechanical-sublayer model is used in the present analysis to model the finite strain, strain-hardening, strain-rate dependent behavior of metals, a brief review of the origins of the model will be given in this subsection.

The mechanical sublayer model, has been also called the "composite model", "subelement model", "subvolume model", "overlay model", and "distributed element model", according to the way in which this model was physically motivated, but most of the mathematical formulations are similar for small strain conditions. The general idea is that the strain-hardening behavior (including the Bauschinger effect) of an elastic-plastic material can be represented by a number of ideal elastic, perfectly-plastic elements having different yield limits but a common strain. As early as 1926, Masing [99] used this model to make some general statements about the behavior of materials; Prandtl [100] in 1928 used a mathematically equivalent model (but with a different physical representation of the model) as a vehicle for the application of kinetic theory to a rather wide range of problems associated with rate effects. The approach was suggested again in 1930 by Timoshenko [101]; in 1935, Duwez [102] applied the model of elastic, perfectly-plastic elements in series to single crystals and showed that the model could be made to give stress-strain curve and hysteretic energy loss results which were in close agreement with experiments.

The model seems to have received little attention until the early 1950's when White [96] in 1950 and Besseling [97] in 1953 used the model to represent elastic, perfectly-plastic behavior exhibiting the Bauschinger effect. Ivlev [103] in 1963 discussed the model, incorporating viscosity effects, and Prager [104] in 1966 further extended Ivlev's work.

In numerical predictions of strain-rate elastic-plastic transient structural response, the mechanical sublayer method was applied first at MIT. This application was carried out by Leech, Balmer, and Witmer during 1962-64 and is reported first in 1964 [105], with more details in 1965 [106] and 1966 [14]. In earlier MIT work reported in 1962 [107], a linear-elastic, linear-strain-hardening approximation with similar rules for loading, unloading, reversed loading, and reloading was used to represent material behavior; however, strictly speaking, this was not the mechanical sublayer model.

Drucker [108] has also discussed this model in 1966 and indicated some of its advantages as well as its shortcomings. The model was again applied by Iwan [109, 95] in 1966 to model the hysteretic behavior of materials and structures. Zienkiewicz [110] considered the isoparametric finite-element implementation of this model in 1972. Hunsaker et al. [94] in 1973 compared the mechanical-sublayer model with other strain-hardening plasticity rules: isotropic hardening, kinematic hardening, and the Mroz model. The mechanical-sublayer model was again utilized in 1976 by McKnight and Sobel [111] to analyze the cyclic thermoplasticity which occurs in areas of strain concentration resulting from the combination of both mechanical and thermal stresses.

It is interesting to note that in the mechanical-sublayer model, the characteristics of the numerical method are used to bypass the necessity for an explicit constitutive relationship. As a matter of fact, by using only elastic, perfectly-plastic sublayers, more satisfactory behavior patterns are achieved than those corresponding to isotropic or kinematic hardening rules; the Bauschinger effect is approximated well by the model.

A "physical" justification for the mechanical-sublayer model can be also found by analogy with a "micro" mechanics approach. The stress-strain behavior in strain-hardening can be attributed to the yielding of individual crystals, each of them experiencing elastic, perfectly-plastic behavior but yielding, however, at different levels of stress.

3.3 Plasticity Theory for Finite Strains

3.3.1 Introduction

As previously noted, the quantities utilized in the small strain theory of plasticity (stress, strain, stress rate, and strain rate) are defined only within the assumption of "small strains". Yet the precise definition of what constitutes "small strain" is always left unstated. Whether or not the strains are "small" cannot be determined by "geometric considerations" a priori; the strains result from loading, and (in general) one cannot know in advance whether for a given loading of a material the "small strain" assumption (always left undefined) will hold or not. Of course, after the problem is solved, this can be established, but if one has solved the problem it is no longer very important whether the strains are small or not. The question of whether the small-strain approximations are valid <u>in advance</u> is always avoided in the "small strain" literature. Furthermore, as R. Hill [112] points out, the really typical plastic problems involve changes in geometry that cannot be disregarded.

In the present subsection, the quantities involved in the particular finite-strain-plasticity theory chosen for the present analysis are discussed in detail; they were defined precisely in Section 2. Now, however, the reasons for this particular choice of variables are stated in Subsection 3.3.2.

3.3.2 General Concepts

The constitutive law to be used in the present analysis can be expressed in functional form as:

$$\overset{\circ}{\bar{\bar{\tau}}} = f(\bar{\bar{D}}, \bar{\bar{\tau}}) \tag{3.21}$$

where the actual form of this function will be made explicit in the next subsection (the purpose of the present subsection is to show the reasons for this particular choice of variables). The quantity $\bar{\bar{\tau}}$ is the Kirchhoff stress, previously defined in Subsection 2.5.2 as:

$$\bar{\bar{\tau}} = \frac{\rho_o}{\rho} \bar{\bar{\sigma}} \tag{3.22}$$

where $\bar{\bar{\sigma}}$ is the Cauchy ("true") stress tensor, and $\rho(\rho_o)$ is the mass density in the present (reference) configuration. Also, the circle over $\bar{\bar{\tau}}$ denotes the co-rotational+ stress rate defined in Subsection 2.6.4. The rate-of-deformation tensor $\bar{\bar{D}}$ is defined in Subsection 2.4.2.1.

This constitutive law (Eq. 3.21) involves quantities associated with the present configuration of the material, with the only exception being the mass

---

+Also known as the "Jaumann stress rate".

density ρ_o which is a constant for a fixed reference configuration and, therefore, does not depend on the deformation history.

The Kirchhoff stress $\bar{\bar{\tau}}$ is used instead of the Cauchy stress $\bar{\bar{\sigma}}$, since it is known to be more suitable for defining the constitutive equations, particularly when thermodynamic principles are used to formulate a constitutive relation. Some of the reasons for the use of this stress measure are:

(a) The Kirchhoff stress is the stress (associated with the present configuration of the material) that is related to a unit of mass, instead of a unit of volume, since as shown in Subsection 2.7, the power per unit mass is expressed simply by

$$\text{Power per Unit Mass} = \frac{\bar{\bar{\tau}} : \bar{\bar{D}}}{\rho_o(\bar{r}, t_o)} \tag{3.23}$$

where ρ_o is a constant for the entire deformation process for a fixed reference configuration, while the power per unit mass expressed in terms of the Cauchy stress is expressed by:

$$\text{Power per Unit Mass} = \frac{\bar{\bar{\sigma}} : \bar{\bar{D}}}{\rho(\bar{R}, t)} \tag{3.24}$$

where $\rho(\overleftarrow{R},t)$ is a variable in the deformation process.

(b) For this reason, the thermodynamic expressions that the constitutive relations must satisfy are simpler when expressed in terms of the Kirchhoff stress.

(c) The co-rotational rate of the Kirchhoff stress has a rate potential while the co-rotational rate of the Cauchy stress has not. As shown by Hill [113]

$$\text{Rate Potential} = \frac{1}{2}\,\overset{\circ}{\bar{\bar{\tau}}} : \bar{\bar{D}} \tag{3.25}$$

(d) The existence of a rate potential is of importance in an incremental finite element analysis since it implies the existence of an incremental variational principle and symmetric tangent stiffness matrices.

(e) The Kirchhoff stress can be easily measured in experiments. As shown in Subsection 2.8.3, in uniaxial experiments it is simply expressed as

$$\tau_u = \frac{P}{A_o}\left(1 + E_u\right) \tag{3.26}$$

where P is the load applied to the specimen, A_o is the original cross sectional area and E_u is the change in length divided by the original length: $E_u = \frac{\ell - \ell_o}{\ell_o}$, the quantity that extensometers and strain gages can provide.

(f) The Kirchhoff stress is the quantity which was computed from experimental data and used in the presentation of results in many of the classic experiments in plasticity of metals by G.I. Taylor [114] and also by A. Nadai [115]. As a matter of fact, it is frequently confused with the true stress in experiments for metals, since for practical purposes one can assume incompressibility ($\rho = \rho_o$) for metals; hence, the Cauchy ("true") stress is approximately equal to the Kirchhoff stress.

(g) When used in conjunction with the logarithmic strain, it produces an approximately symmetric stress-strain response for the uniaxial loading of metals*, unlike other stress measures, like the 1st and 2nd Piola-Kirchhoff stresses which produce significantly asymmetric stress-strain responses for the uniaxial loading of metals.

The co-rotational rate (overscript "o") of the Kirchhoff stress ($\overset{o}{\underline{\underline{\tau}}}$) is used instead of the fixed-in-space observer rate, convected rates, or other stress rates, since:

(a) It satisfies the principle of material frame-indifference as defined by Truesdell and Noll [40] when used in conjunction with the (frame-indifferent) rate-of-deformation tensor in a constitutive law. One implication of this is that the

*For metals with a cubic structure, since slip is their primary deformation mechanism, and it can operate equally well forward or backward.

constitutive law is invariant under arbitrary rigid body motions; the co-rotational rate of the Kirchhoff stress $\overset{\Omega}{\bar{T}}$ vanishes when a material point of the continuum with its environment performs a rigid-body motion and the Kirchhoff stress tensor $\bar{\bar{T}}$ does not vary in time intrinsically with respect to the material point.

(b) The co-rotational rate of the stress tensor is a tensor quantity of the same type as the original stress tensor, since the Kirchhoff stress tensor $\bar{\bar{T}}$ is symmetric, the co-rotational rate $\overset{\Omega}{\bar{\bar{T}}}$ is also symmetric.

(c) Vanishing of the co-rotational derivative of a tensor induces vanishing of the co-rotational derivative of its arbitrary invariant.

(d) In a uniaxial, irrotational deformation, it reduces to the material rate of the tensor.

The rate-of-deformation $\bar{\bar{D}}$ is used in the constitutive expressions since it is defined completely and uniquely by the present state of the material and, unlike strain rates, its description does not involve any reference state. Since plasticity has some similarities* with a flow problem, and the rate-of-deformation tensor $\bar{\bar{D}}$ is the rate quantity used in hydrodynamics, the appropriateness of a description of large strain plasticity in terms of $\bar{\bar{D}}$ is seen at once.

In the case of a uniaxial, irrotational, homogeneous deformation, the rate-of-deformation tensor becomes the rate of the logarithmic strain tensor, as shown in Subsection 2.8.2. The logarithmic strain ranges in value between zero and infinity, both for tension and compression, as shown in Subsection 2.8.2. This provides a measure of strain which has "symmetric" properties for tension and compression. The relative elongation, the Green ("Lagrangian") strain, and the Almansi ("Eulerian") strains do not enjoy this useful property.

*These similarities are only formal in the case of time-independent plasticity, since there is really no rate-dependence or viscosity implied by the plasticity equations. However, in the present treatment, strain-rate dependence of the constitutive equations was taken into account.

Also note that the rate-of-deformation tensor $\bar{\bar{D}}$ is "conjugate" to the Kirchhoff stress tensor $\bar{\bar{T}}$ in the sense that their scalar product is proportional to the rate of work per unit mass, as shown previously.

The constitutive law

$$\overset{\circ}{\bar{\bar{\tau}}} = f(\bar{\bar{D}}, \bar{\bar{\tau}}) \tag{3.27}$$

is a hypoelastic law (references in hypoelasticity are: page 731 of [15], page 401 of [40], and [116-122]). In the general multiaxial case, it is a path-dependent material law, since it cannot be integrated+ in terms of an initial and a final state; it depends on the path connecting these states. To consider finite-elastic-strain response, in addition to finite-plastic-strain response, it is necessary to introduce a finite-strain measure in the constitutive law (that measures deformation by comparing a reference and a present configuration, irrespective of the paths connecting these configurations). It is not difficult to include this finite-elastic-strain response in the constitutive law, for example, by including the Almansi strain $\bar{\bar{e}}$:

$$\overset{\circ}{\bar{\bar{\tau}}} = g(\bar{\bar{D}}, \bar{\bar{\tau}}, \bar{\bar{e}}) \tag{3.28}$$

as done by Lehmann [123], who assumed a linear relationship between stress and strain, with no experimental basis for large-elastic-strains.

For metals, experiments have shown only small elastic strains, even for cases of unloading from large plastic strains. No experimental data seems to exist from which a finite-elastic strain law for metals could be deduced. Moreover, whether elastic strains++ do exist at all for metals is still a matter of discussion. E. H. Lee [124] indicates that under large strain-rate conditions, finite-elastic-strains can be expected in metals. However, these strains could be visco-elastic and not purely elastic, by the very nature of the strain-rate dependence. The experimental information available is not precise enough to determine if these strains are visco-elastic

---

+It can be integrated, under some assumptions, in the cases of uniaxial stress-strain, and pure volumetric deformation.

++In the sense of Green, an elastic material is one for which a strain-energy function exists.

or visco-hypoelastic. In view of the present state of experimental information, the hypoelastic law will be used in the analysis, since it is convenient for the numerical analysis of the elastic-plastic problems; also, for small elastic strains there is practically no difference between hypoelastic and elastic laws, as shown, for example, by Lehmann [123].

3.3.3 A Finite-Strain Elastic-Plastic Strain-Rate-Dependent Theory

This subsection is concerned with the finite-strain elastic-plastic strain-rate-dependent theory utilized in this analysis. The constitutive equations of this theory are discussed in the spirit of modern continuum mechanics. It should be remarked that even within the limitation of the infinitesimal or the "small" strain theory of plasticity, there does not appear to be complete agreement among the various schools of plasticity in the United States, Great Britain, and the Soviet Union; therefore, no attempt at reviewing the literature in <u>finite-strain</u> plasticity will be carried out, since there is little that has become widely accepted, and active theoretical research on the subject is still taking place. Rather, the specific theory used in the numerical analysis of the problems with which this work deals will be examined in detail. In the previous subsection, the reasons why the particular variables used in the constitutive equations were chosen were explained. The previous rough description is made precise in the present subsection.

The present description of the behavior of an elastic-plastic continuum is based on the work of Hill [112-113, 125-131] and of Lehmann [87, 123, 132-137], and can be interpreted as a special case of the general theory of an elasto-plastic continuum by Green and Naghdi [138]. However, strain-rate effects are included in the present analysis, and strain-hardening behavior is treated with a "mechanical sublayer " method properly modified to take into account finite strains.

The present subsection shows the theory in terms of the "primary" variables:

$$\overset{\circ}{\overline{\overline{\tau}}} = f(\overline{\overline{D}}, \overline{\overline{\tau}})$$

as previously specified in Eq. 3.21. However, it should be mentioned that in the actual implementation of the theory, this equation is transformed to

$$\dot{\bar{\bar{S}}} = g\left(\dot{\bar{\bar{\gamma}}}, \bar{\bar{S}}, \bar{\bar{\gamma}}\right) \tag{3.29}$$

according to the tensor transformation rules of Section 2, since the analysis is implemented in the referential (Lagrangian) description of motion with a fixed reference configuration. In Eq. 3.29, $\bar{\bar{S}}$ is the Second Piola Kirchhoff stress tensor, $\dot{\bar{\bar{S}}}$ is its material rate, $\bar{\bar{\gamma}}$ is the Green (Lagrangian) strain tensor, and $\dot{\bar{\bar{\gamma}}}$ is its material rate.

Returning to Eq. 3.21, it is assumed that the Kirchhoff stress $\bar{\bar{\tau}}$ at a material point can be considered as the sum of n components (${}^{s}\bar{\bar{\tau}}$; s = 1 to n) with weighting factors* A_s:

$$\boxed{\bar{\bar{\tau}} = \sum^{n} A_s \, {}^{s}\bar{\bar{\tau}}} \tag{3.30a}$$

where prescript "s" refers to the sth sublayer.

Since the weighting factors A_s are assumed to be independent of time, the co-rotational rate $\overset{\circ}{\bar{\bar{\tau}}}$ of the Kirchhoff stress at a material point can also be considered as the sum of n components (${}^{s}\overset{\circ}{\bar{\bar{\tau}}}$, s = 1 to n) with the same weighting factors A_s:

$$\boxed{\overset{\circ}{\bar{\bar{\tau}}} = \sum^{n} A_s \, {}^{s}\overset{\circ}{\bar{\bar{\tau}}}} \tag{3.30b}$$

Each component ${}^{s}\overset{\circ}{\bar{\bar{\tau}}}$ of the co-rotational rate of the Kirchhoff stress is assumed to be linearly related through a fourth order* "elasticity tensor" ${}^{s}\bar{\bar{\bar{\bar{E}}}}$ to a component ${}^{s}\bar{\bar{D}}^{e}$ of an "elastic" rate of deformation tensor $\bar{\bar{D}}^{e}$:

$${}^{s}\overset{\circ}{\bar{\bar{\tau}}} = {}^{s}\bar{\bar{\bar{\bar{E}}}} : {}^{s}\bar{\bar{D}}^{e} \tag{3.31}$$

---

*These weighting factors are discussed explicitly in Subsection 3.3.4.

**This fourth order "elasticity" tensor has the same symmetric properties as does the usual elasticity tensor (since the $\overset{\circ}{\bar{\bar{\tau}}}$ with the $\bar{\bar{D}}^{e}$ have a potential); this fourth order tensor is a "tensor-tensor", a quantity which plays the same role for tensors of second order as second-order tensors do for vectors (p. 145 of Schouten [61]).

The rate-of-deformation tensor $\overline{\overline{D}}$ is assumed to be decomposed into an "elastic part" ${}^{s}\overline{\overline{D}}^{e}$ and a plastic part ${}^{s}\overline{\overline{D}}^{p}$ for each sublayer "s":

$$ {}^{s}\overline{\overline{D}} = \overline{\overline{D}} = {}^{s}\overline{\overline{D}}^{e} + {}^{s}\overline{\overline{D}}^{p} \tag{3.32} $$

Observe that <u>each</u> sublayer "s" experiences the <u>same</u> rate of deformation $\overline{\overline{D}}$, but different amounts of "elastic" ${}^{s}\overline{\overline{D}}^{e}$ and plastic ${}^{s}\overline{\overline{D}}^{p}$ components. The decomposition of the deformation rate assumes different proportions in each sublayer "s". From Eq. 3.32 one can express Eq. 3.31 as:

$$ {}^{s}\overset{\circ}{\overline{\overline{\tau}}} = {}^{s}\overline{\overline{\overline{\overline{E}}}} : \left(\overline{\overline{D}} - {}^{s}\overline{\overline{D}}^{p}\right) \tag{3.33} $$

Next, the existence of a loading function ${}^{s}\Phi$ (yield surface in stress space) is assumed to exist for each sublayer "s", as a function of the Kirchhoff stress component ${}^{s}\overline{\overline{\tau}}$ of that sublayer, and the total rate of deformation tensor $\overline{\overline{D}}$:

$$ {}^{s}\Phi = {}^{s}\Phi\left({}^{s}\overline{\overline{\tau}}, \overline{\overline{D}}\right) \tag{3.34} $$

This loading function ${}^{s}\Phi$ will define the "elastic" ${}^{s}\overline{\overline{D}}^{e}$ and plastic ${}^{s}\overline{\overline{D}}^{p}$ parts of the rate of deformation $\overline{\overline{D}}$ in each sublayer "s", according to the following rule:

$$ {}^{s}\overline{\overline{D}}^{p} = 0 \quad \text{when} \quad \begin{cases} {}^{s}\Phi < 0 \\ {}^{s}\Phi = 0 \quad \text{and} \quad {}^{s}\dot{\Phi} < 0 \end{cases} \tag{3.35} $$

$$ {}^{s}\overline{\overline{D}}^{p} = {}^{s}\dot{\lambda}\,\frac{\partial\,{}^{s}\Phi}{\partial\,{}^{s}\overline{\overline{\tau}}} \quad \text{when} \quad \left\{\, {}^{s}\Phi = 0 \quad \text{and} \quad {}^{s}\dot{\Phi} = 0 \right. \tag{3.36} $$

which implies that the plastic part ${}^{s}\overline{\overline{D}}^{p}$ of the rate-of-deformation tensor $\overline{\overline{D}}$, for sublayer "s" is normal to the loading surface ${}^{s}\Phi$ of sublayer "s". In the present work, a von Mises loading function (yield surface in stress space) is assumed to exist. This loading function is most readily expressed in terms of the deviatoric stress ${}^{s}\overline{\overline{\tau}}^{D}$ defined as

$$ {}^{s}\overline{\overline{\tau}}^{D} \equiv {}^{s}\overline{\overline{\tau}} - {}^{s}\overline{\overline{\tau}}^{sp} \tag{3.37} $$

where ${}^{s}\overline{\overline{\tau}}^{sp}$ is the spherical (superscript "sp") stress, defined as

$$ {}^{s}\overline{\overline{\tau}}^{sp} \equiv \frac{1}{3}\left(\mathrm{tr}\ {}^{s}\overline{\overline{\tau}}\right)\overline{\overline{I}} \tag{3.38} $$

and (tr ${}^{s}\overline{\overline{\tau}}$) stands for the trace operator:

$$\mathrm{tr}\,{}^s\overline{\overline{\tau}} = \overline{\overline{1}} : {}^s\overline{\overline{\tau}} = {}^s\overline{\overline{\tau}} : \overline{\overline{1}} \tag{3.39}$$

Hence, the deviatoric Kirchhoff stress of the sth sublayer is:

$$\boxed{{}^s\overline{\overline{\tau}}^D = {}^s\overline{\overline{\tau}} - \frac{1}{3}(\mathrm{tr}\,{}^s\overline{\overline{\tau}})\,\overline{\overline{1}}} \tag{3.40}$$

In terms of the deviatoric stress, the von Mises loading function can be expressed as:

$${}^s\Phi = {}^s\overline{\overline{\tau}}^D : {}^s\overline{\overline{\tau}}^D - \frac{2}{3}\left({}^s\tau_u^y\right)^2 \tag{3.41}$$

where

$${}^s\tau_u^y = {}^s\tau_u^y\left(\overline{\overline{D}}^D\right) \tag{3.42}$$

is the deformation-rate-dependent yield stress of a specimen in <u>uniaxial tension</u>. Denoting by ${}^s\tau_{u_o}^y$ the <u>static</u> (rate independent) yield stress of a specimen in uniaxial tension, the rate-dependent yield stress ${}^s\tau_u^y$ is assumed to be related to the deviatoric rate-of-deformation tensor, $\overline{\overline{D}}^D$ by

$${}^s\tau_u^y = {}^s\tau_{u_o}^y\left(1 + \left(\frac{\sqrt{\frac{3}{2}\left(\overline{\overline{D}}^D : \overline{\overline{D}}^D\right)}}{{}^sd}\right)^{\frac{1}{{}^sp}}\right) \tag{3.43}$$

where

$$\overline{\overline{D}}^D = \overline{\overline{D}} - \frac{1}{3}\left(\mathrm{tr}\,\overline{\overline{D}}\right)\overline{\overline{1}} \tag{3.44}$$

and ${}^sd$ and ${}^sp$ are material "rate" constants. Therefore, the von Mises strain-rate dependent loading function becomes:

$$\boxed{{}^s\Phi = {}^s\overline{\overline{\tau}}^D : {}^s\overline{\overline{\tau}}^D - \frac{2}{3}\left({}^s\tau_{u_o}^y\right)^2\left(1 + \left(\frac{\sqrt{\frac{3}{2}\left(\overline{\overline{D}}^D : \overline{\overline{D}}^D\right)}}{{}^sd}\right)^{\frac{1}{{}^sp}}\right)^2} \tag{3.45}$$

The gradient $(\partial({}^s\Phi))/(\partial({}^s\overline{\overline{\tau}}))$ of the loading function ${}^s\Phi$ of sublayer s, with respect to the Kirchhoff stress ${}^s\overline{\overline{\tau}}$ also at sublayer "s", will be needed in the analysis. For the von Mises loading function ${}^s\Phi$, one obtains:

$$\frac{\partial({}^s\Phi)}{\partial({}^s\overline{\overline{\tau}})} = \frac{\partial}{\partial({}^s\overline{\overline{\tau}})}\left({}^s\overline{\overline{\tau}}^D : {}^s\overline{\overline{\tau}}^D - \frac{2}{3}\left({}^s\tau_u^y\right)^2\right)$$

$$= 2\,{}^s\overline{\overline{\tau}}^D \frac{\partial}{\partial({}^s\overline{\overline{\tau}})}\left({}^s\overline{\overline{\tau}} - \frac{1}{3}\left(\mathrm{tr}\,{}^s\overline{\overline{\tau}}\right)\overline{\overline{1}}\right)$$

$$= 2\,{}^s\overline{\overline{\tau}}^D (1-0) = 2\,{}^s\overline{\overline{\tau}}^D \tag{3.46}$$

Also, from Eq. 3.36:

$$\boxed{{}^s\overline{\overline{D}}^P = {}^s\dot{\lambda}\,{}^s\overline{\overline{\tau}}^D} \tag{3.47}$$

Observe that the parameter ${}^s\dot{\lambda}$ can be expressed in terms of the plastic power per unit mass $\dot{U}^P$ of sublayer s, as:

$$\begin{aligned} {}^s\dot{U}^P &= \frac{1}{\rho_o}\left({}^s\overline{\overline{\tau}}\right) : \left({}^s\overline{\overline{D}}^P\right) = \frac{1}{\rho_o}\left({}^s\overline{\overline{\tau}}\right) : \left({}^s\dot{\lambda}\,{}^s\overline{\overline{\tau}}^D\right) \\ &= \frac{{}^s\dot{\lambda}}{\rho_o}\left({}^s\overline{\overline{\tau}}\right) : \left({}^s\overline{\overline{\tau}}^D\right) = \frac{{}^s\dot{\lambda}}{\rho_o}\left({}^s\overline{\overline{\tau}}^D\right) : \left({}^s\overline{\overline{\tau}}^D\right) \end{aligned} \tag{3.48}$$

Since

$${}^s\Phi = 0\,,$$

$$\left({}^s\overline{\overline{\tau}}^D\right) : \left({}^s\overline{\overline{\tau}}^D\right) = \frac{2}{3}\left({}^s\tau_{u_o}^y\right)^2\left(1 + \left(\frac{\sqrt{\frac{3}{2}\left(\overline{\overline{D}}^D : \overline{\overline{D}}^D\right)}}{{}^s d}\right)^{\frac{1}{{}^s p}}\right)^2 \tag{3.49}$$

for

$${}^s\overline{\overline{D}}^P \neq \overline{\overline{0}} \tag{3.50}$$

Then, Eq. 3.48 becomes:

$${}^s\dot{U}^P = \frac{{}^s\dot{\lambda}}{\rho_o}\,\frac{2}{3}\left({}^s\tau_{u_o}^y\right)^2\left(1 + \left(\frac{\sqrt{\frac{3}{2}\left(\overline{\overline{D}}^D : \overline{\overline{D}}^D\right)}}{{}^s d}\right)^{\frac{1}{{}^s p}}\right)^2 \tag{3.51}$$

Hence, one can express ${}^s\dot{\lambda}$ as:

$$
{}^s\dot{\lambda} = \wp_0 \frac{{}^s\dot{\bar{U}}^p}{\frac{2}{3}\left({}^s\tau^y_{u_0}\right)^2\left(1+\left(\frac{\sqrt{\frac{3}{2}\left(\bar{\bar{D}}^D:\bar{\bar{D}}^D\right)}}{{}^sd}\right)^{\frac{1}{{}^sp}}\right)^2}
$$

(3.52)

Equation 3.52 implies that the scalar parameter ${}^s\dot{\lambda}$ characterizes the plastic dissipation ${}^s\dot{\bar{U}}^p$ of sublayer s, which in turn restricts ${}^s\dot{\lambda}$ to be positive semidefinite:

$$
\boxed{{}^s\dot{\lambda} \geq 0 \qquad \text{since} \qquad {}^s\dot{\bar{U}}^p \geq 0} \tag{3.53}
$$

Finally, to summarize, one can express these finite strain, "elastic"-plastic, strain-hardening, strain-rate-dependent constitutive equations as:

$$
\begin{gathered}
\bar{\bar{\tau}} = \sum^{n} A_s \, {}^s\bar{\bar{\tau}} \\
\overset{\circ}{\bar{\bar{\tau}}} = \sum^{n} A_s \, {}^s\overset{\circ}{\bar{\bar{\tau}}} \\
{}^s\bar{\bar{\tau}}^D = {}^s\bar{\bar{\tau}} - \frac{1}{3}\left(\mathrm{tr}\,{}^s\bar{\bar{\tau}}\right)\bar{\bar{1}} \qquad \qquad \bar{\bar{D}}^D = \bar{\bar{D}} - \frac{1}{3}\left(\mathrm{tr}\,\bar{\bar{D}}\right)\bar{\bar{1}} \\
{}^s\Phi = \left({}^s\bar{\bar{\tau}}^D\right):\left({}^s\bar{\bar{\tau}}^D\right) - \frac{2}{3}\left({}^s\tau^y_{u_0}\right)^2\left(1+\left(\frac{\sqrt{\frac{3}{2}\left(\bar{\bar{D}}^D\right):\left(\bar{\bar{D}}^D\right)}}{{}^sd}\right)^{\frac{1}{{}^sp}}\right)^2 \\
{}^s\bar{\bar{D}} = \bar{\bar{D}} = {}^s\bar{\bar{D}}^e + {}^s\bar{\bar{D}}^p \\
{}^s\overset{\circ}{\bar{\bar{\tau}}} = {}^s\bar{\bar{\bar{\bar{E}}}}:\bar{\bar{D}} \quad \text{if} \quad \left\{\begin{array}{l} {}^s\Phi < 0 \\ \qquad \text{or} \\ {}^s\Phi = 0 \quad \text{and} \quad {}^s\dot{\Phi} < 0 \end{array}\right. \\
{}^s\overset{\circ}{\bar{\bar{\tau}}} = {}^s\bar{\bar{\bar{\bar{E}}}}:\left(\bar{\bar{D}} - {}^s\dot{\lambda}\,{}^s\bar{\bar{\tau}}^D\right) \quad \text{if} \quad \left\{ {}^s\Phi = 0 \quad \text{and} \quad {}^s\dot{\Phi} = 0 \right.
\end{gathered}
$$

(3.54)

where:

${}^{s}\overline{\overline{\overline{\overline{E}}}}$	is the fourth order "elasticity" tensor of sublayer s
A_s	is the weighting factor of sublayer s
${}^{s}d$ and ${}^{s}p$	are material strain-rate constants of sublayer s
${}^{s}\tau^{y}_{u_o}$	is the Kirchhoff stress at yield in uniaxial loading, in static conditions, of sublayer s
${}^{s}\dot{\lambda}$	scalar factor that characterizes the dissipation of sublayer s.

It is evident that by considering different values of the material constants ${}^{s}d$ and ${}^{s}p$, and of the "elasticity" tensor ${}^{s}\overline{\overline{\overline{\overline{E}}}}$ for each sublayer s, a very complex material behavior could be represented. However, in the present numerical calculations these parameters have been considered to be the same for each sublayer s; that is,

$$\begin{aligned} \overline{\overline{\overline{\overline{E}}}} &= {}^{s}\overline{\overline{\overline{\overline{E}}}} = {}^{1}\overline{\overline{\overline{\overline{E}}}} = {}^{2}\overline{\overline{\overline{\overline{E}}}} = {}^{3}\overline{\overline{\overline{\overline{E}}}} = \ldots = {}^{(n)}\overline{\overline{\overline{\overline{E}}}} \\ d &= {}^{s}d = {}^{1}d = {}^{2}d = {}^{3}d = \ldots = {}^{(n)}d \\ p &= {}^{s}p = {}^{1}p = {}^{2}p = {}^{3}p = \ldots = {}^{(n)}p \end{aligned} \tag{3.55}$$

for the present analysis.

In addition, for a few numerical calculations* the material has been considered to be strain-rate independent, in which case:

$${}^{s}\Phi = \left({}^{s}\overline{\overline{\tau}}^{D}\right) : \left({}^{s}\overline{\overline{\tau}}^{D}\right) - \frac{2}{3}\left({}^{s}\tau^{y}_{u_o}\right)^2 \tag{3.56}$$

It should also be mentioned that the loading conditions of Eq. 3.35, 3.36, and 3.54 are not the actual loading conditions used in the numerical model, and for these, the reader should turn to Sections 4 and 5.

---

*Impact analysis of 6061-T651 aluminum alloy structures.

3.3.4 Computation of Mechanical-Sublayer-Model Weighting Factors

3.3.4.1 Application to Uniaxial Stress-Strain Conditions

The determination of the mechanical-sublayer-model weighting factor A_s will be considered in the following. As indicated in Eq. 3.29, it is assumed that the Kirchhoff stress $\overline{\overline{T}}$ at a material point can be considered as the sum of n components ($^s\overline{\overline{T}}$, s = 1, ..., n) with weighting factors A_s:

$$\overline{\overline{\tau}} = \sum^{n} A_s \, {}^s\overline{\overline{\tau}} \tag{3.57}$$

The weighting factors A_s may be selected for either one-dimensional, two-dimensional, or three-dimensional stress conditions. Considering one-dimensional stress conditions, the uniaxial (denoted by subscript u) static stress-strain curve of the material is assumed to be perfectly antisymmetric in Kirchhoff stress (τ_{u_o}) versus logarithmic strain (ε^*_u) space, as shown approximately by the classic experiments of G.I. Taylor [114], among others. From Eq. 2.402, the logarithmic strain is

$$\varepsilon^*_u = \ln\left(\frac{\ell}{\ell_o}\right) = \ln\left(1 + E_u\right) \tag{3.58}$$

where $\ell(\ell_o)$ is the final (original) gage length and

$$E_u = \frac{\ell - \ell_o}{\ell_o} \tag{3.59}$$

is the relative elongation, or "engineering strain" that strain gages or extensometers can provide.

From Eq. 2.424, the uniaxial Kirchhoff stress is:

$$\tau_u = \frac{P}{A_o}\frac{\ell}{\ell_o} = \frac{P}{A_o}\left(1 + E_u\right) \tag{3.60}$$

This static stress-strain curve is first approximated by n+1 piecewise-linear segments which are defined at coordinates [$^s(\tau_{u_o})$, $^s(\varepsilon^*_u)$, s = 1, 2, ..., n]; see Fig. 2a. Next, the material is envisioned as consisting, at any point in the material, of n equally-strained sublayers of elastic, perfectly-plastic material, with each sublayer having the same[+] elastic modulus E as the idealized material, but an appropriately different yield stress (denoted by superscript y). For example, the static (subscript o in τ_{u_o}) yield stress (superscript y) of the s sublayer is given by (see Fig. 2b):

$$\boxed{{}^{s}(\tau_{u_o})^{y} = E\,{}^{s}(\varepsilon_u^{*})} \tag{3.61}$$

Then, the Kirchhoff stress value under static conditions, ${}^{s}(\tau_{u_o})$, associated with the sth sublayer can be defined uniquely by the strain history and the value of the strain ε_u^{*} at that material point. Taken collectively with an appropriate weighting factor A_s for each sublayer, the stress (τ_{u_o}) at the material point corresponding to logarithmic strain (ε_u^{*}) may be expressed as:

$$\tau_{u_o} = \sum_{s=1}^{n} A_s\,{}^{s}(\tau_{u_o}) \tag{3.62}$$

where the uniaxial weighting factor A_s for the sth sublayer may readily be confirmed to be:

$$\boxed{A_s = \frac{E_s^T - E_{s+1}^T}{E}} \tag{3.63}$$

where

$$E_1^T = E \qquad \text{(Young's modulus of the material)}$$

$$E_s^T = \frac{{}^{s}\tau_{u_o} - {}^{s-1}\tau_{u_o}}{{}^{s}\varepsilon_u^{*} - {}^{s-1}\varepsilon_u^{*}} \qquad (s = 2, 3, \ldots, n)$$

$$E_{n+1}^T = 0$$

The elastic perfectly-plastic and the elastic linear strain-hardening constitutive relations may be treated as special cases. In the case of

[+] As previously mentioned this assumption is not necessary; by employing different elastic moduli ${}^{s}E$, more complicated material behavior can be represented.

elastic perfectly-plastic behavior, there is only one sublayer; in the case of linear strain-hardening material there are two sublayers and the limit of the second sublayer is taken sufficiently high so that the deformation in that sublayer remains elastic. However, the main advantage of the mechanical-sublayer method is realized if three or more sublayers are utilized, since with proper adjustment of the yield stresses ${}^{s}(\tau_{u_0})^{y}$ of the sublayers, complex material behavior can be represented, including elastic-plastic unloading, the Bauschinger effect, and hysteresis; see Fig. 2c.

For a strain-rate dependent, elastic strain-hardening material, the rate dependence is described by+:

$$ {}^{s}(\tau_u)^{y} = {}^{s}(\tau_{u_0})^{y}\left(1 + \left|\frac{D_u}{d}\right|^{\frac{1}{p}}\right) \tag{3.64} $$

where D_u is the uniaxial component of the rate-of-deformation tensor:

$$ D_u = \frac{\dot{\ell}}{\ell} = \dot{\varepsilon}_u^{*} = \frac{\dot{E}_u}{(1+E_u)} \tag{3.65} $$

that is equal to the material rate of the logarithmic strain ε_u^{*}, as previously shown in Eq. 2.405, and ${}^{s}(\tau_u)^{y}$ is the strain-rate dependent yield stress of sublayer s.

Equation 3.65 is the Cowper-Symonds strain-rate equation developed in 1957 [139] at Brown University to represent the strain-rate effect on the uniaxial stress-strain response of metals. The material strain-rate constants d and p are obtained from experiments. When the material strain-rate constants d and p are chosen to be equal for each sublayer, the stress-strain curve at a given deformation rate $\dot{\varepsilon}_u^{*}$ is simply a constant magnification of the static stress-strain curve along rays emanating from the Kirchhoff stress versus logarithmic strain origin (see Fig. 3).

3.3.4.2 Application to Multiaxial Stress-Strain Conditions

Generally, a somewhat different description for the mechanical-sublayer model is needed when multiaxial stress-strain conditions occur. Fowler [140] has derived the weighting coefficients based on a biaxial stress state using expressions given by Pian [141] in 1966. In

+As previously mentioned the material strain-rate constants d and p, can be assumed to be different for each sublayer s, thereby representing very complicated strain-rate material behavior.

1974 Stalk [142] derived the weighting coefficients based on a triaxial stress state.

Both Fowler and Stalk concluded that the differences between the stress-strain diagrams obtained from the weighting coefficients based on a uniaxial state of stress-strain and the diagrams obtained from the coefficients based on a multiaxial state were very small. Fowler [140] concluded "the error resulting from this difference, certainly, should be smaller than that resulting from the use of a straight-line-segment approximation of the stress-strain curve, ... it is concluded that the use of the uniaxial model weights in a biaxial model does not lead to any significant errors". Stalk [141] concluded that the errors introduced by using the one-dimensional weights for three-dimensional stress states is of the order of 1 to 4 per cent in the sublayer weights.

More recently, Hunsaker et al. [143] discussed the calculation of the sublayer weights when multiaxial states of stress are present. No comparisons of stress-strain curves produced from weighting coefficients based on uniaxial and multiaxial states are shown, or even discussed. However, Hunsaker [144] obtained a closed-form solution for the case of a two sublayer (linear strain hardening) model. The example shown by Hunsaker [143]shows differences between the uniaxial and multiaxial procedures which are of the order of the typical experimental errors in the determination of the material properties.

Besseling [97] in 1953 had already obtained a closed form solution of the sublayer properties (for <u>any</u> number of sublayers) for a general state of stress-strain. It is easy to show that (when only two sublayers are present), Hunsaker's closed-form solution coincides with Besseling's formula.

One can readily show, that upon replacing the deviatoric strains and stresses by the total strains and stresses, Besseling's formulae become:

$$
{}^{s}\left(\tau_{u_o}^{y}\right) = E\,{}^{s}(\epsilon_u^*) + \frac{E}{(1+\nu)}\left(\frac{1}{2}-\nu\right)\sum_{j=1}^{s}\left(1-\frac{E_j^T}{E}\right)\left[{}^{j}(\epsilon_u^*) - {}^{j-1}(\epsilon_u^*)\right] \tag{3.66a}
$$

$$
A_s = 1 - \frac{\frac{2}{3}(1+\nu)}{\frac{E}{E_{s+1}^T} - \frac{2}{3}\left(\frac{1}{2}-\nu\right)} - \sum_{j=1}^{s-1} A_j \tag{3.66b}
$$

It is easily seen from these equations, that for $\nu = 1/2$ (i.e., assuming elastic incompressibility), the sublayer properties become identical with those derived from uniaxial stress-strain conditions (Eqs. 3.61 and 3.63). Also, it is interesting to note that the difference between the sublayer properties derived from uniaxial (Eqs. 3.61 and 3.63) and multiaxial (Eqs. 3.66a and 3.66b) conditions is directly related to the factor $(\frac{1}{2} - \nu)$, which expresses the difference between the elastic[+] (ν) and plastic (assumed to be equal to 1/2 in the analysis) Poisson's ratios. Moreover, in the present analysis for beams, plates, and shells, incompressibility[++] is assumed in calculating the changes in thickness; hence, the calculation of sublayer properties from the uniaxial procedure (Eqs. 3.61 and 3.63) is consistent (under the incompressibility assumption) for the plate (and beam) FE calculations of this report.

3.3.5 Comments on Strain-Rate Behavior Modeling

Because of physical as well as theoretical reasons (as indicated, for example, by Perzyna [145-152]), the plastic strain rate rather than the total strain rate should govern the dynamic (non-stationary) yield condition (Eq. 3.45) if the initial yield condition is to remain the

---

[+] The elastic ν is to be used in Eqs. 3.66a and 3.66b. Note that these equations hold for $s > 1$; for $s = 1$, only the first term of Eq. 3.66a and only the first two terms of Eq. 3.66b apply.

[++] Both for plastic and elastic strains, since the elastic strains are assumed to be small.

same as in plasticity theory. In order to relate the equation for the dynamical yield condition of this work with the equations of Perzyna [147], it is convenient to express Eq. 3.49 in terms of the following invariants:

$$ {}^{s}J_2 = \frac{1}{2}\, {}^{s}\bar{\bar{\tau}}^{D} : {}^{s}\bar{\bar{\tau}}^{D} = \frac{1}{2} \left({}^{s}\tau^{D}\right)^{I}_{J} \left({}^{s}\tau^{D}\right)^{J}_{I} \tag{3.67} $$

$$ I_2^{D} = \frac{1}{2}\, \bar{\bar{D}}^{D} : \bar{\bar{D}}^{D} = \frac{1}{2} \left(D^{D}\right)^{I}_{J} \left(D^{D}\right)^{J}_{I} \tag{3.68} $$

and the yield stress in shear, defined as:

$$ {}^{s}k_o = \frac{{}^{s}\tau^{Y}_{u_o}}{\sqrt{3}} \quad \text{or} \quad \left({}^{s}k_o\right)^2 = \frac{\left({}^{s}\tau^{Y}_{u_o}\right)^2}{3} \tag{3.69} $$

Then, from Eq. 3.49+

$$ {}^{s}\bar{\bar{\tau}}^{D} : {}^{s}\bar{\bar{\tau}}^{D} = 2\, {}^{s}J_2 = \frac{2}{3} \left({}^{s}\tau^{Y}_{u_o}\right)^2 \left[1 + \left(\frac{\sqrt{\frac{3}{2}\left(\bar{\bar{D}}^{D} : \bar{\bar{D}}^{D}\right)}}{{}^{s}d} \right)^{\frac{1}{{}^{s}\alpha}} \right]^2 \tag{3.70} $$

$$ {}^{s}J_2 = \left({}^{s}k_o\right)^2 \left[1 + \left(\frac{\sqrt{I_2^{D}}}{{}^{s}d/\sqrt{3}} \right)^{\frac{1}{{}^{s}\alpha}} \right]^2 \tag{3.71} $$

or

$$ \sqrt{{}^{s}J_2} = {}^{s}k_o \left[1 + \left(\frac{\sqrt{I_2^{D}}}{{}^{s}\gamma} \right)^{\frac{1}{{}^{s}\alpha}} \right] \tag{3.72} $$

which would be identical with Eq. 2.68 of Perzyna [147] if the second invariant of the <u>plastic</u> strain rate

$$ {}^{s}I_2^{p} \equiv \frac{1}{2}\, {}^{s}\bar{\bar{D}}^{p} : {}^{s}\bar{\bar{D}}^{p} = \frac{1}{2} \left({}^{s}D^{p}\right)^{I}_{J} \left({}^{s}D^{p}\right)^{J}_{I} \tag{3.72a} $$

+Since superscript "p" is used here to denote plastic components, the strain-rate constant ${}^{s}p$ for sublayer "s" (see Eq. 3.49) is replaced only in Subsection 3.3.5 by the symbol ${}^{s}\alpha$ to avoid confusion.

were used instead of the second invariant of the deviatoric strain rate I_2^D. Also observe, that the relation between the viscosity coefficient in simple tension ${}^s d$ and the viscosity coefficient in shear ${}^s\gamma$ is the same as the relation between the yield stress in tension and in shear (compare with Eq. 3.69):

$$ {}^s\gamma = \frac{{}^s d}{\sqrt{3}} \tag{3.73}$$

The equation [3.52] for the scalar factor of proportionality ${}^s\dot{\lambda}$ relating the plastic strain rate to the deviatoric stress:

$$ {}^s\bar{\bar{D}}^p = {}^s\dot{\lambda}\; {}^s\bar{\bar{\tau}}^D \tag{3.74}$$

can also be related to the equations of Perzyna [147], by expressing the dissipated (viscoplastic) work per unit mass as:

$$ {}^s\dot{U}^p = \frac{1}{\rho_o}\, {}^s\bar{\bar{\tau}}^D : {}^s\bar{\bar{D}}^p = \frac{2}{\rho_o}\sqrt{{}^sJ_2}\;\sqrt{{}^sI_2^p} \tag{3.75}$$

Then, using Eqs. 3.75, 3.72, 3.69, and 3.52, one obtains

$$ {}^s\dot{\lambda} = \frac{\rho_o \frac{2}{\rho_o}\sqrt{{}^sJ_2}\;\sqrt{{}^sI_2^p}}{\frac{2}{3}\,3\left({}^sk_o\right)^2 \frac{\sqrt{{}^sJ_2}}{{}^sk_o}\left[1+\left(\frac{\sqrt{I_2^p}}{{}^s\gamma}\right)^{\frac{1}{{}^s\alpha}}\right]} \tag{3.76}$$

or

$$ {}^s\dot{\lambda} = \frac{\sqrt{{}^sI_2^p}}{{}^sk_o}\left[1+\left(\frac{\sqrt{I_2^D}}{{}^s\gamma}\right)^{\frac{1}{{}^s\alpha}}\right]^{-1} \tag{3.77}$$

which is identical with Eq. 2.77 of Perzyna [147] if I_2^D is replaced by ${}^sI_2^p$.

The strain rate equation+

$$ \frac{\tau_u}{\tau_{u_o}^Y} = 1 + \left|\frac{\dot{\varepsilon}_u^*}{d}\right|^{\frac{1}{\alpha}} \tag{3.78}$$

+This equation applies only for $(\dot{\varepsilon}_u^*)^p \neq 0$; then, $\tau_u = \tau_u^Y > \tau_{u_o}^Y$.

used in the present work can represent secondary creep, since for constant stress

$$\dot{\tau}_u = 0 \tag{3.79}$$

the elastic strain rate is zero:

$$\left(\dot{\epsilon}_u^*\right)^e = \frac{\dot{\tau}_u}{E} = 0 \tag{3.80}$$

Hence, the total strain rate is equal to the plastic strain rate

$$\dot{\epsilon}_u^* = \left(\dot{\epsilon}_u^*\right)^e + \left(\dot{\epsilon}_u^*\right)^p = \left(\dot{\epsilon}_u^*\right)^p \tag{3.81}$$

Thus, Eq. 3.78 can be expressed as

$$\left(\dot{\epsilon}_u^*\right)^p = d\left|\frac{\tau_u}{\tau_{u_o}^y} - 1\right|^\alpha \tag{3.82}$$

which is the power law (also known as Norton's law) of secondary creep.[+] However, the strain rate equation used in the present work cannot represent relaxation effects. In effect, for relaxation, the total strain rate is zero:

$$\dot{\epsilon}_u^* = 0 \tag{3.83}$$

and Eq. 3.78 expresses the condition that the stress τ_u relaxes instantaneously to the static yield stress $\tau_{u_o}^y$

$$\tau_u = \tau_{u_o}^y \quad \text{for} \quad \dot{\epsilon}_u^* = 0 \tag{3.84}$$

However, if the plastic strain rate $(\dot{\epsilon}_u^*)^p$ rather than the total strain rate $\dot{\epsilon}_u^*$ were used in Eq. 3.78,

[+]However, secondary creep is present only for $\tau_u > \tau_{u_o}^y$. Also, d and α are temperature dependent.

$$\frac{\tau_u}{\tau_{u_o}^y} = 1 + \left| \frac{(\dot{\epsilon}_u^*)^p}{d} \right|^{\frac{1}{\alpha}} \tag{3.85}$$

Then, for relaxation:

$$\dot{\epsilon}_u^* = 0 = \frac{\dot{\tau}_u}{E} + d \left| \frac{\tau_u}{\tau_{u_o}^y} - 1 \right|^{\alpha} \tag{3.86}$$

For example, this equation can be solved for $\alpha = 1$, yielding an exponential relaxation:

$$\tau_u = \bar{\tau}_u \, e^{-\frac{t}{R}} + \tau_{u_o}^y \tag{3.87}$$

where the relaxation constant R is

$$R = \frac{\tau_{u_o}^y}{E\,d} \tag{3.88}$$

If many sublayers are present rather than one, it can be shown that creep recovery, and primary as well as secondary creep, can be represented by Eq. 3.85.

Only total strain rates (rather than plastic strain rates) are usually measured in strain rate tests; therefore, it is necessary to assume that the elastic strain rates are small in those experiments, as indicated by Campbell (page 52 of [153]), for example. When the material strain-rate constants d and p are chosen to be equal for each sublayer, the present mechanical sublayer model produces as a result stress-strain curves at a given strain rate that are simply a constant magnification of the static (rate-independent) stress-strain curve along rays emanating from the origin of the Kirchhoff stress vs.

logarithmic strain curve. This is the behavior that was observed by MacGregor [154] and by Wulf [155] in a number of experiments, among others.

In any case, the difference between the total and the plastic strain rates can be deduced from the following argument for a uniaxial test:

$E_u = \dfrac{l - l_o}{l_o}$	relative elongation
$\varepsilon_u^* = \ln(1 + E_u)$	total uniaxial logarithmic strain
$\dot{\varepsilon}_u^* = \dfrac{d}{dt}(\varepsilon_u^*)$	material rate of ε_u^*
$(\dot{\varepsilon}_u^*)^e$, $(\dot{\varepsilon}_u^*)^p$	elastic and plastic parts of ε_u^*, respectively
$\tau_u = \dfrac{P}{A_o}(1 + E_u)$	uniaxial Kirchhoff stress
E	Young's (elastic) modulus

Decomposing the total strain rate $\dot{\varepsilon}_u^*$ into elastic and plastic parts:

$$\dot{\varepsilon}_u^* = (\dot{\varepsilon}_u^*)^e + (\dot{\varepsilon}_u^*)^p \tag{3.89}$$

where since

$$(\varepsilon_u^*)^e = \frac{1}{E}\,\tau_u \tag{3.90}$$

the elastic strain rate $(\dot{\varepsilon}_u^*)^e$ is related to the stress as:

$$(\dot{\varepsilon}_u^*)^e = \frac{1}{E}\,\dot{\tau}_u \tag{3.91}$$

one obtains

$$\dot{\varepsilon}^* = \frac{1}{E}\,\dot{\tau}_u + (\dot{\varepsilon}_u^*)^p \tag{3.92}$$

Hence, one can express the plastic-strain rate $(\dot{\varepsilon}_u^*)^p$ as

$$\begin{aligned}(\dot{\varepsilon}_u^*)^p &= \dot{\varepsilon}_u^* - \frac{1}{E}\,\dot{\tau}_u \\ &= \dot{\varepsilon}_u^* - \frac{1}{E}\,\frac{d\tau_u}{d\varepsilon_u^*}\,\dot{\varepsilon}_u^*\end{aligned} \tag{3.93}$$

Defining the tangent modulus E^T as

$$E^T = \frac{d\tau_u}{d\varepsilon_u^*} \tag{3.94}$$

one obtains

$$\boxed{(\dot{\varepsilon}_u^*)^p = \left(1 - \frac{E^T}{E}\right)\dot{\varepsilon}_u^*} \tag{3.95}$$

Since the tangent modulus $E^T = (d\tau_u)/(d\varepsilon_u^*)$ of the Kirchhoff stress τ_u versus logarithmic strain ε_u^* curve is small for most metals, the quantity $E^T/E = (d\tau_u/d\varepsilon_u^*)/E$ is small compared with unity. For example, the calculations in the present work have been carried out with the following materials:

<u>For 6061-T651 aluminum:</u>

$$\left.\begin{aligned} \frac{E^T}{E} &= \frac{1}{E}\frac{d\tau_u}{d\varepsilon_u^*} = 0.00699 \\ (\dot{\varepsilon}_u^*)^p &= 0.993\,\dot{\varepsilon}_u^* \end{aligned}\right\} \quad \text{for} \quad .0044 < \varepsilon_u^* < .076$$

$$\left.\begin{aligned} \frac{E^T}{E} &= \frac{1}{E}\frac{d\tau_u}{d\varepsilon_u^*} = 0.00505 \\ (\dot{\varepsilon}_u^*)^p &= 0.995\,\dot{\varepsilon}_u^* \end{aligned}\right\} \quad \text{for} \quad .076 < \varepsilon_u^* < .615$$

Therefore, for 6061-T651 aluminum, the relative difference $\dfrac{\dot{\varepsilon}_u^* - (\dot{\varepsilon}_u^*)^p}{\dot{\varepsilon}_u^*}$ between the total strain rate and the plastic strain rate is less than 0.7%.

<u>For National Forge 4130 cast steel:</u>

$$\left.\begin{aligned} \frac{E^T}{E} &= \frac{1}{E}\frac{d\tau_u}{d\varepsilon_u^*} = 0.04069 \\ (\dot{\varepsilon}_u^*)^p &= 0.959\,\dot{\varepsilon}_u^* \end{aligned}\right\} \quad \text{for} \quad .00289 < \varepsilon_u^* < .0225$$

$$\left.\frac{E^T}{E} = \frac{1}{E}\frac{d\tau_u}{d\varepsilon_u^*} = 0.00961 \;,\; (\dot{\varepsilon}_u^*)^p = 0.990\,\dot{\varepsilon}_u^* \right\} \text{for } .0225 < \varepsilon_u^* < .06$$

$$\left.\begin{aligned} \frac{E^T}{E} &= \frac{1}{E}\,\frac{d\tau_u}{d\varepsilon_u^*} = 0.00378 \\ (\dot{\varepsilon}_u^*)^p &= 0.996\,\dot{\varepsilon}_u^* \end{aligned}\right\} \text{for} \qquad .060 < \varepsilon_u^* < .557$$

Hence, for this National Forge 4130 cast steel, the relative difference between the total and plastic strain rates is 4% for strains smaller than 2%, and the difference is less than 1% for strains larger than 2%. The experimental error in the calculation of total strain rates in strain-rate experiments is of the same or larger order than the difference between the plastic and total strain rates.

SECTION 4

CURVED BEAMS AND RINGS

4.1 Introduction

Section 4 deals with the strain-displacement equations and the constitutive equations used for the numerical analysis of curved beams and rings.

These strain-displacement relations for finite strains and rotations also take into account thickness change and seem to be "new" (not found in the literature). The decomposition of the total strain into a "membrane" and a "bending" part is discussed, and it is seen to be dependent on the definition of the strain measure. Also, the decomposition of the deformation gradient into a rotation and a pure stretch is shown for illustrative purposes. Equivalent equations for "small membrane strains" are displayed. Finally, the constitutive equations for curved beams are shown together with the corresponding incremental procedure which can be used in solving the equations of motion stepwise in small increments Δt in time.

4.2 Strain-Displacement Relations for Finite Strains and Rotations

4.2.1 Strain-Displacement Relations for the Bernoulli-Euler Displacement Field

4.2.1.1 Formulation

The previous general results of Subsection 2.4 for the kinematics of a deformable medium are specialized to the case of a curved beam, as pictured in Figs. 4a and 4b, with the following definitions:

- **Fixed-in-Space System** (Inertial)
  - Rectangular Cartesian Coordinates
    - Reference Configuration ($t = t_o$): x_1, x_2, x_3
    - Present Configuration ($t = t$): X_1, X_2, X_3
  - Base Vectors: $\bar{\iota}_1$, $\bar{\iota}_2$, $\bar{\iota}_3$
- **Body-Fixed System** (Convected, Intrinsic or Embedded)
  - Curvilinear Coordinates: $\xi \equiv \xi^1$, $\eta \equiv \xi^2$, $\zeta^o \equiv \xi^3$
  - Base Vectors
    - Reference Configuration ($t = t_o$): $\bar{g}_1$, $\bar{g}_2$, $\bar{n} \equiv \bar{g}_3$
    - Present Configuration ($t = t$): $\bar{G}_1$, $\bar{G}_2$, $\lambda^* \bar{N} = \bar{G}_3$

The coordinate $\eta \equiv \xi^2$ defines the (curvilinear) reference axis of the curved beam and $\zeta^o \equiv \xi^3$ measures the distance along an outwardly-directed normal to η. All deformations take place in the η, ζ^o two-dimensional plane.

For the body-fixed convected system, the base vectors $\bar{g}_i$ and $\bar{G}_I$ are functions of the coordinates η and ζ^o, and the $\bar{G}_I$ are also functions of time t:

$$\bar{g}_2 = \bar{g}_2(\eta, \zeta^o; t_o); \quad \bar{G}_2 = \bar{G}_2(\eta, \zeta^o; t) \tag{4.1}$$

The base vectors of the body-fixed convected system at the reference curvilinear axis η (that is, at $\zeta^{o} = 0$) are given special names:

$$\bar{a}_2 \equiv \bar{g}_2(\eta, \zeta^{\circ}=0) = \bar{a}_2(\eta)$$

$$\bar{A}_2 \equiv \bar{G}_2(\eta, \zeta^{\circ}=0, t) = \bar{A}_2(\eta, t) \tag{4.2}$$

The base vectors associated with the coordinate $\zeta^{o} \equiv \xi^{3}$ are:

$$\bar{n} \equiv \bar{g}_3 \qquad\qquad \lambda^{*}\bar{N} = \bar{G}_3 \tag{4.3}$$

Here, $\bar{n}$ is the unit normal vector to $\bar{a}_2$ in the reference configuration and $\bar{N}$ is the unit normal vector to $\bar{A}_2$ in the <u>present</u> configuration. Since they are unit vectors, they are only a function of the coordinate η:

$$\bar{n} = \bar{n}(\eta) \qquad\qquad \bar{N} = \bar{N}(\eta, t) \tag{4.4}$$

The quantity λ^{*} is a parameter that is associated with the thickness change of the curved beam, and hence is a function of ζ^{o} as well as η:

$$\lambda^{*} = \lambda^{*}(\eta, \zeta^{\circ}, t) \tag{4.5}$$

Hence

$$\bar{G}_3 = \lambda^{*}(\eta, \zeta^{\circ}, t)\,\bar{N}(\eta, t) = \bar{G}_3(\eta, \zeta^{\circ}, t)$$

$$\bar{g}_3 = \bar{n}(\eta) = \bar{g}_3(\eta) \tag{4.6}$$

Any point in the reference configuration of the curved beam is located by the position vector $\bar{r}_o$ to the reference axis η and the unit vector $\bar{n}$ normal to the reference axis η in the form:

$$\bar{r} = \bar{r}_o + \zeta^{\circ}\bar{n} \tag{4.7}$$

Any point in the present (deformed) configuration of the curved beam is located by the position vector $\bar{R}_o$ to the reference axis η and the vector $\bar{G}_3 = \lambda^{*}\bar{N}$ normal to the reference axis η in the form:

$$\bar{R} = \bar{R}_o + \zeta^{\circ}\lambda\bar{N} \tag{4.8}$$

The base vector $\bar{a}_2$ at the reference axis η (at $\zeta^o = 0$) in the reference configuration is the unit vector tangent to the reference axis coordinate η:

$$\bar{a}_2 = \frac{\partial \bar{r}_o}{\partial \xi^2} = \frac{\partial \bar{r}_o}{\partial \eta} \qquad a_{22} = \bar{a}_2 \cdot \bar{a}_2 = 1 = a^{22} \tag{4.9}$$

The base vector $\bar{A}_2$ at the reference axis η (at $\zeta^o = 0$) in the present configuration is:

$$\bar{A}_2 = \frac{\partial \bar{R}_o}{\partial \xi^2} = \frac{\partial \bar{R}_o}{\partial \eta} \tag{4.10}$$

and it is not (in general) a unit vector.

The covariant base vectors of the "curved beam space" in the reference configuration are:

$$\bar{g}_2 = \frac{\partial \bar{r}}{\partial \xi^2} = \frac{\partial \bar{r}}{\partial \eta} = \frac{\partial \bar{r}_o}{\partial \eta} + \zeta^o \frac{\partial \bar{n}}{\partial \eta} = \bar{a}_2 + \frac{\zeta^o}{R}\bar{a}_2 = \left(1 + \frac{\zeta^o}{R}\right)\bar{a}_2 \tag{4.11}$$

$$\bar{g}_3 = \frac{\partial \bar{r}}{\partial \xi^3} = \frac{\partial \bar{r}}{\partial \zeta^o} = \frac{\partial \bar{r}_o}{\partial \zeta^o} + \bar{n} = \bar{n}$$

where R is the radius of curvature in the reference configuration, taken here positive when the center of curvature lies in the negative direction of $\bar{n}$ (which is opposite in sign to that given in some books on tensors).

Note that:

$$\bar{a}_2 = \bar{g}_2 (\zeta^o = 0) \tag{4.12}$$

The (metric) tensor components of the unit tensor $\mathbf{I}$ in the convected coordinate system are:

$$g_{ij} = \bar{g}_i \cdot \bar{g}_j = \begin{Vmatrix} \left(1 + \frac{\zeta^o}{R}\right)^2 & 0 \\ 0 & 1 \end{Vmatrix} \tag{4.13}$$

$$g^{ij} = [g_{ij}]^{-1} = \left\| \begin{matrix} \dfrac{1}{\left(1+\dfrac{\zeta^\circ}{R}\right)^2} & 0 \\ 0 & 1 \end{matrix} \right\| \tag{4.14}$$

The displacement field at any point $\xi^2 = \eta$, $\xi^3 = \zeta^\circ$ in a curved beam can be expressed as follows (as depicted in Fig. 4b):

$$\bar{u}(\eta, \zeta^\circ) = \bar{u}_\circ(\eta) + \zeta^\circ\left[\lambda(\zeta^\circ; \eta)\bar{N}(\eta) - \bar{n}(\eta)\right] \tag{4.15}$$

where

$$\begin{aligned} \bar{u}_\circ &= \bar{R}_\circ - \bar{r}_\circ = \overset{\circ}{u}{}^2 \bar{a}_2 + \overset{\circ}{u}{}^3 \bar{n} \\ \bar{u} &= \bar{R} - \bar{r} \end{aligned} \tag{4.16}$$

or defining $v \equiv \overset{\circ}{u}{}^2$ and $w \equiv \overset{\circ}{u}{}^3$, one may write

$$\bar{u}_\circ = v\,\bar{a}_2 + w\,\bar{n} \tag{4.17}$$

In the case of no extension of the normals (no thinning or thickening of the beam):

$$\lambda = \lambda^* = 1 \tag{4.18}$$

Accordingly, one obtains a "Kirchhoff" or "Bernoulli-Euler" displacement field (see Fig. 5):

$$\bar{u} = \bar{u}_\circ + \zeta^\circ(\bar{N} - \bar{n}) = v\,\bar{a}_2 + (w - \zeta^\circ)\bar{n} + \zeta^\circ \bar{N} \tag{4.19}$$

It can be shown that[+]:

$$\zeta^\circ \bar{N} = \frac{\zeta^\circ}{\overset{\circ}{U}{}^2_2}\left[(1+\chi)\bar{n} + (-\psi)\bar{a}_2\right] \tag{4.20}$$

[+]From geometrical considerations; in particular, it can be obtained from a specialization of Eq. 5.84 of Section 5.

where

$$\overset{\circ}{U}{}^2_2 = \sqrt{\overset{\circ}{C}{}^2_2} = \sqrt{1+2\overset{\circ}{\gamma}{}^2_2} \qquad (4.21)$$

$\overset{\circ}{U}{}^2_2$ = mixed component of the right stretch tensor at the reference axis $\eta(\zeta^o = 0)$

$\overset{\circ}{C}{}^2_2$ = mixed component of the Cauchy-Green tensor at the reference axis $\eta(\zeta^o = 0)$

$\overset{\circ}{\gamma}{}^2_2$ = mixed component of the Green strain tensor at the reference axis $\eta(\zeta^o = 0)$

$$\chi = \frac{\partial v}{\partial \eta} + \frac{w}{R} \qquad \psi = \frac{\partial w}{\partial \eta} - \frac{v}{R} \qquad (4.22)$$

Hence,

$$\begin{aligned} \bar{u} &= \left(v - \frac{\zeta^o}{\overset{\circ}{U}{}^2_2}\psi\right)\bar{a}_2 + \left[w + \frac{\zeta^o}{\overset{\circ}{U}{}^2_2}(1+\chi) - \zeta^o\right]\bar{n} \\ &= \tilde{v}\,\bar{a}_2 + \tilde{w}\,\bar{n} \end{aligned} \qquad (4.23)$$

Then, the deformation gradient tensor $\bar{\bar{F}}$ has the following components with respect to the base vectors of the reference configuration:

$$F^{i\cdot}_{\cdot j} = \begin{Vmatrix} (1+\chi)\left(1 + \frac{\zeta^o}{(\overset{\circ}{U}{}^2_2)^3}\mathcal{K}\right) & -\frac{\psi}{\overset{\circ}{U}{}^2_2} \\ \psi\left(1+\frac{\zeta^o}{(\overset{\circ}{U}{}^2_2)^3}\mathcal{K}\right) & \frac{(1+\chi)}{\overset{\circ}{U}{}^2_2} \end{Vmatrix} \qquad (4.24)$$

$$= \begin{Vmatrix} F^{2\cdot}_{\cdot 2} & F^{2\cdot}_{\cdot 3} \\ F^{3\cdot}_{\cdot 2} & F^{3\cdot}_{\cdot 3} \end{Vmatrix} \qquad (4.25)$$

where

$$\boxed{\mathcal{K} = \left(-\frac{\partial \psi}{\partial \eta}\right)(1+\chi) + \frac{\partial \chi}{\partial \eta}\psi} \qquad (4.26)$$

From Eq. 4.24 and Eq. 2.132, the right Cauchy-Green deformation tensor components C^i_j in the body fixed coordinate system in the reference configuration can be obtained as follows:

$$\bar{\bar{C}} = \bar{\bar{F}}^T \cdot \bar{\bar{F}}$$

$$C^{i}_{j} = (F^{\cdot i}_{\cdot k})^T F^{k \cdot}_{\cdot j} = \begin{Vmatrix} (1+\chi)\left(1+\frac{\zeta^o}{(\overset{o}{U}{}^2_2)^3}K\right) & \psi\left(1+\frac{\zeta^o}{(\overset{o}{U}{}^2_2)^3}K\right) \\ -\frac{\psi}{\overset{o}{U}{}^2_2} & \frac{(1+\chi)}{\overset{o}{U}{}^2_2} \end{Vmatrix} \begin{Vmatrix} (1+\chi)\left(1+\frac{\zeta^o}{(\overset{o}{U}{}^2_2)^3}K\right) & -\frac{\psi}{\overset{o}{U}{}^2_2} \\ \psi\left(1+\frac{\zeta^o}{(\overset{o}{U}{}^2_2)^3}K\right) & \frac{1+\chi}{\overset{o}{U}{}^2_2} \end{Vmatrix} \tag{4.27}$$

which reduces to

$$C^{i}_{j} = \begin{Vmatrix} \left[(1+\chi)^2+\psi^2\right]\left[1+\frac{\zeta^o}{(\overset{o}{U}{}^2_2)^3}K\right]^2 & 0 \\ 0 & \frac{\psi^2+(1+\chi)^2}{(\overset{o}{U}{}^2_2)^2} \end{Vmatrix} \tag{4.28}$$

Hence, the right Cauchy-Green deformation tensor mixed components at the reference axis η (at $\zeta^o = 0$) are:

$$\overset{o}{C}{}^2_2 \equiv C^2_2(\eta, \zeta^o = 0) = (1+\chi)^2 + \psi^2 \tag{4.29}$$

Also, note that

$$\overset{o}{C}{}^2_2 = (\overset{o}{U}{}^2_2)^2 \tag{4.30}$$

Placing Eq. 4.30 into Eq. 4.28, one can express the mixed components C^i_j of the right Cauchy-Green deformation tensor anywhere in the curved beam space η, ζ^o in terms of the mixed component $\overset{o}{C}{}^i_j$ at the reference axis ($\zeta^o = 0$), the "curvature" κ, and the normal coordinate ζ^o:

$$C^i_j = \begin{Vmatrix} \overset{o}{C}{}^2_2 \left[1 + \dfrac{\zeta^o}{(\overset{o}{C}{}^2_2)^{3/2}} \kappa\right]^2 & 0 \\ 0 & 1 \end{Vmatrix} \tag{4.31}$$

The classical Green (Lagrangian) strain tensor $\overline{\overline{\gamma}}$ can be obtained readily from the right Cauchy-Green deformation tensor (Eqs. 2.136 and 2.140):

$$\overline{\overline{\gamma}} = \frac{1}{2}\left(\overline{\overline{C}} - \overline{\overline{1}}\right)$$

$$\gamma^i_j = \frac{1}{2}\left(C^i_j - \delta^i_j\right)$$

$$\gamma^i_j = \begin{Vmatrix} \dfrac{1}{2}\left(\overset{o}{C}{}^2_2 \left[1 + \dfrac{\zeta^o}{(\overset{o}{C}{}^2_2)^{3/2}} \kappa\right]^2 - 1\right) & 0 \\ 0 & 0 \end{Vmatrix} \tag{4.32}$$

or, using Eq. 4.21, namely $\overset{o}{\gamma}{}^2_2 = \frac{1}{2}(\overset{o}{C}{}^2_2 - 1)$, then

$$\boxed{\gamma^i_j = \begin{Vmatrix} \left(\overset{o}{\gamma}{}^2_2 + \dfrac{\zeta^o}{\sqrt{1 + 2\overset{o}{\gamma}{}^2_2}} \kappa + \dfrac{(\zeta^o)^2 \kappa^2}{(1 + 2\overset{o}{\gamma}{}^2_2)^2}\right) & 0 \\ 0 & 0 \end{Vmatrix}} \tag{4.33}$$

where the Green strain component at the reference axis $\eta(\zeta^o=0$ superscript "o"), or the membrane strain component is

$$\boxed{\overset{o}{\gamma}{}^2_2 = \chi + \frac{1}{2}\psi^2 + \frac{1}{2}\chi^2} \tag{4.34}$$

4.2.1.2 Membrane, Bending, and Polar Decompositions

No assumptions as far as the magnitude of the strains or rotations have been made in Eq. 4.33. One can decompose Eq. 4.33 additively as follows:

$$\boxed{\underbrace{\gamma^2_2 = \overset{o}{\gamma}{}^2_2}_{\text{"MEMBRANE"}} + \underbrace{\frac{\zeta^o K}{\sqrt{1+2\overset{o}{\gamma}{}^2_2}}\left[1+\zeta^o\frac{K}{(1+2\overset{o}{\gamma}{}^2_2)^{3/2}}\right]}_{\text{"BENDING"="CHANGE OF CURVATURE"}}} \tag{4.35}$$

Otherwise, one can apply a multiplicative decomposition of the deformation gradient tensor into a "membrane" part (defined at $\zeta^o = 0$ and denoted by the superscript "o") and a "bending" part (denoted by the over script "κ"):

$$F^{i}_{\cdot j} = \overset{o}{F}{}^{i}_{\cdot k}\,\overset{K}{F}{}^{k}_{\cdot j} = \underbrace{\begin{Vmatrix} (1+\chi) & -\dfrac{\psi}{\overset{o}{\mathfrak{U}}{}^2_2} \\ \psi & \dfrac{(1+\chi)}{\overset{o}{\mathfrak{U}}{}^2_2} \end{Vmatrix}}_{\text{"MEMBRANE"}} \underbrace{\begin{Vmatrix} \left(1+\dfrac{\zeta^o}{(\overset{o}{\mathfrak{U}}{}^2_2)^3}K\right) & 0 \\ 0 & 1 \end{Vmatrix}}_{\text{"BENDING"}} \tag{4.36}$$

Hence, the "membrane" right Cauchy-Green deformation tensor component $\overset{o}{C}{}^i_j$ is:

$$\overset{o}{C}{}^{i}_{j} = \left(\overset{o}{F}{}^{i}_{\cdot k}\right)^{T} \left(\overset{o}{F}{}^{k}_{\cdot j}\right) = \begin{Vmatrix} (1+\chi) & \psi \\ -\dfrac{\psi}{\overset{o}{u}{}^{2}_{2}} & \dfrac{(1+\chi)}{\overset{o}{u}{}^{2}_{2}} \end{Vmatrix} \begin{Vmatrix} (1+\chi) & -\dfrac{\psi}{\overset{o}{u}{}^{2}_{2}} \\ \psi & \dfrac{(1+\chi)}{\overset{o}{u}{}^{2}_{2}} \end{Vmatrix} \tag{4.37}$$

or

$$\overset{o}{C}{}^{i}_{j} = \begin{Vmatrix} [(1+\chi)^2 + \psi]^2 & 0 \\ 0 & 1 \end{Vmatrix} = \underbrace{\begin{Vmatrix} \overset{o}{C}{}^{2}_{2} & 0 \\ 0 & 1 \end{Vmatrix}}_{\text{"MEMBRANE"}} \tag{4.38}$$

Similarly, the "bending" right Cauchy-Green deformation tensor component $\overset{K}{C}{}^{i}_{j}$ is:

$$\overset{K}{C}{}^{i}_{j} = \left(\overset{K}{F}{}^{i}_{\cdot k}\right)^{T} \overset{K}{F}{}^{k}_{\cdot j} = \begin{Vmatrix} \left(1 + \dfrac{\zeta^{o} K}{(\overset{o}{u}{}^{2}_{2})^{3}}\right) & 0 \\ 0 & 1 \end{Vmatrix} \begin{Vmatrix} \left(1 + \dfrac{\zeta^{o} K}{(\overset{o}{u}{}^{2}_{2})^{3}}\right) & 0 \\ 0 & 1 \end{Vmatrix} \tag{4.39}$$

or

$$\overset{K}{C}{}^{i}_{j} = \underbrace{\begin{Vmatrix} \left(1 + \dfrac{\zeta^{o}}{(\overset{o}{C}{}^{2}_{2})^{3/2}} K\right)^{2} & 0 \\ 0 & 1 \end{Vmatrix}}_{\text{"BENDING"}} \tag{4.40}$$

Thus, in accordance with Eq. 4.31

$$\boxed{C^i_j = \overset{\circ}{C}{}^i_k \, C^k_j = \underbrace{\begin{Vmatrix} [(1+\chi)^2+\psi^2] & 0 \\ 0 & 1 \end{Vmatrix}}_{\text{"MEMBRANE"}} \underbrace{\begin{Vmatrix} \left(1+\dfrac{z^0}{(\overset{\circ}{C}{}^2_2)^{3/2}} K\right)^2 & 0 \\ 0 & 1 \end{Vmatrix}}_{\text{"BENDING"}}} \tag{4.41}$$

From the polar decomposition of the deformation gradient tensor, one can obtain expressions for the displacement gradients χ and ψ in terms of (1) a rotation angle θ from the reference configuration and (2) a stretch, (see Eq. 2.122):

$$\overset{\circ}{F}{}^{i}_{\cdot j} = R^{i}_{\cdot k} \, \overset{\circ}{U}{}^k_j \tag{4.42}$$

or, in matrix form, Eq. 4.42 becomes

$$\underbrace{\begin{Vmatrix} (1+\chi) & -\dfrac{\psi}{\overset{\circ}{U}{}^2_2} \\ \psi & \dfrac{(1+\chi)}{\overset{\circ}{U}{}^2_2} \end{Vmatrix}}_{\text{DEFORMATION GRADIENT}} = \underbrace{\begin{Vmatrix} \cos\theta & -\sin\theta \\ \sin\theta & \cos\theta \end{Vmatrix}}_{\text{ROTATION}} \underbrace{\begin{Vmatrix} \overset{\circ}{U}{}^2_2 & 0 \\ 0 & 1 \end{Vmatrix}}_{\text{STRETCH}} \tag{4.43}$$

which shows that:

$$(1+\chi) = \overset{\circ}{U}{}^2_2 \cos\theta \tag{4.44}$$

$$\psi = \overset{\circ}{U}{}^2_2 \sin\theta \tag{4.45}$$

These relations are very important in the finite element analysis since χ and ψ are used: (1) as some of the degrees of freedom of each finite element and (2) in the strain-displacement relations. It is seen from Eqs. 4.44 and 4.45 that <u>both</u> χ and ψ are related to the stretch <u>and</u> to the rotation.

Observe, that <u>for "small rotations"</u>:*

$$\cos\theta \approx 1 \qquad \sin\theta \approx \theta \tag{4.46}$$

and, <u>for "small membrane strains"</u>:*

$$\overset{\circ}{\tilde{E}}{}^2_2 < 1 \qquad \overset{\circ}{U}{}^2_2 = 1 + \overset{\circ}{\tilde{E}}{}^2_2 = \sqrt{1+2\overset{\circ}{\gamma}{}^2_2} \approx 1 \tag{4.47}$$

Hence, one obtains

$$\chi \approx \overset{\circ}{\tilde{E}}{}^2_2 \quad \text{"relative elongation"} \qquad \psi \approx \theta \quad \text{"rotation"} \tag{4.48}$$

This indicates that the displacement gradient χ is approximately the relative elongation, and the displacement gradient ψ is approximately the rotation angle θ <u>only for small strains and small rotations</u>. Observe, however, that for finite rotations, <u>both</u> χ and ψ are related to the strains <u>and</u> rotations. Also, note that one can obtain Eqs. 4.44 and 4.45 from geometrical arguments as indicated, for example, in Fig. 5 and the following observations:

$$\overset{\circ}{U}{}^2_2 = 1 + \overset{\circ}{\tilde{E}}{}^2_2 \quad \text{"membrane" right stretch} \tag{4.49}$$

$$\Delta s = \overset{\circ}{U}{}^2_2\, \Delta\eta \tag{4.50}$$

---

*Here, the precise meaning of "small" rotations and "small" strains is made clear in this context.

The Bernoulli-Euler-Kirchhoff displacement field may be expressed as:

$$\tilde{V} = V - \zeta_i^{\circ} \sin\theta \tag{4.51}$$

$$\tilde{W} = W - \zeta_i^{\circ}(1 - \cos\theta) \tag{4.52}$$

$$\cos\theta = \lim_{\Delta s \to 0} \left(\frac{\Delta\eta + \Delta v}{\Delta s} \right) \tag{4.53}$$

$$\cos\theta = \lim_{\Delta\eta \to 0} \left(\frac{1}{\overset{\circ}{U}_2^2} \frac{\Delta\eta + \Delta v}{\Delta\eta} \right) = \frac{1}{\overset{\circ}{U}_2^2}\left(1 + \frac{\partial v}{\partial\eta}\right) \tag{4.54}$$

$$\sin\theta = \lim_{\Delta s \to 0} \left(\frac{\Delta w}{\Delta s} \right) \tag{4.55}$$

$$\sin\theta = \lim_{\Delta\eta \to 0} \left(\frac{1}{\overset{\circ}{U}_2^2} \frac{\Delta w}{\Delta\eta} \right) = \frac{1}{\overset{\circ}{U}_2^2} \frac{\partial w}{\partial\eta} \tag{4.56}$$

Hence, defining

$$\chi \equiv \frac{\partial v}{\partial\eta} \qquad \psi \equiv \frac{\partial w}{\partial\eta} \tag{4.57}$$

one obtains

$$\cos\theta = \frac{1}{\overset{\circ}{U}_2^2}(1 + \chi) \tag{4.58}$$

$$\sin\theta = \frac{1}{\overset{\circ}{U}_2^2}\psi \tag{4.59}$$

Thus, the Bernoulli-Euler-Kirchhoff displacement field becomes:

$$\tilde{v} = v - \zeta^{\circ} \frac{\psi}{\overset{\circ}{U}{}_2^2} \tag{4.60}$$

$$\tilde{w} = w + \zeta^{\circ} \frac{(1+\chi)}{\overset{\circ}{U}{}_2^2} - \zeta^{\circ} \tag{4.61}$$

which compares with Eq. 4.23.

At this point it is convenient to use Eqs. 4.44 and 4.45 to show that the expressions for the right Cauchy-Green deformation tensor component C_2^2 of Eq. 4.31 and the Green strain tensor component γ_2^2 of Eq. 4.35 <u>are, indeed, invariant under arbitrarily large rotations</u>.

For this, it suffices to show that the right Cauchy-Green deformation tensor component $\overset{\circ}{C}{}_2^2$ at the reference axis $\eta(\zeta^{\circ} = 0)$, and the "curvature" κ are invariants under rotation. From Eq. 4.29: $\overset{\circ}{C}{}_2^2 = (1 + \chi)^2 + \psi^2$. Placing Eqs. 4.44 and 4.45 into this expression, one obtains:

$$\overset{\circ}{C}{}_2^2 = \left(\overset{\circ}{U}{}_2^2 \cos\theta\right)^2 + \left(\overset{\circ}{U}{}_2^2 \sin\theta\right)^2 = \left(\overset{\circ}{U}{}_2^2\right)^2 \left(\cos^2\theta + \sin^2\theta\right)$$
$$= \left(\overset{\circ}{U}{}_2^2\right)^2 \tag{4.62}$$

which is an identity, from Eq. 4.21. Hence $\overset{\circ}{C}{}_2^2$ is <u>invariant under arbitrarily large rotations</u>. Next, from Eq. 4.26:

$$\kappa = \left(-\frac{\partial\psi}{\partial\eta}\right)(1+\chi) + \frac{\partial\chi}{\partial\eta}\psi \tag{4.63}$$

Placing Eqs. 4.44 and 4.45 into Eq. 4.63, one obtains:

$$\frac{\partial\psi}{\partial\eta} = \overset{\circ}{U}{}_2^2 \cos\theta \frac{\partial\theta}{\partial\eta} + \sin\theta \frac{\partial \overset{\circ}{U}{}_2^2}{\partial\eta} \tag{4.64}$$

$$\frac{\partial\chi}{\partial\eta} = -\overset{\circ}{U}{}_2^2 \sin\theta \frac{\partial\theta}{\partial\eta} + \cos\theta \frac{\partial \overset{\circ}{U}{}_2^2}{\partial\eta} \tag{4.65}$$

$$
\begin{aligned}
K &= -\left(\mathring{U}^2_2 \cos\theta \frac{\partial\theta}{\partial\eta} + \sin\theta \frac{\partial \mathring{U}^2_2}{\partial\eta}\right)\left(\mathring{U}^2_2 \cos\theta\right) \\
&\quad + \left(-\mathring{U}^2_2 \sin\theta \frac{\partial\theta}{\partial\eta} + \cos\theta \frac{\partial \mathring{U}^2_2}{\partial\eta}\right)\left(\mathring{U}^2_2 \sin\theta\right) \\
&= -\left(\mathring{U}^2_2\right)^2 \cos^2\theta \frac{\partial\theta}{\partial\eta} - \cancel{\mathring{U}^2_2 \sin\theta\cos\theta \frac{\partial \mathring{U}^2_2}{\partial\eta}} - \mathring{U}^2_2 \sin^2\theta \frac{\partial\theta}{\partial\eta} \\
&\quad + \cancel{\mathring{U}^2_2 \cos\theta \sin\theta \frac{\partial \mathring{U}^2_2}{\partial\eta}} \\
&= -\left(\mathring{U}^2_2\right)^2 \frac{\partial\theta}{\partial\eta}\left(\cos^2\theta + \sin^2\theta\right) = -\left(\mathring{U}^2_2\right) \frac{\partial\theta}{\partial\eta}
\end{aligned}
\tag{4.66}
$$

Equation 4.66 shows that the "curvature" expression $\underline{K}$ of Eq. 4.26 is <u>invariant under arbitrarily large rigid-body motions</u>.

It can also be shown that the expression

$$
K/\left(\mathring{U}^2_2\right)^3 \tag{4.67}
$$

appearing in the expressions for the deformation gradient tensor components of Eq. 4.24 and Eq. 4.36 and in the right Cauchy-Green deformation tensor, Eq. 4.31 and Eq. 4.40, is the <u>actual curvature</u>* $\partial\theta/\partial s$, as follows. Since

$$
\mathring{U}^2_2 = \frac{\partial s}{\partial\eta} \tag{4.68}
$$

and

$$
\frac{\partial\theta}{\partial\eta} = \mathring{U}^2_2 \frac{\partial\theta}{\partial s} \tag{4.69}
$$

---

*Here s is the "deformed" arc length (the arc length in the <u>present</u> configuration).

One finds from Eq. 4.66 that

$$K = -\left(\overset{\circ}{U}{}_2^2\right)^2 \frac{\partial\theta}{\partial\eta} = -\left(\overset{\circ}{U}{}_2^2\right)^3 \frac{\partial\theta}{\partial s} \tag{4.70}$$

Hence

$$\frac{\partial\theta}{\partial s} = -\frac{K}{\left(\overset{\circ}{U}{}_2^2\right)^3} = -\frac{K}{\left(\overset{\circ}{C}{}_2^2\right)^{3/2}} = -\frac{K}{\left(1+2\overset{\circ}{\gamma}{}_2^2\right)^{3/2}} \tag{4.71}$$

Therefore, one can express Eq. 4.36 as:

$$F^{i\cdot}_{\cdot j} = \underbrace{\begin{Vmatrix} (1+\chi) & -\dfrac{\psi}{\overset{\circ}{U}{}_2^2} \\ \psi & \dfrac{(1+\chi)}{\overset{\circ}{U}{}_2^2} \end{Vmatrix}}_{\text{"MEMBRANE"}} \underbrace{\begin{Vmatrix} \left(1-\zeta^\circ \dfrac{\partial\theta}{\partial s}\right) & 0 \\ 0 & 1 \end{Vmatrix}}_{\text{"BENDING"}} \tag{4.72}$$

Also, the expression for the right Cauchy-Green deformation tensor component C^i_j, Eq. 4.41, can be expressed as:

$$C^i_j = \underbrace{\begin{Vmatrix} \overset{\circ}{C}{}_2^2 & 0 \\ 0 & 1 \end{Vmatrix}}_{\text{"MEMBRANE"}} \underbrace{\begin{Vmatrix} \left(1-\zeta^\circ \dfrac{\partial\theta}{\partial s}\right)^2 & 0 \\ 0 & 1 \end{Vmatrix}}_{\text{"BENDING"}} \tag{4.73}$$

Equivalently, one can express the Green strain tensor component γ^2_2, from Eq. 4.35, as:

$$\gamma^2_2 = \underbrace{\overset{\circ}{\gamma}{}^2_2}_{\text{"MEMBRANE"}} - \underbrace{\zeta^\circ\left(1+2\overset{\circ}{\gamma}{}^2_2\right)\frac{\partial\theta}{\partial s}\left(1-\zeta^\circ\frac{\partial\theta}{\partial s}\right)}_{\text{"BENDING"}} \tag{4.74}$$

Or, defining a "curvature" measured per unit length of the reference configuration, as in Eq. 4.69:

$$\frac{\partial\theta}{\partial\eta} = \sqrt{1+2\overset{\circ}{\gamma}{}^2_2}\;\frac{\partial\theta}{\partial s} \tag{4.75}$$

$$\gamma^2_2 = \overset{\circ}{\gamma}{}^2_2 - \zeta^\circ\sqrt{1+2\overset{\circ}{\gamma}{}^2_2}\;\frac{\partial\theta}{\partial\eta}\left(1 - \zeta^\circ\frac{1}{\sqrt{1+2\overset{\circ}{\gamma}{}^2_2}}\frac{\partial\theta}{\partial\eta}\right) \tag{4.76}$$

$$\underbrace{\gamma^2_2 = \overset{\circ}{\gamma}{}^2_2}_{\text{"MEMBRANE"}} - \underbrace{\zeta^\circ\frac{\partial\theta}{\partial\eta}\left(\sqrt{1+2\overset{\circ}{\gamma}{}^2_2} - \zeta^\circ\frac{\partial\theta}{\partial\eta}\right)}_{\text{"BENDING"}} \tag{4.77}$$

This equation holds for arbitrarily large rotations and strains.

4.2.1.3 Specialization to Small Membrane Strains

If, instead of the exact equations for arbitrarily large rotations and strains, one assumes "small membrane strains" at the outset (a common assumption in the engineering literature*), the displacement field (Eq. 4.23) becomes altered. For convenient reference, Eq. 4.23 follows as Eq. 4.78:

$$\bar{u} = \left(v - \frac{\zeta^\circ}{\overset{\circ}{U}{}^2_2}\psi\right)\bar{a}_2 + \left(w + \frac{\zeta^\circ}{\overset{\circ}{U}{}^2_2}(1+\chi) - \zeta^\circ\right)\bar{n} \tag{4.78}$$

For "small membrane strains", one has

$$\overset{\circ}{U}{}^2_2 = 1 + \overset{\circ}{\tilde{E}}{}^2_2 = \sqrt{1+2\overset{\circ}{\gamma}{}^2_2} \approx 1 \tag{4.79}$$

Hence, Eq. 4.78 becomes

$$\boxed{\bar{u} \approx (v - \zeta^\circ\psi)\,\bar{a}_2 + (w + \zeta^\circ\chi)\,\bar{n}} \tag{4.80}$$

In this (approximate) Bernoulli-Euler-Kirchhoff displacement field, the only assumption made is that the membrane strains are small, but no assumption is made regarding the magnitudes of the displacements.

*For example, as in Novozhilov's book on the Nonlinear Theory of Elasticity [156], or as in [28].

From this displacement field, one obtains the following deformation gradient tensor components:

$$F^{i\cdot}_{\cdot j} = \begin{Vmatrix} \left(1+\chi - \zeta^{\circ}\frac{\partial \psi}{\partial \eta}\right) & -\psi \\ \left(\psi + \zeta^{\circ}\frac{\partial \chi}{\partial \eta}\right) & (1+\chi) \end{Vmatrix} \tag{4.81}$$

From $F^{i\cdot}_{\cdot j}$, the following right Cauchy-Green deformation tensor components are obtained:

$$C^{i}_{j} = \left(F^{i\cdot}_{\cdot k}\right)^{T}\left(F^{k\cdot}_{\cdot j}\right) = \begin{Vmatrix} \left(1+\chi-\zeta^{\circ}\frac{\partial \psi}{\partial \eta}\right) & \left(\psi+\zeta^{\circ}\frac{\partial \chi}{\partial \eta}\right) \\ -\psi & (1+\chi) \end{Vmatrix} \begin{Vmatrix} \left(1+\chi-\zeta^{\circ}\frac{\partial \psi}{\partial \eta}\right) & -\psi \\ \left(\psi+\zeta^{\circ}\frac{\partial \chi}{\partial \eta}\right) & (1+\chi) \end{Vmatrix} \tag{4.82}$$

$$= \begin{Vmatrix} \left(1+\chi-\zeta^{\circ}\frac{\partial \psi}{\partial \eta}\right)^{2} + \left(\psi+\zeta^{\circ}\frac{\partial \chi}{\partial \eta}\right)^{2} & -\psi\left(1+\chi-\zeta^{\circ}\frac{\partial \psi}{\partial \eta}\right)+(1+\chi)\left(\psi+\zeta^{\circ}\frac{\partial \chi}{\partial \eta}\right) \\ -\psi\left(1+\chi-\zeta^{\circ}\frac{\partial \psi}{\partial \eta}\right)+(1+\chi)\left(\psi+\zeta^{\circ}\frac{\partial \chi}{\partial \eta}\right) & \psi^{2}+(1+\chi)^{2} \end{Vmatrix}$$

$$C^{i}_{j} = \begin{Vmatrix} \left\{\overset{\circ}{C}{}^{2}_{2} + 2\zeta^{\circ}\kappa + (\zeta^{\circ})^{2}\left[\left(\frac{\partial \psi}{\partial \eta}\right)^{2} + \left(\frac{\partial \chi}{\partial \eta}\right)^{2}\right]\right\} & \zeta^{\circ}\left[\psi\frac{\partial \psi}{\partial \eta} + (1+\chi)\frac{\partial \chi}{\partial \eta}\right] \\ \zeta^{\circ}\left[\psi\frac{\partial \psi}{\partial \eta} + (1+\chi)\frac{\partial \chi}{\partial \eta}\right] & \overset{\circ}{C}{}^{2}_{2} \end{Vmatrix} \tag{4.83}$$

where, as before

$$\overset{\circ}{C}{}_2^2 = C_2^2(\eta, \zeta^\circ = 0) = (1+\chi)^2 + \Psi^2 \tag{4.84}$$

$$K = \left(-\frac{\partial \Psi}{\partial \eta}\right)(1+\chi) + \Psi \frac{\partial \chi}{\partial \eta} \tag{4.85}$$

Observe that the introduction of the "small membrane strains" assumption in the Bernoulli-Euler-Kirchhoff displacement field is responsible for producing spurious shear strains and normal strains*. The spurious normal strain is just as large as the membrane strain, although the shear and normal strains had been assumed to be zero. Also, the introduction of the "small membrane strains" assumption in the displacement field results in an expression for the quadratic terms in ζ^o that needs the extra assumption of small membrane strain gradients $((\partial \overset{\circ}{U}{}_2^2/\partial\eta) << (\partial\theta/\partial\eta))$ to be correct.

From Eqs. 4.64 and 4.65, one finds that

$$(\zeta^\circ)^2\left[\left(\frac{\partial \Psi}{\partial \eta}\right)^2 + \left(\frac{\partial \chi}{\partial \eta}\right)^2\right] = (\zeta^\circ)^2\left[(\overset{\circ}{U}{}_2^2)^2\left(\frac{\partial \theta}{\partial \eta}\right)^2 + \left(\frac{\partial \overset{\circ}{U}{}_2^2}{\partial \eta}\right)^2\right] \tag{4.86}$$

The Green strain tensor components can be obtained from this displacement field as:

$$\gamma^i_j = \frac{1}{2}\left(C^i_j - \delta^i_j\right)$$

Hence,

$$\gamma^i_j = \begin{Vmatrix} \left\{\overset{\circ}{\gamma}{}^2_2 + \zeta^\circ K + \frac{1}{2}(\zeta^\circ)^2\left[\left(\frac{\partial \Psi}{\partial \eta}\right)^2 + \left(\frac{\partial \chi}{\partial \eta}\right)^2\right]\right\} & \frac{1}{2}\zeta^\circ\left[\Psi\frac{\partial \Psi}{\partial \eta} + (1+\chi)\frac{\partial \chi}{\partial \eta}\right] \\ \frac{1}{2}\zeta^\circ\left[\Psi\frac{\partial \Psi}{\partial \eta} + (1+\chi)\frac{\partial \chi}{\partial \eta}\right] & \overset{\circ}{\gamma}{}^2_2 \end{Vmatrix} \tag{4.87}$$

---

*This observation has already been made in [28].

where, as before

$$\mathring{\gamma}_2^2 = \chi + \frac{1}{2}\psi^2 + \frac{1}{2}\chi^2 \tag{4.88}$$

$$\kappa = \left(-\frac{\partial \psi}{\partial \eta}\right)(1+\chi) + \psi \frac{\partial \chi}{\partial \eta} \tag{4.89}$$

Several subsets of the strain-displacement equation for the Green strain tensor component γ_2^2 were used and studied in Ref. 28.

For convenient reference, these relations are shown concisely in the following:

$$\gamma_2^2 = \overbrace{\chi + \frac{1}{2}\psi^2 + \frac{1}{2}\chi^2}^{\mathring{\gamma}_2^2} + \zeta^\circ \overbrace{\left[\left(-\frac{\partial \psi}{\partial \eta}\right)(1+\chi) + \psi \frac{\partial \chi}{\partial \eta}\right]}^{\kappa} + \frac{1}{2}(\zeta^\circ)^2\left[\left(\frac{\partial \psi}{\partial \eta}\right)^2 + \left(\frac{\partial \chi}{\partial \eta}\right)^2\right]$$

TYPE "A"

TYPE "B"

TYPE "D"

TYPE "E"

TYPE "C"

(4.90)

Strain-displacement relation Type "A" is used in the JET 3 computer program [24] . It is restricted by <u>small strains</u> <u>and</u> by <u>small angles of rotation</u>:

<u>Strain-Displacement Relation Type "A" (JET 3):</u>

$$\gamma_2^2\Big|_{\text{"A"}} = \chi + \frac{1}{2}\psi^2 + \zeta^\circ\left(-\frac{\partial \psi}{\partial \eta}\right) \tag{4.91}$$

Placing Eqs. 4.44, 4.45, and 4.64 into Eq. 4.91, one obtains:

$$\gamma_2^2\Big|_{\text{"A"}} = \sqrt{1+2\mathring{\gamma}_2^2}\,\cos\theta - 1 + \frac{1}{2}\left(1+2\mathring{\gamma}_2^2\right)\sin^2\theta$$

$$-\zeta^\circ\left[\sqrt{1+2\mathring{\gamma}_2^2}\,\cos\theta \frac{\partial \theta}{\partial \eta} + \sin\theta\, \frac{\partial\left(\sqrt{1+2\mathring{\gamma}_2^2}\right)}{\partial \eta}\right] \tag{4.92}$$

So that only, for small membrane strains:

$$1+2\overset{\circ}{\gamma}{}_2^2 \approx 1 \tag{4.93}$$

small angles of rotation:

$$\cos\theta \approx 1$$
$$\sin\theta \approx \theta \tag{4.94}$$

and small membrane strain gradients:

$$\theta \frac{\partial \overset{\circ}{\gamma}{}_2^2}{\partial \eta} < \frac{\partial \theta}{\partial \eta} \tag{4.95}$$

one obtains

$$\gamma_2^2 \Big|_{\text{"A"}} \approx \overset{\circ}{\gamma}{}_2^2 - \zeta^\circ \frac{\partial \theta}{\partial \eta} \tag{4.96}$$

Strain-displacement relation Type "B" is used in the CIVM-JET 4B computer program [27]. For strictly membrane deformations (no bending deformations at all), it is valid for large strains and rotations. Otherwise, it is also restricted by small strains and small rotations, as follows:

Strain-Displacement Relation Type "B" (CIVM-JET 4B)

$$\gamma_2^2 \Big|_{\text{"B"}} = \overset{\circ}{\gamma}{}_2^2 + \zeta^\circ \left(- \frac{\partial \psi}{\partial \eta}\right) \tag{4.97}$$

It was shown previously in Eq. .62 that the membrane part $(\overset{\circ}{\gamma}{}_2^2 = \frac{1}{2}(\overset{\circ}{C}{}_2^2 - 1))$ of this strain-displacement equation is valid for large strains and large rotations. But the bending part is not. From Eqs. 4.64 and 4.97, one finds that

$$\gamma_2^2 \Big|_{\text{"B"}} = \overset{\circ}{\gamma}{}_2^2 + \zeta^\circ \left[\sqrt{1+2\overset{\circ}{\gamma}{}_2^2}\, \cos\theta \frac{\partial \theta}{\partial \eta} + \sin\theta \frac{\partial \sqrt{1+2\overset{\circ}{\gamma}{}_2^2}}{\partial \eta}\right] \tag{4.98}$$

It is obvious from this that, only for

(a) no rotations (and therefore no change of curvature)

$$\cos\theta = 1 \qquad \sin\theta = 0 \qquad \frac{\partial\theta}{\partial\eta} = 0 \tag{4.99}$$

or

(b) <u>small membrane strains:</u>

$$1 + 2\overset{\circ}{\gamma}{}^2_2 \approx 1 \tag{4.100}$$

and

(c) <u>small angles of rotation:</u>

$$\cos\theta \approx 1 \qquad \sin\theta \approx \theta \tag{4.101}$$

and

(d) <u>small membrane strain gradients:</u>

$$\theta \frac{\partial \overset{\circ}{\gamma}{}^2_2}{\partial\eta} < \frac{\partial\theta}{\partial\eta} \tag{4.102}$$

one obtains:

$$\gamma^2_2\Big|_{"B"} \approx \overset{\circ}{\gamma}{}^2_2 - \zeta^\circ \frac{\partial\theta}{\partial\eta} \tag{4.103}$$

For example, see Fig. 5, suppose that a clamped beam is bent at the free end by the application of pure moment, to 90°. In this case, one would obtain from the application of strain-displacement relation type "B":

For: $\theta = 90^\circ$ and $\overset{\circ}{\gamma}{}^2_2 \approx 0 \;,\; \frac{\partial \overset{\circ}{\gamma}{}^2_2}{\partial\eta} \approx 0$

then

$$\gamma^2_2\Big|_{"B"} = 0 + \zeta^\circ \left[\sqrt{1+0}\,(0)\frac{\partial\theta}{\partial\eta} + 1\,(0)\right] = 0 \tag{4.104}$$

which indicates that strain-displacement relation type "B" would produce zero bending strain no matter how large the curvature $\partial\theta/\partial\eta$ is.

Clearly, this is a spurious result produced by the use of the equation beyond its range of validity.

It is evident from Eqs. 4.86, 4.66, and 4.62 that the only subsets of Eq. 4.90 that are valid for arbitrarily large rotations are strain-displacement relations Types "B" and "C"; although these relations apply for arbitrarily large membrane strains, the assumed displacement field given by Eq. 4.80 which is employed to compute the bending strain implies small membrane strain.

<u>4.2.2 Inclusion of Thickness Change Associated with Finite Strains</u>

As previously mentioned, <u>no assumptions</u> regarding the magnitude of <u>strains</u> and/or <u>rotations</u> are present in Eqs. 4.31 and 4.33. However, these equations are subject to the kinematical restrictions imposed by the assumed-displacement field of Eq. 4.23 which does not allow any shear deformations or normal (to the reference axis η) strains, as is evident from the strain matrix displayed in Eq. 4.33, for example.

A theory of thin bodies which is subjected to the kinematic constraint that the thickness before and after deformation remains the same, is not realistic when finite strains are admitted in the deformation process. To enforce such a constraint, the density of the material would have to change in a special way during deformation. Since for most materials the ratio of the deformed to the undeformed mass density is very nearly equal to unity even for large strains, such an unrealistic density change (as enforced by the constraint of constant thickness) cannot be admitted in the characterization of the deformation process of an actual material at finite strains.

The formulation to be presented here can be derived from the general shell formulation of Section 5. Thickness changes will be introduced in the formulation by means of the assumption of no volume change.

The assumed-displacement field will contain only the zeroth order term in a (thickness-coordinate) asymptotic expansion of the factor $\lambda(\eta, \zeta^{o})$ appearing in Eq. 4.8. This zeroth order term provides only a <u>symmetric</u> thickness change (with respect to the reference axis η) and excludes antisymmetric thickness changes that can be provided by higher order terms in the asymptotic series expansion.

It turns out that the retention of just the zeroth order term is equivalent to satisfying the incompressibility condition in an exact fashion only at the reference axis η (at $\zeta^{o} = 0$). Higher order terms in the thickness coordinate (ζ^{o}) are not included at the present time so as not to complicate the analysis unduly. These higher order terms affect the axial strain-displacement equation in terms of the order of the square of the thickness coordinate and higher. For sufficiently "thin" bodies, these terms should be negligible. Also, the practical usefulness of including such higher order terms (that serve to satisfy with increasing degrees of accuracy the incompressibility assumption along the thickness of the thin body) is of questionable validity in a theory such as the present one that does not include any shear deformations and is restricted to deformations in 2-D space.

Let an asymptotic expansion for the factor $\lambda(\eta,\zeta^{o})$ of Eq. 4.8 be assumed in the form:

$$\lambda(\eta,\zeta^{o}) = \lambda_0(\eta) + \zeta^{o}\lambda_1(\eta) + \ldots O(\zeta^{o})^2 \tag{4.105}$$

Keeping only the zeroth order term,

$$\lambda(\eta,\zeta^{o}) = \lambda_0(\eta) \tag{4.106}$$

Eq. 4.8 becomes

$$\bar{R} = \bar{R}_0 + \zeta^{o}\lambda_0\bar{N} \tag{4.107}$$

Also, Eq. 4.6 becomes

$$\bar{G}_3 = \frac{\partial\bar{R}}{\partial\xi^3} = \frac{\partial\bar{R}}{\partial\zeta^{o}} = \lambda_0\bar{N} \tag{4.108}$$

Thus, the displacement field, Eq. 4.15 becomes:

$$\bar{u}(\eta,\zeta^{o}) = \bar{u}_0(\eta) + \zeta^{o}\left[\lambda_0(\eta)\bar{N}(\eta) - \bar{n}(\eta)\right] \tag{4.109}$$

From Eq. 4.108, one can obtain the deformation and strain tensors in the thickness direction:

$$G_{33} = C_{33} = g_{33} + 2\gamma_{33} = \bar{G}_3 \cdot \bar{G}_3 = (\lambda_o)^2 \qquad (4.110)$$

Since terms of order ζ^o and higher were neglected in the expansion given in Eq. 4.105, they should also be neglected in Eq. 4.110 to be consistent; hence,

$$C_{33} = [\lambda_o(\eta)]^2$$

$$C^3_3 = \overset{o}{C}{}^3_3 = C_{33} = \overset{o}{C}_{33} = (\lambda_o)^2 \qquad (4.111)$$

where

$$\overset{o}{C}{}^3_3 = C^3_3(\zeta^o = 0)$$

$$\overset{o}{C}_{33} = C_{33}(\zeta^o = 0)$$

The thickness deformation is measured by the parameter λ_o, which is a function of the curvilinear axis coordinate η, and is not a function of the thickness coordinate ζ^o. The thickness deformation is assumed to be homogeneous through the thickness. The deformation tensor component C^3_3 has the same value anywhere in the thickness ζ^o at a given location η. One can express the deformation tensor C^3_3 in terms of the stretch tensor U^3_3 as

$$U^3_3 = \overset{o}{U}{}^3_3 = \sqrt{C^3_3} = \lambda_o \qquad (4.112)$$

Imposing no volume deformation at the reference axis $\eta(\zeta^o = 0)$ for this thin body deforming in 2-D space is tantamount to writing

$$U^2_2 U^3_3 = 1 \qquad \text{at} \quad \zeta^o = 0 \qquad (4.113)$$

or

$$\overset{o}{U}{}^2_2 \overset{o}{U}{}^3_3 = 1 \qquad (4.114)$$

Employing Eq. 4.112, one obtains

$$\overset{o}{U}{}^2_2 \lambda_o = 1 \qquad (4.115)$$

Hence,

$$\boxed{\lambda_o = \mathcal{U}^3_3 = \frac{1}{\overset{\circ}{\mathcal{U}}{}^2_2} = \frac{1}{\sqrt{\overset{\circ}{C}{}^2_2}} = \frac{1}{\sqrt{1+2\overset{\circ}{\gamma}{}^2_2}}} \tag{4.116}$$

which expresses the thickness change λ_o in terms of the membrane axial strain $\overset{\circ}{\gamma}{}^2_2$.

Placing this result into the displacement field equation (4.109), one obtains

$$\bar{u} = \bar{u}_o + \frac{1}{\overset{\circ}{\mathcal{U}}{}^2_2} \zeta^\circ \bar{N} - \zeta^\circ \bar{n} \tag{4.117}$$

Hence, using Eqs. 4.19 and 4.20, Eq. 4.117 becomes

$$\bar{u} = V\bar{a}_2 + (w - \zeta^\circ)\bar{n} + \frac{\zeta^\circ}{(\overset{\circ}{\mathcal{U}}{}^2_2)^2}\left[(1+\chi)\bar{n} + (-\Psi)\bar{a}_2\right]$$

$$= \left(V - \frac{\zeta^\circ}{\overset{\circ}{C}{}^2_2}\Psi\right)\bar{a}_2 + \left[w + \frac{\zeta^\circ}{\overset{\circ}{C}{}^2_2}(1+\chi) - \zeta^\circ\right]\bar{n}$$

$$= \tilde{V}\bar{a}_2 + \tilde{W}\bar{n} \tag{4.118}$$

Thus one obtains the following strain matrix (<u>to the order of ζ°</u>):

$$\gamma^i_j = \left\| \begin{matrix} \left(\overset{\circ}{\gamma}{}^2_2 + \dfrac{\zeta^\circ}{(1+2\overset{\circ}{\gamma}{}^2_2)}\kappa\right) & \left(-\dfrac{\zeta^\circ}{(1+2\overset{\circ}{\gamma}{}^2_2)^2}\dfrac{\partial\overset{\circ}{\gamma}{}^2_2}{\partial\eta}\right) \\ \left(-\dfrac{\zeta^\circ}{(1+2\overset{\circ}{\gamma}{}^2_2)^2}\dfrac{\partial\overset{\circ}{\gamma}{}^2_2}{\partial\eta}\right) & \dfrac{1}{2}\left[\dfrac{1}{(1+2\overset{\circ}{\gamma}{}^2_2)} - 1\right] \end{matrix} \right\| \tag{4.119}$$

where $\overset{o}{\gamma}{}_2^2$ and κ were defined in Eqs. 4.26 and 4.34.

This expression shows that nonzero transverse shear strains are present away from the reference axis η (at $\zeta^o \neq 0$). This transverse shear strain is caused by the normal strain (thickness change) gradient in the η direction and disappears entirely when this gradient is zero (see Fig. 6 for this effect). The expression for this transverse shear strain can be expressed either in terms of the membrane strain gradient $\partial\overset{o}{\gamma}{}_2^2/\partial\eta$ or in terms of the normal strain gradient $\partial\gamma_3^3/\partial\eta$ as follows:

$$\gamma_3^2 = -\frac{\zeta^o}{(1+2\overset{o}{\gamma}{}_2^2)^2}\frac{\partial\overset{o}{\gamma}{}_2^2}{\partial\eta} = \zeta^o\frac{\partial\overset{o}{\gamma}{}_3^3}{\partial\eta} = \zeta^o\frac{\partial\gamma_3^3}{\partial\eta} \tag{4.120}$$

Since transverse shear deformations were neglected to start with, it will be assumed that the transverse shear strain produced by the normal strain gradient in the axial direction is negligible:

$$\gamma_3^2 = \gamma_2^3 \approx 0 \tag{4.121}$$

This is equivalent to

$$\zeta^o\frac{\partial\gamma_3^3}{\partial\eta} \approx 0 \tag{4.122}$$

which implies the assumption that the membrane strain gradient is small enough:

$$\frac{\zeta^o}{(1+2\overset{o}{\gamma}{}_2^2)^2}\frac{\partial\overset{o}{\gamma}{}_2^2}{\partial\eta} \approx 0 \tag{4.123}$$

Hence, the transverse shear strain created by the normal strain gradient in the axial direction is neglected in the Principle of Virtual Work. Likewise, although normal strains are considered in the analysis, the terms that correspond to it in the Principle of Virtual Work are neglected under the assumption of an approximate state of plane stress throughout the thin body. Or, what is equivalent, the normal (through-the-thickness direction) stresses are considered to be negligible.

An evident shortcoming of the present analysis is its restriction to two-dimensional space. In the physical world all phenomena take place in a three-dimensional space. Incompressibility (or equivalently, no change in volume) is a three-dimensional concept.

In the present analysis, incompressibility was imposed in a two-dimensional space; that is, not allowing any deformations in the direction normal to this two-dimensional η, ζ^o surface. One can examine the consequences of satisfying incompressibility in the three-dimensional case, in an approximate fashion, by replacing Eq. 4.114 by:

$$\overset{\circ}{\mathcal{U}}{}^1_1 \overset{\circ}{\mathcal{U}}{}^2_2 \overset{\circ}{\mathcal{U}}{}^3_3 = 1 \tag{4.124}$$

where the index "1" refers to the ξ^1 direction, normal to the $\xi^2 \equiv \eta$ and $\xi^3 \equiv \zeta^o$ directions. Therefore, from Eq. 4.112 and Eq. 4.124, one obtains:

$$\overset{\circ}{\mathcal{U}}{}^1_1 \overset{\circ}{\mathcal{U}}{}^2_2 \lambda_o = 1 \tag{4.125}$$

$$\lambda_o = \overset{\circ}{\mathcal{U}}{}^3_3 = \frac{1}{\overset{\circ}{\mathcal{U}}{}^1_1 \overset{\circ}{\mathcal{U}}{}^2_2} \tag{4.126}$$

Assuming that

$$\overset{\circ}{\mathcal{U}}{}^1_1 = f(\overset{\circ}{\mathcal{U}}{}^2_2) \tag{4.127}$$

then

$$\lambda_o = \frac{1}{\overset{\circ}{\mathcal{U}}{}^2_2 f(\overset{\circ}{\mathcal{U}}{}^2_2)} = \frac{1}{g(\overset{\circ}{\mathcal{U}}{}^2_2)} \tag{4.128}$$

In the case of a <u>very narrow beam</u>, with isotropic properties, and with a width exactly equal to its thickness, it is natural to expect:

$$\overset{\circ}{\mathcal{U}}{}^1_1 = \overset{\circ}{\mathcal{U}}{}^3_3 \tag{4.129}$$

Hence,

$$\overset{\circ}{\mathcal{U}}{}^1_1 = \lambda_o \tag{4.130}$$

Hence, from Eq. 4.125:

$$\overset{\circ}{U}{}^{2}_{2}(\lambda_o)^2 = 1 \tag{4.131}$$

$$\lambda_o = \frac{1}{\sqrt{\overset{\circ}{U}{}^{2}_{2}}} = \frac{1}{(\overset{\circ}{C}{}^{2}_{2})^{1/4}} = \frac{1}{(1+2\overset{\circ}{\gamma}{}^{2}_{2})^{1/4}} \tag{4.132}$$

Placing λ_o into Eq. 4.109 for the displacement field, one can obtain, after some manipulations the following strain-displacement equations:

$$\boxed{\gamma^3_3 = \gamma^1_1 = \frac{1}{2}\left[\frac{1}{\sqrt{1+2\overset{\circ}{\gamma}{}^{2}_{2}}} - 1\right]} \tag{4.133}$$

$$\boxed{\gamma^2_2 = \overset{\circ}{\gamma}{}^{2}_{2} + \frac{\zeta^o}{(1+2\overset{\circ}{\gamma}{}^{2}_{2})^{3/4}}\,K} \tag{4.134}$$

Here, $\overset{\circ}{\gamma}{}^{2}_{2}$ and κ have the same definitions as in Eqs. 4.34 and 4.26, respectively.

In general, one would expect a behavior that is bounded between Eqs. 4.134 and 4.119; that is, between the case in which (1) the strain in the ξ^1 direction is equal to the strain in the $\xi^3 \equiv \zeta^o$ direction and (2) that in which the strain in the ξ^1 direction is equal to 0.

4.2.3 Summary of Strain-Displacement Equations

For convenient reference, the strain-displacement equations for thin curved beams $(1 + (\zeta^o/R) \stackrel{\sim}{\sim} 1)$ will be reproduced in the following for certain specific situations.

4.2.3.1 Strain-Displacement Relations for Small Strains

From Eq. 4.80, the assumed displacement field (implying small membrane strain) is:

$$\boxed{\bar{u} = (v - \zeta^o \psi)\,\bar{a}_2 + (w + \zeta^o \chi)\,\bar{n}} \tag{4.135}$$

This field leads to the following strain-displacement equation (Eq. 4.90):

$$\gamma_2^2 = \overbrace{\chi + \frac{1}{2}\psi^2 + \frac{1}{2}\chi^2}^{\overset{\circ}{\gamma}{}_2^2} + \zeta^\circ \overbrace{\left[\left(-\frac{\partial\psi}{\partial\eta}\right)(1+\chi) + \psi\frac{\partial\chi}{\partial\eta}\right]}^{\kappa} + \frac{(\zeta^\circ)^2}{2}\left[\left(\frac{\partial\psi}{\partial\eta}\right)^2 + \left(\frac{\partial\chi}{\partial\eta}\right)^2\right] \tag{4.90}$$

TYPE "A"

TYPE "B"

TYPE "D"

TYPE "E"

TYPE "C"

where

$$\gamma_1^1 \approx \gamma_3^3 \approx \gamma_2^3 \approx \gamma_3^2 \approx \gamma_2^1 \approx \gamma_1^2 \approx \gamma_3^1 \approx \gamma_1^3 \approx 0$$

and

$$\chi = \frac{\partial v}{\partial\eta} + \frac{w}{R} = \sqrt{1 + 2\overset{\circ}{\gamma}{}_2^2}\,\cos\theta - 1$$

$$\psi = \frac{\partial w}{\partial\eta} - \frac{v}{R} = \sqrt{1 + 2\overset{\circ}{\gamma}{}_2^2}\,\sin\theta$$

The displacement gradients are χ and ψ, and θ is the angle of rotation of the reference axis η(at $\zeta^o = 0$).

Note from Eqs. 4.74 and 4.77 that the bending contribution to the Green strain γ_2^2 involves also the membrane strain $\overset{o}{\gamma}{}_2^2$. Hence, the bending contribution can be approximated in various ways depending upon one's assumption (in the bending part) concerning the size of $\overset{o}{\gamma}{}_2^2$. For example, if one assumes that $1 + 2\,\overset{o}{\gamma}{}_2^2 \approx 1$ only in the bending part as in Eqs. 4.79 and 4.80, the resulting strain-displacement relations are restricted, therefore, to small membrane strains insofar as the bending contribution itself is concerned; this applies to strain-displacement relations A, B, C, D, and E. For the membrane part of γ_2^2, arbitrarily large membrane strains and rotations are taken into account in Eq. 4.90 except for Type A. For the bending part of γ_2^2 in Eq. 4.90, arbitrarily large rotations apply only for Types C and E. Type A is the curved-beam equivalent of von Karman's nonlinear plate equations [157] and Sanders' nonlinear shell equations [158].

4.2.3.2 Strain-Displacement Relations for Finite Strains and Finite Rotations

As before, let the Green ("Lagrangian") membrane strain be defined as

$$\overset{\circ}{\gamma}{}_2^2 = \chi + \frac{1}{2}\psi^2 + \frac{1}{2}\chi^2 \tag{4.136}$$

and the "curvature" as

$$K = \left(-\frac{\partial \psi}{\partial \eta}\right)(1+\chi) + \psi \frac{\partial \chi}{\partial \eta} \tag{4.137}$$

The following displacement field:

$$\boxed{\bar{u} = \left(v - \frac{\zeta^{\circ}}{(1+2\overset{\circ}{\gamma}{}_2^2)^{\alpha}}\psi\right)\bar{a}_2 + \left(w + \zeta^{\circ}\frac{(1+\chi)}{(1+2\overset{\circ}{\gamma}{}_2^2)^{\alpha}} - \zeta^{\circ}\right)\bar{n}} \tag{4.138}$$

produces the following strain-displacement equations (to the order of ζ°):

$$\gamma_2^2 = \overset{\circ}{\gamma}{}_2^2 + \frac{\zeta^{\circ}}{(1+2\overset{\circ}{\gamma}{}_2^2)^{\alpha}} K \tag{4.139}$$

$$\gamma_3^3 = \frac{1}{2}\left[\frac{1}{(1+2\overset{\circ}{\gamma}{}_2^2)^{\beta}} - 1\right] \tag{4.140}$$

$$\gamma_1^1 = \frac{1}{2}\left[\frac{1}{(1+2\overset{\circ}{\gamma}{}_2^2)^{\mu}} - 1\right] \tag{4.145}$$

with

$$\gamma_2^1 \approx \gamma_1^2 \approx \gamma_1^3 \approx \gamma_3^1 \approx \gamma_3^2 \approx \gamma_2^3 \approx 0$$

The following special cases can be identified:

(a) No changes in thickness or lateral dimensions ($\gamma_1^1 = \gamma_3^3 = 0$); then,

$$\alpha = 1 \qquad \beta = 0 \qquad \mu = 0$$

(b) Thickness change only ($\gamma_1^1 = 0$, $\gamma_3^3 \neq 0$); then,

$$\alpha = 1 \qquad \beta = 1 \qquad \mu = 0$$

(c) Equal strains in the thickness and the lateral direction: ($\gamma_3^3 = \gamma_1^1 \neq 0$); then

$$\alpha = \frac{3}{4} \qquad \beta = \frac{1}{2} \qquad \mu = \frac{1}{2}$$

The case in which $\alpha = 1$, $\beta = 1$, $\mu = 0$ is called strain displacement relation Type F and is the one used in the analysis of beams and rings of Section 7; that is

$$\left.\begin{aligned} \gamma_2^2 &= \overset{\circ}{\gamma}{}_2^2 + \frac{\overset{\circ}{\tau}}{(1+2\overset{\circ}{\gamma}{}_2^2)} K \\ \gamma_3^3 &= \frac{1}{2}\left[\frac{1}{(1+2\overset{\circ}{\gamma}{}_2^2)} - 1\right] \\ \gamma_1^1 &= 0 \end{aligned}\right\} \text{TYPE "F"} \tag{4.146}$$

This equation is valid for arbitrarily large membrane strains, rotations, and displacements for incompressible thickness-changing B-E 2-D structures with $\gamma_1^1 = 0$.

4.3 Constitutive Equations for Finite Strains and Rotations

4.3.1 Introduction

The general theory for finite-strain elastic-plastic strain-rate dependent deformations of a solid presented in Section 3 will be specialized to curved beams, for which only the axial (circumferential) component of stress is considered to be important.

4.3.2 Constitutive Equations

In the particular case in consideration, the stress-strain relation is one-dimensional (no shear strains are considered and normal through-the-thickness stresses are disregarded, considering a state of plane stress). Hence, the problem simplifies considerably. The co-rotational rate of the mixed components of stress in convected coordinates becomes equal to the material rate of the mixed components of stress in convected coordinates.

In convected coordinates:

$$ {}^{s}\overset{\circ}{\tau}{}^{2}_{2} = {}^{s}\dot{\tau}^{2}_{2} \tag{4.147}$$

Also, the mixed components of the rate-of-deformation tensor in convected coordinates become equal to the material rate of the mixed components of logarithmic strain in convected coordinates:

$$ D^{2}_{2} = \dot{H}^{2}_{2} = \overset{\circ}{H}{}^{2}_{2} \tag{4.148}$$

Hence, Eq. 3.31 for the case of a <u>one-dimensional</u> stress-strain relation in convected coordinates becomes*

$$ {}^{s}\overset{\circ}{\tau}{}^{2}_{2} = {}^{s}E\; {}^{s}(D^{2}_{2})^{e} \tag{4.149}$$

or, equivalently:

$$ {}^{s}\dot{\tau}^{2}_{2} = {}^{s}E\; {}^{s}(D^{2}_{2})^{e} \tag{4.150}$$

where

$$ D^{2}_{2} = {}^{s}(D^{2}_{2})^{e} + {}^{s}(D^{2}_{2})^{p} = \dot{H}^{2}_{2} = {}^{s}(\dot{H}^{2}_{2})^{e} + {}^{s}(\dot{H}^{2}_{2})^{p} \tag{4.151}$$

Equation 4.150 can be integrated to obtain

$$ {}^{s}\tau^{2}_{2}(t) = {}^{s}E\; {}^{s}(H^{2}_{2})^{e}(t) + {}^{s}\tau^{2}_{2}(t_0) \tag{4.152}$$

Therefore, in this special case of a one-dimensional stress-strain relation expressed in the body-fixed convected coordinates, the constitutive law (Eq. 3.27) does have an <u>elastic potential</u>:

$$ {}^{s}\Psi = \frac{1}{\rho_0}\,\frac{1}{2}\,{}^{s}\tau^{2}_{2}\;{}^{s}(H^{2}_{2})^{e} = \frac{1}{\rho_0}\,\frac{1}{2}\,{}^{s}E\left[{}^{s}(H^{2}_{2})^{e}\right]^{2} \tag{4.153}$$

---

*Here, as in previous subsections, prescript "s" refers to a quantity pertaining to the sth sublayer of the mechanical-sublayer model.

and

$$ {}^{s}\tau_{2}^{2} = \rho_{0} \frac{\partial\, {}^{s}\psi}{\partial\, {}^{s}(H_{2}^{2})^{e}} \tag{4.154}$$

where ${}^{s}\psi$ is the Holmholtz free internal energy per unit mass, under isothermal conditions, of sublayer s.

The governing equations, expressed in the body-fixed convected coordinate system, are (compare with Eq. 3.54):

$$ \begin{aligned} \tau_{2}^{2} &= \sum^{n} A_{s}\, {}^{s}\tau_{2}^{2} \\ \dot{\tau}_{2}^{2} &= \sum^{n} A_{s}\, {}^{s}\dot{\tau}_{2}^{2} \end{aligned} \tag{4.155}$$

$$ {}^{s}\Phi = \left({}^{s}\tau_{2}^{2}\right)^{2} - \left({}^{s}\tau_{u_0}^{y}\right)^{2} \left(1 + \left|\frac{D_{2}^{2}}{d}\right|^{\frac{1}{p}}\right)^{2} \tag{4.156}$$

$$ {}^{s}\dot{\tau}_{2}^{2} = E\, D_{2}^{2} \quad \text{if} \left\{ \quad {}^{s}\Phi \leq 0 \right. \tag{4.157}$$

$$ {}^{s}\tau_{2}^{2} = +{}^{s}\tau_{u_0}^{y}\left(1 + \left|\frac{D_{2}^{2}}{d}\right|^{1/p}\right) \quad \text{if} \left\{ \quad {}^{s}\tau_{2}^{2} > {}^{s}\tau_{u_0}^{y}\left(1 + \left|\frac{D_{2}^{2}}{d}\right|^{\frac{1}{p}}\right) \right. \tag{4.158}$$

$$ {}^{s}\tau_{2}^{2} = -{}^{s}\tau_{u_0}^{y}\left(1 + \left|\frac{D_{2}^{2}}{d}\right|^{1/p}\right) \quad \text{if} \left\{ \quad {}^{s}\tau_{2}^{2} < -{}^{s}\tau_{u_0}^{y}\left(1 + \left|\frac{D_{2}^{2}}{d}\right|^{\frac{1}{p}}\right) \right. \tag{4.159}$$

These equations have to be transformed to the stress and strain quantities used in the numerical analysis; for these, one uses the following previously-derived equations (2.269, 2.352, and 2.188) to obtain:

$$\tau_2^2 = S_2^2\left(1+2\gamma_2^2\right) \tag{4.160}$$

$$\overset{\circ}{\tau}{}_2^2 = \dot{\tau}_2^2 = \dot{S}_2^2\left(1+2\gamma_2^2\right) + 2\,S_2^2\,\dot{\gamma}_2^2 \tag{4.161}$$

$$D_2^2 = \frac{\dot{\gamma}_2^2}{\left(1+2\gamma_2^2\right)} \tag{4.162}$$

It will be shown that since each sublayer experiences the <u>same strain</u> as the actual material, the mechanical sublayer model is easily represented in terms of the Second Piola-Kirchhoff stress component S_2^2:

$$\begin{aligned}
\tau_2^2 &= \sum_{s=1}^{m} A_s\ {}^s\tau_2^2 \\
\tau_2^2 &= S_2^2\left(1+2\gamma_2^2\right) \\
{}^s\tau_2^2 &= {}^sS_2^2\left(1+2\gamma_2^2\right)
\end{aligned} \tag{4.163}$$

Hence,

$$\begin{aligned}
S_2^2\left(1+2\gamma_2^2\right) &= \sum_{s=1}^{m}\left[{}^sS_2^2\left(1+2\gamma_2^2\right)\right]A_s \\
&= \left(1+2\gamma_2^2\right)\sum_{s=1}^{m} A_s\ {}^sS_2^2
\end{aligned} \tag{4.164}$$

Therefore, also the Second Piola-Kirchhoff stress S_2^2 can be considered as the sum of n components (${}^{s}S^2_2$, s = 1, ..., n) with the same weighting factors A_s as used for the Kirchhoff stress T^2_2:

$$\boxed{S^2_2 = \sum^{n} A_s \, {}^{s}S^2_2} \tag{4.165}$$

Now, expressing Eq. 4.157 in terms of the Second Piola-Kirchhoff stress component S^2_2 and the Green strain component γ^2_2, by use of Eqs. 4.160-4.162, one obtains:

$$ {}^{s}\dot{S}^2_2 \left(1+2\gamma^2_2\right) + 2\,{}^{s}S^2_2\,\dot{\gamma}^2_2 = E\,\frac{\dot{\gamma}^2_2}{\left(1+2\gamma^2_2\right)} \tag{4.166}$$

or

$$ d\left({}^{s}S^2_2\right) = \frac{\left[E - 2\left(1+2\gamma^2_2\right)\left({}^{s}S^2_2\right)\right]}{\left(1+2\gamma^2_2\right)^2}\, d\left(\gamma^2_2\right) \tag{4.167}$$

Integrating this differential expression by the trapezoidal rule, from the time instant t - Δt to the incrementally close time instant t, and defining for the time being:

$$ {}^{s}S \equiv {}^{s}S^2_2 \tag{4.168}$$

$$ \gamma \equiv \gamma^2_2 \tag{4.169}$$

$$ \Delta\,{}^{s}S \equiv \left({}^{s}S^2_2\right)^{t} - \left({}^{s}S^2_2\right)^{t-\Delta t} \tag{4.170}$$

$$ \Delta\gamma \equiv \left(\gamma^2_2\right)^{t} - \left(\gamma^2_2\right)^{t-\Delta t} \tag{4.171}$$

one obtains:

$$ \Delta\,{}^{s}S = \frac{\left\{E - 2\,{}^{s}S^{t-\Delta t}\left[\left(1+2\gamma^{t}\right) - \Delta\gamma\right]\right\}}{\left[\left(1+2\gamma^{t}\right)^2 - \left(1+2\gamma^{t}\right)\Delta\gamma + 2\left(\Delta\gamma\right)^2\right]}\,\Delta\gamma \tag{4.172}$$

An illustration of the method of computing the axial stress at a given thru-the-thickness integration station* is presented as follows. One begins by knowing the sublayer stress ${}^{s}S^{t-\Delta t}$ at time $(t - \Delta t)$ for the sth sublayer at the integration station, and the strain increment $\Delta\gamma$ at the same integration station; therefore, the strain γ^{t} at time t at that integration station is also known.

One takes a trial value (superscript T) of ${}^{s}S^{t}$ (the stress at sublayer s at time t) which is computed by assuming an incrementally-elastic path:

$$({}^{s}S^{t})^{T} = {}^{s}S^{t-\Delta t} + \frac{\{E - 2\,{}^{s}S^{t-\Delta t}[(1+2\gamma^{t}) - \Delta\gamma]\}}{[(1+2\gamma^{t})^{2} - (1+2\gamma^{t})\Delta\gamma + 2(\Delta\gamma)^{2}]}\Delta\gamma \tag{4.173}$$

A check is then performed to see what the correct value of ${}^{s}S^{t}$ must be:

If

$$[({}^{s}S^{t})^{T}(1+2\gamma^{t})]^{2} \leq ({}^{s}\tau_{u_{o}}^{y})^{2}\left(1+\left|\frac{\Delta\gamma}{d\,(1+2\gamma^{t})\Delta t}\right|^{\frac{1}{P}}\right)^{2}$$

then

$${}^{s}S^{t} = ({}^{s}S^{t})^{T} \tag{4.174}$$

*Gaussian integration is utilized in the analysis.

If

$$\left({}^{s}S^{t}\right)^{T}\left(1+2\gamma^{t}\right) > {}^{s}\tau_{u_o}^{y}\left(1+\left|\frac{\Delta\gamma}{d\left(1+2\gamma^{t}\right)\Delta t}\right|^{\frac{1}{p}}\right)$$

then

$${}^{s}S^{t} = \frac{{}^{s}\tau_{u_o}^{y}\left(1+\left|\frac{\Delta\gamma}{d\left(1+2\gamma^{t}\right)\Delta t}\right|^{\frac{1}{p}}\right)}{\left(1+2\gamma^{t}\right)} \tag{4.175}$$

If

$$\left({}^{s}S^{t}\right)^{T}\left(1+2\gamma^{t}\right) < -\,{}^{s}\tau_{u_o}^{y}\left(1+\left|\frac{\Delta\gamma}{d\left(1+2\gamma^{t}\right)\Delta t}\right|^{\frac{1}{p}}\right)$$

then

$${}^{s}S^{t} = -\,\frac{{}^{s}\tau_{u_o}^{y}\left(1+\left|\frac{\Delta\gamma}{d\left(1+2\gamma^{t}\right)\Delta t}\right|^{\frac{1}{p}}\right)}{\left(1+2\gamma^{t}\right)} \tag{4.176}$$

This procedure is applied to <u>all sublayers</u> at that numerical integration station, and at <u>every integration station</u>.

SECTION 5

PLATES AND SHELLS

5.1 Introduction

Strain-displacement relations for general thin shells valid for finite strains and rotations are derived here. The main references that have been consulted for this derivation are: Mar [159], Dugundji [160], Koiter [161], and Biricikoglu and Kalnins [162].

The classical theory of shells is subjected to the kinematic constraint that the thickness of the shell before and after deformation remains the same, but this is not realistic when large strains are present. Since most materials which are capable of undergoing large strains are nearly incompressible, the constraint of incompressibility (no volume change) seems to be a physically-plausible and mathematically-convenient assumption; accordingly, this assumption is made in the present analysis. The analysis of thickness change by this kinematical constraint saves numerical computation and reduces the number of degrees of freedom required to analyze a given problem (in comparison with the existing finite-strain three-dimensional finite element analyses). The assumption of incompressible behavior of shells, as enforced in the present analysis, will not result in the existing critical numerical problem [163] associated with large severe thickness distortion associated with three-dimensional incompressible behavior present in the assumed-displacement finite-element analysis of large plastic strain three-dimensional, plane-strain or axisymmetric problems. The assumption of incompressibility is enforced in the analysis by means of an asymptotic series expansion in powers of the normal thickness coordinate. The corresponding finite-strain, finite-rotation, strain-displacement relations are believed to be original. These equations are then specialized to the case of an initially-flat shell; that is, a "plate".

In Subsection 5.3, constitutive equations which are valid for (1) finite strains and rotations, (2) elastic-plastic materials with strain-hardening and strain-rate properties -- are derived under the assumption of plane stress conditions for general thin shells. These equations are written in terms of the variables associated with the fixed reference configuration, and the finite element incremental procedure for the evaluation of the stresses is presented.

5.2 Strain-Displacement Relations for Finite Strains and Rotations

5.2.1 Formulation for General Shells

Let the location of each material point of the continuum be defined by the same two systems indicated in Subsection 2.4; namely, the space-fixed and the body-fixed (embedded) coordinate systems. A surface in three-dimensional Euclidean space is defined by the curvilinear coordinates ξ^1 and ξ^2 of the body-fixed coordinate system; this surface is called the "reference surface"* of a "thin shell". The coordinate $\xi^3 \equiv \zeta^o$ measures the distance along an outwardly-directed normal to the reference surface ($\zeta^o = 0$). The unit normal vector to the reference surface in the reference configuration is denoted by $\bar{n}$, while the unit normal vector to the reference surface in the present configuration is denoted by $\bar{N}$. Any material point p in the reference configuration of the shell is located by the position vector $\bar{r}_o$ to the reference surface ($\zeta^o = 0$) and the unit normal vector $\bar{n}$ to the reference surface, in the form (Fig. 7):

$$\bar{r}(\xi^1,\xi^2,\zeta^o) = \bar{r}_o(\xi^1,\xi^2) + \zeta^o\,\bar{n}(\xi^1,\xi^2) \tag{5.1}$$

Observe that the position vector $\bar{r}$ (as well as $\bar{r}_o$) is not a function of time:

$$\bar{r}(\xi^1,\xi^2,\zeta^o) = \bar{r}(\xi^1,\xi^2,\zeta^o,t_o) \tag{5.2}$$

where t_o is some reference (fixed) time.

The material point p in the reference configuration of the shell (at time t_o) is identified by the letter P in the present configuration of the shell (at time t). The material point P is located by the position vector

---

* It turns out that the best location for this surface for the purposes of this work is the middle surface of the shell.

$\bar{R}$ expressed in terms of $\bar{R}_o$ to the reference surface ($\zeta^o = 0$) and the unit vector $\bar{N}$ normal to the reference surface, as well as the scalar parameter λ that measures the thickness change:

$$\bar{R}(\xi^1,\xi^2,\zeta^o) = \bar{R}_o(\xi^1,\xi^2) + \zeta^o\lambda(\xi^1,\xi^2,\zeta^o)\bar{N}(\xi^1,\xi^2) \qquad (5.3)$$

Observe that the position vector $\bar{R}$ (as well as $\bar{R}_o$) is a function of time, of course:

$$\bar{R}(\xi^1,\xi^2,\zeta^o) = \bar{R}(\xi^1,\xi^2,\zeta^o,t) \qquad (5.4)$$

Equation 5.3 is tantamount to the assumption that the resulting deformation is such that the lines normal to the reference surface in the reference configuration remain normal to the present reference surface, but the surfaces originally parallel to the reference surface at time t_o need not remain parallel to the present reference surface at time t. Moreover, the distance of a material point to the reference surface is permitted to change with the deformation of the shell.

The displacement field at any point ξ^1, ξ^2, ζ^o in a shell may be written as follows:

$$\bar{u}(\xi^1,\xi^2,\zeta^o) = \bar{R}(\xi^1,\xi^2,\zeta^o) - \bar{r}(\xi^1,\xi^2,\zeta^o) \qquad (5.5)$$

$$= \bar{R}_o - \bar{r}_o + \zeta^o\lambda\bar{N} - \zeta^o\bar{n}$$

$$\boxed{\bar{u} = \bar{u}_o + \zeta^o(\lambda\bar{N} - \bar{n})} \qquad (5.6)$$

The covariant base vectors of the reference surface in the reference and present configurations are, respectively:

$$\bar{a}_\alpha = \bar{r}_{o,\alpha} = \frac{\partial\bar{r}_o}{\partial\xi^\alpha} \qquad \bar{A}_\alpha = \bar{R}_{o,\alpha} = \frac{\partial\bar{R}_o}{\partial\xi^\alpha} \qquad (5.7)$$

and they are tangent to the reference surface.* Note that one can express

*Greek minuscules α, β, ... take on values 1 and 2, corresponding to the reference surface coordinates ξ^1 and ξ^2, respectively.

the base vector $\bar{A}_\alpha$ to the reference surface in the present configuration in terms of the displacement vector $\bar{u}_o$:

$$\bar{A}_\alpha = \frac{\partial \bar{R}_o}{\partial \xi^\alpha} = \frac{\partial \bar{r}_o}{\partial \xi^\alpha} + \frac{\partial \bar{u}_o}{\partial \xi^\alpha} = \bar{a}_\alpha + \frac{\partial \bar{u}_o}{\partial \xi^\alpha} \tag{5.8}$$

The reference surface metric tensor components associated with these base vectors are:

$$a_{\alpha\beta} = \bar{a}_\alpha \cdot \bar{a}_\beta \tag{5.9}$$

$$A_{\alpha\beta} = \bar{A}_\alpha \cdot \bar{A}_\beta = a_{\alpha\beta} + \bar{a}_\alpha \cdot \frac{\partial \bar{u}_o}{\partial \xi^\beta} + \bar{a}_\beta \cdot \frac{\partial \bar{u}_o}{\partial \xi^\alpha} + \frac{\partial \bar{u}_o}{\partial \xi^\alpha} \cdot \frac{\partial \bar{u}_o}{\partial \xi^\beta} \tag{5.10}$$

One can introduce the contravariant base vectors $\bar{a}^\alpha$, $\bar{A}^\alpha$ by the relations:

$$\bar{a}^\alpha \cdot \bar{a}_\beta = \delta^\alpha_\beta = \bar{A}^\alpha \cdot \bar{A}_\beta \tag{5.11}$$

where

$$\delta^\alpha_\beta \begin{cases} 1 & \text{if } \alpha = \beta \\ 0 & \text{if } \alpha \neq \beta \end{cases} \tag{5.12}$$

is the previously defined Kronecker delta. Therefore, one can write the following tensor components:

$$a^{\alpha\beta} = \bar{a}^\alpha \cdot \bar{a}^\beta \qquad\qquad A^{\alpha\beta} = \bar{A}^\alpha \cdot \bar{A}^\beta \tag{5.13}$$

The determinants of these metric tensors are:

$$a = \begin{vmatrix} a_{11} & a_{12} \\ a_{21} & a_{22} \end{vmatrix} = a_{11}a_{22} - (a_{12})^2$$

$$A = \begin{vmatrix} A_{11} & A_{12} \\ A_{21} & A_{22} \end{vmatrix} = A_{11}A_{22} - (A_{12})^2 \tag{5.14}$$

The contravariant base vectors $\bar{a}^{\alpha}$ and $\bar{A}^{\alpha}$ are related to the covariant base vectors as:

$$\bar{a}^1 = \frac{\bar{a}_2 \times \bar{n}}{(\bar{a}_1 \times \bar{a}_2)\cdot\bar{n}} \qquad \bar{A}^1 = \frac{\bar{A}_2 \times \bar{N}}{(\bar{A}_1 \times \bar{A}_2)\cdot\bar{N}} \tag{5.15}$$

$$\bar{a}^2 = \frac{\bar{n} \times \bar{a}_1}{(\bar{a}_1 \times \bar{a}_2)\cdot\bar{n}} \qquad \bar{A}^2 = \frac{\bar{N} \times \bar{A}_1}{(\bar{A}_1 \times \bar{A}_2)\cdot\bar{N}} \tag{5.16}$$

It is also true that:

$$[(\bar{a}_1 \times \bar{a}_2)\cdot\bar{n}]^2 = a \qquad [(\bar{A}_1 \times \bar{A}_2)\cdot\bar{N}]^2 = A \tag{5.17}$$

Hence, one can express Eqs. 5.15 and 5.16 as:

$$\bar{a}^1 = \frac{\bar{a}_2 \times \bar{n}}{\sqrt{a}} \qquad \bar{A}^1 = \frac{\bar{A}_2 \times \bar{N}}{\sqrt{A}} \tag{5.18}$$

$$\bar{a}^2 = \frac{\bar{n} \times \bar{a}_1}{\sqrt{a}} \qquad \bar{A}^2 = \frac{\bar{N} \times \bar{A}_1}{\sqrt{A}} \tag{5.19}$$

and

$$a^{11} = \frac{a_{22}}{a} \qquad A^{11} = \frac{A_{22}}{A} \tag{5.20}$$

$$a^{22} = \frac{a_{11}}{a} \qquad A^{22} = \frac{A_{11}}{A} \tag{5.21}$$

$$a^{12} = a^{21} = -\frac{a_{12}}{a} \qquad A^{12} = A^{21} = -\frac{A_{12}}{A} \tag{5.22}$$

The "second fundamental tensor of the reference surface" is the tensor that expresses the curvature of th reference surface; its components are obtained either by differentiation of the (tangent) base vectors of the surface, or by differentiation of the unit normal vectors to the surface:

$$b_{\alpha\beta} \equiv \bar{n} \cdot \frac{\partial \bar{a}_\alpha}{\partial \xi^\beta} = -\bar{a}_\beta \cdot \frac{\partial \bar{n}}{\partial \xi^\alpha} = -\bar{a}_\alpha \cdot \frac{\partial \bar{n}}{\partial \xi^\beta} \tag{5.23}$$

$$B_{\alpha\beta} \equiv \bar{N} \cdot \frac{\partial \bar{A}_\alpha}{\partial \xi^\beta} = -\bar{A}_\beta \cdot \frac{\partial \bar{N}}{\partial \xi^\alpha} = -\bar{A}_\alpha \cdot \frac{\partial \bar{N}}{\partial \xi^\beta} \tag{5.24}$$

Associated with this tensor are two important sets of invariants (k, h, b and K, H, B):

$$k = \frac{b}{a} \tag{5.25}$$

$$h = \frac{1}{2} a^{\alpha\beta} b_{\alpha\beta} = \frac{1}{2} b^\alpha_\alpha$$

$$b = |b_{\alpha\beta}| = b_{11} b_{22} - (b_{12})^2 \tag{5.26}$$

$$K = \frac{B}{A} \tag{5.27}$$

$$H = \frac{1}{2} A^{\alpha\beta} B_{\alpha\beta} = \frac{1}{2} B^\alpha_\alpha \tag{5.28}$$

$$B = |B_{\alpha\beta}| = B_{11} B_{22} - (B_{12})^2$$

Here k and K are the "Gaussian curvatures" of the reference surface in the reference and present configurations, respectively, while h and H are the "mean curvatures" of the reference surface in the reference and present configurations, respectively.

The differential elements of reference surface area, can be shown to be:

$$d\mathcal{A}_0 = |\bar{a}_1 \times \bar{a}_2| \, d\xi^1 d\xi^2 = \sqrt{a} \, d\xi^1 d\xi^2 \qquad (5.29)$$

$$d\mathcal{A} = |\bar{A}_1 \times \bar{A}_2| \, d\xi^1 d\xi^2 = \sqrt{A} \, d\xi^1 d\xi^2 \qquad (5.30)$$

in the reference and present configurations, respectively. Thus, the ratio of the determinants of the metric tensors of the reference and present configurations is equal to the ratio of the differential elements of area:

$$\sqrt{\frac{a}{A}} = \frac{d\mathcal{A}_0}{d\mathcal{A}} \qquad (5.31)$$

Likewise, one defines base vectors of the "shell space" $\bar{g}_\alpha$, $\bar{g}_3$, that are tangent to surfaces at a distance ζ^o from the reference surface in the reference configuration:

$$\bar{g}_\alpha = \frac{\partial \bar{r}}{\partial \xi^\alpha} \qquad \bar{g}_3 = \frac{\partial \bar{r}}{\partial \xi^3} = \frac{\partial \bar{r}}{\partial \zeta^o} \qquad (5.32)$$

and base vectors $\bar{G}_\alpha$, $\bar{G}_3$, that are tangent to surfaces at a distance ζ^o from the reference surface in the present configuration:

$$\bar{G}_\alpha = \frac{\partial \bar{R}}{\partial \xi^\alpha} \qquad \bar{G}_3 = \frac{\partial \bar{R}}{\partial \zeta^o} \qquad (5.33)$$

These base vectors have the following determinants:

$$g = \begin{vmatrix} g_{11} & g_{12} & g_{13} \\ g_{12} & g_{22} & g_{23} \\ g_{13} & g_{23} & g_{33} \end{vmatrix} \qquad (5.34)$$

$$G = \begin{vmatrix} G_{11} & G_{12} & G_{13} \\ G_{12} & G_{22} & G_{23} \\ G_{13} & G_{23} & G_{33} \end{vmatrix} \tag{5.35}$$

The base vectors $\bar{g}_1$, $\bar{g}_2$, $\bar{g}_3$ as well as $\bar{G}_1$, $\bar{G}_2$, $\bar{G}_3$ describe the metric properties of three dimensional Euclidean space. The base vectors $\bar{a}_1$, $\bar{a}_2$ describe the metric properties of the reference surface embedded in the three dimensional space.

It is interesting to observe that the unit (metric) tensor $\bar{\bar{I}}$ of the three-dimensional Euclidean space can be expressed as:

$$\begin{aligned} \bar{\bar{I}} &= g_{ij}\,\bar{g}^i\bar{g}^j = \delta^i_j\,\bar{g}_i\bar{g}^j = g^{ij}\,\bar{g}_i\bar{g}_j \\ &= G_{IJ}\,\bar{G}^I\bar{G}^J = \delta^i_j\,\bar{G}_I\bar{G}^J = G^{IJ}\,\bar{G}_I\bar{G}_J \\ &= a_{\alpha\beta}\,\bar{a}^\alpha\bar{a}^\beta + \bar{n}\,\bar{n} = \delta^\alpha_\beta\,\bar{a}_\alpha\bar{a}^\beta + \bar{n}\,\bar{n} \end{aligned} \tag{5.36}$$

And that:

$$\sqrt{\frac{g}{a}} = 1 - 2\zeta^\circ h + (\zeta^\circ)^2 k \tag{5.37}$$

The differential elements of volume are:

$$dV_o = \sqrt{g}\; d\xi^1 d\xi^2 d\zeta^\circ \tag{5.38}$$

$$dV = \sqrt{G}\; d\xi^1 d\xi^2 d\zeta^\circ \tag{5.39}$$

in the reference and present configurations, respectively.

One can express the base vectors of the "shell space" in terms of the base vectors of the reference surface as:

$$\bar{g}_\alpha = \frac{\partial \bar{r}}{\partial \xi^\alpha} = \frac{\partial \bar{r}_o}{\partial \xi^\alpha} + \zeta^\circ \frac{\partial \bar{n}}{\partial \xi^\alpha} = \bar{a}_\alpha + \zeta^\circ \frac{\partial \bar{n}}{\partial \xi^\alpha} \tag{5.40}$$

$$\bar{g}_3 = \frac{\partial \bar{r}}{\partial \zeta^\circ} = \bar{n} \tag{5.41}$$

$$\bar{G}_\alpha = \frac{\partial \bar{R}}{\partial \xi^\alpha} = \frac{\partial \bar{R}_\circ}{\partial \xi^\alpha} + \zeta^\circ \frac{\partial(\lambda \bar{N})}{\partial \xi^\alpha}$$

$$= \bar{A}_\alpha + \zeta^\circ \frac{\partial \lambda}{\partial \xi^\alpha} \bar{N} + \zeta^\circ \lambda \frac{\partial \bar{N}}{\partial \xi^\alpha} \tag{5.42}$$

$$\bar{G}_3 = \frac{\partial \bar{R}}{\partial \zeta^\circ} = \zeta^\circ \frac{\partial \lambda}{\partial \zeta^\circ} \bar{N} + \lambda \bar{N} \tag{5.43}$$

Likewise, these expressions can be written in terms of the curvature tensors and the base vectors, by means of Eqs. 5.23 and 5.24, obtaining:

$$\boxed{\begin{aligned} \bar{g}_\alpha &= \bar{a}_\alpha - \zeta^\circ b^\beta_\alpha \bar{a}_\beta && (5.44) \\ \bar{g}_3 &= \bar{n} && (5.45) \\ \bar{G}_\alpha &= \bar{A}_\alpha - \zeta^\circ \lambda B^\beta_\alpha \bar{A}_\beta + \zeta^\circ \frac{\partial \lambda}{\partial \xi^\alpha} \bar{N} && (5.46) \\ \bar{G}_3 &= \left(\lambda + \zeta^\circ \frac{\partial \lambda}{\partial \zeta^\circ}\right) \bar{N} && (5.47) \end{aligned}}$$

where

$$B^\beta_\alpha = B_{\alpha\gamma} A^{\gamma\beta} \tag{5.48}$$

$$b^\beta_\alpha = b_{\alpha\gamma} a^{\gamma\beta} \tag{5.49}$$

Finally, with these equations, one can write the metric tensor components, from which the Cauchy-Green deformation tensor, or the Green strain tensor can be easily obtained as follows. Since

$$\bar{a}_\alpha \cdot \bar{a}_\beta = a_{\alpha\beta} \qquad \bar{A}_\alpha \cdot \bar{A}_\beta = A_{\alpha\beta}$$

$$\bar{a}_\alpha \cdot \bar{n} = 0 \qquad \bar{A}_\alpha \cdot \bar{N} = 0 \tag{5.50}$$

then:

$$g_{\alpha\beta} = \bar{g}_\alpha \cdot \bar{g}_\beta = a_{\alpha\beta} - 2\zeta^\circ b_{\alpha\beta} + (\zeta^\circ)^2 b^\delta_\alpha b_{\delta\beta} \tag{5.51}$$

$$g_{\alpha 3} = 0 \tag{5.52}$$

$$g_{33} = 1 \tag{5.53}$$

$$G_{\alpha\beta} = \bar{G}_\alpha \cdot \bar{G}_\beta = A_{\alpha\beta} - 2\zeta^\circ \lambda B_{\alpha\beta} + (\zeta^\circ)^2 B^\delta_\alpha B_{\delta\beta} (\lambda)^2 + (\zeta^\circ)^2 \frac{\partial\lambda}{\partial\xi^\alpha}\frac{\partial\lambda}{\partial\xi^\beta} \tag{5.54}$$

$$G_{3\alpha} = \zeta^\circ \lambda \frac{\partial\lambda}{\partial\xi^\alpha} + (\zeta^\circ)^2 \frac{\partial\lambda}{\partial\xi^\alpha}\frac{\partial\lambda}{\partial\xi^\beta} \tag{5.55}$$

$$G_{33} = (\lambda)^2 + 2\zeta^\circ \lambda \frac{\partial\lambda}{\partial\zeta^\circ} + (\zeta^\circ)^2 \left(\frac{\partial\lambda}{\partial\zeta^\circ}\right)^2 \tag{5.56}$$

The assumption of no change in volume can be expressed mathematically as:

$$\frac{dV_o}{dV} = \sqrt{\frac{g}{G}} = 1 \tag{5.57}$$

This assumption will be utilized to express the parameter λ in terms of the variables at the reference surface. From Eqs. 5.51-5.53, one finds

$$g = \begin{vmatrix} g_{11} & g_{12} & 0 \\ g_{12} & g_{22} & 0 \\ 0 & 0 & 1 \end{vmatrix} = g_{11} g_{22} - (g_{12})^2 \tag{5.58}$$

Therefore,

$$\begin{aligned} g = a &- 2\zeta^\circ (b_{11} a_{22} + b_{22} a_{11} - 2 b_{12} a_{12}) \\ &+ (\zeta^\circ)^2 [b_1^\delta b_{\delta 1} a_{22} + b_2^\delta b_{\delta 2} a_{11} + 4 b_{11} b_{22} \\ &- 2 b_1^\delta b_{\delta 2} a_{12} - 4 (b_{12})^2] + O(\zeta^\circ)^3 \end{aligned} \tag{5.59}$$

$$g = a \left[1 - 2\zeta^\circ h + \zeta^\circ k \right]^2 \tag{5.60}$$

Also, from Eqs. 5.54-5.56, one finds that

$$\begin{aligned} G = A (\lambda)^2 &- 2\zeta^\circ C (\lambda)^3 + 2\zeta^\circ A \lambda \frac{\partial \lambda}{\partial \zeta^\circ} \\ &+ (\zeta^\circ)^2 \Big\{ A \left(\frac{\partial \lambda}{\partial \zeta^\circ}\right)^2 + (\lambda)^4 [B_1^\delta B_{\delta 1} A_{22} + B_2^\delta B_{\delta 2} A_{11} \\ &+ 4 B_{11} B_{22} - 2 B_1^\delta B_{\delta 2} A_{12} - 4 (B_{12})^2] \\ &- 4 (\lambda)^2 \frac{\partial \lambda}{\partial \zeta^\circ} C \Big\} + O(\zeta^\circ)^3 \end{aligned} \tag{5.61}$$

where:

$$C \equiv B_{11} A_{22} + B_{22} A_{11} - 2 B_{12} A_{12} \tag{5.62}$$

To solve Eq. 5.57 in terms of λ, the following asymptotic expansion is assumed:

$$\lambda(\xi^1, \xi^2, \zeta^\circ) = \lambda_0(\xi^1, \xi^2) + \zeta^\circ \lambda_1(\xi^1, \xi^2) + (\zeta^\circ)^2 \lambda_2(\xi^1, \xi^2) + \cdots \tag{5.63}$$

This asymptotic expansion will turn out to be a Taylor series expansion in powers of ζ^0 around $\zeta^0 = 0$:

$$\lambda(\zeta^0) = \lambda(\zeta^0 = 0) + \zeta^0\left[\frac{\partial\lambda}{\partial\zeta^0}(\zeta^0 = 0)\right] + \ldots \qquad (5.64)$$

It is easy to show, using Eqs. 5.57, 5.59, 5.61, and 5.64, by expansion matching, that:

$$\lambda_0 = \lambda(\zeta^0 = 0) = \sqrt{\frac{a}{A}} \qquad (5.65)$$

$$\lambda_1 = \frac{\partial\lambda}{\partial\zeta^0}(\zeta^0 = 0) = \frac{1}{2}\left[\frac{C\,a}{(A)^2} - \frac{c}{\sqrt{aA}}\right] \qquad (5.66)$$

where

$$c = b_{11}a_{22} + b_{22}a_{11} - 2b_{12}a_{12} \qquad (5.67)$$

Hence, from Eq. 5.63:

$$\boxed{\lambda(\zeta^0) = \sqrt{\frac{a}{A}} + \frac{\zeta^0}{2}\left[\frac{C\,a}{(A)^2} - \frac{c}{\sqrt{aA}}\right] + O(\zeta^0)^2} \qquad (5.68)$$

is the asymptotic expansion for λ in integral powers of ζ^0 that satisfies the condition of no change in volume.

Observe that substituting this expression for λ into Eq. 5.6, one obtains the following displacement field:

$$\boxed{\bar{u} = \bar{u}_0 + \zeta^0\left(\sqrt{\frac{a}{A}}\,\bar{N} - \bar{n}\right) + (\zeta^0)^2\lambda_1\bar{N} + O(\zeta^0)^3} \qquad (5.68)$$

where λ_1 is defined in Eq. 5.66. Also, substituting Eq. 5.68 into Eqs. 5.54-5.56, one obtains the metric tensor components of the present configuration:

$$G_{\alpha\beta} = A_{\alpha\beta} - 2\zeta^o\sqrt{\frac{a}{A}}\,B_{\alpha\beta} - 2(\zeta^o)^2\lambda_1 B_{\alpha\beta} + (\zeta^o)^2\frac{a}{A}B^{\delta}_{\alpha}B_{\delta\beta} + (\zeta^o)^2\frac{\partial\left(\sqrt{\frac{a}{A}}\right)}{\partial\xi^\alpha}\frac{\partial\left(\sqrt{\frac{a}{A}}\right)}{\partial\xi^\beta} + 0(\zeta^o)^3 \tag{5.69*}$$

$$G_{3\alpha} = \zeta^o\sqrt{\frac{a}{A}}\,\frac{\partial\sqrt{\frac{a}{A}}}{\partial\xi^\alpha} + (\zeta^o)^2\lambda_1\frac{\partial\sqrt{\frac{a}{A}}}{\partial\xi^\alpha} + (\zeta^o)^2\sqrt{\frac{a}{A}}\,\frac{\partial\lambda_1}{\partial\xi^\alpha} + (\zeta^o)^2\frac{\partial\sqrt{\frac{a}{A}}}{\partial\xi^\alpha}\frac{\partial\sqrt{\frac{a}{A}}}{\partial\xi^\beta} + 0(\zeta^o)^3 \tag{5.70*}$$

$$G_{33} = \frac{a}{A} + 4\zeta^o\sqrt{\frac{a}{A}}\,\lambda_1 + 0(\zeta^o)^2 \tag{5.71*}$$

The curvature tensor components $B_{\alpha\beta}$ were defined in Eq. 5.24 in terms of the reference surface base vectors and the normal to the reference surface in the present configuration. Hence, all that remains in order to write the metric tensor components of the present configuration in terms of the reference surface displacements is to express the normal $\bar{N}$ and vectors $\bar{A}_\alpha$ as a function of those displacements. The reference surface displacement field in terms of its components u_o^α along the coordinates ξ^α and its component w along the normal to the reference surface is:

$$\bar{u} = u_o^\alpha\,\bar{a}_\alpha + w\bar{n} \tag{5.72}$$

Hence,

$$\bar{A}_\alpha = \frac{\partial\bar{R}_o}{\partial\xi^\alpha} = \bar{a}_\alpha + \frac{\partial}{\partial\xi^\alpha}\left(u_o^\gamma\,\bar{a}_\gamma + w\bar{n}\right) \tag{5.73}$$

*These expressions are shown to illustrate the nature of the terms involved when all terms to a given order of ζ^o are retained. However, these expressions are not intended to form a consistent approximation to the strain energy.

Since

$$\frac{\partial \bar{a}_\alpha}{\partial \xi^\beta} = \left\{ {\delta \atop \alpha \ \beta} \right\} \bar{a}_\delta + b_{\alpha\beta}\bar{n} \tag{5.74}$$

$$\frac{\partial \bar{n}}{\partial \xi^\beta} = - b^\sigma_\beta \, \bar{a}_\sigma \tag{5.75}$$

where

$$\left\{ {\delta \atop \alpha \ \beta} \right\} \equiv \bar{a}^\delta \cdot \frac{\partial \bar{a}_\alpha}{\partial \xi^\beta} \tag{5.76}$$

are the surface Christoffel symbols, Eq. 5.73 becomes

$$\bar{A}_\alpha = \bar{a}_\alpha + \left(u_o{}^\sigma{}_{,\alpha} - w\, b^\sigma_\alpha\right)\bar{a}_\sigma + \left(\frac{\partial w}{\partial \xi^\alpha} + u_o^\gamma\, b_{\gamma\alpha}\right)\bar{n} \tag{5.77}$$

Thus, defining the displacement gradients:*

$$\theta^{\sigma\cdot}_{\cdot\alpha} \equiv u_o{}^\sigma{}_{,\alpha} - w\, b^\sigma_\alpha \tag{5.78}$$

$$\theta_\alpha \equiv \frac{\partial w}{\partial \xi^\alpha} + u_o^\gamma\, b_{\gamma\alpha} \tag{5.79}$$

one obtains:

$$\bar{A}_\alpha = \bar{a}_\alpha + \theta^{\sigma\cdot}_{\cdot\alpha}\, \bar{a}_\sigma + \theta_\alpha \bar{n} \tag{5.80}$$

The components of the deformation gradient tensor of the surface

$$\ell^{\sigma\cdot}_{\cdot\alpha} = \delta^\sigma_\alpha + \theta^{\sigma\cdot}_{\cdot\alpha} \tag{5.81}$$

---

*These displacement gradients are the covariant derivatives in three-dimensional Euclidean space of the three-dimensional Euclidean vector $\bar{u}_o$.

are also useful, and enable one to write:

$$\bar{A}_\alpha = \ell^{\sigma \cdot}_{\cdot \alpha} \, \bar{a}_\sigma + \theta_\alpha \bar{n} \tag{5.82}$$

Since

$$\bar{N} = \frac{\bar{A}_1 \times \bar{A}_2}{\sqrt{A}} \tag{5.83}$$

substituting Eq. 5.82 for $\bar{A}_\alpha$ into this equation for $\bar{N}$, one obtains:

$$\begin{aligned} \bar{N} = \sqrt{\frac{a}{A}} \Big[& \left(\theta_\lambda \ell^{\lambda \cdot}_{\cdot \mu} - \theta_\mu \ell^{\lambda \cdot}_{\cdot \lambda}\right) a^{\mu\nu} \bar{a}_\nu \\ & + \frac{1}{2}\left(\ell^{\lambda \cdot}_{\cdot \lambda} \ell^{\mu \cdot}_{\cdot \mu} - \ell^{\lambda \cdot}_{\cdot \mu} \ell^{\mu \cdot}_{\cdot \lambda}\right) \bar{n} \Big] \end{aligned} \tag{5.84}$$

$$\begin{aligned} = \sqrt{\frac{a}{A}} \Big[& \left(\ell^{1 \cdot}_{\cdot 1} \ell^{2 \cdot}_{\cdot 2} - \ell^{2 \cdot}_{\cdot 1} \ell^{1 \cdot}_{\cdot 2}\right) \bar{n} \\ & + \left(\theta_2 \ell^{2 \cdot}_{\cdot 1} - \theta_1 \ell^{2 \cdot}_{\cdot 2}\right) \bar{a}^1 \\ & + \left(\theta_1 \ell^{1 \cdot}_{\cdot 2} - \theta_2 \ell^{1 \cdot}_{\cdot 1}\right) \bar{a}^2 \Big] \end{aligned} \tag{5.85}$$

This is an <u>exact</u> expression for the normal to the reference surface in the present configuration and is completely independent of the assumed-displacement field.

From Eq. 5.82, one can obtain the expression for the metric tensor of the reference surface with components $A_{\alpha\beta}$ in the present configuration, as a function of the displacements:

$$\boxed{A_{\alpha\beta} = \bar{A}_\alpha \cdot \bar{A}_\beta = a_{\sigma\gamma} \, \ell^{\sigma \cdot}_{\cdot \alpha} \ell^{\gamma \cdot}_{\cdot \beta} + \theta_\alpha \theta_\beta} \tag{5.90}$$

Hence, one can define the components of a Green strain tensor at the reference surface as:

$$\boxed{\overset{\circ}{\gamma}_{\alpha\beta} = \frac{1}{2}\left(A_{\alpha\beta} - a_{\alpha\beta}\right)} \tag{5.91}$$

Also, the ratio of the determinants of the metric tensor of the reference surface in the present and reference configurations can be expressed in terms of the reference surface strain components as*

$$\frac{A}{a} = 1 + 2\overset{\circ}{\gamma}{}^{\alpha}_{\alpha} + 2\,\varepsilon^{\alpha\lambda}\varepsilon^{\beta\mu}\overset{\circ}{\gamma}_{\alpha\beta}\overset{\circ}{\gamma}_{\lambda\mu} \tag{5.92}$$

or

$$\boxed{\frac{A}{a} = \left(1 + 2\overset{\circ}{\gamma}{}^{1}_{1}\right)\left(1 + 2\overset{\circ}{\gamma}{}^{2}_{2}\right) - \left(2\overset{\circ}{\gamma}{}^{1}_{2}\right)\left(2\overset{\circ}{\gamma}{}^{2}_{1}\right)} \tag{5.93}$$

where $\overset{\circ}{\gamma}{}^{\alpha}_{\beta}$ are the mixed components of the Green strain tensor:

$$\overset{\circ}{\gamma}{}^{\alpha}_{\beta} = \frac{1}{2}\left(a^{\alpha\sigma}A_{\sigma\beta} - \delta^{\alpha}_{\beta}\right) \tag{5.94}$$

Differentiating Eq. 5.82 covariantly with respect to ξ^{β}, one obtains:

$$\frac{\partial \bar{A}_{\alpha}}{\partial \xi^{\beta}} = \frac{\partial l^{\sigma\cdot}_{\cdot\alpha}}{\partial \xi^{\beta}}\bar{a}_{\sigma} + l^{\sigma\cdot}_{\cdot\alpha}\frac{\partial \bar{a}_{\sigma}}{\partial \xi^{\beta}} + \frac{\partial \theta_{\alpha}}{\partial \xi^{\beta}}\bar{n} + \theta_{\alpha}\frac{\partial \bar{n}}{\partial \xi^{\beta}} \tag{5.95}$$

$$\frac{\partial \bar{A}_{\alpha}}{\partial \xi^{\beta}} = \left(\frac{\partial l^{\sigma\cdot}_{\cdot\alpha}}{\partial \xi^{\beta}} - b^{\sigma}_{\beta}\theta_{\alpha}\right)\bar{a}_{\sigma} + \left(\frac{\partial \theta_{\beta}}{\partial \xi^{\beta}} + b_{\sigma\beta}l^{\sigma\cdot}_{\cdot\alpha}\right)\bar{n} \tag{5.96}$$

From Eqs. 5.96, 5.85, and 5.24, one can express the curvature tensor components $B_{\alpha\beta}$ in terms of the displacements as:

$$\boxed{\begin{aligned} B_{\alpha\beta} = \sqrt{\frac{a}{A}}\Big[&\frac{1}{2}\left(l^{\lambda\cdot}_{\cdot\lambda}l^{\mu\cdot}_{\cdot\mu} - l^{\lambda\cdot}_{\cdot\mu}l^{\mu\cdot}_{\cdot\lambda}\right)\left(\frac{\partial \theta_{\alpha}}{\partial \xi^{\beta}} + b_{\sigma\beta}l^{\sigma\cdot}_{\cdot\alpha}\right) \\ &+ \left(\theta_{\lambda}l^{\lambda\cdot}_{\cdot\sigma} - \theta_{\sigma}l^{\lambda\cdot}_{\cdot\lambda}\right)\left(\frac{\partial l^{\sigma\cdot}_{\cdot\alpha}}{\partial \xi^{\beta}} - b^{\sigma}_{\beta}\theta_{\alpha}\right)\Big]\end{aligned}} \tag{5.97}$$

*Where $\varepsilon^{\alpha\beta} = 1$ if $\alpha = 1$, $\beta = 2$; $\varepsilon^{\alpha\beta} = -1$ if $\alpha = 2$, $\beta = 1$; and $\varepsilon^{\alpha\beta} = 0$ if $\alpha = \beta$.

Therefore, one can express the Green strain tensor components as:

$$\gamma_{\alpha\beta} = \frac{1}{2}\left(G_{\alpha\beta} - g_{\alpha\beta}\right) \tag{5.98}$$

$$\gamma_{3\alpha} = \frac{1}{2} G_{3\alpha} \tag{5.99}$$

$$\gamma_{33} = \frac{1}{2}\left(G_{33} - 1\right) \tag{5.100}$$

Finally, using Eqs. 5.97, 5.93, 5.91, 5.90, 5.81, 5.79, 5.78, 5.71, 5.70, 5.69, 5.66, 5.62, and 5.14, one can relate these strain components to the displacements for general thin shells.

5.2.2 Strain-Displacement Relations for Plates

At this point, these equations are specialized for a shell with no initial curvature; that is, a plate. The reference surface coordinates ξ^1 and ξ^2 and the normal coordinate ζ^o are chosen so as to form a rectangular Cartesian coordinate system (in the reference configuration), where:

$$\begin{array}{ll} \xi^1 \equiv x \qquad \xi^2 \equiv y & g_{\alpha\beta} = a_{\alpha\beta} = \delta_{\alpha\beta} \\ b_{\alpha\beta} = b^{\delta}_{\sigma} = b^{\gamma\lambda} = 0 & u_o^1 \equiv u \qquad u_o^2 \equiv v \\ g = a = 1 & c = h = k = 0 \end{array} \tag{5.101}$$

Expression 5.68 for the parameter λ that characterizes the thinning or thickening of the plate becomes

$$\lambda(\zeta^o) = \sqrt{\frac{1}{A}} + \frac{\zeta^o}{2}\left[\frac{B_{11}A_{22} + B_{22}A_{11} - 2B_{12}A_{12}}{(A)^2}\right] + O(\zeta^o)^2 \tag{5.102}$$

Taking the middle surface as the reference surface of the plate, the zeroth order term in ζ^o characterizes the (symmetric) thinning due to membrane strains; while the first order term in ζ^o characterizes the (antisymmetric) thinning produced by changes of curvature. Defining a "curvature" $\kappa_{\alpha\beta}$ as:

$$K_{\alpha\beta} \equiv -\sqrt{A}\, B_{\alpha\beta} \tag{5.103}$$

one can obtain, after some manipulations, the following expressions for the components of the Green strain tensor:

$$\gamma_{\alpha\beta} = \overset{\circ}{\gamma}_{\alpha\beta} + \frac{\zeta^\circ}{A} K_{\alpha\beta} + \frac{1}{2}(\zeta^\circ)^2 \frac{1}{(A)^3}\Big\{(\delta_{\alpha\beta} + 2\overset{\circ}{\gamma}_{\alpha\beta})\big[(K_{12})^2 - K_{11}K_{22}\big] + \Big(\frac{1}{2}\frac{\partial A}{\partial \xi^\alpha}\Big)\Big(\frac{1}{2}\frac{\partial A}{\partial \xi^\beta}\Big)\Big\} + O(\zeta^\circ)^3 \tag{5.104}$$

$$\gamma_{3\alpha} = -\frac{\zeta^\circ}{(A)^2}\Big(\frac{1}{2}\frac{\partial A}{\partial \xi^\alpha}\Big) + O(\zeta^\circ)^2 \tag{5.105}$$

$$\gamma_{33} = \frac{1}{2}\Big(\frac{1}{A} - 1\Big) + \frac{\zeta^\circ}{(A)^3}\Big\{(1+2\overset{\circ}{\gamma}_{22})K_{11} + (1+2\overset{\circ}{\gamma}_{22})K_{22} - 2K_{12}\,2\overset{\circ}{\gamma}_{12}\Big\} + O(\zeta^\circ)^2 \tag{5.106}$$

Observe that the transverse shear strain $\gamma_{3\alpha}$ is associated with the strain gradient with respect to the ξ^α coordinates on the reference surface:

$$\begin{aligned}\gamma_{3\alpha} &= -\frac{\zeta^\circ}{(A)^2}\Big(\frac{1}{2}\frac{\partial A}{\partial \xi^\alpha}\Big) \\ &= -\frac{\zeta^\circ}{(A)^2}\Big((1+2\overset{\circ}{\gamma}_{11})\frac{\partial \overset{\circ}{\gamma}_{22}}{\partial \xi^\alpha} + (1+2\overset{\circ}{\gamma}_{22})\frac{\partial \overset{\circ}{\gamma}_{11}}{\partial \xi^\alpha} - 2(2\overset{\circ}{\gamma}_{12})\frac{\partial(2\overset{\circ}{\gamma}_{12})}{\partial \xi^\alpha}\Big)\end{aligned} \tag{5.107}$$

and that it can also be expressed in terms of the gradient of the transverse normal strain γ_{33}:

$$\gamma_{3\alpha} = -\frac{\zeta^\circ}{2(A)^2}\frac{\partial A}{\partial \xi^\alpha} = \frac{\zeta^\circ}{2}\frac{\partial (A)^{-1}}{\partial \xi^\alpha} = \frac{\zeta^\circ}{2}\frac{\partial (2\gamma_{33})}{\partial \xi^\alpha} \tag{5.108}$$

$$\boxed{\gamma_{3\alpha} = \zeta^\circ \frac{\partial \gamma_{33}}{\partial \xi^\alpha}} \tag{5.109}$$

In the present analysis, the following <u>simplifying assumptions</u> are made:

(a) The second order terms in the thickness coordinate ζ° in the expression for $\gamma_{\alpha\beta}$ are negligible

$$K_{\alpha\beta} > \frac{1}{2}\frac{\zeta^\circ}{(A)^2}\Big\{(\delta_{\alpha\beta} + 2\overset{\circ}{\gamma}_{\alpha\beta})\big[(K_{12})^2 - K_{11}K_{22}\big] + \Big(\frac{1}{2}\frac{\partial A}{\partial \xi^\alpha}\Big)\Big(\frac{1}{2}\frac{\partial A}{\partial \xi^\beta}\Big)\Big\} \tag{5.110}$$

and hence Eq. 5.104 reduces to:

$$\gamma_{\alpha\beta} = \overset{\circ}{\gamma}_{\alpha\beta} + \frac{\zeta^\circ}{A}K_{\alpha\beta} + O(\zeta^\circ)^2 \tag{5.111}$$

(b) The "thinning" parameter λ can be characterized by:

$$\lambda = \frac{1}{\sqrt{A}} + O(\zeta^\circ) \tag{5.112}$$

and hence Eq. 5.106 reduces to:

$$\gamma_{33} = \frac{1}{2}\Big(\frac{1}{A} - 1\Big) + O(\zeta^\circ) \tag{5.113}$$

and (c) the transverse shear strains are small:

$$\gamma_{3\alpha} = \zeta^\circ \frac{\partial \gamma_{33}}{\partial \xi^\alpha} = -\frac{\zeta^\circ}{(A)^2}\Big(\frac{1}{2}\frac{\partial A}{\partial \xi^\alpha}\Big) \approx C \tag{5.114}$$

Assumptions (a) and (b) are made since the present formulation is intended to apply to thin shells, and for problems in which the symmetric (with respect to the middle surface) part of the transverse normal strain is the dominant factor in the thickness change. Assumption (c) is made since otherwise (as shown in the next subsection) a general state of multiaxial 2nd Piola-Kirchhoff stress would exist in the shell (even though a state of <u>plane</u> Kirchhoff stress may exist simultaneously). Assumption (c) precludes a detailed analysis of necking. The incorporation of thinning effects under assumptions (a), (b), and (c) does <u>not</u> represent any extra effort in the analysis. The only quantity that needs to be computed to include thinning effects ($A^{1/2}$) would have to be computed anyway for finite strains even if thinning effects were not included, as is evident from Eq. 5.97.

Under these simplifying assumptions, the following plate equations, for finite strains and rotations, and including approximate thinning effects are expressed finally in terms of the reference surface displacements (u, v) and the displacement component (w) along the unit normal to the reference surface, along the Lagrangian (material) vectors $\bar{a}_1$, $\bar{a}_2$ and $\bar{n}$, respectively:

$$\gamma_{\alpha\beta} = \overset{\circ}{\gamma}_{\alpha\beta} + \frac{\overset{\circ}{\zeta}}{A} K_{\alpha\beta} \tag{5.115}$$

$$\gamma_{33} = \frac{1}{2}\left(\frac{1}{A} - 1\right) \tag{5.116}$$

$$A = \left(\frac{ds}{ds_0}\right)^2 = \left(1 + 2\underline{\overset{\circ}{\gamma}_{11}}\right)\left(1 + 2\underline{\overset{\circ}{\gamma}_{22}}\right) - \underline{\left(2\overset{\circ}{\gamma}_{12}\right)^2} \tag{5.117}$$

where $\overset{\circ}{\gamma}_{11}$, $\overset{\circ}{\gamma}_{22}$, $\overset{\circ}{\gamma}_{12}$ are the "membrane" strains at the middle surface. These strains are given by:*

$$\overset{\circ}{\gamma}_{11} = \frac{\partial u}{\partial x} + \underline{\frac{1}{2}\left(\frac{\partial u}{\partial x}\right)^2} + \underline{\frac{1}{2}\left(\frac{\partial v}{\partial x}\right)^2} + \frac{1}{2}\left(\frac{\partial w}{\partial x}\right)^2 \tag{5.118}$$

---

*The underlined terms will be discussed presently.

$$\overset{\circ}{\gamma}_{22} = \frac{\partial v}{\partial y} + \frac{1}{2}\left(\frac{\partial v}{\partial y}\right)^2 + \frac{1}{2}\left(\frac{\partial u}{\partial y}\right)^2 + \frac{1}{2}\left(\frac{\partial w}{\partial y}\right)^2 \tag{5.119}$$

$$2\overset{\circ}{\gamma}_{12} = 2\overset{\circ}{\gamma}_{21} = \frac{\partial u}{\partial y}\left(1 + \frac{\partial u}{\partial x}\right) + \frac{\partial v}{\partial x}\left(1 + \frac{\partial v}{\partial y}\right) + \frac{\partial w}{\partial x}\frac{\partial w}{\partial y} \tag{5.120}$$

and the "bending" expressions κ_{11}, κ_{22}, and κ_{12} are:

$$K_{11} = \alpha\left(-\frac{\partial^2 w}{\partial x^2}\right) + \beta\left(-\frac{\partial^2 u}{\partial x^2}\right) + \eta\left(-\frac{\partial^2 v}{\partial x^2}\right) \tag{5.121}$$

$$K_{22} = \alpha\left(-\frac{\partial^2 w}{\partial y^2}\right) + \beta\left(-\frac{\partial^2 u}{\partial y^2}\right) + \eta\left(-\frac{\partial^2 v}{\partial y^2}\right) \tag{5.122}$$

$$K_{12} = K_{21} = \alpha\left(-\frac{\partial^2 w}{\partial x \partial y}\right) + \beta\left(-\frac{\partial^2 u}{\partial x \partial y}\right) + \eta\left(-\frac{\partial^2 v}{\partial x \partial y}\right) \tag{5.123}$$

where

$$\alpha \equiv 1 + \frac{\partial u}{\partial x} + \frac{\partial v}{\partial y} \tag{5.124}$$

$$\beta \equiv -\frac{\partial w}{\partial x}\left(1 + \frac{\partial v}{\partial y}\right) + \frac{\partial w}{\partial y}\frac{\partial v}{\partial x} \tag{5.125}$$

$$\eta \equiv -\frac{\partial w}{\partial y}\left(1 + \frac{\partial u}{\partial x}\right) + \frac{\partial w}{\partial x}\frac{\partial u}{\partial y} \tag{5.126}$$

Subscripts 1, 2 and 3 stand for the Lagrangian (material) coordinates x, y, and ζ^o, respectively.

The terms underlined by $\sim$ are terms not appearing in von Karman's equations [157] for "large displacements". The much-used von Karman nonlinear plate equations [157], and the popular Sanders shell equation for "moderately small rotations" [158] as well as Koiter's nonlinear shell equation for "small finite deflections" [161], despite its successes, have these inherent limitations: (a) small strain, (b) moderately small rotations, and (c) no transverse normal strains. These equations are very important for analytical purposes, but for a general numerical analysis, the more comprehensive expressions 5.115 through 5.126 should be used, since the extra amount of numerical computation is amply compensated for by the generality of arbitrarily large rotations and finite strains that one accommodates by the use of these equations.

Observe that the following displacement field is associated with expressions 5.115 through 5.126:

$$\bar{u} = u^{\alpha}\bar{a}_{\alpha} + u^{3}\bar{n} \tag{5.127}$$

$$u^{1} = u - \frac{\zeta^{\circ}}{A}\eta \tag{5.128}$$

$$u^{2} = v - \frac{\zeta^{\circ}}{A}\beta \tag{5.129}$$

$$u^{3} = w + \frac{\zeta^{\circ}}{A}\mu - \zeta^{\circ} \tag{5.130}$$

where

$$\mu \equiv \alpha + \frac{\partial u}{\partial x}\frac{\partial v}{\partial y} - \frac{\partial u}{\partial y}\frac{\partial v}{\partial x} \tag{5.131}$$

$$\eta^{2} + \beta^{2} + \mu^{2} = A \tag{5.132}$$

$$\sqrt{\left(\frac{\eta}{\sqrt{A}}\right)^{2} + \left(\frac{\beta}{\sqrt{A}}\right)^{2} + \left(\frac{\mu}{\sqrt{A}}\right)^{2}} = 1 \tag{5.133}$$

5.3 Constitutive Equations for Finite Strains and Rotations

5.3.1 Introduction

Constitutive equations which are valid for finite strains and large displacements are derived for general thin shells under the assumption of plane stress. This assumption is critically examined in terms of the "pseudo-stress" measure (the 2nd Piola-Kirchhoff stress) used in the present analysis. The von Mises strain-rate dependent loading function introduced in Section 3 is derived in terms of the stress and strain quantities associated with the reference configuration for the case of plane stress. The "elastic" and plastic parts of the constitutive relations for strain-hardening, strain-rate dependent materials are shown in explicit form in terms of the stress and strain measures associated with the reference configuration as well as the material constants (to be measured experimentally). Finally, the incremental procedure for the evaluation of the stresses in the finite element analysis is shown. Note that, although the present work is concerned with the numerical analysis of initially flat plates, the theory presented is valid for general thin shells.

5.3.2 Constitutive Equations

5.3.2.1 Plane Stress Assumption for Thin Shells at Finite Strains

An approximate state of plane stress is assumed to exist in the shell. F. John [164] has established that the state of stress in an elastic thin shell, in the absence of surface loads, is indeed approximately plane, by means of concrete estimates of the errors involved. Exploiting modern developments on the behavior of the solutions of elliptic systems of partial differential equations, he published a rigorous proof that the state of stress in the interior domain of an elastic shell (i.e., at a sufficient distance from the edge of a shell) and in the absence of surface loads is approximately plane with an approximately linear distribution through the thickness of the stress parallel to the middle surface. The approximate equations of F. John hold for any magnitude of the deflections, provided the strains remain small everywhere. Unfortunately, a similar proof for large strains does not appear to exist. It seems reasonable that, if a state of plane stress should exist for a thin shell for finite strains, that state of plane stress should be expressed in terms of the Kirchhoff stress components:

$$\tau^3_3 = \tau^3_2 = \tau^2_3 = \tau^3_1 = \tau^1_3 = 0 \tag{5.134}$$

with respect to the present configuration; that is,

$$\bar{\bar{\tau}} = \tau^I_J \, \bar{G}_I \bar{G}^J \tag{5.135}$$

$$\tau^3_J = \tau^J_3 = 0 \tag{5.136}$$

If this condition should be satisfied at all times, the co-rotational rate of the out-of-plane Kirchhoff stress components should vanish:

$$\overset{\circ}{\tau}{}^3_J = \overset{\circ}{\tau}{}^J_3 = 0 \tag{5.137}$$

Since the present analysis is formulated in terms of the reference configuration, these plane-Kirchhoff-stress equations are expressed in terms of the 2nd Piola-Kirchhoff stress components and the Green (Lagrangian) strain, from Eq. 2.270 as:

$$\tau^I_K = (g_{k\ell} + 2\gamma_{k\ell}) S^{\ell i} \tag{5.138}$$

$$\begin{aligned} \tau^3_3 = 0 &= (g_{3\ell} + 2\gamma_{3\ell}) S^{\ell 3} \\ &= (1 + 2\gamma_{33}) S^{33} + 2\gamma_{23} S^{23} + 2\gamma_{13} S^{13} \end{aligned} \tag{5.139}$$

$$\begin{aligned} \tau^3_2 = 0 &= (g_{2\ell} + 2\gamma_{2\ell}) S^{\ell 3} \\ &= (g_{22} + 2\gamma_{22}) S^{23} + 2\gamma_{12} S^{13} + 2\gamma_{23} S^{33} \end{aligned} \tag{5.140}$$

$$\tau_3^2 = 0 = \left(g_{3\ell} + 2\gamma_{3\ell}\right) S^{\ell 2}$$

$$= \left(1 + 2\gamma_{33}\right) S^{23} + 2\gamma_{13} S^{12} + 2\gamma_{23} S^{22} \tag{5.141}$$

$$\tau_1^3 = 0 = \left(g_{1\ell} + 2\gamma_{1\ell}\right) S^{\ell 3}$$

$$= \left(g_{11} + 2\gamma_{11}\right) S^{13} + 2\gamma_{12} S^{23} + 2\gamma_{13} S^{33} \tag{5.142}$$

$$\tau_3^1 = 0 = \left(g_{3\ell} + 2\gamma_{3\ell}\right) S^{\ell 1}$$

$$= \left(1 + 2\gamma_{33}\right) S^{13} + 2\gamma_{23} S^{12} + 2\gamma_{13} S^{11} \tag{5.143}$$

It is clear that the condition of "plane 2nd Piola-Kirchhoff stress"

$$S^{33} = S^{23} = S^{32} = 0 \tag{5.144}$$

satisfies Eqs. 5.139, 5.140, and 5.142, but still Eqs. 5.141 and 5.143:

$$\tau_3^2 = 0 = 2\gamma_{13} S^{12} + 2\gamma_{23} S^{22} \tag{5.145}$$

$$\tau_3^1 = 0 = 2\gamma_{23} S^{12} + 2\gamma_{13} S^{11} \tag{5.146}$$

are not satisfied, in general, unless the transverse shear strains are negligible:

$$\gamma_{13} = \gamma_{23} = 0 \tag{5.147}$$

From Eq. 5.109, this is equivalent to:

$$\zeta^{o}\frac{\partial\gamma_{33}}{\partial\xi^{1}}=\zeta^{o}\frac{\partial\gamma_{33}}{\partial\xi^{2}}=0 \qquad (5.148)$$

which are satisfied exactly at the reference surface ($\zeta^{o} = 0$).

These quantities (γ_{13} and γ_{23}) can be made as small as one pleases by restricting the shell thickness to be sufficiently thin. If the conditions

$$S^{33}=S^{23}=S^{13}=0 \qquad (5.149)$$

$$\gamma_{13}=\gamma_{23}=0 \qquad (5.150)$$

are satisfied at all times, then the material rates of those quantities also vanish; hence,

$$\dot{S}^{33}=\dot{S}^{23}=\dot{S}^{13}=0 \qquad (5.151)$$

$$\dot{\gamma}_{13}=\dot{\gamma}_{23}=0 \qquad (5.152)$$

and, therefore, the co-rotational rate of the out-of-plane Kirchhoff stresses vanishes:

$$\overset{o}{\tau}{}^{3}_{J}=\overset{o}{\tau}{}^{J}_{3}=0 \qquad (5.153)$$

as can be shown from Eq. 2.353:

$$\overset{o}{\tau}{}^{I}_{J}=\dot{S}^{im}C_{mj}+\frac{1}{2}S^{km}\dot{C}_{m\ell}\left[\delta^{i}_{k}\delta^{\ell}_{j}+(C^{-1})^{\ell i}C_{kj}\right] \qquad (5.154)$$

In this expression, C_{ij} and $(C_{ij})^{-1}$ are defined as:

$$C_{ij}=G_{IJ}=g_{ij}+2\gamma_{ij} \qquad (5.155)$$

$$(C^{-1})^{ij} = (g_{ij} + 2\gamma_{ij})^{-1} \tag{5.156}$$

where

$$C_{13} = C_{23} = \dot{C}_{13} = \dot{C}_{23} = (C^{-1})^{13} = (C^{-1})^{23} = 0 \tag{5.157}$$

with matrices:

$$\|C_{ij}\| = \begin{Vmatrix} C_{11} & C_{12} & 0 \\ C_{12} & C_{22} & 0 \\ 0 & 0 & C_{33} \end{Vmatrix} = \begin{Vmatrix} (g_{11}+2\gamma_{11}) & 2\gamma_{12} & 0 \\ 2\gamma_{12} & (g_{22}+2\gamma_{22}) & 0 \\ 0 & 0 & (1+2\gamma_{33}) \end{Vmatrix} \tag{5.158}$$

$$\|(C^{-1})^{ij}\| = \begin{Vmatrix} (C^{-1})^{11} & (C^{-1})^{12} & 0 \\ (C^{-1})^{12} & (C^{-1})^{22} & 0 \\ 0 & 0 & (C^{-1})^{33} \end{Vmatrix} = \begin{Vmatrix} \frac{C_{22}}{\det} & -\frac{C_{12}}{\det} & 0 \\ -\frac{C_{12}}{\det} & \frac{C_{22}}{\det} & 0 \\ 0 & 0 & \frac{1}{C_{33}} \end{Vmatrix} \tag{5.159}$$

$$\det \equiv C_{11}C_{22} - (C_{12})^2 = (g_{11} + 2\gamma_{11})(g_{22} + 2\gamma_{22}) - (2\gamma_{12})^2 \tag{5.160}$$

From Eqs. 5.157 and 5.151, it follows that

$$\begin{aligned} \overset{\circ}{\mathcal{T}}{}^3_J &= \dot{S}^{3m}C_{mj} + \frac{1}{2}S^{km}\dot{C}_{m\ell}\left[\delta^3_k\delta^\ell_j + (C^{-1})^{\ell 3}C_{kj}\right] \\ &= 0 \\ \overset{\circ}{\mathcal{T}}{}^I_3 &= \dot{S}^{im}C_{m3} + \frac{1}{2}S^{km}\dot{C}_{m\ell}\left[\delta^i_k\delta^\ell_3 + (C^{-1})^{\ell i}C_{k3}\right] \\ &= 0 \end{aligned}$$

Hence,

$$S^{33} = S^{23} = S^{13} = 0$$

$$\gamma_{13} = \gamma_{23} = 0 \tag{5.161}$$

are sufficient conditions for the existence of a state of plane stress and are assumed in the present analysis to hold at all times.

5.3.2.2 von Mises Strain-Rate-Dependent Loading Function for Plane Stress and Finite Strains

In the finite-strain elastic-plastic strain-rate dependent theory displayed in Subsection 3.3.3, a loading function ${}^{s}\Phi$ (yield surface in stress space) was assumed to exist for each sublayer s of the mechanical sublayer model. This loading function ${}^{s}\Phi$ was assumed to be expressible in terms of the deviatoric Kirchhoff stress ${}^{s}\bar{\bar{\tau}}^{D}$ of sublayer s and a parameter ${}^{s}\tau_{u}$ which depends on material properties of sublayer s and the deviatoric rate of deformation tensor $\bar{\bar{D}}^{D}$, as expressed in Eq. 3.45 and repeated here for convenience:

$${}^{s}\Phi = {}^{s}\bar{\bar{\tau}}^{D} : {}^{s}\bar{\bar{\tau}}^{D} - \frac{2}{3}\left({}^{s}\tau_{u_0}^{y}\right)^2 \left(1 + \left(\frac{\sqrt{\frac{3}{2}\bar{\bar{D}}^{D} : \bar{\bar{D}}^{D}}}{{}^{s}d}\right)^{\frac{1}{{}^{s}p}}\right) \tag{5.162}$$

This loading function ${}^{s}\Phi$ will be expressed in terms of the nonzero components of stress S^{ij} and strain C_{ij} under the plane stress condition of Eq. 5.161. Equation 5.162 can be rewritten as:

$$\begin{aligned} {}^{s}\Phi &= \frac{2}{3}\left(\frac{3}{2}\,{}^{s}\bar{\bar{\tau}}^{D} : {}^{s}\bar{\bar{\tau}}^{D} - \left({}^{s}\tau_{u}^{y}\right)^2\right) \\ &= \frac{2}{3}\left({}^{s}\Phi_{1} - {}^{s}\Phi_{2}\right) \end{aligned} \tag{5.163}$$

The <u>first term</u> of this expression, namely (subscript "1")

$${}^{s}\Phi_{1} \equiv \frac{3}{2}\,{}^{s}\bar{\bar{\tau}}^{D} : {}^{s}\bar{\bar{\tau}}^{D} \tag{5.164}$$

can be written as

$$ {}^{s}\Phi_1 = \frac{3}{2}\left({}^{s}\bar{\bar{\tau}} - \frac{1}{3}\left(tr\,{}^{s}\bar{\bar{\tau}}\right)\bar{\bar{1}}\right):\left({}^{s}\bar{\bar{\tau}} - \frac{1}{3}\left(tr\,{}^{s}\bar{\bar{\tau}}\right)\bar{\bar{1}}\right) \tag{5.165} $$

$$ = \frac{3}{2}\left({}^{s}\bar{\bar{\tau}} : {}^{s}\bar{\bar{\tau}} - \frac{1}{3}\left(tr\,{}^{s}\bar{\bar{\tau}}\right)^2\right) \tag{5.166} $$

by means of the definition of ${}^{s}\bar{\bar{T}}^{D}$, Eq. 3.40, and making use of these facts:

$$ \bar{\bar{1}} : \bar{\bar{1}} = 3 \tag{5.167} $$

$$ {}^{s}\bar{\bar{\tau}} : \bar{\bar{1}} = \bar{\bar{1}} : {}^{s}\bar{\bar{\tau}} = tr\ {}^{s}\bar{\bar{\tau}} \tag{5.168} $$

Equation 5.166 for ${}^{s}\Phi_1$ can be written in terms of the components of ${}^{s}\bar{\bar{T}}$ in the present configuration of the body-fixed convected coordinate system:

$$ {}^{s}\bar{\bar{\tau}} = {}^{s}\tau^{I}_{J}\,\bar{G}_{I}\,\bar{G}^{J} \tag{5.169} $$

Hence,

$$ {}^{s}\Phi_1 = \frac{3}{2}\left({}^{s}\tau^{I}_{J}\,{}^{s}\tau^{J}_{I} - \frac{1}{3}\left(\tau^{K}_{K}\right)^2\right) \tag{5.170} $$

or

$$ \boxed{{}^{s}\Phi_1 = \frac{3}{2}\,{}^{s}\tau^{I}_{J}\,{}^{s}\tau^{J}_{I} - \frac{1}{2}\left(\tau^{K}_{K}\right)^2} \tag{5.171} $$

Under plane stress

$$ \tau^{3}_{3} = \tau^{3}_{2} = \tau^{2}_{3} = \tau^{1}_{3} = \tau^{3}_{1} = 0\ , \tag{5.172} $$

Eq. 5.171 becomes

$$ \boxed{{}^{s}\Phi_1 = \left({}^{s}\tau^{1}_{1}\right)^2 + \left({}^{s}\tau^{1}_{2}\right)^2 + 3\left({}^{s}\tau^{1}_{2}\right)\left({}^{s}\tau^{2}_{1}\right) - {}^{s}\tau^{1}_{1}\,{}^{s}\tau^{2}_{2}} \tag{5.173} $$

Since, from Eq. 2.270:

$$\tau_K^I = C_{kl} S^{li} \tag{5.174}$$

and, from Eqs. 5.161 and 5.165:

$$S^{33} = S^{23} = S^{13} = 0$$

$$C_{13} = C_{23} = 0$$

then, Eq. 5.173 is equivalent to:

$$\boxed{\begin{aligned} {}^s\Phi_1 = {} & (C_{11}S^{11})^2 + (C_{22}S^{22})^2 + \left[(C_{12})^2 + 3C_{11}C_{22}\right](S^{12})^2 \\ & + \left[C_{11}S^{11} + C_{22}S^{22}\right]4C_{12}S^{12} + \left[3(C_{12})^2 - C_{11}C_{22}\right]S^{11}S^{22} \end{aligned}} \tag{5.175}$$

where the components C_{ij} of the right Cauchy-Green deformation tensor were defined in Eq. 5.158 in terms of the components γ_{ij} of the Green strain tensor.

The second term in the loading function ${}^s\Phi$ is (from Eq. 5.163):

$$ {}^s\Phi_2 \equiv ({}^s\tau_u^y)^2 = ({}^s\tau_{u_o}^y)^2 \left(1 + \left(\frac{\sqrt{\frac{3}{2}\bar{\bar{D}}^D : \bar{\bar{D}}^D}}{{}^sd}\right)^{\frac{1}{{}^sp}}\right)^2 \tag{5.176}$$

where ${}^s\tau_{uo}$ is the static (rate independent) Kirchhoff stress yield of a specimen in uniaxial tension, and ${}^sd$ and ${}^sp$ are material strain-rate constants, as discussed in Subsection 3.3. Equation 5.176 can be rewritten as:

$$ {}^s\Phi_2 = ({}^s\tau_{u_o}^y)^2 \left(1 + \left(\frac{\sqrt{D}}{{}^sd}\right)^{\frac{1}{{}^sp}}\right)^2 \tag{5.177}$$

where D is an "equivalent deformation rate" defined by:

$$D = \frac{3}{2}\bar{\bar{D}}^D : \bar{\bar{D}}^D \tag{5.178}$$

which, being the scalar product of two deviatoric tensors, can be expressed as:

$$D = \frac{3}{2} D^I_J D^J_I - \frac{1}{2} (D^K_K)^2$$

$$\bar{\bar{D}} = D^I_J \bar{G}_I \bar{G}^J \tag{5.179}$$

just as the scalar product of the deviatoric Kirchhoff stress tensors were expressed in the form of Eq. 5.171. From Eq. 2.188 one can express the components D^I_J of the rate-of-deformation tensor in terms of the material rate of the Green strain components $\dot{\gamma}_{ij}$:

$$D^I_J = (C^{-1})^{i\ell} \dot{\gamma}_{\ell j} \tag{5.180}$$

where the components $(C^{-1})^{i\ell}$ were defined in Eq. 5.159. Since

$$(C^{-1})^{\alpha 3} = \dot{\gamma}_{\alpha 3} = 0 \qquad \alpha = 1,2 \tag{5.181}$$

from Eq. 5.157, then:

$$D^1_3 = D^3_1 = D^2_3 = D^3_2 = 0 \tag{5.182}$$

and hence, Eq. 5.179 becomes:

$$\boxed{D = (D^1_1)^2 + (D^2_2)^2 + 3(D^1_2)(D^2_1) - (D^1_1)(D^2_2) + D^3_3(D^3_3 - D^1_1 - D^2_2)} \tag{5.183}$$

Since the present analysis is formulated in terms of the strain components γ_{ij}, Eq. 5.183 will be expressed in terms of these quantities. From Eqs. 5.180 and 5.158:

$$D^3_3 = (C^{-1})^{33} \dot{\gamma}_{33} = \frac{\dot{\gamma}_{33}}{C_{33}} = \frac{\dot{\gamma}_{33}}{(1+2\gamma_{33})} \tag{5.184}$$

It can be shown, after some tedious algebra, that

$$\boxed{\begin{aligned} D^3_3 = &-(\mathring{C}^{-1})^{11}\frac{d}{dt}(\mathring{\gamma}_{11}) - (\mathring{C}^{-1})^{22}\frac{d}{dt}(\mathring{\gamma}_{22}) \\ &-(\mathring{C}^{-1})^{12}\frac{d}{dt}(\mathring{C}_{12}) \end{aligned}} \tag{5.185}$$

where

$$\mathring{C}_{ij} = a_{ij} + 2\mathring{\gamma}_{ij} \tag{5.186}$$

$$\|\mathring{C}_{ij}\| = \begin{Vmatrix} \mathring{C}_{11} & \mathring{C}_{12} & 0 \\ \mathring{C}_{12} & \mathring{C}_{22} & 0 \\ 0 & 0 & C_{33} \end{Vmatrix} = \begin{Vmatrix} (a_{11}+2\mathring{\gamma}_{11}) & 2\mathring{\gamma}_{12} & 0 \\ 2\mathring{\gamma}_{12} & (a_{22}+2\mathring{\gamma}_{22}) & 0 \\ 0 & 0 & (1+2\gamma_{33}) \end{Vmatrix} \tag{5.187}$$

$$\|(\mathring{C}^{-1})^{ij}\| = \begin{Vmatrix} (\mathring{C}^{-1})^{11} & (\mathring{C}^{-1})^{12} & 0 \\ (\mathring{C}^{-1})^{12} & (\mathring{C}^{-1})^{22} & 0 \\ 0 & 0 & (C^{-1})^{33} \end{Vmatrix} = C_{33}\begin{Vmatrix} \mathring{C}_{22} & -\mathring{C}_{12} & 0 \\ -\mathring{C}_{12} & \mathring{C}_{11} & 0 \\ 0 & 0 & \dfrac{1}{(C_{33})^2} \end{Vmatrix} \tag{5.188}$$

$$C_{33} = 1 + 2\gamma_{33} = \frac{a}{A} = \frac{1}{(1+2\mathring{\gamma}^1_1)(1+2\mathring{\gamma}^2_2) - (2\mathring{\gamma}^1_2)(2\mathring{\gamma}^2_1)} \tag{5.189}$$

and

$$
\begin{aligned}
\mathcal{D} = {} & \left[(C^{-1})^{11}\dot{\gamma}_{11}\right]^2 + \left[(C^{-1})^{22}\dot{\gamma}_{22}\right]^2 \\
& + \left\{\left[(C^{-1})^{12}\right]^2 + 3\,(C^{-1})^{11}(C^{-1})^{22}\right\}(\dot{\gamma}_{12})^2 \\
& + 4\left[(C^{-1})^{11}\dot{\gamma}_{11} + (C^{-1})^{22}\dot{\gamma}_{22}\right](C^{-1})^{12}\dot{\gamma}_{12} \\
& + \left\{3\left[(C^{-1})^{12}\right]^2 - (C^{-1})^{11}(C^{-1})^{22}\right\}\dot{\gamma}_{11}\dot{\gamma}_{22} \\
& + D_3^3\left[D_3^3 - (C^{-1})^{11}\dot{\gamma}_{11} - (C^{-1})^{22}\dot{\gamma}_{22} - (C^{-1})^{12}\dot{\gamma}_{12}\right]
\end{aligned}
\tag{5.190}
$$

where the components $[C^{-1}]^{ij}$ are defined in Eq. 5.159 and D_3^3 is defined by Eq. 5.185. Therefore,

$$
{}^s\Phi = \frac{2}{3}\left({}^s\Phi_1 - {}^s\Phi_2\right)
$$

is defined in terms of S^{ij}, γ_{ij} and $\dot{\gamma}_{ij}$ by Eqs. 5.175, 5.158, 5.177, 5.185, 5.187, 5.188, 5.159, and 5.190.

5.3.2.3 "Elastic" Part of the Constitutive Relations for Plane Stress and Finite Strains

Consider Eq. 3.31; namely,

$$
{}^s\overset{\circ}{\overline{\overline{\tau}}} = {}^s\overline{\overline{\overline{\overline{E}}}} : {}^s\overline{\overline{D}}^e \tag{5.191}
$$

where ${}^s\overset{\circ}{\overline{\overline{T}}}$ is the co-rotational rate of the Kirchhoff stress ${}^s\overline{\overline{T}}$ of sublayer s, ${}^s\overline{\overline{\overline{\overline{E}}}}$ is the fourth order "elasticity tensor", considered here to be the same for each sublayer s:

$$
\overline{\overline{\overline{\overline{E}}}} = {}^s\overline{\overline{\overline{\overline{E}}}} \tag{5.192}
$$

and $\overline{\overline{D}}^e$ the "elastic" part of the rate-of-deformation tensor. Expression 5.192 will be made explicit in terms of the components in the present configuration of the body-fixed convected coordinate system:

$$
{}^s\overset{\circ}{\overline{\overline{\tau}}} = {}^s\overset{\circ}{\tau}{}^I_J\, \overline{G}_I \overline{G}^J \tag{5.193}
$$

$$\overline{\overline{\overline{E}}} = E^{I\,K}_{J\,L}\, \overline{G}_I \overline{G}^J \overline{G}_K \overline{G}^L \tag{5.194}$$

$$^s\overline{\overline{D}}^e = {}^sD^L_K\, \overline{G}_L \overline{G}^K \tag{5.195}$$

Hence, one obtains

$$\boxed{{}^s\overset{\circ}{\tau}{}^I_J = E^{I\,K}_{J\,L}\, ({}^sD^e)^L_K} \tag{5.196}$$

For plane-stress conditions of an isotropic material, the classical plane-stress elasticity relations are generalized to finite strains and rotations as follows:

$$^s\overset{\circ}{\tau}{}^1_1 = E^{11}_{11}\,({}^sD^e)^1_1 + E^{12}_{12}\,({}^sD^e)^2_2 \tag{5.197}$$

$$^s\overset{\circ}{\tau}{}^2_2 = E^{22}_{22}\,({}^sD^e)^2_2 + E^{21}_{21}\,({}^sD^e)^1_1 \tag{5.198}$$

$$^s\overset{\circ}{\tau}{}^1_2 = E^{12}_{21}\,({}^sD^e)^1_2 \tag{5.199}$$

$$^s\overset{\circ}{\tau}{}^2_1 = E^{21}_{12}\,({}^sD^e)^2_1 \tag{5.200}$$

where the mixed components of the fourth order elasticity tensor $\overline{\overline{\overline{E}}}$ are:

$$E^{11}_{11} = E^{22}_{22} = \frac{E}{(1-\nu^2)} \tag{5.201}$$

$$E^{12}_{12} = E^{21}_{21} = \frac{E\,\nu}{(1-\nu^2)} = \nu\, E^{11}_{11} \tag{5.202}$$

$$E^{12}_{21} = E^{21}_{12} = \frac{E}{1+\nu} = E^{11}_{11} - E^{12}_{12} = (1-\nu)E^{11}_{11} \tag{5.203}$$

The physical components* of a fourth order tensor are,

$$\left(E^{IK}_{JL}\right)^{physical} = \sqrt{\frac{G_{KK}}{G_{LL}}\;\frac{G_{II}}{G_{JJ}}}\; E^{IK}_{JL} \tag{5.204}$$

Hence,

$$\left(E^{11}_{11}\right)^{physical} = \sqrt{\frac{G_{11}}{G_{11}}\;\frac{G_{11}}{G_{11}}}\; E^{11}_{11} = E^{11}_{11} \tag{5.205}$$

$$\left(E^{22}_{22}\right)^{physical} = \sqrt{\frac{G_{22}}{G_{22}}\;\frac{G_{22}}{G_{22}}}\; E^{22}_{22} = E^{22}_{22} \tag{5.206}$$

$$\left(E^{12}_{12}\right)^{physical} = \sqrt{\frac{G_{22}}{G_{22}}\;\frac{G_{11}}{G_{11}}}\; E^{12}_{12} = E^{12}_{12} \tag{5.207}$$

$$\left(E^{21}_{21}\right)^{physical} = \sqrt{\frac{G_{11}}{G_{11}}\;\frac{G_{22}}{G_{22}}}\; E^{21}_{21} = E^{21}_{21} \tag{5.208}$$

$$\left(E^{12}_{21}\right)^{physical} = \sqrt{\frac{G_{22}}{G_{11}}\;\frac{G_{11}}{G_{22}}}\; E^{12}_{21} = E^{12}_{21} \tag{5.209}$$

$$\left(E^{21}_{12}\right)^{physical} = \sqrt{\frac{G_{11}}{G_{22}}\;\frac{G_{22}}{G_{11}}}\; E^{21}_{12} = E^{21}_{12} \tag{5.210}$$

---

*As defined by Truesdell [37].

The components E^{IK}_{JL} in Eqs. 5.197-5.200 are, indeed, physical components and, therefore, E and ν are Young's modulus and Poisson's ratio, respectively, as measured from experiments.

Expressions 5.197-5.200 are written in terms of the co-rotational Kirchhoff stress rate and the rate-of-deformation tensor, both quantities associated with the present configuration. Since the present finite element analysis is formulated in terms of a reference configuration, one has to express Eqs. 5.197-5.200 in terms of the 2nd Piola-Kirchhoff stress and the Green strain.

Before doing this, an important point will be mentioned. In Section 3, Eq. 3.32, the following additive decomposition of the rate-of-defomation tensor $\bar{\bar{D}}$ was assumed:

$$ {}^s\bar{\bar{D}} = \bar{\bar{D}} = {}^s\bar{\bar{D}}^e + {}^s\bar{\bar{D}}^p \tag{5.211} $$

From Eq. 2.182:

$$ \dot{\bar{\bar{\gamma}}} = \bar{\bar{F}}^T \cdot \bar{\bar{D}} \cdot \bar{\bar{F}} \tag{5.212} $$

Hence, one can express the additive decomposition of the rate-of-deformation tensor $\bar{\bar{D}}$ in terms of the material rate of the Green strain tensor $\dot{\bar{\bar{\gamma}}}$ as follows:

$$ \dot{\bar{\bar{\gamma}}} = \bar{\bar{F}}^T \cdot \bar{\bar{D}} \cdot \bar{\bar{F}} = \bar{\bar{F}}^T \cdot \left({}^s\bar{\bar{D}}^e + {}^s\bar{\bar{D}}^p\right) \cdot \bar{\bar{F}} $$

$$ \boxed{\dot{\bar{\bar{\gamma}}} = \bar{\bar{F}}^T \cdot {}^s\bar{\bar{D}}^e \cdot \bar{\bar{F}} + \bar{\bar{F}}^T \cdot {}^s\bar{\bar{D}}^p \cdot \bar{\bar{F}}} \tag{5.213} $$

If one wishes, one may define the "elastic" Green strain rate as:

$$ \boxed{{}^s\dot{\bar{\bar{\gamma}}}^e \equiv \bar{\bar{F}}^T \cdot {}^s\bar{\bar{D}}^e \cdot \bar{\bar{F}}} \tag{5.214} $$

and the "plastic" Green strain rate as:

$$ \boxed{{}^s\dot{\bar{\bar{\gamma}}}^p \equiv \bar{\bar{F}}^T \cdot {}^s\bar{\bar{D}}^p \cdot \bar{\bar{F}}} \tag{5.215} $$

Therefore, from Eq. 5.213:

$$\boxed{\overset{\bullet}{\overset{=}{\gamma}} = {}^{s}\overset{\bullet}{\overset{=}{\gamma}}{}^{e} + {}^{s}\overset{\bullet}{\overset{=}{\gamma}}{}^{p}} \tag{5.216}$$

the Green strain material rate $\overset{\bullet}{\overset{=}{\gamma}}$ can be decomposed, as well as $\overset{=}{D}$, into additive elastic and plastic parts.

Since this was shown to be true in the absolute tensor notation, it is true for <u>any coordinate system</u>. In particular, for the body-fixed convected coordinate system one obtains:

$$D^{I}_{J} = {}^{s}(D^{I}_{J})^{e} + {}^{s}(D^{I}_{J})^{p} \tag{5.217}$$

$$D^{I}_{J} G_{IK} = {}^{s}(D^{I}_{J})^{e} G_{IK} + {}^{s}(D^{I}_{J})^{p} G_{IK} \tag{5.218}$$

$$D_{JK} = {}^{s}(D_{JK})^{e} + {}^{s}(D_{JK})^{p} \tag{5.219}$$

From Eq. 2.175:

$$\dot{\gamma}_{ij} = D_{IJ} \tag{5.220}$$

Therefore,

$$\dot{\gamma}_{ij} = {}^{s}(\dot{\gamma}_{ij})^{e} + {}^{s}(\dot{\gamma}_{ij})^{p} \tag{5.221}$$

or, from Eq. 2.188:

$$D^{I}_{J} = (C^{-1})^{i\ell} \dot{\gamma}_{\ell j} \tag{5.222}$$

Hence,

$$D^{I}_{J} = {}^{s}(D^{I}_{J})^{e} + {}^{s}(D^{I}_{J})^{p} = (C^{-1})^{i\ell}\, {}^{s}(\dot{\gamma}_{\ell j})^{e} + (C^{-1})^{i\ell}\, {}^{s}(\dot{\gamma}_{\ell j})^{p} \tag{5.223}$$

where

$$ {}^{s}(D^{I}_{J})^{e} = (C^{-1})^{i\ell}\; {}^{s}(\dot{\gamma}_{\ell j})^{e} \tag{5.224} $$

$$ {}^{s}(D^{I}_{J})^{p} = (C^{-1})^{i\ell}\; {}^{s}(\dot{\gamma}_{\ell j})^{p} \tag{5.225} $$

Note, that the deformation gradient tensor $\overline{\overline{F}}$ appearing in expressions 5.213, 5.214, and 5.215 is the total deformation gradient tensor that measures the total deformation from the reference configuration to the present configuration. Also, the Cauchy-Green deformation tensor components $(C^{-1})^{i\ell}$ appearing in expressions 5.223, 5.224, and 5.225 are the total deformation tensor components. The decompositions

$$ \overline{\overline{D}} = {}^{s}\overline{\overline{D}}^{e} + {}^{s}\overline{\overline{D}}^{p} \tag{5.226} $$

$$ \dot{\overline{\overline{\gamma}}} = {}^{s}\dot{\overline{\overline{\gamma}}}^{e} + {}^{s}\dot{\overline{\overline{\gamma}}}^{p} \tag{5.227} $$

are exact. The first decomposition (Eq. 5.226) measures the "elastic" and plastic deformation rates with respect to the differential length of the differential line element in the present configuration, while the second measures it with respect to the reference configuration differential line element.

The basic assumption is that the differential line element dS in the present configuration can be decomposed into "elastic" and "plastic" parts:

$$ (dS)^{2} = d\overline{R} \cdot d\overline{R} \tag{5.228} $$

$$ dS = {}^{s}(dS)^{e} + {}^{s}(dS)^{p} \tag{5.229} $$

Hence, the material rate of the differential line element dS in the present configuration can also be decomposed into elastic and plastic parts:

$$\frac{d}{dt}(dS) = d\dot{S} \tag{5.230}$$

$$d\dot{S} = {}^{s}(d\dot{S})^{e} + {}^{s}(d\dot{S})^{p} \tag{5.231}$$

Dividing this relation by the length of the differential line element in the present configuration, one obtains the additive decomposition of the rate-of-deformation tensor (Eq. 5.226):

$$\boxed{\begin{aligned} \frac{(d\dot{S})}{dS} &= \frac{{}^{s}(d\dot{S})^{e}}{dS} + \frac{{}^{s}(d\dot{S})^{p}}{dS} \\ \overline{\overline{D}} &= {}^{s}\overline{\overline{D}}^{e} + {}^{s}\overline{\overline{D}}^{p} \end{aligned}} \tag{5.232}$$

Since the Green strain tensor compares lengths in the present and reference configurations:

$$\gamma = \frac{1}{2}\left(\frac{(dS)^2 - (ds)^2}{(ds)^2}\right) = \frac{1}{2}\left(\frac{(dS)^2}{(ds)^2} - 1\right) \tag{5.233}$$

$$C = \frac{(dS)^2}{(ds)^2} = 1 + 2\gamma = (U)^2 \tag{5.234}$$

its material rate is:

$$\dot{\gamma} = \frac{d}{dt}\left(\frac{1}{2}\left(\left(\frac{dS}{ds}\right)^2 - 1\right)\right) = \frac{dS}{ds}\left(\frac{d\dot{S}}{ds}\right) \tag{5.235}$$

$$\dot{\gamma} = \frac{1}{2}\dot{C} \tag{5.236}$$

Multiplying Eq. 5.231 by $C = 1 + 2\gamma = (\frac{dS}{ds})^2$, one obtains:

$$\left(\frac{dS}{ds}\right)\left(\frac{d\dot{S}}{ds}\right) = \frac{dS}{ds}\,\frac{{}^{s}(d\dot{S})^{e}}{ds} + \frac{dS}{ds}\,\frac{{}^{s}(d\dot{S})^{p}}{ds} \tag{5.237}$$

$$\dot{\bar{\bar{\gamma}}} = {}^{s}\dot{\bar{\bar{\gamma}}}^{e} + {}^{s}\dot{\bar{\bar{\gamma}}}^{p} \tag{5.238}$$

which in equivalent to:

$$\boxed{\begin{aligned} \frac{d\dot{S}}{ds} &= \frac{{}^{s}(d\dot{S})^{e}}{ds} + \frac{{}^{s}(d\dot{S})^{p}}{ds} \\ \dot{\bar{\bar{\gamma}}} &= {}^{s}\dot{\bar{\bar{\gamma}}}^{e} + {}^{s}\dot{\bar{\bar{\gamma}}}^{p} \end{aligned}} \tag{5.239}$$

Therefore, the additive decomposition of the rate-of-deformation tensor $\bar{\bar{D}}$ into "elastic" and plastic parts ${}^{s}\bar{\bar{D}}^{e}$ and ${}^{s}\bar{\bar{D}}^{p}$ is equivalent to the additive decomposition of the material rate $(d\dot{S})$ of the differential line element dS in the present configuration into "elastic" $({}^{s}d\dot{S}^{e})$ and plastic $({}^{s}d\dot{S}^{p})$ parts, which are measured with respect to the total differential line element dS in the present configuration. The additive decomposition of the material rate $\dot{\bar{\bar{\gamma}}}$ of the Green strain tensor $\bar{\bar{\gamma}}$ into "elastic" ${}^{s}\dot{\bar{\bar{\gamma}}}^{e}$ and plastic ${}^{s}\dot{\bar{\bar{\gamma}}}^{p}$ parts is tantamount to the additive decomposition of the material rate $(d\dot{S})$ of the differential line element (dS) in the present configuration into "elastic" $({}^{s}d\dot{s}^{e})$ and plastic $({}^{s}d\dot{s}^{p})$ parts, which are measured with respect to differential line element ds in the reference configuration.

Consider, for the moment, that the deformation in sublayer s is totally elastic, then

$$^{s}(D^{I}_{J})^{e} = D^{I}_{J} \tag{5.240}$$

$$^{s}(\dot{\gamma}_{ij})^{e} = \dot{\gamma}_{ij} \tag{5.241}$$

$$D^{I}_{J} = (C^{-1})^{il}\,\dot{\gamma}_{lj} \tag{5.242}$$

By means of Eq. 5.242 and Eq. 2.353; namely,

$$\overset{e}{\tau}{}^{I}_{J} = \dot{S}^{im} C_{mj} + \frac{1}{2} S^{km} \dot{C}_{m\ell}\left[\delta^{i}_{k}\delta^{\ell}_{j} + (C^{-1})^{\ell i} C_{kj}\right] \quad (5.243)$$

one can express Eqn. 5.197-5.200 in terms of the 2nd Piola-Kirchhoff components ${}^{s}S^{ij}$ and Green strain $\gamma_{ij} = \frac{1}{2}(C_{ij} - g_{ij})$, to obtain after some lengthy algebra:

$$\begin{aligned}{}^{s}\dot{S}^{11} = {}& \dot{\gamma}_{11}\left\{E^{11}_{11}\left[(C^{-1})^{11}\right]^2 - 2\,{}^{s}S^{11}(C^{-1})^{11}\right\} \\ &+ (2\dot{\gamma}_{12})\left\{E^{11}_{11}(C^{-1})^{12}(C^{-1})^{11} - {}^{s}S^{12}(C^{-1})^{11} - {}^{s}S^{11}(C^{-1})^{12}\right\} \\ &+ \dot{\gamma}_{22}\left\{E^{12}_{12}(C^{-1})^{11}(C^{-1})^{22} + E^{12}_{21}\left[(C^{-1})^{12}\right]^2 - 2\,{}^{s}S^{12}(C^{-1})^{12}\right\} \quad (5.244)\end{aligned}$$

$$\begin{aligned}{}^{s}\dot{S}^{22} = {}& \dot{\gamma}_{22}\left\{E^{11}_{11}\left[(C^{-1})^{22}\right]^2 - 2\,{}^{s}S^{22}(C^{-1})^{22}\right\} \\ &+ (2\dot{\gamma}_{12})\left\{E^{11}_{11}(C^{-1})^{12}(C^{-1})^{22} - {}^{s}S^{12}(C^{-1})^{22} - {}^{s}S^{22}(C^{-1})^{12}\right\} \\ &+ \dot{\gamma}_{11}\left\{E^{12}_{12}(C^{-1})^{22}(C^{-1})^{11} + E^{12}_{21}\left[(C^{-1})^{12}\right]^2 - 2\,{}^{s}S^{12}(C^{-1})^{12}\right\}\end{aligned}$$

(5.245)

$$\begin{aligned}{}^{s}\dot{S}^{12} = {}& \dot{\gamma}_{11}\left\{E^{11}_{11}(C^{-1})^{11}(C^{-1})^{12} - {}^{s}S^{11}(C^{-1})^{12} - {}^{s}S^{12}(C^{-1})^{11}\right\} \\ &+ \frac{1}{2}(2\dot{\gamma}_{12})\Big\{\left(E^{11}_{11} + E^{12}_{12}\right)\left[(C^{-1})^{12}\right]^2 + E^{12}_{21}(C^{-1})^{11}(C^{-1})^{22} - 2\,{}^{s}S^{12}(C^{-1})^{12} \\ &- {}^{s}S^{12}(C^{-1})^{12} - {}^{s}S^{11}(C^{-1})^{22} - {}^{s}S^{22}(C^{-1})^{11}\Big\} \\ &+ \dot{\gamma}_{22}\left\{E^{11}_{11}(C^{-1})^{22}(C^{-1})^{12} - {}^{s}S^{22}(C^{-1})^{12} - {}^{s}S^{12}(C^{-1})^{22}\right\}\end{aligned}$$

(5.246)

where

$$E^{11}_{11} = \frac{E}{(1-\nu^2)} \tag{5.247}$$

$$E^{12}_{12} = \frac{\nu E}{(1-\nu^2)} = \nu E^{11}_{11} \tag{5.248}$$

$$E^{12}_{21} = \frac{E}{1+\nu} = (1-\nu) E^{11}_{11} \tag{5.249}$$

as defined in Eqs. 5.201-5.203, and the inverse of the right Cauchy-Green deformation tensor $[C^{-1}]^{ij}$ was defined in Eq. 5.159. Compare Eqs. 5.244-5.246 with their "small strain" approximation:

$${}^s\dot{S}^{11} = \dot{\gamma}_{11} E^{11}_{11} + \dot{\gamma}_{22} E^{12}_{12} \tag{5.250}$$

$${}^s\dot{S}^{22} = \dot{\gamma}_{22} E^{11}_{11} + \dot{\gamma}_{11} E^{12}_{12} \tag{5.251}$$

$${}^s\dot{S}^{12} = \dot{\gamma}_{12} E^{12}_{21} \tag{5.252}$$

to evaluate the errors incurred in such an approximation.

5.3.2.4 "Plastic" Part of the Constitutive Relations for Plane Stress and Finite Strains

From Section 3, Eq. 3.33, the constitutive relations of the sth sublayer is:

$${}^s\overset{\circ}{\underline{\underline{\tau}}} = \underline{\underline{\underline{\underline{E}}}} : (\underline{\underline{D}} - {}^s\underline{\underline{D}}^P) \tag{5.253}$$

or

$${}^s\overset{\circ}{\underline{\underline{\tau}}} = \underline{\underline{\underline{\underline{E}}}} : \underline{\underline{D}} - \underline{\underline{\underline{\underline{E}}}} : {}^s\underline{\underline{D}}^P$$

$${}^s\overset{\circ}{\underline{\underline{\tau}}} = ({}^s\overset{\circ}{\underline{\underline{\tau}}})_1 - ({}^s\overset{\circ}{\underline{\underline{\tau}}})_2 \tag{5.254}$$

The first part of this relationship; namely,

$$\left({}^{s}\overset{\circ}{\overline{\overline{\tau}}}\right)_1 = \overline{\overline{\overline{\overline{E}}}} : \overline{\overline{D}} \tag{5.255}$$

$$\left({}^{s}\overset{\circ}{\tau}{}^{I}_{J}\right)_1 = E^{I\ K}_{J\ L}\, D^{L}_{K} \tag{5.256}$$

was treated extensively in the previous subsection, and was expressed in terms of the 2nd Piola-Kirchhoff stress components ${}^{s}S^{ij}$ and the material rate of the Green strain tensor with components γ_{ij} in Eqs. 5.244-5.246. In this subsection the second part of expression 5.254; namely, the term

$$\left({}^{s}\overset{\circ}{\overline{\overline{\tau}}}\right)_2 = \overline{\overline{\overline{\overline{E}}}} : {}^{s}\overline{\overline{D}}{}^{p} \tag{5.257}$$

will be studied.

From Eq. 3.47, the plastic rate-of-deformation tensor ${}^{s}\overline{\overline{D}}{}^{p}$ of sublayer s can be expressed as:

$${}^{s}\overline{\overline{D}}{}^{p} = {}^{s}\dot{\lambda}\ {}^{s}\overline{\overline{\tau}}{}^{D} \tag{5.258}$$

Hence, one can write Eq. 5.257 as

$$\left({}^{s}\overset{\circ}{\overline{\overline{\tau}}}\right)_2 = \overline{\overline{\overline{\overline{E}}}} : {}^{s}\dot{\lambda}\ {}^{s}\overline{\overline{\tau}}{}^{D} \tag{5.259}$$

or, in the body-fixed convected coordinate system, in the present configuration:

$$\left({}^{s}\overset{\circ}{\tau}{}^{I}_{J}\right)_2 = {}^{s}\dot{\lambda}\, E^{I\ K}_{J\ L}\left({}^{s}\tau^{D}\right)^{L}_{K} \tag{5.260}$$

For plane stress conditions, this equation becomes

$$\left({}^{s}\overset{\circ}{\tau}{}^{I}_{J}\right)_2 = {}^{s}\dot{\lambda}\, E^{12}_{21}\left({}^{s}\tau^{L}_{K} - \frac{1-2\nu}{3(1-\nu)}\,\delta^{L}_{K}\left({}^{s}\tau^{1}_{1} + {}^{s}\tau^{2}_{2}\right)\right) \tag{5.261}$$

where, as before,

$$E^{12}_{21} = \frac{E}{1+\nu} \tag{5.262}$$

Defining,

$$\boxed{{}^{s}\dot{\lambda}^{*} = \frac{1}{3} E^{11}_{21}\, {}^{s}\dot{\lambda} = \frac{E}{3(1+\nu)}\, {}^{s}\dot{\lambda}} \qquad (5.263)$$

expression 5.253 becomes:

$$\left({}^{s}\overset{\circ}{\tau}{}^{1}_{1}\right)_{2} = {}^{s}\dot{\lambda}^{*}\left(3\,{}^{s}\tau^{1}_{1} - \left(\frac{1-2\nu}{1-\nu}\right)\left({}^{s}\tau^{1}_{1} + {}^{s}\tau^{2}_{2}\right)\right) \qquad (5.264)$$

$$\left({}^{s}\overset{\circ}{\tau}{}^{2}_{2}\right)_{2} = {}^{s}\dot{\lambda}^{*}\left(3\,{}^{s}\tau^{2}_{2} - \left(\frac{1-2\nu}{1-\nu}\right)\left({}^{s}\tau^{1}_{1} + {}^{s}\tau^{2}_{2}\right)\right) \qquad (5.265)$$

$$\left({}^{s}\overset{\circ}{\tau}{}^{1}_{2}\right)_{2} = {}^{s}\dot{\lambda}^{*}\, 3\, {}^{s}\tau^{1}_{2} \qquad (5.266)$$

$$\left({}^{s}\overset{\circ}{\tau}{}^{2}_{1}\right)_{2} = {}^{s}\dot{\lambda}^{*}\, 3\, {}^{s}\tau^{2}_{1} \qquad (5.267)$$

Using Eq. 2.270, and the conditions of plane-stress (Eq. 5.161)

$$\tau^{i}_{k} = C_{kl}\, S^{li} \qquad (5.268)$$

$$S^{33} = S^{23} = S^{13} = 0 \qquad (5.269)$$

$$\gamma_{13} = C_{13} = \gamma_{23} = C_{23} = 0 \qquad (5.270)$$

one obtains

$${}^{s}\tau^{1}_{1} = C_{1l}\, {}^{s}S^{l1} = C_{11}\, {}^{s}S^{11} + C_{12}\, {}^{s}S^{12} \qquad (5.271)$$

$${}^{s}\tau^{2}_{2} = C_{2l}\, {}^{s}S^{l2} = C_{12}\, {}^{s}S^{12} + C_{22}\, {}^{s}S^{22} \qquad (5.272)$$

$${}^{s}\tau^{1}_{2} = C_{2l}\, {}^{s}S^{l1} = C_{12}\, {}^{s}S^{11} + C_{22}\, {}^{s}S^{12} \qquad (5.273)$$

$${}^{s}\tau^{2}_{1} = C_{1l}\, {}^{s}S^{l2} = C_{11}\, {}^{s}S^{12} + C_{12}\, {}^{s}S^{22} \qquad (5.274)$$

Hence,

$$\left({}^{s}\overset{\circ}{\tau}{}^{1}_{1}\right)_2 = {}^{s}\dot{\lambda}^{*}\left(3C_{11}{}^{s}S^{11} + 3C_{12}{}^{s}S^{12} - \frac{(1-2\nu)}{(1-\nu)}\left(C_{11}{}^{s}S^{11} + C_{22}{}^{s}S^{22} + 2C_{12}{}^{s}S^{12}\right)\right) \tag{5.275}$$

$$\left({}^{s}\overset{\circ}{\tau}{}^{2}_{2}\right)_2 = {}^{s}\dot{\lambda}^{*}\left(3C_{22}{}^{s}S^{22} + 3C_{12}{}^{s}S^{12} - \frac{(1-2\nu)}{(1-\nu)}\left(C_{11}{}^{s}S^{11} + C_{22}{}^{s}S^{22} + 2C_{12}{}^{s}S^{12}\right)\right) \tag{5.276}$$

$$\left({}^{s}\overset{\circ}{\tau}{}^{1}_{2}\right)_2 = {}^{s}\dot{\lambda}^{*}\left(3C_{22}{}^{s}S^{12} + 3C_{12}{}^{s}S^{11}\right) \tag{5.277}$$

$$\left({}^{s}\overset{\circ}{\tau}{}^{2}_{1}\right)_2 = {}^{s}\dot{\lambda}^{*}\left(3C_{11}{}^{s}S^{12} + 3C_{12}{}^{s}S^{22}\right) \tag{5.278}$$

Also, from Eqs. 5.197-5.200, 5.191 and 5.254, one obtains:

$$\left({}^{s}\overset{\circ}{\tau}{}^{1}_{1}\right)_1 = E^{11}_{11}D^{1}_{1} + E^{12}_{12}D^{2}_{2} \tag{5.279}$$

$$\left({}^{s}\overset{\circ}{\tau}{}^{2}_{2}\right)_1 = E^{11}_{11}D^{2}_{2} + E^{12}_{12}D^{1}_{1} \tag{5.280}$$

$$\left({}^{s}\overset{\circ}{\tau}{}^{1}_{2}\right)_1 = E^{12}_{21}D^{1}_{2} \tag{5.281}$$

$$\left({}^{s}\overset{\circ}{\tau}{}^{2}_{1}\right)_1 = E^{12}_{21}D^{2}_{1} \tag{5.282}$$

Hence,

$${}^{s}\overset{\circ}{\tau}{}^{1}_{1} = E^{11}_{11}D^{1}_{1} + E^{12}_{12}D^{2}_{2} - \left({}^{s}\overset{\circ}{\tau}{}^{1}_{1}\right)_2 \tag{5.283}$$

$${}^{s}\overset{\circ}{\tau}{}^{2}_{2} = E^{11}_{11}D^{2}_{2} + E^{12}_{12}D^{1}_{1} - \left({}^{s}\overset{\circ}{\tau}{}^{2}_{2}\right)_2 \tag{5.284}$$

$${}^{s}\overset{\circ}{\tau}{}^{1}_{2} = E^{12}_{21}D^{1}_{2} - \left({}^{s}\overset{\circ}{\tau}{}^{1}_{2}\right)_2 \tag{5.285}$$

$$ {}^{s}\overset{\circ}{\tau}{}^{2}_{1} = E^{12}_{21} D^{2}_{1} - ({}^{s}\overset{\circ}{\tau}{}^{2}_{1})_{2} \tag{5.286} $$

One can express Eqs. 5.283-5.286 in terms of the material rates of s^{ij} and γ_{ij} by means of Eq. 2.188, which for these plane stress conditions

$$ S^{31} = S^{32} = S^{33} = 0 \tag{5.287} $$

$$ (C^{-1})^{13} = (C^{-1})^{23} = C_{13} = C_{23} = 0 \tag{5.288} $$

becomes

$$ D^{1}_{1} = (C^{-1})^{11}\dot{\gamma}_{11} + (C^{-1})^{12}\dot{\gamma}_{12} \tag{5.289} $$

$$ D^{2}_{2} = (C^{-1})^{12}\dot{\gamma}_{12} + (C^{-1})^{22}\dot{\gamma}_{22} \tag{5.290} $$

$$ D^{1}_{2} = (C^{-1})^{11}\dot{\gamma}_{12} + (C^{-1})^{12}\dot{\gamma}_{22} \tag{5.291} $$

$$ D^{2}_{1} = (C^{-1})^{12}\dot{\gamma}_{11} + (C^{-1})^{22}\dot{\gamma}_{12} \tag{5.292} $$

and by means of Eq. 2.353, which for the plane stress conditions (Eq. 5.287) becomes:

$$ \begin{aligned} {}^{s}\overset{\circ}{\tau}{}^{1}_{1} = {}& {}^{s}\dot{S}^{11}C_{11} + {}^{s}\dot{S}^{12}C_{12} \\ & + \dot{\gamma}_{11}\left\{{}^{s}S^{11} + {}^{s}S^{11}(C^{-1})^{11}C_{11} + {}^{s}S^{12}(C^{-1})^{11}C_{12}\right\} \\ & + (2\dot{\gamma}_{12})\left\{{}^{s}S^{12} + {}^{s}S^{11}(C^{-1})^{12}C_{11} - {}^{s}S^{22}(C^{-1})^{12}C_{22}\right\} \\ & + \dot{\gamma}_{22}\left\{(C^{-1})^{12}({}^{s}S^{12}C_{11} + {}^{s}S^{22}C_{12})\right\} \end{aligned} \tag{5.293} $$

$$
\begin{aligned}
{}^{s}\overset{\circ}{\tau}{}^{2}_{2} = {} & {}^{s}\dot{S}^{22} C_{22} + {}^{s}\dot{S}^{12} C_{12} \\
& + \dot{\gamma}_{22}\left\{{}^{s}S^{22} + {}^{s}S^{22}(C^{-1})^{22} C_{22} + {}^{s}S^{12}(C^{-1})^{22} C_{12}\right\} \\
& + (2\dot{\gamma}_{12})\left\{{}^{s}S^{12} + {}^{s}S^{22}(C^{-1})^{12} C_{22} - {}^{s}S^{11}(C^{-1})^{12} C_{11}\right\} \\
& + \dot{\gamma}_{11}\left\{(C^{-1})^{12}\left({}^{s}S^{12} C_{22} + {}^{s}S^{11} C_{12}\right)\right\}
\end{aligned}
\tag{5.294}
$$

$$
\begin{aligned}
{}^{s}\overset{\circ}{\tau}{}^{1}_{2} = {} & {}^{s}\dot{S}^{11} C_{12} + {}^{s}\dot{S}^{12} C_{22} \\
& + \dot{\gamma}_{11}\left\{(C^{-1})^{11}\left({}^{s}S^{11} C_{12} + {}^{s}S^{12} C_{22}\right)\right\} \\
& + \frac{1}{2}(2\dot{\gamma}_{12})\left\{{}^{s}S^{11} + {}^{s}S^{11}(C^{-1})^{12} C_{12} + {}^{s}S^{22}(C^{-1})^{11} C_{22}\right\} \\
& + \dot{\gamma}_{22}\left\{{}^{s}S^{12} + (C^{-1})^{12}\left({}^{s}S^{12} C_{12} + {}^{s}S^{22} C_{22}\right)\right\}
\end{aligned}
\tag{5.295}
$$

$$
\begin{aligned}
{}^{s}\overset{\circ}{\tau}{}^{2}_{1} = {} & {}^{s}\dot{S}^{22} C_{12} + {}^{s}\dot{S}^{12} C_{11} \\
& + \dot{\gamma}_{22}\left\{(C^{-1})^{22}\left({}^{s}S^{22} C_{12} + {}^{s}S^{12} C_{11}\right)\right\} \\
& + \frac{1}{2}(2\dot{\gamma}_{12})\left\{{}^{s}S^{22} + {}^{s}S^{22}(C^{-1})^{12} C_{12} \right. \\
& \qquad \left. + S^{11}(C^{-1})^{22} C_{11}\right\} \\
& + \dot{\gamma}_{11}\left\{{}^{s}S^{12} + (C^{-1})^{12}\left({}^{s}S^{12} C_{12} + {}^{s}S^{11} C_{11}\right)\right\}
\end{aligned}
\tag{5.296}
$$

This results in a system of 4 coupled equations in $\dot{\gamma}_{11}$, $\dot{\gamma}_{22}$, $\dot{\gamma}_{12}$, $\dot{s}^{11}$, $\dot{s}^{22}$ and $\dot{s}^{12}$. Solving for the 2nd Piola-Kirchoff stress rates $\dot{s}^{11}$, $\dot{s}^{22}$ and $\dot{s}^{12}$ in terms of the stresses, strain rates, and strains, one finally obtains:

$$\boxed{\begin{aligned} {}^{s}\dot{S}^{11} = {} & \dot{\gamma}_{11}\left\{E^{11}_{11}\left[(C^{-1})^{11}\right]^{2} - 2\,{}^{s}S^{11}(C^{-1})^{11}\right\} \\ & + (2\dot{\gamma}_{12})\left\{E^{11}_{11}(C^{-1})^{12}(C^{-1})^{11} - {}^{s}S^{12}(C^{-1})^{11} - {}^{s}S^{11}(C^{-1})^{12}\right\} \\ & + \dot{\gamma}_{22}\left\{E^{12}_{12}(C^{-1})^{11}(C^{-1})^{22} + E^{12}_{21}\left[(C^{-1})^{12}\right]^{2} - 2\,{}^{s}S^{12}(C^{-1})^{12}\right\} \\ & - {}^{s}\dot{\lambda}^{*}\left\{3\,{}^{s}S^{11} - \left(\frac{1-2\nu}{1-\nu}\right)(C^{-1})^{11}\left({}^{s}S^{11}C_{11} + {}^{s}S^{22}C_{22} + 2\,{}^{s}S^{12}C_{12}\right)\right\} \end{aligned}} \qquad (5.297)$$

$$\boxed{\begin{aligned} {}^{s}\dot{S}^{22} = {} & \dot{\gamma}_{22}\left\{E^{11}_{11}\left[(C^{-1})^{22}\right]^{2} - 2\,{}^{s}S^{22}(C^{-1})^{22}\right\} \\ & + (2\dot{\gamma}_{12})\left\{E^{11}_{11}(C^{-1})^{12}(C^{-1})^{22} - {}^{s}S^{12}(C^{-1})^{22} - {}^{s}S^{22}(C^{-1})^{12}\right\} \\ & + \dot{\gamma}_{11}\left\{E^{12}_{12}(C^{-1})^{22}(C^{-1})^{11} + E^{12}_{21}\left[(C^{-1})^{12}\right]^{2} - 2\,{}^{s}S^{12}(C^{-1})^{12}\right\} \\ & - {}^{s}\dot{\lambda}^{*}\left\{3\,{}^{s}S^{22} - \left(\frac{1-2\nu}{1-\nu}\right)(C^{-1})^{22}\left({}^{s}S^{11}C_{11} + {}^{s}S^{22}C_{22} + 2\,{}^{s}S^{12}C_{12}\right)\right\} \end{aligned}} \qquad (5.298)$$

$$\boxed{\begin{aligned} {}^{s}\dot{S}^{12} = {} & \dot{\gamma}_{11}\left\{E^{11}_{11}(C^{-1})^{11}(C^{-1})^{12} - {}^{s}S^{11}(C^{-1})^{12} - {}^{s}S^{12}(C^{-1})^{11}\right\} \\ & + \frac{1}{2}(2\dot{\gamma}_{12})\left\{(E^{11}_{11} + E^{12}_{12})\left[(C^{-1})^{12}\right]^{2} + E^{12}_{21}(C^{-1})^{11}(C^{-1})^{22}\right. \\ & \qquad \left. - 2\,{}^{s}S^{12}(C^{-1})^{12} - {}^{s}S^{11}(C^{-1})^{22} - {}^{s}S^{22}(C^{-1})^{11}\right\} \\ & + \dot{\gamma}_{22}\left\{E^{11}_{11}(C^{-1})^{22}(C^{-1})^{12} - {}^{s}S^{22}(C^{-1})^{12} - {}^{s}S^{12}(C^{-1})^{22}\right\} \\ & - {}^{s}\dot{\lambda}^{*}\left\{3\,{}^{s}S^{12} - \frac{(1-2\nu)}{(1-\nu)}(C^{-1})^{12}\left({}^{s}S^{11}C_{11} + {}^{s}S^{22}C_{22} + 2\,{}^{s}S^{12}C_{12}\right)\right\} \end{aligned}} \qquad (5.299)$$

where

$$E^{11}_{11} = \frac{E}{(1-\nu^2)}$$

$$E^{12}_{12} = \frac{\nu E}{(1-\nu^2)} = \nu E^{11}_{11}$$

$$E^{12}_{21} = \frac{E}{(1+\nu)} = (1-\nu) E^{11}_{11}$$

as previously defined in Eqs. 5.201-5.203. The right Cauchy-Green deformation tensor components C_{ij} and their inverse $(C^{-1})^{ij}$ are defined by Eqs. 5.158 and 5.159.

5.3.2.5 Incremental Procedure for the Evaluation of Stresses

In the following, the procedure employed to determine the stress components at any integration point in the volume integrals necessary for the finite element analysis, is described. In the previous subsection this procedure was described for the case in which differential changes in strains and stresses occur. In the present case, however, those rules are applied directly for finite incremental rather than differential changes. Hence, attention must be given to computational difficulties which might, therefore, arise. This matter will be discussed further, presently.

Let it be assumed that at time $(t - \Delta t)$, all stresses, strains, and displacements are known at all shell locations of interest. Further, let it be assumed that the displacement increments Δq_i and strain increments $\Delta\gamma_{ij}$ from time $(t - \Delta t)$ to time t have been calculated. In order to integrate the differential expressions 5.297-5.299, a "mixed rectangle rule" which uses the Cauchy-Green deformation tensor components $(C^{-1})^{ij}$ and C_{ij} computed at time t, and the stress tensor components $^sS^{ij}$ computed at time $t - \Delta t$ is employed. The trapezoidal rule would be ideally suited for this integration, since it entails a much lower truncation error than the integration method used. However, as it is evident from Eqs. 5.297-5.299, that the system to be integrated has many terms (many more than in the small strain approximation of the constitutive equations) and it is highly coupled. In order to apply the trapezoidal rule (as previously done in Section 4 for the curved beam equation), this system of three coupled equations would have to be solved in terms of the stress increments $\Delta^s s^{11}$, $\Delta^s s^{22}$, and $\Delta^s s^{12}$. For the present analysis, these equations are expressed in incremental form by replacing:

$$ {}^s\dot{S}^{11} = \frac{\Delta^s S^{11}}{\Delta t} \qquad {}^s\dot{S}^{22} = \frac{\Delta^s S^{22}}{\Delta t} \qquad {}^s\dot{S}^{12} = \frac{\Delta^s S^{12}}{\Delta t} \tag{5.300} $$

$$ \dot{\gamma}_{11} = \frac{\Delta\gamma_{11}}{\Delta t} \qquad \dot{\gamma}_{22} = \frac{\Delta\gamma_{22}}{\Delta t} \qquad \dot{\gamma}_{12} = \frac{\Delta\gamma_{12}}{\Delta t} \tag{5.301} $$

$$ (C^{-1})^{ij} = \left[(C^{-1})^{ij}\right]_t \qquad C_{ij} = \left[C_{ij}\right]_t \tag{5.302} $$

$$ {}^sS^{ij} = \left({}^sS^{ij}\right)_{t-\Delta t} \tag{5.303} $$

in Eqs. 5.297-5.299.

It is convenient in the computational process for determining the stress components $({}^ss^{ij})_t$ at time t to perform an initial examination by forming a <u>trial value</u> of the stress (overscript T) by assuming that the stress increment arises from wholly-"elastic" behavior:

$$ \left({}^s\overset{T}{S}{}^{ij}\right)_t = \Delta^s\overset{T}{S}{}^{ij} + \left({}^sS^{ij}\right)_{t-\Delta t} \tag{5.304} $$

where

$$ \begin{aligned} \Delta^s\overset{T}{S}{}^{11} = {} & \Delta\gamma_{11}\left\{\frac{E}{(1-\nu^2)}\left[(C^{-1})^{11}_t\right]^2 - 2\,{}^sS^{11}_{t-\Delta t}(C^{-1})^{11}_t\right\} \\ & + (2\Delta\gamma_{12})\left\{\frac{E}{(1-\nu^2)}(C^{-1})^{12}_t(C^{-1})^{11}_t - {}^sS^{12}_{t-\Delta t}(C^{-1})^{11}_t - {}^sS^{11}_{t-\Delta t}(C^{-1})^{12}\right\} \\ & + \Delta\gamma_{22}\left\{\frac{E\nu}{(1-\nu^2)}(C^{-1})^{11}_t(C^{-1})^{22}_t + \frac{E}{1+\nu}\left[(C^{-1})^{12}_t\right]^2 - 2\,{}^sS^{12}_{t-\Delta t}(C^{-1})^{12}_t\right\} \end{aligned} \tag{5.305} $$

$$\Delta {}^s\overset{T}{S}{}^{22} = \Delta\gamma_{22}\left\{\frac{E}{(1-\nu^2)}\left[(C^{-1})^{22}_t\right]^2 - 2\,{}^sS^{22}_{t-\Delta t}\,(C^{-1})^{22}_t\right\}$$

$$+(2\,\Delta\gamma_{12})\left\{\frac{E}{(1-\nu^2)}(C^{-1})^{12}_t(C^{-1})^{22}_t - {}^sS^{12}_{t-\Delta t}\,(C^{-1})^{22}_t - {}^sS^{22}_{t-\Delta t}\,(C^{-1})^{12}_t\right\}$$

$$+\Delta\gamma_{11}\left\{\frac{\nu E}{(1-\nu^2)}(C^{-1})^{22}_t(C^{-1})^{11}_t + \frac{E}{1+\nu}\left[(C^{-1})^{12}_t\right]^2 - 2\,{}^sS^{12}_{t-\Delta t}(C^{-1})^{12}_t\right\} \quad (5.306)$$

$$\Delta {}^s\overset{T}{S}{}^{12} = \Delta\gamma_{11}\left\{\frac{E}{(1-\nu^2)}(C^{-1})^{11}_t(C^{-1})^{12}_t - {}^sS^{11}_{t-\Delta t}(C^{-1})^{12}_t - {}^sS^{12}_{t-\Delta t}\,(C^{-1})^{11}_t\right\}$$

$$+\frac{1}{2}(2\Delta\gamma_{12})\left\{\frac{E}{(1-\nu)}\left[(C^{-1})^{12}_t\right]^2 + \frac{E}{(1+\nu)}(C^{-1})^{11}_t\,(C^{-1})^{22}_t\right.$$

$$\left. - 2\,{}^sS^{12}_{t-\Delta t}\,(C^{-1})^{12}_t - {}^sS^{11}_{t-\Delta t}\,(C^{-1})^{22}_t - {}^sS^{22}_{t-\Delta t}\,(C^{-1})^{11}_t\right\}$$

$$+\Delta\gamma_{22}\left\{\frac{E}{(1-\nu^2)}(C^{-1})^{22}_t\,(C^{-1})^{12}_t - {}^sS^{22}_{t-\Delta t}(C^{-1})^{12}_t - {}^sS^{12}_{t-\Delta t}(C^{-1})^{11}_t\right\} \quad (5.307)$$

It should be noted that the symmetry of these expressions is fully exploited in the computer implementation of the analysis.

Next, a test is performed to determine whether or not the $({}^s\overset{T}{S}{}^{ij})_t$ are within the "elastic" region bounded by the loading function $({}^s\overset{T}{\Phi})_t$ defined by Eqs. 5.175, 5.177, 5.185, and 5.190. Thus, one forms a trial (T) value of the loading function $({}^s\overset{T}{\Phi})_t$ of the sth sublayer at time t:

$$({}^s\overset{T}{\Phi})_t = ({}^s\overset{T}{\Phi}_1)_t - \left[({}^s\tau^{y}_{u})_t\right]^2 \quad (5.308)$$

where

$$({}^s\overset{T}{\Phi}_1)_t = \left[(C_{11})_t\,({}^s\overset{T}{S}{}^{11})_t\right]^2 + \left[(C_{22})_t\,({}^s\overset{T}{S}{}^{22})_t\right]^2 +$$

$$+\left\{\left[(C_{12})_t\right]^2+3(C_{11})_t\,(C_{22})_t\right\}\left[({}^s\overset{T}{S}{}^{12})_t\right]^2$$

$$+\left[(C_{11})_t\,({}^s\overset{T}{S}{}^{11})_t+(C_{22})_t\,({}^s\overset{T}{S}{}^{22})_t\right]4\,(C_{12})_t\,({}^s\overset{T}{S}{}^{12})_t$$

$$+\left[3\left[(C_{12})_t\right]^2-(C_{11})_t\,(C_{22})_t\right]({}^s\overset{T}{S}{}^{11})_t\,({}^s\overset{T}{S}{}^{22})_t \tag{5.309}$$

$$\left[({}^s\tau^{y}_{u})_t\right]^2=({}^s\tau^{y}_{u_o})^2\left[1+\left(\frac{\sqrt{D_t}}{d\,\Delta t}\right)^{\frac{1}{p}}\right]^2 \tag{5.310}$$

$$D_t=\left[(C^{-1})^{11}_t\,\Delta\gamma_{11}\right]^2+\left[(C^{-1})^{22}_t\,\Delta\gamma_{22}\right]^2$$

$$+\left\{\left[(C^{-1})^{12}_t\right]^2+3(C^{-1})^{11}_t\,(C^{-1})^{22}_t\right\}(\Delta\gamma_{12})^2$$

$$+2\left[(C^{-1})^{11}_t\,\Delta\gamma_{11}+(C^{-1})^{22}_t\,\Delta\gamma_{22}\right](C^{-1})^{12}_t\,\Delta 2\gamma_{12} \tag{5.311}$$

$$+\left\{3\left[(C^{-1})^{12}_t\right]^2-(C^{-1})^{11}_t\,(C^{-1})^{22}_t\right\}\Delta\gamma_{11}\,\Delta\gamma_{22}$$

$$+(D^3_3)_t\left[(D^3_3)_t+(C^{-1})^{11}_t\,\Delta\gamma_{11}+(C^{-1})^{22}_t\,\Delta\gamma_{22}+(C^{-1})^{12}_t\,\Delta 2\gamma_{12}\right]$$

$$(D^3_3)_t=(\mathring{C}^{-1})^{11}_t\,\Delta\mathring{\gamma}_{11}+(\mathring{C}^{-1})^{22}_t\,\Delta\mathring{\gamma}_{22}+(\mathring{C}^{-1})^{12}_t\,\Delta 2\mathring{\gamma}_{12} \tag{5.312}$$

In these expressions:

${}^s\tau^{y}_{u_o}$ = static yield (Kirchhoff) stress of the sth sublayer in an uniaxial test.

d,p = material strain rate constants

If $({}^s\overset{T}{\Phi})_t \leq 0$, the trial stress state $({}^s\overset{T}{S}{}^{ij})_t$ lies within the "elastic" domain bounded by the loading function (yield surface in stress space) or it lies exactly on it. Therefore, for this time step Δt, there has been no plastic flow and the actual stress increments $\Delta({}^sS^{ij})$ did, in fact, arise from wholly-elastic behavior as initially assumed in the trial examination. Hence, the actual stress $({}^sS^{ij})_t$ is equal to the trial stress; thus,

$$({}^sS^{ij})_t = ({}^s\overset{T}{S}{}^{ij})_t = \Delta({}^s\overset{T}{S}{}^{ij}) + ({}^sS^{ij})_{t-\Delta t} \tag{5.313}$$

If, on the contrary, $({}^s\overset{T}{\Phi})_t > 0$, the trial stress state $({}^s\overset{T}{S}{}^{ij})_t$ lies outside of the loading function (i.e., in the forbidden region). Therefore, the trial assumption that the entire strain increment is an elastic strain increment is not valid. Plastic flow has occurred within this time step and the actual stress state $({}^sS^{ij})_t$ must lie on the loading function $({}^s\Phi)_t = 0$. Then the calculation proceeds as follows. As shown in expressions 5.221 and 5.239, the total strain rate $\dot{\gamma}_{k\ell}$ can be decomposed exactly into elastic and plastic components for each sublayer s:

$${}^s\dot{\gamma}^e_{k\ell} = \dot{\gamma}_{k\ell} - {}^s\dot{\gamma}^p_{k\ell} \tag{5.314}$$

From expressions 5.297-299, one may see at once that the stress rate ${}^s\dot{S}^{ij}$ can be decomposed into two parts, one dependent on the total strain rates $\dot{\gamma}_{k\ell}$ and another part dependent on the plastic strain rate ${}^s\dot{\gamma}^p_{k\ell}$ which is:

$${}^s\dot{\lambda}^*\left\{3S^{ij} - \frac{(1-2\nu)}{(1-\nu)}(C^{-1})^{ij}\left({}^sS^{11}C_{11} + {}^sS^{22}C_{22} + 2\,{}^sS^{12}C_{12}\right)\right\} \tag{5.315}$$

Since the stress $({}^sS^{ij})_{t-\Delta t}$ at the previous time increment $t - \Delta t$ satisfied the loading function condition

$$({}^s\Phi)_{t-\Delta t} \leq 0 \tag{5.316}$$

Eq. 5.315 will be integrated during a finite time increment Δt by taking the stresses ${}^sS^{ij}$ and strains $(C^{-1})^{ij}$, C_{ij} to be

$$ {}^{s}S^{ij} = ({}^{s}S^{ij})_{t-\Delta t} \tag{5.317} $$

$$ (C^{-1})^{ij} = (C^{-1})^{ij}_{t} \tag{5.318} $$

$$ C_{ij} = (C_{ij})_{t} \tag{5.319} $$

Therefore, one obtains the following expression for the actual stress increment $\Delta({}^{s}S^{ij})$:

$$ \Delta({}^{s}S^{ij}) = \underbrace{\Delta({}^{s}\overset{T}{S}{}^{ij})}_{\text{due to } \Delta {}^{s}\gamma_{ij}} - \underbrace{\Delta({}^{s}\lambda^{*})\overbrace{\left\{3({}^{s}S^{ij})_{t-\Delta t} - (C^{-1})^{ij}_{t}\,{}^{s}S^{P}\right\}}^{{}^{s}\overset{\approx}{S}{}^{ij}}}_{\text{due to } \Delta {}^{s}\gamma_{ij}^{P}} \tag{5.320} $$

where

$$ {}^{s}S^{P} \equiv \frac{1-2\vartheta}{1-\vartheta}\left[({}^{s}S^{11})_{t-\Delta t}(C_{11})_{t} + ({}^{s}S^{22})_{t-\Delta t}(C_{22})_{t} + 2({}^{s}S^{12})_{t-\Delta t}(C_{12})_{t}\right] \tag{5.321} $$

The actual stress at time t is

$$ \begin{aligned} ({}^{s}S^{ij})_{t} &= \Delta({}^{s}S^{ij}) + ({}^{s}S^{ij})_{t-\Delta t} \\ &= ({}^{s}\overset{T}{S}{}^{ij})_{t} - \Delta({}^{s}\lambda^{*})\underbrace{\left\{3({}^{s}S^{ij})_{t-\Delta t} - (C^{-1})^{ij}_{t}\,{}^{s}S^{P}\right\}}_{({}^{s}\overset{\approx}{S}{}^{ij})} \end{aligned} \tag{5.322} $$

The parameter $\Delta({}^{s}\lambda^{*})$ will be obtained from the solution of a second degree polynomial in $\Delta({}^{s}\lambda^{*})$. This second degree polynomial is obtained from the condition that the actual stresses $({}^{s}S^{ij})_{t}$ at time t must satisfy the loading function $({}^{s}\Phi)_{t} = 0$. This condition insures that the stress $({}^{s}S^{ij})_{t}$ at time t is, indeed, located exactly on the yield surface. Expressing this mathematically:

$$({}^s\Phi)_t = 0 = \left[(C_{11})_t\,({}^sS^{11})_t\right]^2 + \left[(C_{22})_t\,({}^sS^{22})_t\right]^2$$
$$+\left\{\left[(C_{12})_t\right]^2 + 3\,(C_{11})_t\,(C_{22})_t\right\}\left[({}^sS^{12})_t\right]^2$$
$$+\left[(C_{11})_t\,({}^sS^{11})_t + (C_{22})_t\,({}^sS^{22})_t\right]4\,(C_{12})_t\,(S^{12})_t \tag{5.323}$$
$$+\left\{3\left[(C_{12})_t\right]^2 - (C_{11})_t\,(C_{22})_t\right\}({}^sS^{11})_t\,({}^sS^{22})_t$$
$$-\left[({}^s\tau_u^{\vartheta})_t\right]^2$$

where $({}^s\tau_u^{\vartheta})_t$ is obtained from Eq. 5.310. Substituting Eq. 5.322 into Eq. 5.323 and solving for $\Delta({}^s\lambda^*)$ one obtains the physically valid value:

$$\Delta({}^s\lambda^*) = \frac{B - \sqrt{B^2 - AC}}{A} \equiv \frac{C}{B + \sqrt{B^2 - AC}} \tag{5.324}$$

where:

$$A = \left[(C_{11})_t\right]^2\left[{}^s\overset{D}{S}{}^{11}\right]^2 + \left[(C_{22})_t\right]^2\left[{}^s\overset{D}{S}{}^{22}\right]^2$$
$$+\left\{\left[(C_{12})_t\right]^2 + 3\,(C_{11})_t(C_{22})_t\right\}({}^s\overset{D}{S}{}^{12})^2 \tag{5.325}$$
$$+\left[(C_{11})_t\,({}^s\overset{D}{S}{}^{11}) + (C_{22})_t\,({}^s\overset{D}{S}{}^{22})\right]4\,(C_{12})_t\,({}^s\overset{D}{S}{}^{12})$$
$$+\left\{3\left[(C_{12})_t\right]^2 - (C_{11})_t\,(C_{22})_t\right\}({}^s\overset{D}{S}{}^{11})\,({}^s\overset{D}{S}{}^{22})$$

$$B = \left[(C_{11})_t\right]^2({}^s\overset{T}{S}{}^{11})_t\,({}^s\overset{D}{S}{}^{11}) + \left[(C_{22})_t\right]^2({}^s\overset{T}{S}{}^{22})_t\,({}^s\overset{D}{S}{}^{22})$$
$$+\left\{\left[(C_{12})_t\right]^2 + 3\,(C_{11})_t(C_{22})_t\right\}({}^s\overset{T}{S}{}^{12})_t\,({}^s\overset{D}{S}{}^{12}) + \left[(C_{11})_t({}^s\overset{T}{S}{}^{11})_t\right.$$
$$\left.+\,(C_{22})_t({}^s\overset{T}{S}{}^{22})_t\right]2(C_{12})_t({}^s\overset{D}{S}{}^{12}) + \left[(C_{11})_t({}^s\overset{D}{S}{}^{11}) + (C_{22})_t({}^s\overset{D}{S}{}^{22})\right]2\,(C_{12})_t({}^s\overset{T}{S}{}^{12})_t$$
$$+\tfrac{1}{2}\left\{3\left[(C_{12})_t\right]^2 - (C_{11})_t\,(C_{22})_t\right\}\left\{({}^s\overset{T}{S}{}^{11})_t({}^s\overset{D}{S}{}^{22}) + ({}^s\overset{D}{S}{}^{11})({}^s\overset{T}{S}{}^{22})_t\right\} \tag{5.326}$$

$$C = ({}^s\overset{T}{\Phi})_t \tag{5.327}$$

The coefficient C was already displayed in Eqs. 5.308-5.312. The following requirements must be satisfied:

$$B^2 - AC \geq 0 \tag{5.328}$$

$$B - \sqrt{B^2 - AC} > 0 \tag{5.329}$$

During the operation of the solution process for intense loading problems, instances of large strain increments may occur which lead to an imaginary value of ${}^s\lambda^*$. A subincremental procedure to circumvent this difficulty as developed by Huffington [165] is employed. The basic time increment Δt, is divided into a number, say L, of equal <u>subincrements</u>; the size of the subincrements is chosen to be sufficiently small so that a positive real value of $\Delta^s\lambda^*$ for each subincrement can be derived successively, as follows. The value of the strain increments $\Delta\gamma_{ij}$ during the time interval Δt are also divided into L equal parts, $\Delta\gamma_{ij}/L$. It is assumed that during each subincrement of length $\Delta t/L$ this change in strain is approximately correct. Then, by employing the previously mentioned procedure, a valid value for $\Delta^s\lambda^*$ along with stress increments $\Delta({}^sS^{ij})$ are calculated for each subinterval, and in the meanwhile, the stresses and plastic strains are kept updated. The process is continued until either (a) the information needed at time t is calculated or (b) a complex or negative $\Delta^s\lambda^*$ is encountered. In the latter case, the process is repeated from time $(t - \Delta t)$ using a larger value of L. If the stresses at time t can be derived successfully, the solution procedure continues with L henceforth set to unity until an imaginary or negative $\Delta^s\lambda^*$ is again encountered.

SECTION 6

GOVERNING EQUATIONS AND SOLUTION PROCEDURES

6.1 Introduction

In this investigation, attention is restricted to methods for analyzing dynamic structural response, with principal attention devoted to the transient responses of structures which are subjected to transient external loads such as those arising from gusts, blast, impact, etc. Explicitly excluded from consideration is the "short time" or "early time" response which is often called "material response", and which pertains to the nature, propagation, and effects of stress waves in the material as a result of severe impact or impulsive loads applied to the structure; roughly the time span of interest for this type of response is of the order of from 1 to 100 microseconds. Only the "late time" response which is usually termed "structural response" (in contrast with "material response") is discussed here; such responses involve times of interest extending from time zero to 1 millisecond or perhaps to several hundred milliseconds; this type of response pertains to the transient bending and/or stretching behavior of overall structures or of structural components such as beams, rings, plates, and shells.

Furthermore, principal interest in this study centers upon transient structural responses involving finite strains including large rotations and deflections, as well as path-dependent and time-dependent elastic-plastic material behavior. Sought is information on both the peak transient responses (deflections and strains, with primary interest on strains) together with the time of occurrence of that peak and the permanent deformation condition of the structure after subsidence of the externally-applied transient loading.

In this section, the finite element equations of motion are derived from a variational statement consisting of the Principle of Virtual Work and D'Alembert's Principle. The resulting equations can be solved in three ways: (a) the pure vector form (characteristic of explicit solution by methods like the central-difference operator), (b) the constant stiffness, and (c) the tangent stiffness form; these last two forms are often used with implicit operators which exhibit better stability properties than do explicit operators.

For the transient, path-dependent, time-dependent problems of interest in the present work, the first two forms are used, since they are more efficient computationally. For the "pure vector" form of the equations of motion, the so-called "unconventional" formulation is the best to use; however, for the "constant stiffness" form of the equations of motion, the resulting equations are developed in two forms: (a) the "conventional" form and (b) the "modified unconventional" form. The new "modified unconventional" formulation is shown to be applicable for any kind of material behavior, while the usual "conventional" formulation is valid only for small-strain, elastic-plastic materials. In addition, it is shown that the "modified unconventional formulation" is more efficient and economical (although it takes more computer storage) than is the conventional formulation.

A brief review is made of different timewise finite-difference operators suitable for the problem being investigated. Also, the solution of the governing equations of motion is discussed.

6.2 Equations of Motion

6.2.1 Variational Formulation

In the present investigation, the assumed-displacement version of the finite element method was used. The finite-element method can be developed most systematically and conveniently within the framework of variational principles as shown, for example, by Pian and Tong [166]. Variational principles, as expressions of physical laws, have the following advantages: (a) they are statements about a system as a whole, rather than the parts that it comprises, (b) since they refer to the extremum of a scalar, they are invariant, and may be used to derive the special forms appropriate to any particular description, (c) they imply boundary conditions as well as differential equations, (d) they automatically include the effects of constraints, without requiring that the corresponding reactions be known,

(e) they have heuristic value for suggesting generalizations, (f) they are elegant, and (g) they may be used to calculate or prove existence of solutions.

Consider a continuum in equilibrium under the action of body forces, externally-applied surface tractions, and with arbitrary deformation conditions consistent with the prescribed geometric boundary conditions. Let this equilibrium configuration be subjected to an arbitrary and independent set of infinitesimal virtual displacements $\delta\bar{u}$ without violating the geometric boundary conditions. The displacement variations $\delta\bar{u}$ are called virtual because they need not be actual physical displacements $\bar{u}$ which would occur under the given loads, but merely hypothetical, kinematically possible displacements. The Principle of Virtual Work* (page 595 of [7], 237 of [50], [167] and [168]) states that the virtual work, δW, done by the external forces (body forces and surface tractions), is equal to the virtual work, δU, of the internal stresses, i.e.,

$$\delta U = \delta W \tag{6.1}$$

$$\delta U - \delta W = 0 \tag{6.2}$$

with

$$\delta U = \int_{V_0} \bar{\bar{S}} : \delta\bar{\bar{\gamma}}\, dV_0 \tag{6.3}$$

$$= \int_{V_0} S^{ij}\, \delta\gamma_{ij}\, dV_0 \tag{6.4}$$

$$\delta W = \int_{V_0} \rho_0 \bar{B} \cdot \delta\bar{u}\, dV_0 + \int_{A_{0\bar{t}}} \bar{t} \cdot \delta\bar{u}\, dA_0 \tag{6.5}$$

---

*Seemingly first formulated for a continuum by Piola in 1848 [169].

or

$$\delta W = \int_{V_o} \rho_o B^i \delta u_i \, dV_o + \int_{A_{o\bar{t}}} t^i \delta u_i \, dA_o \tag{6.6}$$

In this equation, $\bar{\bar{S}}$ is the second Piola-Kirchhoff stress tensor, introduced in Subsection 2.5.3, $\bar{B}$ is the body-force vector (inertia, gravitational, magnetic, etc.) per unit mass, $\bar{t}$ is the externally-applied surface traction vector, introduced in Subsection 2.5, Eq. 2.209, $\bar{\bar{\gamma}}$ is the Green (Lagrangian) strain tensor, introduced in Subsection 2.4.2.3, $\bar{u}$ is the displacement vector introduced in Subsection 2.4, Eq. 2.76, and ρ_o is the mass density in the reference configuration, introduced in Subsection 2.5.2, Eq. 2.218. In the Eqs. 6.1 - 6.6 only displacement variations $\delta\bar{u}$ are permitted, and for that reason this principle also goes by the name "Principle of Virtual Displacements". By dividing through by δt, one obtains an alternative statement of the Principle of Virtual Work called the "Principle of Virtual Velocities", the only advantage of this formulation is that the virtual velocities $\delta\bar{u}/\delta t$ can be considered as arbitrary finite quantities, without invoking the imprecise notion of "infinitesimal" virtual displacements.

In the present formulation, <u>all</u> pertinent quantities used in the final form of the analysis are described <u>consistently</u> with respect to the <u>fixed</u> reference configuration. The integrations extend over the entire volume V_o in the reference configuration* of the continuum which is bounded by the surface (area) A_o in the reference configuration. The boundary surface A_o may be divided into a prescribed surface-traction boundary $A_{\sigma_{\bar{t}}}$, and a prescribed-displacement boundary $A_{\sigma_{\bar{u}}}$.

---

*As previously indicated, one must always bear in mind that the choice of the reference configuration is <u>arbitrary</u> [22, page 79], that the reference configuration is merely some shape that the body has occupied or might occupy. If the last configuration that the body has occupied is employed as the reference configuration, the corresponding description is sometimes called "updated Lagrangian"; while if a fixed reference configuration is employed, the description is sometimes called "total Lagrangian". In the present treatment, a <u>fixed</u> reference configuration is going to be used for the description of the motion.

By employing the concept of D'Alembert's Principle, the body force vector $\bar{B}$ may be regarded as consisting of D'Alembert inertia force vector $(-\ddot{u})$ and other body forces $\bar{f}$ (gravitational, magnetic, etc.). Thus, one may write:

$$\bar{B} = -\ddot{\bar{u}} + \bar{f} = -\dot{\bar{v}} + \bar{f}$$
$$B^i = -\ddot{u}^i + f^i = -\dot{v}^i + f^i \tag{6.7}$$

where $\bar{v}$ is the velocity vector, defined in Eq. 2.79, and $(\dot{\ })$ denotes the material rate. Observe that the $\bar{u}$ appearing in the acceleration $\ddot{u}$ are not subject to variation since this pertains to the existing force.

The Green (Lagrangian) strain tensor $\bar{\bar{\gamma}}$ can be expressed as a function of the deformation gradient tensor $\bar{\bar{F}}$, from Eq. 2.133, as

$$\bar{\bar{\gamma}} = \frac{1}{2}\left(\bar{\bar{F}}^T \cdot \bar{\bar{F}} - \bar{\bar{I}}\right) \tag{6.8}$$

or, in the body-fixed convected coordinate system (Eq. 2.139) the tensor components are

$$\gamma_{ij} = \frac{1}{2}\left(u_{i,j} + u_{j,i} + u_{k,i}\, u^k{}_{,j}\right) \tag{6.9}$$

where $(\ )_{,i}$ denotes covariant differentiation with respect to the convected coordinates ξ^i using the metric tensor g_{ij} of the reference configuration (Eqs. 2.53 and 2.55). Then, the variation in the strain tensor $\bar{\bar{\gamma}}$ may be expressed as

$$\delta\bar{\bar{\gamma}} = \frac{1}{2}\left(\bar{\bar{F}}^T \cdot \delta\bar{\bar{F}} + \delta\bar{\bar{F}}^T \cdot \bar{\bar{F}}\right) \tag{6.10}$$

or

$$\delta\gamma_{ij} = \frac{1}{2}\left[\left(\delta^k_i + u^k{}_{,i}\right)\delta u_{k,j} + \left(\delta^k_j + u^k{}_{,j}\right)\delta u_{k,i}\right] \tag{6.11}$$

where δ^k_i is the Kronecker delta defined by Eq. 2.8.

This basic variational formulation, the Principle of Virtual Work, holds independently of the material constitutive equations and the possible existence of potential functions for the external forces. Also, it embodies the equation of equilibrium of the continuum:

$$\operatorname{div}\left(\bar{\bar{S}}\cdot\bar{\bar{F}}^{T}\right)+\rho_0\bar{f}=\rho_0\ddot{\bar{u}}=\rho_0\dot{\bar{V}} \tag{6.12}$$

where "div" stands for the divergence operator with respect to the reference configuration. This equation has the following components in the body-fixed convected coordinate system:

$$\left[S^{jk}\left(\delta_k^i+u^i{}_{,k}\right)\right]_{,j}+\rho_0 f^i=\rho_0\ddot{u}^i=\rho_0\dot{V}^i \tag{6.13}$$

and the prescribed surface traction boundary condition on A_{σ_t} (Eq. 2.229, 2.246, 2.262) are

$$\bar{n}\cdot\left(\bar{\bar{S}}\cdot\bar{\bar{F}}^{T}\right)=\bar{t} \tag{6.14}$$

$$\bar{\tilde{t}}\cdot\bar{\bar{F}}^{T}=\bar{t} \tag{6.15}$$

$$n_j\,S^{jk}\left(\delta_k^i+u^i{}_{,k}\right)=t^i \tag{6.16}$$

where $\bar{n}$ is the unit outward normal vector to the boundary surface in the reference configuration, and $\tilde{t}$ is the pseudo-traction vector both defined in Eq. 2.209.

6.2.2 Finite Element Formulation for the Assumed Displacement Model

In the finite-element-analysis method, the entire domain of the continuum is subdivided into a finite number of regions called "finite elements" or "discrete elements", each having a finite number of "nodes" as control points. The behavior of the actual continuum which has an infinite number of degrees of freedom is thereby described approximately in terms of a finite number of degrees of freedom (DOF) at each of the finite number of nodes. The generalized displacements within each finite element are expressed in terms of (a) such variables called "generalized degrees of freedom" q which are defined at the node points in conjunction with (b) suitably-selected interpolation functions to describe the distribution of each quantity throughout the interior of each finite element. Applying this approach within the framework of the Principle of Virtual Work and D'Alembert's Principle results in a finite-sized system of second-order ordinary differential equations. The unknowns in the equations are the generalized degrees of freedom at each node of the complete assembled discretized structure (or continuum).

In the assumed-displacement-type of finite-element analysis, one selects appropriate interpolation functions "anchored to" control-point values which are the nodal generalized displacements. Let it be assumed that the continuum (or structure) being analyzed has been subdivided conceptually into n finite elements. Then, one may write Eq. 6.1 as the sum of the contributions from each of the finite elements as follows:

$$\sum_{e=1}^{n} (\delta \mathcal{U})_e = \sum_{e=1}^{n} (\delta W)_e \qquad (6.17)$$

where for any element e:

$$(\delta \mathcal{U})_e = \int_{(V_o)_e} \overline{\overline{S}} : \delta \overline{\overline{\gamma}} \, dV_o \qquad (6.18)$$

$$= \int_{(V_o)_e} S^{ij} \, \delta \gamma_{ij} \, dV_o \qquad (6.19)$$

$$(\delta W)_e = \int_{(V_o)_e} \rho_o \left(-\ddot{\overline{u}} + \overline{f}\right) \cdot \delta \overline{u} \, dV_o \qquad (6.20)$$

$$+ \int_{(A_o \overline{t})_e} \overline{t} \cdot \delta \overline{u} \, dA_o$$

$$= \int_{(V_o)_e} \rho_o \left(-\ddot{u}^i + f^i\right) \delta u_i \, dV_o \qquad (6.21)$$

$$+ \int_{(A_o \overline{t})_e} t^i \, \delta u_i \, dA_o$$

In these equations, $(V_o)_e$ is the volume in the fixed reference configuration of the eth discrete element, and $(A_{o_{\bar{t}}})_e$ is the portion of the surface area $(A_o)_e$ in the fixed reference configuration of element e, over which the surface traction $\bar{t}$ is prescribed. The summation Σ extends over the n elements of the continuum.

For each element e, let an assumed displacement field u_i of the following form be selected:

$$u_i(\xi^j,t) = \lfloor N_i(\xi^j) \rfloor \{\alpha(t)\} \tag{6.22}$$

where $N_i(\xi^j)$ is an appropriately assumed interpolation function expressed in terms of convected coordinates ξ^j of a generic point within the element (a row vector is identified here by the symbol $\lfloor\ \rfloor$). Also, $\{\alpha(t)\}$ represents a column vector (symbol $\{\ \}$) of independent parameters which are a function of time t only. Hence, it follows that the vector of nodal generalized displacements $\{q\}$ is defined in terms of the local coordinate system of each element and can be obtained by substituting the coordinates of the nodal points into Eq. 6.22. Accordingly, one may write:

$$\{q(t)\} = [G]\{\alpha(t)\} \tag{6.23}$$

If one takes the same number of displacement parameters $\alpha(t)$ as the nodal generalized displacements $q(t)$, the transformation matrix $[G]$ is a square matrix. By inverting Eq. 6.23 for $\{\alpha(t)\}$ and then substituting into Eq. 6.22, one has

$$u_i(\xi^j,t) = \lfloor N_i(\xi^j) \rfloor [G]^{-1}\{q(t)\} = \lfloor \Phi_i(\xi^j) \rfloor \{q\} \tag{6.24}$$

where*

$$\lfloor \Phi_i(\xi^j) \rfloor = \lfloor N_i(\xi^j) \rfloor [G]^{-1} \tag{6.25}$$

*One should not confuse the interpolation function $\Phi_i(\xi^1)$ with the earlier Φ symbol used to denote the loading function (yield surface).

Because N_i and G are a priori chosen functions expressed in the ξ^j coordinates only, they are not subjected to variation; hence

$$\delta u_i = \lfloor \Phi_i \rfloor \{\delta q\} \tag{6.26}$$

Also, the time derivatives of Eq. 6.24 becomes

$$\ddot{u}_i = \lfloor \Phi_i \rfloor \{\ddot{q}\} \tag{6.27}$$

By using Eqs. 6.9 and 6.24, one may obtain the corresponding strain γ_{ij} at any point in the element e as a function of position ξ^k and the nodal generalized displacements {q} as follows*:

$$\gamma_{ij}(\xi^k, t) = \lfloor D_{ij}(\xi^k) \rfloor \{q(t)\} + \frac{1}{2} \lfloor q(t) \rfloor \{D_{\ell i}(\xi^k)\} \lfloor D_j^\ell(\xi^k) \rfloor \{q\} \tag{6.28}$$

It follows that

$$\delta \gamma_{ij} = \lfloor D_{ij} \rfloor \{\delta q\} + \lfloor q \rfloor \{D_{\ell i}\} \lfloor D_j^\ell \rfloor \{\delta q\} \tag{6.29}$$

where D_{ij}, $D_{\ell i}$, and D_j^ℓ are the appropriate differential (gradient) operators which may be expressed symbolically in the form:

$$\lfloor D_{ij}(\xi^k) \rfloor = \frac{1}{2} \lfloor \Phi_{i,j}(\xi^k) + \Phi_{j,i}(\xi^k) \rfloor \tag{6.30}$$

$$\lfloor D_{\ell i}(\xi^k) \rfloor = \lfloor \Phi_{\ell,i}(\xi^k) \rfloor \tag{6.31}$$

$$\lfloor D_j^\ell(\xi^k) \rfloor = \lfloor \Phi^\ell{}_{,j}(\xi^k) \rfloor \tag{6.32}$$

*Here the three-dimensional continuum equations are utilized for clarity, instead of the more complicated strain-displacement equations for shells.

Employing Eqs. 6.24 through 6.32, Eqs. 6.17, 6.19, and 6.21 become:

$$\sum_{e=1}^{n} \lfloor \delta q \rfloor \Big(\Big(\int_{(V_o)_e} \{D_{ij}\} S^{ij} dV_o + \int_{(V_o)_e} \{D_{\ell i}\} \lfloor D^{\ell}{}_{j} \rfloor S^{ij} dV_o \; \{q\}$$

$$- \int_{(V_o)_e} \rho_o \{\Phi_i\} f^{i} dV_o - \int_{(A_o\bar{t})_e} \{\Phi_i\}_b \, t^{i} dA_o + \int_{(V_o)_e} \{\Phi_i\} \rho_o \lfloor \Phi^{i} \rfloor dV_o \{\ddot{q}\} \Big)$$

$$= 0 \tag{6.33}$$

where subscript "b" is used to signify that the $\{\Phi_i\}$ are evaluated along the element boundaries.

Equation 6.33 is a convenient finite-element form of the Principle of Virtual Work and D'Alembert's Principle from which one can obtain the "equations of motion".

6.2.3 Computational Strategies

One can divide the numerical schemes for the solution of initial boundary-value problems into three categories which differ primarily in the preconditioning of the numerical solution, as pointed out by Argyris [170]. According to this criterion, one distinguishes between:

(i) The pure vector approach, describing the kinematic motion by state vectors without resorting to gradient matrices. This approach is characteristic of explicit forward strategies, like the central difference time operator.

(ii) The constant stiffness approach describes the solution path in terms of gradient matrices which remain constant. This is characteristic of combined explicit-implicit solution schemes, like the Houbolt implicit time operator with linear extrapolation of the nonlinear terms due to plasticity or geometry.

(iii) The variable stiffness approach (tangential stiffness method) describes the solution path in terms of gradient matrices which are updated with the evolution of the solution. This is characteristic of fully implicit strategies, like the use of an implicit time operator with Newton-Raphson iteration of the nonlinear terms.

The pure vector approach is traditionally used in connection with finite difference explicit methods [23, 171, 172, for example]. A system stiffness matrix is never constructed, and the equations of motion are expressed simply in terms of vector equations which read:

$$[M]\underbrace{\{\ddot{q}\}}_{\text{UNKNOWN}} = \underbrace{-\{I(q)\} + \{F\}}_{\text{"KNOWN"}} \tag{6.34}$$

where [M] is the global mass matrix, {F} represents the generalized nodal load vector accounting for externally-applied distributed or concentrated loads and body forces, and {I} is a vector of internal forces (elastic and plastic) and nonlinear geometric effects. The pure vector approach which results from the use of the explicit time-marching scheme has strict stability limitations and very restrictive convergence behavior for the iterative solution of nonlinear structural equilibrium equations. Therefore, the range of application is restricted to small increments of time. It has the advantage that, for a given time step that provides stability and convergence, it presents the smallest computational effort of all of the computational techniques being reviewed. In some kinds of analyses (notably in the analysis of short-term shocks and wave propagation problems in which the higher frequencies play a significant role), it is the most effective technique.

The constant stiffness approach was the natural computational procedure to use at the time that finite elements were introduced into nonlinear analysis [23 and 173, for example]. Just as in linear finite element analysis, a system gradient matrix called the stiffness matrix [K] remains constant (hence the name "constant stiffness") during the whole solution procedure. The effects of nonlinearities are treated as pseudo forces; therefore, this method is also called the "pseudo force method". These pseudo forces are functions of the displacements $\{q\}$ and are placed on the right-hand side (the "known" side) of the equations of equilibrium. The basic equations of equilibrium, as obtained by this method, may be expressed mathematically as:

$$\underbrace{[M]\{\ddot{q}\} + [K]\{q\}}_{\text{UNKNOWN}} = \underbrace{\{F_q^{NL}\} + \{F_p\} + \{F\}}_{\text{"KNOWN"}} \qquad (6.35)$$

where $\{F_q^{NL}\}$ is a pseudo-force vector arising from nonlinear geometric effects and $\{F_p\}$ is a pseudo-force vector stemming from plastic effects. Since the pseudo-forces are not known in advance, one resorts to either an extrapolation of the pseudo forces from previous increments (in an incremental procedure), or to an iterative correction of this implicit prediction. The constant stiffness method, thus leads to a combined implicit-explicit formulation of the equations of motion. One iterative scheme that keeps the gradient matrices (the matrices on the left-hand side of the equation) constant is the method of successive approximations. However, this iteration scheme imposes restrictions on the amount of nonlinearities that the scheme can handle (if the structure stiffness becomes larger than the original stiffness, then the method will not converge). Also, the convergence rate is very slow. Further, self-correcting procedures can be utilized, as shown by Stricklin [174]. Of course, the Newton-Raphson method can be utilized, but this will involve refactoring of the left-hand side of the equation.

Finally, the tangent stiffness approach [74 and 175, for example] follows the concept of tangential linearization of the solution path by introducing time variable system properties. The form of the incremental equations is:

$$\underbrace{[M]\{\Delta\ddot{q}\} + [K^T]\{\Delta q\}}_{\text{UNKNOWN}} = \underbrace{\{\Delta F\} + \{f_u\}}_{\text{KNOWN}} \qquad (6.36)$$

where $\{f_u\}$ is an unbalance load added to the right-hand side to satisfy equilibrium. Here $[K^T]$ is a tangent stiffness matrix that includes nonlinear geometric effects as well as elastic-plastic effects. This procedure has been used, for example, by McNamara and Marcal [175] who show that larger time increments can be used by this method than with the previous ones. Of course, a considerable amount of computer time is involved in the evaluation of $[K^T]$ and the refactoring of the left-hand side of the equation. In connection with an unconditionally stable time operator and the Newton-Raphson iteration, this solution method provides the most reliable computational technique for long term response analyses with large nonlinearities. The Newton-Raphson technique is very often modified in order to reduce the computational effort whereby the system gradients are updated only occasionally. In this case, however, the convergence properties deteriorate (in the limit, when the initial stiffness matrix remains unaltered, the constant stiffness method is recovered).

Finally, one can summarize the three schemes, as done by Argyris [170] by expressing the reliability of the three methods in terms of stability and convergence restrictions of the underlying nonlinear time-marching scheme and where the computational effort accounts for the programming effort as well as the numerical cost of the solution of typical reference problems:

Computational Procedure	Stability Properties	Convergence Behavior	Computational Effort
Pure Vector (Explicit Operators)	Very restrictive	Very restrictive+	Small
Constant Stiffness (Implicit-Explicit)	Not restrictive	Restrictive	Medium
Tangent Stiffness (Implicit)	Not restrictive	Not restrictive	Large

One can observe that the constant stiffness procedure converts nonlinear deviations from the linear prediction into equivalent pseudo-load

+Numerical experience, however, shows that when the Δt is chosen small enough to insure stability, convergence is also achieved.

vectors (nonlinear correction), thereby combining the simplicity of the vector formulation with the reliability of the gradient methods. For the purposes of the present study, the pure vector approach with the central-difference explicit time operator and the constant stiffness approach with the implicit Houbolt time operator are used. These two approaches have been chosen (1) because of their inherent numerical advantage (the stiffness matrix is never formed or used in the vector approach, and it is formed and factored only once in the constant stiffness approach) and (2) since the present study is concerned with the strain predictions of time-dependent plasticity.

Since the present class of nonlinear elastic-plastic transient structures exhibits strictly path-dependent responses, it is impossible to guarantee the return to the true solution path by residual correction at the end of the time increment without integration of the prior history. Hence, one has either to use small increments of time (as is necessary with the pure-vector approach and constant stiffness method) or to integrate the nonlinear history of deformation within each time increment, which will always involve numerical truncation errors. Moreover, since higher frequencies are more important in the strain response than in the displacement response of the structure, it may be possible to follow the displacement response with fairly large increments, but to follow the strain response, smaller time increments are necessary.

6.2.3.1 Pure Vector Form

Observe that Eq. 6.33 may be written more compactly as follows [23] for the so-called "unconventional" formulation:

$$\sum_{e=1}^{n} \lfloor \delta q \rfloor \left([m]\{\ddot{q}\} + \{p\} + [h]\{q\} - \{f\} \right) = 0 \qquad (6.37)$$

where the following are evaluated for each finite element:

$$[m] = \int_{(V_0)_e} \rho_0 \{\Phi_i\} \lfloor \Phi^i \rfloor \, dV_0 \qquad (6.38)$$

$$\{p\} = \int_{(V_0)_e} \{D_{ij}\} S^{ij} dV_0 \tag{6.39}$$

$$[h] = \int_{(V_0)_e} \{D_{\ell i}\} \lfloor D^{\ell}_{j} \rfloor S^{ij} dV_0 \tag{6.40}$$

$$\{f\} = \int_{(V_0)_e} \rho_0 \{\Phi_i\} f^i dV_0 + \int_{(A_0\bar{t})_e} \{\Phi_i\} t^i dA_0 \tag{6.41}$$

Note that {p} and [h] involve <u>stress</u> information, and that they are time dependent:

$$\{p\} = \{p(t)\} \tag{6.42}$$

$$[h] = [h(t)] \tag{6.43}$$

Since the element nodal generalized displacements {q} for different elements are not completely independent, a transformation is required to relate the element nodal displacements {q} to independent global (or common) nodal generalized displacements {q*} for the discrete-element assemblage by

$$\{q\} = [J]\{q^*\} \tag{6.44}$$

The quantity [J] includes the effect of transferring from local coordinates from each individual element to global reference coordinates for the system as a whole.

Applying Eq. 6.44 to Eqs. 6.38-6.41 to describe the system in terms of the independent global generalized displacements {q*}, one obtains:

$$\sum_{e=1}^{n} \lfloor \delta q^* \rfloor \left([m^*]\{\ddot{q}^*\} + \{p^*\} + [h^*]\{q^*\} - \{f^*\} \right) = 0 \tag{6.45}$$

where

$$[m^*] = [J]^T [m] [J] \tag{6.46}$$

$$\{p^*\} = [J]^T \{p\} \tag{6.47}$$

$$[h^*] = [J]^T [h] [J] \tag{6.48}$$

$$\{f^*\} = [J]^T \{f\} \tag{6.49}$$

Since the square matrix [h] is not a constant, and since <u>both</u> {p} <u>and</u> [h] involve nonlinear geometric effects as well as plastic effects, there is no practical reason to calculate the matrix [h] explicitly in the analysis, and <u>this is not done</u>. It is more convenient to express

$$\lfloor D^{\ell}_{j} \rfloor \{q\} = \lfloor D^{\ell}_{j} \rfloor [J] \{q^*\} \equiv \chi^{\ell}_{j} \tag{6.50}$$

and hence

$$\{i\} \equiv \{p\} + [h]\{q\} = \int_{(V_0)_e} \{D_{ij}\} S^{ij} dV_0 + \int_{(V_0)_e} \{D_{\ell i}\} S^{ij} \chi^{\ell}_{j} dV_0 \tag{6.51}$$

Therefore, Eqs. 6.37 and 6.45 become:

$$\sum_{e=1}^{n} \lfloor \delta q \rfloor \left([m]\{\ddot{q}\} + \{i\} - \{f\} \right) = 0 \tag{6.52}$$

$$\sum_{e=1}^{n} \lfloor \delta q^* \rfloor \left([m^*]\{\ddot{q}^*\} + \{i^*\} - \{f^*\} \right) = 0 \tag{6.53}$$

where

$$\{i^*\} = [J]^T \{i\} \tag{6.54}$$

Performing the summation in Eq. 6.53, invoking the appropriate element function generalized displacement compatibilities, and because the $\{\delta q^*\}$ are independent and arbitrary, the following vector equations of motion are obtained for the complete assembled discretized structure:

$$\boxed{[M]\{\ddot{q}^*\} = -\{I\} + \{F\}} \tag{6.55}$$

where [M] is the global mass matrix, {I} is a vector of internal forces associated with linear and nonlinear terms of the strain displacement relations as well as elastic and plastic forces; and {F} represents the generalized load vector accounting for externally-applied distributed or concentrated loads. In terms of element information, [M], {I} and {F} may be expressed as:

$$[M] = \begin{bmatrix} [m_1^*] & & & & \\ & [m_2^*] & & & \\ & & [m_3^*] & & \\ & & & \ddots & \\ & & & & [m_n^*] \end{bmatrix} \tag{6.56}$$

$$\{I(t)\} = \begin{Bmatrix} \{i_1^*(t)\} \\ \{i_2^*(t)\} \\ \{i_3^*(t)\} \\ \vdots \\ \{i_n^*(t)\} \end{Bmatrix} \tag{6.57}$$

$$\{F(t)\} = \begin{Bmatrix} \{f_1^*(t)\} \\ \{f_2^*(t)\} \\ \{f_3^*(t)\} \\ \vdots \\ \{f_n^*(t)\} \end{Bmatrix} \tag{6.58}$$

6.2.3.2 Constant Stiffness Form

Two types of constant stiffness formulations will be presented. The first type is the "conventional" pseudo force formulation, which may be obtained by replacing the stress tensor S^{ij} in Eq. 6.33 by the following expression in terms of the strains $\gamma_{k\ell}$

$$S^{ij} = E^{ijk\ell}(\gamma_{k\ell} - \gamma_{k\ell}^{P}) \tag{6.59}$$

where $E^{ijk\ell}$ consists of elastic constants and $\gamma_{k\ell}^{P}$ represents the components of the total plastic strain (or other given initial strains such as thermal strain, etc.). Of course, it should be evident that this formulation is valid only for infinitesimal strains, since for finite strains $E^{ijk\ell}$ <u>cannot</u> be a constant,+ but it will depend on the total strain (<u>both</u> the elastic and plastic parts). For finite strains the decomposition of the <u>total</u> Green strain into elastic and plastic parts is not a useful concept, since the Green "elastic" strain will <u>not</u> have the usual meaning of elastic strains, but will be a quantity affected by the <u>total</u> deformation.

By means of the strain-displacement equations (6.28), one can express Eq. 6.59 as:

$$S^{ij} = E^{ijk\ell}\left(\lfloor D_{k\ell}\rfloor\{q\} + \frac{1}{2}\lfloor q\rfloor\{D_{ck}\}\lfloor D_{\ell}^{c}\rfloor\{q\} - \gamma_{k\ell}^{P}\right) \tag{6.60}$$

+Since experiments on polycrystals with a cubic crystal structure confirm that the constant elastic modulus relates the Kirchhoff stress and the logarithmic strain, and <u>not</u> the 2nd Piola-Kirchhoff stress and the Green (Lagrangian) strain when finite strains are present (see Eqs. 4.167 and 5.297-5.299).

Applying Eqs. 6.60 and 6.55 to Eq. 6.33 one obtains:

$$\sum_{e=1}^{n} \lfloor \delta q^* \rfloor \left([m^*]\{\ddot{q}^*\} + [k^*]\{q^*\} - \{f^*\} - \{f_q^{NL*}\} - \{f_p^{L*}\} - \{f_p^{NL*}\} \right) = 0 \tag{6.61}$$

where

$$[m^*] = [J]^T \int_{(V_o)_e} \rho_o \{\Phi_i\} \lfloor \Phi^i \rfloor \, dV_o \, [J] \tag{6.62}$$

$$[k^*] = [J]^T \int_{(V_o)_e} \{D_{ij}\} E^{ijkl} \lfloor D_{kl} \rfloor \, dV_o \, [J] \tag{6.63}$$

$$\{f^*\} = [J]^T \left(\int_{(V_o)_e} \rho_o \{\Phi_i\} f^i dV_o + \int_{(A_{ot})_e} \{\Phi_i\}_b t^i dA_o \right) \tag{6.64}$$

$$\begin{aligned}\{f_q^{NL*}\} = [J]^T \Big(& -\int_{(V_o)_e} \{D_{ij}\} E^{ijkl} \tfrac{1}{2} \lfloor q^* \rfloor \{D_{ck}\} \lfloor D_l^c \rfloor \{q^*\} dV_o \\ & - \int_{(V_o)_e} \{D_{ai}\} \lfloor D_j^a \rfloor E^{ijkl} \left(\lfloor D_{kl} \rfloor \{q^*\} + \tfrac{1}{2} \lfloor q^* \rfloor \{D_{ck}\} \lfloor D_l^c \rfloor \{q^*\} \right) dV_o \{q^*\} \Big)\end{aligned} \tag{6.65}$$

$$\{f_p^{L*}\} = -[J]^T \int_{(V_o)_e} \{D_{ij}\} E^{ijkl} \gamma_{kl}^P \, dV_o \tag{6.66}$$

$$\{f_p^{NL*}\} = -[J]^T \int_{(V_o)_e} \{D_{ai}\} \lfloor D_j^a \rfloor E^{ijkl} \gamma_{kl}^P \, dV_o \{q^*\} \tag{6.67}$$

Performing the summation invoking interelement generalized displacement compatibility, and because the variation $\{\delta q^*\}$ can be independent and arbitrary, the following conventional equilibrium equation, which is valid only for small strains is obtained:

$$\boxed{[M]\{\ddot{q}^*\} + [K]\{q^*\} = \{F\} + \{F_q^{NL}\} + \{F_p^L\} + \{F_p^{NL}\}} \tag{6.68}$$

where [M] is the global mass matrix, [K] is the usual small-strain linear-elastic global (constant) stiffness matrix, {F} is the generalized load vector representing externally applied distributed or concentrated loads, $\{F_q^{NL}\}$ represents a pseudo load vector arising from the nonlinear terms in the strain-displacement equations, $\{F_p^L\}$ and $\{F_p^{NL}\}$ are the pseudo load vectors due to plastic (small) strains and are associated, respectively, with the linear and nonlinear terms of the strain-displacement equations.

Not only does this formulation have the drawback that is applicable only to small strains, but if an adequate description of the structural behavior requires one to employ nonlinear strain-displacement relations (specially for finite rotations of beams, plates, and shells), it is evident that the "conventional formulation" involves much more computational work than the "modified unconventional" formulation to be presented next.

The "unconventional" formulation of Eq. 6.55 is valid for small and finite strains, for any kind of material. The reason for this is that the "unconventional" formulation is an exact expression of the Principle of Virtual Work. No assumptions whatsoever have been made in the "unconventional" formulation about the constitutive equations. On the other hand, the "conventional" formulation is valid only for the special kind of material that obeys the constitutive equation given as Eq. 6.59, which is not valid for finite strains of elastic-plastic materials. However, the "unconventional" formulation, as expressed by Eq. 6.55, has stability and convergence problems, since the only gradient matrix (the matrix on the left hand side of the equation) is the mass matrix. Therefore, to be able to have stability and convergence properties similar to the constant stiffness method, while at the same time preserving the useful properties of the "unconventional" formulation, the small-strain linear-elastic, constant-stiffness matrix [K] is added to both sides of the Eq. 6.55 to obtain the following modified unconventional form of the equations of motion:

$$[M]\{\ddot{q}^*\} + [K]\{q^*\} = [K]\{q^*\} - \{I\} + \{F\} \qquad (6.69)$$

Observe that this equation is valid for finite strains, and for any kind of material, since no constitutive assumptions have been made. Defining

$$\boxed{\{F^{NL}\} = [K]\{q^*\} - \{I\}} \tag{6.70}$$

where $\{F^{NL}\}$ is a pseudo-force arising from finite strain elastic-plastic behavior as well as all (linear and nonlinear) terms of the strain-displacement equations, one can express Eq. 6.69 as:

$$\boxed{[M]\{\ddot{q}^*\} + [K]\{q^*\} = \{F^{NL}\} + \{F\}} \tag{6.71}$$

This expression is called the "modified unconventional" form of the equations of motion.

In the next subsection, this "modified unconventional" formulation is to be used with implicit time operators, while the "unconventional" formulation of Eq. 6.55 is to be used with explicit time operators.

6.2.3.3 Tangent Stiffness Form

The tangent stiffness form of the equations of motion will be derived here from the Principle of Virtual Work for completeness purposes, but the reader is reminded that the tangent stiffness formulation is not utilized in the present report for any computations or predictions.

The vector form of the equations of motion (Eq. 6.55 derived from the Principle of Virtual Work) at time instants t and t-Δt may be written, respectively, as

$$[M]\{\ddot{q}^*\}_t = -\{I\}_t + \{F\}_t \tag{6.72a}$$

$$[M]\{\ddot{q}^*\}_{t-\Delta t} = -\{I\}_{t-\Delta t} + \{F\}_{t-\Delta t} \tag{6.72b}$$

Subtracting Eq. 6.72b from Eq. 6.72a, one obtains the following incremental form of the equations of motion:

$$[M]\{\Delta \ddot{q}^*\} = -\{\Delta I\} + \{\Delta F\} \qquad (6.72c)$$

where

$$\{\Delta \ddot{q}^*\} \equiv \{\ddot{q}^*\}_t - \{\ddot{q}^*\}_{t-\Delta t} \qquad (6.72d)$$

$$\{\Delta I\} \equiv \{I\}_t - \{I\}_{t-\Delta t} \qquad (6.72e)$$

$$\{\Delta F\} \equiv \{F\}_t - \{F\}_{t-\Delta t} \qquad (6.72f)$$

Next, the increment of the internal force vector $\{\Delta I\}$ is treated as a differential:

$$\{\Delta I\} = \frac{\partial\{I\}}{\partial\{q^*\}}\{\Delta q^*\} = [K^T]\{\Delta q^*\} \qquad (6.73)$$

Hence, one obtains the following "tangent stiffness" form of the equations of motion:

$$\boxed{[M]\{\Delta \ddot{q}^*\} + [K^T]\{\Delta q^*\} = \{\Delta F\} + \{f_u\}} \qquad (6.74)$$

where the "unbalanced force" $\{f_u\}$ is due to the error implicit in Eq. 6.73 and consists of writing the residual equation for Eq. 6.55:

$$\{f_u\} = -[M]\{\ddot{q}^*\} - \{I\} + \{F\} \qquad (6.75)$$

This error term consists of evaluating the terms at the state <u>before</u> the current increment (if no errors had been introduced by previous increments the error would be equal to zero). By including this residual load correction in the equations of motion, one may obtain convergent solutions using time increments that are relatively large in comparison with the solutions obtained without the correction.

From Eqs. 6.37, 6.39, 6.40, and 6.51, one obtains

$$\{i\} = \int_{(V_0)_e} \{D_{ij}\} S^{ij} dV_0 + \int_{(V_0)_e} \{D_{\ell i}\} \lfloor D^{\ell}_{j} \rfloor \{q\} S^{ij} dV_0 \tag{6.76}$$

and, since, from Eq. 6.73

$$[k^T] = \frac{\partial\{i\}}{\partial\{q\}} \tag{6.77}$$

it follows that

$$\begin{aligned}[k^T] = & \int_{(V_0)_e} \{D_{ij}\} \left[\frac{\partial S^{ij}}{\partial \gamma_{k\ell}}\right] \left\lfloor \frac{\partial \gamma_{k\ell}}{\partial\{q\}} \right\rfloor dV_0 \\ & + \int_{(V_0)_e} \{D_{\ell i}\} \lfloor D^{\ell}_{j} \rfloor S^{ij} dV_0 \\ & + \int_{(V_0)_e} \{D_{\ell i}\} \lfloor D^{\ell}_{j} \rfloor \{q\} \left[\frac{\partial S^{ij}}{\partial \gamma_{k\ell}}\right] \left\lfloor \frac{\partial \gamma_{k\ell}}{\partial\{q\}} \right\rfloor dV_0\end{aligned} \tag{6.78}$$

By means of the strain-displacement equations, 6.28, one can write:

$$\frac{\partial \gamma_{k\ell}}{\partial\{q\}} = \lfloor D_{k\ell} \rfloor + \tfrac{1}{2} \lfloor q \rfloor \{D_{ck}\} \lfloor D^{c}_{\ell} \rfloor + \tfrac{1}{2} \lfloor q \rfloor \{D^{c}_{\ell}\} \lfloor D_{ck} \rfloor \tag{6.79}$$

Placing Eq. 6.79 into Eq. 6.78, one obtains the following tangent stiffness for finite element "e":

$$\begin{aligned}[k^T] = & \int_{(V_0)_e} \{D_{ij}\} \left[\frac{\partial S^{ij}}{\partial \gamma_{k\ell}}\right] \lfloor D_{k\ell} \rfloor dV_0 \\ & + \int_{(V_0)_e} \{D_{ij}\} \left[\frac{\partial S^{ij}}{\partial \gamma_{k\ell}}\right] \lfloor q \rfloor \{D_{ck}\} \lfloor D^{c}_{\ell} \rfloor dV_0/2 \\ & + \int_{(V_0)_e} \{D_{ij}\} \left[\frac{\partial S^{ij}}{\partial \gamma_{k\ell}}\right] \lfloor q \rfloor \{D^{c}_{\ell}\} \lfloor D_{ck} \rfloor dV_0/2\end{aligned}$$

$$+\int_{(V_0)_e} \{D_{\ell i}\} \lfloor D_j^{\ell} \rfloor S^{ij} \, dV_0 \tag{6.79}$$

$$+\int_{(V_0)_e} \{D_{\ell i}\} \lfloor D_j^{\ell} \rfloor \{q\} \left[\frac{\partial S^{ij}}{\partial \gamma_{k\ell}}\right] \lfloor D_{k\ell} \rfloor \, dV_0$$

$$+\int_{(V_0)_e} \{D_{\ell i}\} \lfloor D_j^{\ell} \rfloor \{q\} \left[\frac{\partial S^{ij}}{\partial \gamma_{k\ell}}\right] \lfloor q \rfloor \{D_{ck}\} \lfloor D_\ell^c \rfloor \, dV_0/2$$

$$+\int_{(V_0)_e} \{D_{\ell i}\} \lfloor D_j^{\ell} \rfloor \{q\} \left[\frac{\partial S^{ij}}{\partial \gamma_{k\ell}}\right] \lfloor q \rfloor \{D_\ell^c\} \lfloor D_{ck} \rfloor \, dV_0/2$$

(6.79)

It should be emphasized that this tangent stiffness matrix $[k^T]$ depends upon the current state of displacement $\{q\}$ and stress. Also, comparing Eqs. 6.79, 6.63, 6.76, and 6.70, it is evident that more calculations are involved in the formulation of the tangent stiffness matrix than in the formation of the internal forces for the modified unconventional and/or for the unconventional formulations.

6.3 Finite Difference Operators

6.3.1 Linear Dynamic Systems

For the timewise numerical solution of undamped linear dynamic structural problems, many finite-difference operators have been explored to assess their attributes and shortcomings. Some schemes are stable no matter how large the time increment Δt is chosen to be -- and hence are termed "unconditionally stable"; others are unstable for Δt larger than some critical value -- and thus are termed "conditionally stable". Some introduce (unintentionally) artificial or false damping whereas others do not exhibit this undesirable feature. All of these methods, however, usually* produce a phase-shift error in the predicted response, depending upon the size of the finite Δt used -- some schemes exhibit more phase-shift error than others for a given Δt. A concise tabulation [177] of

*An exception, however, has been noted in Ref. 176 wherein the 3-point central-difference formula was used to solve the one dimensional wave equation. When Δt was chosen such that $(\Delta t)/(\Delta x) = 1$, a solution which was exact in both amplitude and phase was obtained. Second, the Gurtin averaging operator with $c = 0$ exhibits no phase shift error but only with one (much too large) value of Δt; false damping also is present.

some of the features of the more commonly-used varieties of this method are given below.

SUMMARY OF SOME FD OPERATOR FEATURES

FOR UNDAMPED LINEAR DYNAMIC SYSTEMS (MATH. MODEL)

Method	Allowable Δt for Conditionally Stable Method	Unconditionally Stable	False Damping	Phase Shift Error
EXPLICIT				
Central Diff. 3 Pt.	$\Delta t \leq \frac{2}{\omega_{max}}$	No	No	Yes
3rd Order Runge Kutta	$\Delta t \leq \sqrt{3}/\omega_{max}$	No	Yes	Yes
4th Order Runge Kutta	$\Delta t \leq 2\sqrt{2}/\omega_{max}$	No	Yes	Yes
de Vogelaere (I)	$\Delta t \leq 2\sqrt{2}/\omega_{max}$	No	Yes	Yes
IMPLICIT				
Houbolt	---	Yes	Yes	Yes
+Newmark β				
$\gamma = \frac{1}{2}$, $\beta = \frac{1}{4}$	---	Yes	No	Yes
$\gamma = \frac{1}{2}$; $0<\beta<\frac{1}{4}$	$\Delta t \leq \frac{2}{[\omega_{max}(1-4\beta)^{1/2}]}$	No	No	Yes
Gurtin Averaging	---	Yes	Yes	Yes
Wilson Averaging	---	Yes	Yes	Yes
de Vogelaere (II)	$\Delta t \leq 2\sqrt{2}/\omega_{max}$ or $2\sqrt{3}/\omega_{max} \leq \Delta t \leq 2\sqrt{6}/\omega_{max}$	No	No	Yes

*Here ω_{max} represents the largest natural frequency of the math. model.

+For $\beta = 0$, this reduces to the explicit 3 pt. CD operator.

The selection of a suitable time increment size Δt is governed by (a) the stability criterion -- the condition under which the exponential error growth will be bounded and (b) the convergence requirement -- the closeness of the temporal discretization solution to the exact differential equation solution as the timewise discretization mesh decreases. The mathematical foundations for the questions of convergence and stability of numerical methods are well-developed only for linear systems. Moreover, the problem of practical convergence (the closeness of the solutions for finite Δt) is often neglected.

As previously defined, a finite-difference scheme is said to be convergent, if all values of the finite-difference solution approach the solution of the differential equation of the continuum as the finite difference mesh size approaches zero. The finite-difference scheme is said to be consistent if the finite-difference equation approaches the differential equation as the mesh size approaches zero. Although consistency might seem to be automatically satisfied by the Taylor series method of developing the finite-difference scheme, in fact it is not. The property of consistency is a subtle concept, since it is not concerned with the limit behavior of the whole solution of the differential equation but merely with the limit behavior of the individual terms (differentials) of the equation. For example, a finite-difference simulation of a differential equation may have consistent finite differences but not be convergent.

Lax [178] has stated an equivalence theorem that has fundamental importance for linear systems of equations. This equivalence theorem, states that, for a consistent finite-difference scheme, stability is a necessary and sufficient condition for convergence:

$$\left.\begin{array}{l}\text{Lax equivalence theorem}\\ \text{(for linear systems)}\end{array}\right\}\ \text{consistency + stability = convergence}$$

Although early investigators like O'Brien, Hyman, and Kaplan [179] as well as Eddy [180] have defined stability in terms of the growth or decay of roundoff errors, it is now generally accepted that the definition of Lax and Richtmyer [178] is much to be preferred. This more general definition of stability requires a bounded extent to which <u>any</u> component of the initial data can be amplified in the numerical procedure (by <u>any</u> kind of error, including truncation error as well as gross errors).

As Roache [181, p. 49] points out, <u>stability</u> even for <u>linear</u> systems is <u>not</u> defined with universal applicability. The stability criterion associated with the name of von Neumann is that stability is to be determined from the decay or amplification of <u>each mode</u> of a finite Fourier series expansion of the solution to a model equation. Lax and Richtmyer [178] have demonstrated that this is sufficient for stability for a <u>linear</u> system with <u>constant</u> coefficients. Richtmyer [182] points out that the concept of stability depends on the choice of the <u>norm</u> used to measure stability, and that the use of Fourier analysis as in the von Neumann method implies a root mean square norm, which is somewhat arbitrary.

One can readily construct m-point forward-difference, central-difference, or backward-difference operators by Taylor series representation of the acceleration $\ddot{q}$ and/or velocities $\dot{q}$ in terms of displacement q_m information at m instants in time; the truncation error of each approximation thus selected may be identified, and depends upon the number (m, such as 1,2,3,...etc.) of the time instants used. It can also be shown that: (1) all forward-difference operators are unconditionally unstable, (2) all central difference operators are conditionally stable (a critical Δt exists beyond which error blowup will occur), and (3) all backward difference operators are unconditionally stable. Krieg [183] has shown that there can be no explicit second order method which is unconditionally stable, and, in addition, no explicit second order method can have a critical time step larger than that of the central difference time operator. Morino et al. [18] have shown that the central difference method is the optimal method within the class of explicit n-step predictor methods with different n-step correctors, where $n \leq 3$.

The Houbolt method is a four-point implicit backward-difference method (that is, at time n, $\ddot{q}_n$ and $\dot{q}_n$ are expressed in terms of q_n, q_{n-1}, q_{n-2}, and q_{n-3}); this method, accordingly, is unconditionally stable. However, it introduces false damping.

While error instability is avoided by all of the unconditionally stable methods (permitting one to use as large a Δt as one wishes), the forcing function in a given problem may have severe variations such that one must use a fairly small Δt in order to follow and identify the severe peaks, etc. in the response. Perhaps a Δt of some chosen fraction of the period of the highest significantly-excited mode should be used. However, the problem is: can one make a rational a priori estimate of this situation? In such cases the feature of unconditional stability may not be as much of an advantage over a conditionally-stable method as one might think at first sight. However, for "stiff" equations (a term used by numerical analysts to refer to equations containing widely varying frequency components) like structural dynamics equations, and in particular transient loadings which excite only the lowest modes of the structure, the "larger Δt" permitted by the unconditionally-stable methods compared with the "small Δt" required by the conditionally-stable methods (like the 3 point central-difference scheme) makes the unconditionally-stable methods attractive.

Although one can construct finite-difference operators of the implicit or explicit type having truncation errors as small as one wishes by using information at time stations (t, $t-\Delta t$, $t-2\Delta t,\ldots$), it is evident that one pays a price in the necessity of storing this information in order to march the solution ahead in time. Further, the use of an explicit operator circumvects the iterative (or extrapolation) type of calculation required for the solution of the equations of motion when an implicit time operator is used.

6.3.2 Nonlinear Dynamic Systems

The equivalence theorem of Lax is certainly important for linear systems, but, as Roache [181, p. 50] points out, its significance tends to be overemphasized. Some authors have based arguments for the convergence of nonlinear finite-difference equations on the Lax equivalence theorem for linear systems, "apparently out of desperation". While it is useful to study linear systems as guidelines to nonlinear systems, Lax's equivalence theorem is simply not applicable to nonlinear systems. As Roache

[181, p. 50] points out, a precise stability criterion is not required mathematically. Hicks [185] suggests skipping over the problems of stability criteria and going directly to the heart of the matter which is, after all: convergence. Fundamentally, one wants the finite-difference solution to approach the differential equation solution, and stability definitions are of secondary nature.

None of the criteria or analyses of stability are really adequate for practical computations of nonlinear problems. Usually the stability conditions are applied locally. The shortcomings of this approach should be clear. Several authors [182,186,187, and 188] have reported instabilities caused by nonlinearity, or at least because of variable coefficients. Others [189] have reported the phenomena of time splitting of solutions (Section III-A-6 of [181]) which, though not an instability in the sense of producing unbounded solutions, is an instability in a practical sense of preventing iterative convergence.

It is of fundamental importance to realize that it may be impossible to distinguish between what one might call a "true" instability and just a very poor rate of convergence. In fact, preoccupation with tidy definitions of consistency, convergence, and stability as the mesh size goes to zero ($\Delta t \to 0$) is sometimes rather futile, since computations are not run under these conditions. Various of the explicit methods have been applied to nonlinear problems -- with the corresponding linear system Δt limit being used as a guide for choosing an appropriate Δt -- in typical practice some fraction, usually 0.8 and 0.9, of the analytically-indicated maximum Δt for the linear system. In early time calculations, when transients are large, smaller fractions may be needed.

All of the finite-difference operators which are unconditionally stable for the linear system provide degraded (grossly inaccurate) solutions for nonlinear problems if the time step is too large.

Since there is no reason to extrapolate to nonlinear problems the classical methods used to describe stability limits and convergence for simple linear systems, the complexity of the problem determines that the best way to examine the various approaches at the present time is by numerical means.

6.3.2.1 Implicit Methods without Iteration

Stricklin et al. [190] have compared the explicit fourth order Runge-Kutta method with the implicit Houbolt and Newmark ($\beta = \frac{1}{4}$) methods. The comparisons were made on problems with nonlinear strain-displacement relations and linear elastic material behavior, solved by the finite element method. The "conventional" form of the equations of motion was used. Therefore, the equilibrium equations consisted of a constant stiffness matrix on the left-hand (unknown) side of the equations, and the nonlinear terms were expressed as pseudo-load vectors on the right-hand ("known") side of the equations. The nonlinear terms on the right-hand side of the equation were extrapolated from the previous increments, thus avoiding iteration. For the extrapolation of the pseudo-loads, both linear and quadratic extrapolations were explored. The linear extrapolation was felt to be more accurate since the quadratic extrapolation led to numerical instabilities. The Houbolt and Newmark ($\beta = \frac{1}{4}$) implicit methods are unconditionally stable for linear problems, while the fourth order Runge Kutta method is explicit and conditionally stable. For the nonlinear response of an elastic shell of revolution subjected to a step pressure loading, direct preference was established for the Houbolt operator since it was stable and accurate for a larger time step Δt than that required for stability with the Newmark ($\beta = \frac{1}{4}$) method. The time increment Δt demanded by the Runge-Kutta operator was extremely small in comparison with the other two. Later on, Stricklin et al. [191] extended their investigation to include elastic-plastic behavior.

Wu and Witmer [23] also compared the Houbolt and Newmark $\beta = \frac{1}{4}$ methods. They demonstrated that the Houbolt method is more accurate for a larger time increment Δt size than the Newmark method, for linear elastic or elastic-plastic, geometrically nonlinear structural problems, and that the 3 point central-difference method remains conditionally stable but the stability criterion becomes more severe (a smaller Δt is required) than for linear problems. The equations of motion were cast in both the "unconventional" and the "conventional" form for use with the (explicit) central difference time operator; only* the "conventional" form of the equations of motion could be used with the (implicit) Houbolt and Newmark time operators, and the pseudo-loads were extrapolated linearly.

Weeks [192] examined the Houbolt, Newmark $\beta = \frac{1}{4}$, and central-difference operators. Based on a one-degree-of-freedom system, he showed that the Houbolt method provides accurate solutions for a larger time step Δt than the Newmark $\beta = \frac{1}{4}$ method when linear extrapolation of the pseudo-forces is used. For the linear elastic, geometrically nonlinear response of a cantilevered rod, the results obtained indicated the same characteristics as for the one-degree-of-freedom system, and with large time increments both the Houbolt and Newmark operators gave grossly inaccurate answers.

McNamara [193] studied the central-difference, Newmark, Houbolt, and Wilson time operators. Unlike the previously-mentioned authors, McNamara used the tangent-stiffness formulation of the equations of motion, where the stress-strain relations for nonlinear material behavior are suitably linearized during an increment, and all nonlinearities are taken together in one total stiffness matrix; this tangent stiffness matrix has to be reassembled and refactorized frequently throughout the solution. McNamara points out: "the computer time required can become substantial for large problems, and much thought has been given to avoiding this drawback". He proposes the pseudo-load extrapolation method with constant stiffness (the "conventional" formulation) as an alternative, but does not use this method in the solutions presented. The tangent stiffness matrix was kept constant throughout the increment. When no equilibrium iteration was used, the Houbolt method again proved to be the method that gave accurate solutions for larger time steps of all the methods compared. The comparisons included a linear elastic beam clamped at both ends with a point step-load applied at the midspan of the beam. This problem is geometrically nonlinear. The Newmark $\beta = \frac{1}{4}$ and Wilson $\theta = 1.5$ methods became unstable,

---

*The "unconventional" form of the equations of motion cannot be used with an implicit operator, since the initial guess afforded by the "unconventional" method is quite poor because the gradient matrix is just the mass matrix.

while the Houbolt method was stable for all checked values (those values of Δt were as much as five times larger than the values of Δt that produced unstable behavior for the Newmark operator, and thirty times larger than the values that produced instability for the central-difference operator). Another comparison was established for an impulsively-loaded beam clamped at both ends, with elastic-plastic material behavior, and deflections reaching a value of more than four times the original thickness. For this problem the Newmak ($\beta = \frac{1}{4}$) method proved to be the most "unstable" of the implicit operators examined, and again, the Houbolt operator was given an edge over all of the other operators examined.

Recently, Park [194] has devised an attractive implicit method. Two numerical examples are shown for the nonlinear dynamic response of structures. A shallow spherical cap with clamped edges under a step load at the apex was solved by the Park and Houbolt operators. This problem has geometrical nonlinearities but the material is considered to be linear. Park concludes that his method provides a maximum "stable" step size of 0.5 μsec, while this value is 0.3 μsec for the Houbolt operator. Since these are the only two Δt values displayed, it is not clear what it is considered to be stable or unstable behavior in this case. Also, a simply-supported cylindrical shell under uniform external impulse, with nonlinear material (elastic-plastic) behavior as well as geometric nonlinearities was solved by the Park and Houbolt methods by the DYNAPLAS code. The same problem was solved by a <u>different</u> computer code, named SHORE, that utilizes the central-difference time operator. The solution of the SHORE code was utilized by Park as the bench-mark solution. Park concluded that the solution obtained with his method with $\Delta t = 8$ μ sec was more accurate than by the Houbolt method with $\Delta t = 5$ μsec. This conclusion is intriguing, since different computer codes are utilized, and again, only the Houbolt method solution for one Δt value is displayed. The equations of motion for this comparison are cast in the "conventional" form, and the pseudo-loads are extrapolated linearly. Finally, Park's operator is at least as stable locally and has less false damping and frequency distortion than the Houbolt operator; accordingly, its use for the present class of nonlinear transient response problems deserves further investiation.

6.3.2.2 Implicit Methods with Iteration

It is very important to distinguish between two types of quasistatic problems according to the path-dependence of the solution. As pointed out by Argyris [170], path-independent problems readily lend themselves to a total equilibrium formulation in which the incremental linearization errors are under full control via residual load iteration. In contrast, path-dependent problems (for example, plastic problems) make it <u>impossible</u> to compute residual loads without integration of the prior history. While path-independent problems guarantee a return to the true solution path within a given tolerance, path-dependent problems provide no possibility of reducing the numerical integration errors without reanalyzing the process with smaller increments. The numerical solution of the path-dependent problems poses computational problems which are fundamentally different from path-independent problems. The error control and the development of time step strategies which assure <u>accuracy</u> as well as stability are far more complicated. It is a common mistake to believe that residual correction at the end of the increment will guarantee the return to the true solution path. It is of fundamental importance that the truncation error <u>cannot be reduced</u> by residual <u>iteration</u> for path-dependent problems.

<u>Path-Independent Nonlinear Problems</u>

Weeks [192] observed that, for the nonlinear, path-independent response of a one-degree-of-freedom system, the Houbolt operator provides more accurate solutions when linear extrapolation of the pseudo-loads is used than when (Newton-Raphson) iteration is used, for sufficiently large time step sizes Δt. The numerical damping of the Houbolt operator is compensated by the weak instability produced by the linear extrapolation of the pseudo-loads; thus, extrapolation provides more accurate solutions than iteration. When the Newton-Raphson iteration method was used to converge for a nonlinear solution at each time step, the Newmark and Houbolt operators were always stable, at least for the time step sizes investigated (time steps that were small enough to trace the response adequately). In contrast, the Newmark operator became unstable when using load extrapolation and larger time steps, whereas the Houbolt operator was always stable with load extrapolation.

For the elastic (path-independent) nonlinear response of a cantilevered beam, Weeks found that, the Houbolt operator is stable (but exhibits considerable damping) when Newton-Raphson iteration is used at each time step, while the Newmark method exhibits no artificial damping but does exhibit a slight shift, and was stable for the time step sizes investigated.

McNamara [193] studied the linear elastic (path-independent) geometrically nonlinear response of a beam clamped at both ends and subjected to a point step-load at midspan. He used the tangent stiffness form of the equations of motion. The iteration method he used is the so-called modified Newton-Raphson iteration. This method is just the well-known method of succesive approximations, applied at each time step. The gradient matrix is the tangent stiffness matrix, which is kept constant within the time step, and hence, is kept constant within the iteration loop. He found the interesting results that (for large time steps Δt): (a) the Houbolt operator provides better results when iteration is not used and (b) the Newmark operator becomes stable for this nonlinear problem when iteration is used, but the results are not as accurate as the results obtained with the Houbolt operator.

Path-Dependent Problems

For the path-dependent (elastic-plastic) and geometrically nonlinear problem exam. 1 (the impulsive loading of a beam clamped at both ends) by McNamara [193], he could not achieve convergence for the iteration scheme used (the modified Newton-Raphson method).

However, Belytschko and Schoeberle [195] report to have obtained "stable" results for the same problem. They also used the tangent stiffness form of the equations of motion, as well as the modified Newton-Raphson iteration scheme (the tangent stiffness is kept constant within each iteration loop, and recomputed at each time step). Belytschko and Schoeberle used a different computational procedure which ensures that the energy is conserved within a given "energy error criterion". The average number of iterations per time step was not reported, but it is reported that when large time steps are used, from 50 to 100 iterations are required in the first time step because the yield value is exceeded quite a bit within that time step. The Newmark β method was used, with values of $\beta = \frac{1}{4}, \frac{3}{8}$ and $\frac{1}{8}$. The Newmark $\beta = \frac{1}{8}$ method is unstable, just as for linear systems. The results for $\beta = \frac{1}{4}$ and $\beta = \frac{3}{8}$ are "stable" but deteriorate as the time step size is increased, with the amplitude of the response increasing as the time step is increased. The three problems shown exhibit "stability" and "accuracy" for time steps much larger (10-1000 times) than the stability limit of the central-difference time operator. However, in order to have comparable computing times as for the central-difference time operator, time steps more than twenty times the size of the allowable time step size for the certral-difference operator were required for the implicit scheme. Belytschko and Schoeberle conclude that the path-dependence for the problems investigated was quite weak, and that in problems with two or three dimensional states of stress, the accuracy will deteriorate more rapidly with increasing time step size.+

6.4 Solution of the Governing Equations

In order to obtain the timewise solution of a set of equations of dynamic equilibrium such as Eqs. 6.71, 6.68, or 6.55, one may resort to analytical techniques or numerical techniques depending upon the mathematical (and/or physical) nature of the problem.

For small-deflection linear-elastic behavior, for example, one may recast these equations into normal mode form and solve the resulting equations of motion analytically, mode by mode if the forcing functions are modally uncoupled or are properly sequentially coupled. Superposition of the forced responde of each mode then provides the total response of the system. Alternatively, if desired, one may solve these equations by using a finite-difference numerical procedure whereby one obtains a recurrence equation which provides a solution step-by-step in finite-time increments.

If the stiffness matrix varies with time as in the present class of nonlinear problems, the normal modes also vary in time; of course, one

+Since the plasticity itself becomes path dependent in stress space for non-proportional loading in multidimensional states of stress.

could retain the linear part of the internal force terms -- thereby identifying time-invariant "normal modes" and treat the remainder of the internal force terms as pseudo-loads. However, the normal mode approach may become impractical. Accordingly, the numerical finite-difference method is employed in the present study for solving equations of motion like Eqs. 6.71, 6.68, or 6.55.

In particular, the central-difference finite-difference time operator is employed for purposes of illustrating the solution process for the "unconventional" formulation described in Subsection 6.4.1. Since the central-difference time operator is an explicit scheme, the solution of the equations of motion is best handled by the pure vector form described in Subsection 5.2.3.1, which is denoted here as the "unconventional" formulation; of course, other methods like the constant stiffness method ("conventional" formulation) can be and were used in the past, but these methods are not as efficient as the "unconventional" formulation.

In Subsection 6.4.2, the Houbolt (finite-difference) time operator is employed to describe the solution process for the "conventional" or for the "modified unconventional" formulation.

6.4.1 Explicit Solution Process of the Equations of Motion

As indicated earlier, the equations of motior (Eq. 6.55) in the pure vector form are:

$$\boxed{[M]\{\ddot{q}^*\} = -\{I\} + \{F\}} \tag{6.72}$$

where [M] is the global mass matrix, $\{I\}$ is a vector of internal forces associated with linear and nonlinear terms of the strain-displacement relations as well as elastic and plastic forces; and $\{F\}$ represents the generalized load vector accounting for externally-app d distributed or concentrated loads. These equations are to be solved at a sequence of instants in time Δt apart y employing the following central-difference (explicit) (finite-difference) simulation for the acceleration $\ddot{q}_t$ at any instant t:

$$\ddot{q}^*_t = \frac{q^*_{t+\Delta t} - 2q^*_t + q^*_{t-\Delta t}}{(\Delta t)^2} + O(\Delta t)^2 \tag{6.73}$$

Also, one may approximate the velocity $\dot{q}^*_t$ at time t by:

$$\dot{q}^*_t = \frac{q^*_{t+\Delta t} - q^*_{t-\Delta t}}{2\ \Delta t} + O(\Delta t)^2 \tag{6.74}$$

Now note that at any time instant t, Eq. 6.72 can be written exactly as:

$$[M]\{\ddot{q}^*\}_t = -\{I\}_t + \{F\}_t \tag{6.75}$$

In this equation, all quantities except [M] change, in general, with time. If the solution has been obtained for earlier instants of time, one may compute $\{\ddot{q}^*\}_t$ from this equation (Eq. 6.75), and then use Eq. 6.73 to obtain $\{q^*\}_{t+\Delta t}$ as:

$$\{q^*\}_{t+\Delta t} = \{\ddot{q}^*\}_t(\Delta t)^2 + 2\{q^*\}_t - \{q^*\}_{t-\Delta t} \tag{6.76}$$

Assuming that at t = 0, the structure is at a known condition such as

$$\{q^*\}_0 = \{0\}\ ;\ \{\dot{q}^*\}_0 = \{A\}\ ;\ \{\ddot{q}^*\}_0 = \{B\} \tag{6.77}$$

one can readily obtain $\{q^*\}_{\Delta t}$ from the following Taylor series expansion:

$$\{q^*\}_{\Delta t} = \{q^*\}_0 + \{\dot{q}^*\}_0\Delta t + \{\ddot{q}^*\}_0\frac{(\Delta t)^2}{2} + O(\Delta t)^3 \tag{6.78}$$

since $\{F\}_0$ is prescribed and all other quantities are known.

In the timewise step-by-step solution process involving geometric (path-independent) nonlinearities as well as material (path-dependent) elastic-plastic transient responses, the vector of internal forces $\{I\}_t$ changes with time and hence must be reevaluated, in general, at each instant in time. This vector, in turn, is composed by assembling the contributions (see Eq. 6.51):

$$\{i\} = \int_{(V_0)_e} \{D_{ij}\} S^{ij} dV_0 + \int_{(V_0)_e} \{D_{\ell i}\} S^{ij} \chi_j^\ell \, dV_0 \quad (6.79)$$

where

$$\chi_j^\ell = \lfloor D_j^\ell \rfloor \{q\} \quad (6.80)$$

for each finite element "e", (see Eqs. 6.51, 6.50, 6.54, and 6.55). It is seen that these quantities involve volume integrals of information involving the stress state S^{ij}. In practice, these evaluations are carried out by appropraite numerical integration -- Gaussian quadrature. This requires that the stresses S^{ij} and displacement gradients $\lfloor D_j^\ell \rfloor \{q\}$ be evaluated at a finite number of Gaussian integration points over the "spanwise" or "areawise" and the "depthwise" region of each finite element.

At any instant of time t, one needs to solve Eq. 6.75 for $\{\ddot{q}\}_t$, which is of the form:

$$[M]\{x(t)\}_t = \{b(t)\}_t \quad \text{for } t = 0, \Delta t, 2\Delta t, \ldots \quad (6.81)$$

where

[M] is a known banded positive definite symmetric matrix

$\{x(t)\}_t$ is a vector of unknowns which must be determined by solving Eq. 6.81

$\{b(t)\}_t$ is a known vector (representing all terms except $[M]\ \{\ddot{q}^*\}_t$ in Eq. 6.75)

In order to solve Eq. 6.81, the Choleski method is used. Briefly, the well known Choleski method [196] involves factoring the matrix [M] to form a lower triangular matrix and an upper triangular matrix, which is the transpose of the former. If a diagonal ("lumped") mass matrix is used, then the solution of Eq. 6.81 is trivial, and hence extremely fast.

An alternate solution scheme is the triple-factorization and sequential solution method (see pp. 162-167 of Ref. 196) and is more efficient and better conditioned numerically than the standard Cholesky method. This method is also called the Gauss-Doolittle decomposition with sequential solution (see pp. 21-22 of Ref. 197) and consists of two major steps:

1. The global mass matrix is factored into a triple product (triple factorization or Gauss-Doolittle decomposition).

2. The displacements are solved for sequentially, in three sub-steps.

The global mass matrix $[M]$ is factored into the form:

$$[M] = [L][D][L]^T \tag{6.82}$$

where $[L]$ is a lower triangular matrix with zeros in its upper triangular portion and unity on the diagonal, and $[D]$ is a pure diagonal matrix. By direct substitution and comparison, one can show readily that

$$D_m = M_{mm} - \sum_{p=1}^{m-1} L^2_{mp} D_p \tag{6.82a}$$

and

$$L_{im} = \frac{1}{D_m}\left[M_{im} - \sum_{p=1}^{m-1} L_{ip} L_{mp} D_p\right] \tag{6.82b}$$

Note that for m = 1, there are no summation terms. By the use of Eq. 6.82, Eq. 6.81 may be rewritten as

$$[L][D][L]^T \{x\} = \{b\} \tag{6.83}$$

Next, let

$$[L]\{R\} = \{b\} \tag{6.84}$$

where

$$\{R\} = [D][L]^T\{x\} \tag{6.84a}$$

Solving Eq. 6.84 for $\{R\}$, one obtains by forward solution

$$R_m = \frac{1}{L_{mm}}\left[b_m - \sum_{p=1}^{m-1} L_{mp} R_p\right] \tag{6.85}$$

Next, rewrite Eq. 6.84a as

$$[D]\{P\} = \{R\} \tag{6.86}$$

where

$$[L]^T\{x\} = \{P\} \tag{6.86a}$$

Solving Eq. 6.86, one finds

$$\{P\} = [D]^{-1}\{R\} = \begin{Bmatrix} R_1/D_1 \\ R_2/D_2 \\ \vdots \\ R_n/D_n \end{Bmatrix} \tag{6.87}$$

Finally, Eq. 6.86a is solved by backward substitution to obtain:

$$\begin{aligned} x_n &= \frac{P_n}{L_{nn}} \\ x_{n-1} &= \frac{1}{L_{n-1\,n-1}}\left(P_{n-1} - L_{n\,n-1}\, x_n\right) \\ &\vdots \\ x_1 &= \frac{1}{L_{11}}\left(P_1 - L_{21}x_2 - L_{31}x_3 - \dots - L_{n1}x_n\right) \end{aligned} \tag{6.88}$$

Sequentially, the "computing and storing" process involves (a) solving Eq. 6.84 for $\{R\}$ and replacing $\{b\}$ by $\{R\}$ (b) solving Eq. 6.86 for $\{P\}$ and replacing $\{R\}$ by $\{P\}$, and (c) solving Eq. 6.86a for $\{x\}$ and replacing $\{P\}$ by $\{x\}$.

6.4.2 Implicit Solution Process of the Equations of Motion

The constant stiffness form of the equations of motion is to be used with implicit operators.+ From Eqs. 6.71 and 6.68, these equations of motion are:

$$\boxed{[M]\{\ddot{q}^*\} + [K]\{q^*\} = \{F\} + \{F^{NL}\}} \tag{6.89}$$

where [M] is the global mass matrix, [K] is the usual small strain, linear-elastic, global (constant) stiffness matrix, and {F} is the load vector representing externally applied distributed or concentrated loads. The vector $\{F^{NL}\}$ is, for the "conventional" formulation

$$\{F^{NL}\} = \{F_p^L\} + \{F_p^{NL}\} + \{F_q^{NL}\} \tag{6.90}$$

a pseudo-load vector representing internal forces, which for small strains can be decomposed into three vectors: $\{F_q^{NL}\}$ a vector arising from the nonlinear terms in the strain-displacement equations, and $\{F_p^L\}$ and $\{F_p^{NL}\}$ pseudo-load vectors due to plastic (small) strains and associated respectively, with the linear and nonlinear terms of the strain-displacement relations.

For the "modified unconventional" formulation, the vector

$$\{F^{NL}\} = [K]\{q^*\} - \{I\} \tag{6.91}$$

is a pseudo-load vector representing internal forces arising from (small and finite strain) elastic-plastic behavior as well as all (linear and nonlinear) terms of the strain-displacement relations. In Eq. 6.91, the matrix [K] is the same global (constant) stiffness matrix appearing on the left-hand side of Eq. 6.89, and {I} is the same pseudo load vector of internal forces used for the "unconventional" vector form of the equations of motion, Eq. 6.72. The "modified unconventional" form of the equations of motion (Eq. 6.91) is more efficient than the "conventional" form of the equations of motion, as well as being valid for finite strain

+Of course, one can also use a variable stiffness formulation with implicit operators, like the tangent stiffness form of the equations of motion.

material behavior of any kind, while the "conventional" form is valid only for small-strain elastic-plastic material behavior.

The solution of the dynamic equation of motion (Eq. 6.89) can be accomplished by applying an implicit integration scheme. In this scheme, the time derivatives of the nodal displacement vector $\{q^*\}$ (that is, $\{\ddot{q}^*\}$ and $\{\dot{q}^*\}$) are expressed at a discrete time instant in terms of the nodal displacements at several nearby discrete time instants. When substituted into the governing equation of motion, a recurrence relation is obtained from which displacements can be calculated at each discrete time instant.

The acceleration $\{\ddot{q}^*\}_{t+\Delta t}$ at time $t + \Delta t$ is expressed by a 4-point backward-difference formula in the <u>Houbolt operator</u>:

$$\{\ddot{q}^*\}_{t+\Delta t} = \frac{1}{(\Delta t)^2}\left(2\{q^*\}_{t+\Delta t} - 5\{q^*\}_t + 4\{q^*\}_{t-\Delta t} - \{q^*\}_{t-2\Delta t}\right) + O(\Delta t)^2 \tag{6.92}$$

The velocity $\{\dot{q}^*\}_{t+\Delta t}$ at time $t + \Delta t$ can be expressed by the following 3-point backward-difference formula having the same truncation error as $\{\ddot{q}^*\}_{t+\Delta t}$:

$$\{\dot{q}^*\}_{t+\Delta t} = \frac{1}{2\Delta t}\left(3\{q^*\}_{t+\Delta t} - 4\{q^*\}_t + \{q^*\}_{t-\Delta t}\right) + O(\Delta t)^2 \tag{6.93}$$

For computational convenience, the terms in Eq. 6.92 can be regrouped so that $\{\ddot{q}\}_{t+\Delta t}$ at time $t + \Delta t$ can also be related to $\{\dot{q}^*\}_t$ at time t:

$$\{\ddot{q}\}_{t+\Delta t} = \frac{1}{(\Delta t)^2}\Big[2\left(\{q^*\}_{t+\Delta t} - \{q^*\}_t\right) + \left(-3\{q^*\}_t + 4\{q^*\}_{t-\Delta t} - \{q^*\}_{t-2\Delta t}\right)\Big] \tag{6.94}$$

or

$$\boxed{\{\ddot{q}\}_{t+\Delta t} = \frac{2}{(\Delta t)^2}\left(\{q^*\}_{t+\Delta t} - \{q^*\}_t\right) - \frac{2}{\Delta t}\{\dot{q}^*\}_t} \tag{6.95}$$

Equation 6.89 can be written to express dynamic equilibrium at time $t + \Delta t$ as

$$[M]\{\ddot{q}^*\}_{t+\Delta t} + [K]\{q^*\}_{t+\Delta t} = \{F\}_{t+\Delta t} + \{F^{NL}\}_{t+\Delta t} \qquad (6.96)$$

Equation 6.95 is then substituted into Eq. 6.96 and the terms regrouped to give

$$\boxed{\left(\frac{2}{(\Delta t)^2}[M] + [K]\right)\{q^*\}_{t+\Delta t} = \{F\}_{t+\Delta t} + \{F^{NL}\}_{t+\Delta t} + \frac{2}{\Delta t}[M]\left(\{\dot{q}^*\}_t + \frac{1}{\Delta t}\{q^*\}_t\right)} \qquad (6.97)$$

The recurrence relation given by Eq. 6.97 can be solved at each time step for the unknown displacements $\{q^*\}_{t+\Delta t}$ at time $t + \Delta t$, based on the knowledge of $\{F\}_{t+\Delta t}$, $\{F^{NL}\}_{t+\Delta t}$, $\{\dot{q}\}_t$, and $\{q^*\}_t$. The quantities $\{F\}_{t+\Delta t}$, $\{\dot{q}^*\}_t$, and $\{q^*\}_t$ on the right-hand side of the equilibrium equation (Eq. 6.97) are known at time $t + \Delta t$, but the vector of pseudo-forces $\{F^{NL}\}_{t+\Delta t}$ is a function of $\{q^*\}_{t+\Delta t}$ and, thus, is not known. Consequently, either some form of extrapolation or iteration is required to calculate $\{F^{NL}\}_{t+\Delta t}$ as will be discussed in Subsection 6.4.2.1 and 6.4.2.2.

Once $\{q^*\}_{t+\Delta t}$ is determined, the velocities, $\{\dot{q}^*\}_{t+\Delta t}$ can be obtained from Eq. 6.93, and the solution advanced to the next time instant. This process is repeated until some specified termination point is reached. The process is self-starting, since once the initial conditions, $\{\dot{q}^*\}_o$ and $\{q^*\}_o$ at time $t = 0$ are specified, the solution for $\{q^*\}_{\Delta t}$ is obtained directly from Eq. 6.97. However, in order to evaluate the velocity $\{\dot{q}^*\}_{\Delta t}$ at time $t = \Delta t$ (needed to calculate $\{q^*\}_{t+2\Delta t}$) from Eq. 6.93, $\{q^*\}_{-\Delta t}$ is needed but is not known. Thus, some form of "starting sequence" is required. In the present case, $\{q^*\}_{-\Delta t}$ is calculated from a central-difference expression for $\{\dot{q}^*\}_o$

$$\{\dot{q}^*\}_o = \frac{1}{2\Delta t}\left(\{q^*\}_{\Delta t} - \{q^*\}_{-\Delta t}\right) + O(\Delta t)^2 \qquad (6.98)$$

which when solved for $\{q^*\}_{-\Delta t}$ gives

$$\{q^*\}_{-\Delta t} = \{q^*\}_{\Delta t} - 2\Delta t \{\dot{q}^*\}_0 \tag{6.99}$$

and substituting this into Eq. 6.93 (for t = 0) gives the required expression for $\{\dot{q}^*\}_{\Delta t}$:

$$\{\dot{q}\}_{\Delta t} = \frac{2}{\Delta t}\left(\{q^*\}_{\Delta t} - \{q^*\}_0\right) - \{\dot{q}^*\}_0 \tag{6.100}$$

After the first time step, the solution progresses using Eq. 6.97 for $\{q^*\}_{t+\Delta t}$ and Eq. 6.93 for $\{\dot{q}^*\}_{t+\Delta t}$.

The matrices [M] and [K], and the time step size Δt, are held constant throughout the timewise solution. In order to solve Eq. 6.97 for $\{q^*\}_{t+\Delta t}$, the triple-factoring form of Gauss-Jordan elimination is used, as reviewed in Subsection 6.4.1. The matrix sum $(\frac{2}{(\Delta t)^2}[M] + [K])$ is thus formed and factored only once, prior to the first time step. At each time step, $\{q^*\}_{t+\Delta t}$ is obtained by back-substitution operations.

6.4.2.1 Extrapolation

Using a first order Taylor's series expansion about time t, one obtains:

$$\{F^{NL}\}_{t+\Delta t} = \{F^{NL}\}_t + \frac{\partial}{\partial t}\{F^{NL}\}_t \Delta t + O(\Delta t)^2 \tag{6.101}$$

Approximating the partial derivative $\frac{\partial}{\partial t}\{F^{NL}\}_t$ by a first-order backwards difference expression gives:

$$\frac{\partial}{\partial t}\{F^{NL}\} = \frac{1}{\Delta t}\left(\{F^{NL}\}_t - \{F^{NL}\}_{t-\Delta t}\right) \tag{6.102}$$

substituting this back into Eq. 6.101 produces the following "linear extrapolation expression":

$$\{F^{NL}\}_{t+\Delta t} = 2\{F^{NL}\}_t - \{F^{NL}\}_{t-\Delta t} \tag{6.103}$$

This expression has an inherent truncation error of order $(\Delta t)^2$ which is the same as the order of error inherent in the Houbolt approximations for both the acceleration (Eq. 6.92) and the velocity (Eq. 6.93); hence, it is a consistent approximation of the pseudo-load vector $\{F^{NL}\}_{t+\Delta t}$. Equation 6.103 corresponds to a linear extrapolation of the loads from the two previous time instants.

Substituting expression 6.103 into the recursive relation (Eq. 6.97) for the equations of motion with the Houbolt operator produces:

$$\boxed{\begin{aligned}\left(\frac{2}{(\Delta t)^2}[M]+[K]\right)\{q^*\}_{t+\Delta t} &= \{F\}_{t+\Delta t} \\ &+\frac{2}{\Delta t}[M]\left(\{\dot{q}^*\}_t+\frac{1}{\Delta t}\{q^*\}_t\right)+2\{F^{NL}\}_t-\{F^{NL}\}_{t-\Delta t}\end{aligned}} \quad (6.104)$$

where:

$$\{F^{NL}\}_t = [K]\{q^*\}_t - \{I\}_t \quad (6.105)$$

$$\{F^{NL}\}_{t-\Delta t} = [K]\{q^*\}_{t-\Delta t} - \{I\}_{t-\Delta t} \quad (6.106)$$

for the "modified unconventional formulation with linear extrapolation" (MULE) form of the equations of motion, and

$$\{F^{NL}\}_t = \{F_p^L\}_t + \{F_p^{NL}\}_t + \{F_q^{NL}\}_t \quad (6.107)$$

$$\{F^{NL}\}_{t-\Delta t} = \{F_p^L\}_{t-\Delta t} + \{F_p^{NL}\}_{t-\Delta t} + \{F_q^{NL}\}_{t-\Delta t} \quad (6.108)$$

for the "conventional linear extrapolation" form of the equations of motion. The linear extrapolation of the pseudo-force vector arising from nonlinearities has significant advantages: no iteration for convergence is necessary, and only a vector ($\{F^{NL}\}_{t-\Delta t}$) needs to be stored, rather than the complete Jacobian matrix, as it would be necessary with the Newton-Raphson method.

6.4.2.2 Iteration and Convergence

The iteration method that is used in this work is the method of successive substitutions, also known as the method of successive approximations. This iterative technique, one of the easiest methods to apply, was used since it does not involve the formation and refactoring of the gradient matrix, which is consistent with the spirit of the constant stiffness form of the equations of motion. For the Houbolt operator, the equations of motion are (see Eq. 6.97):

$$\left(\frac{2}{(\Delta t)^2}[M] + [K]\right)\{q^{*n+1}\}_{t+\Delta t} = \{F\}_{t+\Delta t} + \frac{2}{\Delta t}[M]\left(\{\dot{q}^*\}_t + \frac{1}{\Delta t}\{q^*\}_t\right) + \{F^{NL\,n}\}_{t+\Delta t} \qquad n = 0, 1, \ldots N \tag{6.109}$$

In this recursive relation, n denotes the nth iteration and the variable N indicates the total number of iterative cycles required for "convergence" during a given Δt time step. The procedure starts (superscript "o") with an initial estimate $\{F^{NL_o}\}_{t+\Delta t}$ of the pseudo-load vector. It is natural to use the extrapolated load from the previous two increments as the first estimate; hence,

$$\{F^{NL_o}\}_{t+\Delta t} = 2\{F^{NL}\}_t - \{F^{NL}\}_{t-\Delta t} \tag{6.110}$$

Then a value of the displacement vector is obtained from Eq. 6.109

$$[A]\{q^{*1}\}_{t+\Delta t} = \{B\} + \{F^{NL\,o}\}_{t+\Delta t} \tag{6.111}$$

where

$$[A] = \frac{2}{(\Delta t)^2}[M] + [K] \tag{6.112}$$

$$\{B\} = \{F\}_{t+\Delta t} + \frac{2}{\Delta t}[M]\left(\{\dot{q}^*\}_t + \frac{1}{\Delta t}\{q^*\}_t\right) \tag{6.113}$$

From this value $\{q^{*1}\}_{t+\Delta t}$, a new estimate $\{F^{NL_1}\}_{t+\Delta t}$ of the pseudo-load vector can be obtained, and then a new estimate $\{q^{*2}\}_{t+\Delta t}$ from the solution of

$$[A]\{q^{*2}\}_{t+\Delta t} = \{B\} + \{F^{NL_1}\}_{t+\Delta t} \tag{6.114}$$

can also be obtained, and so on. This iterative process is continued until either convergence of two successive displacement vectors is noted or a specified number of iterations is reached. The method of successive substitutions is severely limited by its inability to converge for problems exhibiting a significant degree of nonlinearity.

For a one-degree-of-freedom system:

$$A q^* = F(q^*) \tag{6.115}$$

it is easy to show that if $F(q^*)$ possess a continuous derivative, it is necessary for convergence of the method of successive substitutions, that

$$\left|\frac{\partial F}{\partial q^*}(\alpha)\right| \leqslant A \tag{6.116}$$

where α is a root of Eq. 6.115. Moreover, since the gradient matrix [A] stays constant during the iteration, this method has a very slow rate of convergence when it does converge. Furthermore, when unloading of an elastic-plastic solid occurs, even the Newton-Raphson method (which has proven itself to be one of the best solution methods available for static, geometrically nonlinear analysis) fails to converge in many cases, as pointed out by Stricklin and Haisler [198], who anticipate that this lack of convergence arises from the discontinuity produced by elastic unloading.

A nested double iteration procedure using an inner loop Newton-Raphson procedure has been employed successfully in materially nonlinear static analysis by Bushnell [199]. The outer loop updates (for a given value of the load) the material properties and strain components while the inner one ensures equilibrium for that set of material properties. The problems solved in Ref. 199 did not involve cases of severe unloading and were not dynamic. Stricklin and Haisler [198] conclude "The research conducted to date tends to indicate that additional refinements are necessary before the direct application of the Newton-Raphson method can be made for plasticity problems with complex loading and unloading patterns".

For the present work, the following compromise procedure was devised. Knowing in advance that the method of successive substitutions will fail to converge for the complex geometrically and materially nonlinear dynamic problem being analyzed (that involves complex loading and unloading patterns), it is still hoped that the first few iterations will be "asymptotically convergent" in the sense that the first few estimates of the solution may be closer and closer to the solution until the method <u>begins</u> to diverge. Monitoring the rate of convergence, the iteration loop is stopped once divergence commences and the last "converged" estimate of the solution is taken as the solution (in "equilibrium") for that time step. In order to monitor the convergence, two criteria were applied. The first criterion is

$$\frac{\left(\left\|\left\{q^{*n+1}\right\}_{t+\Delta t}\right\|\right)^2-\left(\left\|\left\{q^{*n}\right\}_{t+\Delta t}\right\|\right)^2}{\left(\left\|\left\{q^{*n}\right\}_{t+\Delta t}\right\|\right)^2}<\varepsilon \tag{6.117}$$

where $\left\|\{q^{*n}\}_{t+\Delta t}\right\|$ is the Euclidean norm of the vector $\{q^{*n}\}_{t+\Delta t}$:

$$\left\|\left\{q^{*n}\right\}_{t+\Delta t}\right\| = \left(\sum_i \left[{}^i\left(\left(q^{*n}\right)_{t+\Delta t}\right)\right]\right)^{1/2} \tag{6.118}$$

It is easy to show that the convergence criterion Eq. 6.117 is more stringent (by a factor of 2) than the convergence criterion obtained from the difference of the Euclidean norms:

$$\left(\frac{\left\|\{q^{*\,n+1}\}_{t+\Delta t}\right\|}{\left\|\{q^{*\,n}\}_{t+\Delta t}\right\|}\right)^2 < 1+\varepsilon \tag{6.119}$$

$$\frac{\left\|\{q^{*\,n+1}\}_{t+\Delta t}\right\| - \left\|\{q^{*\,n}\}_{t+\Delta t}\right\|}{\left\|\{q^{*\,n}\}_{t+\Delta t}\right\|} < \sqrt{1+\varepsilon} - 1 \tag{6.120}$$

which, for small ε is approximately:

$$\boxed{\frac{\left\|\{q^{*\,n+1}\}_{t+\Delta t}\right\| - \left\|\{q^{*\,n}\}_{t+\Delta t}\right\|}{\left\|\{q^{*\,n}\}_{t+\Delta t}\right\|} < \frac{1}{2}\varepsilon} \tag{6.121}$$

Hence, if convergence criterion Eq. 6.117 (used in the present work) is satisfied to a given tolerance ε, then convergence criterion Eq. 6.121 (used, for example, in Ref. 200) is satisfied to $\frac{1}{2}\varepsilon$. In the present work, the convergence criterion was taken to be

$$\varepsilon = 1 \times 10^{-4} \tag{6.122}$$

The second convergence criterion examined in the present study was:

$$\boxed{\frac{\left\|\{q^{*\,n+1}\}_{t+\Delta t} - \{q^{*\,n}\}_{t+\Delta t}\right\|}{\left\|\{q^{*\,n}\}_{t+\Delta t}\right\|} < \delta} \tag{6.123}$$

It is easy to show that this convergence criterion is more stringent than the previous ones, since, from the triangle inequality:

$$\left\| \{q^{*n+1}\}_{t+\Delta t} - \{q^{*n}\}_{t+\Delta t} \right\| + \left\| \{q^{*n}\}_{t+\Delta t} \right\| \geqslant \left\| \{q^{*n+1}\}_{t+\Delta t} \right\| \tag{6.124}$$

or

$$\boxed{\left\| \{q^{*n+1}\}_{t+\Delta t} - \{q^{*n}\}_{t+\Delta t} \right\| \geqslant \left\| \{q^{*n+1}\}_{t+\Delta t} \right\| - \left\| \{q^{*n}\}_{t+\Delta t} \right\|} \tag{6.125}$$

Hence, if the Eq. 6.123 criterion is met within a given solerance δ, it certainly meets criterion Eq. 6.121 to within a smaller or equal tolerance.

The convergence criterion Eq. 6.123 is to be preferred to Eq. 6.121 since, for any norm $||\{q^{n+1}\} - \{q^n\}||$ is a measure of the deviation of the approximation in vector space.

In the present work, the quantity δ was taken to be

$$\delta = 1 \times 10^{-4} \tag{6.126}$$

If the iteration scheme were convergent, it would take a certain number of iterations to meet a given criterion; however, since the present iteration sceme will not always converge, the following test is made: if the condition of Eq. 6.117 or Eq. 6.123 is not met, the iterative process is continued <u>if</u>

$$\frac{\left(\left\| \{q^{*n+1}\}_{t+\Delta t} \right\|\right)^2 - \left(\left\| \{q^{*n}\}_{t+\Delta t} \right\|\right)^2}{\left(\left\| \{q^{*n}\}_{t+\Delta t} \right\|\right)^2} \leqslant \frac{\left(\left\| \{q^{*n}\}_{t+\Delta t} \right\|\right)^2 - \left(\left\| \{q^{*n-1}\}_{t+\Delta t} \right\|\right)^2}{\left(\left\| \{q^{*n-1}\}_{t+\Delta t} \right\|\right)^2} \tag{6.127}$$

for Eq. 6.117, or <u>if</u>

$$\frac{\left\| \{q^{*n+1}\}_{t+\Delta t} - \{q^{*n}\}_{t+\Delta t} \right\|}{\left\| \{q^{*n}\}_{t+\Delta t} \right\|} \leqslant \frac{\left\| \{q^{*n}\}_{t+\Delta t} - \{q^{*n-1}\}_{t+\Delta t} \right\|}{\left\| \{q^{*n-1}\}_{t+\Delta t} \right\|} \tag{6.128}$$

for Eq. 6.123.

Otherwise, if conditions Eq. 6.127, 6.128 are not satisfied, the iteration process is stopped, and

$$\boxed{\left\{q^{*}\right\}_{t+\Delta t} = \left\{q^{*n}\right\}_{t+\Delta t}} \qquad (6.127)$$

the previous estimate that satisfied Eq. 6.127 or 6.128 is taken as the "equilibrium" solution for that time step.

SECTION 7

EVALUATION AND DISCUSSION

7.1 Introduction

In order to evaluate the present finite-strain formulation and implemented computational procedure for predicting transient structural responses produced by severe transient external loads or impact, several well-defined problems for which independent predictions and/or reliable experimental data are available for comparison are investigated. This discussion is divided, for convenience and clarity, into two categories: (1) impulsively-loaded structures and (2) fragment-impacted structures. Further, under each of these categories, there are two types of structural response and modeling: (a) two-dimensional (or planar) and (b) three-dimensional (non-planar) structural deflections.

Impulsively-loaded structures discussed in Subsections 7.2, 7.3, and 7.4, respectively, are a narrow plate (or beam), an initially circular ring, and an initially-flat square thin aluminum plate with all four sides ideally-clamped. These first two structures exhibit essentially two-dimensional deformation behavior, while the third one involves distinct three-dimensional structural deflections as well as large levels of strain. These examples are especially important since the conditions responsible for producing the large transient deflections are very clear and well defined -- each represents a well-defined initial-value problem. Accordingly, these examples provide a clear and stringent test of the accuracy and reliability of the present finite-strain formulation and computational procedure.

Discussed in Subsections 7.5 and 7.6 are structural responses produced by fragment impact. A steel containment ring which was subjected to simultaneous impact by 3 equal-size bladed-disk fragments from a T58 aircraft engine turbine rotor is examined in Subsection 7.5, and is found to exhibit essentially two-dimensional structural response. Hence, this containment ring was represented for analysis by curved-ring finite elements which pertain strictly to two-dimensional response.

Considered in Subsection 7.6 is a narrow aluminum plate having both ends ideally clamped, both sides free, and subjected to perpendicular impact at its midwidth-midspan location by a solid steel sphere of 1-inch diameter. Near the "impact station" the structure exhibits severe three-dimensional structural deformations; elsewhere, except very near the clamped ends, the specimen displays essential two-dimensional deflection behavior. Accordingly, this narrow-plate specimen was analyzed in two different ways. First, the structure and the attacking fragment were idealized as a strictly 2-D problem -- the structure was modeled with 2-D beam elements and the fragment was regarded as being a solid cylindrical fragment extending across the entire width of the beam. In the second analysis, the structure was represented by flat-plate elements which can accommodate three-dimensional structural deflection behavior, and the fragment was represented as a non-deformable sphere of 1-inch diameter. Each of these cases is discussed in the following.

7.2 Impulsively-Loaded Narrow Plate

7.2.1 Problem Definition

To provide a well-defined initial-value problem which would furnish reliable experimental data on large-deflection elastic-plastic transient structural responses involving significantly large peak and permanent strains, narrow aluminum plates with both ends ideally clamped and both sides free were subjected to known impulse loading [1]; see Fig. 8. In particular, a 6061-T651 aluminum narrow plate (or beam) specimen denoted as CB-4 with 8.005-in span, 1.497-in width, and 0.102-in thickness was loaded uniformly impulsively over its entire width and a 1.80-in spanwise region centered at midspan by the sheet explosive loading technique. This resulted in essentially a uniform initial lateral velocity of 10,590 in/sec of the loaded portion of the specimen; accordingly, the initial kinetic energy was 3930 in-lb. Spanwise oriented strain gages were attached to the upper (non-loaded) surface at various distances measured from the midspan location. These strains were displayed and recorded photographically from oscilloscopes. Post-test measurements of the permanently-deformed configuration were made. Large transient and permanent deflections were produced. These data are reported in Ref. 1.

Uniaxial static tensile test specimens whose axes were parallel to the spanwise direction of specimen CB-4 were made from the thick-plate stock from which specimen CB-4 was prepared. High-elongation strain gages were used to measure the relative elongation E_u of these specimens in static tensile tests as a function of the applied load P; the initial cross-sectional area A_o of each specimen was known. For use in the "small strain" and in the "finite strain" calculations, the uniaxial static stress-strain information is approximated as described in Subsection 7.2.2 for beam-finite-element modeling and in Subsection 7.2.3 for plate-finite-element modeling of the CB-4 narrow-plate specimen.

Finite element analyses of specimen CB-4 have been carried out to compare predictions based upon (a) the (previous) small-strain procedure and (b) the present consistent finite-strain procedure versus the experimental results. Further, for each case the specimen has been finite-element modeled in two ways: (1) by assumed-displacement cubic-cubic (CC) beam elements and (2) by assumed-displacement linear-linear-cubic (LLC) flat plate elements. These two types of finite element modelings of narrow-plate specimen CB-4 and the resulting predictions are discussed in Subsections 7.2.2 and 7.2.3, respectively.

7.2.2 Comparison of Small-Strain vs Finite-Strain Predictions for Structural Modeling by Beam Finite Elements

Since there is symmetry about the midspan location y = 0, only the half span of specimen CB-4 was modeled by 4 DOF/node beam type finite elements. The use of beam elements implies the assumption that the displacement behavior is two-dimensional (or planar). Studies reported in Refs. 28 and 30 indicate that the use of 20 equal-length 4 DOF/node beam elements provides a reasonable modeling - permitting one to obtain essentially converged predictions for the displacements. The use of a finer mesh in order to obtain converged strain predictions would have been preferable, but the unduly large computing time for a significantly finer mesh was outside the range of what the present financial resources would allow.

For analysis the uniaxial tensile static stress-strain behavior of this lot of 6061-T651 aluminum (see Fig. 29a of Ref. 2 and Fig. 18 of Ref. 30) was modeled by piecewise linear segments for use in the mechanical sublayer model. This strain-hardening model, as implemented in the small-strain JET3 computer program [24], requires that the stress-strain curve being modeled must be monotonically increasing -- the stress associated with the stress-strain curve must not decrease with increasing strain -- and unloading must proceed elastically at the same slope or modulus as the original elastic modulus. Since the uniaxial Kirchhoff stress τ_u versus uniaxial Lagrangian strain γ_u exhibits this type of monotonic behavior whereas the 2nd Piola-Kirchhoff stress S_u does not, the uniaxial tensile static stress-strain data from Fig. 29a of Ref. 2 was cast into the form $\tau_u \equiv \sigma_{E_u}^{o}(1 + E_u)$ vs γ_u and fitted in a piecewise linear fashion by the following stress-strain pairs $(\tau_u, \gamma_u)^o = (0,0)$, (41,000 psi, 0.0041 in/in), (45,000 psi, 0.0120), and (53,000 psi, 0.1000); note that $\sigma_{E_u} \equiv P/A_o$ is the uniaxial engineering stress and E_u is the axial relative elongation: $E_u = [(1 + 2\gamma_u)^{1/2} - 1] = (\ell - \ell_o)/\ell_o$. In the JET 3 computer program [24] used for the analysis, the resulting stress τ_u was used as playing the role of the proper second Piola-Kirchhoff stress S_u (or $\overline{\overline{S}}$) upon which the basic finite-element formulation was based. Since the JET 3 computer code is valid only for small strains, this is consistent because for small strains $\tau_u \simeq S_u$. In view of the above considerations as well as the data scatter in experimental uniaxial stress-strain measurements, this adopted compromise procedure (not fully consistent) was believed likely to provide reasonable predictions of structural response involving small strains, but was expected to be significantly in error at large strain levels. At what strain levels these computer-implemented approximations lead to unreliable predictions was (until now) very uncertain. Accordingly, this compromise procedure has been termed the "small-strain analysis" here and in Ref. 30. Also, it is assumed that strain rate effects can be approximated satisfactorily by an expression of the form

$$^{s}\tau_{u}^{y} = {}^{s}\tau_{u_o}^{y}\left(1 + \left|\frac{\dot{\gamma}_u}{d}\right|^{\frac{1}{p}}\right) \tag{7.1}$$

where ${}^{s}\tau_{u_o}^{y}$ and ${}^{s}\tau_{u}^{y}$ are, respectively, the static and the strain-rate-dependent yield stress of the s̲th elastic, perfectly-plastic mechanical sublayer, and $\dot{\gamma}_u = \frac{d}{dt}\gamma_u$ = material rate of the u̲niaxial Green (Lagrangian) strain γ_u. The strain rate constants d and p for aluminum as cited in Refs. 201 and 202 were used as: $d = 6500\ \mathrm{sec}^{-1}$ and $p = 4$.

For a consistent finite strain representation and computer implementation of tne correct stress-strain behavior, the uniaxial tensile stress-strain data of Fig. 29a of Ref. 2 was recast into τ_{u_o} versus $\varepsilon_u^* \equiv \ell n \frac{\ell}{\ell_o}$ = logarithmic ("natural" or "true") strain $\equiv \ell n\ (1 + E_u)$. This curve was then fitted in a piecewise-linear fashion by the following τ_{u_o}, ε_u^* pairs for use in the mechanical-sublayer model: $(\tau_{u_o}, \varepsilon_u^*) = (0,0)$, (44,200 psi, 0.00442 in/in), (49,200 psi, 0.076), and (76,400 psi, 0.615). It is assumed that strain-rate effects can be approximated by:

$$^{s}\tau_{u}^{y} = {}^{s}\tau_{u_o}^{y}\left(1 + \left|\frac{\dot{\varepsilon}_u^*}{d}\right|^{\frac{1}{p}}\right) \tag{7.2}$$

where

${}^{s}\tau_{u_o}^{y}$ = static (subscript "o") uniaxial yield stress of the s̲th elastic, perfectly-plastic mechanical sublayer

${}^{s}\tau_{u}^{y}$ = strain-rate-dependent yield stress of the s̲th mechanical sublayer

$\dot{\varepsilon}_u^* \equiv \frac{d\varepsilon_u^*}{dt} = \frac{\dot{\ell}}{\ell}$ = longitudinal component of the rate of deformation tensor

For illustrative purposes, the material strain rate constants d and p for aluminum cited in Refs. 201 and 202 are used: $d = 6500\ sec^{-1}$, and $p = 4$.

For analysis, the half span of specimen CB-4 was modeled by using 20 equal-length 4 DOF/node (cubic-cubic) assumed-displacement finite elements, and symmetry conditions were imposed at midspan. Four spanwise and four depthwise Gaussian stations were used for the volume integration of the finite-element property equations. A consistent mass (CM) matrix was employed for each element. A time increment size of 0.25 microseconds (approximately equal to $1.6/\omega_{max}$ where ω_{max} is the maximum natural frequency of the finite-element model or the structure for purely linear behavior) was used; the explicit central-difference timewise finite difference operator was used to solve the unconventional form of the equations of motion. The aluminum material was treated as behaving in an elastic, strain hardening (EL-SH) rate-independent fashion or as EL-SH-SR where SR denotes strain-rate sensitive behavior; the material rate constants were assumed to be $d = 6500\ sec^{-1}$ and $p = 4$. The mass per unit volume ρ_o was taken as $0.25384 \times 10^{-3}\ (lb\text{-}sec^2)/in^4$.

Response predictions were carried out by the "small-strain procedure" and by the "finite-strain procedure" as follows:

Small-Strain Procedure

(a) The uniaxial static tensile stress-strain data for 6061-T651 aluminum [2] were expressed as τ_{u_o} vs γ_u and fitted in a piecewise linear fashion as described earlier.

(b) Strain-displacement relation Type C in conjunction with an assumed displacement field which is valid for small membrane strains (see Eq. 490) was used. Hence, this equation is valid for arbitrarily large rotations but only for "small strains".

Finite-Strain Procedure

(a) The uniaxial static tensile stress-strain data were expressed as τ_{u_o} vs ϵ_u^* and fitted in a piecewise-linear fashion as described earlier.

(b) Strain-displacement relation Type F given by Eq. 4.14b for finite strains, arbitrarily large rotations, and incompressible material behavior was used.

(c) The proper transformations of the stresses and strains to the forms demanded by the correct finite-element formulation (Eqs. 4.173 - 4.176) were employed as described in Subsection 4.3.

Indicated in the following tabulation are the comparisons of those two predictions with each other (and/or versus experimental data) as shown in the indicated figures for the time histories of the longitudinal Green strain tensor component* γ_2^2 on the upper (non-loaded) and/or the lower (impulsively-loaded) surface at various spanwise stations of narrow-plate (or beam) specimen CB-4:

Figure	Station $\lvert y \rvert$ (in)	Time Histories of γ_2^2 on Surface: Upper (U) or Lower (L)	
		Predicted	Measured
9a	0 (midspan)	U and L	-
9b	1.4	U and L	U
9c	2.2	U	U
9d	3.0	U	U

At all stations except for the midspan, the plotted strain is the average of the values given by the two elements at those nodal-junction station locations. At midspan, the predicted strain is the value at the element node located there. Each of these stations is located at a nodal station of the finite element model.

It is seen that, of the spanwise stations shown, the major differences between the two procedures occur at the midspan station y = 0 in, where the finite-strain formulation shows that between 150 μsec and 500 μsec the lower (loaded) surface experiences larger strains than the upper surface while the former "small-strain" formulation indicates the opposite behavior. Also, at this midspan station, the strains predicted by the finite-strain

---

*Beam specimen CB-4 was originally straight; hence, 1/R = 0 and, therefore, $\gamma^{22} = \gamma_2^2 = \gamma_{22}$.

procedure are considerably larger than the strains predicted by the small-strain procedure. At the other stations, where smaller strains occur, the differences between the two predictions are correspondingly smaller.

Shown in Fig. 9e is the spanwise strain distribution at t = 300 μsec from y = 0 in (midspan) to y = 4.00 in (clamped end) of the upper (non-loaded) surface. This time instant is taken as typical, since the strains have already achieved their peak and about 97% of the initial kinetic energy has been transformed into strain energy by that time. The strains predicted by the finite-strain formulation are larger than those predicted by the small-strain formulation with the exception of a region at the end of the impulsively-loaded zone (y = 0.9 in) and a region at the middle of the half-span (y = 2.0 in to y = 2.4 in). The nodal strain discontinuities typical of the 4 DOF/node finite element (employed in the JET 3 and CIVM-JET 4B programs) are evident from the graph. This assumed-displacement finite-element model involves cubic polynomials in the assumed-displacement field for v (the axial displacement) and w (the lateral displacement). The degrees-of-freedom (DOF) involved at each end of the finite-element are the displacements v and w and the displacement gradients $\chi = \frac{\partial v}{\partial \eta} + \frac{w}{R}$ and $\psi = \frac{\partial w}{\partial \eta} - \frac{v}{R}$. These degrees-of-freedom provide continuity of displacement (v and w) and continuity of membrane strain ($\overset{o}{\gamma}{}_2^2 = \chi + 1/2\ \chi^2 + 1/2\ \psi^2$) but the bending strain ($\zeta^o \kappa = \zeta^o [(-\frac{\partial \psi}{\partial \eta})(1+\chi) + \psi \frac{\partial \chi}{\partial \eta}]$) is not continuous at the nodes since $\frac{\partial \psi}{\partial \eta}$ and $\frac{\partial \chi}{\partial \eta}$ are not degrees-of-freedom. Hence, strain jumps appear at each finite-element node since inside each element the displacement function is continuous to derivatives of all orders but at the nodes only continuities of displacement and its first derivative are preserved.* The strain-displacement equations (Eqs. 4.146 and 4.90) involve the displacement gradients $\chi = \frac{\partial v}{\partial \eta} + \frac{w}{R}$ and $\psi = \frac{\partial w}{\partial \eta} - \frac{v}{R}$ and their derivatives $\frac{\partial \psi}{\partial \eta}$ and $\frac{\partial \chi}{\partial \eta}$. The degree of the polynomial involved in the displacement gradients χ and ψ is quadratic for an initially-straight beam. The degree of the polynomial involved in the representation of the first

---

* See Ref. 28 for an evaluation of a formulation which includes element-junction continuity of bending strain.

derivatives of the displacement gradients $\frac{\partial\psi}{\partial\eta} = \frac{\partial^2 w}{\partial\eta^2} - \frac{\partial}{\partial\eta}\left(\frac{v}{R}\right)$ and $\frac{\partial\chi}{\partial\eta} = \frac{\partial^2 v}{\partial\eta^2} + \frac{\partial}{\partial\eta}\left(\frac{w}{R}\right)$ is of the first order or linear, for an initially-straight beam (using the 4 DOF/node cubic-cubic element). From Fig. 9c it is observed that the degree of the polynomials involved in the spanwise strain distribution is (mainly) either quadratic or linear.

It is also observed that the largest discontinuities occur at locations where bending strains are largest: at the end of the impulsively-loaded zone (y = 0.9 in) and at the immediate zone adjacent to the clamped end (y = 3.8 in to y = 4.0 in). At the clamped zone, a very large strain discontinuity is evident. The reason for this is that this region involves high levels of nonlinearity. The strain discontinuity at the clamped zone is significantly larger with the finite-strain formulation, which involves a more nonlinear representation of the behavior than the "small-strain" formulation. It is evident that a finer mesh of finite elements is needed in this clamped-zone region to represent accurately this nonlinear behavior. However, time and fund restrictions have prevented a more thorough study of this matter at this time.

The predicted transient midspan transverse displacement w for each of these EL-SH-SR predictions is shown in Fig. 10. It is seen that the finite-strain formulation and small-strain formulation predictions are in fairly good agreement with each other.

The computing time required for the two formulations for explosively-impulsed beam CB-4 is displayed conveniently in the following tabulation for 4000 time steps with a time step size of 0.25 microseconds; all runs were conducted on an IBM 370/168 computer with double precision arithmetic:

Formulation	No. of FE	No. of Gaussian Sta. per Elem.		Total No. of Unknown DOF
		Spanwise	Depth	
Small Strain	20	4	4	79
Finite Strain	20	4	4	79

Formulation	Strain-Displ. Relation Type	Mass Matrix	No. of Cycles	CPU Time (min)	CPU (min) / (DOF) (Cycles)
Small Strain	C (Eq.4.90)	CM	4000	8.63	27.3×10^{-6}
Finite Strain	F (Eq.4.146)	CM	4000	11.07	35.0×10^{-6}

The effects on CPU time of the more lengthy expressions used and manipulations required for the finite-strain calculations are evident from an inspection of the last column. Note here that the efficient "unconventional" formulation of the equations of motion was used for both the small- and finite-strain procedures.

Finally, compared in Fig. 11 are finite-strain predictions for the transient w-displacement at the midspan location of specimen CB-4 for the same modeling as before but for the two cases in which the 6061-T651 aluminum material is assumed to behave as (a) EL-SH-SR or (b) EL-SH, where the latter case assumed no strain rate effect upon the mechanical behavior of the material. It is seen that the predicted midspan deflection w is much larger for the EL-SH than for the EL-SH-SR case even though the rate-sensitivity used for the EL-SH-SR is rather "weak" since large strain-rates are present. Note that the finite-strain EL-SH-SR prediction compares favorably with the observed experimental permanent deformation. It is evident also that the strains predicted for the finite-strain EL-SH are much larger than for the finite strain EL-SH-SR case. Accordingly, the former are not shown since the latter have been displayed and demonstrate the behavior adequately -- and also have been shown to compare favorably with experiment.

7.2.3 Modeling by Plate Finite Elements

7.2.3.1 Modeling Description and Outline of Analysis

Impulsively-loaded narrow plate specimen CB-4 was also analyzed by using a finite-element model consisting of initially-flat plate elements of the assumed displacement type [31]. These elements consisted of rectangular flat plate elements with linear in-plane (u,v) and cubic out-of-plane (w) displacements for the assumed displacement field; accordingly, each corner node has 6 degrees of freedom.* To "minimize" the computations, only one quarter of specimen CB-4 was modeled: 27 uniform-length elements covered the half span, with each element extending from the midwidth to the free edge of narrow-plate CB-4. This modeling provides a comparable number of degrees of freedom in the v,w plane as used for the beam-element modeling. For the 4 DOF/node beam element, with 20 elements in the axial "y" direction, there are [4 x (20+1) - 5) = 79 unrestrained degrees of freedom, while the linear-linear cubic plate element is "equivalent" to a 3 DOF/node beam element when $u = \frac{\partial w}{\partial x} = \frac{\partial^2 w}{\partial x \partial y} = 0$ having then [3 x (27+1)-5] = 79 unrestrained degrees of freedom. Thus, the assembled "unrestrained" finite element model consisted of 336 DOF, which reduced to 238 DOF by imposing (1) symmetry conditions along $x = 0$ and $y = 0$ and (2) the ideally-clamped condition at the end. With this FE model, it turns out that the maximum natural frequency of this mathematical model is $\omega_{max} = 0.739 \times 10^7$ rad/sec. Thus, if one were to predict the transient response of this finite element model by using the very convenient explicit central-difference timewise operator, the Δt required to avoid calculation instability would be $\Delta t \leq 0.8 \frac{2}{\omega_{max}} = 0.2$ microseconds. Since one may need to study the structural response for a time duration of up to perhaps 900 microseconds, one would need to carry out some 4500 solution time steps on this 238 DOF nonlinear system; this may be viewed in some circles as a rather substantial calculation.

On the other hand, one might be able to use some other finite-difference operator which would permit the use of a substantially larger time step Δt while still providing "proper results". For stiff systems such as the present one involving large deflections and nonlinear material behavior with many regions of loading, unloading, reloading, etc., one has available a number of implicit-type finite-difference operators which are unconditionally stable (Δt is not limited by calculation stability or blow up) for linear system response analysis but which become ill-behaved for the present type of nonlinear system if Δt is "too large". Nevertheless,

*The DOF are u, v, w, $\frac{\partial w}{\partial x}$, $\frac{\partial w}{\partial y}$, and $\frac{\partial^2 w}{\partial x \partial y}$.

it turns out that some of these operators will permit one to use a much larger Δt than needed for the central-difference operator while still providing transient response predictions which compare favorably with (converged) central-difference predictions. Because these operators are of the implicit type, the solution procedure at each time step must employ either (a) iteration (hopefully to convergence) or (b) extrapolation of "internal force" information. The latter, of course, represents an approximation to the correct internal force terms needed for the proper solution; this approximation becomes worse as one attempts to use a larger and larger Δt.

Many iteration methods are available for the solution of simultaneous nonlinear equations. Unlike single degree-of-freedom nonlinear equations, always-convergent methods are just not available for solution of systems of nonlinear equations. Convergence itself is such a serious problem for systems of nonlinear equations that if the initial approximation is not quite close to the solution, the method will not converge. One of the most simple methods, the method of successive substitution (also called Piccard's method) enjoys linear convergence (under some conditions). Examples of higher-order methods are the Newton method, that has quadratic convergence and the secant or quasi-Newton methods (like the BFGS method [203,204]) that possess superlinear convergence (which is faster than linear but slower than quadratic convergence). The higher order methods (like the BFGS or the Newton methods) use variable-gradient matrices that may become singular (for example, in the course of unloading in elastic-plastic problems, these gradients become discontinuous), and may impede convergence of the method. The computational effort for iteration methods is large, as compared with extrapolation of the nonlinear internal pseudo forces.

The point at which an iteration method would be competitive computationally with the extrapolation method would be for large time step sizes; however, under those condition, the path-dependency of elastic-plastic strain-rate-dependent transient response problems could be significantly lost (because of integration error that iteration methods cannot reduce -- see Subsection 6.3.2.2) unless higher order integration rules (like the fourth order Runge-Kutta method) are utilized to integrate the differential equations of plasticity.[+] Moreover, the use of a suitably lax convergence criterion can give one the illusion of having achieved convergence when this has not actually been accomplished.

Among the attractive implicit methods are those of Newmark [205], Houbolt [206], Park [194], and others. Since studies reported in Refs. 23, 174, and 194 indicate that the Houbolt method for problems of the present type provides "well-behaved predictions" for (a) Δt sizes larger than needed for comparable performance by Newmark $\beta = \frac{1}{4}$ operator or (b) comparable to those needed for Park's operator -- and also since the authors have appropriate computer programs [24,31] available using the Houbolt operator, it was decided to employ this timewise solution operator for the CB-4 narrow-plate transient response predictions reported in the following. Similar studies involving the use of the very attractive Park operator [194] would be useful, but time and effort constraints have not permitted this in the present investigation.

In this study, calculations have been carried out to demonstrate the necessity for using double-precision calculations with the present solution method when one uses a digital computer with the significant-figure retention capability of the IBM 370/168 at MIT, which was used for these calculations. For this demonstration, the Houbolt operator with $\Delta t = 1$ μsec and linear extrapolation (not iteration) for the "internal loads" were utilized. Calculations were carried out for both the small-strain procedure and the finite-strain procedure, and are discussed in Subsection 7.2.3.2.

Next, a study was made to investigate the use of:

(a) the linear-extrapolation procedure for Δt values ranging from 0.5 to 20 μsec; and

---

[+] However, a subincrementation procedure (see Subsection 5.3.2.5) as used in this study partly relieves this problem.

(b) the use of iteration during a given Δt time step -- again for Δt values ranging from 0.5 to 20 μsec.

Because of the use of very different Δt values, the strain-rate information available in these various calculations will not be of comparable accuracy and meaning. Accordingly, for these comparisons, the CB-4 narrow plate material was assumed to be EL-SH; that is, independent of strain rate. Only in this way can one make a valid comparison among the predictions when one uses various fixed time-step sizes Δt. These studies are discussed in Subsection 7.2.3.3.

Finally, having selected double-precision calculations, an appropriate solution procedure, and an appropriate Δt, predictions were carried out to compare small-strain formulation predictions versus finite-strain formulation predictions, and are discussed in Subsection 7.2.3.4.

7.2.3.2 Single-Precision vs Double-Precision Predictions

Stated concisely in the following are the modeling and solution features employed in these calculations:

Finite Element Model:	Quarter plate modeled by 27 flat-plate LLC elements with 6 DOF/node; consistent mass matrix.
Material Behavior for both Small-Strain and Finite-Strain Calculations	EL-SH-SR with the mechanical sublayer stress-strain fit given by: $({}^{s}\tau_{u_o}, \epsilon^*_u) = \begin{matrix}(44{,}200 \text{ psi}, 0.00442)\\ (49{,}200 \text{ psi}, 0.07500)\\ (76{,}400 \text{ psi}, 0.61500)\end{matrix}$ Strain rate constants: $d = 6500$ sec^{-1} and $p = 4$ for all mechanical sublayers are used for illustrative purposes.
Timewise Finite Difference Operator and Solution Procedure	Houbolt with $\Delta t = 1.0$ microsecond and linear extrapolation of pseudo-loads.

The constant stiffness form[†] of the equations of motion was used with the Houbolt operator. From Eq. 6.90, this expression at time t+Δt is:

$$\left(\frac{2}{(\Delta t)^2}[M]+[K]\right)\{q^*\}_{t+\Delta t}=\{F\}_{t+\Delta t}+\{F^{NL}\}_{t+\Delta t}$$

$$+\frac{2}{\Delta t}[M]\left(\{\dot{q}^*\}_t+\frac{1}{\Delta t}\{q^*\}_t\right) \tag{7.3}$$

where [M] is the global (constant) mass matrix, [K] is the usual small strain, linear-elastic, global (constant) stiffness matrix, $\{F\}_{t+\Delta t}$ is the load vector representing prescribed externally-applied distributed or concentrated loads, evaluated at time $t = t+\Delta t$; and $\{F^{NL}\}_{t+\Delta t}$ is a pseudo-load vector representing internal forces.

For the small-strain computational procedure, the "conventional" form of the equations of motion (Eq. 6.68) was utilized. The vector $\{F^{NL}\}_{t+\Delta t}$ for the "conventional" formulation is

$$\{F^{NL}\}_{t+\Delta t}=\{F_p^{L}\}_{t+\Delta t}+\{F_p^{NL}\}_{t+\Delta t}+\{F_q^{NL}\}_{t+\Delta t} \tag{7.4}$$

where $\{F_q^{NL}\}_{t+\Delta t}$ is a vector arising from the nonlinear terms in the strain-displacement equations, and $\{F_p^{L}\}_{t+\Delta t}$ and $\{F_p^{NL}\}_{t+\Delta t}$ are pseudo-load vectors arising from plastic (small) strains and associated, respectively, with the linear and nonlinear terms of the strain-displacement relations. The reader is reminded that Eq. 7.4 is valid only for small strains.

[†]Also referred to herein as the modified unconventional form.

For the finite strain computational procedure, the "modified unconventional" form of the equations of motion was employed. The vector $\{F^{NL}\}_{t+\Delta t}$ for the "modified unconventional" formulation is

$$\{F^{NL}\}_{t+\Delta t} = [K]\{q^*\}_{t+\Delta t} - \{I\}_{t+\Delta t} \tag{7.5}$$

where [K] is the same global (constant) stiffness matrix appearing on the left-hand side of Eq. 7.3, and $\{I\}_{t+\Delta t}$ is the same pseudo-load vector of internal forces used for the "unconventional" vector form of the equations of motion, Eq. 6.72. It turns out that the "modified unconventional" form of the equations of motion can be used for both small and finite strains, requires less computation, and is also better conditioned numerically than the "conventional" form (Eq. 7.4, which cannot be used for finite strains).

Note that the pseudo-load vector $\{F^{NL}\}_{t+\Delta t}$ appearing in Eq. 7.3 depends upon the displacements $\{q^*\}_{t+\Delta t}$ at time instant $t = t+\Delta t$, but these remain to be determined; thus these "forces" are approximated by linearly extrapolating the known pseudo-forces at two previous time instants $t = t$, and $t = t-\Delta t$ (as explained in Subsection 6.4.2.1) as:

$$\{F^{NL}\}_{t+\Delta t} = 2\{F^{NL}\}_t - \{F^{NL}\}_{t-\Delta t} \tag{7.6}$$

This expression has the same inherent order of error as in the Houbolt operator approximations for both the acceleration (Eq. 6.92) and the velocity (Eq. 6.93); hence, it is a consistent approximation of the pseudo-load vector $\{F^{NL}\}_{t+\Delta t}$.

Note that the pseudo-force extrapolation for the modified unconventional linear extrapolation procedure (MULE) is directly analogous to that used for solving the conventional form of the equations of motion for small-strain problems -- only the pseudo-force vector $\{F^{NL}\}$ is extrapolated, the constant stiffness form providing much better stability proportion than if one attempted to extrapolate the entire pseudo-force vector {I} itself in a vector form of the equations of motion (Eq. 6.34). Computational experiments confirmed this expectation.

Compared in Fig. 12 are the single-precision and the double-precision predictions for the transient lateral displacement w at the plate-center location (x,y) = (0,0) for the small-strain equations and procedure. It is seen that the single-precision calculation deteriorates badly beyond a time of about 300 microseconds. The double-precision prediction appears to be well behaved and compares favorably with the experimentally-observed permanent deflection at this location. Although transient strain predictions are not shown here for these cases, it is evident that these predictions must differ greatly from each other; the computed results do show this.

For the finite-strain equations and procedure, Fig. 13 shows the single-precision and the double-precision predictions for the transient lateral displacement w at the plate-center location (x,y) = (0,0). In this case the single-precision prediction appears to behave in a more plausible fashion than for the small-strain calculation but also has "stabilized" to a permanent deflection value much less than both the double-precision prediction and experiment show. While the finite-strain equations using MULE are much better conditioned numerically than the "conventional equations of motion" employed for the small-strain prediction, the necessity of employing double-precision arithmetic with these equations using the IBM 370/168 system at MIT is evident.

Although the aspect ratio of the finite elements in the present mesh is certainly responsible in part for the inadequacy of single-precision arithmetic for these calculations, many other investigators have concluded in the past that double-precision arithmetic is necessary when using the IBM machine to produce accurate results for the types of transient nonlinear response problems being studied here.

Finally, compared in Fig. 14 are the single-precision predictions for w at (x,y) = (0,0) for (1) the small-strain procedure versus (2) the finite-strain procedure. Here it is apparent that the latter prediction is much better behaved than the former (since many fewer computations are required for the "modified unconventional" formulation than for the "conventional" formulation of the equations of motion), but both predictions are in serious disagreement with experiment. Accordingly, all other calculations in this work have been performed with double-precision arithmetic on the IBM 370/168.

7.2.3.3 Time Increment Size Effects

In using an implicit timewise finite-difference operator (the Houbolt operator) to solve the modified unconventional equations of motion for finite strain, one can (1) employ the convenient (linear) "explicit" extrapolation procedure for the pseudo-loads or (2) resort to "iteration to convergence" within each time step Δt before proceeding for the next time step in the timewise solution process.

LINEAR EXTRAPOLATION

For the modified unconventional linear extrapolation procedure (MULE), it is evident that this approximation for the pseudo-force vector $\{F^{NL}\}$ will become poorer and poorer as Δt increases. On the other hand, the use of the largest Δt which will provide "accurate" transient response predictions will be highly desirable in order to minimize the computing time and expense for a given time duration in which the transient response must be predicted so as to provide, for example, the peak transient strains. To study this "Δt effects question", only EL-SH material behavior is taken into account-- since for time-dependent EL-SH-SR material behavior it is obvious that the time increment size Δt will have a definite effect on the solution behavior. Further, all modeling and computing features used now are the same as summarized in Subsection 7.2.3.2 except that Δt values of 0.5, 2, 10, and 20 μsec are used for the finite-strain MULE procedure.

Compared in Fig. 15 are finite-strain MULE predictions of the transient w displacement at the plate-center location $(x,y) = (0,0)$ for Δt values of 0.5, 2, 10, and 20 microseconds. For $\Delta t = 0.5$ and 2 microseconds, the predicted transient displacement appears to be relatively well behaved for the first 300 μsec. However, for $\Delta t = 10$ and 20 microseconds, the pseudo-forces have been badly overestimated and the transient response is seen to deviate substantially from the "proper" behavior. For $\Delta t = 10$ μsec this predicted transient w displacement became "very smooth" and peaked at a value of about 2.01 in at about 740 μsec; for $\Delta t =$ 20 μsec this predicted transient response was similar but a peak value of 1.82 in was reached at $t \doteq 700$ μsec.

Observe from Fig. 15 that after 300 μsec there are significant differences between the $\Delta t = 0.5$ and 2 microseconds predictions. Also, observe that the transient w displacement at the plate center location does <u>not</u> grow monotonically with increasing time increment size Δt. In fact, the peak transient displacement prediction is smaller for $\Delta t = 2$ μsec than for $\Delta t = 0.5$ μsec; it is larger for $\Delta t = 10$ μsec than for $\Delta t = 2$ μsec and $\Delta t = 0.5$ μsec; and it is <u>smaller</u> for $\Delta t = 20$ μsec than for $\Delta t = 10$ μsec. Therefore, <u>no monotonic exponential instability is observed</u>, but rather the predictions become less and less accurate as Δt increases -- in an <u>oscillatory</u> form. This agrees with the results obtained by McNamara [165] for the Houbolt operator, but with a different formulation of the equations of motion and for a problem with geometrical nonlinearities and with linear material behavior.

These calculations confirm the expectation that large Δt values will lead to poor estimates of the proper pseudo-forces when the linear extrapolation estimate is used. Stricklin et al. [162] observed that quadratic-extrapolation predictions lead to less well-behaved results than do linear-extrapolation predictions; for a given "not-too-small" time step size Δt, for nonlinear dynamic problems. Of course, one could employ higher order extrapolation estimates for the pseudo-forces at the cost of additional storage and computing; however, the benefits of such procedures are uncertain and may well be problem-dependent.

Hence, in view of the MULE predictions shown (1) here for EL-SH behavior with Δt values of 0.5 and 2 μsec and (2) in Subsection 7.2.3.2 for EL-SH-SR predictions with a Δt value of 1 μsec, it appears that plausible well-behaved transient responses are provided by the finite-strain Houbolt-MULE procedure for Δt values of at least up to about 1 μsec. However, there is no proof that one has obtained essentially a "converged" prediction; conversely, it is certain that such has not been achieved, but the predicted response might very well be close enough to convergence for all practical engineering purposes. That assessment could be made, if required, by using the central-difference timewise solution operator together with a suitably small Δt to solve the unconventional form of the equations of motion; for this case, a Δt of about 0.2 microseconds would be required. Whereas with MULE and the Houbolt operator, an "adequate" prediction apparently is achieved by using a 5 times larger Δt; namely, $\Delta t \doteq 1$ μsec -- but the computational saving is not as large as this factor because of the greater required storage and computation needed for Houbolt-MULE vs the central-difference scheme described.

Finally, the merit of Houbolt-MULE becomes evident when one considers transient response problems of the present type but with a finite element model involving perhaps 10 times as many DOF. For such a case the required Δt for a central-difference solution might well be 10^{-3} μsec whereas a satisfactory Houbolt-MULE solution might need a Δt of only about 1 μsec.

ITERATION SOLUTION

Compared here are predicted transient displacements of impulsively-loaded narrow-plate CB-4 specimen obtained by (1) iteration as required during each Δt time interval during Houbolt operator solution of the modified unconventional equations of motion for finite strain (as explained in Subsection 6.4.2.2) and (2) the Houbolt-MULE (non-iterative linear extrapolation) procedure.

Shown on Fig. 16 are Houbolt equilibrium-iteration and Houbolt-MULE transient w-displacement solutions at $(x,y) = (0,0)$ for the 27-element plate model of specimen CB-4, both with $\Delta t = 0.5$ μsec. The iteration convergence criterion used in this case* was (see Eq. 6.117),

$$\alpha = \frac{\left(\left\|\{q^{*\,n+1}\}_{t+\Delta t}\right\|\right)^2 - \left(\left\|\{q^{*\,n}\}_{t+\Delta t}\right\|\right)^2}{\left(\left\|\{q^{*\,n}\}_{t+\Delta t}\right\|\right)^2} < 1 \times 10^{-4} \tag{7.7}$$

where $\|\{q^{*\,n}\}_{t+\Delta t}\|$ is the Euclidean (L^2) norm of the vector $\{q^{*\,n}\}_{t+\Delta t}$. Superscripts n and n+1 denote iterations n and n+1 during a given time step interval Δt.

During a response time of 294.5 μsec (589 Δt cycles), 41 iteration loops (or 7% of the total number of iteration loops) did converge to a mean ratio of $\alpha = 4.7 \times 10^{-5}$ (with a standard deviation of 2.7×10^{-5}). There were 3.4 equilibrium iterations in the mean (with a standard deviation of 1.2) during these 41 iteration loops that satisfied criterion Eq. 7.7. However, as was expected, most iteration loops (548 iteration loops or 93% of the total number of iteration loops) could not satisfy the convergence criterion Eq. 7.7. In these cases the procedure outlined in Eqs. 6.120 - 6.122 was employed. As soon as divergence of the iteration procedure was detected, the iteration loops were stopped (after a mean number of 4.0 iterations with a standard deviation of 1.4), and the previous "convergent" estimate was taken to be the "equilibrium" solution for that time step. This previous "converged" estimate satisfied a mean convergence ratio of $\alpha = 2.7 \times 10^{-3}$ (with a standard deviation of 9.3×10^{-3}). From this figure, the iteration solution is seen to differ somewhat from the Houbolt-MULE linear extrapolation prediction.

---

*Also see Eq. 6.121.

A further comparison of these predictions is given in Fig. 17 where included also are central-difference predictions with $\Delta t = 0.25$ μsec for the half span of specimen CB-4 modeled by 20 4 DOF/node beam elements. Although the finite element models used are different, it is interesting to note that the explicit central-difference beam prediction compares very well with the Houbolt-MULE linear extrapolation prediction, and the modified successive substitution iteration method seems not to have "converged" to the correct solution.

Similar plate finite-element finite-strain equilibrium iteration vs Houbolt-MULE linear-extrapolation predictions are shown on Fig. 18a for $\Delta t = 2$ μsec. These two predictions are very close to each other for the 300 microsecond time span shown. Later on in time, however, as Fig. 18b shows, these two predictions exhibit pronounced differences.

Finally, for a Δt of 20 μsec, Houbolt-MULE linear-extrapolation predictions as well as equilibrium iteration solutions obtained by using two different iteration convergence criteria are shown in Fig. 19. Also shown in Fig. 19 is the Houbolt-MULE linear-extrapolation prediction for the transient w at (x,y) = (0,0) using a Δt of 0.5 μsec; this prediction should be "accurate" and serves as a yardstick against which to measure the "worth" of the other predictions shown. Of the two $\Delta t = 20$ μsec predictions, only the equilibrium iteration scheme in which

$$\beta = \frac{\left\| \{q^{*n+1}\}_{t+\Delta t} - \{q^{*n}\}_{t+\Delta t} \right\|}{\left\| \{q^{*n}\}_{t+\Delta t} \right\|} < 1\times10^{-4} \tag{7.8}$$

is used for "iteration convergence" appears to be plausible over the entire time span shown. Even this prediction exhibits an "excessively smooth" transient response profile, and also seriously overpredicts the permanent deflection. Clearly $\Delta t = 20$ μsec is much too large to provide an acceptable transient response prediction for this structural response problem.

The present (modified successive substitution) iteration procedure does not provide accurate results. Further, the attendant computational expense for the iteration scheme is much larger fc a "given prediction accuracy" than the Houbolt-MULE linear-extrapolatic procedure. It would be useful to investigate the efficiency and practi ality of employing the BFGS iteration method cited in Subsection 7.2.3.1.

7.2.3.4 Small-Strain vs Finite-Strain Predictions

Having determined the necessity of using double-precision arithmetic for the present calculations on the IBM 370 and the superior accuracy/efficiency of using the Houbolt operator with linear extrapolation (compared with the iteration schemes studied), calculations for narrow-plate specimen CB-4 were then carried out using the Houbolt operator and linear extrapolation with a conservative Δt of 1 μsec. Stated concisely, used were:

Houbolt Operator with Linear extrapolation
Double Precision IBM 370/168
27 LLC Elements for the Quarter Plate
Consistent Mass Matrix
EL-SH-SR with $\dot{d} = 6500$ sec^{-1}, p = 4 and the ${}^{s}\tau_{u_o}$, ε_u^* Piecewise-Linear Fit given in Subsection 7.2.3.2
$\Delta t = 1$ microsecond

SMALL STRAIN: von Kármán's Strain-Displacement Equations for Plates (see Eqs. 5.118 - 5.123)
Small-Strain Plasticity Theory
"Conventional" Formulation

FINITE STRAIN: Finite-Strain Strain-Displacement Equations (see Eqs. 5.118 - 5.123)
Finite-Strain Plasticity Theory
"Modified Unconventional" Formulation

For the finite-strain predictions, the terms containing the second-order derivatives of u and v in the strain-displacement equations, Eqs. 5.118 - 5.123, are obviously equal to zero for the assumed displacement element which has linear (u) - linear (v) - cubic (w). Although for general purposes a higher order (cubic-cubic-cubic) plate element should be used to treat arbitrarily-large rotation problems, studies conducted in Ref. 28 reveal that the second-order derivatives of the in-plane displacements u and and v have a very small influence in the predicted strains for the present kind of problems (impulsively-loaded narrow-plate CB-4 being discussed now and fragment-impacted narrow-plate CB-18 to be discussed later).

Predictions for both the small-strain procedure and the finite-strain procedure were made, and are compared here with each other and/or with experimentally-measured data for the permanent deflection and for transient strains at various midwidth spanwise stations on the upper (non-loaded) and/or on the lower (loaded) surface of explosively-impulsed narrow-plate CB-4.

The computing time on the IBM 370/168 for 900 μsec with the same Δt = 1 μsec and the Houbolt operator was:

FINITE STRAIN ("MODIFIED UNCONVENTIONAL" FORMULATION)	71 min
SMALL STRAIN ("CONVENTIONAL" FORMULATION)	70 min

Shown in Fig. 20 are the small-strain and the finite-strain predictions of the w displacement at the plate-center location (x,y) = (0,0); shown also is the observed permanent deflection at this location. It is seen that these two predictions compare very well with each other, and apparently also fairly well with the experimental permanent deflection. This displacement vs time comparison is shown here since this type of comparison is an almost-standard one found in the open technical literature; however, it is a <u>notoriously insensitive</u> measure of the prediction accuracy of <u>any method</u> for the present type of geometrically and materially nonlinear elastic-plastic transient response problem.

A much more meaningful and sensitive comparison involves predicted vs measured <u>strains</u> since for ductile materials the strains are a much better indicator of impending rupture than are displacements. Accordingly, shown in the following figures are the small-strain and finite-strain predictions of the spanwise-direction Green strain* γ_2^2 on the upper and/or the lower surface of specimen CB-4 (see Fig. 8) at the indicated stations** vs the measured strain:

Figure	Station $\|y\|$, (in)	Time Histories of γ_2^2 on Surface Upper (U) or Lower (L)	
		Predicted	Measured
22a,22b	4.00	U,L	--
22c	3.80	L	L
22d	3.80	U	U
22e	3.00	U	U
22f	2.20	U	U
22g	1.40	U	U
22h,22i	0.0	U,L	--

At the clamped end station $(|x|, |y|) = (0, 4.00$ in), at the lower (loaded) surface, a maximum strain $\gamma_2^2 \approx +0.18$ is predicted by the small-strain procedure; see Figs. 22a and 22b.

Station $|y| = 3.8$ in is near the clamped end ($|y| = 4.00$ in); hence, the strain γ_2^2 on each surface (see Figs. 22c and 22d) consists of a significant "bending contribution" in addition to the "membrane part" of the strain. Thus, as expected, this strain exhibits a larger tensile transient peak value at the lower (loaded) surface than on the upper (non-loaded) surface. Further, on this lower surface where larger strains occur, it is seen that the consistent finite-strain prediction differs significantly from the small-strain prediction, and the finite-strain prediction agrees much better with experiment than does the latter. On the upper surface at $|y| = 3.80$ in where smaller levels of strain occur,

---

*Or γ_{22}, since beam CB-4 is initially flat, $\gamma^{22} = \gamma_2^2 = \gamma_{22}$.

**To assist in interpreting these results, Fig. 21 shows a schematic of the finite element model and element numbering.

these two predictions are much closer to each other (see Fig. 22d). The large strains that occur at the lower (loaded) surface, at the clamped end $|y| = 4.00$, $|x| = 0.00$ have a very significant influence on the behavior of the strains at 0.2 in from the clamped end, the finite strains results being much closer to the experimental values.

On the upper surface at station y = 3.00 in, these two predictions compare well with each other in an overall sense as seen from Fig. 22e, but the peak strain predicted by the "proper" finite-strain prediction procedure is about 20 per cent larger than the small-strain calculation result. The experimental value, however, appears to be even larger up to the instant at which the strain trace was lost -- probably because of broken lead wires. Note that the finite strain results are closer to the predicted strains of the beam finite elements (Fig. 9d).

At station $|y| = 2.20$ in, the strains consist mainly of membrane behavior with a small bending contribution. Figure 22f shows that the finite-strain and the small-strain predictions for the upper-surface strain are close to each other. However, the finite-strain prediction is again closer to the overall behavior predicted by the beam finite element modeling (Fig. 9c) since it does not exhibit the strange behavior at t = 300 μsec that the small-strain results display.

Station $|y| = 1.40$ in is nearer than any of the others to the end ($|y| = 0.90$ in) of the spanwise region to which uniform lateral impulse loading was applied. Hence, one expects to see an important bending contribution here in addition to the dominant membrane behavior; accordingly, somewhat greater differences are seen and are expected here between finite-strain and small-strain predictions than at $|x| = 2.20$ in -- which is more remote from station $|x| = 0.90$ in. Larger strains are predicted by the finite-strain than by the small-strain procedure at $|x| = 1.40$ in as seen from Fig. 22g. However, it appears that the peak experimental strain is even larger -- possibly by some 30 per cent than the (better) finite-strain procedure predicts.

Finally, at the plate-center (midspan) station (x,y) = (0,0), one observes from Figs. 22h and 22i for the upper surface and the lower surface, respectively, that there is early-time agreement between the finite-strain and the small-strain predictions. Beyond about 200 microseconds, however, there are some distinct differences in the character of these predictions. Observe that both the small-strain and the finite-strain predictions at the plate center using plate finite-element modeling agree with the finite-strain predictions at the same location when using beam finite-element modeling (Fig. 9a), in that they predict a reverse bending that occurs between 100 μsec and 400 μsec.

Additionally, let it be noted that although many of the traces of the experimentally-measured strains on specimen CB-4 were terminated before the peak values were reached, it appears that the experimental peaks would have been somewhat larger in nearly every case than predicted by the plate finite elements. The cubic-cubic beam finite elements show better strain results. Improved predictions could be achieved by using a greater number of the present (too stiff) linear-linear-cubic (LLC) assumed-displacement elements or by using the fundamentally-better but more costly cubic-cubic-cubic (CCC) assumed-displacement element for the u, v, w displacement fields. As shown in Refs. 23 and 28 and numerous other references, the use of balanced-polynomial assumed-displacement elements leads to predictions of superior accuracy for the present kind of problems compared with unbalanced-polynomial elements. An extension of the present investigation, therefore, is recommended to utilize and assess the benefits to be achieved by the use of CCC elements for finite-strain predictions in the present type of nonlinear transient response problem.

7.3 Impulsively-Loaded Free Circular Ring

Sought is a more stringent test and evaluation of the present finite-strain predictions vs small-strain predictions vs experiment. This is afforded by the experimental data from Ref. 207 for an impulsively-loaded free initially-circular aluminum ring since

(1) larger compressive strains are present (and over a larger circumferential region);

(2) much larger rotations are present; and

(3) bending rather than stretching dominates the response of the structure.

7.3.1 Problem Definition

As reported in Ref. 207 a free initially-circular 6061-T6 aluminum ring (called F15) of 2.937-in midsurface radius, 0.124-in thickness, and a 1.195-in width was loaded impulsively uniformly over a 120-degree sector (centered at $\theta = 0^{\circ}$) of its exterior, resulting in an inward initial velocity of 6853 in/sec for that loaded region. High speed photographic measurements were made of the deforming ring. Also, transient strains were measured at various circumferential stations on the inner surface and/or the outer surface of the ring. Static uniaxial stress-strain tests were conducted on coupons of the 6061-T6 aluminum from which the ring was made. The mass per unit volume of this material is assumed to be $\rho_o = 0.0002526\ (\text{lb-sec}^2)/\text{in}^4$.

For the small-strain analysis, strain-displacement relation Type C which is valid for arbitrarily large rotations but only small strains was employed and the following [23,28] stress-strain pairs (τ_{u_o},γ_u) were used for mechanical sublayer fitting of the static stress-strain data: (τ_{u_o},γ_u) = (42,000 psi, 0.00476 in/in) and (58,219 psi, 0.2000 in/in). The material was assumed to be strain rate sensitive; strain rate constant values $d = 6500\ \text{sec}^{-1}$ and $p = 4$ were assumed for illustrative purposes.

For the finite-strain analysis, strain-displacement relation Type F which is valid for finite strains and finite rotations was used and the static uniaxial stress-strain data were recast into τ_{u_o} vs ε_u^* where $\tau_{u_o} = \sigma_E (1 + E_u)$ and $\varepsilon_u^* = \ln(1 + E_u)$. A piecewise linear fit of this τ_{u_o} vs ε_u^* data of Ref. 207 was made as follows for use in the mechanical-sublayer material model: $(\tau_{u_o}, \varepsilon_u^*)$ = (42,974 psi, 0.0040679), (52,150 psi, 0.07000), and (107,383 psi, 0.615). For this calculation also, it was assumed for illustrative purposes that the material strain rate constants were $d = 6500\ \text{sec}^{-1}$ and $p = 4$.

7.3.2 Comparison of Small-Strain vs Finite-Strain Predictions

For economy and convenience reasons in both calculations, advantage was taken of symmetry by modeling the half ring with 18 uniform-length CC 4DOF/node curved-ring elements, thereby resulting in 72 unknown DOF. The finite element properties were evaluated numerically by Gaussian quadrature with 4 spanwise and 4 depthwise Gaussian stations in each element. A consistent mass matrix was used. Both calculations employed the central-difference timewise operator with $\Delta t = 0.6$ microsecond; for this model $\omega_{max} = 2.5730 \times 10^6$ rad/sec, so $0.8\,(2/\omega_{max}) = 0.62$ μsec has not been exceeded by the selected Δt.

Comparisons of predicted circumferential Green strain γ_2^2 for both the small-strain and the finite-strain procedure are shown versus each other and/or experiment in the following indicated figures at various circumferential locations θ on the inner (non-loaded) surface or on the outer (loaded) surface:

Figure	θ-Location (deg, min)	Surface	
		Inner	Outer
23a	92° 30'	x	
23b	92° 30'		x
23c	87° 20'	x	
23d	86° 10'		x
23e	176°		x
23f	16°	x	
23g	16°		x

At all of these locations except for $\theta = 16^\circ$, the predicted and measured strains indicate the presence of a very significant bending contribution -- the inner-surface and the outer-surface strains are of significant magnitude and of opposite sign. It is seen that finite-strain predictions in nearly all cases differ considerably from the small-strain predictions, and also are in better agreement with experiment than are the latter predictions.

At $\theta = 16^\circ$, note that membrane compression behavior is dominant -- at both surfaces the predicted γ_2^2 is compression and the values of γ_2^2 on the inner surface differ little from those on the outer surface. At these $\theta = 16^\circ$ inner-surface and outer-surface locations, it is seen that the finite-strain and the small-strain predictions are in better agreement with each other than at the other locations - where bending behavior is very prominent.

Shown in Fig. 24 is a comparison of measurements vs predictions of time history of the ring's midplane centerline separation distance. Both predictions are in fairly good agreement with measured values. The finite-strain prediction shows a smaller extreme separation distance than the small-strain prediction and occurs at about 1250 microseconds while that for the small-strain calculation occurs at about 1400 μsec.

Note that near 1500 μsec, the ring is in a severely deformed state. At this condition, it is of some interest to examine the circumferential distribution of the circumferential strain γ_2^2 along both the outer surface and the inner surface. Finite-strain predictions for this information as well as measured values are shown in Fig. 25. It is seen that in the region $3^{\circ} \lesssim \theta \lesssim 105^{\circ}$ there are very severe spatial gradients in the strain along each surface. Regions of (a) mainly membrane, (b) mainly bending, and (c) combined behavior are evident. Despite the severe spatial gradients in the strain, it is seen that the finite-strain predictions are in reasonably good agreement with measurements at this time instant.

7.3.3 Comments

This impulsively-loaded free initially-circular ring is of special interest in the present finite-strain study since not only are strains of significant magnitude produced but also certain regions of the ring undergo very large rotations -- conditions which are accommodated properly in the present theory and analysis. Now one finds significantly improved qualitative and quantitative agreement between measurements and finite-strain predictions compared with the former small-strain predictions. The large differences between the small-strain and the finite-strain predictions at $\theta = 92^{\circ}\ 30'$, $\theta = 87^{\circ}\ 20'$, and $\theta = 86^{\circ}\ 10'$ take place because these locations are close to a region* where compressive strains of more than 14% are present, and hence these locations are also affected appreciably.

Finally, note that in both cases the vector (unconventional) form of the equations of motion was used and solved with the timewise central-difference operator.

*At $\theta \approx 60°$.

7.4 Impulsively-Loaded Square Thin Flat Plate

7.4.1 Problem Definition

As reported in Ref. 2, square thin 6061-T651 aluminum flat panels (nominally 0.060 by 8.00 by 8.00 in -- see Fig. 26) with all four sides ideally clamped were subjected to impulsive loading on the lower surface over a 2-in by 2-in region centered at the panel-center location (x,y) = (0,0). A schematic of this experiment is given in Fig. 27.

Selected for examination here is clamped panel specimen CP-2; its dimensions are 0.0623 in by 8.00 in by 8.00 in. The explosively-imparted impulse resulted in an "initial velocity" of 16,325 in/sec for the 2-in by 2-in HE-loaded region [2]. This condition produced a very large permanent deflection of the panel, measurements for which are reported in Ref. 2. In addition, a portion of the upper surface of specimen CP-2 had on it a mechanically lightly-scribed closely-spaced grid whose pre-test and post-test spacings were measured, thereby providing permanent relative elongation data. Also, at various (x,y) locations on the upper surface at indicated orientations θ (see Fig. 26), high-elongation strain gages were attached and used to measure transient relative elongations; these transient strains were displayed and recorded photographically from oscilloscopes. Finally, permanent relative elongations were measured from all surviving strain gages.

This problem provides a well-defined initial-value problem for a 3-D structural response situation wherein measurements have been made successfully of transient strains as well as large permanent deflections and strains. Moreover, the maximum permanent strains produced are very close to the rupture threshold; in fact near (x,y) = (-0.65 in, -0.7 to +0.7 in) incipient cracking occurred. At a corresponding location (i.e. x = +0.65 in and $-0.7 \lesssim y \lesssim +0.7$ in) very severe straining but no evidence of cracking was observed. Accordingly, specimen CP-2 serves as a stringent test of the accuracy and reliability of the present finite-strain formulation and calculation procedure.

7.4.2 Comparison of Finite-Strain Predictions vs. Experiment

7.4.2.1 Finite-Strain and Finite-Element Analysis Model

For computational economy and efficiency, advantage was taken of double symmetry for this CP-2 plate problem; hence, only one quarter of the plate was modeled by finite elements. The resulting 11 by 11 mesh of 121 quadrilateral flat-plate LLC elements is shown in Fig. 28, including element dimensions, node numbering, and element numbering. Note that the impulsively-loaded 1-in by 1-in quarter-plate region centered at $(x,y) = (0,0)$ has been modeled by 4.5 elements in each direction. Thus, the assembled-structure nodes lying inside this dotted region account for the plate mass to which was imparted a uniform w-direction velocity $\dot{w}_o = 16{,}325$ in/sec; accordingly, each of the cited nodes was given this $\dot{w}_o$, thereby defining an initial kinetic energy $(KE)_o$ for both the actual plate and the finite-element model of the plate to be 8,402 in-lb, where the 6061-T651 aluminum material is assumed to have a mass per unit initial volume ρ_o of 0.000253828 $(\text{lb-sec}^2)/\text{in}^4$.

With the available funds and computing system, this 11 by 11 mesh of finite elements is about the largest feasible size. The .222-in by .222-in element size selected for the impulsively-loaded region where severe straining occurs was expected to be nearly adequate, although CCC elements rather than the present LLC elements would provide a much better representation of the behavior. Also, a continuation of this element size to $(x,y) = (2,2)$ would have permitted a better modeling of the expected strain behavior in this region; however, the resulting total number of degrees of freedom and computer storage would have exceeded that currently "allowable" at the computer facility used. Thus, a coarser mesh was used beyond $(x,y) = (1.111, 1.111)$, as indicated in Fig. 28. Hence, the selected finite-element mesh resulted in a total of 144 nodes at 6 DOF/Node or 864 DOF. Since 23 nodes at 6 DOF/Node are ideally-clamped (along $x = 4$, $y = 4$), a total of 20 nodes involve symmetry at 3 DOF/Node, and the center node at $(x,y) = (0,0)$ has double symmetry imposed at 5 DOF/Node, a total of 203 restrained DOF are involved. Hence, the total number of unknown DOF = 864-203 = 661 DOF.

As reported in Ref. 2, static uniaxial stress-strain measurements were conducted on coupons of material whose axes were (1) parallel (longitudinal, L) with or (2) perpendicular (transverse, T) to the plate-roll direction of the thick-plate stock of 6061-T651 aluminum material from which specimen CP-2 was prepared; the x and the y direction of specimen CP-2 corresponds, respectively, to the T and the L direction. These static stress-strain tests revealed that this 6061-T651 plate-stock material is not exactly isotropic, as Figs. 29a and 29b of Ref.2 show for the L- and the T-direction, respectively. However, since the analysis and the computer program employed assume that <u>initially</u> the material is isotropic, the cited Ref. 2 data were recast into $\tau_{u_o} = \frac{P}{A_o}(1 + E_u)$ vs. $\varepsilon_u^* = \ell n\,(1 + E_u)$ and the average data were fitted in a piecewise-linear fashion by the following $(\tau_{u_o}, \varepsilon_u^*)$ pairs for use in the mechanical-sublayer model: $(\tau_{u_o}, \varepsilon_u^*)$ = (0,0), (45,000 psi, .0045), (52,400 psi, .0960), and (72,000 psi, .585).

Note should be taken of additional information pertaining to the "non-isotropic" character of this 6061-T651 aluminum plate material. First, static tensile tests of coupons revealed that the static relative elongations at fracture were about .75 and .40 for the L and T specimens, respectively; hence, the T-direction exhibits rupture at a substantially smaller level of strain than does the L-direction. Accordingly, incipient rupturing of "T-direction fibers" in a plate specimen such as CP-2 would be expected first before rupturing of "L-direction" fibers; this indeed was the case for specimen CP-2 which exhibited threshold rupturing of T-direction material at x = −0.65 in along y = −.70 to ≈ y = +.70 in.

Because of the very severe impulsive loading to which specimen CP-2 was subjected, certain regions of this specimen will experience very high strain rates at least at early times. Thus, even though the 6061-T651 aluminum might not be particularly strain-rate sensitive, one expects nevertheless a significant effect of the strain rate on the transient structural response. Accordingly, two calculations were carried out (a) one for zero strain-rate sensitivity: [illegible] = p = 0 or EL-SH and (b) EL-SH-SR where the strain rate parameter values assumed were d = 6500 sec^{-1}

and p = 4. For case (a) calculations for 600 microseconds of structural response were carried out, but only 300 μsec for case (b) because of the computational expense involved. For this FE model, it was found that $\omega_{max} = .354328 \times 10^7$ rad/sec; hence, $0.8\ (2/\omega_{max}) = 0.452$ μsec.

Finally, it should be noted that the present LLC assumed displacement element is too stiff and displays only a state of constant displacement gradients+; a higher order element such as a CCC would be better from the viewpoint of accuracy as well as reducing roundoff error but time has not permitted including that type of better element in the present study.

7.4.2.2 Transient Strain Comparisons and Transient Displacements

In the following listed figures, measured transient relative elongations at the indicated (x,y) locations and accompanying θ-orientations on the upper (non-loaded) surface of flat-panel specimen CP-2 are compared with finite-strain predictions obtained from a timewise solution of the modified unconventional equations of motion together with linear extrapolation of the pseudo loads (MULE) and the use of the Houbolt operator with $\Delta t = 1.0$ μsec:

Figure	Upper-Surface Location x(in)	Upper-Surface Location y(in)	Upper-Surface Location θ(deg)	Distance from Plate Center (in)	Strain Gage Data [2] Gage No.	Strain Gage Data [2] Peak Transient Rel. Elong. (per cent)
29a	0	1.50	90	1.50	3, 18*	5.3, 6.7
29b	0	2.00	90	2.00	4	2.7
29c	1.061	1.061	45	1.50	6	6.1
29d	1.414	1.414	45	2.00	-	-
29e	1.50	1.50	45	2.121	7	2.2
29f	2.00	2.00	45	2.828	8	1.03

*Gage 18 was located at (x,y,θ) = (0, -1.50 in, 270 deg.)

Figures 29a and 29b show predicted (EL-SH and EL-SH-SR) and measured transient relative elongations on the upper surface of specimen CP-2 along the θ = 90-deg. direction at (x,y) = (0, 1.50) and (0, 2.00 in), respectively. Since the Fig. 29b location is at a greater distance from the

+The LLC assumed-displacement element used provides displacement gradients $u_{,x}$ and $v_{,x}$ which are constant in the x direction, and displacement gradients $u_{,y}$ and $v_{,y}$ which are constant in the y direction.

plate center than the Fig. 29a location, one expects for this problem that the peak transient strain at the Fig. 29b location will be significantly smaller than that for the Fig. 29a location. Both measurements and predictions confirm this expectation. For the $(x,y) = (0, 1.50)$ location for the Fig. 29a display, one sees that the peak predicted relative elongation for the EL-SH calculation is about 15 per cent and occurs at about 100 μsec, whereas the peak measured values are about 5.2 and 6.2 for gages 3 and 18, respectively, and occurred at about 85 μsec. However, the EL-SH-SR early peak predicted is about 6.9 per cent and occurs at about 60 μsec. Hence, the EL-SH prediction appears to overestimate the magnitude of this early peak very substantially, whereas the EL-SH-SR prediction is in reasonably good agreement with the measured early peak. Note that although the measured relative elongation traces were obtained successfully only to about 150 μsec, the EL-SH-SR predicted transient response appears to be in good agreement both qualitatively and quantitatively with the measured responses.

At the more distant location $(x,y,\theta) = (0, 2.00 \text{ in}, 90 \text{ deg.})$, the EL-SH and the EL-SH-SR prediction give time histories in good qualitative and quantitative agreement with each other. Further, these two finite-strain predictions are in fairly good agrement with the measured transient response data (see Fig. 29b). Also, the longer duration EL-SH prediction indicates that a predicted permanent relative elongation here would be about 2.5 per cent; the measured [2] permanent relative elongation at that location was 1.8 per cent.

Figures 29c, 29d, 29e, and 29f pertain to measured and predicted upper-surface transient relative elongations along a ray at $\theta = 45$ deg from the plate center at distances, respectively, of 1.50, 2.00, 2.121, and 2.828 inches. At these locations the peak and permanent relative elongations are expected to decrease at these 4 "successively more distant locations"; the measured data show this to be the case, as the above-tabulated measured peaks show.

Note that the measured peak relative elongation at 1.50 in from the plate center along $\theta = 90$ deg and $\theta = 45$ deg (see Fig. 29c) are in close agreement; gages 3 and 18 at θ = 90 deg indicate, respectively, 5.3 and 6.7 per cent while gage 6 at θ = 45 deg indicates a peak of about 6.1 per cent. Figure 29c also shows that the EL-SH-SR transient response prediction is in much better agreement with the measured response than is the EL-SH prediction.

Observe from Figs. 29a and 29c, where both locations are 1.50 in from the plate center but the former is oriented at θ = 90 deg while the latter is oriented at θ = 45 deg, that the general magnitude of the measured relative elongation time histories is "the same" but the early portion of the time history at these two "equivalent locations" is distinctly different. Note that the EL-SH-SR prediction also exhibits this qualitatively different early-time response -- in agreement with measurements. From Fig. 29c where a "measured strain trace" was obtained from 0 to about 340 μsec, one sees that the peak (6.1 per cent) was reached before 150 μsec and the strain level changed very little thereafter. It is expected that had this trace been obtained for a much longer duration, very little change in this "subsequent" strain level would have been seen; this is consistent with the fact that this strain gage showed a permanent relative elongation of 5.4 per cent at this location.

At a 2-in distance from the plate center, Fig 29b shows measured and predicted transient relative elongations at (x,y,θ) = (0, 2.00 in, 90 deg) while Fig. 29d shows only predictions at (x,y,θ) = (1.414, 1.414 in, 45 deg). For the former, generally good theoretical-experimental agreement is observed; note also that the measured peak (2.7 per cent) is reached before 170 μsec and the subsequent strain level does not change very much, but the predictions would indicate a somewhat larger value. At the Fig. 29d 2-in location (along θ = 45 deg) no transient response measurement was obtained (only a permanent relative elongation of 2.5 per cent was measured), but the EL-SH and EL-SH-SR predictions appear to be plausible qualitatively compared with the Fig. 29c predictions at the 1.50 in distance along θ = 45 deg. However, the "predicted permanent strain levels" are much higher than one expects (and measures) at this 2.00-in location.

Figure 29e shows measurements and predictions at a somewhat greater distance (2.12 in) from the plate center along $\theta \approx 45$ deg. Here the measured strain trace reaches a peak ($\approx$ 2.2 per cent) before about 170 μsec and changes its level very little thereafter; this gage gave a permanent relative elongation of 1.7 per cent. The EL-SH-SR prediction appears to be plausible for perhaps the first 200 of the 300 μsec duration shown; but the "steady level" achieved before 200 μsec is at about 4 per cent strain level (vs. about 2 per cent experimentally). On the other hand, the EL-SH prediction shows a peak strain level (at about 300 μsec) which is significantly larger than that of this same EL-SH prediction at the closer-in 2.00-in location shown in Fig. 29d. Hence, it is apparent that at these "more distant locations", the EL-SH calculation is exhibiting a numerical deterioration.

Pronounced evidence of this "late time" numerical deterioration is exhibited in Fig. 29f where the measured transient relative elongation at the 2.828-in distance: $(x,y,\theta) = (2.00,\ 2.00\ \text{in},\ 45\ \text{deg})$ is shown and compared with EL-SH and EL-SH-SR predictions at this location. Experimentally, a peak strain of about 1.03 per cent was reached at about 220 μsec, and the strain level changed very little thereafter. On the other hand, at this location the relative elongation predicted by the EL-SH calculations behaves plausibly and exhibits a reasonable level of strain for about the first 200 μsec, but then exhibits an almost-exponential growth with time -- reaching 20 per cent at about 500 μsec. The EL-SH-SR calculation, on the other hand, does not exhibit this type of <u>clear</u> deterioration during its 300 μsec duration, but it indicates a "permanent strain level" of about 3 per cent which is much larger than measured at this location. Based upon the Fig. 29e results (and those of Fig. 29f), the EL-SH and the EL-SH-SR predictions must be regarded with suspicion in the "outer zone" spanned by the finite element region "enclosed" by elements 8 through 10 and 78 through 111 at times beyond about 200 μsec.

Information supplementing these indications of numerical deterioration (despite the use of double precision on the IBM 370/168) is given in Tables 3 and 4 for the EL-SH and the EL-SH-SR calculation, respectively. Shown in these tables are the time histories of the upper-surface γ_1^1 Green strain at each nodal station along y = 0. Also shown are the upper-surface principal Green strains at the centers of element 1 through 6. These tabulations show that plausible time histories of strain are predicted <u>at all times</u> for (a) the "close-in nodal stations" (that is, $x \lesssim 1.00$ in) and (b) the centers of elements 1 through 6 for both the EL-SH and the EL-SH-SR calculation, although the values predicted by the latter are much more reasonable. At nodal locations beyond about x = 1.00 in (except at node 12 (x = 4.00 in)), one observes a progressive deterioration in that the predicted strains continue to grow implausibly to unrealistically large levels.

Shown in Figs. 30a, 30b, and 30c are the EL-SH and EL-SH-SR predicted time histories of the <u>principal strain</u> at the center, respectively, of elements 1, 3, and 6; these elements (see Fig. 28b) lie adjacent to the y = 0 symmetry line and their centers are located at the following respective locations (x,y) = (.111, .111 in), (.333, .111), and (1.298, .111). At the first two locations, these principal strains increase quickly and reach a "plateau" by about 80 μsec, and change very little thereafter; further, in both cases, the "plateau principal strain" levels are substantially smaller for the EL-SH-SR than for the EL-SH calculation, as expected. At the center of element 6, the principal strain time history for the EL-SH calculation is similar to those for elements 1 and 3; however, the EL-SH-SR predicted principal strain first rises rapidly and then increases slowly for the remainder of the 300 μsec time history rather than reaching a plateau. To supplement this information, the principal strain at the center of elements 1 through 6 is given at various time instants in Tables 3 and 4 for, respectively, the EL-SH and the EL-SH-SR calculation.

It is instructive also to examine the spatial distribution of the predicted strain in the panel at various fixed instants in time. Accordingly, shown in Figs. 30d and 30e, respectively, are EL-SH and EL-SH-SR predictions of the x-direction upper-surface Green strain γ_1^1 at nodes 1 through 12 (see Fig. 28a) along the y = 0 symmetry line from the panel center (x,y) = (0,0) to the clamped edge (x,y) = (4.00, 0); this information is also given in Tables 3 and 4, respectively.

For the EL-SH calculation, Fig. 30d shows that γ_1^1 vs. x at 60 μsec is of the expected form for this physical situation -- displaying smoothly varying large values within and just beyond the 1.00-in edge of the impulsive-loading zone, and then decreasing rapidly to small values for $x \gtrsim 1.50$ in. At 100 μsec, the strain has increased significantly at station x = 1.111 and 1.486 in but remains close to the 60 μsec values at the other locations. At 200 μsec, the γ_1^1 strain distribution remains similar to that at 100 μsec except that a substantial increase in the γ_1^1 strain occurs at stations x = 1.861 and 2.486 in where the values are, respectively, 13.21 and 5.17 per cent. At location x = 1.861 in (which is remote from the impulsive-loading zone), this strain value should be very similar to (or perhaps between) those exhibited in Figs. 29a (at x,y = 0, 1.50 in) and 29b (at x,y = 0, 2.00 in) since these locations "span" the station in question, where the respective EL-SH predicted values are 5.7 and 3.7 per cent and the measured values are ≃ 4.0 and 2.0 per cent, whereas a value of 13.2 per cent is EL-SH predicted at station x = 1.861 in. For this x = 1.861-in station, an examination of Table 3 indicates that a numerical deterioration of the calculation is occurring here beyond about 120 μsec since as time progresses the EL-SH predicted strain continues to grow "unrealistically" and reaches a value of 31.2 per cent at 600 μsec, whereas the measured peak [2] at the "spanning stations" did not exceed about 6 and 2.5 per cent, respectively. Further evidence of this calculation deterioration in the mesh region spanned by nodes 8 through 11 and 85 through 121 can be seen by examining (a) the plotted predicted strain profiles at t = 300 μsec and 600 μsec in Fig. 30d and (b) the time histories of the predicted strains at these nodal stations as given in Table 3. Further, the measured permanent strains at $x \gtrsim 1.4$ in were smaller by at least a factor of 4 than the predicted values listed in Table 3 at t = 600 μsec. Also, observe that the predicted strains in the region $0 \leq x \lesssim 1.11$ in quickly reached fairly large values and essentially "retained" these values throughout the 600 μsec time period; strains in this region, therefore, are believed to be valid and not affected by the cited timewise progressive numerical deterioration of the calculation in the indicated mesh portion of this large-DOF problem.

Figure 30e shows a similar sequence of predicted strain profiles for the EL-SH-SR calculation. Although the magnitudes of the predicted strains are considerably smaller than for the corresponding locations and times in the EL-SH calculation, the timewise trends are similar to those of Fig. 30d. For the EL-SH-SR calculation also, there is evidence from Fig. 30e and Table 4 of a progressive deterioration of the numerical predictions in the region spanned by nodes 8 through 11 and 85 through 121.

Given in Tables 3 and 4 for the EL-SH and the EL-SH-SR calculation, respectively, are the values of Green strain γ_1^1 at the nodal stations along y = 0 (nodes 1 through 12) at about 20-μsec intervals. Note that the peak and the permanent strains from nodes 1 through 7 are reached within about 140 μsec. For stations 8, 9, 10, and 11 one observes a "deterioration" in the strain behavior beyond about 120, 240, 350, and 450 μsec for the EL-SH calculation, and beyond about 100 and 260 μsec for stations 8 and 9 for the EL-SH-SR calculation which was carried out for only 300 μsec. Thus, in the region beyond x = 1.86 in (or in the mesh zone bounded by nodes 8 through 11 and 85 through 121) the strains become unrealistically huge. As a result, the gross w displacement time history at "all nodal stations" also degenerates in the sense that these displacements continue to grow in the region $0 \lesssim x \lesssim 2.5$ in in a vigorous manner even though nearly all of the initial kinetic energy has been absorbed already by plastic work; the time history of the quarter-plate kinetic energy is shown in Fig. 31. This "degenerate" w-displacement time history is shown in Fig. 31 at (x,y) = (0,0) for the EL-SH and the EL-SH-SR calculations; both calculations indicate w displacement values which are much larger than observed experimentally. The excessively large strains predicted in the mesh region spanned by nodes 8 through 11 and 85 through 121 because of "numerical deterioration" cause the w-displacement in the region $0 \leq x \lesssim 3.0$ in to become unrealistically large also. Clearly this is a numerical-degeneration problem incurred despite the use of double-precision arithmetic on the IBM 370/168 at MIT. Further study is needed to resolve this difficulty.

7.4.2.3 Permanent Deflections and Strains

Because of the already-cited progressive timewise numerical deterioration of the calculation, the present calculations do not provide valid estimates of the permanent deflection of the CP-2 impulsively-loaded thin aluminum panel. However, it may be of interest to compare EL-SH vs. EL-SH-SR predicted w-displacement profiles vs. x along the fixed-y locations y = 0, 1.111, and 2.486 in at a fixed instant in time. Such comparisons are shown for illustration in Fig. 32a at t = 300 μsec. Because of "strain-rate stiffening", one observes that the EL-SH deflections tend to be much larger than those for the EL-SH-SR calculation along y = 0 and y = 1.111 in. However, along y = 2.486 in, the reverse is true because the "stiffer EL-SH-SR structure" has responded more rapidly (peaks sooner) than has the "EL-SH structure" at this y = 2.486 in station.

That these predicted w-displacement profiles at various fixed-y locations are of generally plausible character (although of invalid too-large magnitude) can be seen by examining the experimentally-measured permanent w-deflection profiles plotted vs. x in Fig. 32b for various fixed-y stations. Note that a permanent plate-center deflection of about 1.1 in occurred on this 0.0623 by 4 by 4-in square clamped-sided panel. It is evident from these permanent-deflection profiles that very large strains must be present over about a central 1.5 by 1.5-in region.

Shown in Fig. 32c are the measured permanent relative elongations on the upper surface of panel specimen CP-2 as a function of pretest distance x from the plate center along y = 0 from mechanically-scribed upper-surface grid measurements. Also included are permanent-elongation data from strain gage measurements [2]. Permanent relative elongation estimates from each of the two present calculations are shown also on Fig. 32c.

A study of the transient strain predictions for the EL-SH case indicated that the strain at the center of the small elements in the row adjacent to $y = 0$ had essentially reached the final state by about 300 μsec; in fact as Table 3 shows, the strains at nodal stations for $0 \leq x \leq 1.00$ in remain almost unchanged to the 600 μsec end of the EL-SH calculation. Thus, the relative elongations at nodes 1 through 5 at 600 μsec were chosen for the permanent strain estimate. For stations with $x \gtrsim 1.00$ in, it is believed that the associated relatively coarse finite element mesh makes the predicted strains unreliable; accordingly, no permanent strain estimates from nodal strains are made in this region. However, at the location of upper-surface strain gage 3: (x,y,θ) = (0, 1.50 in, 90 deg), the EL-SH predicted transient relative elongation as shown in Fig. 29a was used to estimate a permanent y-direction relative elongation there of 6.5 per cent. Strains in the region of evident numerical deterioration are unreliable and, hence, are not employed in making these permanent-strain estimates. It is seen that these predicted EL-SH permanent relative elongations tend to be larger than the measured values.

For the EL-SH-SR calculation which was carried out to only 300 μsec, the permanent relative elongation at this time was used as the "permanent-strain estimate" for nodal and element center stations at $0 \leq x \leq 1.00$ in. Included also was the permanent relative elongation (at 300 μsec) at the outer-surface center of element 6. It is seen that these predicted EL-SH-SR permanent relative elongations are (1) considerably smaller than from the EL-SH prediction and (2) in reasonably good agreement with measured values with a tendency of being in the mean, perhaps, somewhat smaller.

It should be noted that the LLC assumed-displacement elements used provide displacement gradients $u_{,x}$, $v_{,x}$ which are constant in the x direction, and displacement gradients $u_{,y}$, $v_{,y}$ which are constant in the y direction. This element is much too stiff; however, the use of a much finer mesh of the LLC elements could improve the prediction, but at the cost of greater storage and computing expense.

An evaluation was made of the principal strains and associated directions (θ_p) on the upper surface at the center of the "small" elements (see Fig. 28b) for both the EL-SH and the EL-SH-SR calculation. An illustration of these finite-strain-predicted maximum principal strain results are given in Table 5. An inspection of these values indicates that the most extreme values occur at the center of the following elements in each row:

	EL-SH		EL-SH-SR	
Row	Element	Value (Per Cent)	Element	Value (Per Cent)
1	5	37.2	1	14.3
2	16	40.0	12	13.0
3	27	38.0	23	10.6
4	38	30.4	38	9.5
5	57	12.3	56	8.8

Finally, it is of interest to note that the pre-test and post-test measurements of the spacing of the mechanically lightly-scribed grids on the upper surface of specimen CP-2 permitted determining that the permanent relative elongation close to (but not exactly at) the location of incipient rupture ($x \doteq 0.65$ in and $-0.7 \lesssim y \lesssim 0.7$) was about 26.4 per cent for this bi- or tri-axial strain state whereas in the "uniaxial coupon static tests", the rupture value of the relative elongation in the corresponding direction (the transverse, T, direction) averaged about 40 per cent. It would be useful to assess the experimental CP-2 incipient rupture conditions with respect to an independent strain based incipient rupture criterion for this type of aluminum alloy: 6061-T651 and its attendant mill preparation. This matter is left for future study.

The computing times required to carry out the <u>finite-strain</u> Houbolt-MULE predictions of the transient responses of explosively-impulsed 6061-T651 aluminum thin panel specimen CP-2 are summarized in the following for the EL-SH and the EL-SH-SR calculations. These computations were performed in double precision on the IBM 370/168 at MIT; $\Delta t = 1$ μsec was used for both calculations.

Matl. Behavior	No. of Plate FE	Total Unknown DOF	No. of Cycles	CPU Time (min)	CPU (min) / DOF Cycles
EL-SH	121	661	600	260.49	656.8×10^{-6}
EL-SH-SR	121	661	300	131.88	665.1×10^{-6}

Similar comparisons for other examples in the present study are given in Subsections 7.6.5.1 and 7.6.6.

7.5 Containment-Ring Response of T58 Turbine Rotor Tri-Hub Burst Attack

7.5.1 Problem Definition

At the Naval Air Propulsion Center, various aircraft engine rotors have been employed in spin chamber tests in which the rotor has been caused to fail in various ways while rotating at high rpm [208-210]. The resulting rotor fragments have impacted containment rings of single-layer or multi-layer multi-material construction. High speed photography has been used to observe the ring-fragment impact and interaction from initial impact until quite late in the response history. Transient strain and permanent strain measurements at various locations have been made on some of the rings. Also, the permanently deformed ring configurations have been measured.

Selected for analysis here is NAPTC Test 201 in which a 4130 spin-cast steel containment ring* of 0.625-in thickness, 1.50-in axial length, and 15.00-in inside diameter and weighing 12.83 pounds rested horizontally on smooth support wires and encircled a T58 turbine rotor which was caused to fail in three equal 120-degree segments at about 19,859 rpm and to impact against this containment ring. Given in Table 2 are the weight and geometric data defining the containment ring, the rotor burst fragment properties, and the test conditions for NAPTC Test 201 [208,209].

*From ACIPCO billet No.2.

Each fragment consisted of a 120-degree sector of the rim with seventeen attached blades; the distance from the axis of rotation of the rotor to the CG of the fragment was 2.797 in. At the rotor burst rpm of 19,859, the translational velocity at the CG of each fragment was 14,557.2 in/sec. The resulting total kinetic energy of the three released fragments was 908,820 in-lb, of which 476,766 in-lb was translational and 432,054 in-lb was rotational. Hence, each fragment had nominally 158,922 in-lb of translational and 144,018 in-lb of rotational kinetic energy.

The results of an extensive analysis of this test and of various small-strain predictions for the responses of the containment ring and the attacking fragments are reported in Ref. 30. For present purposes, however, only one of the analysis models considered in Ref. 30 will be used. In particular, each fragment is idealized as consisting of a rigid "cylindrical disk" of 2.555-in radius having a mass and a mass moment of inertia matching the actual fragment at its instant of pre-impact release from the rotor; also, the translation velocity at the CG of the idealized fragment and its rotational velocity match those of the actual fragment. The entire ring was modeled (as depicted in Fig. 33) by 48 equal-length 4DOF/node ring elements. Local ring-fragment impact was treated as being perfectly elastic; hence, a coefficient of restitution e = 1 was used. Further, it is assumed for present purposes that the impact-interaction between each fragment and the ring is frictionless.

7.5.2 Comparison of Small-Strain vs Finite-Strain Predictions

For the small-strain calculations reported in Ref. 30, National Forge billet static tensile stress-strain data supplied by the NAPTC [209] were used to analyze the Test 201 ring since according to Ref. 209 the Test 201 ring material is almost identical to the National Forge billet. Accordingly, those τ_{u_o} vs γ_{u_o} static uniaxial tensile stress-strain data+ were approximated by piecewise-linear segments defined by $(\tau_{u_o}, \gamma_{u_o})$ = (0 psi, 0 in/in); (80,950 psi, 0.00279); (105,300 psi, 0.0225); and (121,000 psi, 0.2000) for use in the mechanical sublayer material model. The material

+Material rupture occurred at γ_u = 52.3 per cent.

is assumed to be strain rate sensitive with $d = 40.4\ sec^{-1}$ and $p = 5$ which is reported to be applicable [201] to mild steel. Also, strain-displacement relation Type B and the CIVM-JET 4B computer program [27] which employs the timewise central-difference operator was used for the small-strain analysis.

For the finite-strain analysis+ the basic finite element method and impact-interaction conditions were the same as before. However, strain-displacement relation Type F was used. Also, the National Forge billet uniaxial static tensile stress-strain data were recast into $\tau_{u_o} = \sigma_E (1 + E_u)$ vs $\varepsilon_u^* \equiv \ln (1 + E_u)$, and fitted by piecewise-linear segments with the following $(\tau_{u_o}, \varepsilon_u^*)$ pairs: $(\tau_{u_o}, \varepsilon_u^*)$ = (0,0), (84 240 psi, 0.002890), (107,500 psi, 0.0225), (118,000 psi, 0.0600), and (172,700 psi, 0.557).

This FE-modeled ring consists of 196 unknown DOF. Taking the mass per unit initial volume ρ_o as 0.000733 $(lb\text{-}sec^2)/in^4$ for the 4130 cast steel ring, it was found that the highest natural frequency of this mathematical ring model for small-displacement linear-elastic behavior was ω_{max} = 0.4121789×10^6 rad/sec. To avoid calculation instability, one must select $\Delta t \lesssim 0.8\ (2/\omega_{max}) = 3.88\ \mu sec$; for convenience a Δt of 2.50 μsec was used. The central-difference operator is used to solve the vector (unconventional) form of the equations of motion. Finite element properties are evaluated numerically with three spanwise and four depthwise Gaussian stations.

It was found that the deformed ring configuration and fragment locations in this two-dimensional impact-response problem are very nearly the same at a given time after initial impact for (a) the small-strain prediction and (b) the finite-strain prediction. Hence, such comparisons are omitted here. However, of much greater interest and importance are the circumferential inner-surface and outer-surface strains γ_2^2. Small-strain [30], vs finite-strain predictions++ of the inner-surface and the outer-surface γ_2^2 strains at the midspan stations of elements 1, 4, 6, 9, 11, and 47 are shown, respectively, in Figs. 34a, 34b, 34c, 34d, 34e, and

---

+A finite-strain-modified version of CIVM-JET 4B was employed; this version is called CIVM-JET 4C [.4].

++For the present finite strain calculation, L_{eff} = 0.497 in was chosen since this value was used for the small strain calculations of Ref. 30. Otherwise, the "more plausible" value $L_{eff} = 2h = 1.25$ in would have been preferred.

34f. Shown in Fig. 35 for a time after initial impact of 1180 μsec+ are the small-strain and the finite-strain predictions of the circumferential distribution of outer-surface strains γ_2^2.

Here it is seen that there are distinct differences between the finite-strain predictions and the small-strain predictions at some locations and very little difference in others. Generally, however, larger strains are predicted by the consistent and valid finite-strain formulation-and-solution procedure compared with the former small-strain procedure, which is consistent with the fact that for tensile strains the finite-strain procedure should predict larger strains than the small-strain procedure if the same stress-strain data is used as input for both procedures.

7.6 Steel-Sphere-Impacted Narrow Plate

7.6.1 Problem Definition

As reported in Ref. 1, initially-flat narrow 6061-T651 aluminum plates with both ends ideally clamped have been subjected each to perpendicular impact at its midwidth-midspan location by a 1-inch diameter steel sphere at various velocities, ranging from 1893 to 3075 in/sec. These narrow plates were of nominal 0.1-in thickness, 1.5-in width, and 8.0-in span. Sphere pre-impact velocities in the range 2485 in/sec to about 2800 in/sec were found to produce moderate to large permanent deformations in the plates; rupture of the plate was observed for steel sphere velocities above about 2870 in/sec.

It was noted that except in the near vicinity of the location of initial impact, the narrow-plate specimens exhibited essentially 2-D deflections; for those regions, the 2-D impact-response codes CIVM-JET 4B [27] and/or CIVM-JET 5B [29] would appear to provide useful approximate predictions. However, significant 3-D deformations are present near the "impact location"; hence, modeling of the behavior of the structure by plate rather than beam finite elements would appear to permit one to make more realistic predictions of the actual structural response both near and far from the initial-impact location. Accordingly, small-strain and finite-strain calculations were carried out for both (1) 2-D beam modeling and (2) 3-D plate modeling of the structure.

+This is essentially the time of occurrence of peak straining.

To illustrate these predictions and their comparison with experiment, narrow-plate specimen CB-18 of Ref. 1 will be analyzed. This plate was of 0.097-in thickness, 1.498-in width, and 8.002-in span. A 1-in diameter steel sphere weighing 66.810 grams with a pre-impact velocity of 2794 in/sec impacted specimen CB-18 approximately 0.06-in from the plate-center location. A schematic of the model showing global coordinate directions is given in Fig. 36. In this test transient relative elongation data were measured successfully with strain gages along the y-axis (midwidth location) at $y = \pm 0.6$-in (upper surface), $y = 1.2$-in (upper surface), $y = -1.5$-in (upper surface), and $y = 1.5$-in (upper and lower surfaces).

For both the small-strain and the finite-strain calculations, the uniaxial static stress-strain data for this material were taken to be the same as described in Ref. 30 and in Subsection 7.2.3.2; namely, $(\tau_{u_o}, \epsilon^*_u)$ = (0,0), (44,200 psi, 0.00442 in/in), (49,200 psi, 0.075 in/in), and (76,400 psi, 0.615 in/in) for use in the mechanical sublayer material model. For this 6061-T651 material, the rupture level of Green strain γ_u for uniaxial static test specimens was found [2] to be about 105 percent.

Finally, since both small-strain and finite-strain predictions were reported in Ref. 30 for the impact-induced transient response of specimen CB-18 -- and those calculations were made for 2-D beam element modeling and for <u>EL-SH behavior only</u> -- the predictions to be presented in this report will include mainly EL-SH behavior for the material of narrow-plate specimen CB-18.

First, in Subsection 7.6.2, 2-D beam-element and idealized 2-D impact-interaction modeling and response will be discussed. Next in Subsection 7.6.3, the narrow-plate specimen (CB-18) will be modeled with plate elements to accommodate 3-D structural response; also, the attacking solid-sphere fragment will be modeled faithfully as a spherical fragment (rather than as an "equivalent cylindrical fragment as in the 2-D modeling case).

7.6.2 Modeling by Beam Finite Elements

In modeling the CB-18 narrow plate by beam elements, the structural response is being approximated as being <u>strictly two-dimensional (2-D)</u>. Hence, consistent with this, the attacking fragment is also idealized as a 2-D fragment; that is, the fragment rather than being a 1-inch diameter sphere is idealized and visualized conceptually as a solid non-deformable cylindrical fragment of 1-inch diameter and extending across the entire width of the narrow-plate specimen. This idealized fragment is defined to have the same total mass as the actual fragment.

The entire span of narrow-plate specimen CB-18 has been modeled by 43 equal-length (0.186-in) cubic-cubic assumed-displacement beam elements with 4DOF/node -- based upon extensive studies reported in Ref. 30. The mass per unit initial volume ρ_o of the CB-18 material is assumed to be 0.25384×10^{-3} $(lb\text{-}sec^2)/in^4$. As a result, the finite-element model consists of 157 unknown DOF and its maximum linear-system frequency is $\omega_{max} = 0.2326 \times 10^7$ rad/sec. Accordingly, since the CIVM-JET 4B computer program (and modified versions thereof) utilize the timewise central-difference operator, one must choose a time increment size Δt of about $0.8\ (2/\omega_{max}) = 0.688$ μsec or less to avoid calculation instability; for convenience a Δt of 0.50 μsec was employed and provided converged results. Finally, at each impact between the fragment and the structure, the structure is assumed to receive an impact-imparted momentum increment (see Ref. 27) on a spanwise length of $\Delta t(E/\rho_o)^{1/2} = 0.0993$-in on either side of the station of impact; since initial perpendicular impact occurred at the midspan station of the center element, this criterion resulted (with the resident computer program logic) in the imparting of velocity increments to the two end nodes of that element. Each of these assembled-structure nodes "account for mass" from half of the center element and half of the next element; hence, the effective region of impact influence is one full element length or 0.186-in on each side of the station of impact. This effective region is consistent with that estimated in Ref. 30 on stress-wave propagation arguments as approximately $2h = 2\ (0.097) = 0.194$ inch.

For the small-strain and the finite-strain calculation, strain-displacement relation Type B (Eq. 4.90) and Type F (Eq. 4.146), respectively, was employed. In both cases, three spanwise and four depthwise Gaussian stations were used for the volume numerical integration for the finite-element property matrices. Also, a diagonalized (lumped) mass matrix for each element was used.

These calculations and modeling apply to both the small-strain and the finite-strain predictions. Accordingly, these 2-D predictions can not match the experimental results near the impact station where distinct 3-D structural response occurred. However, elsewhere (except possibly near the clamped ends), one can expect to find reasonable agreement between these predictions and experiment.

7.6.3 Modeling by Plate Finite Elements

To simulate the actual physical situation of the CB-18 steel-sphere-impacted narrow plate more faithfully -- to accommodate the 3-D type of structural or plate deformations which are dominant -- specimen CB-18 was modeled with plate finite elements of the LLC type with 6DOF/node. For computational thrift and economy, only one quarter of specimen CB-18 was modeled by flat-plate elements; symmetry conditions were imposed along both the midspan and the midwidth station: $(x,y) = (0,0)$, and ideally-clamped conditions were imposed at the clamped end. Initial perpendicular impact of a 1-inch diameter non-deformable spherical fragment was assumed to occur at $(x,y) = (0,0)$ -- rather than about 0.06-in from this point as seen in the CB-18 experiment. The element mesh of flat-plate elements employed was the same as reported earlier [210] for the small-strain calculation; namely, the quarter plate was represented by two rows of 11 spanwise flat plate elements each of 0.375-in width and each with spanwise lengths as depicted in Fig. 37a; later calculations used the "refined" finite element mesh shown in Fig. 37b. The flat plate elements used were the same LLC elements as described in Subsection 7.2.3.1.

For the FE plate modeling of specimen CB-18, the small-strain calculations employed the von Karman strain-displacement relations (Eqs. 5.118 - 5.123 and the attendant following paragraph) while the finite-strain calculation utilized the more comprehensive strain-displacement relations given in Eqs. 5.118 - 5.123 (without the terms involving the second order derivatives of the in-plane displacements u and v, since the assumed displacement field for the LLC finite-element is bilinear in u and v). In both cases, three Gaussian stations in each spanwise direction and four depthwise Gaussian stations were used in each flat-plate element to evaluate, by volume numerical integration, the proportion of each element. Also, a diagonalized (lumped) mass matrix was used for each element.

The maximum linear-system frequency ω_{max} of the Fig. 37a finite-element model was found to be 0.2372×10^7 rad/sec. Thus, if one were to compute the impact-induced transient response by using the timewise central-difference operator, a Δt of about $0.8\ (2/\omega_{max}) = 0.67\ \mu sec$ would be required to avoid calculation instability. However, these predictions were carried out by using the CIVM-PLATE program in which the Houbolt operator is employed. Accordingly, a convenient Δt of <u>1.0 μsec</u> was employed which earlier experience and discussion indicated would provide "reliable converged predictions".

At each impact between the fragment and the plate, it is assumed that momentum is transferred by a perfectly-elastic collision to a plate region (from the fragment) defined by a circle of radius $L_{eff} = \Delta t [\frac{E}{\rho_o}]^{1/2} =$ 0.1985-in centered at the impact location; other more rational selections for L_{eff} could be employed, but this one is used for present illustrative purposes.

<u>7.6.4 Comparison of Beam-Model vs. Plate-Model Predictions</u>

First, it is useful to compare small-strain vs. finite-strain predictions for the 2-D idealization (with beam finite elements) of the CB-18 impacted narrow plate. Next, similar comparisons will be made for the case in which the proper 3-D structural response is accommodated by plate-type finite elements and a spherical impacting fragment of the proper size and shape. Finally, it is illuminating to compare 2-D vs. 3-D predictions only for the consistently formulated and implemented finite-strain analysis.

7.6.4.1 Strain Comparisons

Since primary interest centers on the predicted and measured strains, comparisons of longitudinal Green strain γ_2^2 are made in the following indicated figures at the specimen midwidth location at various spanwise locations on the upper (non-impacted) or lower (impacted) surface:

Figure	FE Model		Analysis Strain Type		Location of γ_2^2 Strain Data				
	Beam	Plate	Small	Finite	Station (in)	Prediction		Experiment	
	Δt 0.5 μsec	Δt 1.0 μsec				Upper	Lower	Upper	Lower
38a	X	-	X	X	0	X	-	-	-
38b	X	-	X	X	0	-	X	-	-
38c	X	-	X	X	0.3	X	-	-	-
38d	X	-	X	X	0.3	-	X	-	-
38e	X	-	X	X	0.6	X	-	X	-
38f	X	-	X	X	1.20	X	-	X	-
38g	X	-	X	X	1.50	X	-	X	-
38h	X	-	X	X	1.50	-	X	-	X
38i	X	-	X	X	3.00	X	-	P	-
38j	X	-	X	X	3.00	-	X	-	P
38k	X	-	X	X	3.70	X	-	P	-
38ℓ	X	-	X	X	3.70	-	X	-	P
38m	X	-	X	X	4.00	X	-	-	-
38n	X	-	X	X	4.00	-	X	-	-

P denotes that only permanent strain information was obtained.

Location y = 0 in (at the midspan of the beam) coincides with the midspan Gaussian integration station of a finite element. Location y = $\pm$ 4.0 in is at the clamped end of the beam and coincides with a finite element node at which clamped-end conditions have been imposed (namely that the displacements v and w and the lateral-displacement gradient ψ are zero). All other stations occur at locations intermediate between the end and the midspan of a finite element, and do not coincide with spanwise Gaussian integration points. Also, measured permanent strains are indicated on those figures where available.

These figures show that the strains γ_2^2 predicted (a) by the current "finite-strain procedure" and (b) by the former "small-strain procedure" agree reasonably well with each other and/or with experiment at all of these stations except y = 0, 3.7, and 4.0 in. Large strains do occur at both y = 0 and y = 4.0 in; also, the occurrence of large strains at y = 4.0-in exerts a distinct and pronounced effect at "nearby station" y = 3.7 in (located in the element adjacent to the finite element at which the clamped end condition has been imposed). Although the calculations have been carried out for only 900 microseconds, it appears that the current "finite strain procedure" would provide better permanent strain comparisons with measurements at all spanwise stations (if carried out long enough in time) than by the former "small-strain procedure".

Figure 39 shows that the time histories of the midspan lateral deflection w from these two predictions for beam CB-18 are very close to each other. Finally, the time histories of the support reactions M_x, S_z, and F_y at station x = 4.0 in are shown in Figs. 40a, 40b, and 40c, respectively, for these two predictions. The agreement between these two predictions is very good for the longitudinal support reaction force F_y (associated with the membrane strains), but one observes some differences in the transverse support reaction (shear) force S_z and large differences for the support reaction bending moment M_x. These differences are caused by the fact that the expressions of CIVM-JET 4B for the bending part of the strain are valid only for small rotations and small strains, while the finite strain version of the program does not have this restriction. Of course, the support reaction bending moment M_x is most influenced by the bending part of the strain-displacement relations.

The computing time required to analyze steel-sphere-impacted beam CB-18 by the two procedures, under otherwise-identical conditions, is conveniently displayed in the following tabulation (for a time step of 0.50 microsecond; all runs were conducted on an IBM 370/168 computer):

Formulation	No. of Beam FE	No. of Gaussian Sta. per Elem. Spanwise	Depth	Total No. of Unknown DOF
Small Strain	43	3	4	170
Finite Strain	43	3	4	170

Formulation	Strain-Displ. Relation Type	Mass Matrix	No. of Cycles	CPU Time (min)	$\frac{\text{CPU(min)}}{\text{(DOF)(Cycles)}}$
Small Strain	B	DM	2250	5.11	13.4×10^{-6}
Finite Strain	F	DM	1850	6.81	21.7×10^{-6}

Here again, the finite-strain-formulation calculations require more CPU time per (DOF)(cycle) than the small-strain formulation. The smaller CPU time per (DOF)(cycle) noted here for steel-sphere-impacted narrow plate specimen CB-18 compared with explosively-impulsed narrow plate specimen CB-4 arises from the use in the latter of the more-heavily populated consistent mass matrices vs. diagonalized mass matrices for the CB-18 calculations, and the use of 3 rather than 4 spanwise Gaussian stations for the CB-18 calculations.

It appears that (a) the use of the proper (second Piola-Kirchhoff) stress tensor in the constitutive equations by making proper transformations of certain stress and strain measures, (b) the use of τ_u vs. ε_u^* for representing the monotonic strain-hardening antisymmetric (in tension and compression) mechanical behavior of the material by the mechanical sublayer model, and (c) the use of a finite-strain strain-displacement equation, and (d) the inclusion of thickness changes provide significantly improved predictions of transient strains (the most important and sensitive quantities).

Next, consider the plate-model predictions; see Fig. 41:

Figure	FE Model		Analysis Strain Type		Location of γ_2^2 Strain Data Along the Plate Midwidth Station				
	Beam	Plate	Small	Finite	Station	Prediction		Experiment	
	0.25 μsec	1.0 μsec			y (in)	Upper	Lower	Upper	Lower
41a	-	X	X	X	0	X	-	-	-
41b	-	X	X	X	0	-	X	-	-
41c	-	X	X	X	3.40	X	-	-	-
41d	-	X	X	X	3.70	X	-	P*	-
41e	-	X	X	X	3.70	-	X	-	P*
41f	-	X	X	X	4.00	X	-	-	-
41g	-	X	X	X	4.00	-	X	-	-

At the plate-center location (x,y) = (0,0) where initial impact occurs, it is seen that the transient strain provided by the consistent finite-strain prediction is substantially larger than that given by the (now unreliable) small-strain calculation+. A similar result is observed at station (x,y) = (0, 3.70 in) and (0, 4.00 in) which are, respectively, near and at the clamped end. However, at station (x,y) = (0,3.40 in) which is more "remote" from the clamped end, one observes a much smaller level of impact-induced structural-response strain; a lesser but still significant difference exists between the strains predicted by these two schemes.

7.6.4.2 Deflection Comparisons

Since only permanent deflection data (no transient deflections) were measured in the CB-18 experiment, only permanent deflections can be used

*Only permanent strain was recorded at this location.

+Note that the static-test uniaxial rupture level for γ_u for this material [2] is about 1.05 or 105 per cent.

to compare predictions with experiment. However, it is instructive also to compare various transient displacement predictions with each other. Accordingly, such deflection comparisons are shown on figures indicated in the following tabulation:

Figure	FE Model		Analysis Strain Type		Stress Strain Approx.	Predicted w-Displ. Location (x,y)	Expt. Perm. Displ. Location (x,y), in
	Beam	Plate	Small	Finite			
42a	X	-	X	-	EL-SH and EL-SH-SR	y = 1.00	Avg. at y = 1.00
42b	X	-	X	X	EL-SH	x = 0	-
42c	-	X	X	X	EL-SH	(0,0)	(0,0)
42d	-	X	X	-	EL-SH	At 840 μsec vs. y Along x=0, x=0.375, x=0.75 (Estimated Permanent)	Along x = 0
42e	-	X	-	X	EL-SH	At 840 μsec vs. y Along x=0, x=0.375, x=0.75 (Estimated Permanent)	Along x = 0
42f	-	X	X	X	EL-SH	Along x = 0 at t = 840 μsec	Along x = 0

In Fig. 42a it is seen that the FE beam model small-strain prediction for the transient w-displacement at "2-D location y = 1.00 in" exhibits a larger peak for the EL-SH than for the EL-SH-SR representation of the material behavior; it is seen also that the EL-SH-SR prediction for the permanent displacement at this station is in the better agreement with the experimentally-observed result.

Finite-strain predictions versus small-strain predictions for the transient 2-D w-displacement for the beam-element modeled structure are compared at the midspan "impact station" in Fig. 42b. These two midspan predictions compare well with each other in overall transient response, in peak response, and in the permanent-deformation estimate. However, as noted earlier, the predicted transient strains are significantly different for the small-strain vs. the finite-strain calculation at the important regions which are near midspan and near the clamped end.

For the more-realistic flat plate finite-element modeling of the CB-18 structure, the transient 3-D Houbolt-MULE w-displacement predictions at the plate-center location (x,y) = (0,0) for the small-strain vs. the finite strain calculation are shown in Fig. 42c for EL-SH material behavior. Again these predictions compare well with each other but a larger peak and permanent deflection is predicted by the finite-strain calculation.

The 3-D character of the predicted w-displacement for the small-strain plate-element model calculation is shown in Fig. 42d. Here at t = 840 μsec, the w-displacement is shown as a function of spanwise distance from midspan to the clamped end along the node lines at the plate midwidth (centerline) station, half-way to the free edge, and along the free edge. Beyond about station y = 1.50 in, the w-displacement is seen to be nearly identical along these three widthwise stations, and thus indicates essentially 2-D displacement behavior in this region of the structure. Closer to the plate-center impact location, however, the 3-D character of the w-displacement is clearly evident.

A similar "displacement profile" plot is shown in Fig. 42e for the finite-strain plate-element-model calculation at t = 840 μsec. Both qualitatively and quantitatively these profiles are similar to those shown in Fig. 42d. Finally, the FE plate model small-strain vs. the finite-strain prediction for w is compared only along the midwidth location in Fig. 42f. The more realistic finite strain prediction is seen to exhibit a slightly more "bulgy" profile than the small-strain prediction. As noted earlier, however, the strain predictions are significantly different between the finite-strain and the small-strain calculation, with the former being in much better agreement with experimental measurements.

7.6.5 Finite-Strain Predictions for a Refined Element-Mesh Model

Since the finite element modeling shown in Figs. 37a and 37b for one quarter of narrow-plate specimen CB-18 was rather coarse and thereby limited the response detail which could be accommodated, it was decided to employ a "refined FE mesh" of LLC plate elements to represent the quarter plate as depicted in Figs. 37c and 37d. In this refined-mesh model, elements of 0.1-in by 0.1-in are used near the "initial impact station" $(x,y) = (0,0)$; also near the clamped end ($y = 4.00$ in), two rows of 0.1-in spanwise length LLC elements are employed. These two regions are those in which pronounced 3-D response effects and pronounced strain gradients are to be expected.

The refined-mesh model shown in Fig. 37c consists of 75 LLC quadrilateral plate elements. The assembled structure has 96 nodes with 6 DOF/Node, giving a total of 576 DOF. Symmetry conditions are invoked along the two sides at $x = 0$ and $y = 0$, while clamping is imposed along $y = 4.00$ in; accordingly, the restrained DOF are: 5 from double symmetry at node 1, 3 each at 19 single-symmetry nodes, and 6 at 6 clamped-end nodes. Hence, the unknown DOF = 576-5-(3)(19)-6(6) = 478. For these calculations a diagonalized (lumped) mass model was used. Thus, the maximum linear-system frequency of the Fig. 37c finite-element model was found to be 13.19775×10^6 rad/sec. If one were to compute the impact-induced transient response by using the timewise central-difference operator, a Δt of about $0.8\ (2/\omega_{max}) \doteq 0.12$ μsec would be required to avoid calculation instability. However, the present predictions were carried out by using the CIVM-PLATE program in which the Houbolt operator is employed. Accordingly, a convenient Δt of <u>1.0 μsec</u> was employed, which earlier computational experience with Houbolt-MULE had indicated would provide "converged predictions".

At each impact between the fragment and the plate, it is assumed that momentum is transferred by a perfectly-elastic collision to a plate region (from the fragment) defined by a circle of radius L_{eff} centered at the impact location. From stress-wave propagation arguments given in Subsection 2.2 of Ref. 30, L_{eff} has been chosen to be twice the thickness h of narrow-plate specimen CB-18: $L_{eff} = 2(.097) = 0.194$ in.

For this refined-mesh FE model, all other finite strain formulation-and-calculation procedures, strain-displacement relations, and other data were the same as for the coarse-mesh finite-element plate model computation.

Shown in Fig. 43 are the coarse-mesh vs. refined-mesh plate-element finite-strain EL-SH predictions of the plate-center, (x,y) = (0,0), displacement w of steel-sphere-impacted 6061-T651 aluminum narrow-plate specimen CB-18. As expected, the refined-mesh model exhibits a larger peak deflection later in time compared with the coarse-mesh model prediction:

FE Plate Model	Peak w(in)	Time at Peak (μsec)
Coarse Mesh	0.970	690
Refined Mesh	0.987	750

However, as noted earlier, transient (or permanent) displacements are not a sensitive indicator of the accuracy and/or reliability of the prediction. Strains on the other hand are of primary interest and concern, and provide a much more sensitive and meaningful indication of prediction adequacy. Hence, strain predictions are examined next.

Compared in Figs. 44a through 44o are coarse-mesh vs. refined-mesh plate-element-model finite-strain predictions of transient longitudinal Green (Lagrangian) strain γ_2^2 on the surface at various spanwise stations of steel-sphere-impacted 6061-T651 aluminum narrow-plate specimen CB-18. Experimental transient and/or permanent strains, as appropriate and available, are included also. Summarized in the following are the figure number and associated station/surface at which these γ_2^2 strains are compared:

Figure	Plate FE Model		Location of γ_2^2 Strain Data Along the Plate Midwidth (x=0) Station				
	Coarse	Refined	Station y (in)	Prediction Upper	Prediction Lower	Experiment Upper	Experiment Lower
44a	X	X	0	X	-	-	-
44b	X	X	0	-	X	-	-
44c	X	X	0.30	X	-	-	-
44d	X	X	0.30	-	X	-	-
44e	X	X	0.60	X	-	X	-
44f	X	X	0.60	-	X	-	-
44g	X	X	1.20	X	-	X	-
44h	X	X	1.50	X	-	X	-
44i	X	X	1.50	-	X	-	X
44j	X	X	3.00	X	-	P*	-
44k	X	X	3.00	-	X	-	P*
44ℓ	X	X	3.70	X	-	P*	-
44m	X	X	3.70	-	X	-	P*
44n	X	X	4.00	X	-	-	-
44o	X	X	4.00	-	X	-	-

*Only permanent strain was recorded at this location.

Figure 44 shows that at the upper (non-impacted) surface at the initial-impact station (x,y) = (0,0), the refined-mesh plate-element model predicts a peak γ_2^2 strain of about 59.7 per cent at time after initial impact TAII = 750 μsec, while the corresponding coarse-mesh model predicts a peak γ_2^2 strain of about 35.6 per cent at TAII = 690 μsec. A similar disparity is seen (Fig. 44b) at the lower surface at station (x,y) = (0,0), but the refined-mesh model predicts a compressive strain peak of much <u>smaller</u> magnitude than that from the coarse-mesh model. Hence, the refined-mesh model predicts larger <u>membrane</u> strains at (x,y) = (0,0).

At station (x,y) = (0, 0.30 in), the more accurate refined-mesh model prediction of γ_2^2 differs significantly from the coarse-mesh model prediction, as Figs. 44c and 44d show. Evidence of "reversed curvature" is present -- the lower surface experiences a larger peak strain than does the upper surface, and both are tensile.

At station (x,y) = (0, 0.60 in) which is more remote from the initial-impact station, the predicted peak γ_2^2 (longitudinal) strains are of tensile character on both surfaces (see Figs. 44e and 44f); the peak γ_2^2 strain for the refined-mesh model vs. the coarse-mesh model is about 9.0 and 17.5 per cent higher for, respectively, the upper and the lower surface, where the refined-mesh result is used as a reference. For the upper surface (Fig. 44e), the experimental transient strain trace agrees reasonably well with both predictions until about 500 microseconds when the experimental strain trace was lost. On the upper surface, permanent strain measurements of 2.24 and 2.36 per cent were obtained at respective stations (0, +0.60 in) and (0, -0.60 in); it is evident that the "refined-mesh prediction" of the permanent strain would be close to these values.

It should be noted, however, that for computational efficiency and economy reasons, only one quarter of narrow-plate specimen CB-18 was modeled by finite elements. Furthermore, it was assumed in these calculations that initial impact occurred at station (x,y) = (0,0); in the actual experiment, however, initial impact occurred at about (x,y) = (+.057, -.019 in). Therefore, the locations of strain gages relative to the actual impact location are different from those with respect to the "assumed" initial-impact location (x,y) = (0,0). Therefore, the computed and the measured strains compared here are actually at somewhat different distances from the initial impact point. Accordingly, this effect should be responsible in part for the discrepancies between measured and predicted strains, especially at those stations near the initial impact location. At more distant stations, however, this factor assumes a lesser to negligible importance.

On the upper surface at station (x,y) = (0, 1.20 in), Fig. 44g shows that the peak γ_2^2 strain from the coarse-mesh calculation is about 36 per cent smaller than that for the refined-mesh prediction (3.13 per cent). From 0 to 200 μsec, the measured strain trace agrees very well with both predictions; from 300 to 475 μsec, it agrees better with the coarse-mesh result; and beyond about 475 μsec, the measured transient strain is in better agreement with the refined-mesh prediction. The measured permanent strain agrees reasonably well (and best) with the coarse-mesh calculation. Although the refined-mesh prediction was carried out to only 800 μsec, it appears that the "indicated" permanent strain would be larger than measured; this effect is not unexpected at this particular (less important) location since a rather large (0.50-in long) finite element was used and contains that (x,y) = (0, 1.20 in) station -- the use of smaller elements to span this region would likely improve the prediction in this region of relatively small strains.

More distant from the initial-impact location is station (x,y) = (0, 1.50 in) where γ_2^2 predictions and measurements are shown in Figs. 44h and 44i, respectively, for the upper and the lower surface. At this location, the coarse-mesh calculation indicates larger peak γ_2^2 strains on both surfaces than given by the refined-mesh prediction; in both cases the peak values are less than 2.5 per cent. The measured transient γ_2^2 strain on the upper surface is larger than either prediction, but at the lower surface the measured information is in reasonably good agreement with predictions. Finally, the measured permanent strain at (1) upper-surface stations (x,y) = (0, 1.50 in) and (x,y) = (0, -1.50 in) was 1.48 and 1.13 per cent, respectively and (2) the lower-surface stations (x,y) = (0, 1.50 in) and (x,y) = (0, -1.50 in) was 1.31 and 1.27 per cent, respectively; the refined-mesh prediction is seen to be in good agreement with those measurements.

Coarse-mesh and refined-mesh predictions for the transient γ_2^2 strain at station (x,y) = (0, 3.00 in) are shown in Figs. 44j and 44k, respectively, for the upper and the lower surface. Here the peak strains are small, and the coarse-mesh calculation predicts somewhat larger peak values than does the refined-mesh computation. On the upper surface the refined-mesh prediction indicates the closer agreement with the measured strain.

Of greater importance and interest are the strains at stations close to the clamped end. Here significant spatial strain gradients and strain values themselves must occur. Hence, stations (x,y) = (0, 3.70 in) and (x,y) = (0, 4.00 in) are of particular interest. Coarse-mesh and fine-mesh transient γ_2^2 strain predictions are shown in Figs. 44ℓ and 44m for station (x,y) = (0, 3.70 in) and in Figs. 44n and 44o for station (x,y) = (0, 4.00 in) at, respectively, the upper and the lower surface for each station. Since, a finer element mesh is used in this region for the refined-mesh model compared with the coarse-mesh model, the former is expected to provide substantially more reliable predictions, especially at the clamped end (x,y) = (0, 4.00 in).

On both the upper and the lower surface at station (x,y) = (0, 3.70 in), the peak strains predicted by the refined-model calculation are much smaller than from the coarse-mesh prediction. The measured permanent strains on the (1) upper surface at (x,y) = (0, 3.70 in) and (x,y) = (0, -3.70 in) were 0.56 and 0.68 per cent, respectively, and (2) lower surface at (x,y) = (0, 3.70 in) and (x,y) = (0, -3.70 in) were 1.07 and 0.47 per cent, respectively. It is seen that the refined-mesh predictions are in close agreement with these measured permanent strains.

At the clamped-end station (x,y) = (0, 4.00 in), very severe bending strains occur. As Fig. 44n shows, the upper surface at this station experiences sequential transient compression, tension, compression, and finally tension as the membrane effect overwhelms the bending contribution -- according to the (more reliable) refined-mesh prediction. The coarse-mesh prediction shows a similar sequence except that the final state is one of compression rather than the tension predicted by the refined-mesh calculation.

On the lower surface at (x,y) = (0, 4.00 in), very large tension strains γ_2^2 are expected from the additive effect of membrane and severe bending; this is seen to be the case from the predictions shown in Fig. 44o. Note that the coarse-mesh calculation predicts a peak tensile γ_2^2 strain of 11.5 per cent at this location while the more reliable refined-mesh computation predicts a peak tensile γ_2^2 strain of 22.6 per cent. Although no strain measurements were made at the lower surface at (x,y) = (0, 4.0 in), it is evident from visual inspection of the specimens that the permanent strains there (at the clamped-end lower surface) are large. Nonhomogeneous deformation is present with an orange-peel kind of surface; this kind of surface was noticed in static uniaxial tensile tests of the same batch of 6061-T651 aluminum used for the CB-18 plate specimen for tensile strains of about 18 per cent or more. Recall that the initial-impact station, the refined-mesh calculation predicts a peak tensile γ_2^2 strain of 59.7 per cent. Hence, it is apparent that the 3-D structural response behavior accommodated by the plate-finite-element model would result in predicting incipient rupture of the present type of steel-sphere-impacted 6061-T651 aluminum narrow plate to occur at the midspan initial-impact station rather than at the clamped end as predicted by the 2-D model (compare Figs. 38a and 38n at stations y = 0 and 4.00 in, respectively). The experimental specimen CB-16 did break [1] near the point of impact rather than at the clamped end, when subjected to steel-sphere impact with a velocity slightly higher than than the CB-18 velocity.

One point that deserves further investigation is the "exact distribution" of strain in the impact region. While the computer predictions indicate that the maximum strain occurs at the initial-impact point (the midpoint of the plate), the actual experiments show that the maximum strain takes place at about 0.2 in from that location. One reason for this discrepancy might be the presence of transverse shear strains at that location (the computer predictions do not take this type of straining into account). Another reason may be that the local impact-interaction details between the steel sphere and the plate involve contact and stress wave propagation details that the present impact procedure does not take into account; instead a high simplified-interaction model is used -- as described, for example, in Refs. 23, 27, and 30.

The computing time required to carry out the <u>finite-strain</u> Houbolt-MULE predictions of the transient responses of steel-sphere-impacted 6061-T651 aluminum narrow-plate specimen CB-18 on the IBM 370/168 in double precision at MIT are summarized in the following for both the coarse-mesh and the refined-mesh finite element model; $\Delta t = 1$ μsec was used in both cases:

FE Model	No. of Plate FE	Total Unknown DOF	No. of Cycles	CPU Time (min)	$\frac{\text{CPU(min)}}{\text{DOF Cycles}}$
Coarse Mesh	22	157	900	65.4	462.8×10^{-6}
Refined Mesh	75	478	800	202.6	529.8×10^{-6}

As pointed out in Subsection 7.6.4.1, the computing time in terms of CPU time per (DOF) (cycle) for the finite-strain prediction of specimen CB-18's response when modeled by (2-D) beam elements was 21.7×10^{-6}. Thus, it is seen that the plate-element finite-strain 3-D structural response is about 24 times "more expensive" than the simpler, less reliable 2-D model and calculation.

SECTION 8

SUMMARY AND CONCLUSIONS

8.1 Summary

The present study is devoted principally to developing and validating a method of analysis for thin structures (beams, rings, plates, and shells) that incorporates finite-strain, elastic-plastic, strain-hardening, time-dependent material behavior implemented with respect to a fixed reference configuration (total Lagrangian formulation) and which is consistently valid for finite strains and finite rotations. As a result, accurate finite-element predictions of transient strains and large transient deformations of beams, rings, and plates subjected to known forcing functions have been demonstrated (see Section 7). A practical problem to which the present method of analysis has been applied is that of structural (containment) ring response to engine rotor-fragment impact.

The theory is formulated systematically in a body-fixed system of convected coordinates with materially-embedded vectors that deform in common with the continuum, and in the traditional space-fixed system of variable coordinates and constant vectors used by most books on continuum mechanics. Tensors are considered as linear vector functions, and use is made of the dyadic representation (instead of simply considering tensors as a collection of components), because these concise tools are helpful to clarify the physical laws under which materials deform. The kinematics of a deformable continuum is treated in considerable detail, carefully defining precisely all quantities necessary for the analysis.

The finite-strain plasticity theory of Hill is extended to include very complex material behavior (like elastic-plastic unloading, the Bauschinger effect, and hysteresis) by means of the "mechanical sublayer method" pioneered by Prandtl, Timoshenko, and Duwez. Strain-hardening and complex strain-rate dependence of the material are easily accommodated by this model. This plasticity theory is referred to quantities associated with a fixed reference configuration by means of proper transformations between the tensors associated with the present and with the reference configuration.

Strain-displacement equations which are valid for finite strains and rotations and which include thinning effects are derived for beams, rings, plates, and shells.

The finite element concept is used in conjunction with the Principle of Virtual Work and D'Alembert's Principle to obtain the equations of motion of a general solid continuum which is permitted to undergo arbitrarily large rotations and strains. A new constant stiffness formulation of the finite element equations of motion is developed. This new formulation is more efficient computationally and better conditioned numerically than the conventional pseudo-force formulation. Furthermore, this new formulation is valid for finite-strain behavior of any kind of material, while the conventional pseudo-force formulation is valid only for small-strain elastic-plastic materials.

The resulting equations of motion consist of a finite-size system of second order ordinary (coupled) nonlinear differential equations with the unknowns to be determined being the values of the degrees of freedom (displacements and displacement gradients) at the nodes of the finite-element assemblage which represents the continuum. This set of equations is solved stepwise in time by using a numerical integration scheme with an appropriate finite-difference time operator.

An assessment of this method of analysis is made by means of a sequence of problems for beam, ring, and plate structures which are subjected to initial impulsive loading or to impact by rigid fragments. The present finite-strain predictions are compared with reliable experimental data and with small-strain-theory predictions. The central-difference operator and the Houbolt finite-difference operator are used for the timewise calculations. Either linear extrapolation of the nonlinear internal forces or iteration of the nonlinear equations of motion is employed when the (implicit) Houbolt operator is used.

The predictions of the finite-element computer programs that incorporate the finite-strain elastic-plastic time-dependent theory developed are compared with experimental data. The missiles and targets introduced in these experiments (steel-sphere missile, clamped-end thin beams, and thin square panels with all four sides ideally clamped) pose well-defined configurations and conditions for which transient strain, permanent strain, and permanent deflection data of high quality have been obtained.

These test conditions have included impulse loading or fragment impact with velocities sufficient to produce responses of various severities up to and including threshold rupture conditions; often finite strains well beyond the "small strain" range were observed.

From these comparisons it appears that the use of the present finite-strain elastic-plastic formulation can provide significantly improved predictions of transient strains (the most important and sensitive quantities) in thin 2-D and 3-D structures which are subjected to severe impulse or impact loads, compared with the previously-employed small-strain procedure.

8.2 Conclusions

On the basis of the present study, the following conclusions may be stated:

(1) For general application, finite-strain theory rather than small-strain theory should be used in nonlinear analysis of transient response by computer methods since the former is valid for all levels of strain whereas the latter is valid for only a poorly-defined small level of strain.

(2) Large differences between the finite-strain theory results and the small-strain theory results are found in the cases studied herein for (a) strains of the order of about 5 per cent and larger and (b) at regions where significant strain gradients occur (where the peak strains are larger than about 10 per cent).

(3) The use of the present finite-strain formulation for thin structures (beams, rings, and plates) provides physically realistic and superior strain results compared with small-strain formulation predictions, as the present theoretical-experimental comparisons show.

(4) The use of the present finite-strain formulation involves practically no additional cost over the use of the small-strain formulation for the present types of nonlinear transient structural response problems.

(5) Finite-strain elastic-plastic theory can be (and has been) implemented easily in a total Lagrangian reference frame; this appears not to have been demonstrated and implemented heretofore.

(6) Whereas the use of the proper-and-consistent finite-strain analysis and procedure appears to affect the predicted transient displacements very little compared with small-strain calculations, the predicted strains (the most important data) are affected significantly.

(7) The theoretical-experimental comparisons for the finite-strain calculations show generally good agreement for thin structures subjected to explosive-impulse loadings or to impact by a rigid fragment.

(8) The Kirchhoff stress (not to be confused with the 1st or the 2nd Piola-Kirchhoff stress) should be used in the formulation of finite-strain plasticity problems because of:

   (a) theoretical considerations -- based on the simplicity of the thermodynamic equations which employ the Kirchhoff stress, as well as the existence of a rate potential, and

   (b) numerical considerations -- the existence of an incremental variational principle and a symmetric tangent stiffness matrix.

   Additional merits include:

   (c) the Kirchhoff stress is easily measured in experiments such as, for example, the classical experiments of G.I. Taylor and A. Nadai, and

   (d) the Kirchhoff stress represents the actual behavior of the material in simpler terms than by other stress measures.

(9) The mechanical sublayer model of plasticity is superior theoretically to the popular isotropic and kinematic hardening rules of plasticity. The present strain-rate sensitive mechanical sublayer model of finite strain elasto-viscoplasticity provides a very powerful tool to describe the complex problems of impact and explosive loading of structures.

(10) The new (finite strain) constant stiffness formulation of the finite element equations was shown to be more efficient computationally and better conditioned numerically than the conventional (small-strain) pseudo-force constant stiffness formulation for the problems tested in this work.

(11) The results (displacements and strains) of the analysis (2-D and 3-D) of the explosively-impulsed aluminum structures were much closer to the experimental results when the aluminum alloy was analyzed as being strain-rate sensitive than as strain-rate insensitive. This is so, even though there is considerable uncertainty in the appropriateness of the strain-rate constants used in the analysis. As far as how representative these values are of the actual material properties, and how appropriate it is to consider these strain-rate "constants" as being constant over widely different levels of strain-rate and strain encountered in the course of the transient response remain uncertain. Moreover, the strain-rate dependence was considered to be isotropic, while in the actual material this strain rate dependence could be anisotropic.

(12) The 2-D analysis of steel-sphere impacted narrow beams is quite satisfactory as far as the transient displacement response predictions are concerned. However, if detailed transient and permanent strain information is needed, and in particular if the occurrence of rupture is to be predicted adequately, a 3-D analysis is necessary. In effect, while the 2-D analysis (2-D structure and 2-D fragment) predicts that the highest strains (and hence rupture) of the narrow beams will occur at the clamped ends, the 3-D analysis predicts that the largest strains occur at the region of impact, which agrees with both experimental results and expectations.

8.3 Suggestions for Future Research

It is advisable to pursue the inclusion of the following aspects in future analysis developments:

1. To study the implicit Park operator, that appears to possess better false-damping and frequency-distortion features than those of the Houbolt operator, but its performance costs have not been completely assessed for the present category of problems.

2. To investigate the utilization of quasi-Newton iteration methods (like Broydon's method or the BFGS method) within each time step as required to achieve convergence in accord with specified criteria of the nonlinear equations that have to be solved with implicit operators like the Houbolt or Park operators.

3. The development and implementation of an efficient shell finite-element analysis of finite-strain elastic-viscoplastic problems.

4. The inclusion of transverse shear deformations.

5. The inclusion of anisotropic material effects.

REFERENCES

1. Witmer, E.A., Merlis, F. and Spilker, R.L., "Experimental Transient and Permanent Deformation Studies of Steel-Sphere-Impacted or Impulsively-Loaded Aluminum Beams with Clamped Ends", MIT ASRL TR 154-11, October 1975. (Available as NASA CR-134922.)

2. Witmer, E.A., Merlis, F., Rodal, J.J.A. and Stagliano, T.R., "Experimental Transient and Permanent Deformation Studies of Steel-Sphere-Impacted or Explosively-Impulsed Aluminum Panels", MIT ASRL TR 154-12, May 1977. (Available as NASA CR-135315.)

3. Longcope, D.B. and Key, S.W., "On the Verification of Large Deformation Inelastic Dynamic Calculations Through Experimental Comparisons and Analytic Solutions", Sandia Laboratories, Albuquerque, New Mexico (Presented at the Joint Energy Conference, Houston, Texas, Sept.1977).

4. Bathe, K.J., Ramm, E. and Wilson, E.L., "Finite Element Formulations for Large Deformation Dynamic Analysis", Intl. J. for Num. Methods in Eng., Vol. 9, 1975, pp. 353-386.

5. Nemat-Nasser, S., "Continuum Bases for Consistent Numerical Formulations of Finite Strains in Elastic and Inelastic Structures", AMD Vol. 14, New York, 1975, pp. 75-97.

6. Stricklin, J.A. and Haisler, W.E., "Formulations and Solution Procedures for Nonlinear Structural Analysis", Computer & Structures, Vol. 7, Feb. 1977, pp. 125-136.

7. Truesdell, C. and Toupin, R., "The Classical Field Theories" in Vol. III/I of Encyclopedia of Physics (Handbuch der Physik), edited by S. Flugge. Springer-Verlag, Berlin, 1960.

8. Cauchy, A.L., "Recherches sur l'équilibre et le mouvement intérieur des corps solides ou fluides, élastiques ou non élastiques," Bull. Soc. Philomath., 1823, pp. 9-13, in Oeuvres, Ser. 2, Vol. 2, pp.300-304.

9. Cauchy, A.L., "Sur les équations qui expriment les conditions d'equilibre, ou les lois du mouvement intérieur d'un corps solide, élastique, ou non élastique", Ex. de Math., Vol. 3, 1828, pp. 160-187, in Oeuvres, Ser. 2, Vol. 8, pp. 195-226.

10. Cauchy, A.L., "Sur l'équilibre et le mouvement intérieur des corps considérés comme des masses continues", Ex. de Math., Vol. 4, 1829, pp. 293-319, in Oeuvres, Ser. 2, Vol. 9, pp. 243-369.

11. Cauchy, A.L., "Sur les diverses méthodes à l'aide desquelles on peut établir les équations qui représentent les lois d'équilibre, ou le mouvement intérieur des corps solides ou fluides", Bull. sci. math. soc. prop. conn., Vol. 13, 1830, pp. 169-176.

12. Truesdell, C., "The Rational Mechanics of Flexible or Elastic Bodies, 1638-1788". L. Euleri Opera Omnia, Volume 11, Part 2, 1960.

13. Koiter, W.T., "On the Nonlinear Theory of Thin Elastic Shells", Proceedings of the Koninklyke Nederlandse Akademie van Wetenschappen, B. 69, 1966, pp. 1-54.

14. Leech, J.W., "Finite-Difference Calculation Method for Large Elastic-Plastic Dynamically-Induced Deformations of General Thin Shells", AFFDL-TR-66-171, Dec. 1966.

15. Leech, J.W., Witmer, E.A., and Pian, T.H.H., "Numerical Calculation Technique for Large Elastic-Plastic Transient Deformations of Thin Shells", AIAA Journal, Vol. 6, No. 12, Dec. 1968, pp. 2352-2359.

16. Morino, L., Leech, J.W., and Witmer, E.A., "PETROS 2: A New Finite-Difference Method and Program for the Calculation of Large Elastic-Plastic Dynamically-Induced Deformations of General Thin Shells", BRL CR 12 (MIT-ASRL TR 152-1), December 1969 (In two parts: AD 708773 and AD 708774).

17. Morino, L., Leech, J.W., and Witmer, E.A., "An Improved Numerical Calculation Technique for Large Elastic-Plastic Transient Deformations of Thin Shells", Journal of Applied Mechanics, June 1971, Parts 1 and 2, pp. 423-436.

18. Atluri, S., Witmer, E.A., Leech, J.W., and Morino, L., "PETROS 3: A Finite-Difference Method and Program for the Calculation of Large Elastic-Plastic Dynamically-Induced Deformations of Multilayer, Variable-Thickness Shells', BRL CR 60 (MIT-ASRL TR 152-2), November 1971. AD #890200L.

19. Pirotin, S.D., Berg, B.A. and Witmer, E.A., "PETROS 3.5: "New Developments and Program Manual for the Finite-Difference Calculation of Large Elastic-Plastic Transient Deformations of Multilayer Variable-Thickness Shells", BRL CR 211 (MIT ASRL TR 152-4), February 1975.

20. Pirotin, S.D., Morino, L., Witmer, E.A., and Leech, J.W., "Finite-Difference Analysis for Predicting Large Elastic-Plastic Transient Deformations of Variable-Thickness Kirchhoff, Soft-Bonded Thin and Transverse-Shear-Deformable Thicker Shells", BRL CR 315 (MIT-ASRL TR 152-3), September 1976.

21. Pirotin, S.D., Berg, B.A., and Witmer, E.A., "PETROS 4: New Developments and Program Manual for the Finite-Difference Calculation of Large Elastic-Plastic, and/or Viscoelastic Transient Deformations of Multilayer Variable-Thickness (1) Thin Hard-Bonded, (2) Moderately-Thick Hard-Bonded, or (3) Thin Soft-Bonded Shells", BRL CR 316 (MIT-ASRL TR 152-6), September 1976.

22. Truesdell, C.: "A First Course in Rational Continuum Mechanics" Vol.1, General Concepts, Academic Press, New York 1977.

23. Wu, R.W.-H. and Witmer, E.A., "Finite-Element Analysis of Large Transient Elastic-Plastic Deformations of Simple Structures, with Application to the Engine Rotor Fragment Containment/Deflection Problem", ASRL TR 154-4, Aeroelastic and Structures Research Laboratory, Massachusetts Institute of Technology, Jan. 1972. (Available as NASA CR-120886.)

24. Wu, R.W.-H. and Witmer, E.A., "Computer Program - JET 3 - to Calculate the Large Elastic-Plastic Dynamically-Induced Deformations of Free and Restrained, Partial and/or Complete Structural Rings", ASRL TR 154-7, Aeroelastic and Structures Research Laboratory, Massachusetts Institute of Technology, Aug. 1972. (Available as NASA CR-120993.)

25. Zirin, R.M. and Witmer, E.A., "Examination of the Collision Force Method for Analyzing the Responses of Simple Containment/Deflection Structures to Impact by One Engine Rotor Blade Fragment", ASRL TR 154-6, Aeroelastic and Structures Research Laboratory, Massachusetts Institute of Technology, May 1972. (Available as NASA CR-120952.)

26. Wu, Richard W-H. and Witmer, E.A., "Finite Element Predictions of Transient Elastic-Plastic Large Deflections of Stiffened and/or Unstiffened Rings and Cylindrical Shells", AMMRC CTR 74-31 (MIT ASRL TR 171-4), April 1974.

27. Stagliano, T.R., Spilker, R.L. and Witmer, E.A., "User's Guide to Computer Program CIVM-JET 4B to Calculate the Transient Structural Responses of Partial and/or Complete Structural Rings to Engine Rotor Fragment Impact", MIT ASRL TR 154-9, March 1976 (also available as NASA CR-134907).

28. Rodal, J.J.A. and Witmer, E.A., "Finite Element Nonlinear Transient Response Analysis of Simple 2-D Structures to Impulse or Impact Loads", MIT ASRL TR 182-1, June 1976.

29. Wu, R.W.-H., Stagliano, T.R., Witmer, E.A. and Spilker, R.L., "User's Guide to Computer Programs JET 5A and CIVM-JET 5B to Calculate the Large Elastic-Plastic Dynamically-Induced Deformations of Multilayer Partial and/or Complete Structural Rings", MIT ASRL TR 154-10, November 1978. (Available as NASA CR-159484).

C-5

30. Stagliano, T.R., Witmer, E.A. and Rodal, J.J.A., "Two-Dimensional Finite-Element Analyses of Simulated Rotor-Fragment Impacts Against Rings and Beams Compared with Experiments", MIT ASRL TR 154-13, December 1979. (Available as NASA CR-159645.)

31. Spilker, R.L., Witmer, E.A., French, S. and Rodal, J.J.A., "Finite Element Nonlinear Transient Response Analysis of Panels Subjected to Impulse or Impact Loads", MIT ASRL TR 154-14 (in preparation).

32. Truesdell, C., "Second Order Effects in the Mechanics of Materials", in Second Order Effects in Elasticity, Plasticity, and Fluid Dynamics, IUTAM Symposium, Haifa, Israel, April 1962. Edited by M. Reiner and D. Abir, MacMillan, New York, 1964.

33. Truesdell, C., "The Mechanical Foundations of Elasticity and Fluid Dynamics", Journal of Rational Mechanics and Analysis, Volume 1, 1952, pp. 125-300 (corrected reprint in The Mechanical Foundations of Elasticity and Fluid Dynamics. New York: Gordon & Breach, 1966).

34. Truesdell, C., The Elements of Continuum Mechanics, Springer Verlag, New York, 1965.

35. Truesdell, C., Continuum Mechanics (reprints). Gordon & Breach, New York, Vol. 1 1966; Vols. 2,3,4, 1965.

36. Truesdell, C., Six Lectures on Modern Natural Philosophy, Springer Verlag, New York, 1966.

37. Truesdell, C., "The Physical Components of Vectors and Tensors", ZAMM, Vol. 33, 1953, pp. 345-355.

38. Truesdell, C., Rational Thermodynamics, McGraw Hill, 1969.

39. Wang, C.C. and Truesdell, C., Introduction to Rational Elasticity, Noordhoff, Leyden, 1973.

40. Truesdell, C. and Noll, W., The Non-Linear Field Theories of Mechanics, in Encyclopedia of Physics (Handbuch der Physik), Volume III/3, edited by S. Flugge. Springer-Verlag, Berlin, 1965.

41. Sedov, L.I., Foundations of the Non-Linear Mechanics of Continua, English translation edited by J.E. Adkins and A.J.M. Spencer, Pergamon Press, Oxford, 1966.

42. Sedov, L.I., A Course in Continuum Mechanics, Vol. I: Basic Equations and Analytical Techniques, Vol. II: Physical Foundations and Formulations of Problems, Vol. III: Fluids, Gases and the Generation of Thrust Vol. IV: Elastic and Plastic Solids and the Formation of Cracks. Translation from the Russian, Edited by Prof. J. Radok, Wolters-Noordhoff Publishing, Groningen, The Netherlands, 1971.

43. Sedov, L.I., "The Concepts of Different Rates of Change of Tensors" (Prik. Matem. i Mekh.) Applied Matematics and Mechanics, Vol. 24, No. 3, 1960.

44. Sedov, L.I., "Some Problems of Designing New Models of Continuum Media" Proceedings of the 11th International Congress of Applied Mechanics, Munich (Germany) 1964, Springer Verlag 1966.

45. Lokhin, V. and Sedov, L.I., "Nonlinear Tensor Functions of Several Tensor Arguments", in (Prik. Matem. i Mekh.) Applied Mathematics and Mechanics, Volume 27, Number 3, 1963.

46. Berdichevskii, V.L. and Sedov, L.I., "Dynamic Theory of Continuously Distributed Dislocations. Its Relation to Plasticity Theory", in (Prik. Matem. i Mekh.) Applied Mathematics and Mechanics, Volume 31, Number 6, 1967.

47. Sedov, L.I., "Variational Methods of Constructing Models of Continuous Media" in Symposium on Irreversible Aspects of Continuum Mechanics, Vienna, June 1966, Springer Verlag, 1968.

48. Sedov, L.I., "Models of Continuous Media with Internal Degrees of Freedom", in (Prik. Matem. i Mekh.) Applied Mathematics and Mechanics, Volume 32, Number 5, 1968.

49. Sedov, L.I., "On Prospective Trends and Problems in Mechanics of Continuous Media", in (Prik. Matem. i Mekh.) Applied Mathematics and Mechanics, Volume 40, Number 6, 1976.

50. Malvern, L.E., "Introduction to the Mechanics of a Continuous Medium", Prentice Hall, 1969.

51. Jaunzemis, W., Continuum Mechanics, MacMillan Co., New York, 1967.

52. Leigh, D.C., Nonlinear Continuum Mechanics, McGraw Hill, 1968.

53. Eringen, A.C., Nonlinear Theory of Continuous Media, McGraw Hill, New York, 1962.

54. Eringen, A.C., Mechanics of Continua, John Wiley & Sons, Inc., New York, 1967.

55. Biot, M.A., Mechanics of Incremental Deformations, John Wiley & Sons, Inc., New York, 1965.

56. Green, A.E., and Zerna, W., Theoretical Elasticity, 2nd Edition, Clarendon Press, Oxford, 1968.

57. Green, A.E. and Adkins, J.E., Large Elastic Deformations, 2nd Edition revised by A.E. Green, Clarendon Press, Oxford, 1970.

58. Green, A.E. and Adkins, J.E., Large Elastic Deformations and Non-Linear Continuum Mechanics, Clarendon Press, Oxford, 1960.

59. Prager, W., Introduction to Mechanics of Continua, Dover, New York, 1973 (originally published by Ginn and Company in 1961).

60. Fung, Y.C., Foundations of Solids Mechanics, Prentice Hall, New Jersey, 1965.

61. Schouten, J.A., Tensor Analysis for Physicists, Clarendon Press, Oxford, 1951.

62. Einsenhart, L.P., Introduction to Differential Geometry, Princeton University Press, 1940.

63. McConnell, A.J., Applications of the Absolute Differential Calculus, Blackie Company, 1931. (Republished as "Applications of Tensor Analysis" by Dover Publications, New York, 1957).

64. Synge, J.L. and Schild, A., Tensor Calculus, University of Toronto Press, Toronto, 1949.

65. Willmore, T.J., An Introduction to Differential Geometry, Clarendon Press, Oxford, 1959.

66. Sokolnikoff, I.S., Tensor Analysis: Theory and Applications to Geometry and Mechanics of Continua, John Wiley & Sons, New York, 2nd Edition, 1964.

67. Ericksen, J.L., "Tensor Fields", Appendix to Ref. 7.

68. Bowen, R.M. and Wang, C.C., Introduction to Vectors and Tensors, 2 volumes, Plenum Press, New York, 1976.

69. Halmos, P.R., Finite Dimensional Vector Spaces, 2nd. Edition, Van Nostrand, 1958.

70. Weissenberg, K., Geometry of Rheological Phenomena (1946-1947), The Principles of Rheological Measurement, London, pp. 36-65.

71. Biot, M.A., "Theory of Elasticity with Large Displacements and Rotations", Proc. 5th Int. Cong. Appl. Mech., New York, 1939.

72. Swainger, K., "Stress-Strain Compatibility in Greatly Deformed Engineering Metals". Phil. Mag. Number 7, Vol. 38, 1947, pp. 422-439.

73. Hencky, H., "Über die Form des Elastizitätsgesetzes bei ideal Elastichen Stoffen", Z. Techn. Phys., 9, 1928, pp. 214-223.

74. Spivack, M., Calculus on Manifolds, Benjamin, New York, 1965.

75. Rudin, W., Real and Complex Analysis, McGraw-Hill, New York, 2nd Ed., 1974.

76. Zhong-heng, Guo, "Time Derivatives of Tensor Fields in Non-Linear Continuum Mechanics", Archiwum Mechaniki Stosowanej, (Archives de Mecanique Appliquee), Volume 15, 1963, pp. 131-161.

77. Oldroyd, J.G., "On the Formulation of Rheological Equations of State", Proc. Roy. Soc., Ser. A, Vol. 200, 1950, pp. 523-541.

78. Cotter, B., and Rivlin, R.S., "Tensors Associated with Time-Dependent Stress", Quart. Appl. Math., Vol. 13, 1955, pp. 177-182.

79. Masur, E.F., "On the Definition of Stress Rate", Quart. Appl. Math. Vol. 19, 1961, pp. 160-163.

80. Masur, E.F., "On Tensor Rates in Continuum Mechanics", ZAMP, Vol. 16, 1965, pp. 191-201.

81. Zaremba, S., "Sur une Forme Perfectionnée de la Theorie de la Relaxation", Bull. Int. Acad. Sci. Cracovie, Vol. 8, 1903, pp. 594-614.

82. Jaumann, G., Grundlagen der Bewegungslehre, Leipzig, 1905.

83. Noll, W., "On the Continuity of Solid and Fluid States", J. Ratl. Mech. Anal., Vol. 4, 1955, pp. 3-81.

84. Thomas, T.Y., "On the Structure of the Stress-Strain Relations", Proc. Nat. Acad. Sci., Vol. 41, 1955, pp. 716-720.

85. Thomas, T.Y., "Kinematically Preferred Coordinate Systems," Proc. Nat. Acad. Sci., Vol. 41, 1955, pp. 762-770.

86. Prager, W., "An Elementary Discussion of Definitions of Stress Rate", Quart. Appl. Math., Vol. 18, 1961, pp. 403-407.

87. Lehmann, Th., "Formänderungen eines Klassischen Kontinuums in Vierdimensionaler Darstellung", in Proc. 11th Int. Cong. of Appl. Mech., Munich, 1964, pp. 376-382.

88. Thomas, T.Y., Plastic Flow and Fracture in Solids, Academic Press, New York, 1961.

89. Hill, R., The Mathematical Theory of Plasticity, Clarendon, Oxford, 1950.

90. Drucker, D.C., "A More Fundamental Approach to Stress-Strain Relations", Proc. First. U.S. National Congress of Applied Mechanics, Am. Soc. Mech. Engrs., 1951, pp. 487-491.

91. Prager, W., "A New Method of Analyzing Stress and Strain in Work-Hardening Solids", J. App. Mech., Vol. 23, 1956, pp. 493-496 - Discussions by Budiansky and Hodge, Vol. 24, 1957, pp. 481-482, 482-484.

92. Ziegler, H., "A Modification of Prager's Hardening Rule", Quart. Appl. Math., Vol. 17, 1959, pp. 55-65.

93. Almroth, B.O., "Evaluation of Available Technology for Prediction of Plastic Strain", in "Constitutive Equations in Viscoplasticity", ASME, AMD Vol. 20, 1976, pp. 201-211.

94. Hunsaker, B. Jr., Vaughan, D.K., Stricklin, J.A. and Haisler, W.E., " A Comparison of Current Work-Hardening Models Used in the Analysis of Plastic Deformations", Texas A & M University, Department of Aerospace Engineering, TEES-RPT-2926-73-3, Oct. 1973.

95. Iwan, W.D., "On a Class of Models for the Yielding Behavior of Continuous and Composite Systems", Journal of Applied Mechanics, Sept. 1967, pp. 612-716.

96. White, G.N. Jr., "Application of the Theory of Perfectly Plastic Solids to Stress Analysis of Strain Hardening Solids," Brown University Tech. Rep. A11/51, Aug. 1950.

97. Besseling, J.F., "A Theory of Plastic Flow for Anisotropic Hardening in Plastic Deformation of an Initially Isotropic Material," Rep.S410, National Aeronautical Research Institute, Amsterdam, 1953.

98. Mroz, A., "On the Description of Anisotropic Work-Hardening", Journal of the Mechanics and Physics of Solids, Vol. 15, 1967, pp. 163-175.

99. Masing, G., "Eigenspannungen und Verfestigung beim Messing", Proceedings of the Second International Congress of Applied Mechanics, 1926, pp. 332-335.

100. Prandtl, L., "Ein Gedankemodell zur kinetischen Theorie der festen Korper", Zeitschrift fur angewandte mathematik und mechanik, Vol. 8, No. 2, Apr. 1928, pp. 85-106.

101. Timoshenko, S.P., <u>Strength of Materials</u>, Part 2, First Edition, D. Van Nostrand Company, New York, N.Y., 1930, pp. 679-680.

102. Duwez, P., "On the Plasticity of Crystals", Physical Review, Vol. 47, 1935, pp. 494-501.

103. Ivlev, D.D., "The Theory of Complex Media", Soviet Physics-Doklady, Vol. 8, No. 1, July 1963, pp. 28-30.

104. Prager, W., "Models of Plastic Behavior", Proceedings of the Fifth U.S. National Congress of Applied Mechanics, ASME, 1966, pp. 447-448.

105. Balmer, H.A. and Witmer, E.A., "Theoretical-Experimental Correlation of Large Dynamic and Permanent Deformations of Impulsively-Loaded Simple Structures", Air Force Flight Dynamics Laboratory, FDL-TDR-64-108. July 1964.

106. Balmer, H.A., "Improved Computer Programs -- DEPROSS 1, 2, and 3 -- to Calculate the Dynamic Elastic-Plastic Two-Dimensional Responses of Impulsively-Loaded Beams, Rings, Plates and Shells of Revolution". Massachusetts Institute of Technology, ASRL TR 128-3, August 1965.

107. Leech, J.W., Pian, T.H.H., Witmer, E.A. and Herrmann, W., "Dynamic Response of Shells to Externally-Applied Dynamic Loads", Massachusetts Institute of Technology, ASD-TDR-62-610, 1962.

108. Drucker, D.C., "On the Continuum as an Assemblage of Homogeneous Elements or States", Proc. IUTAM Symposium on Irreversible Aspects of Continuum Mechanics and Transfer of Physical Characteristics in Moving Fluids, Springer Verlag, 1966.

109. Iwan, W.D., "A Distributed-Element Model for Hysteresis and its Steady-State Dynamic Response", Journal of Applied Mechanics, Dec. 1966, pp. 893-900.

110. Zienkiewicz, O.C., Nayak, G.C., and Owen, K.R.J., "Composite and Overlay Models in Numerical Analysis of Elasto-Plastic Continua,' in Foundations of Plasticity, A. Sawczuk, ed., Noordhoff, Leyden, 1973

111. McKnight, R.L. and Sobel, L.H., "Finite Element Cyclic Thermoplasticity Anal 's by the method of Subvolumes", Computers and Structures, Vol. 7, 197., pp. 189-196.

112. Hill, R., "A General Theory of Uniqueness and Stability in Elastic-Plastic Solids", J. Mech. Phys. Solids, Vol. 6, 1958, pp. 236-249.

113. Hill, R., "Eigenmodal Deformations in Elastic/Plastic Continua", J. Mech. Phys. Solids, Vol. 15, 1967, pp. 371-396.

114. Taylor, G.I. and Quinney, H., "The Latent Energy Remaining in a Metal after Cold Working", Proc. Roy. Soc. of London, England, Ser. A, Vol. 143, 1934, pp. 307-326.

115. Nadai, W., Theory of Flow and Fracture of Solids, McGraw-Hill, 1950.

116. Thomas, T.Y., "On the Structure of the Stress-Strain Relations", Proc. N.A.S., Vol. 41, 1955, pp. 716-720.

117. Thomas, T.Y., "Combined Elastic and Prandtl-Reuss Stress-Strain Relations", Proc. N.A.S., Vol. 41, 1955, pp. 720-726.

118. Thomas, T.Y., "Combined Elastic and Von Mises Stress-Strain Relations", Proc. N.A.S., Vol. 41, 1955, pp. 908-910.

119. Green, A.E., "Hypo-Elasticity and Plasticity", Proc. Roy. Soc. London, Ser A., Vol. 234, 1956, pp. 46-59.

120. Green, A.E., "Hypo-Elasticity and Plasticity. II", J. Rat. Mech. Anal. Vol. 5, 1956, pp. 725-734.

121. Tokuoka, T., "A Theoretical Study of Fracture and Yield Conditions Derived from the Hypo-Elasticity", in Proc. Int. Conf. Mech. Beh. Mat., Kyoto, 1971, Soc. Mat. Sci. Japan, 1972.

122. Tokuoka, T., "Fundamental Relations of Plasticity Derived from Hypo-Elasticity", in Foundations of Plasticity, edited by Sawczuk, Noordhoff, Leyden, 1972.

123. Lehmann, Th., "On Large Elastic-Plastic Deformations", in Foundations of Plasticity, edited by Sawczuk, Noordhoff, Leyden, 1972, pp. 571-585.

124. Lee, E.H., "Elastic-Plastic Deformation at Finite Strains", Journal of Applied Mechanics, March 1969, p. 106.

125. Hill, R., "Some Basic Principles in the Mechanics of Solids without a Natural Time", J. Mech. Phys. Solids, Vol. 7, 1959, pp. 209-225.

126. Hill, R., "The Essential Structure of Constitutive Laws for Metal Composites and Polycrystals", J. Mech. Phys. Solids, Vol. 15, 1967, pp. 79-95.

127. Hill, R., "On the Classical Constitutive Relations for Elastic/Plastic Solids", in Recent Progress in Applied Mechanics, the Folque Odqvist Volume, John Wiley, New York, 1967, pp. 241-249.

128. Hill, R., "On Constitutive Inequalities for Simple Materials', J. Mech. Phys. Solids, Vol. 16, 1968, part I, pp. 229-242, part II, pp. 315-322.

129. Hill, R., "On Constitutive Macro-Variables for Heterogeneous Solids at Finite Strains", Proc. R. Soc. Lond., Ser. A., Vol. 326, 1972, pp. 131-147.

130. Hill, R. and Rice, J.R., "Constitutive Analysis of Elastic-Plastic Crystals at Arbitrary Strain", J. Mech. Phys. Solids, Vol. 20, 1972, pp. 401-413.

131. Hill, R. and Rice, J.R., "Elastic Potentials and the Structure of Inelastic Constitutive Laws", SIAM J. Appl. Math., Vol. 25, No. 3, Nov. 1973, pp. 448-461.

132. Lehmann, Th. , "Some Thermodynamic Considerations at Phenomenological Theory of Non-Isothermal Elastic-Plastic Deformations", Archives of Mechanics, Vol. 24, 1972, pp. 975-989.

133. Lehmann, Th., "Einige Betrachtungen zur Thermodynamik grosser elasto-plasticher Formänderungen", Acta Mechanica, Vol. 20, 1974, pp. 187-207.

134. Lehmann, Th. and Zander, G., "Non-Isothermic Large Elastic-Plastic Deformations", Archives of Mechanics, Vol. 27, 1975, pp. 759-772.

135. Lehmann, Th., "On the Theory of Large, Non-Isothermic, Elastic-Plastic and Elastic-Visco-Plastic Deformations", Archives of Mechanics, Vol. 29, 1977, pp. 393-409.

136. Lehmann, Th., "Einige Bemerkungen zu einer allgemeinen Klasse von Stoffgesetzen für grosse elasto-plastiche Formänderungen", Ing. Arch., Vol. 41, 1972, pp. 297-310.

137. Lehmann, Th., "Anisotrope Plastiche Formänderungen", Rheologica Acta, Vol. 3, 1964, pp. 281-285.

138. Green, A.E. and Naghdi, P.M., "A General Theory of an Elastic-Plastic Continuum", Arch. Rat. Mech. Anal., Vol. 18, 1965, pp. 251-281.

139. Cowper, G.R. and Symonds, P.S., "Strain Hardening and Strain-Rate Effects in the Impact Loading of Cantilever Bea[illegible]", Tech. Report No. 28, ONR Contr[illegible]t Nr 562 (10), NR-062-406, Div. of Appl. Math., Brown University, Sept. 1957.

140. Fowler, J.N., "Elastic-Plastic Discrete-Element Analysis of Axi-symmetrically-Loaded Shells of Revolution", MIT ASRL TR-146-3, BSD-TR-67-193, July 1967.

141. Pian, T.H.H., "Advanced Topics in Structural Me[illegible]nics", class notes for course 16.25, Dept. of Aeronautics and Astronautics, Massachusetts Institute of Technology, 1966.

142. Stalk, G., "Determination of Mechanical Sublayer Model Weighting Coefficients Considering Triaxial Effects", class project for course 16.28, Prof. T.H.H. Pian, Dept. of Aeronautics and Astronautics, Massachusetts Institute of Technology, May 1974.

143. Hunsaker, B. Jr., Haisler, W.E., and Stricklin, J.A., "On the Use of Two Hardening Rules of Plasticity in Incremental and Pseudo Force Analysis", AMD Vol. 20, ASME, 1976, pp. 139-140.

144. Hunsaker, B. Jr., "The Application of Combined Kinematic-Isotropic Hardening and the Mechanical Sublayer Model to Small Strain Inelastic Structural Analysis by the Finite Element Method", Ph.D. Dissertation, Texas A & M University, Aug. 1976.

145. Perzyna, P., "The Constitutive Equations for Rate Sensitive Plastic Materials", Quart. Appl. Math., Vol. 20, No. 4, 1963, pp. 321-332.

146. Perzyna, P., "The Study of the Dynamic Behavior of Rate Sensitive Plastic Materials", Archiwum Mechaniki Stosowanej, 1963, pp. 113-129.

147. Perzyna, P., "Fundamental Problems in Viscoplasticity", in Advances in Applied Mechanics, Vol. 9, 1966, pp. 243-377.

148. Perzyna, P., "Internal Variable Description of Plasticity", in Problems of Plasticity, Noordhoff, Leyden, 1972, pp. 145-176.

149. Perzyna, P., "The Constitutive Equations Describing Thermomechanical Behaviour of Materials at High Rates of Strain", in Mechanical Properties at High Rates of Strain, Proc. Conf. Mech. Prop. Mat. High Rates of Strain, Oxford, April 1974, pp. 138-153.

150. Perzyna, P., "On Material Isomorphism in Description of Dynamic Plasticity", Arch. of Mechanics, (Archiwum Mechaniki Stosowanej) Vol. 27, No. 3, 1975, pp. 473-484.

151. Perzyna, P., "Thermodynamics of a Unique Material Structure" Archives of Mechanics (Archiwum Mechaniki Stosowanej), Vol. 27, No. 5-6, 1975, pp. 791-806.

152. Perzyna, P., "Coupling of Dissipative Mechanisms of Viscoplastic Flow", Archives of Mechanics, (Archiwum Mechaniki Stosowanej), Vol. 29, No.4, 1977, pp. 607-624.

153. Campbell, J.D., Dynamic Plasticity of Metals, International Centre for Mechanical Sciences, Courses and Lectures No. 46, Springer-Verlag, 1970.

154. MacGregor, C.W. and Fisher, J.C., "Tension Tests at Constant True Strain Rates", Journal of Applied Mechanics, Vol. 12, No. 4, Dec. 1945, pp. A-217-A-227.

155. Wulf, G.L., "Dynamic Stress-Strain Measurements at Large Strains", in Mechanical Properties at High Rates of Strain, Proc. Conf. Mech. Prop. Mat. High Rates of Strain, Oxford, April 1974, pp. 48-52, 83.

156. Novozhilov, V.V., Foundations of the Nonlinear Theory of Elasticity, (translated from the 1947 Russian edition) Rochester, N.Y., Graylock Press, 1953.

157. Timoshenko, S.P. and Woinowsky-Krieger, S., Theory of Plates and Shells, McGraw Hill, 2nd Ed., 1959.

158. Sanders, J.L. Jr., "Nonlinear Theories for Thin Shells", Quart. Appl. Math. 21, 1963, pp. 21-36.

159. Mar, J.W., "Shell Structures", class notes for Courses 16.22 and 16.23, Dept. of Aeronautics and Astronautics, Massachusetts Institute of Technology, 1973.

160. Dugundji, J., "Shell Structures", class notes for Courses 16.22 and 16.23 Dept. of Aeronautics and Astronautics, Massachusetts Institute of Technology, 1973.

161. Koiter, W.T., "On the Nonlinear Theory of Thin Elastic Shells", Proceedings of the Koninklyke Nederlandse Akademie van Wetenschappen, B 69, 1966, pp. 1-54.

162. Biricikoglu, V. and Kalnins, A., "Large Elastic Deformations of Shells with the Inclusion of Transverse Normal Strain", Int. J. Solids Structures, Vol. 7, 1971, pp. 431-444.

163. McMeeking, R.M. and Rice, J.R., "Finite Element Formulations for Problems of Large Elastic-Plastic Deformation", Int. J. Solids Structures, Vol. 11, 1975, pp. 601-616.

164. John, F., "Estimates for the Derivatives of the Stresses in a Thin Shell and Interior Shell Equations", Comm. Pure and Appl. Math., Vol. 18, 1965, pp. 235-267.

165. Huffington, N.J. Jr., "Numerical Analysis of Elastoplastic Stress", U.S. Army Ballistic Research Laboratory, Aberdeen Proving Ground, Maryland, Memorandum Report No. 2006, Sept. 1969.

166. Pian, T.H.H. and Tong, P., "Basis of Finite Element Methods for Solid Continua", Int. J. Num. Methods Eng. Vol. 1, 1963, pp. 3-28.

167. Washizu, K., Variational Methods in Elasticity and Plasticity, 2nd Edition, Pergamon Press, 1974.

168. Lanczos, C., The Variational Principles of Mechanics, 4th Edition, Univ. of Toronto Press, 1974.

169. Piola, G., "Intorno alle equazioni fondamentali del movimento di corpi qualsivogliono, considerati secondo la naturale loro forma e constituzione", Mem. Mat. Fis. Soc. Ital. Modena, Vol. 24, 1848, pp. 1-186.

170. Argyris, J.H., Vaz, L.E., and Willam, K.J., "Improved Solution Methods for Inelastic Rate Problems", Computer Methods in Applied Mechanics and Engineering, Vol. 16, 1978, pp. 231-277.

171. Argyris, J.H., Dunne, P.C. and Angelopoulos, T., "Nonlinear Oscillations Using the Finite Element Technique", J. Comp. Meths. Appl. Mech. Eng., 2, 1973, pp. 203-250.

172. Key, S.W., "A Finite Element Procedure for the Large Deformation Dynamic Response of Axisymmetric Solids", J. Comp. Meths. Appl. Mech. Eng., 4, 1974, pp. 195-218.

173. Stricklin, J.A., Martinez, J.E., Tillerson, J.R., Hong, J.H., and Haisler, W.E., "Nonlinear Dynamic Analysis of Shells of Revolution by Matrix Displacement Method", NASA CR 110406. National Aeronautics and Space Administration, Washington, D.C., 1971.

174. Stricklin, J.A., Haisler, W.E., and Riesemann, W.A., "Evaluation of Solution Procedures for Material and/or Geometrically Nonlinear Structural Analysis by the Direct Stiffness Method", AIAA/ASME/SAE Structures, Structural Dynamics and Materials, 13th Conference, San Antonio, Texas, April 1972.

175. McNamara, J.F. and Marcal, P.V., "Incremental Stiffness Method for Finite Element Analysis of Nonlinear Dynamic Problems", in Numerical and Computer Methods in Structural Mechanics (Edited by S.J. Fenves), Academic Press, New York, 1973, pp. 353-376.

176. Leech, J.W., "Some Experiments with the Wave Equation", Massachusetts Institute of Technology, May 1964.

177. Wu, R. and Witmer, E.A., "Stability of the De Vogelaere Method for Timewise Numerical Integration", AIAA Journal, Vol. 11, No. 10, Oct. 1973, pp. 1432-1436.

178. Lax, P.D. and Richtmyer, R.D., "Survey of the Stability of Linear Finite Difference Equations", Communications on Pure and Applied Mathematics, Vol. 9, 1956, pp. 267-293.

179. O'Brien, G.G., Hyman, M.A. and Kaplan, S., "A Study of the Numerical Solution of Partial Differential Equations," J. Mathematics and Physics, Vol. 29, 1950, pp. 223-251.

180. Eddy, E.P., "Stability in the Numberical Solution of Initial Value Problems in Partial Differential Equations," NOLM 10232, Naval Ordnance Laboratory, White Oak, Silver Spring, Maryland, 1949.

181. Roache, P.J., "Computational Fluid Mechanics", Hermosa Publishers, Albuquerque, N.M., 1976.

182. Richtmyer, R.D., "A Survey of Difference Methods for Nonsteady Fluid Dynamics", NCAR Technical Note 63-2, Boulder, Colorado, 1963.

183. Krieg, R.D., "Unconditional Stability in Numerical Time Integration Methods", J. Appl. Mech., June 1973, pp. 417-421.

184. Morino, L., Leech, J.W. and Witmer, E.A., "Optimal Predictor-Corrector Method for Systems of Second-Order Differential Equations", AIAA Journal, Vol. 12, No. 10, Oct. 1974, pp. 1343-1347.

185. Hicks, D.L., "One-Dimensional Lagrangian Hydrodynamics and the IDLH Hydrocode", SC-RR-60-728, Sandia Laboratories, Albuquerque, New Mexico, 1969.

186. Phillips, N.A., "An Example of Non-Linear Computational Instability", Atmosphere and Sea in Motion, Rossby Memorial Volume, (B.Bolin Ed.), Rockefeller Institute Press, New York, 1959.

187. Hirt, C.W., "Heuristic Stability Theory for Finite Difference Equations", Journal of Computational Physics, Vol. 2, 1968, pp.33[illegible]

188. Gourlay, A. R. and Morris, J.L., "Finite-Difference [illegible]ds for Non-linear Hyperbolic Systems", Mathematics of Co[illegible]tion, Vol. 22, No. 101, 1968, pp. 28-39.

189. Lilly, D.K., "On the Computational Stability of Numerical Solutions of Time-Dependent Non-Linear Geophysical Fluid Dynamics Problems", U.S. Weather Bureau Monthly Weather Review, Vol. 93, No.1, 1965, pp.11-26.

190. Stricklin, J.A., Martinez, J.E., Tillerson, J.R., Hong, J.H. and Haisler, W.E., "Nonlinear Dynamic Analysis of Shells of Revolution by Matrix Displacement Method," AIAA Journal, Vol. 9, No. 4, April 1971 pp. 629-636.

191. Stricklin, J.A. et al., "Large Deflection Elastic-Plastic Dynamic Response of Stiffened Shells of Revolution", Department of Aerospace Engineering, Texas A & M University, Report 72-25, Dec. 1972.

192. Weeks, G., "Temporal Operators for Nonlinear Structural Dynamics Problems", Journal of the Engineering Mechanics Division, Proc. Amer. Soc. Civil Eng., October, 1972, pp. 1087-1104.

193. McNamara, J.F., "Solution Schemes for Problems of Nonlinear Structural Dynamics", Journal of Pressure Vessel Technology, May 1974, pp.96-102.

194. Park, K.C., "Evaluating Time Integration Methods for Nonlinear Dynamic Analysis", in Finite Element Analysis of Transient Nonlinear Structural Behavior, (Edited by T. Belytschko et al) ASME Applied Mechanics Symposia Series, AMD-14, 1975, pp.35-58.

195. Belytschko, T. and Schoeberle, D.F., "On the Unconditional Stability of an Implicit Algorithm for Nonlinear Structural Dynamics", Journal of Applied Mechanics, Dec. 1975, pp. 865-869.

196. Dahlquist, G. and Bjorck, A., Numerical Methods, translated by Ned Anderson, Prentice-Hall, New Jersey, 1975.

197. Desai, C.S. and Abel, J., Introduction to the Finite Element Method, Von Nostrand Reinhold Company, 1972.

198. Stricklin, J.A. and Haisler, W.E., "Formulations and Solution Procedures for Nonlinear Structural Analysis", Computers & Structures, Vol. 7, pp. 125-136, Feb. 1977.

199. Bushnell, D., "A Subincremental Strategy for olving roblems nvolving Large Deflections, Plasticity and Creep", in "Constitutive Equations in Viscoplasticity: Computational and Engineering Aspects", AMD Vol. 20, 1976, pp. 171-199.

200. Bathe, K.J., "Static and Dynamic Geometric and Material Nonlinear Analysis Using ADINA", Report 82448-2, Acoustics and Vibrations Laboratory, Department of Mechanical Engineering, MIT, May 1977.

201. Ting, T.C.T., "The Plastic Deformation of a Cantilever Beam with Strain Rate Sensitivity under Impulsive Loading", Brown University TR 70, Contract Monr-562(10), July 1961.

202. Bodner, S.R. and Symonds, P.S., "Experimental and Theoretical Investigation of the Plastic Deformation of Cantilever Beams Subjected to Impulsive Loading", Journal of Applied Mechanics, December, 1962, pp. 719-728.

203. Bathe, K.J. and Cimento, A.P., "Some Practical Procedures for the Solution of Nonlinear Finite Element Equations", J. Computer Meth. in Appl. Mech. and Eng., in press.

204. Matthies, H. and Strang, G., "The Solution of Nonlinear Finite Element Equations", Int. J. Num. Meth. in Eng., Vol. 14, 1979, pp. 1613-1626.

205. Newmark, N.M., "A Method of Computation for Structural Dynamics", Journal of the Eng. Mech. Div., Proc. Am. Soc. Civ. Eng., Vol. 85, July 1959, pp. 67-94.

206. Houbolt, J.C., "A Recurrence Matrix Solution for the Dynamic Response of Elastic Aircraft", Journal of the Aero. Sciences, Vol. 17, 1950, pp. 540-550.

207. Clark, E.N., Schmitt, F.H. and Nicolaides, S., "Plastic Deformation of Structures, II. Plastic Deformation of Rings", FDL-TDR 64-64 Vol. II, Eng. Sci. Lab., Picatinny Arsenal, Dover, New Jersey, March 1968.

208. Anon., "Rotor Burst Protection Program". (Study for NASA Lewis Research Center on NASA DPR-105 and NASA Interagency Agreement C-41581-B), U.S. Naval Air Propulsion Test Center, Aeronautical Engine Dept. Progress Reports Sept. 1969-Jan. 1977.

209. Private communications from G.J. Mangano, R. DeLucia and J. Salvino, U.S. Naval Air Propulsion Test Center, Philadelphia, Pennsylvania, 1975-76.

210. Mangano, G.J., Salvino, J.T. and DeLucia, R.A., "Rotor Burst Protection Program -- Experimentation to Provide Guidelines for the Design of Turbine Rotor Burst Fragment Containment Rings", Proceedings of the Workshop on An Assessment of Technology for Turbojet Engine Rotor Failures, NASA CP-2017, 1977, pp. 107-149.

211. Spilker, R.L. and Witmer, E.A., "Theoretical and Experimental Studies of the Nonlinear Transient Responses of Plates Subjected to Fragment Impact", Paper presented at the Fourth International Conference on Structural Mechanics in Reactor Technology, San Francisco, Calif., 15-19, August 1977.

212. Epstein, M. and Murray, D.W., "Large Deformation In-Plane Analysis of Elastic Beams", Computers and Structures, Vol. 6, 1976, pp. 1-9.

213. Strang, G. and Fix, G., An Analysis of the Finite Element Method, Prentice-Hall, New Jersey, 1973.

214. Rodal, J.J.A., French, S.E., Witmer, E.A. and Stagliano, T.R., "Instructions for the Use of the CIVM-JET 4C Finite-Strain Computer Code to Calculate the Transient Responses of Partial and/or Complete Arbitrarily-Curved Rings Subjected to Fragment Impact", MIT ASRL MR 154-1, December 1979. (Available as NASA CR-159873.)

215. Dennis, J.E. and Moré, J., "Quasi-Newton Methods: Motivation and Theory", SIAM Rev. 19, 1977, pp. 46-89.

216. Bell, J.F., The Experimental Foundations of Solid Mechanics, Handbuch der Physik, Volume VI 2/1, Springer Verlag, Berlin, 1973.

217. Bridgman, P.W., "The Stress Distribution at the Neck of a Tension Specimen", Trans. ASM, Vol. 32, 1944, p. 553.

218. Lubahn, J.D. and Felgar, R.P., Plasticity and Creep of Metals, John Wiley, 1961, pp. 114-127.

219. Norris, D., Moran, B., Scudder, J. and Quiñones, D., "A Computer Simulation of the Tension Test", Journal of the Mechanics and Physics of Solids, Vol. 26, 1978, pp. 1-19.

220. Saje, M., "Necking of a Cylindrical Bar in Tension", Int. Journal of Solids and Structures, Vol. 15, 1979, pp. 731-742.

221. Hutchinson, J.W., "Survey of Some Recent Work on the Mechanics of Necking", Proceedings of the Eight U.S. National Congress of Applied Mechanics, Los Angeles, June 26-30, 1978, Editor: R.E. Kelly, Western Periodicals Co., North Hollywood, 1979.

TABLE 1

COMPARISON OF NOTATIONS EMPLOYED IN DIFFERENT BOOKS AND PAPERS

THIS WORK	TRUESDELL & TOUPIN (Ref. 7)	TRUESDELL & NOLL (Ref.40)	MALVERN (Ref.50)	JAUNZEMIS (Ref.51)	GREEN & ZERNA (Ref.56)	SEDOV (Ref.41)	ERINGEN (Ref.53)	FUNG (Ref.60)	PRAGER (Ref. 59)	HILL (Ref 112-113, 125-131)
$\overline{\overline{D}}$	$\mathbf{d}$ (348)	$\mathbf{D}$ (54)	$\mathbf{D}$ (147)	$\mathbf{D}$ (158)	—	$\mathfrak{E}$ (97)	—	—	—	$\boldsymbol{\epsilon}$
D^{I}_{J}	d^{i}_{j} (348)	D^{i}_{j} (56)	—	—	—	e^{i}_{j} (97)	d^{i}_{j} (70)	—	—	ϵ^{i}_{j}
$\hat{D}_{IJ}$	d_{ij} (348)	D_{ij} (56)	D_{ij} (147)	D_{ij} (158)	d_{ij} (55)	—	d_{ij} (70)	V_{ij} (142)	V_{ij} (64)	ϵ_{ij}
$\overline{\overline{\gamma}}$	$\mathbf{E}$ (266)	$\mathbf{E}$ (221)	$\mathbf{E}$ (158)	—	—	$\mathring{\boldsymbol{\mathcal{E}}}$ (85)	—	—	—	E
γ^{i}_{j}	E^{I}_{J} (267)	E^{I}_{J}	—	—	γ^{i}_{j} (57)	ε^{i}_{j} (85)	E^{I}_{J} (15)	E^{i}_{j} (92)	—	e^{i}_{j}
$\hat{\gamma}_{ij}$	E_{IJ} (267)	E_{IJ}	E_{IJ} (158)	—	e_{ij} (73)	—	E_{IJ} (13)	E_{ij} (93)	$\overline{U}_{ij}$ (194)	e_{ij}
$\overline{\overline{e}}$	$\mathbf{e}$ (266)	—	$\mathbf{E}^{*}$ (158)	—	—	$\hat{\boldsymbol{\mathcal{E}}}$ (85)	—	—	—	F
e^{I}_{J}	e^{i}_{j} (267)	—	—	—	—	ε^{i}_{j} (85)	e^{i}_{j} (15)	e^{i}_{j} (92)	—	e^{i}_{j}
$\hat{e}_{IJ}$	e_{ij} (267)	—	E^{*}_{ij} (158)	—	—	—	e_{ij} (13)	e_{ij} (93)	U_{ij} (190)	—
$\overline{T}$	$\mathbf{t}_{(n)}$ (537)	$\mathbf{t}_{(n)}$ (40)	$\mathbf{t}$ (65)	$\mathbf{t}_{(n)}$ (205)	$\mathbf{t}$ (58)	$\mathbf{P}_{(n)}$ (121)	$\mathbf{t}_{(n)}$ (97)	$\dot{\mathbf{T}}$ (59)	$\mathbf{T}^{(\nu)}$ (44)	$\mathbf{t}$
$\overline{\overline{\sigma}}$	$\mathbf{t}$ (542)	$\mathbf{T}$ (40)	$\mathbf{T}$ (71)	$\mathbf{T}$ (212)	—	$\mathbf{P}$ (125)	—	—	—	$\boldsymbol{\sigma}$

TABLE 1--CONCLUDED

COMPARISON OF NOTATIONS EMPLOYED IN DIFFERENT BOOKS AND PAPERS										
THIS WORK	TRUESDELL & TOUPIN (Ref. 7)	TRUESDELL & NOLL (Ref.40)	MALVERN (Ref.50)	JAUNZEMIS (Ref.51)	GREEN & ZERNA (Ref.56)	SEDOV (Ref.41)	ERINGEN (Ref.53)	FUNG (Ref.60)	PRAGER (Ref.59)	HILL (Ref 112-113, 125-131)
σ^I_J	t^i_j (542)	T^i_j (40)	—	—	τ^i_j (60)	P^i_j (125)	t^i_j (99)	τ^i_j (82)	—	σ^i_j
$\hat{\sigma}_{IJ}$	t_{ij} (542)	T_{ij} (40)	T_{ij} (72)	T_{ij} (207)	σ_{ij} (68)	—	t_{ij} (99)	σ_{ij} (58)	T_{ij} (200)	σ_{ij}
$\overline{\overline{\overline{\tau}}}$	—	—	—	—	—	$\rho_0 \boldsymbol{\sigma}$ (22c)	—	—	—	$\boldsymbol{\tau}$
τ^I_J	—	—	—	—	s^i_j (65)	$\rho_0 \sigma^i_j$ (22c)	—	—	—	τ^i_j
$\hat{\tau}_{IJ}$	—	—	—	—	—	--	—	—	—	τ_{ij}
$\overline{\overline{\overline{S}}}$	—	$\tilde{\mathbf{T}}$ (124)	$\tilde{\mathbf{T}}$ (222)	—	—	$\frac{\rho_0}{\rho}\mathring{\mathbf{P}}$ (125)	—	—	—	—
S^i_j	T^I_J (554)	$\tilde{T}^I_J$ (124)	—	—	—	$\frac{\rho_0}{\rho}\mathring{P}^i_j$ (125)	T^I_J (109)	—	—	—
$\hat{S}_{ij}$	T_{IJ} (554)	$\tilde{T}_{IJ}$ (124)	$\tilde{T}_{IJ}$ (223)	—	—	—	T_{IJ} (109)	S_{ij} (438)	$\bar{S}_{ij}$ (200)	—
$\overline{\overline{\overline{T}}}$	—	$\mathbf{T}^T_R$ (124)	$\mathbf{T}^{\circ}$ (222)	$\tilde{\mathbf{T}}$ (360)	—	—	—	—	—	$\mathbf{S}$
$T^{i\cdot}_{\cdot J}$	$T^{T\,I\cdot}_{\cdot j}$ (553)	$T^{T\,I\cdot}_{R\,\cdot j}$ (124)	—	—	$t^{i}_{\cdot j}$ (66)	—	$T^{T\,I\cdot}_{\cdot j}$ (109)	—	—	—
$\hat{T}_{iJ}$	T^T_{Ij} (553)	T^T_{RIj} (124)	T°_{Ij} (223)	$\tilde{T}_{ij}$ (360)	—	—	T^T_{Ij} (109)	T_{ij} (438)	$\bar{\bar{T}}_{ij}$ (200)	S_{ij}

TABLE 2

DATA CHARACTERIZING NAPTC TEST 201 FOR T58 TURBINE ROTOR TRI-HUB BURST AGAINST A STEEL CONTAINMENT RING

Containment Ring Data

Inside Diameter (in)	15.00
Radial Thickness (in)	0.625
Axial Length (in)	1.50
Material	4130 cast steel
Elastic Modulus (psi)	29×10^6
4130 Cast Steel	

Fragment Data*

Type T58 Tri-Hub Bladed Disk Fragments
Material Disk: A-286 Blades: SEL-15

Outer Radius (in)	7.00
Fragment Centroid from Rotor Axis (in)	2.797
Fragment Pre-Test Tip Clearance from Ring (in)	0.50
Fragment CG to Blade Tip Distance (in)	4.203
Fragment Weight Each (lbs)	3.627
Fragment Mass Moment of Inertia about its CG (in lb sec^2)	666×10^{-4}
Rotor Burst Speed (rpm)	19,859
Fragment Tip Velocity (ips)	14,557.2
Fragment CG Velocity (ips)	5816.7
Fragment Initial Angular Velocity (rad/sec)	2079.6
Fragment Translational KE (in-lb)	
Each Fragment	158,922
Total for Three Fragments	476,766
Fragment Rotational KE (in lb)	
Each Fragment	144,018
Total for Three Fragments	432,054

*Applies to each fragment unless specified otherwise.

TABLE 3

EL-SH PREDICTED UPPER-SURFACE γ_1^1 STRAINS AT NODAL STATIONS ALONG y=0 AND PRINCIPAL STRAINS AT SELECTED ELEMENT-CENTER LOCATIONS OF PANEL CP-2

	UPPER-SURFACE γ_1^1 STRAIN (PER CENT)											
Node	1	2	3	4	5	6	7	8	9	0	11	12
Loc., x(in)	0	.222	.444	.666	.888	1.111	1.486	1.861	2.486	3.111	3.555	4.000
Time (μsec)												
20	.43	.19	2.48	7.75	19.77	-11.5	.27	1.45	.26	.29	.22	.20
40	2.24	4.67	11.02	16.21	17.16	1.65	.73	1.33	.94	.17	.18	.17
60	14.52	19.97	20.15	15.90	21.93	20.73	2.81	1.00	1.34	.43	.11	.23
80	20.89	22.49	18.04	14.08	22.32	29.93	13.81	1.38	.14	.55	.33	-.06
100	20.82	22.70	17.21	12.75	21.45	30.81	21.01	1.94	.20	.37	.47	-.23
120	20.76	22.69	17.27	12.74	20.40	28.29	17.27	5.03	1.57	.17	.07	.61
140	20.75	22.69	17.43	12.72	20.67	24.56	16.92	9.47	2.17	-.12	-.56	1.32
160	20.78	22.65	17.57	12.83	20.89	22.16	17.58	11.31	3.52	-.31	-.23	1.14
180	20.75	22.68	17.63	12.82	20.78	22.05	16.31	11.18	5.28	-.13	-.07	.53
200	20.76	22.67	17.57	12.93	20.87	22.21	15.44	13.21	5.17	.41	-.35	.21
220	20.76	22.66	17.67	13.01	21.00	22.38	16.37	15.66	5.34	.63	-.09	-.89
240	20.75	22.64	17.66	13.08	21.06	22.55	16.18	17.28	6.59	.84	.33	-2.46
260	20.74	22.63	17.71	13.13	21.10	22.55	15.67	17.24	7.81	.96	.37	-3.84
280	20.73	22.64	17.72	13.18	21.16	22.60	15.44	15.66	9.25	1.01	.47	-4.92
300	20.73	22.64	17.74	13.21	21.19	22.76	15.62	15.25	11.30	1.11	.84	-6.06
350	20.73	22.63	17.82	13.37	21.38	23.15	15.84	17.84	16.69	2.83	1.99	-6.56
400	20.71	22.63	17.89	13.45	21.45	23.46	16.44	21.57	23.83	8.32	1.99	-6.18
450	20.71	22.64	17.96	13.60	21.57	23.84	17.11	24.01	28.32	14.41	3.49	-6.09
500	20.70	22.64	18.05	13.63	21.73	24.08	17.86	25.83	32.46	19.30	4.41	-5.96
550	20.72	22.65	18.17	13.65	21.98	24.17	18.82	27.73	36.63	22.77	5.38	-5.85
600	20.71	22.64	18.26	13.56	22.14	24.22	19.33	31.24	41.16	25.35	6.06	-5.79

TABLE 3 -- CONCLUDED (EL-SH)

Element	UPPER-SURFACE PRINCIPAL GREEN STRAIN (PER CENT)					
	1	2	3	4	5	6
Center Loc., x(in)	.111	.333	.555	.777	.999	1.298
Time (μsec)						
20	.35	1.01	5.15	10.29	34.50	.12
40	3.92	7.93	12.10	21.16	35.54	10.06
60	16.73	20.94	24.61	23.24	37.02	10.81
80	21.06	26.21	23.57	22.16	37.17	11.02
100	21.13	26.12	23.17	21.40	36.99	11.44
120	21.11	26.05	23.24	21.28	36.12	10.93
140	21.08	26.11	23.35	21.43	35.18	10.94
160	21.07	26.15	23.38	21.56	34.96	10.60
180	21.06	26.20	23.42	21.52	34.58	10.27
200	21.06	26.20	23.37	21.48	34.63	10.04
220	21.06	26.22	23.42	21.57	34.69	10.17
240	21.05	26.18	23.36	21.52	34.72	10.25
260	21.05	26.18	23.37	21.50	34.66	10.22
280	21.05	26.18	23.38	21.49	34.64	10.18
300	21.06	26.20	23.37	21.46	34.63	10.20
350	21.07	26.20	23.37	21.47	34.68	10.27
400	21.08	26.20	23.38	21.44	34.65	10.29
450	21.08	26.21	23.38	21.43	34.68	10.34
500	21.09	26.23	23.41	21.47	34.74	10.42
550	21.09	26.26	23.43	21.56	34.79	10.61
600	21.10	26.26	23.42	21.57	34.82	10.71

TABLE 4

EL-SH-SR PREDICTED UPPER-SURFACE γ_1^1 STRAINS AT NODAL STATIONS ALONG y=0 AND PRINCIPAL STRAINS AT SELECTED ELEMENT-CENTER LOCATIONS OF PANEL CP-2

	UPPER-SURFACE γ_1^1 STRAIN (PER CENT)											
Node	1	2	3	4	5	6	7	8	9	10	11	12
Loc., x(in)	0	.222	.444	.666	.888	1.111	1.486	1.861	2.486	3.111	3.555	4.000
Time (μsec)												
20	.79	.98	4.19	6.89	8.55	1.37	.21	2.27	.51	.48	.46	.44
40	9.68	11.20	10.81	8.88	9.68	14.08	3.15	.59	1.77	.35	.24	.26
60	15.50	13.64	8.96	7.88	8.18	28.48	10.15	1.98	.83	.70	.13	.10
80	15.66	14.44	8.10	5.62	7.36	27.52	12.14	3.97	.31	.41	.56	-.31
100	15.37	14.26	8.54	6.20	7.50	24.01	13.69	8.21	.32	-.41	.34	.40
120	15.33	14.18	8.77	6.30	7.93	23.23	15.31	11.25	-.36	-.36	-.82	1.74
140	15.43	14.29	8.47	5.68	7.81	24.45	14.83	12.23	.20	-.55	-.92	1.48
160	15.39	14.26	8.56	6.07	8.22	24.69	16.04	12.18	.95	-.56	-.23	.20
180	15.38	14.36	8.70	6.03	8.16	24.98	17.50	12.27	1.86	.50	-.55	-.47
200	15.40	14.18	8.48	5.82	8.09	24.87	17.70	13.35	2.21	.82	.34	-2.68
220	15.43	14.32	8.67	5.82	7.97	26.16	19.15	14.85	2.53	.83	1.37	-5.19
240	15.39	14.19	8.60	5.96	8.18	26.20	20.78	17.52	2.83	1.41	1.04	-5.52
260	15.40	14.22	8.50	5.62	7.80	26.69	21.73	20.35	3.90	1.98	.90	-5.65
280	15.39	14.24	8.55	5.64	7.74	26.52	23.51	22.72	5.81	2.58	.91	-5.97
300	15.40	14.23	8.55	5.72	7.84	26.88	24.84	24.95	8.06	3.34	.80	-5.86

TABLE 4 -- CONCLUDED (EL-SH-SR)

Element	UPPER-SURFACE PRINCIPAL GREEN STRAIN (PER CENT)					
	1	2	3	4	5	6
Center Loc., x(in)	.111	.333	.555	.777	.999	1.298
Time (μsec)						
20	.89	3.00	6.12	6.88	4.90	1.39
40	10.28	10.93	10.5[illegible]	8.98	6.30	4.69
60	13.87	12.73	10.03	7.65	8.44	5.99
80	14.27	12.90	9.44	7.27	8.60	6.25
100	14.07	12.86	9.77	7.37	7.41	6.78
120	14.01	12.91	9.92	7.50	7.04	7.25
140	14.13	12.87	9.59	7.30	7.39	7.22
160	14.08	12.90	9.77	7.50	7.28	7.36
180	14.14	13.00	9.88	7.45	7.23	7.56
200	14.05	12.82	9.63	7.44	7.49	7.61
220	14.15	12.97	9.76	7.42	7.55	7.94
240	14.05	12.87	9.74	7.51	7.49	8.24
260	14.09	12.84	9.59	7.35	7.66	8.38
280	14.11	12.88	9.63	7.34	7.59	8.66
300	14.11	12.87	[illegible].65	7.39	7.59	8.81

TABLE 5

FINITE-STRAIN PREDICTION OF THE MAXIMUM PRINCIPAL STRAINS AND ASSOCIATED DIRECTIONS ON THE UPPER SURFACE AT THE CENTER OF CERTAIN ELEMENTS OF EXPLOSIVELY-IMPULSED 6061-T651 THIN ALUMINUM PANEL CP-2

Element				Principal Green Strain			
				EL-SH		EL-SH-SR	
No.	Center Location x(in)	y(in)	θ (deg)	Value (in/in)	Orient. θ_p (deg)	Value (in/in)	Orient. θ_p (deg)
1	.111	.111	45.00	.2113	45.08	.1427	45.00
2	.333	"	18.43	.2626	13.86	.1300	9.91
3	.555	"	11.31	.2461	4.59	.1055	3.59
4	.777	"	8.13	.2324	1.28	.0898	2.14
5	.999	"	6.34	.3717	1.87	.0860	16.40
6	1.298	"	4.89	.1144	1.70	.0881	37.51
12	.111	.333	71.57	.2719	76.78	.1301	80.09
13	.333	"	45.00	.1910	45.00	.09[illegible]1	45.00
14	.555	"	30.96	.1611	11.06	.0899	2.87
15	.777	"	23.20	.2179	3.44	.0850	2.54
16	.999	"	18.43	.3997	5.72	.0880	28.00
17	1.298	"	14.40	.1234	26.74	.0803	-32.78
23	.111	.555	78.69	.2466	85.15	.1055	86.42
24	.333	"	59.04	.1611	78.94	.0899	87.13
25	.555	"	45.00	.1345	45.00	.0688	45.00
26	.777	"	35.54	.1776	8.72	.0828	-6.62
27	.999	"	29.05	.3798	8.09	.0864	16.95
28	1.298	"	23.17	.0722	-41.32	.0712	31.15
34	.111	.777	81.87	.2324	88.72	.0898	87.86
35	.333	"	66.80	.2179	86.56	.0850	87.46
36	.555	"	54.46	.1776	81.28	.0828	-83.38
37	.777	"	45.00	.1103	45.03	.0700	-45.00
38	.999	"	37.87	.3036	14.23	.0946	26.92
39	1.298	"	30.93	.0995	20.93	.0661	9.39
45	.111	.999	83.66	.3733	88.15	.0860	73.60
46	.333	"	71.57	.3997	84.28	.0880	62.00
47	.555	"	60.95	.3798	81.91	.0864	73.05
48	.777	"	52.13	.3035	75.77	.0946	63.11
49	.999	"	45.00	.2155	44.79	.0738	45.04
50	1.298	"	37.61	.1053	[illegible].61	.0809	31.79
56	.111	1.298	85.11	.1142	88.31	.0882	52.53
57	.333	"	75.60	.1231	63.19	.0806	-57.24
58	.555	"	66.83	.0715	-43.97	.0668	72.03
59	.777	"	59.07	.1002	68.43	.0661	80.52
60	.999	"	52.39	.1059	52.48	.0806	58.09
61	1.298	"	45.00	.0710	46.61	.0482	-44.88

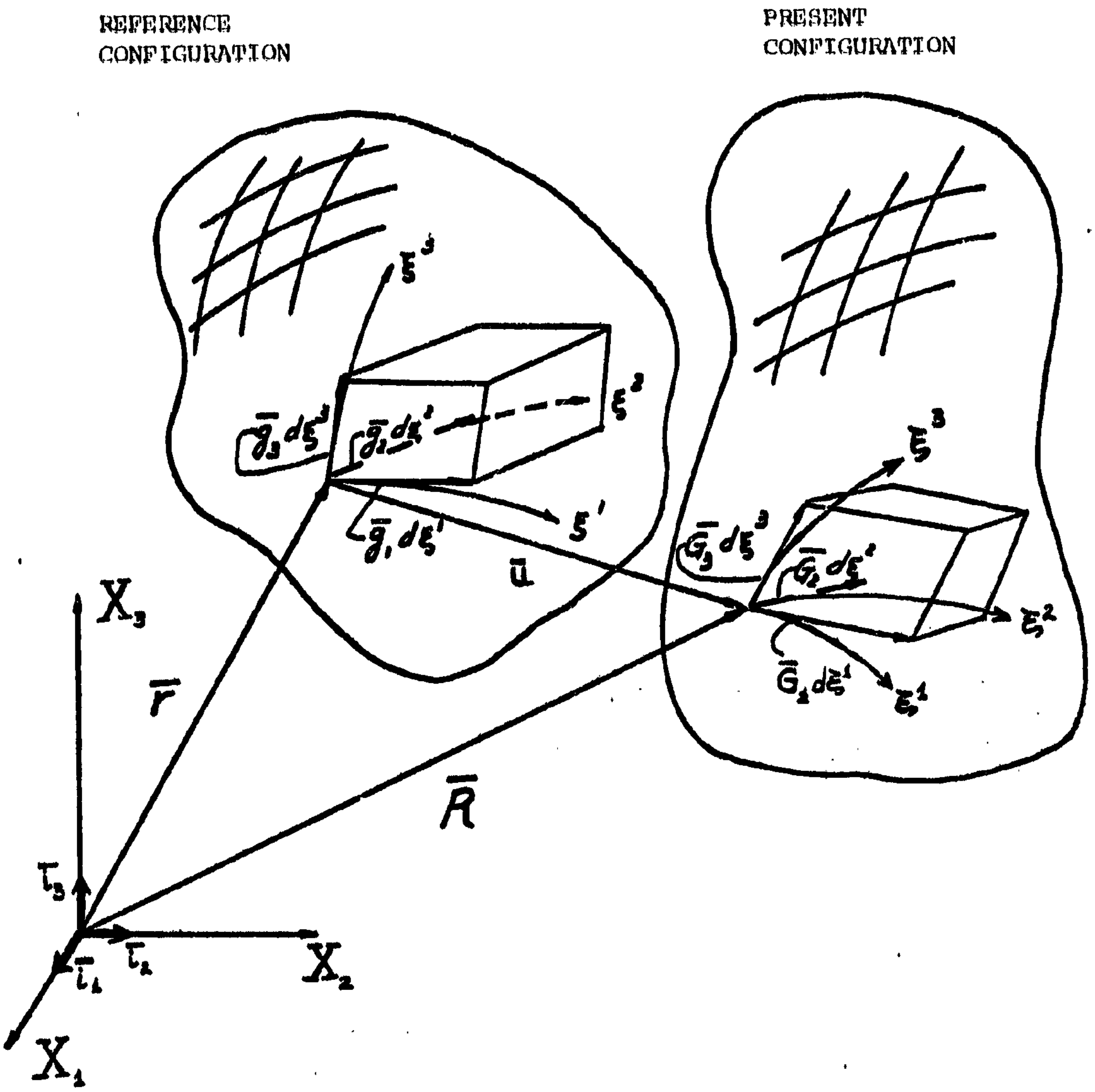

FIG.1 NOMENCLATURE FOR SPACE COORDINATES AND DEFORMATION

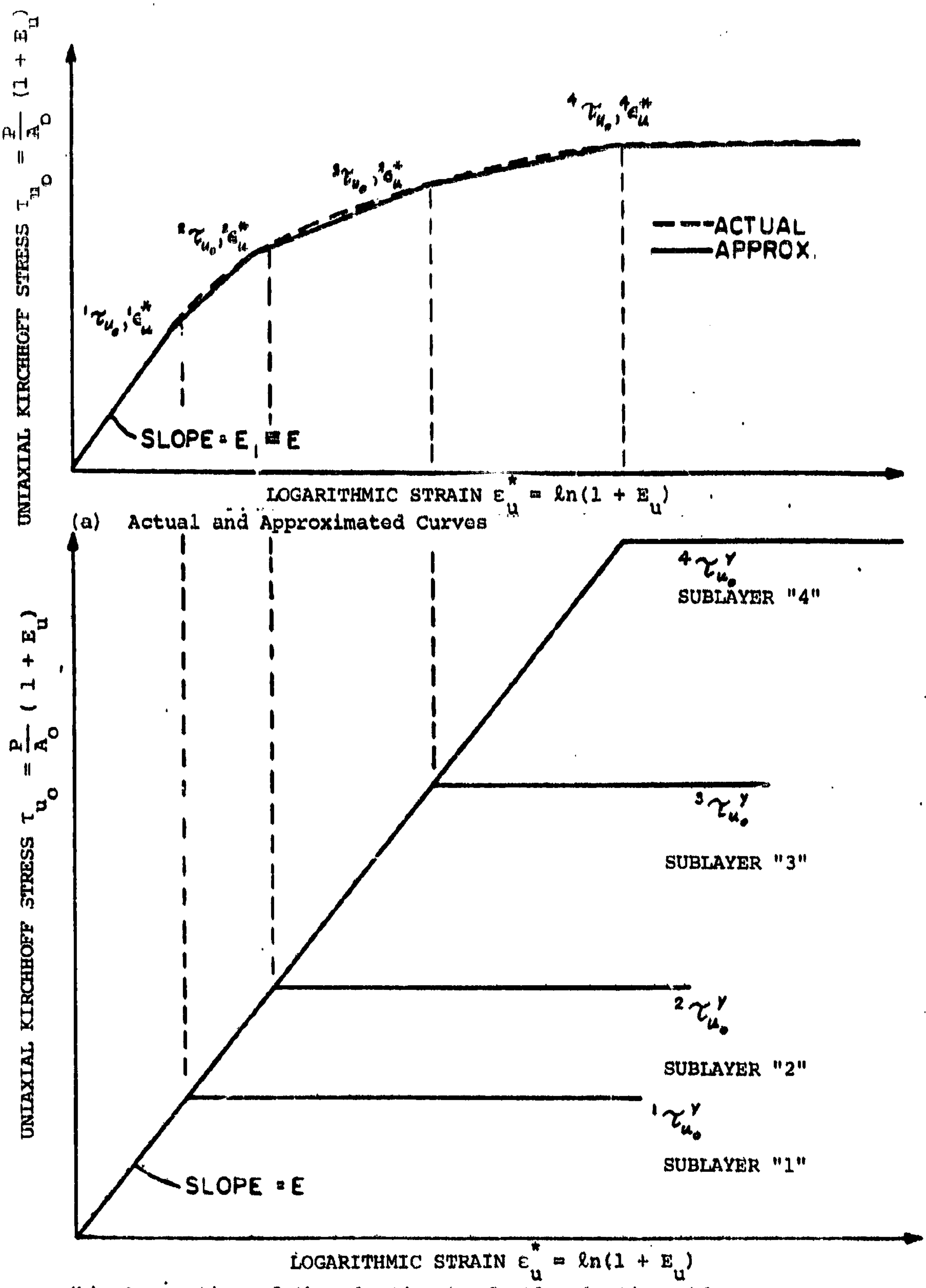

(a) Actual and Approximated Curves

(b) Properties of the Elastic, Perfectly-Plastic Sublayers

FIG. 2 APPROXIMATION OF A UNIAXIAL STRESS-STRAIN CURVE BY THE MECHANICAL-SUBLAYER MODEL

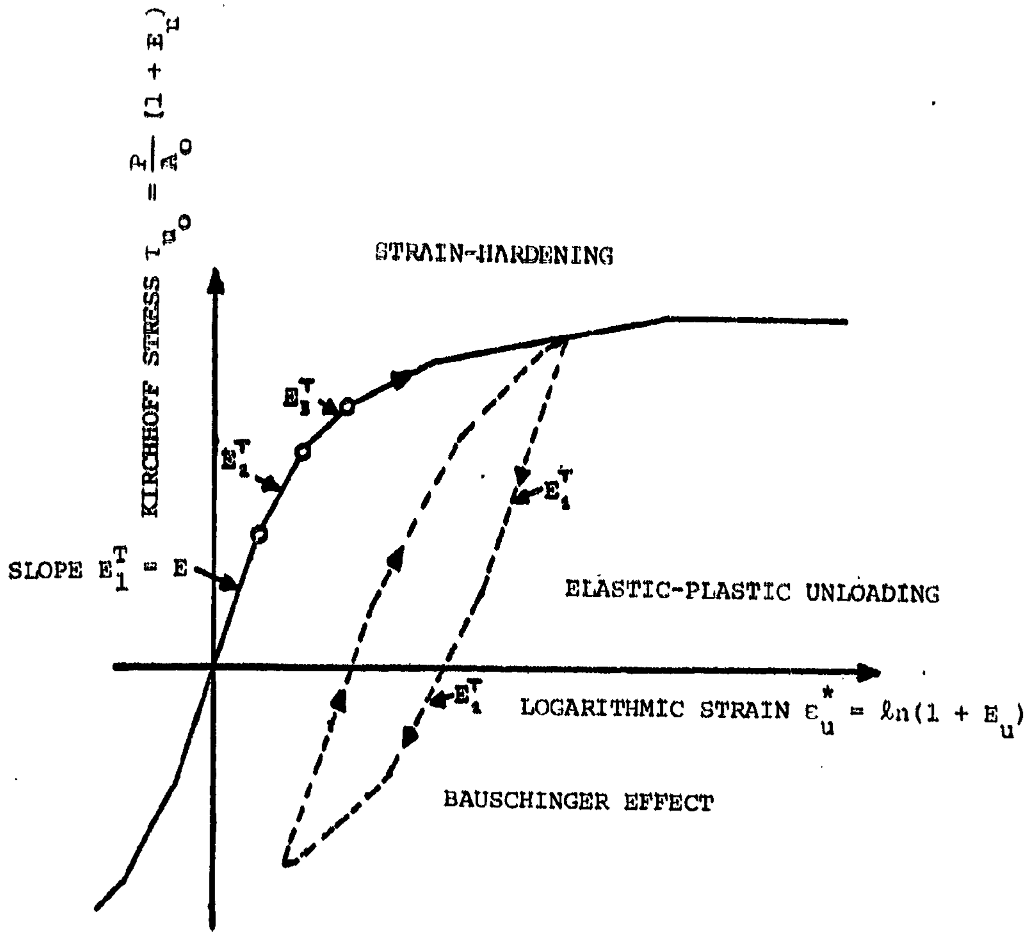

(c) Schematic of Loading, Unloading, and Reloading Paths

FIG. 2 CONCLUDED

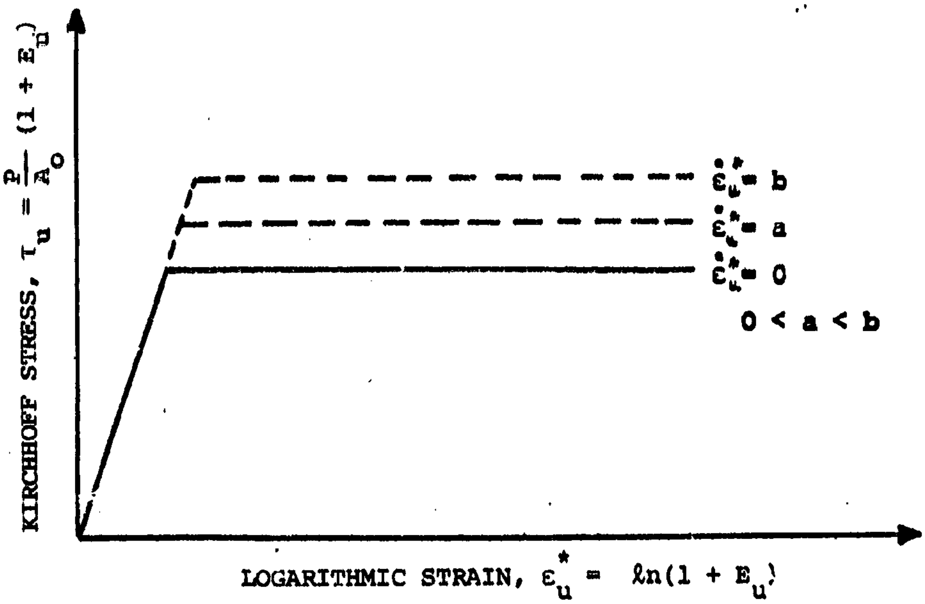

(a) Elastic, Perfectly-Plastic Material

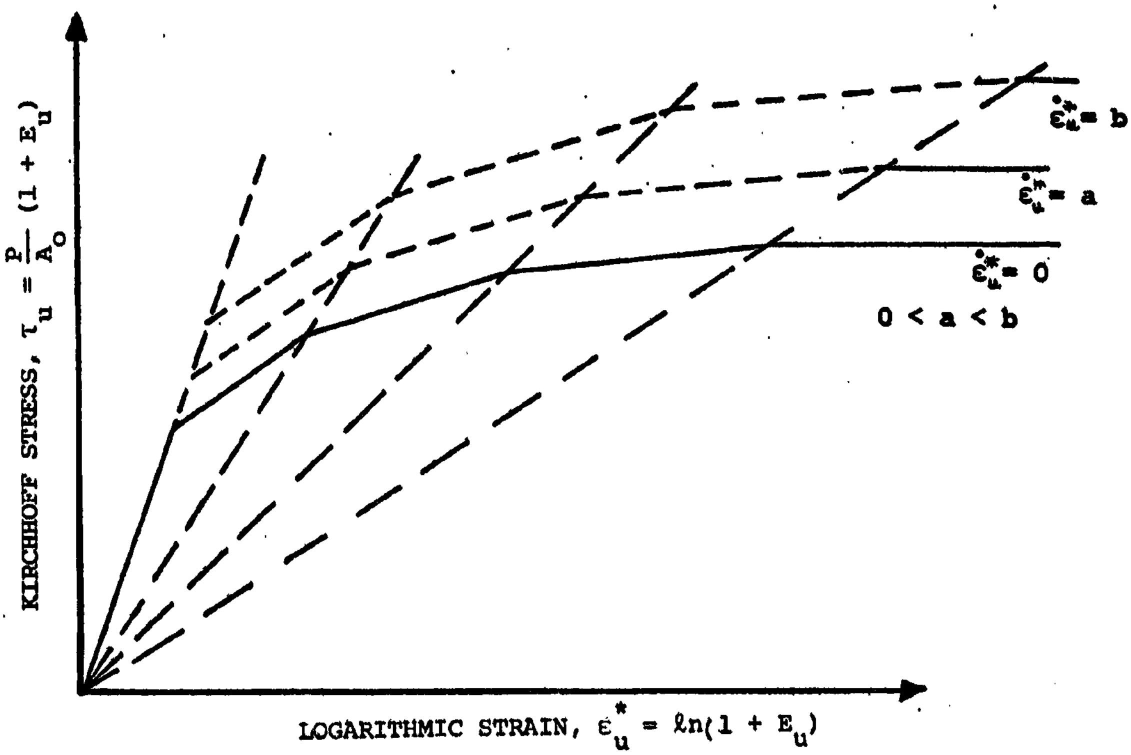

(b) Special Strain Hardening Material

FIG. 3 SCHEMATIC OF STRAIN-RATE DEPENDENT UNIAXIAL STRESS-STRAIN CURVES

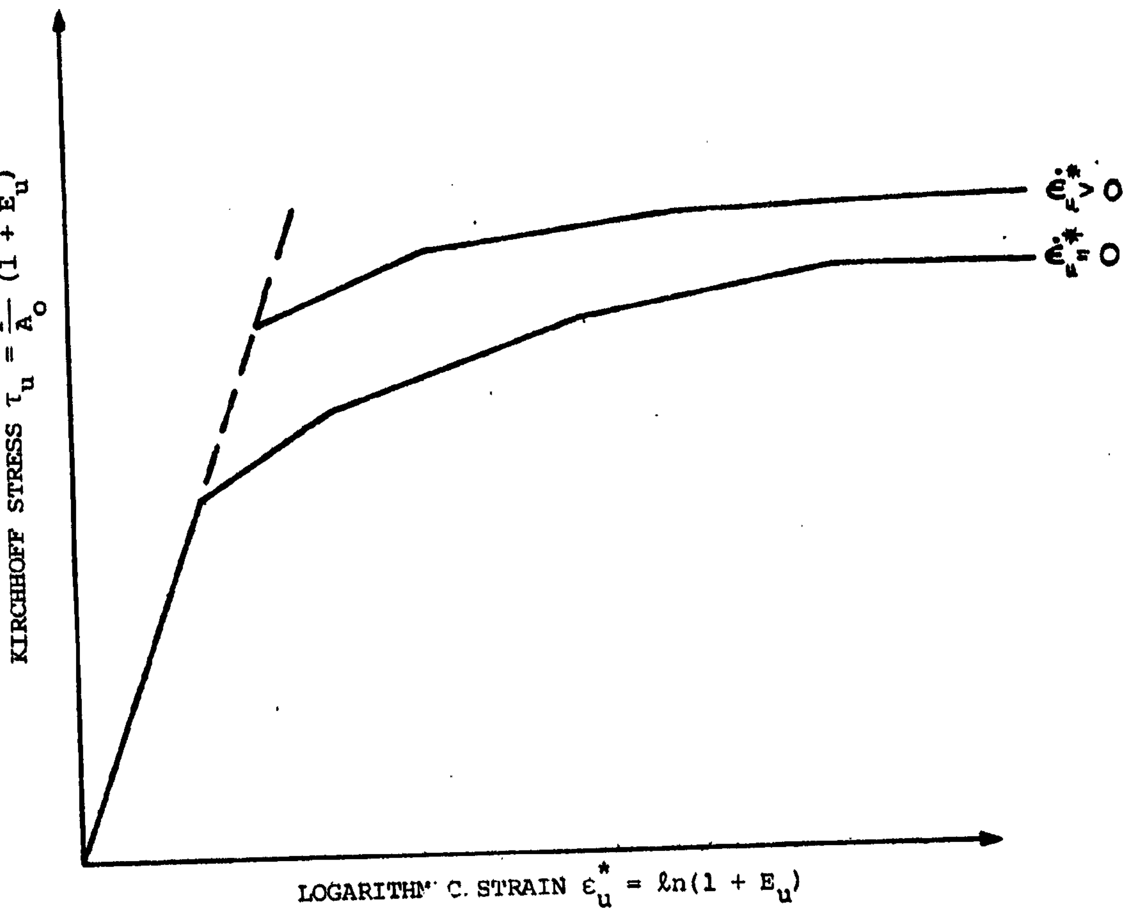

(c) More General Strain-Hardening Material

FIG. 3 CONCLUDED

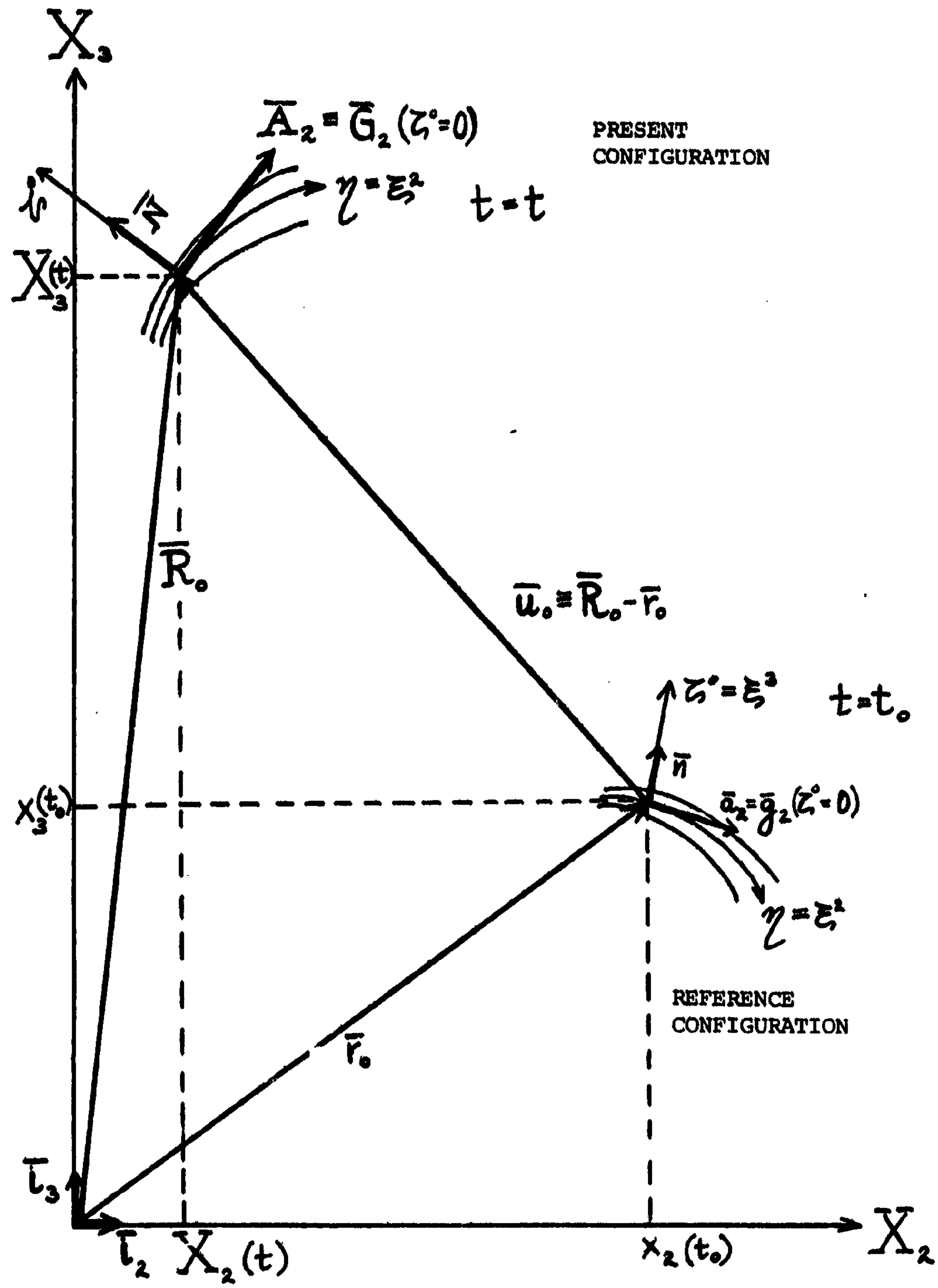

FIG. 4 ILLUSTRATION OF POSITION, DISPLACEMENT, AND BASE VECTORS FOR THE REFERENCE AND THE PRESENT CONFIGURATION

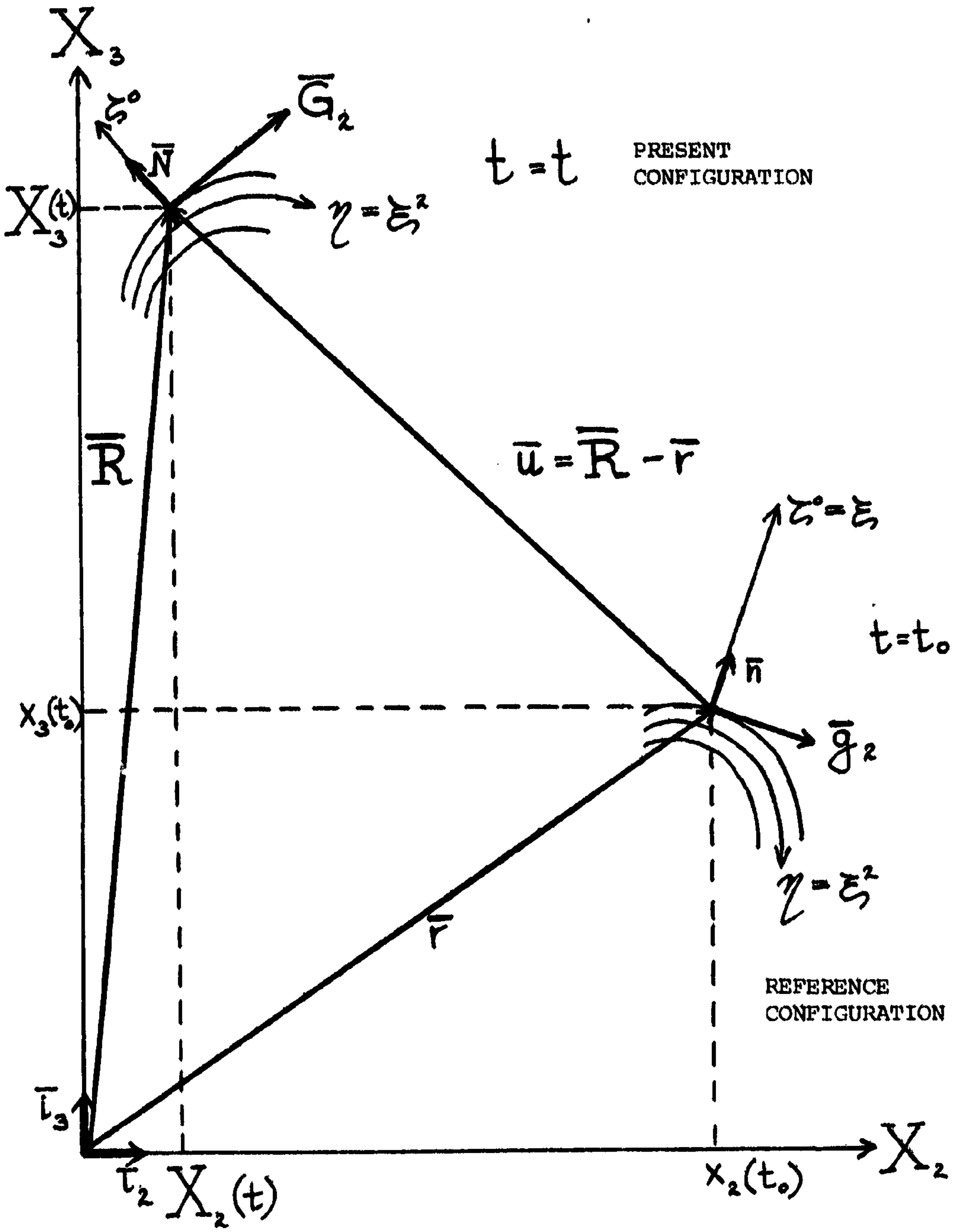

FIG. 4 CONCLUDED

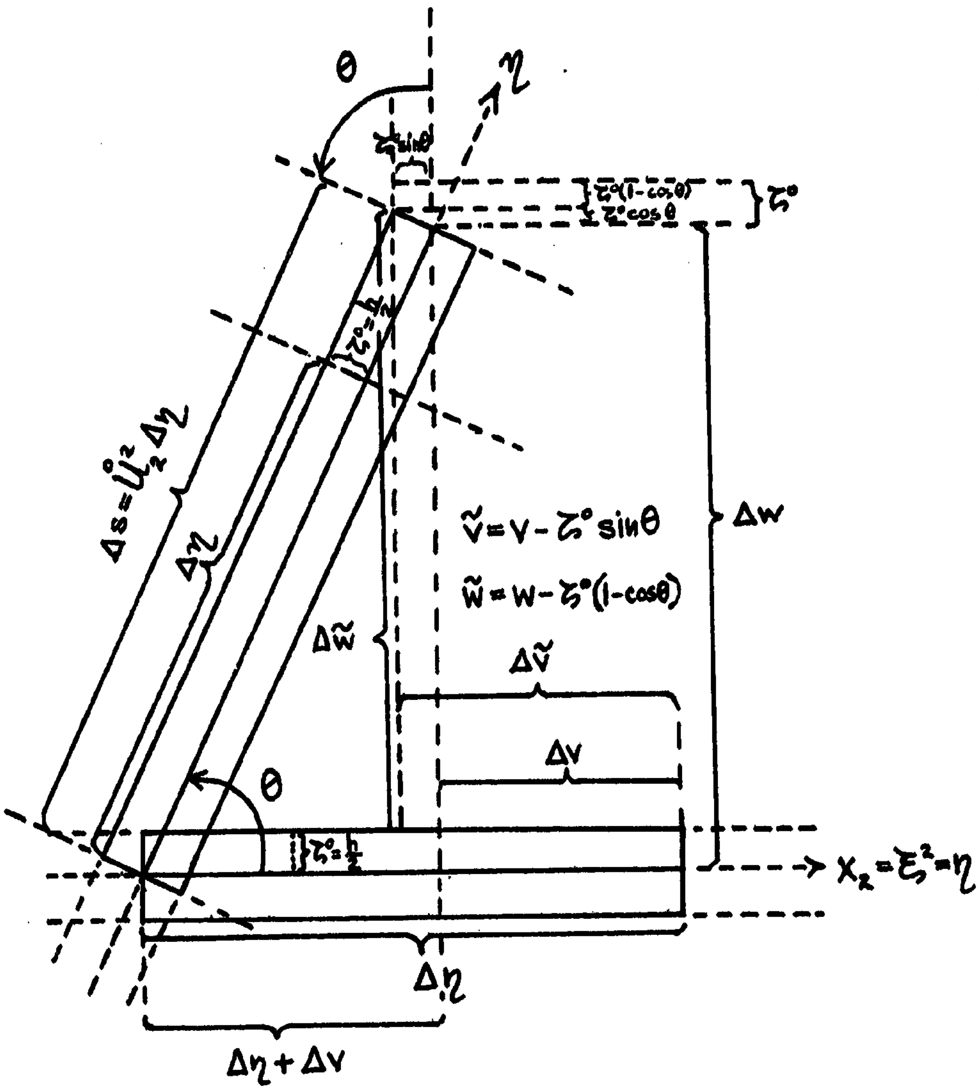

FIG. 5 BERNOULLI-EULER DISPLACEMENT FIELD AND POLAR DECOMPOSITION OF THE DISPLACEMENT GRADIENTS χ AND ψ

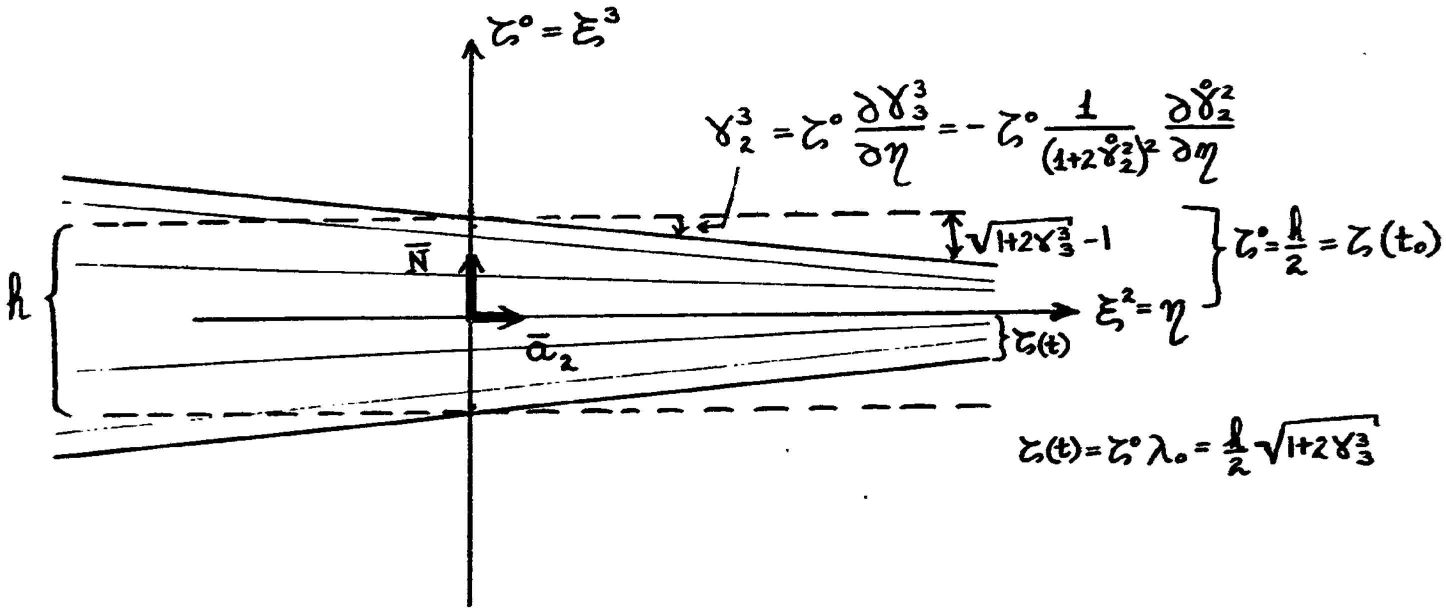

FIG. 6 ILLUSTRATION OF TRANSVERSE SHEAR STRAIN CAUSED BY TRANSVERSE NORMAL STRAIN GRADIENTS

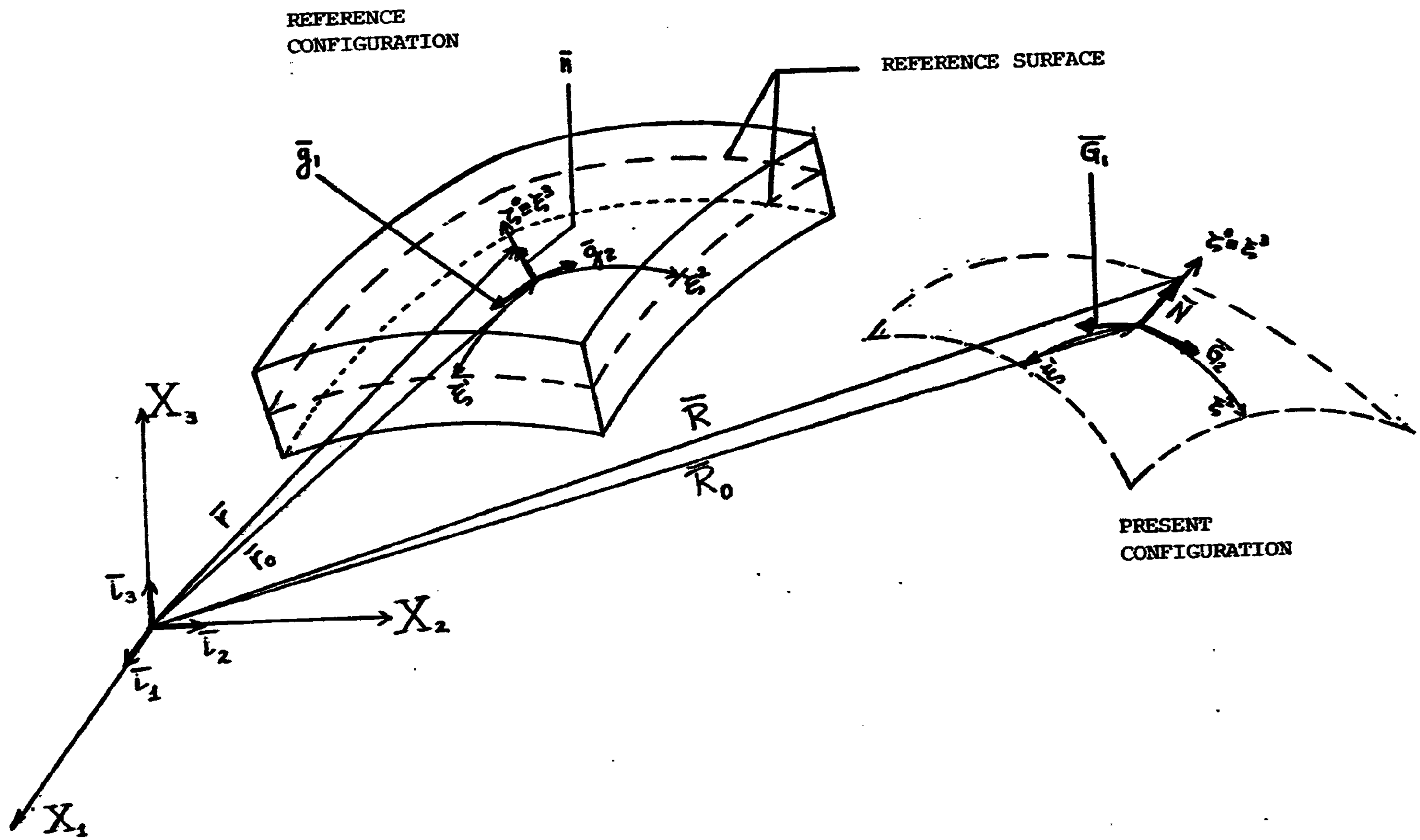

FIG. 7 NOMENCLATURE FOR SHELL GEOMETRY AND DISPLACEMENTS

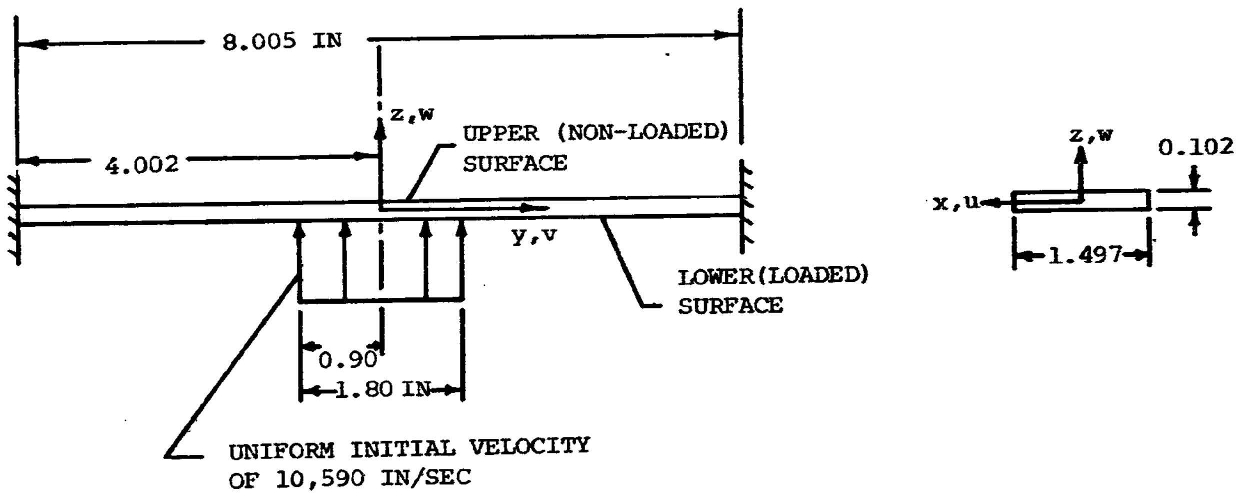

FIG. 8 SCHEMATIC OF IMPULSIVELY-LOADED 6061-T651 ALUMINUM NARROW-PLATE SPECIMEN CB-4

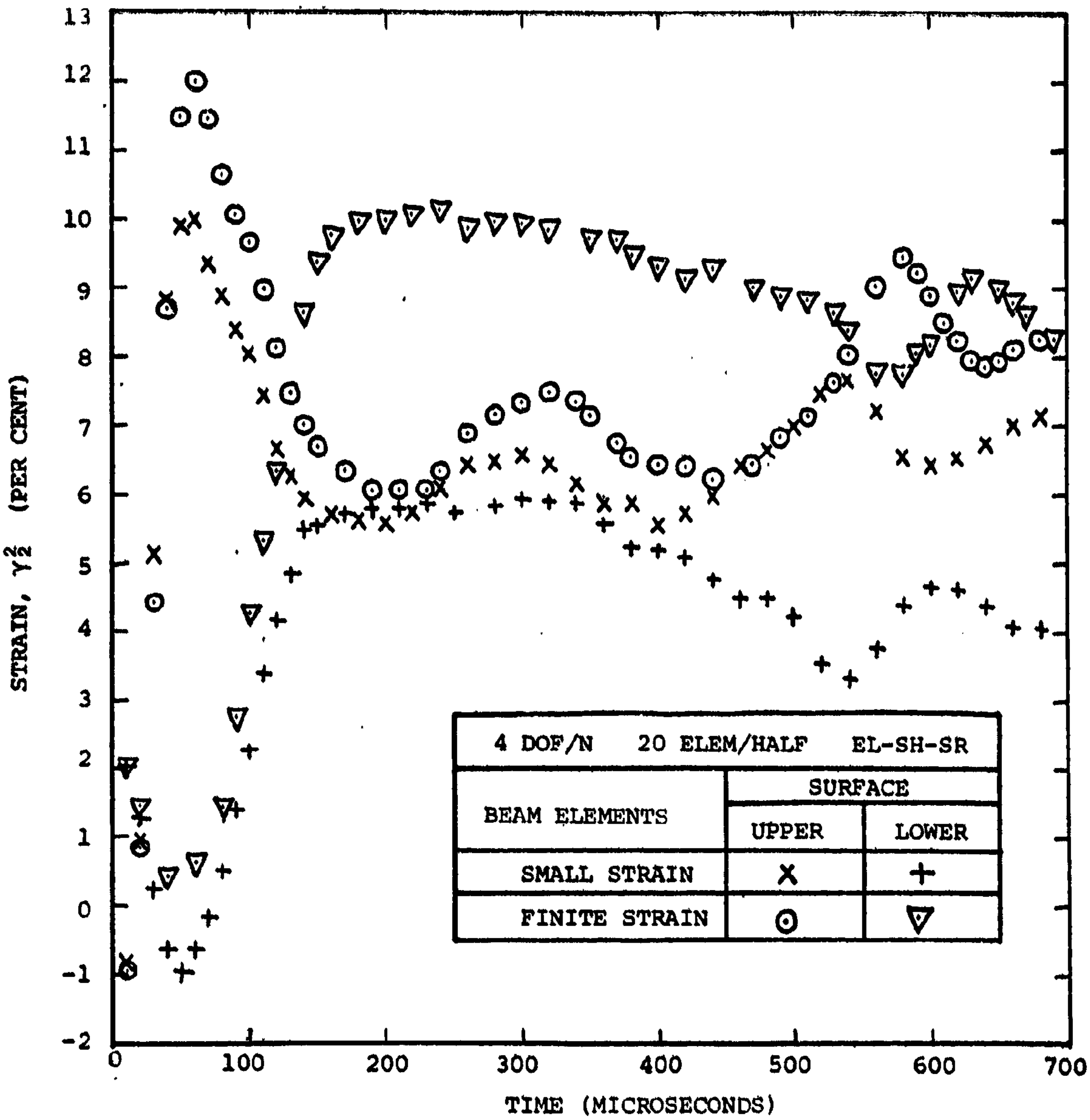

(a) Transient Strain at Station y=0

FIG. 9 MEASUREMENTS AND/OR PREDICTIONS OF TRANSIENT LONGITUDINAL GREEN (LAGRANGIAN) STRAIN ON THE SURFACE FOR VARIOUS SPANWISE STATIONS OF EXPLOSIVELY-IMPULSED 6061-T651 ALUMINUM NARROW - PLATE (BEAM) CB-4 MODELED BY BEAM ELEMENTS

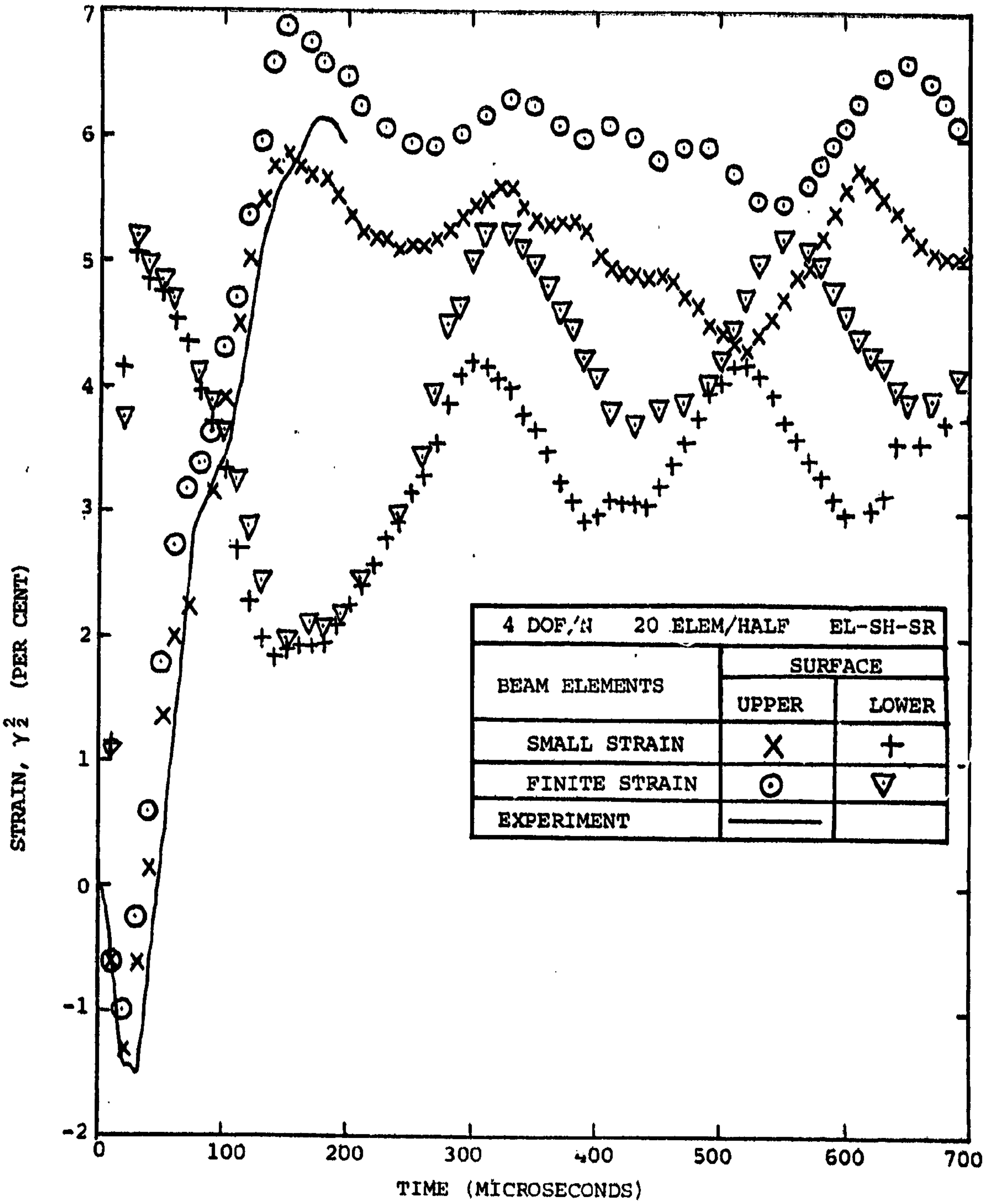

(b) Transient Strain at Station Y=1.40 in

FIG. 9 CONTINUED (CB-4)

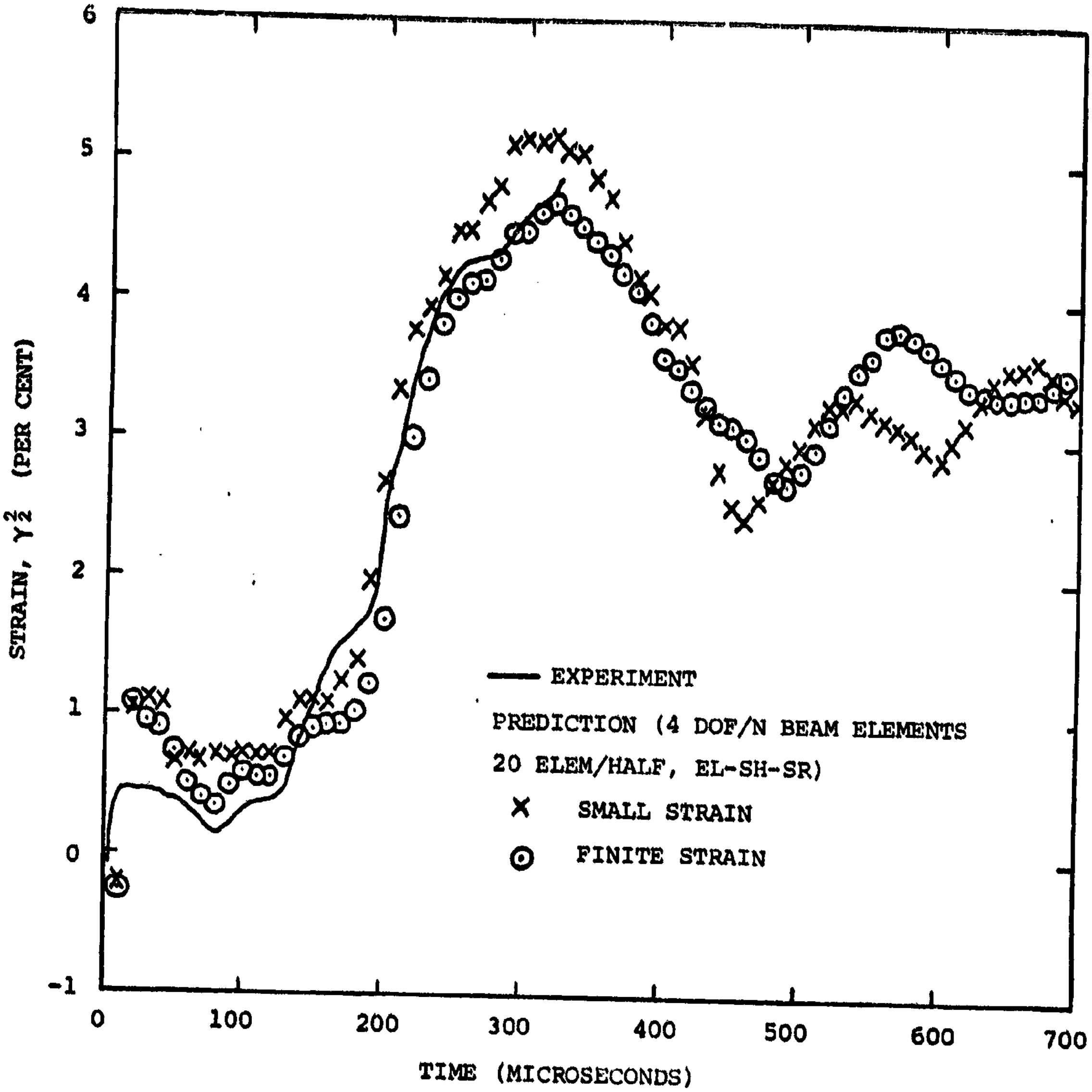

(c) Upper-Surface Transient Strain at y =2.20 in

FIG. 9 CONTINUED (CB-4)

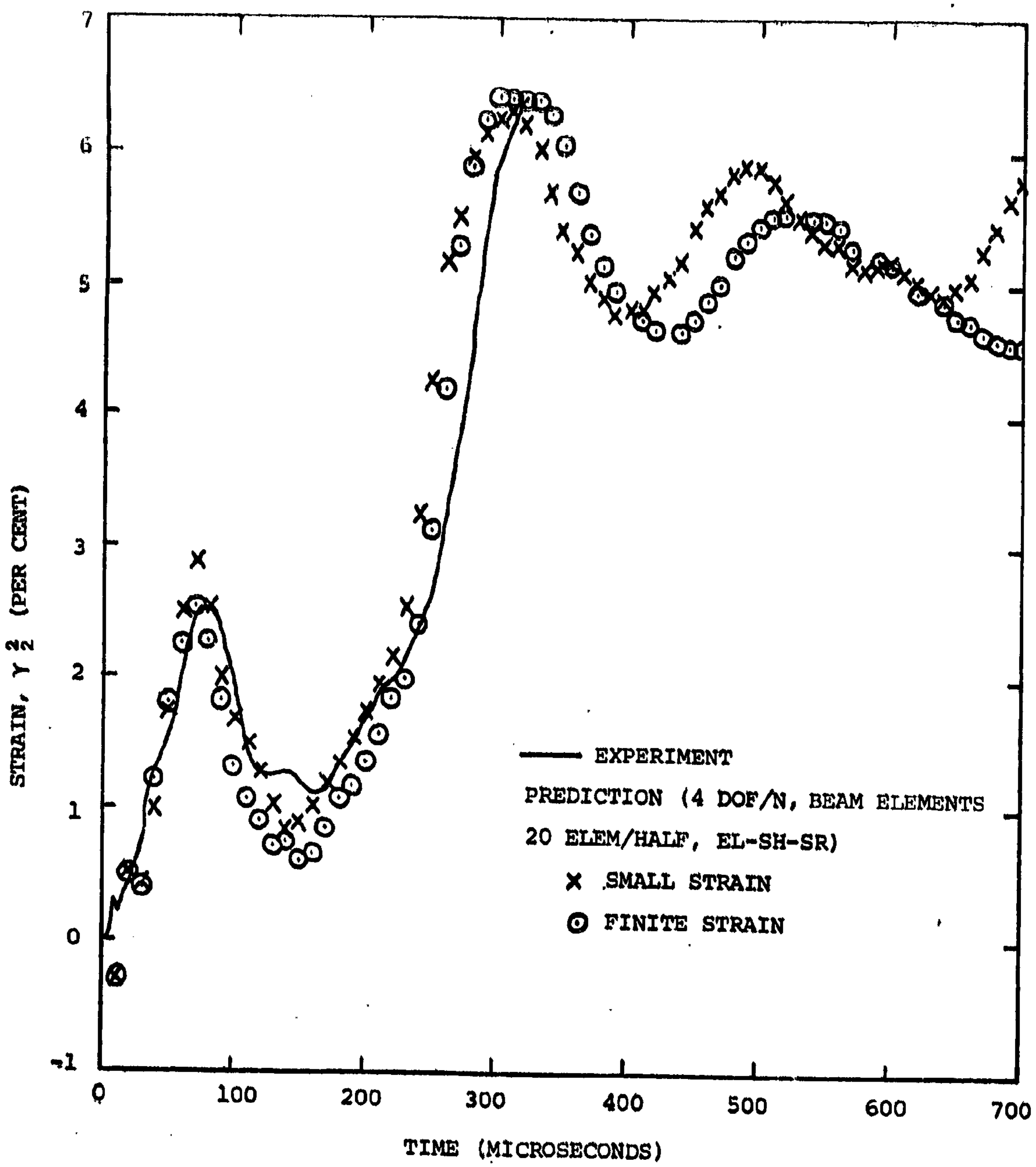

(d) Upper-Surface Transient Strain at Station y=3.00 in

FIG. 9 CONTINUED (CB-4)

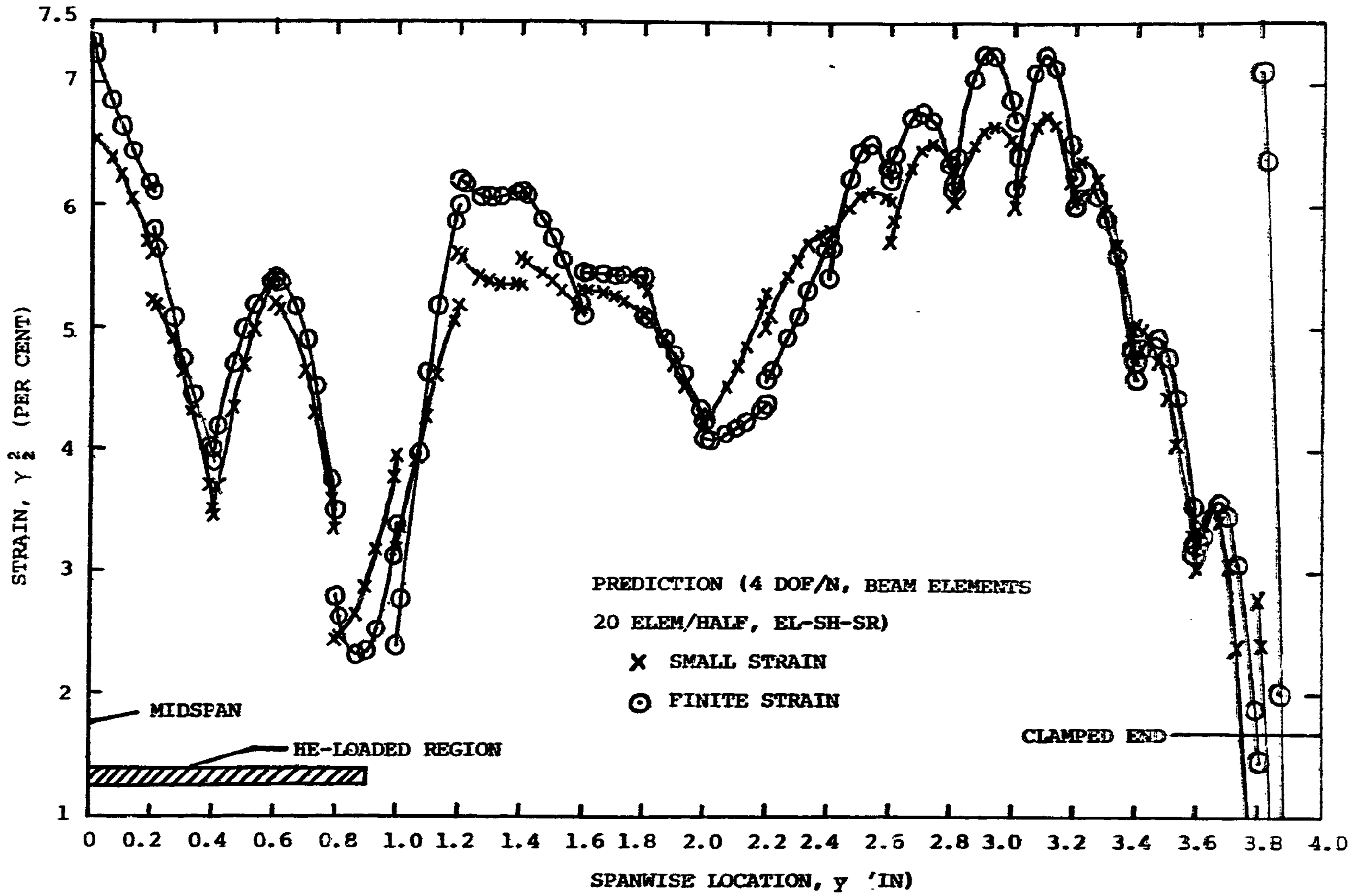

(e) Spanwise Distribution of Upper-Surface Strain at t=300 μsec

FIG. 9 CONCLUDED (CB-4)

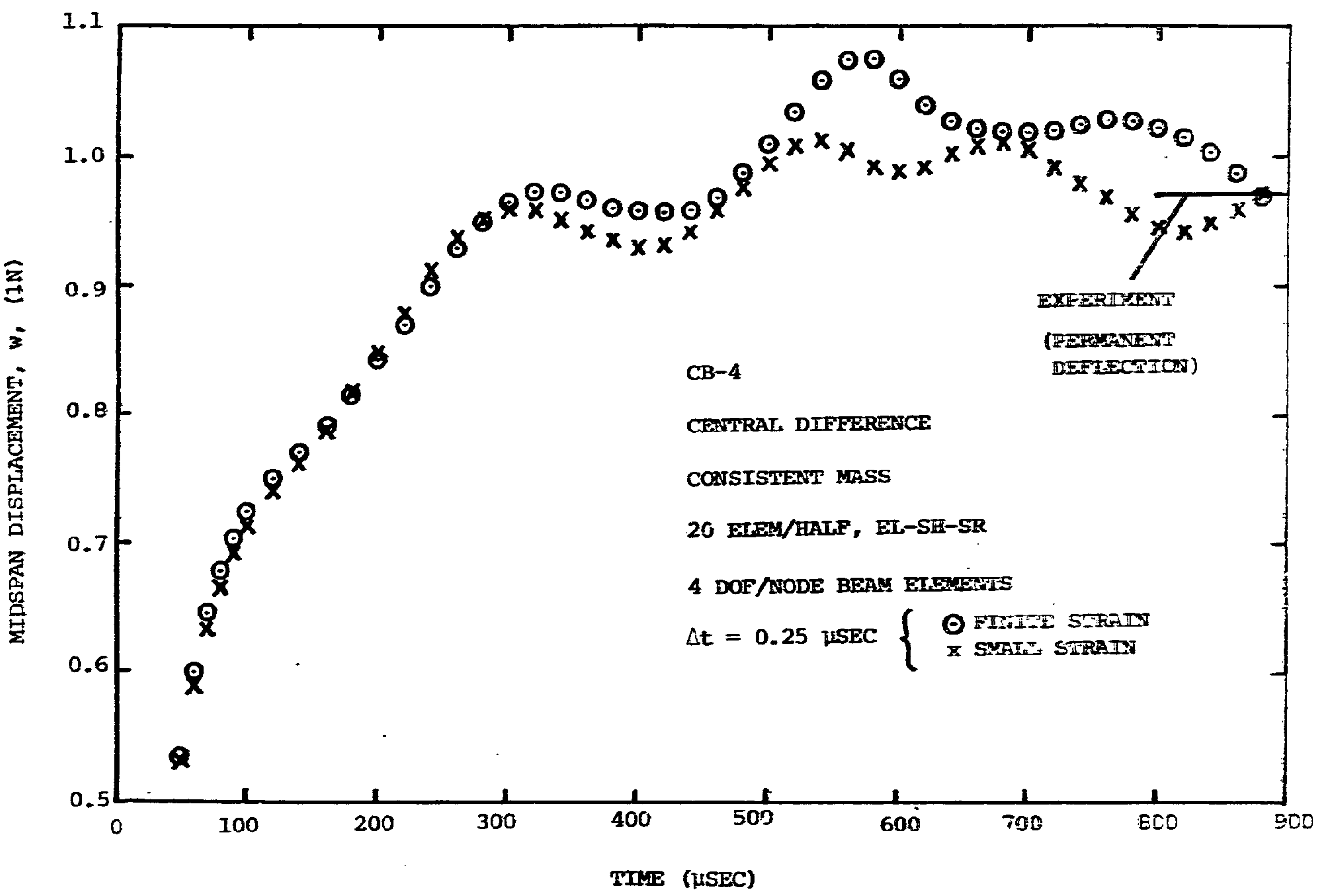

FIG. 10 BEAM-ELEMENT MODEL EL-SH-SR SMALL-STRAIN AND FINITE-STRAIN PREDICTIONS FOR THE TRANSIENT MIDSPAN DISPLACEMENT w OF EXPLOSIVELY-IMPULSED NARROW PLATE SPECIMEN CB-4

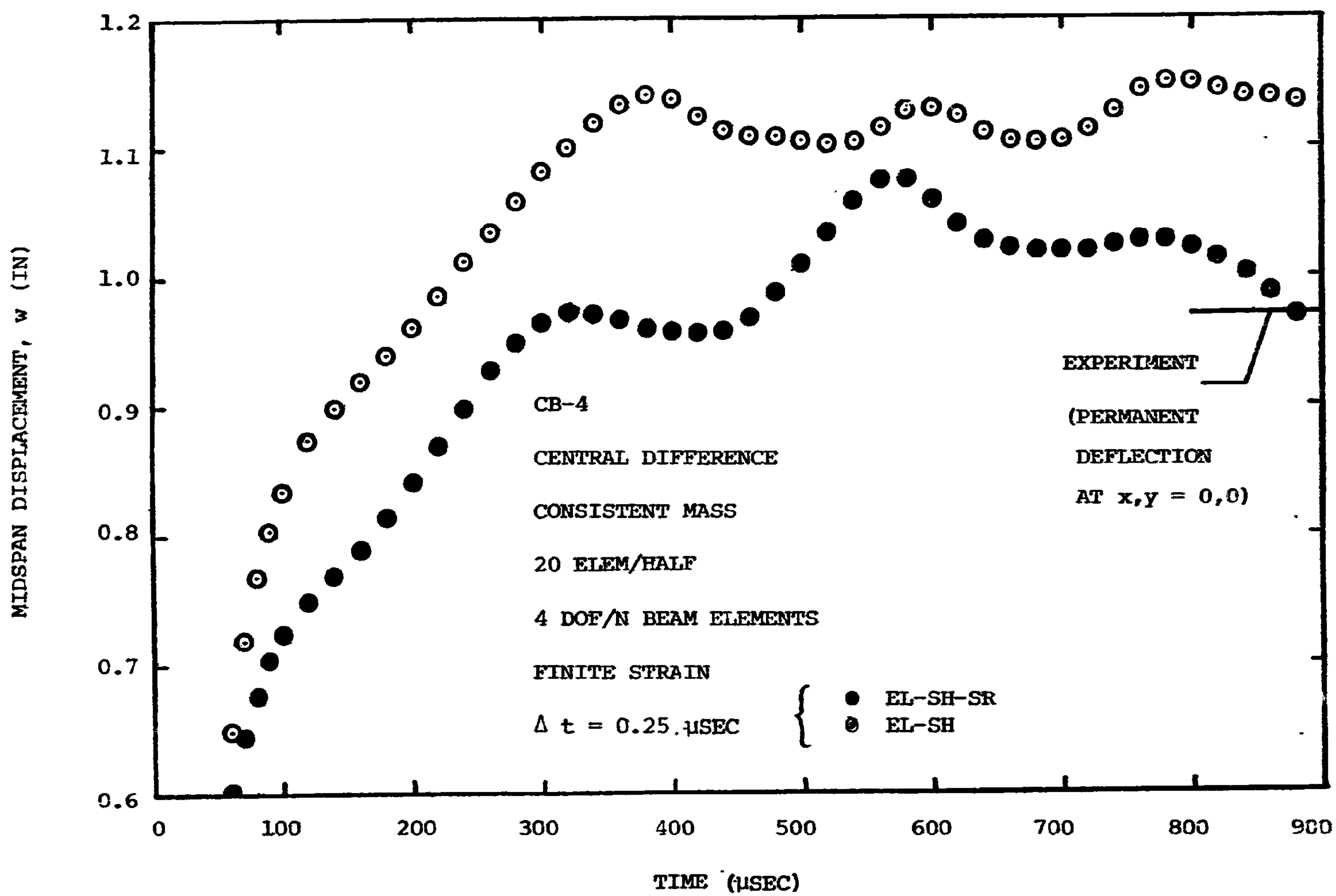

FIG. 11 BEAM-ELEMENT MODEL EL-SH AND EL-SH-SR FINITE-STRAIN PREDICTIONS FOR THE TRANSIENT MIDSPAN DISPLACEMENT w OF EXPLOSIVELY-IMPULSED NARROW-PLATE SPECIMEN CB-4

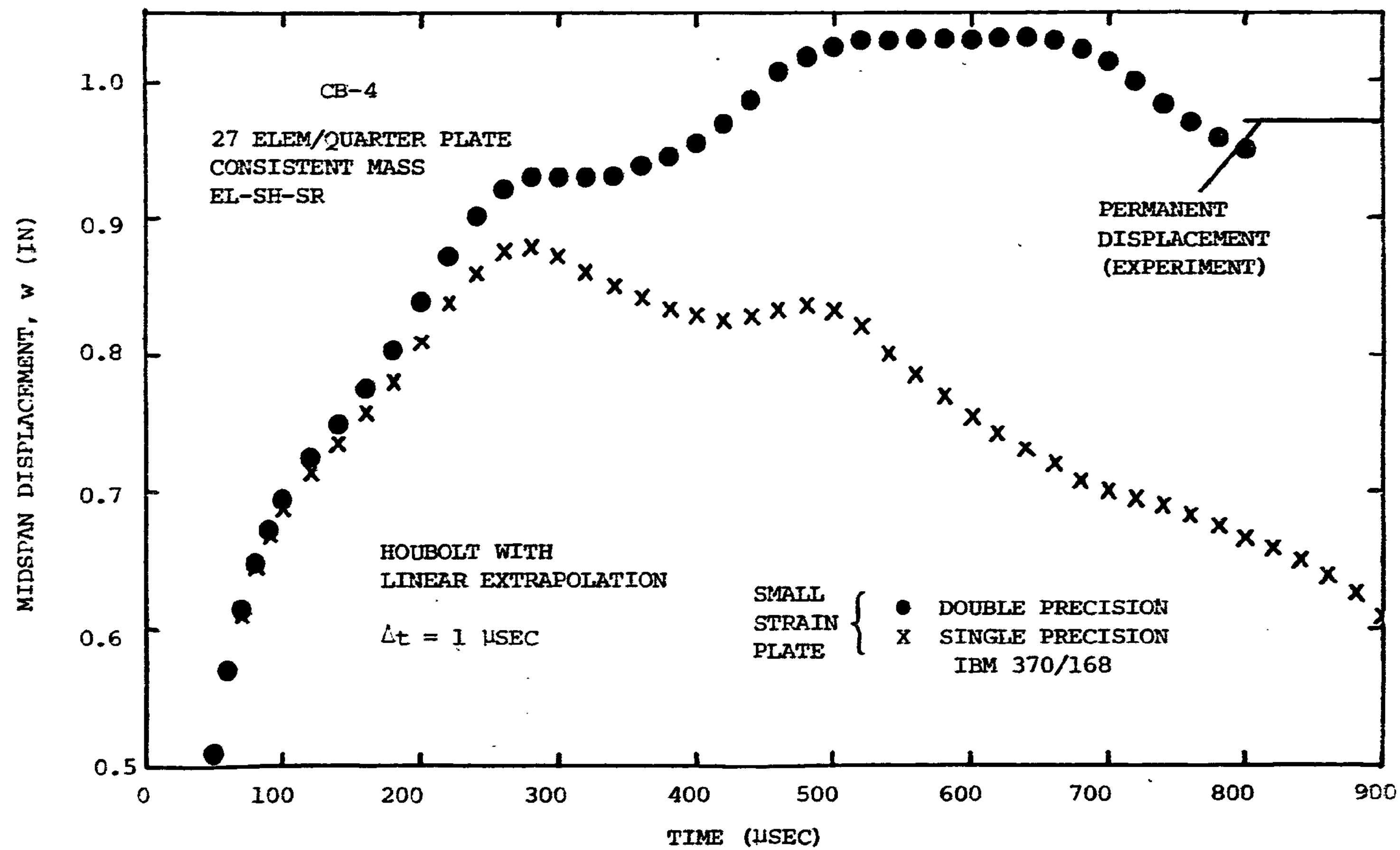

FIG. 12 COMPARISON OF SINGLE-PRECISION vs. DOUBLE-PRECISION SMALL-STRAIN PLATE-ELEMENT MODEL PREDICTIONS FOR THE TRANSIENT PLATE-CENTER DISPLACEMENT w OF EXPLOSIVELY-IMPULSED NARROW-PLATE SPECIMEN CB-4

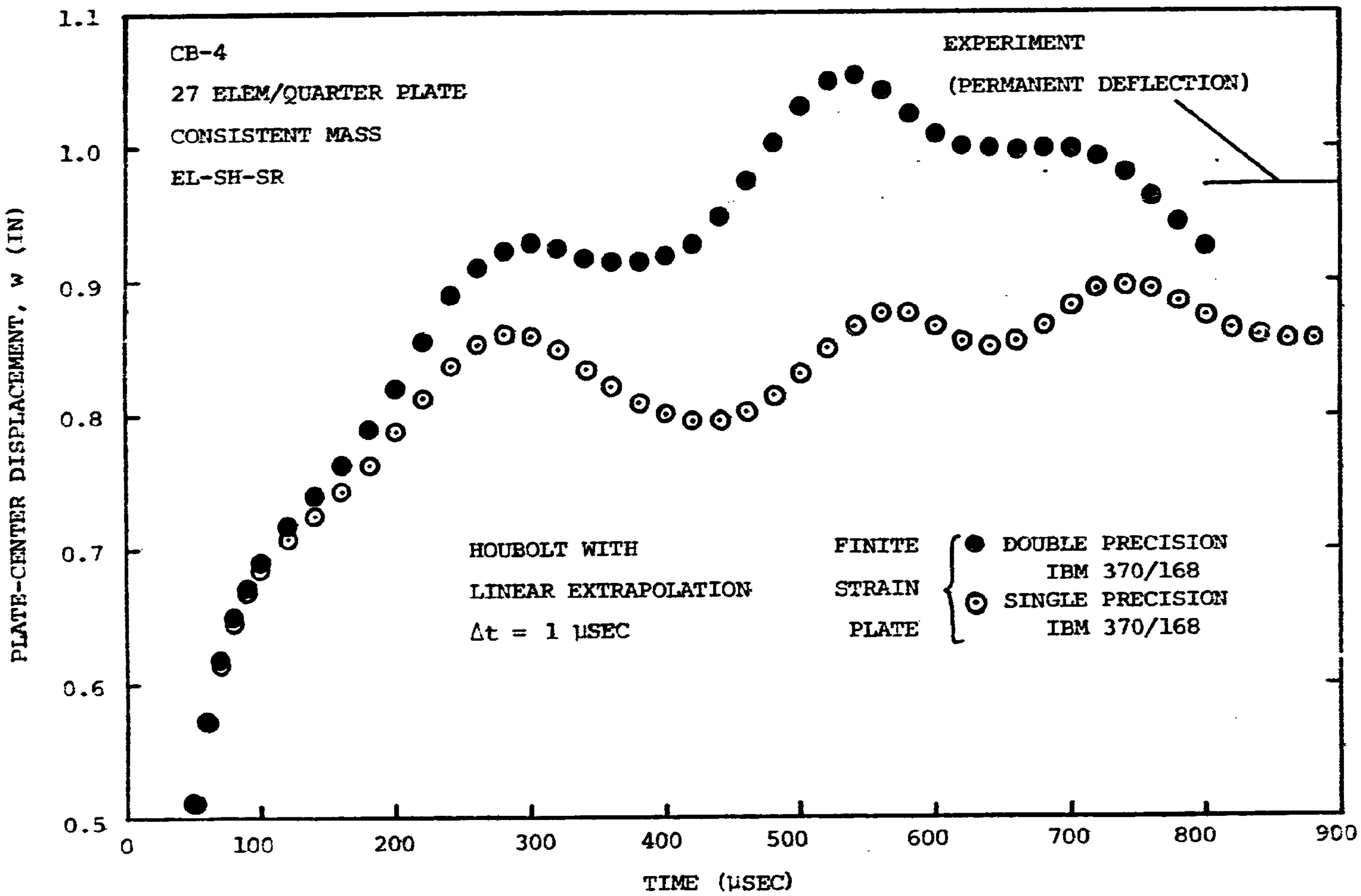

FIG. 13 COMPARISON OF SINGLE-PRECISION vs. DOUBLE-PRECISION FINITE-STRAIN PLATE-ELEMENT MODEL PREDICTIONS FOR THE TRANSIENT PLATE-CENTER DISPLACEMENT w OF EXPLOSIVELY-IMPULSED NARROW-PLATE SPECIMEN CB-4

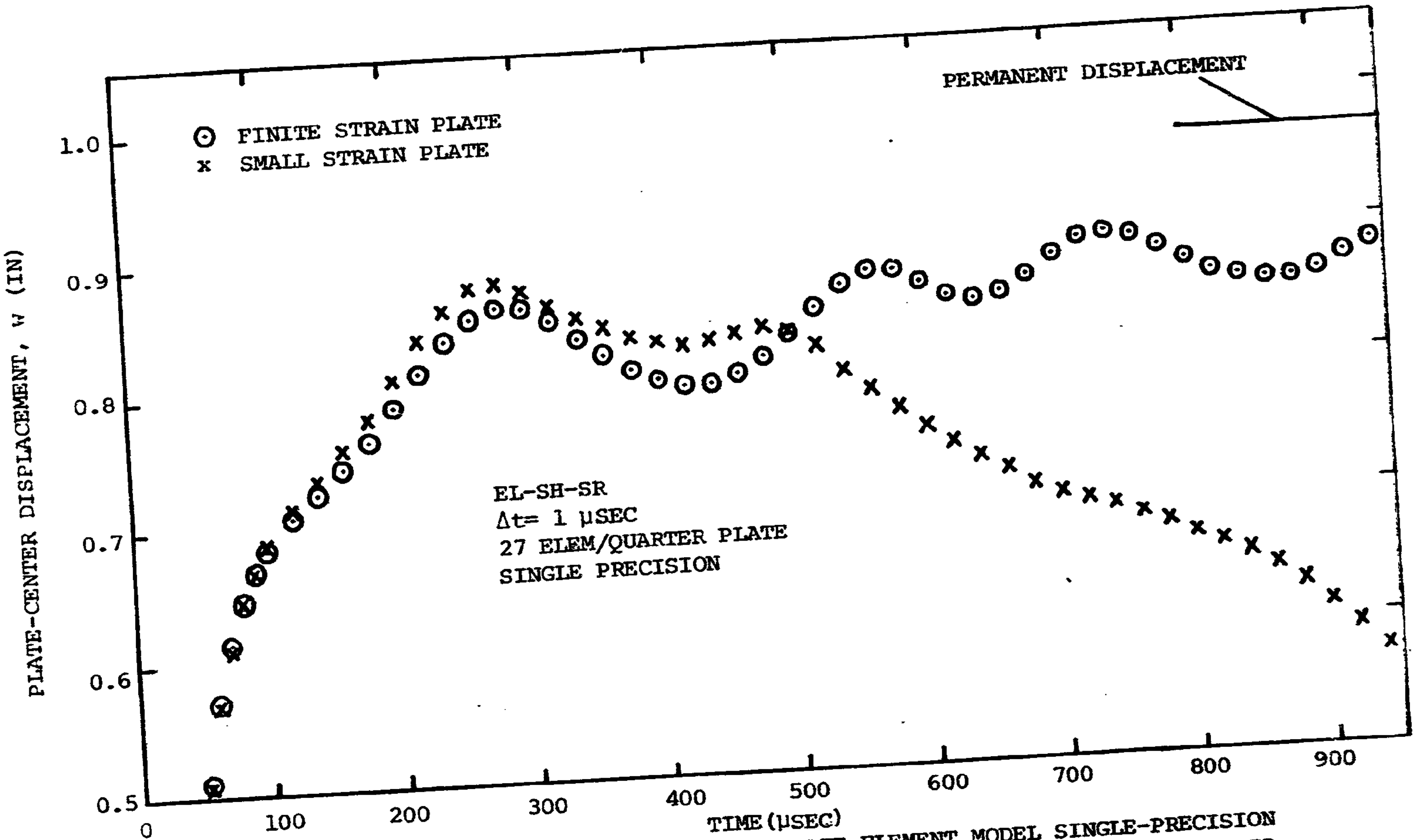

FIG.14 COMPARISON OF SMALL-STRAIN vs. FINITE-STRAIN PLATE-ELEMENT MODEL SINGLE-PRECISION PREDICTIONS FOR THE TRANSIENT PLATE-CENTER DISPLACEMENT w OF EXPLOSIVELY-IMPULSED NARROW-PLATE SPECIMEN CB-4

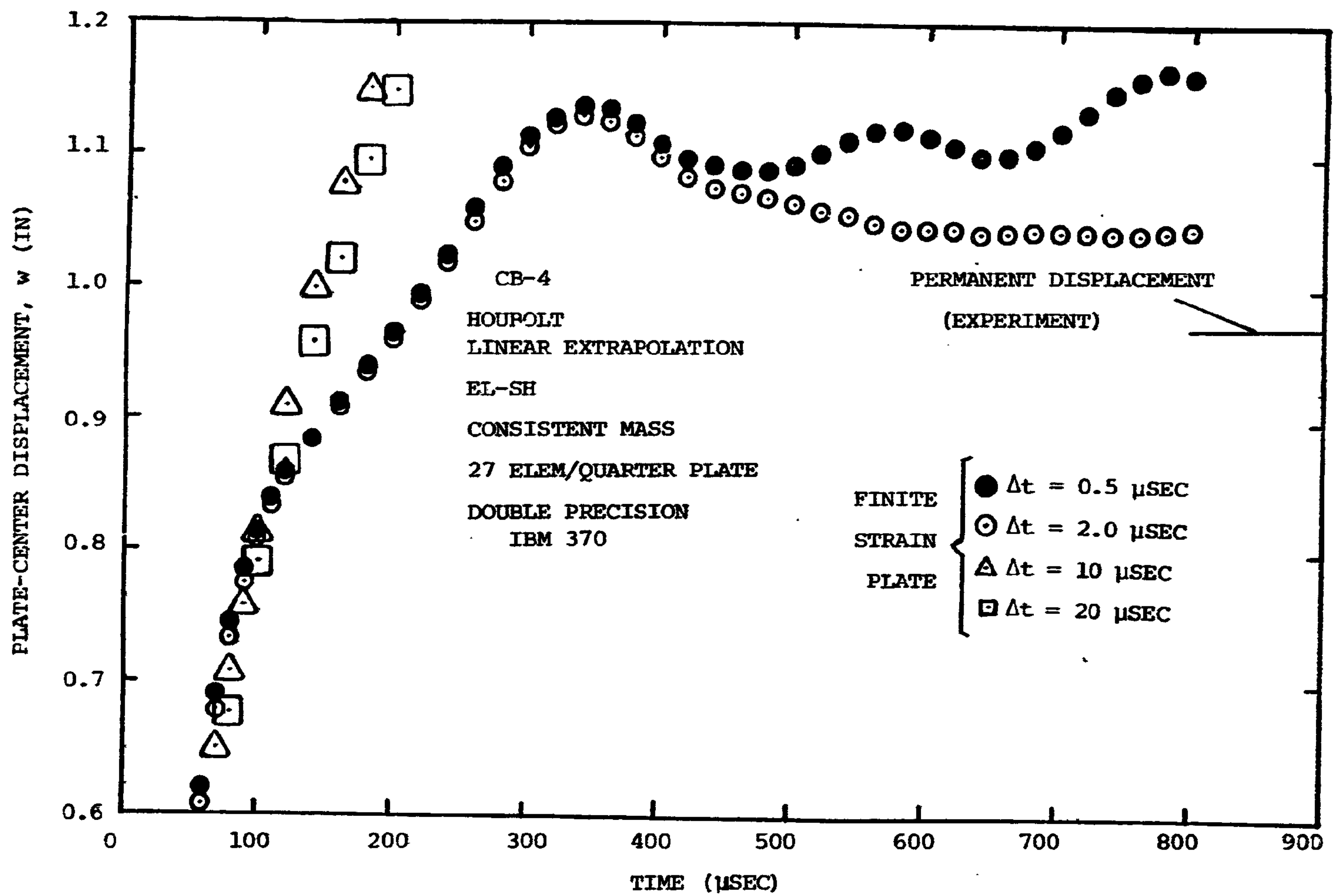

FIG. 15 FINITE-STRAIN PLATE-ELEMENT MODEL PREDICTIONS FOR THE TRANSIENT PLATE-CENTER DISPLACEMENT w OF EXPLOSIVELY-IMPULSED NARROW-PLATE SPECIMEN CB-4 FOR VARIOUS TIME-STEP SIZES Δt BY USING THE HOUBOLT-MULE PROCEDURE

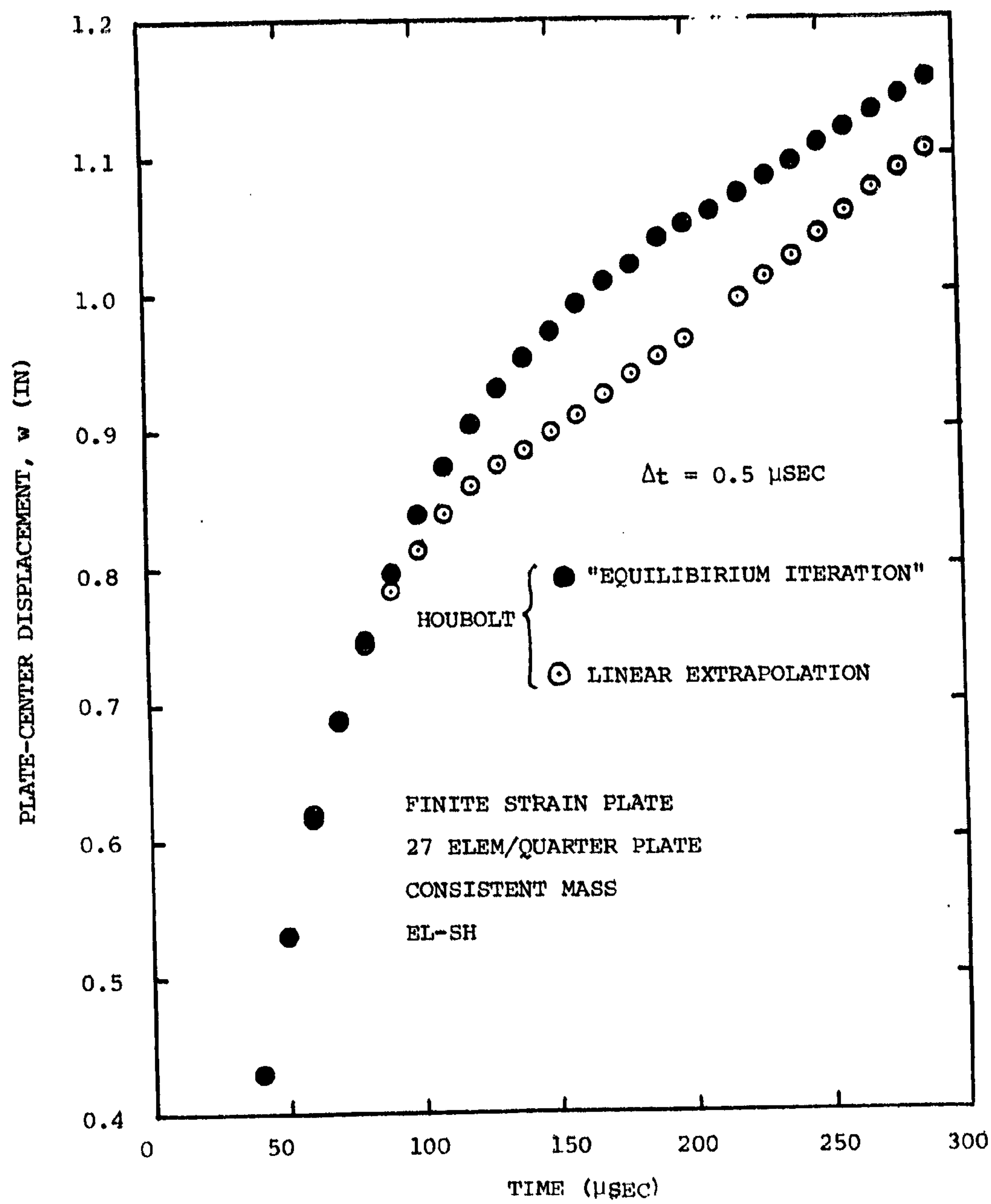

FIG. 16 FINITE-STRAIN PLATE-ELEMENT MODEL PREDICTIONS FOR THE PLATE-CENTER DISPLACEMENT w OF IMPULSIVELY-LOADED NARROW-PLATE SPECIMEN CB-4 BY USING "EQUILIBRIUM ITERATION" WITH THE HOUBOLT OPERATOR OR BY USING THE HOUBOLT-MULE PROCEDURE, WITH Δt = 0.5 MICROSECOND

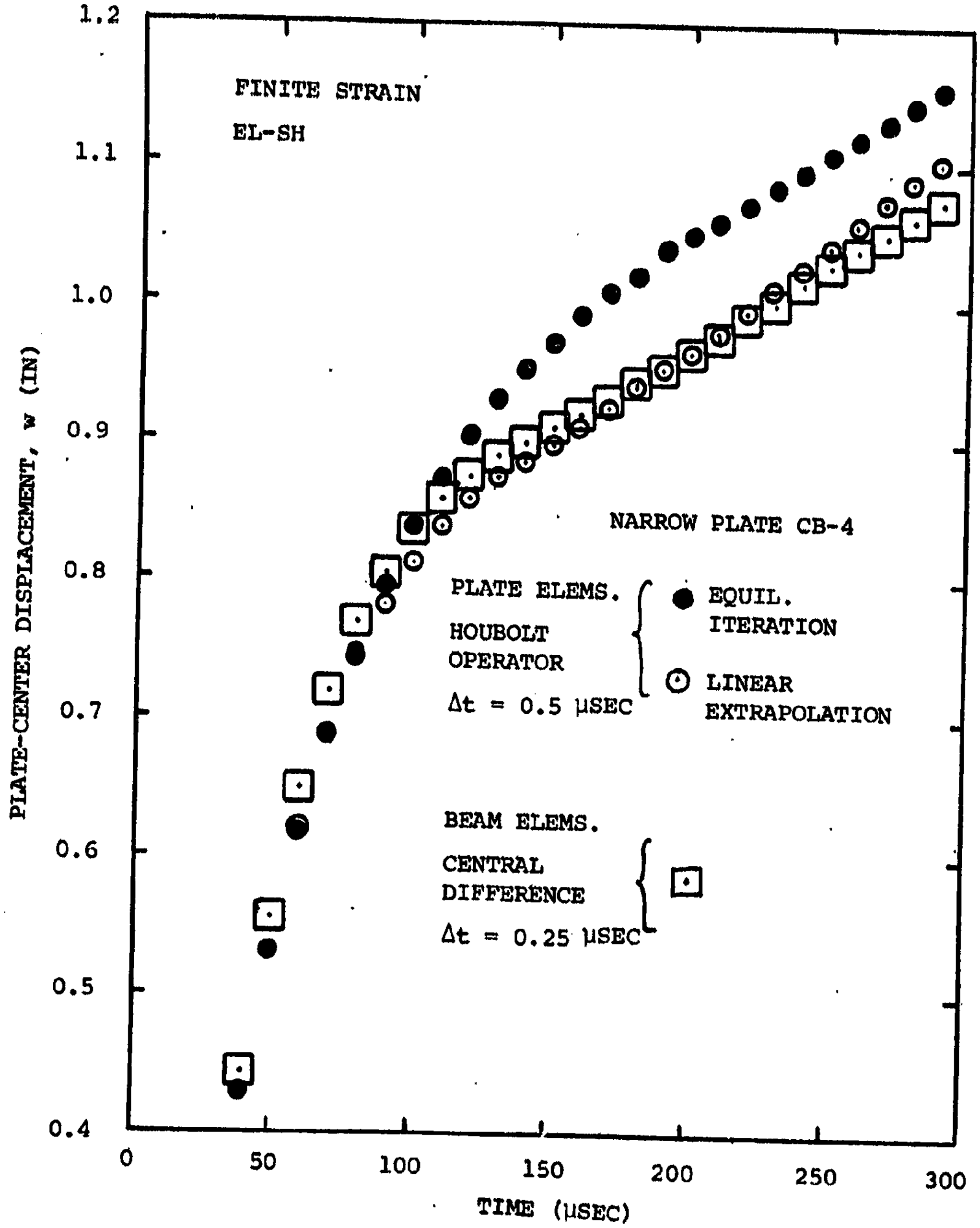

FIG. 17 COMPARISON OF BEAM-ELEMENT MODEL CENTRAL-DIFFERENCE PREDICTIONS vs. PLATE-ELEMENT MODEL PREDICTIONS BY HOUBOLT-MULE AND BY "EQUILIBRIUM ITERATION" WITH THE HOUBOLT OPERATOR FOR THE FINITE-STRAIN TRANSIENT PLATE-CENTER DISPLACEMENT w OF EXPLOSIVE-IMPULSED NARROW-PLATE SPECIMEN CB-4

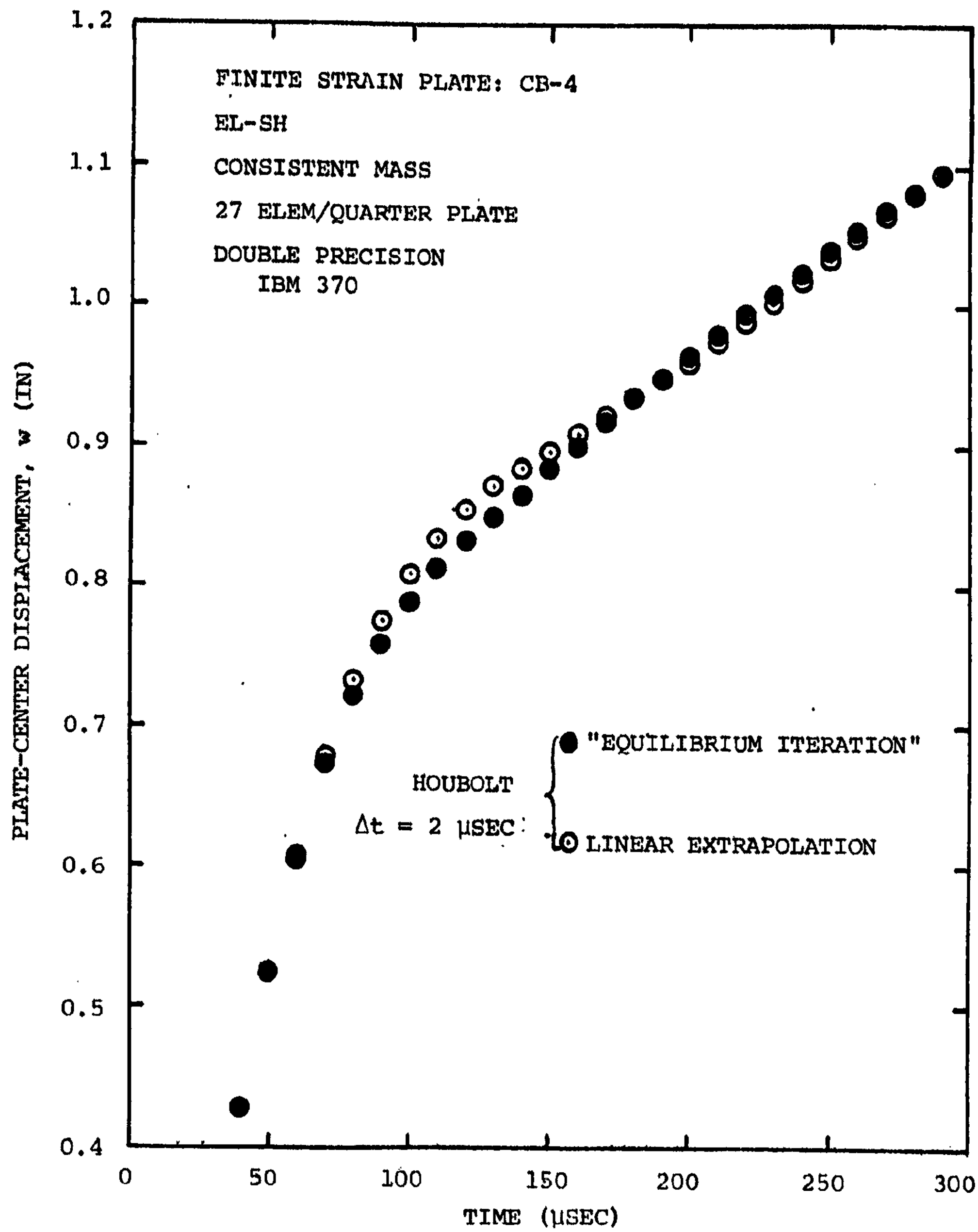

(a) Response for $t < 300$ μsec

FIG. 18 FINITE-STRAIN PLATE-ELEMENT MODEL PREDICTIONS FOR THE TRANSIENT PLATE-CENTER DISPLACEMENT w OF EXPLOSIVELY-IMPULSED NARROW-PLATE SPECIMEN CB-4 BY USING "EQUILIBRIUM ITERATION" WITH THE HOUBOLT OPERATOR OR BY USING THE HOUBOLT-MULE PROCEDURE, WITH Δt = 2.0 MICROSECONDS

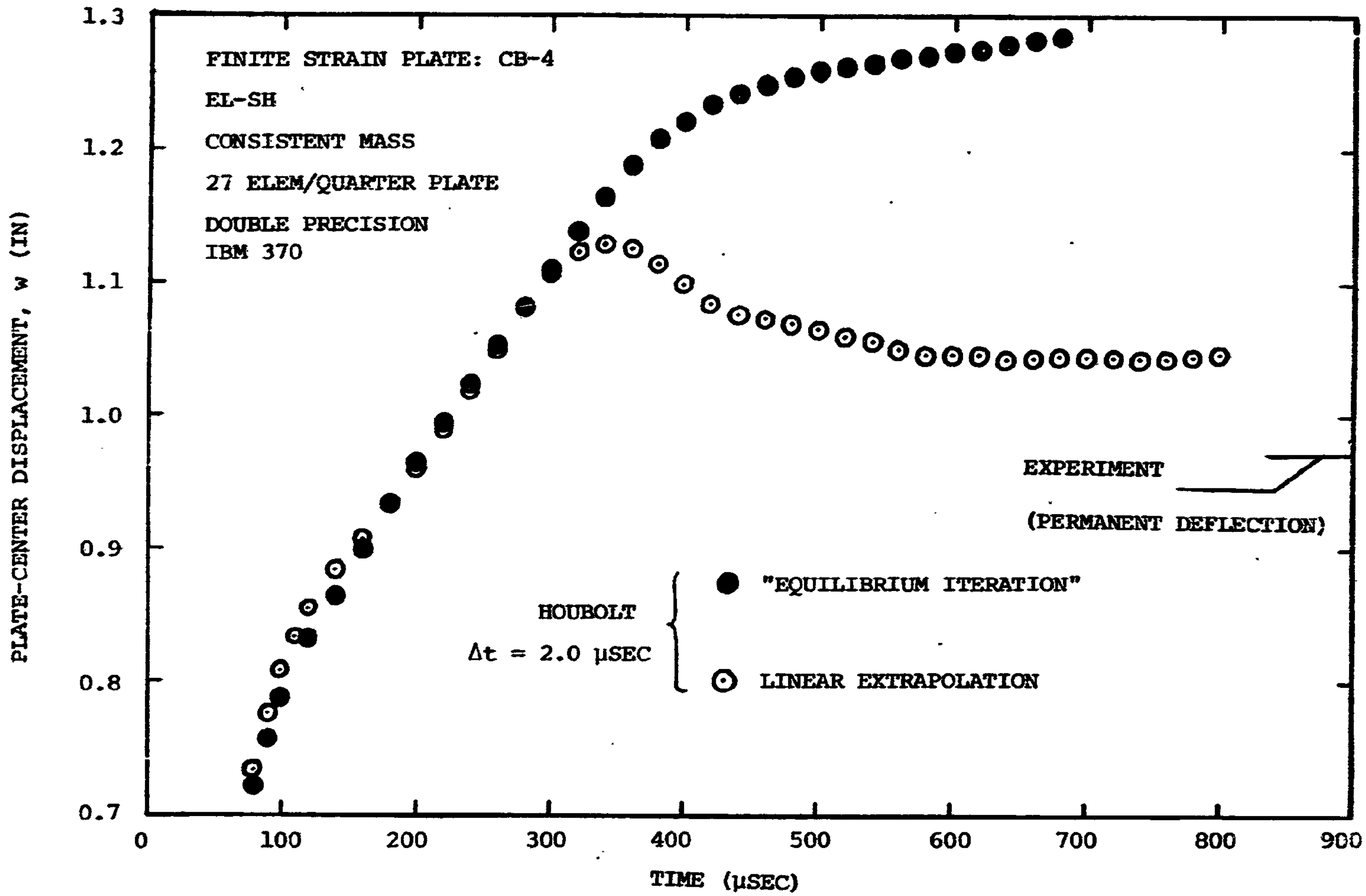

(b) Response for Longer Duration

FIG. 18 (CONCLUDED)

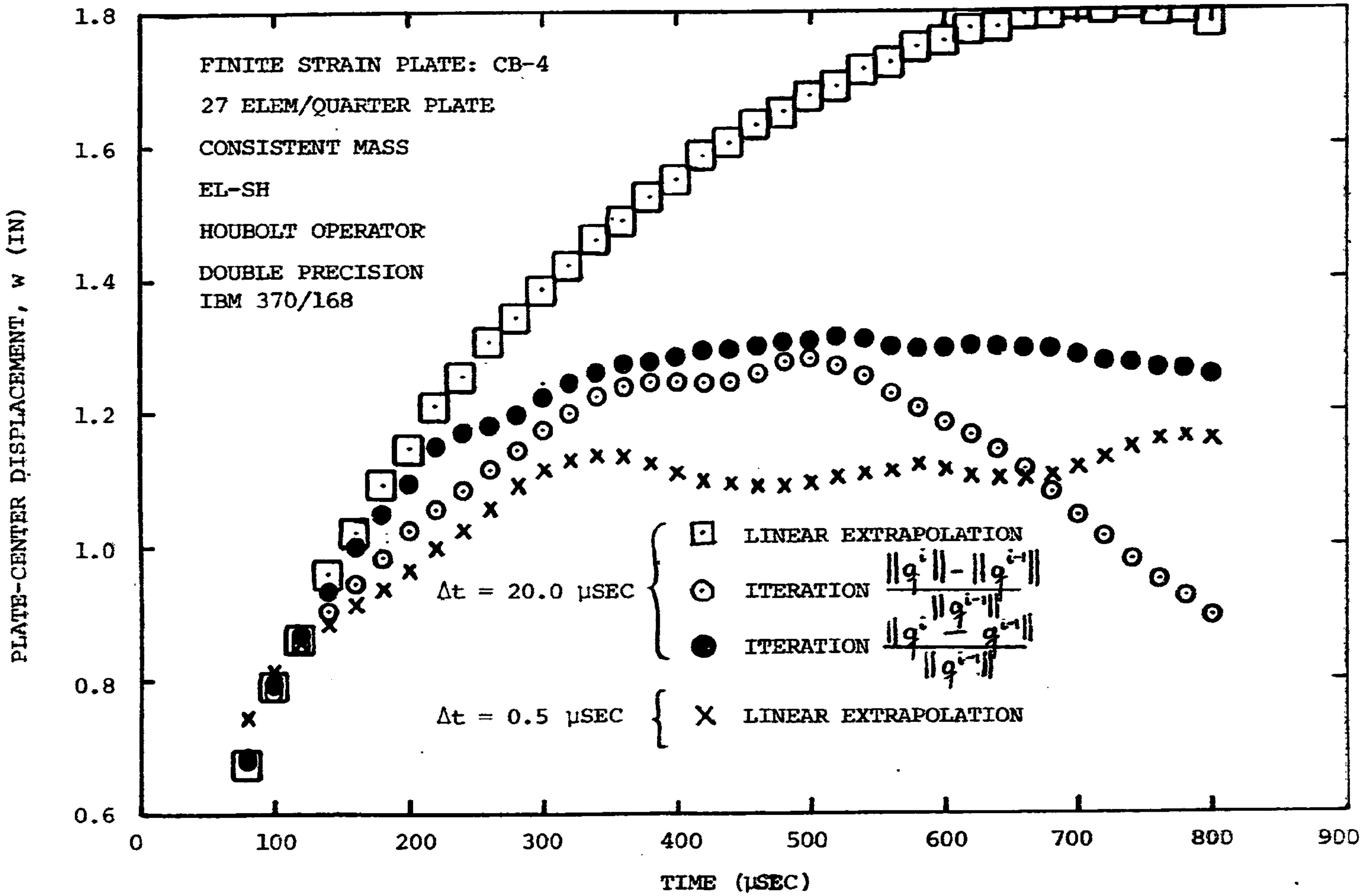

FIG. 19 COMPARISON OF PLATE-ELEMENT MODEL FINITE-STRAIN PREDICTIONS FOR THE TRANSIENT PLATE-CENTER DISPLACEMENT w OF EXPLOSIVELY-IMPULSED NARROW-PLATE SPECIMEN CB-4 BY USING Δt = 20 MICROSECONDS WITH "EQUILIBRIUM ITERATION" HOUBOLT AND WITH HOUBOLT-MULE, AND FOR HOUBOLT-MULE WITH Δt = 0.5 MICROSECOND

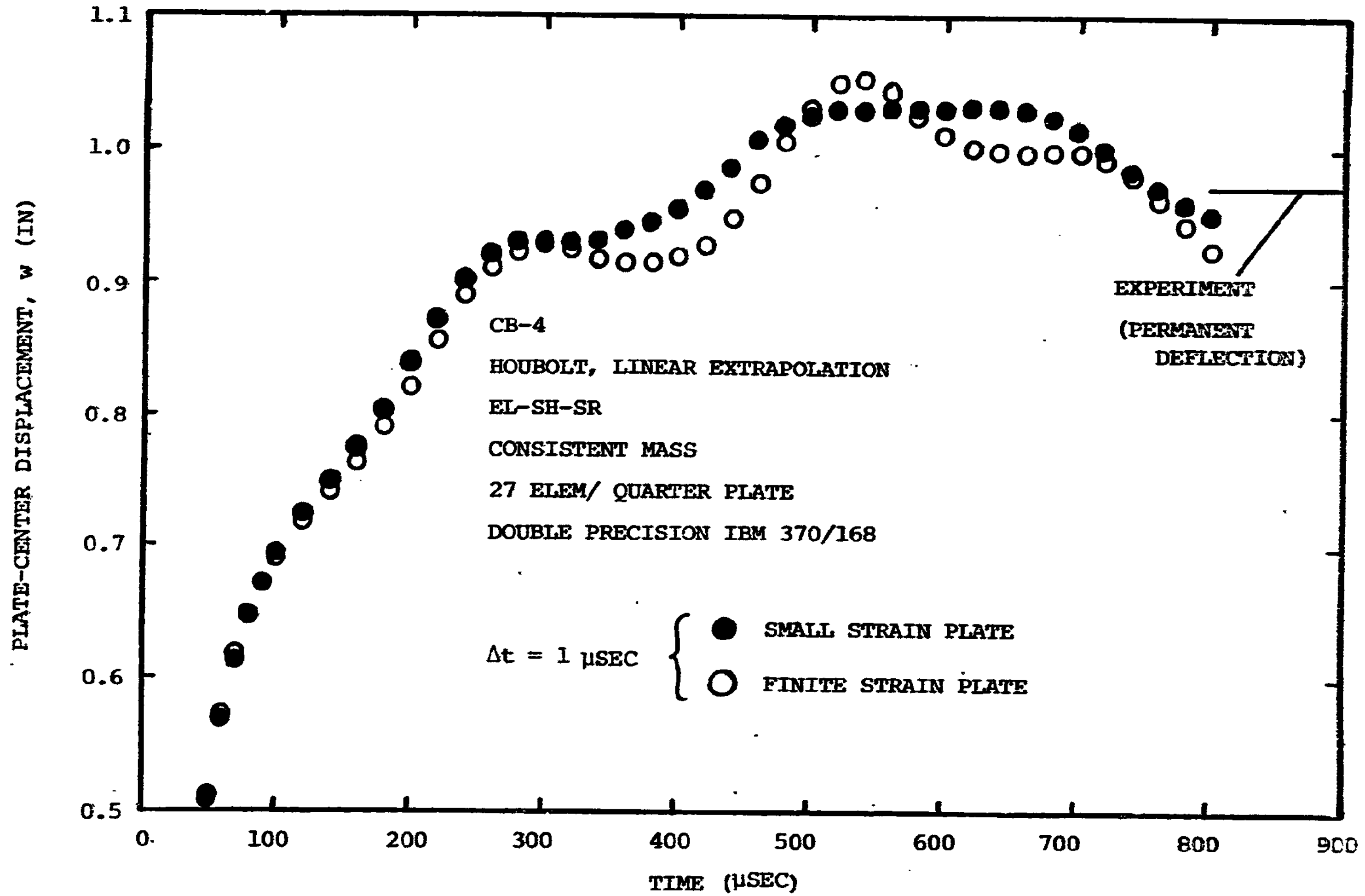

FIG. 20 COMPARISON OF FINITE-STRAIN vs. SMALL-STRAIN PLATE-ELEMENT MODEL PREDICTIONS FOR THE TRANSIENT PLATE-CENTER DISPLACEMENT w OF EXPLOSIVELY-IMPULSED NARROW-PLATE SPECIMEN CB-4

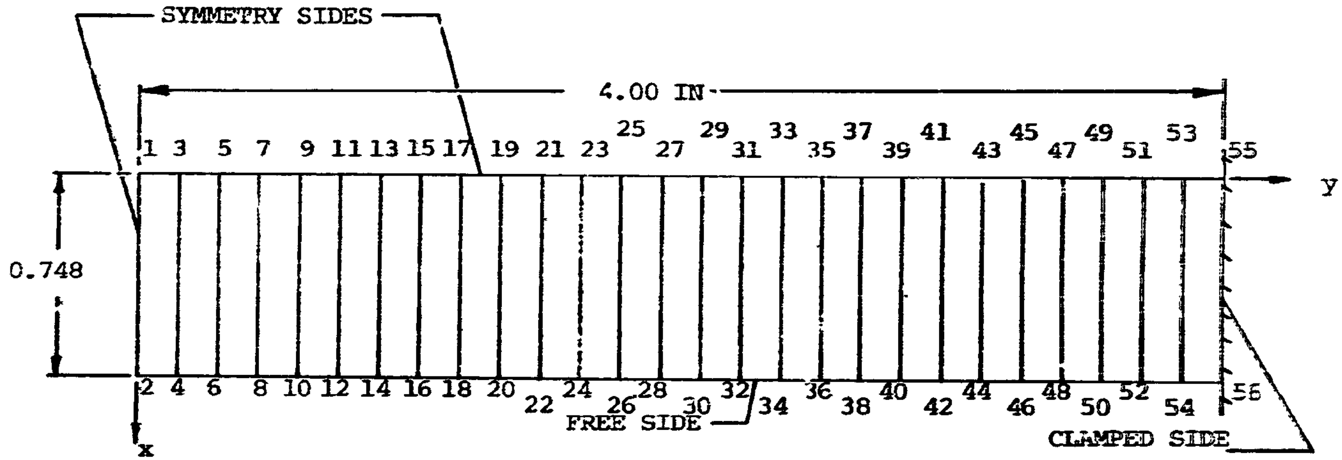

(a) Element Sizes and Node Numbers

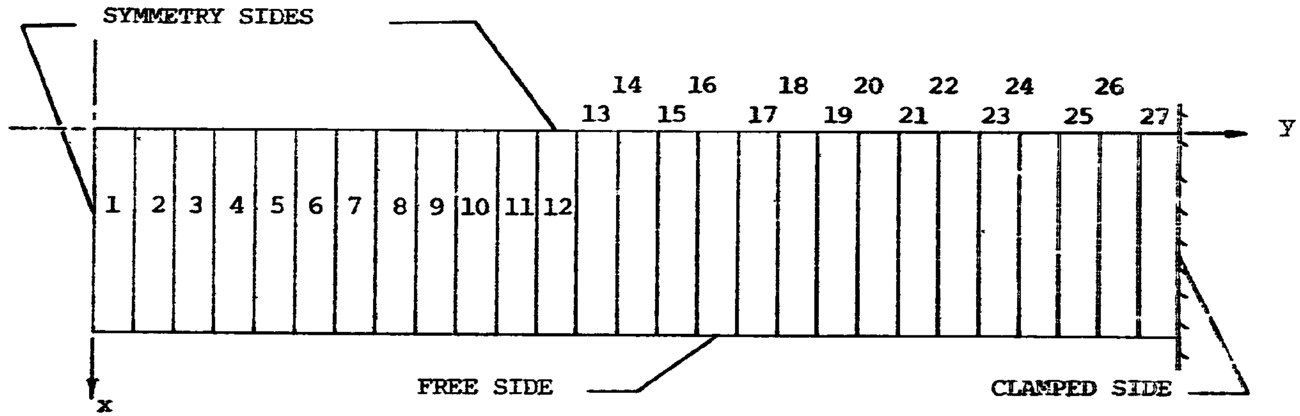

(b) Element Numbering

FIG. 21 PLATE-ELEMENT MODEL OF THE QUARTER PLATE OF EXPLOSIVELY-IMPULSED NARROW-PLATE SPECIMEN CB-4

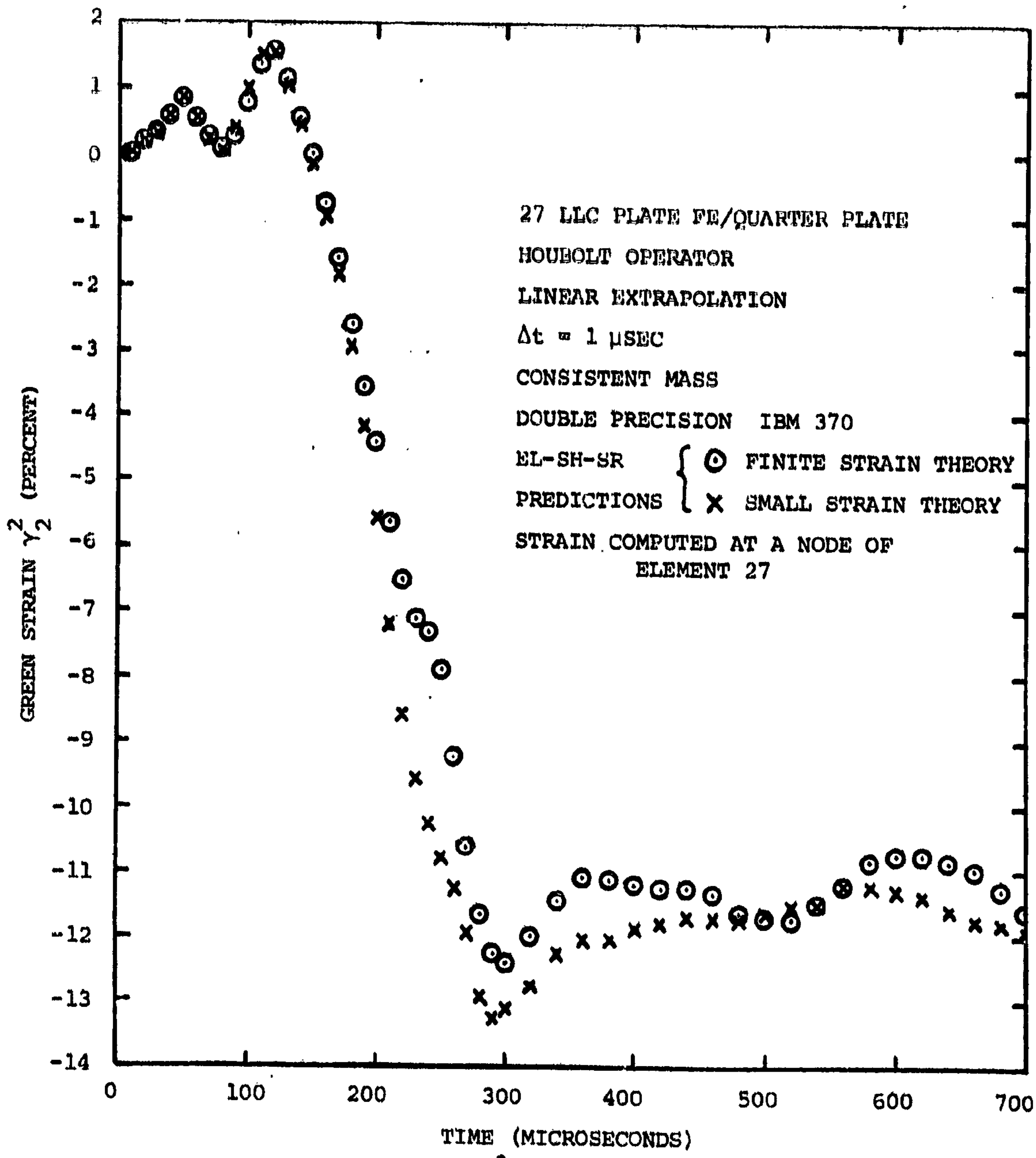

(a) Upper-Surface Strain γ_2^2 at Station $(x,y) = (0,4.00\text{in})$

FIG. 22 COMPARISON OF FINITE-STRAIN PREDICTIONS, SMALL-STRAIN PREDICTIONS, AND MEASUREMENTS OF THE TRANSIENT LONGITUDINAL STRAIN AT VARIOUS SPANWISE STATIONS ON THE UPPER- AND/OR THE LOWER-SURFACE OF EXPLOSIVELY-IMPULSED NARROW-PLATE SPECIMEN CB-4

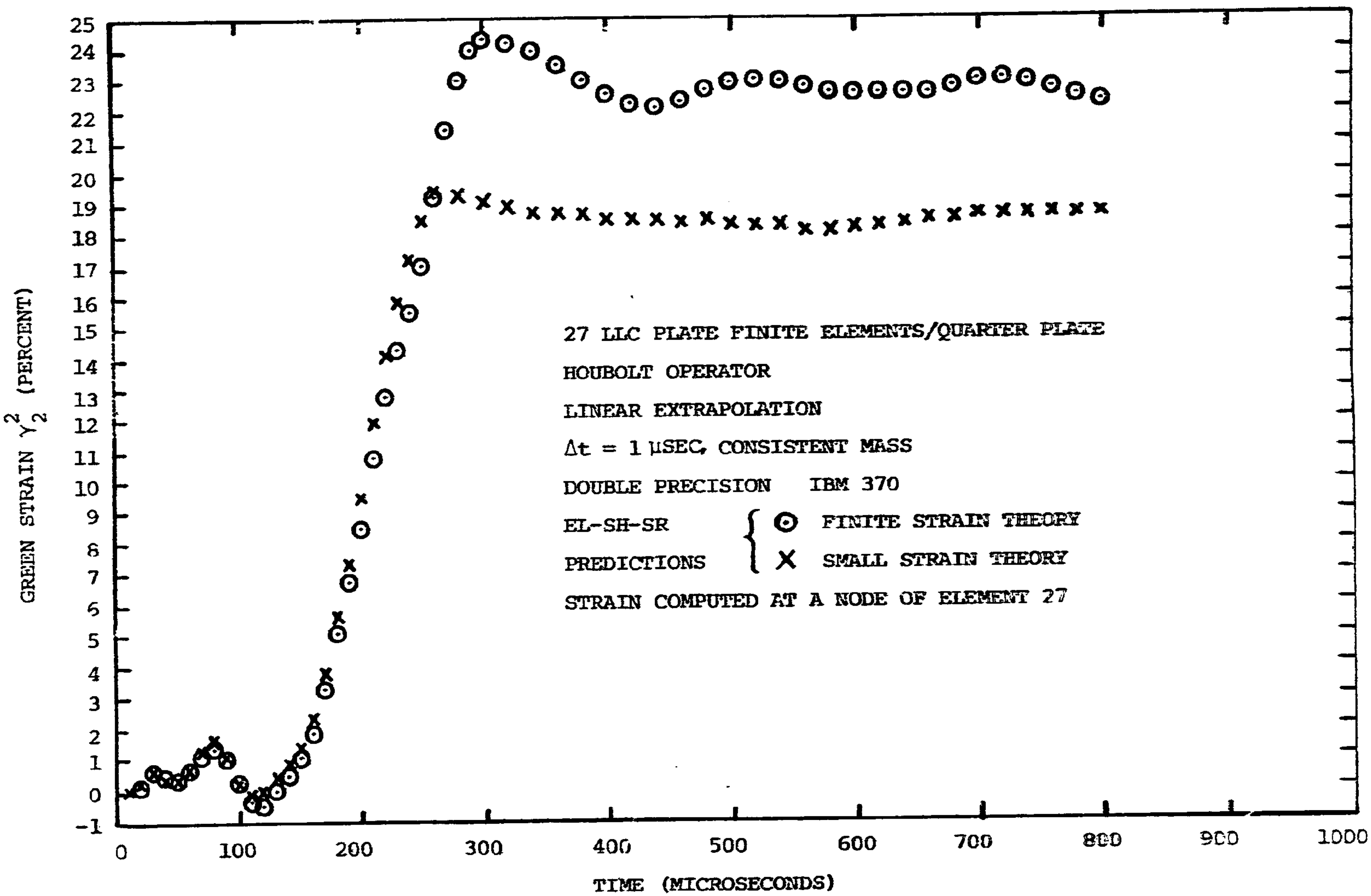

(b) Lower-Surface Strain γ_2^2 at Station $(x,y) = (0,4.00in)$

FIG. 22 CONTINUED (FINITE STRAIN, SMALL STRAIN, EXPT., CB-4)

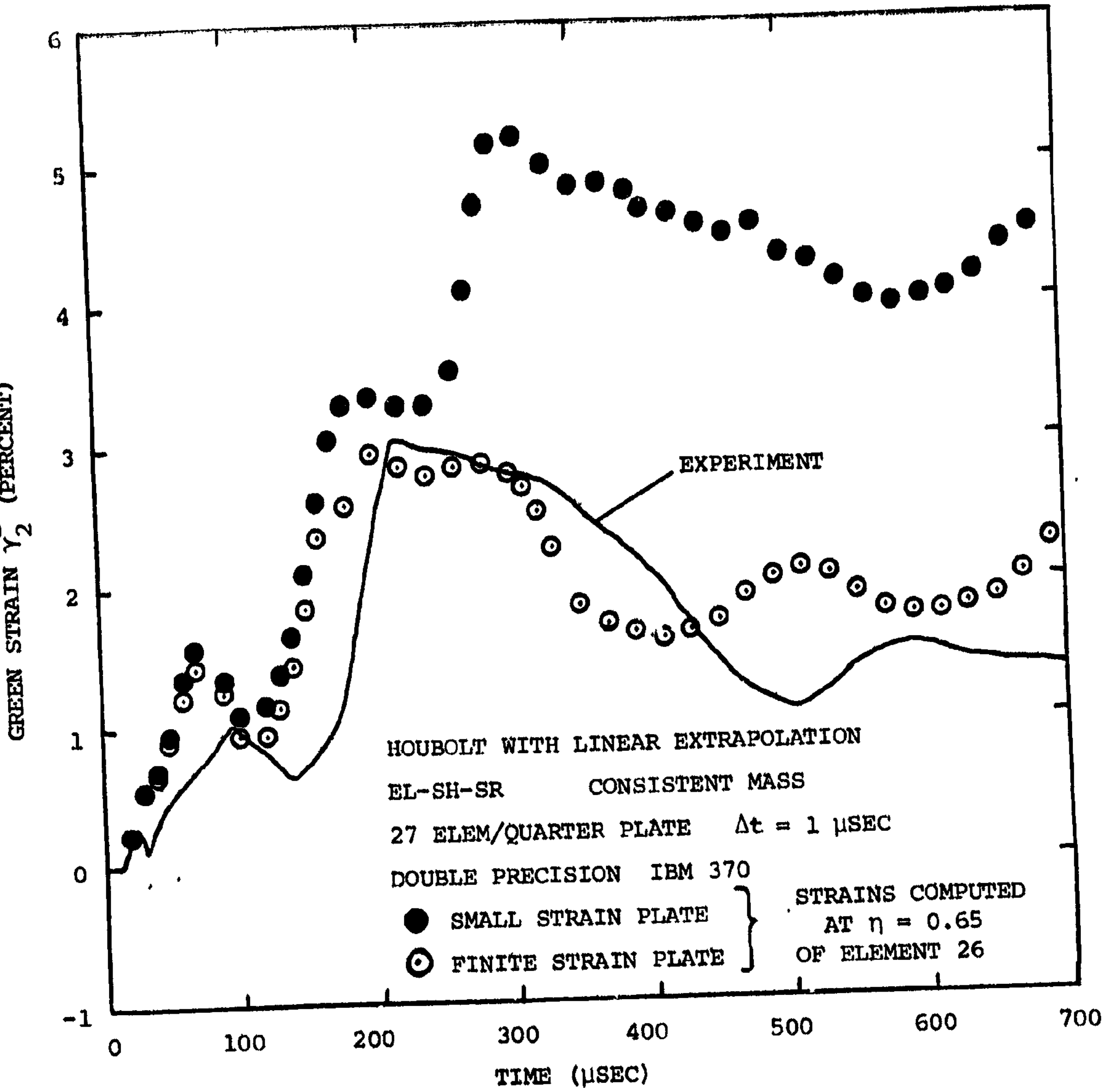

(c) Lower Surface Strain γ_2^2 at Station (x,y) = (0,3.80in)

FIG. 22 CONTINUED (FINITE STRAIN, SMALL STRAIN, EXPT., CB-4)

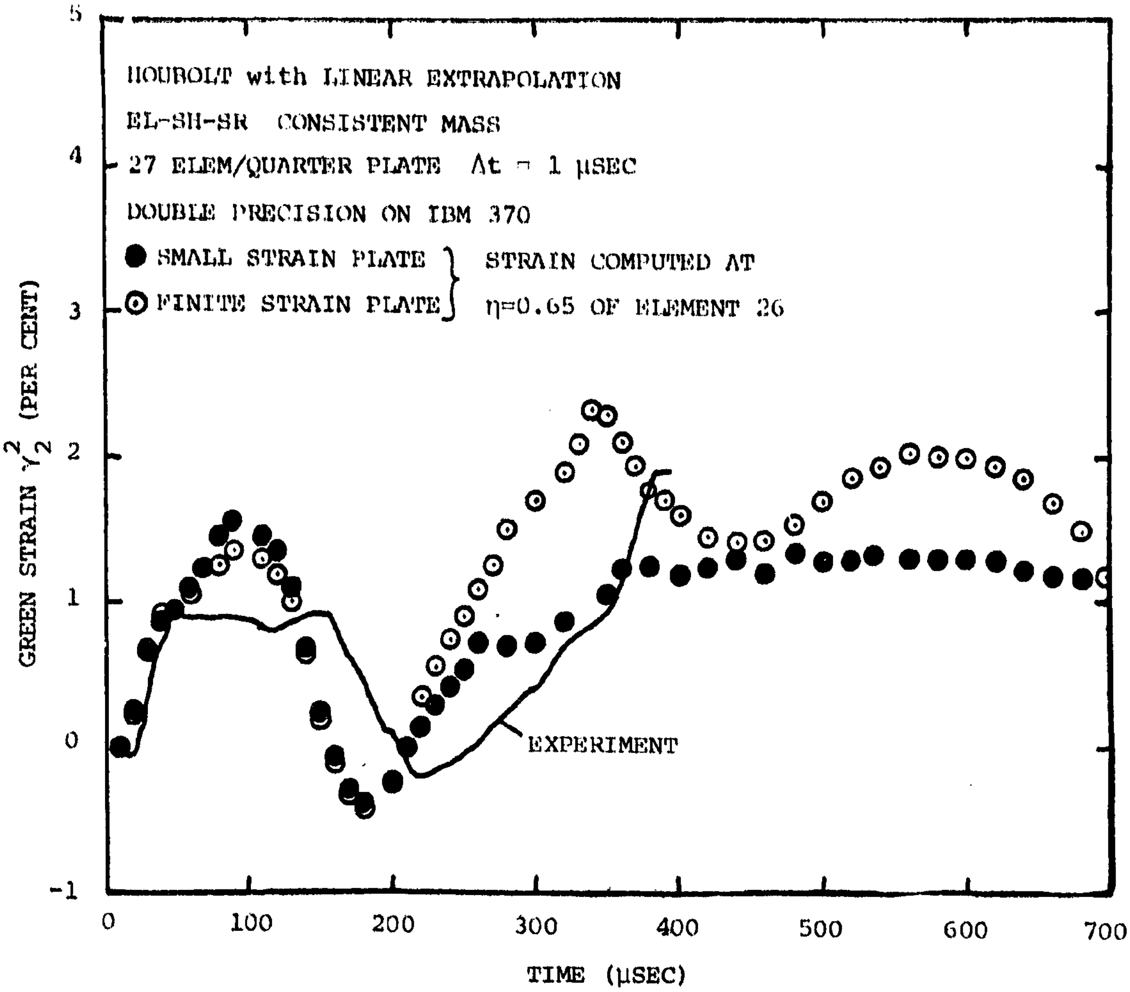

(d) Upper-Surface Strain γ_2^2 at Station (x,y)=(0,3.80in)

FIG. 22 CONTINUED (FINITE STRAIN, SMALL STRAIN, EXPT., CB-4)

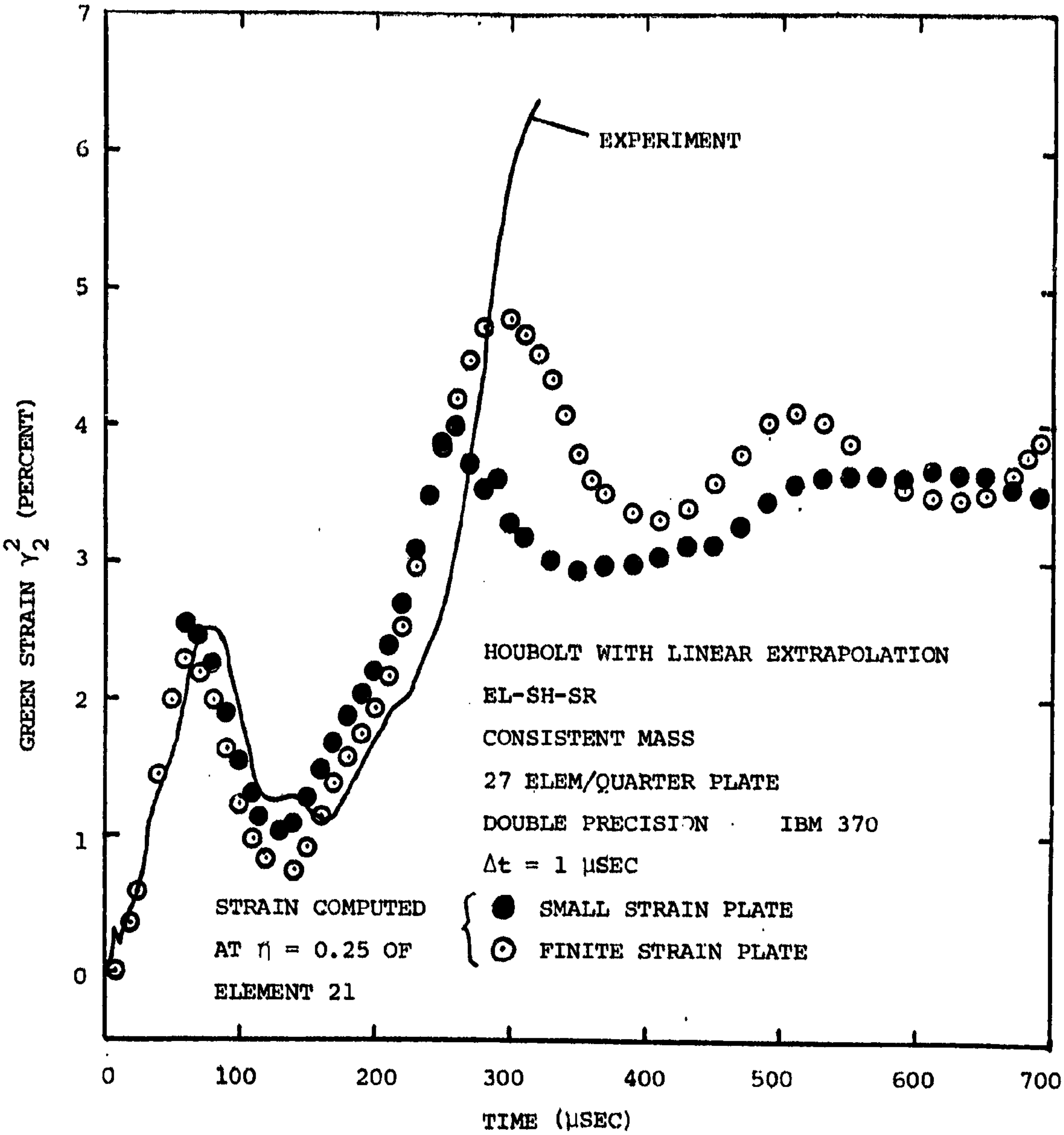

(e) Upper-Surface Strain γ_2^2 at Station (x,y) = (0,3.00in)

FIG. 22 CONTINUED (FINITE STRAIN, SMALL STRAIN, EXPT., CB-4)

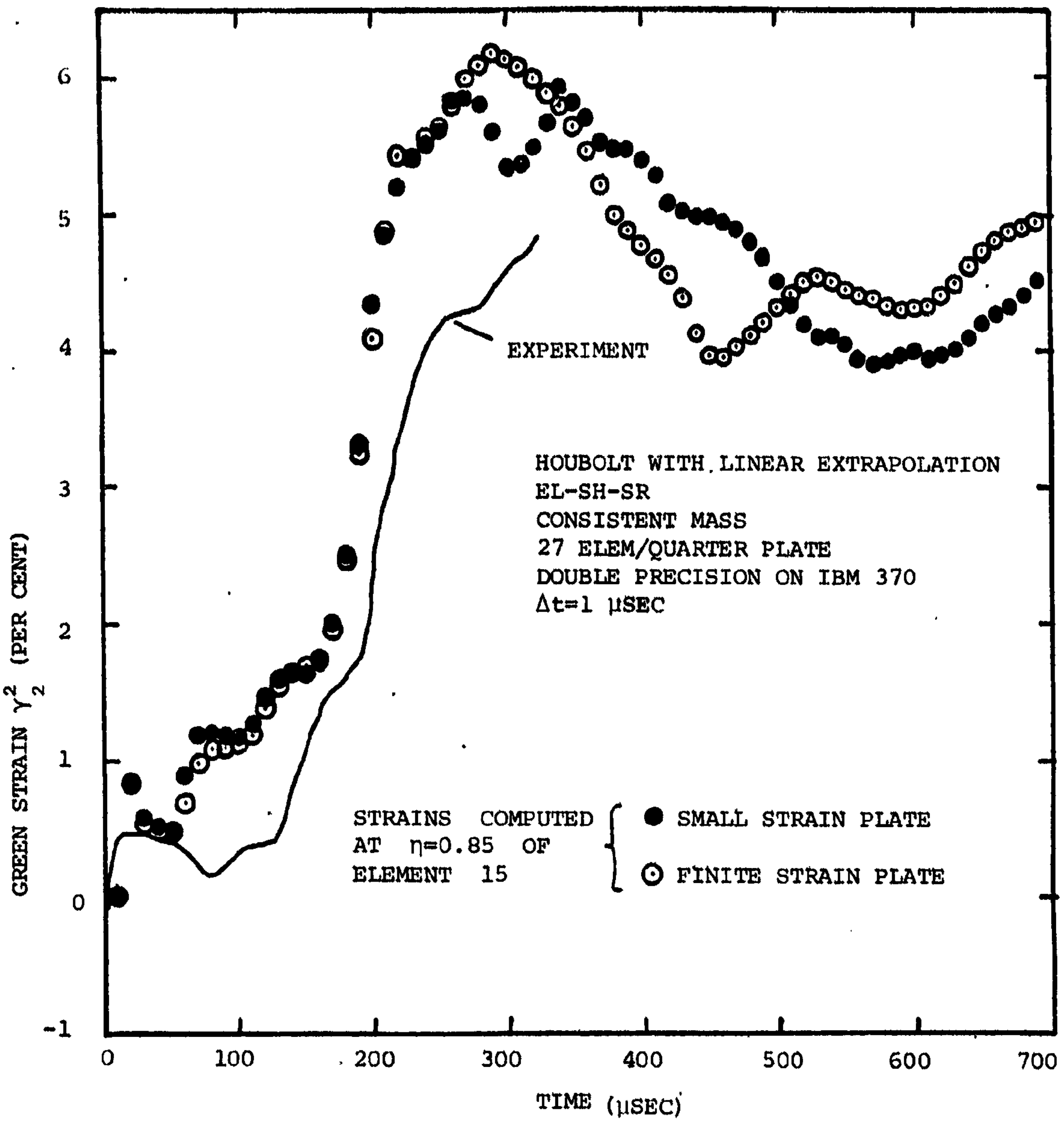

(f) Upper Surface Strain γ_2^2 at Station (x,y)=(0,2.20in)

FIG.22 CONTINUED (FINITE STRAIN, SMALL STRAIN, EXPT., CB-4)

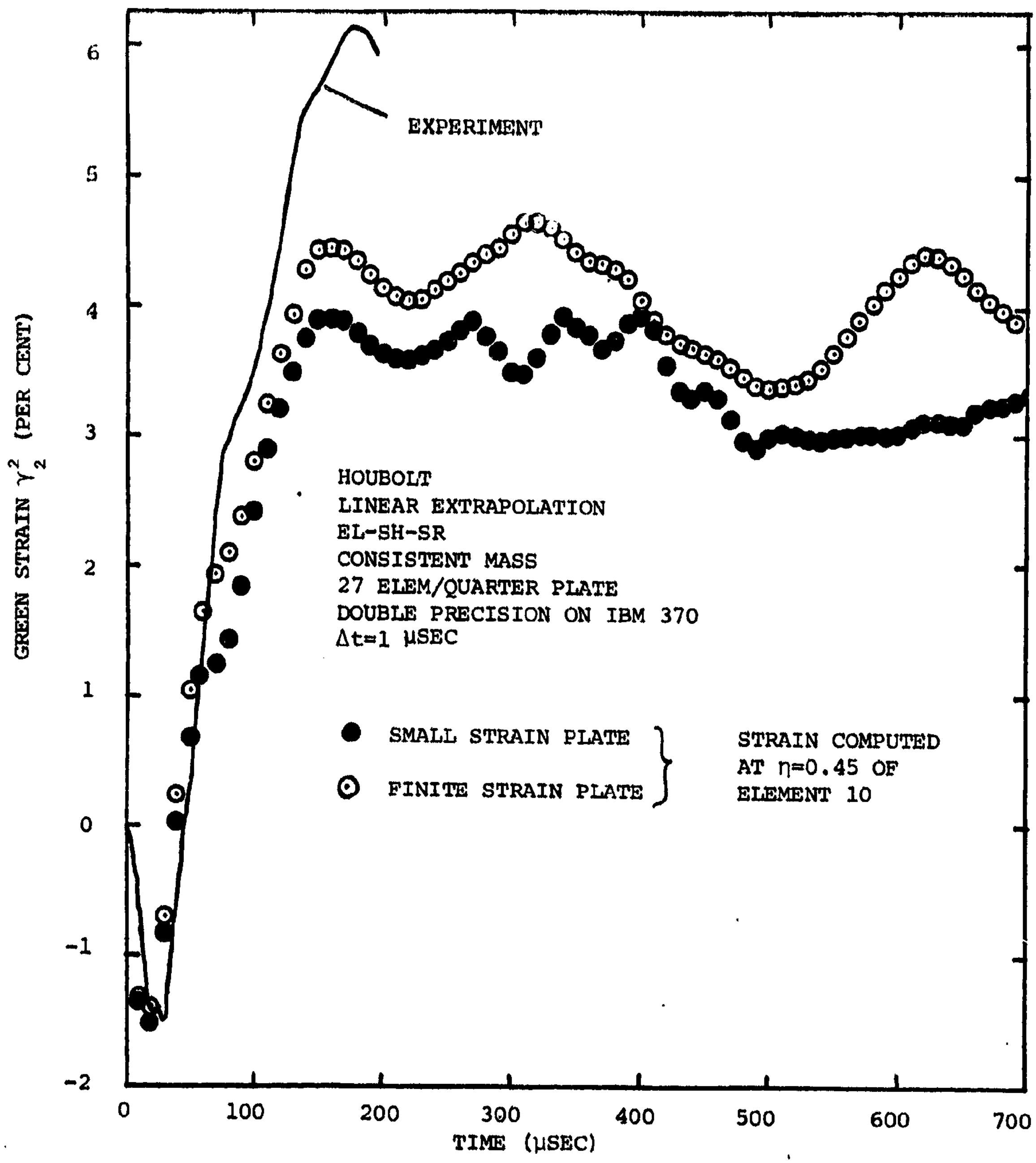

(g) Upper-Surface Strain γ_2^2 at Station (x,y)=(0,1.40in)

FIG.22 CONTINUED (FINITE STRAIN, SMALL STRAIN, EXPT., CB-4)

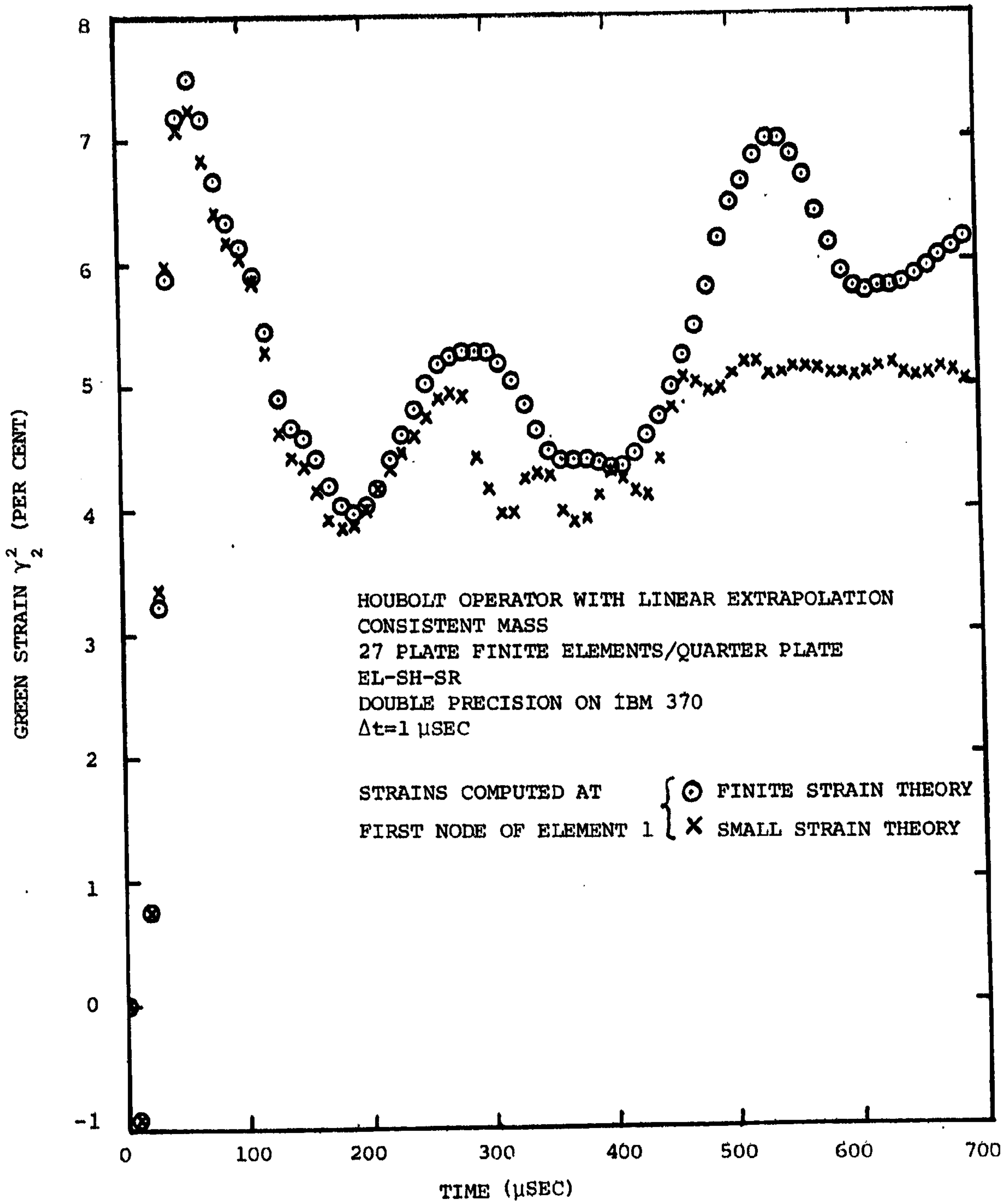

(h) Upper-Surface Strain γ_2^2 at Station (x,y)=(0,0)

FIG.22 CONTINUED (FINITE STRAIN, SMALL STRAIN, EXPT., CB-4)

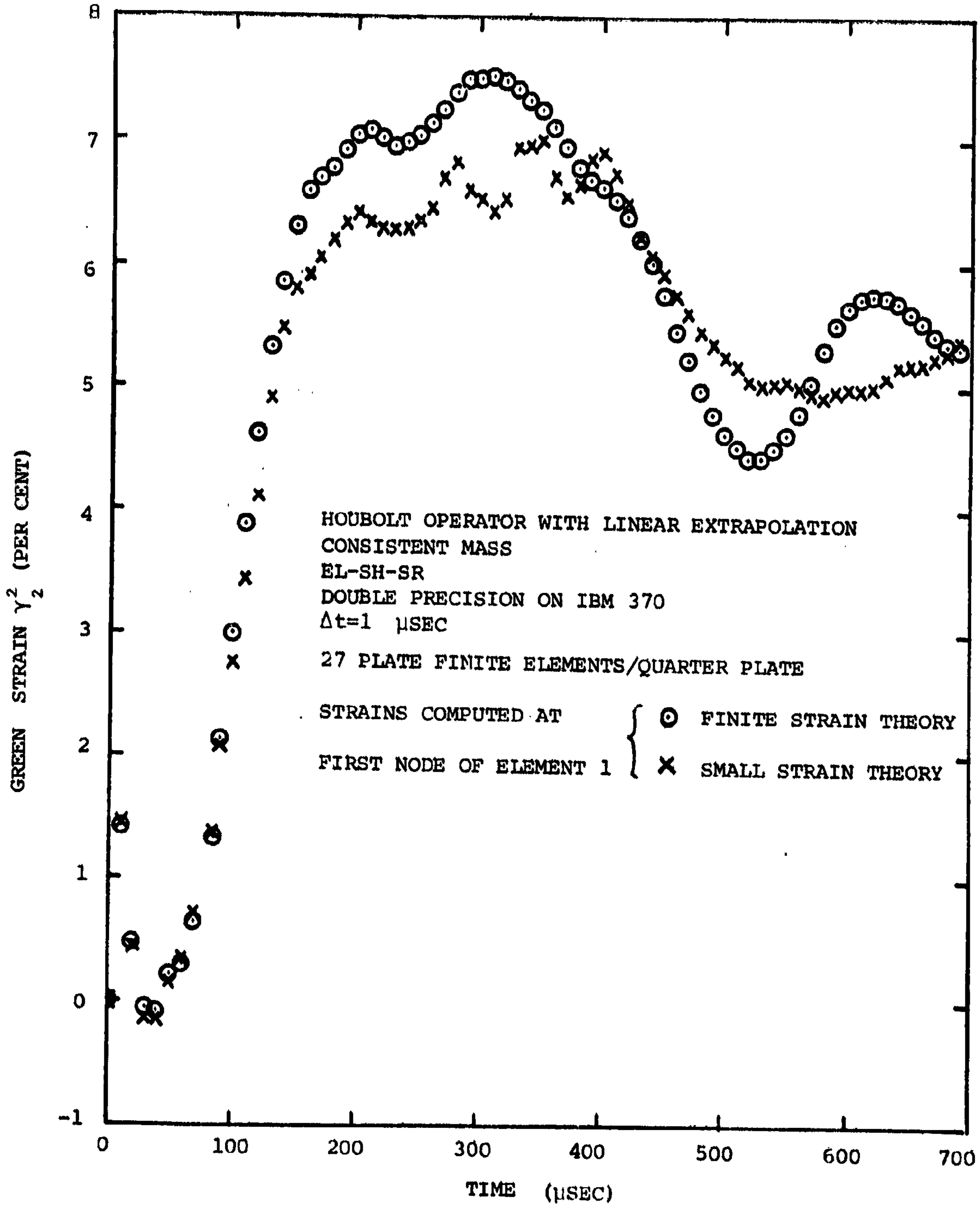

(i) Lower-Surface Strain γ_2^2 at Station (x,y)=(0,0)

FIG.22 CONCLUDED (FINITE STRAIN, SMALL STRAIN, EXPT., CB-4)

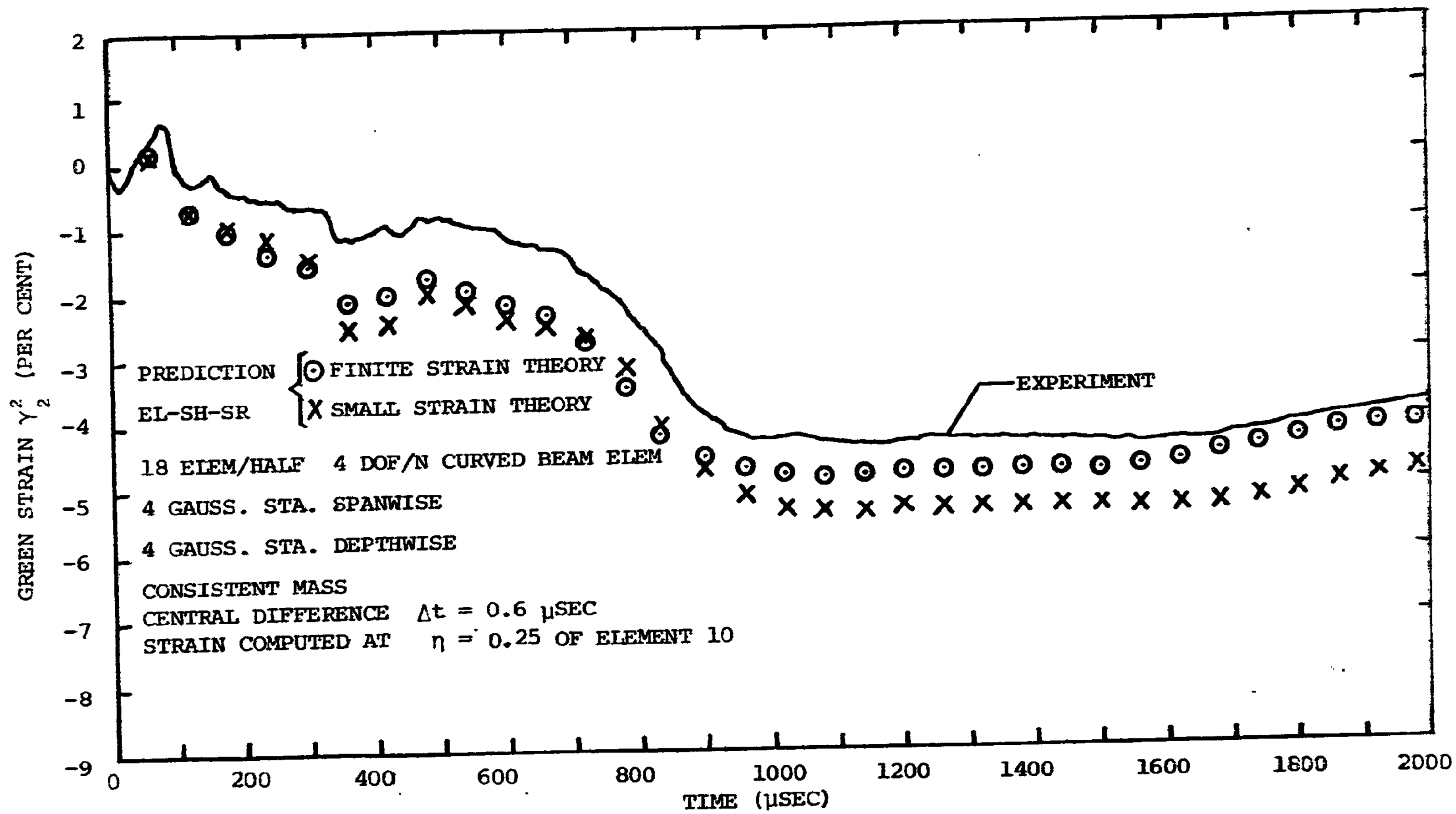

(a) Inner (Non-Loaded) Surface at θ=92° 30'

FIG. 23 COMPARISONS OF EXPERIMENTAL AND PREDICTED STRAINS ON THE INNER AND OUTER SURFACES OF IMPULSIVELY-LOADED FREE CIRCULAR 6061-T6 ALUMINUM RING F-15

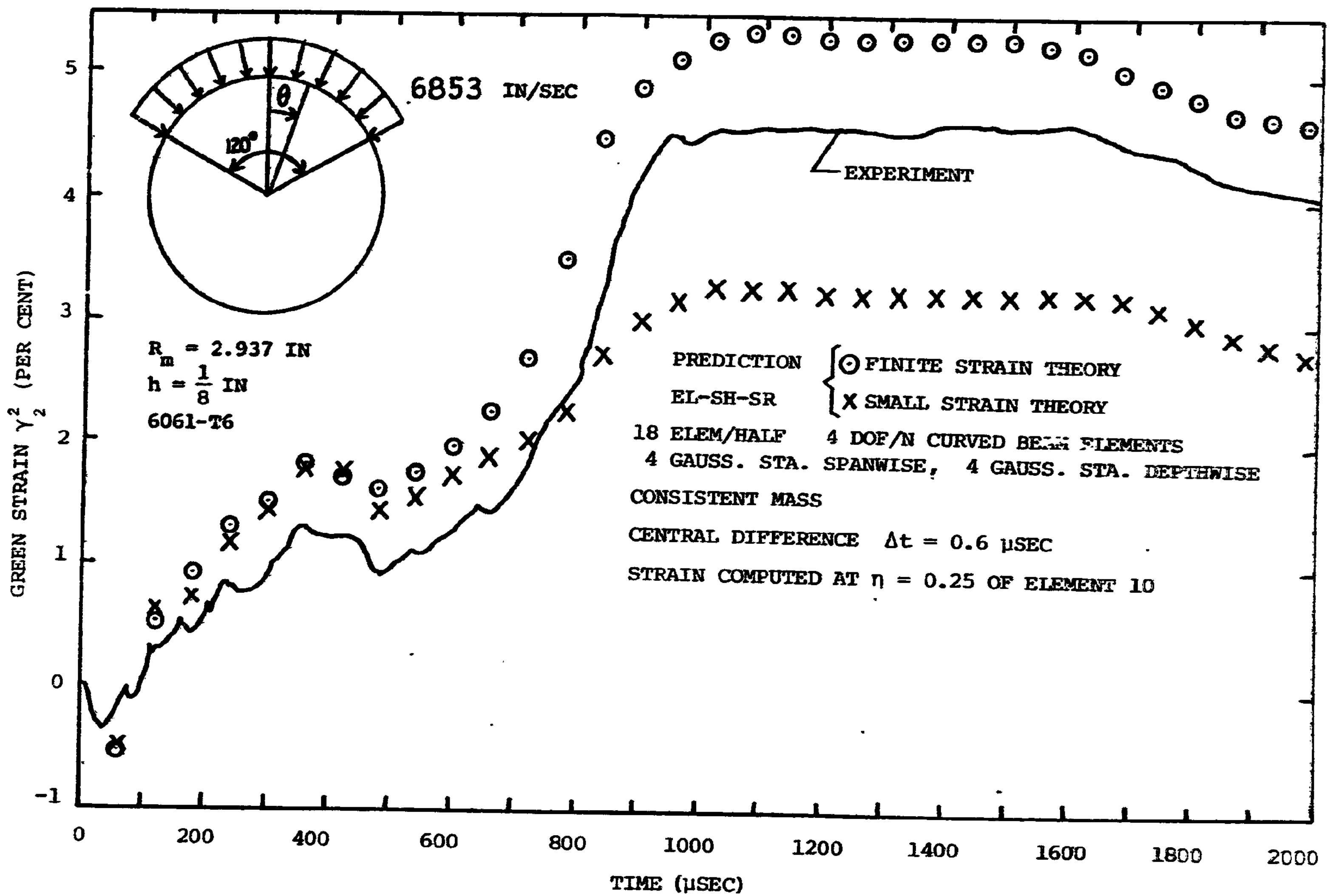

(b) Outer (Loaded) Surface at θ=92° 30'

FIG.23 CONTINUED (FREE RING, EXPT., PREDICTION)

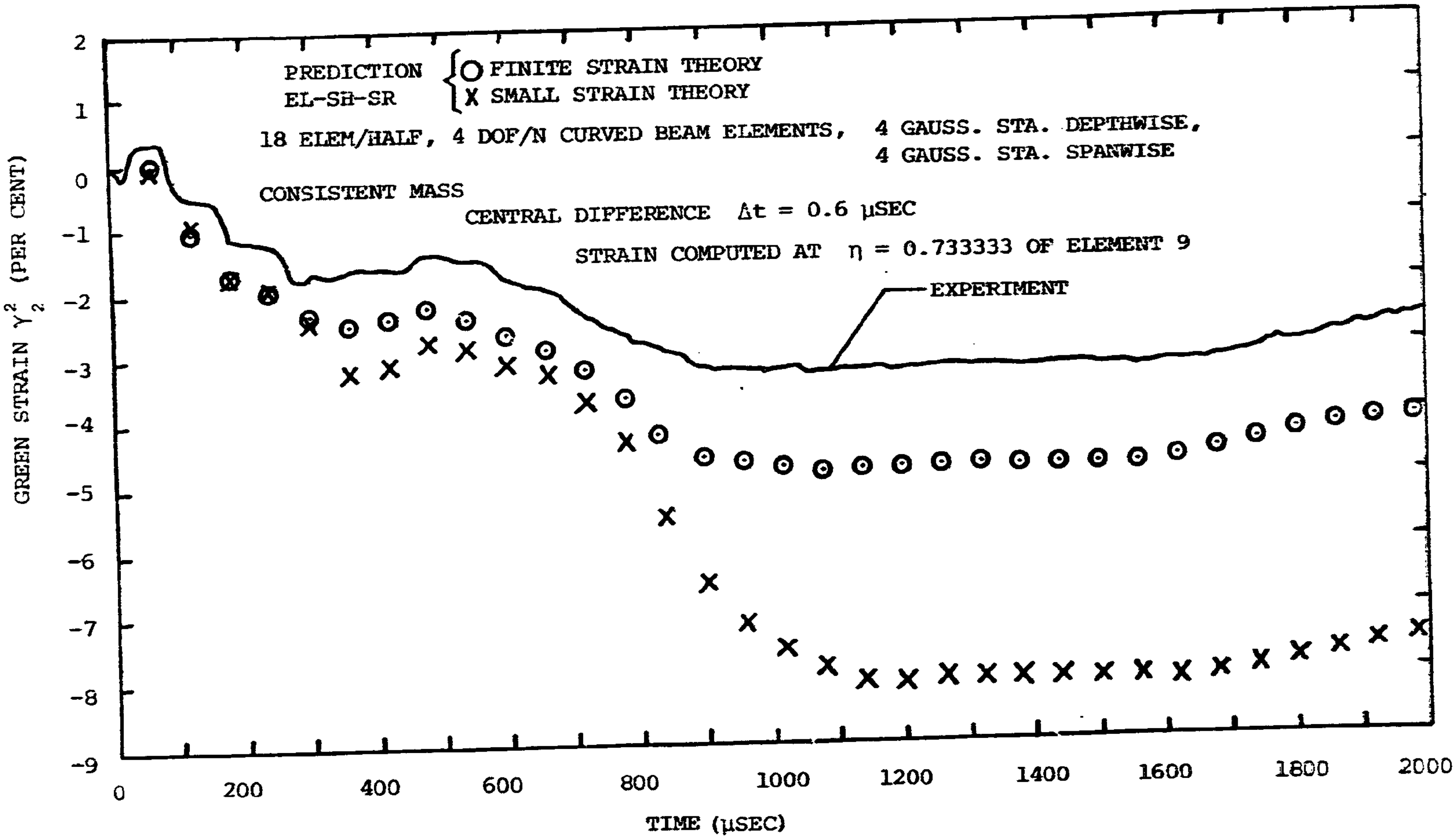

(c) Inner (Non-Loaded) Surface at θ=87° 20'

FIG.23 CONTINUED (FREE RING, EXPT., PREDICTION)

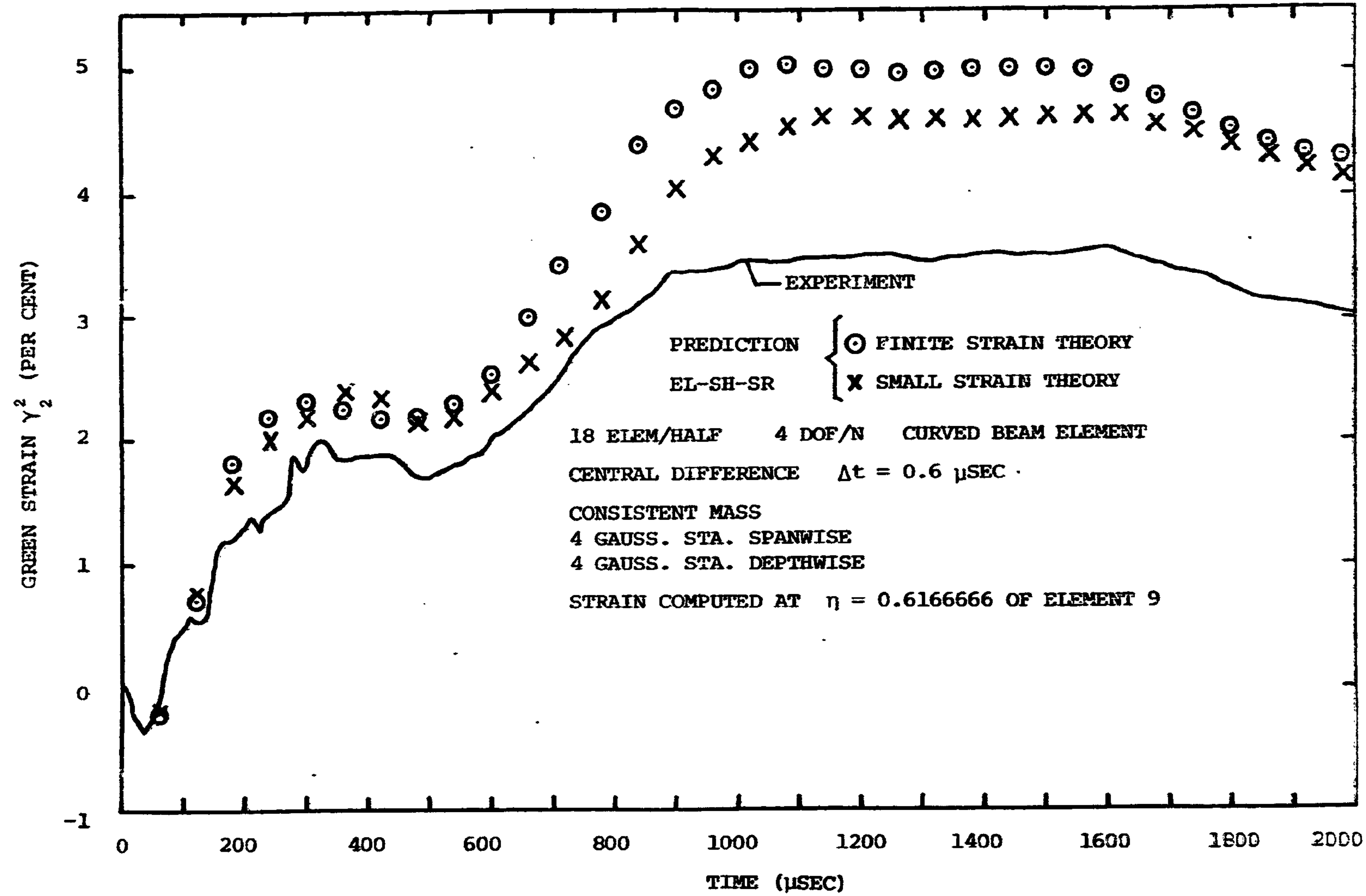

(d) Outer (Loaded) Surface at θ=86° 10'

FIG.23 CONTINUED (FREE RING, EXPT., PREDICTION)

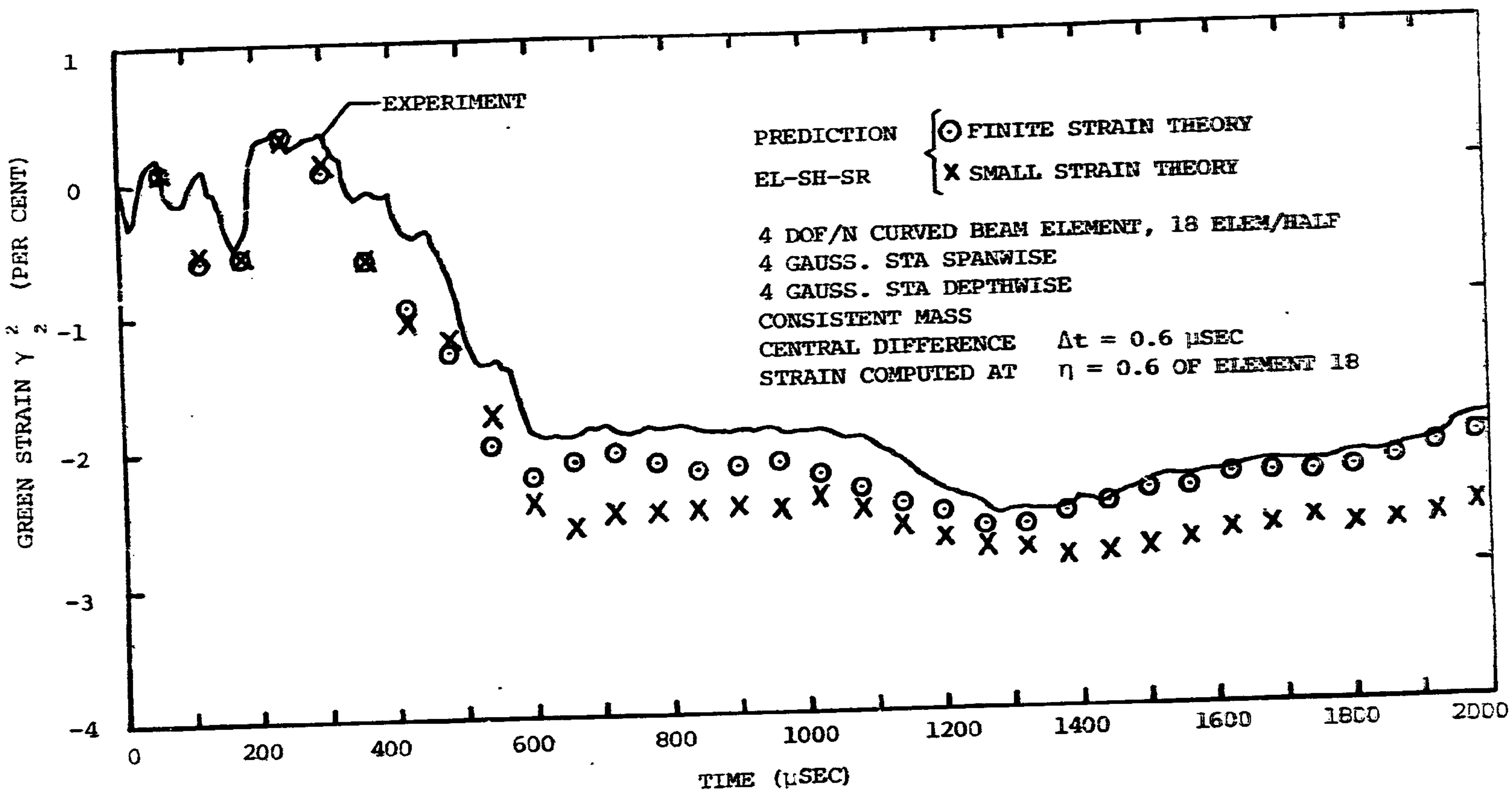

(e) Outer (Loaded) Surface at θ=176°

FIG.23 CONTINUED (FREE RING, EXPT., PREDICTION)

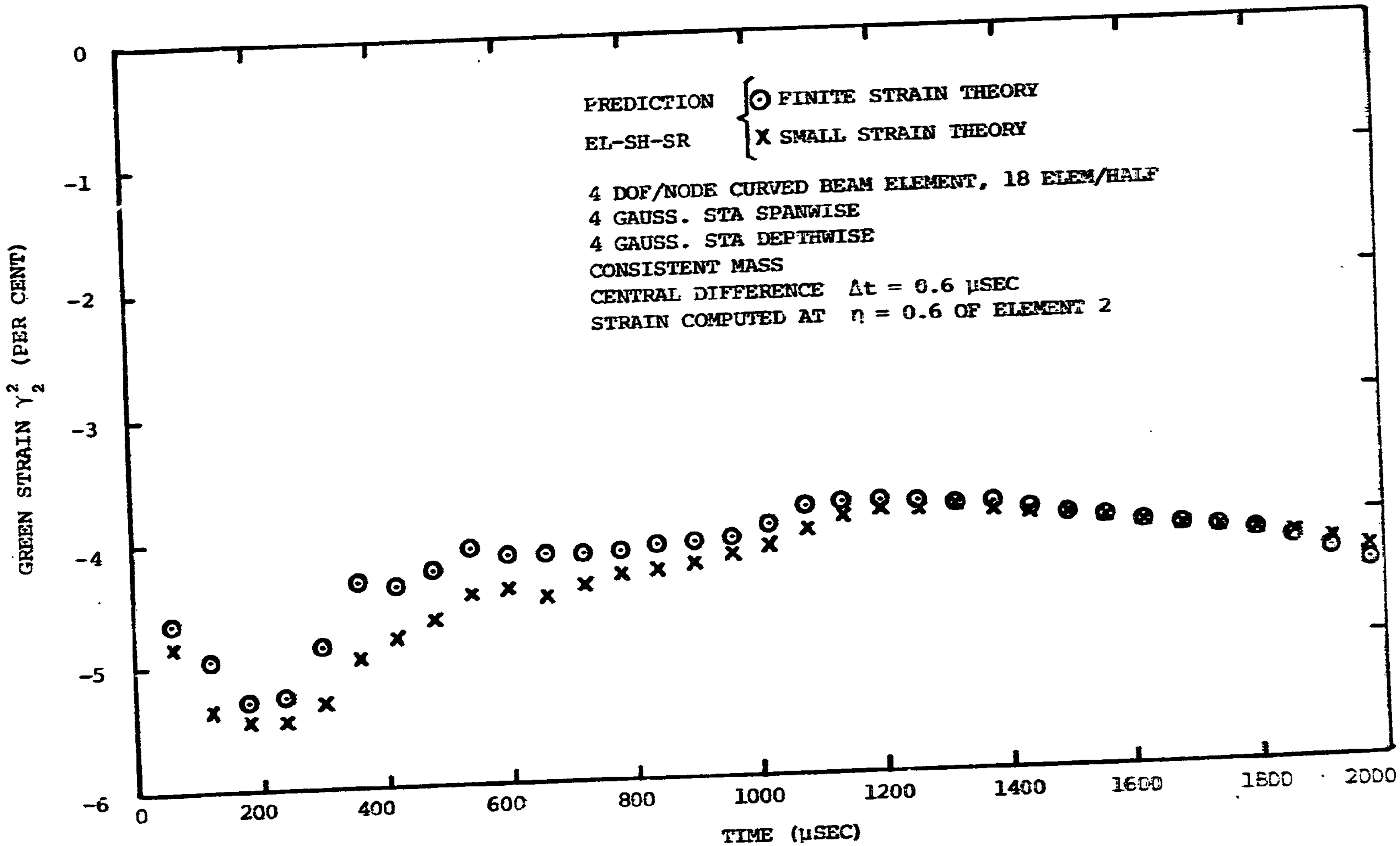

(f) Inner (Non-Loaded) Surface at $\theta=16°$

FIG.23 CONTINUED (FREE RING, EXPT., PREDICTION)

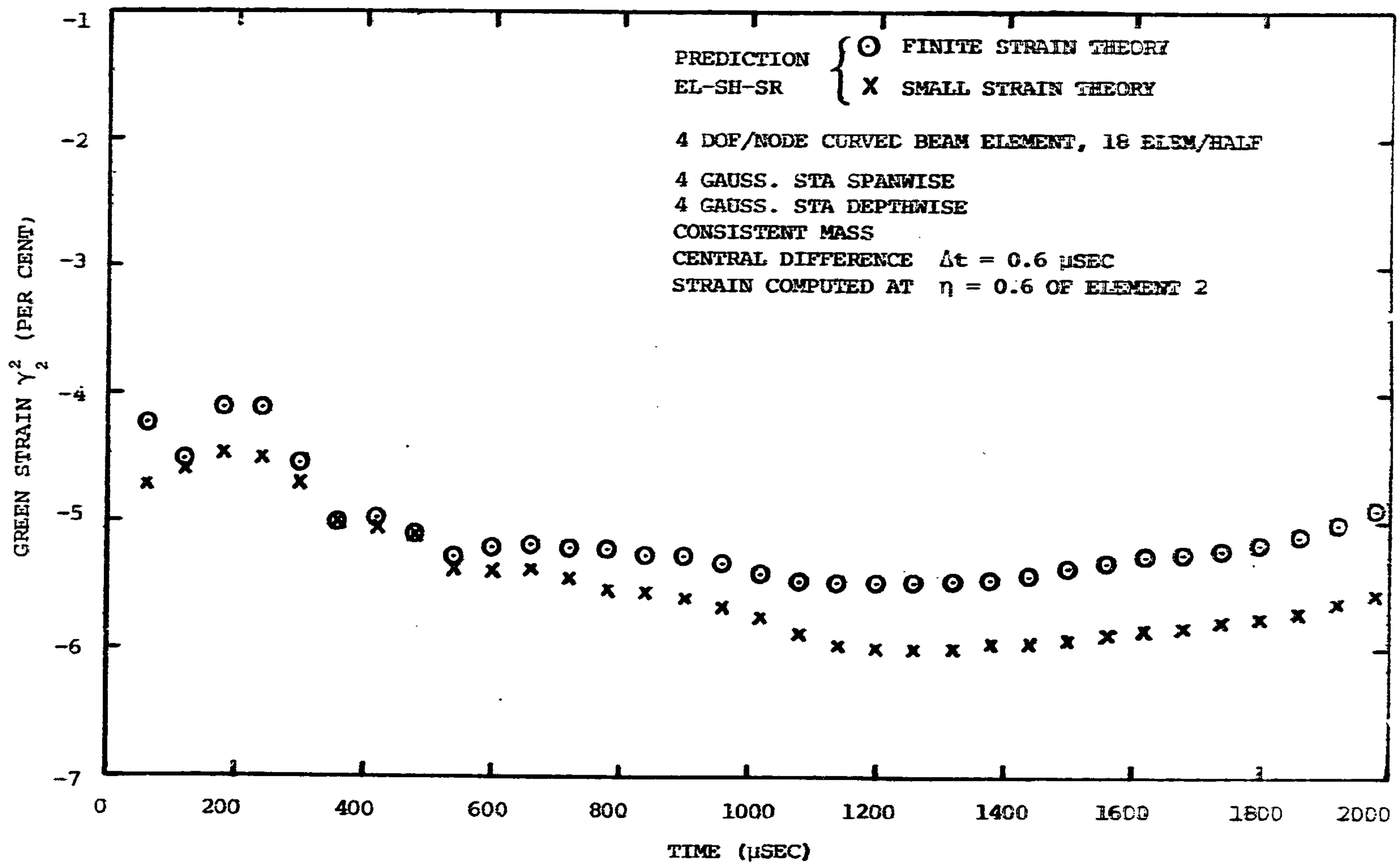

(g) Outer (Loaded) Surface at θ=16°

FIG.23 CONCLUDED (FREE RING, EXPT., PREDICTION)

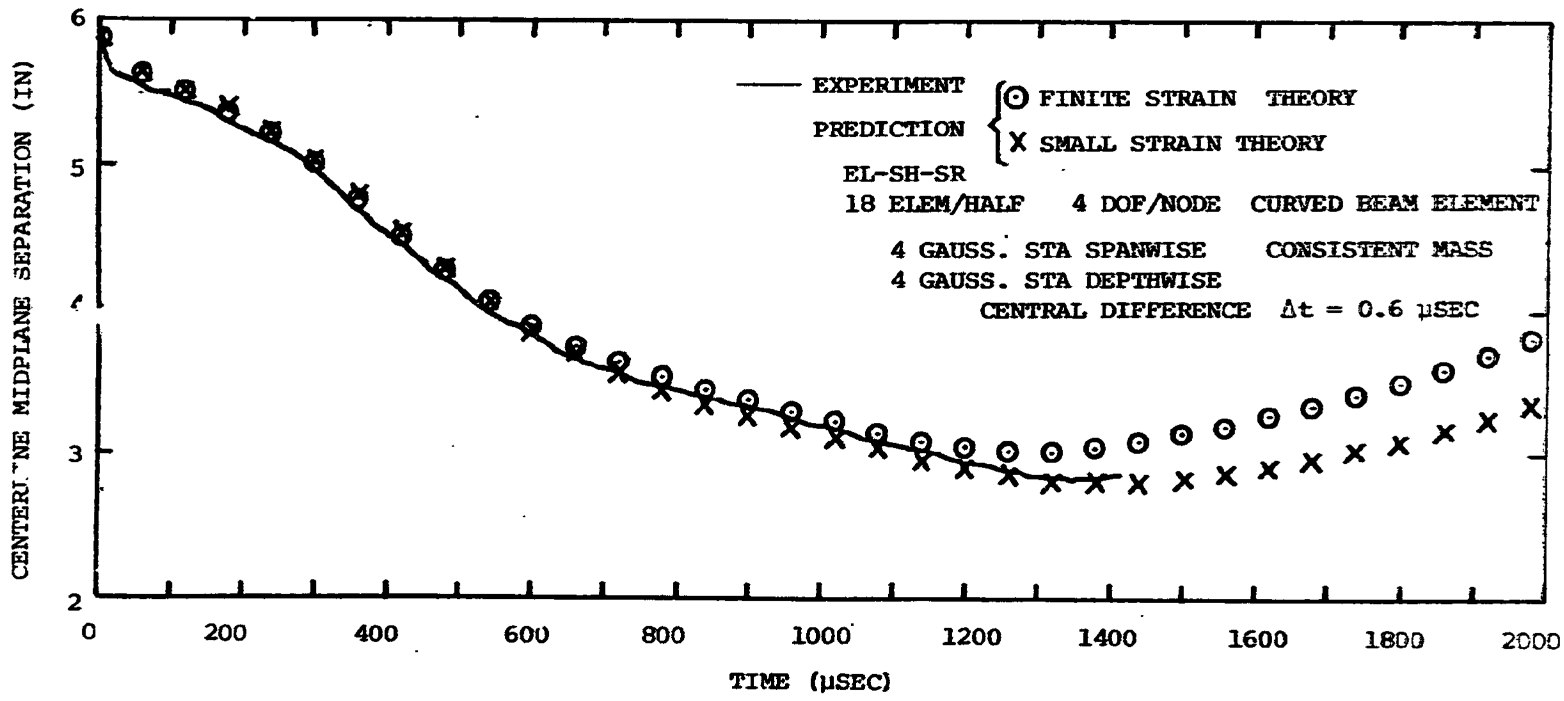

FIG.24 COMPARISON OF EXPERIMENTAL AND PREDICTED CENTERLINE MIDPLANE SEPARATION FOR THE IMPULSIVELY-LOADED FREE CIRCULAR 6061-T6 ALUMINUM RING F-15

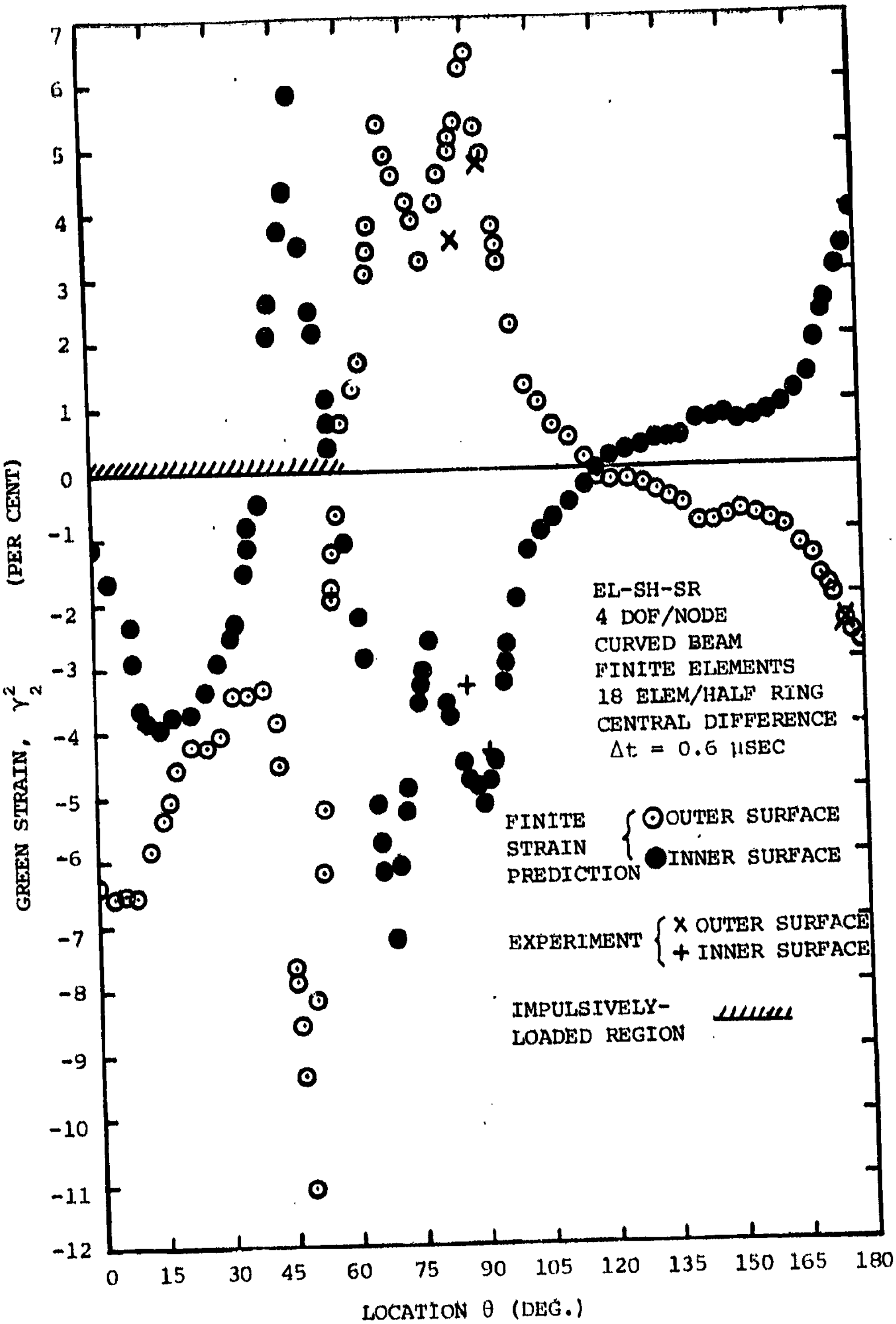

FIG. 25 PREDICTED CIRCUMFERENTIAL DISTRIBUTION OF INNER-SURFACE AND OUTER-SURFACE STRAIN AT 1500 MICROSECONDS FOR IMPULSIVELY-LOADED FREE CIRCULAR 6061-T6 ALUMINUM RING F-1'

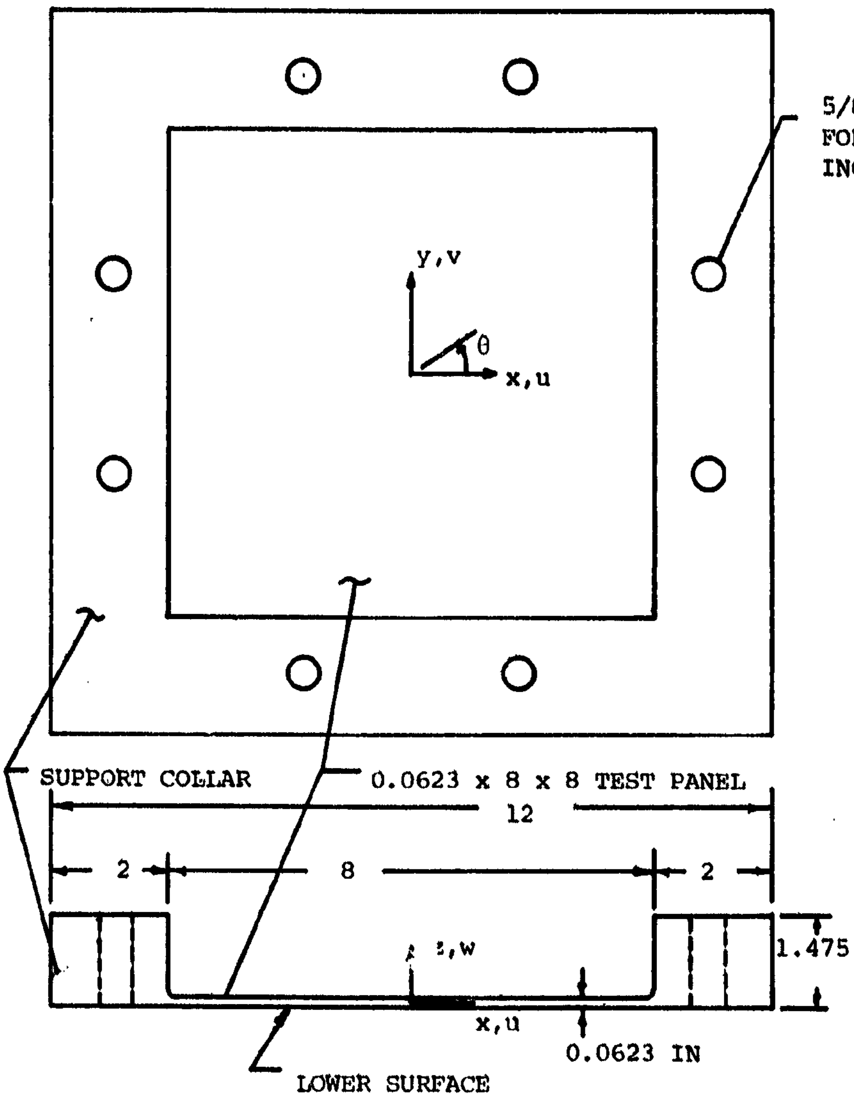

FIG. 26 GEOMETRY AND NOMINAL DIMENSIONS OF UNIFORM-THICKENSS 6061-T651 ALUMINUM PANEL MODEL CP-2

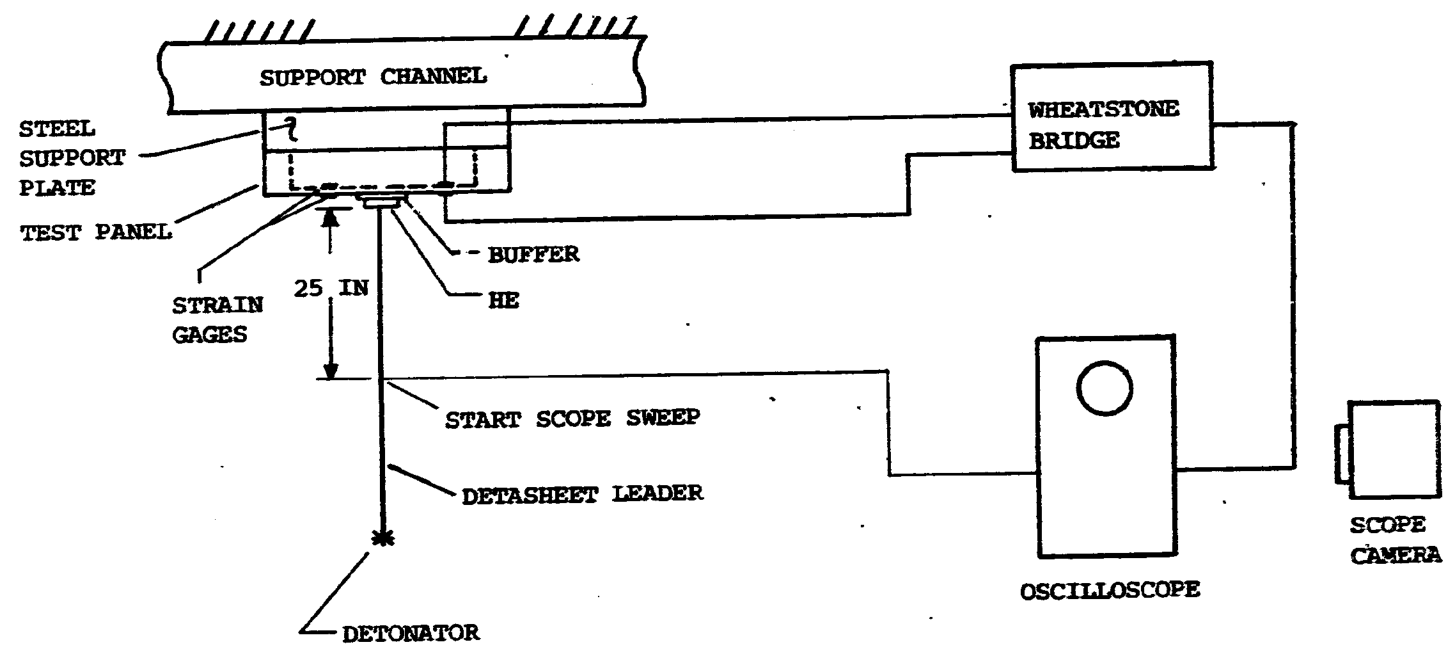

FIG. 27 SCHEMATIC OF IMPULSIVE-LOADING TESTS ON 6061-T651 ALUMINUM PANELS WITH CLAMPED SIDES

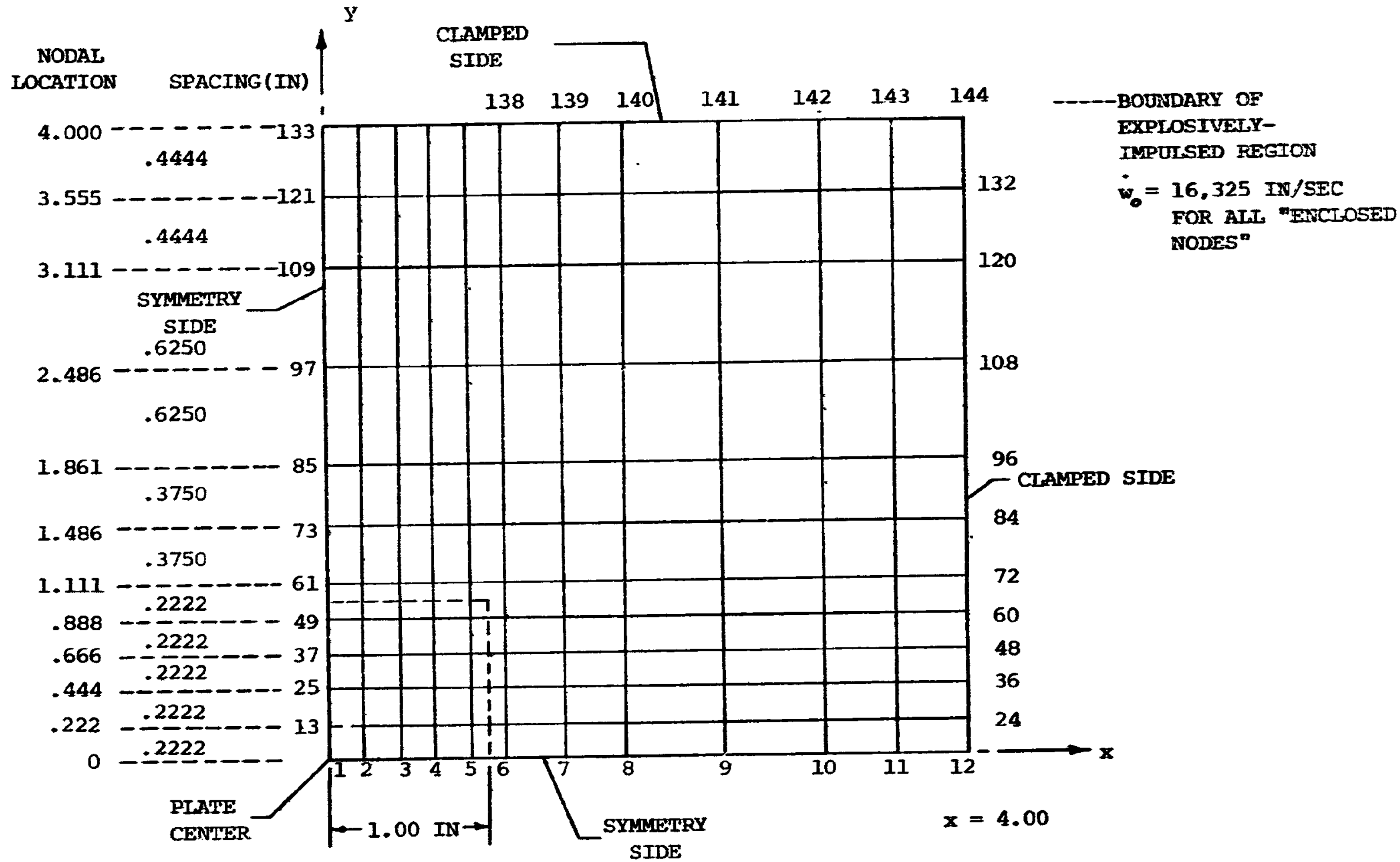

(a) Geometry and Node Numbers

FIG. 28 GEOMETRY, FINITE ELEMENT MESH, NODE NUMBERS, AND ELEMENT NUMBERS FOR ONE QUARTER OF SQUARE CLAMPED-EDGE 6061-T651 THIN ALUMINUM PANEL CP-2 EXPLOSIVELY IMPULSED OVER A CENTERED 2-IN BY 2-IN REGION

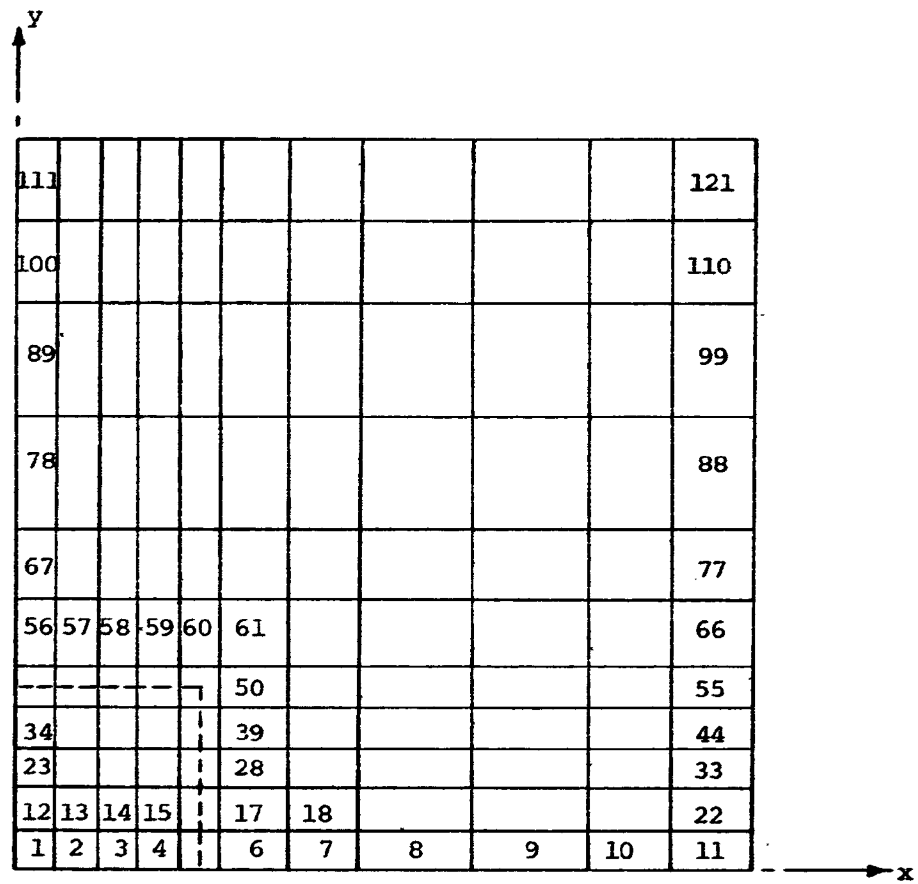

(b) Element Numbers

FIG. 28 CONCLUDED (CP-2)

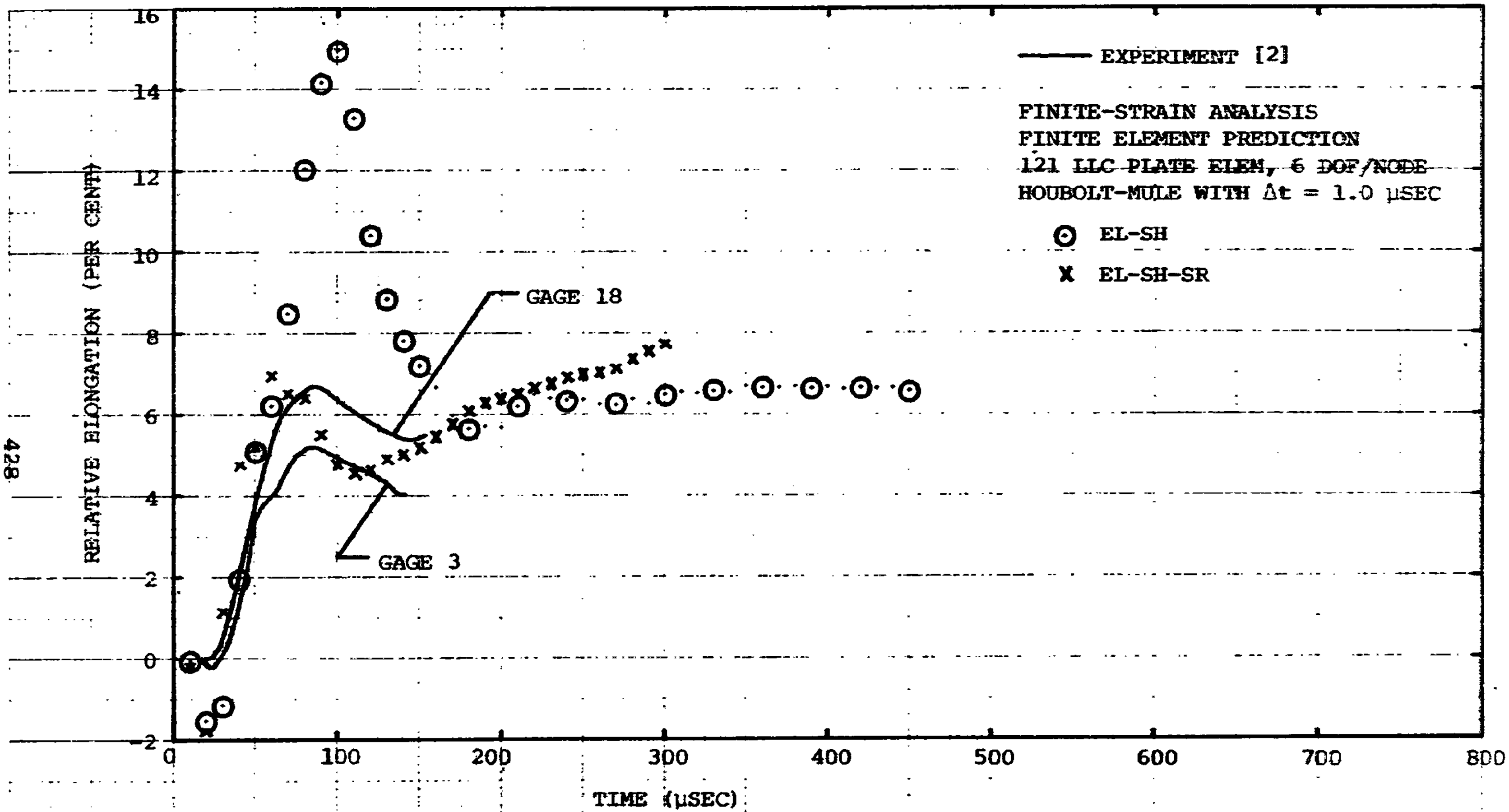

(a) Location (x, y, θ) = (0, 1.50 in, 90 deg.), Upper Surface

FIG. 29 COMPARISON OF FINITE-STRAIN-PREDICTED VS. MEASURED TRANSIENT RELATIVE ELONGATION ON THE UPPER (NON-LOADED) SURFACE OF EXPLOSIVELY-IMPULSED 6061-T651 THIN ALUMINUM PANEL CP-2

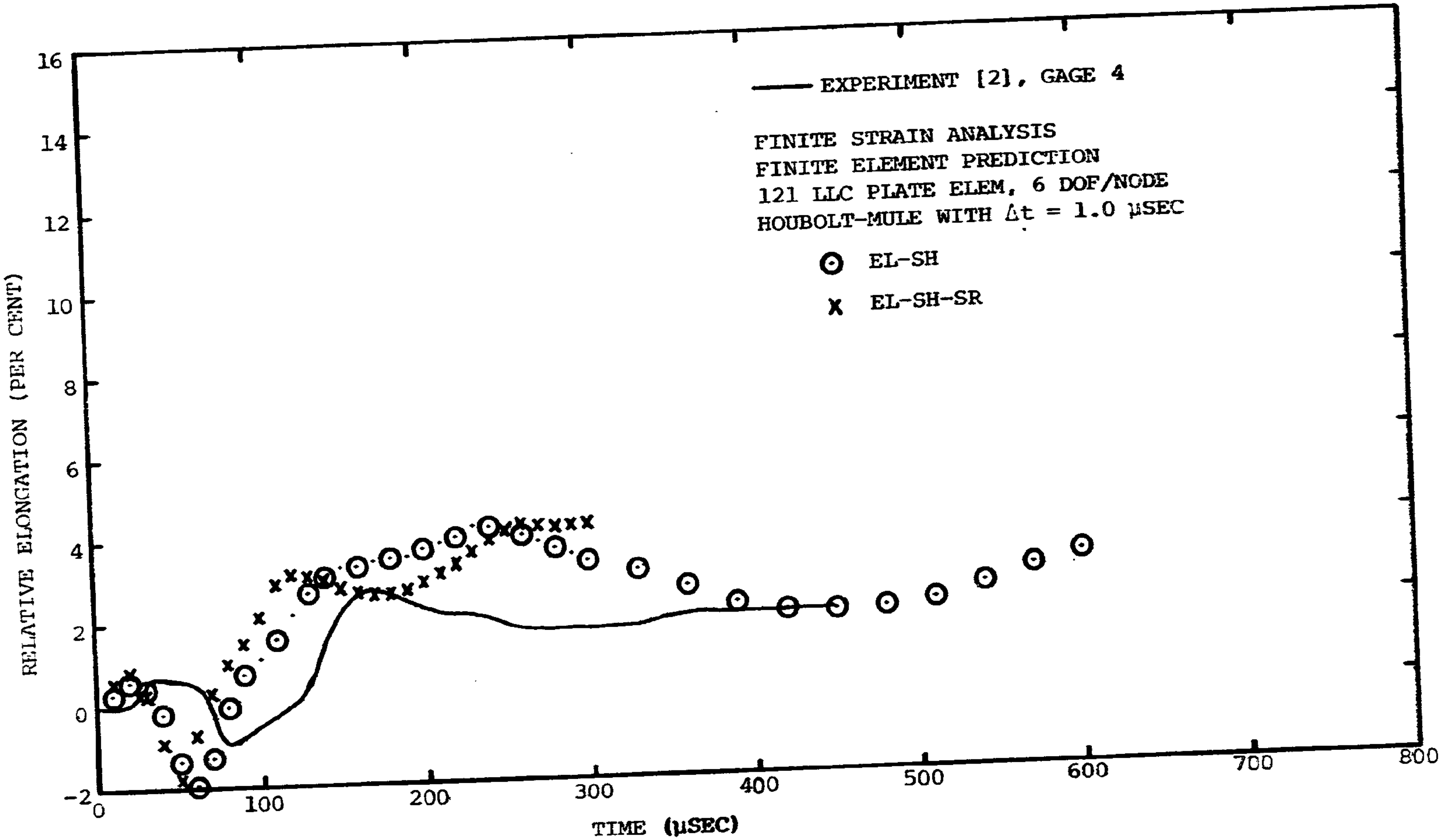

(b) Location (x,y,θ) = (0, 2.00 in, 90 deg), Upper Surface

FIG. 29 CONTINUED (CP-2, FINITE STRAIN PREDICTION, EL-SH, EL-SH-SR, EXPT)

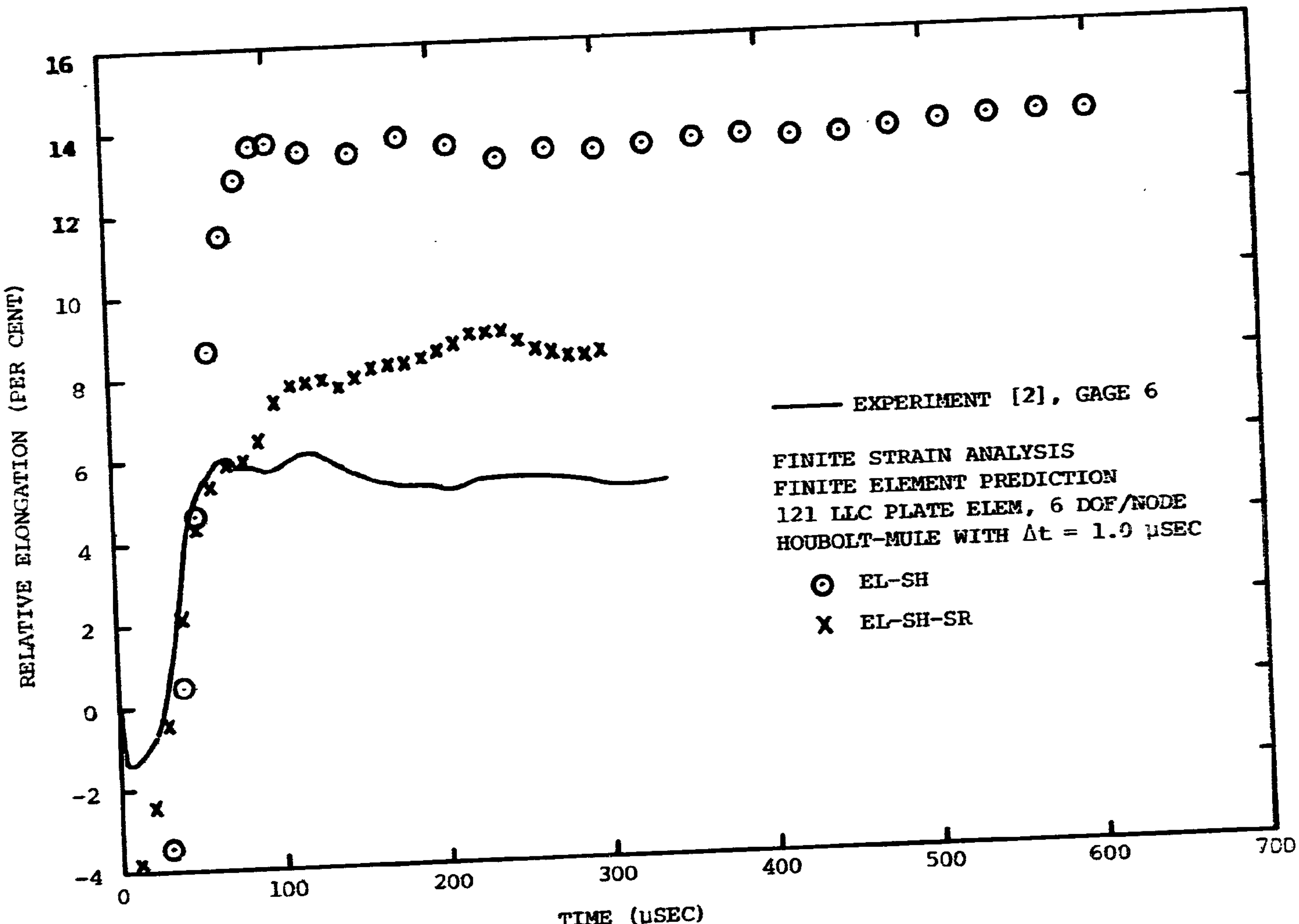

(c) Location (x,y,θ) = (1.061, 1.061 in, 45 deg), Upper Surface

FIG. 29 CONTINUED (CP-2, FINITE STRAIN PREDICTION, EL-SH, EL-SH-SR, EXPT.)

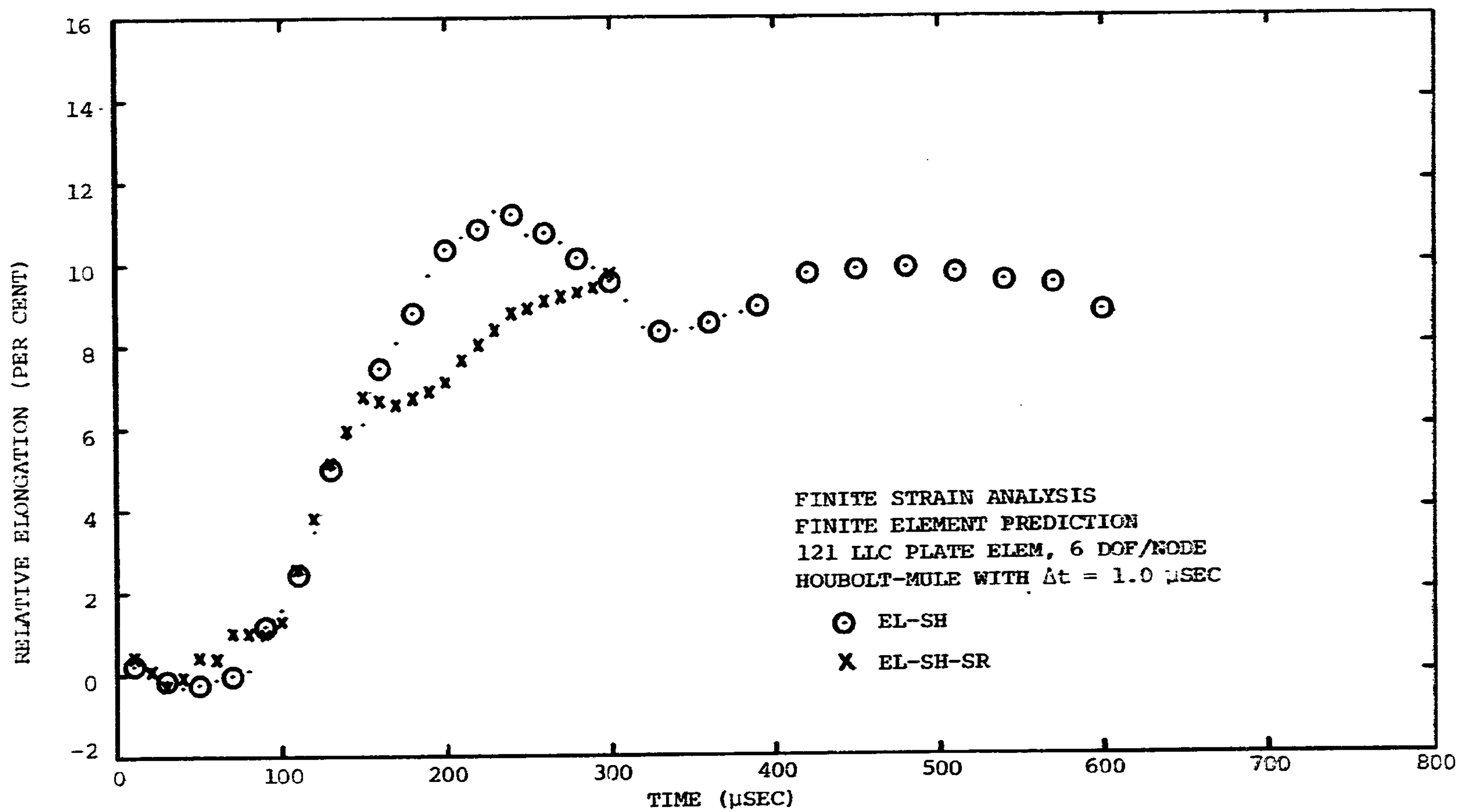

(d) Location (x,y,θ) = (1.414, 1.414 in, 45 deg), Upper Surface

FIG. 29 CONTINUED (CP-2, FINITE STRAIN PREDICTION, EL-SH, EL-SH-SR, EXPT)

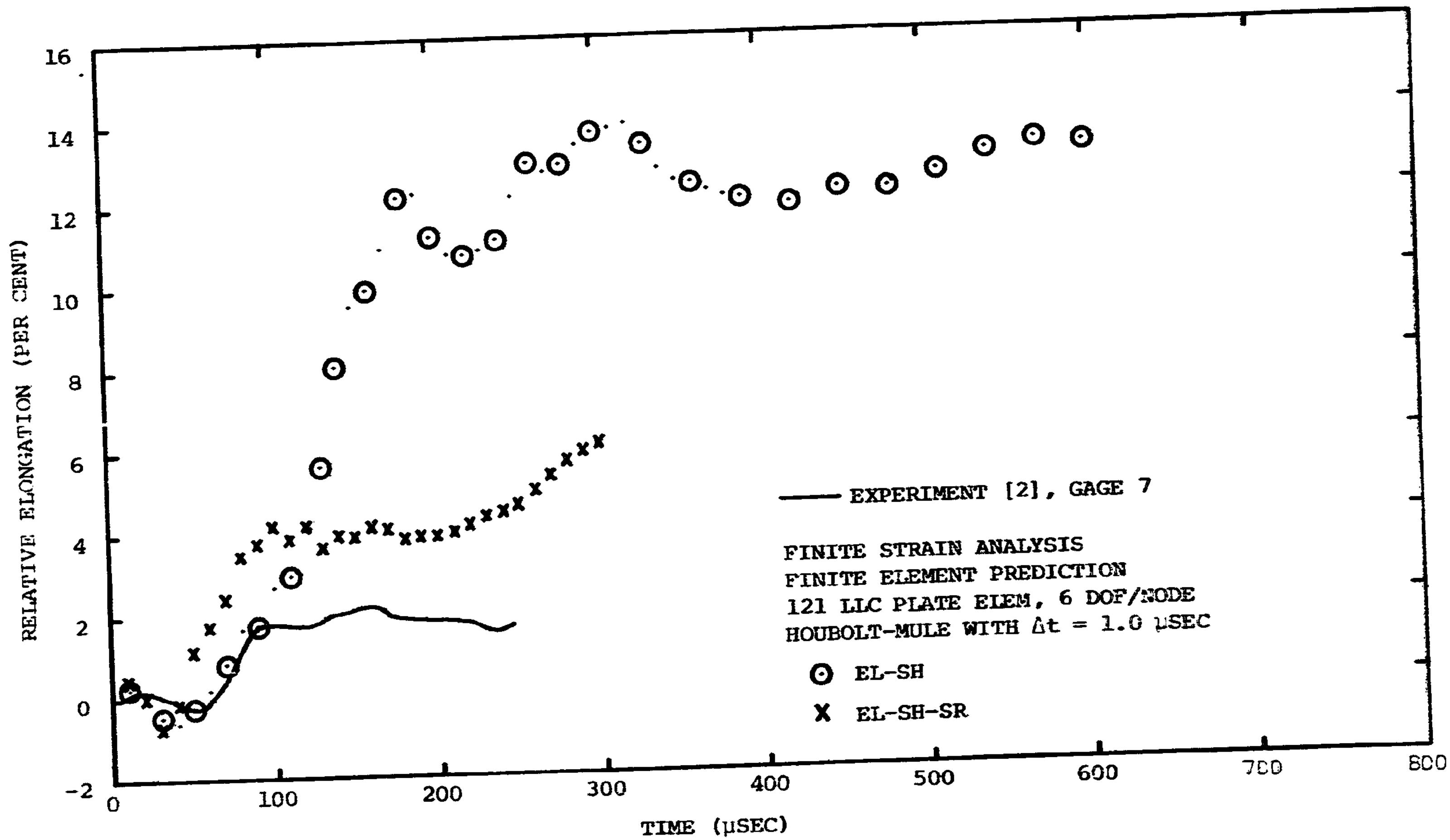

(e) Location (x,y,θ) = (1.50, 1.50 in, 45 deg), Upper Surface

FIG. 29 CONTINUED (CP-2, FINITE STRAIN PREDICTION, EL-SH, EL-SH-SR, EXPT)

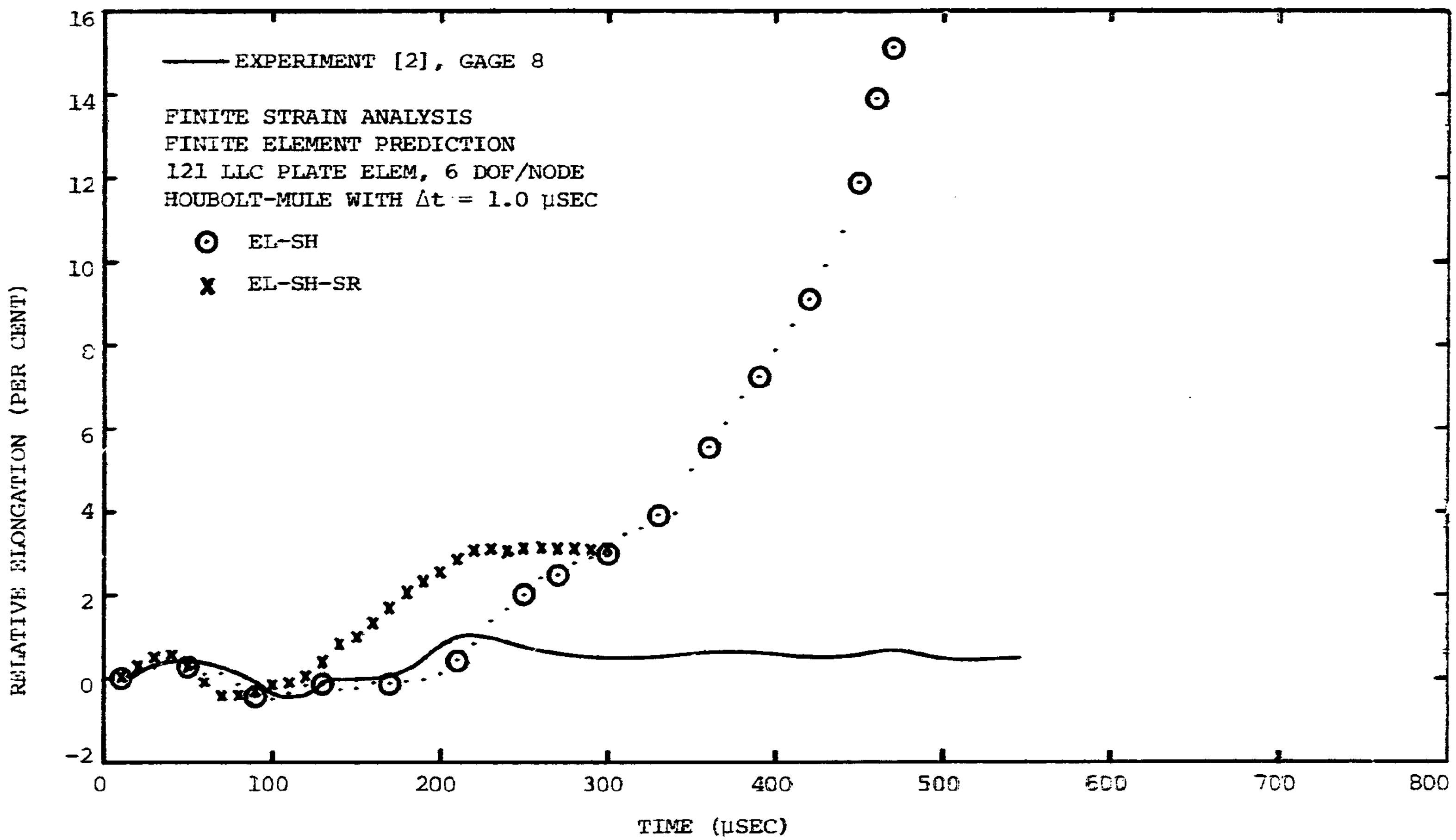

(f) Location (x,y,θ) = (2.00, 2.00 in, 45 deg), Upper Surface

FIG. 29 CONCLUDED (CP-2, FINITE STRAIN PREDICTION EL-SH, EL-SH-SR, EXPT)

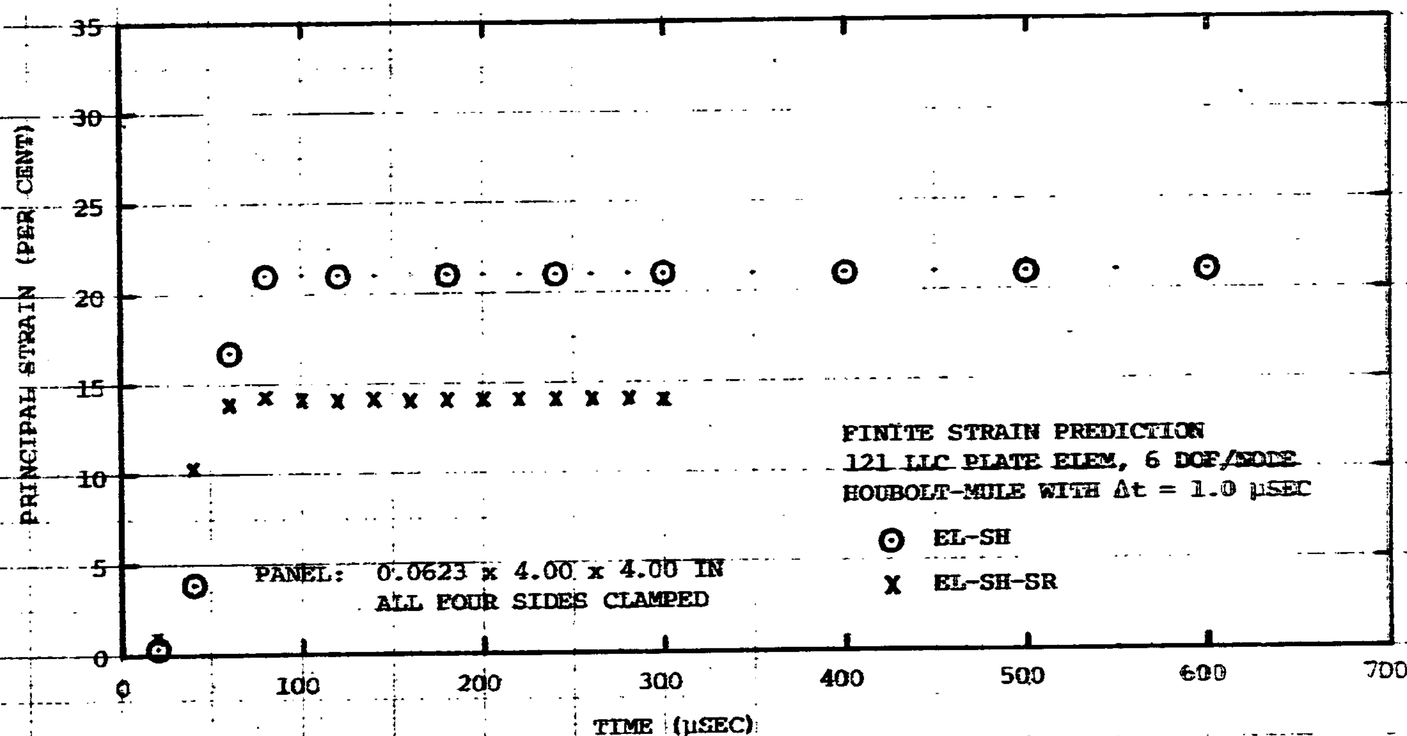

(a) Predicted Upper-Surface Transient Principal Strain at Station (x,y) = (0.111, 0.111 in) — Center of Element 1

FIG. 30 FINITE-STRAIN PREDICTION OF UPPER-SURFACE STRAINS AT VARIOUS STATIONS AND TIMES FOR EXPLOSIVELY-IMPULSED 6061-T651 ALUMINUM PANEL CP-2

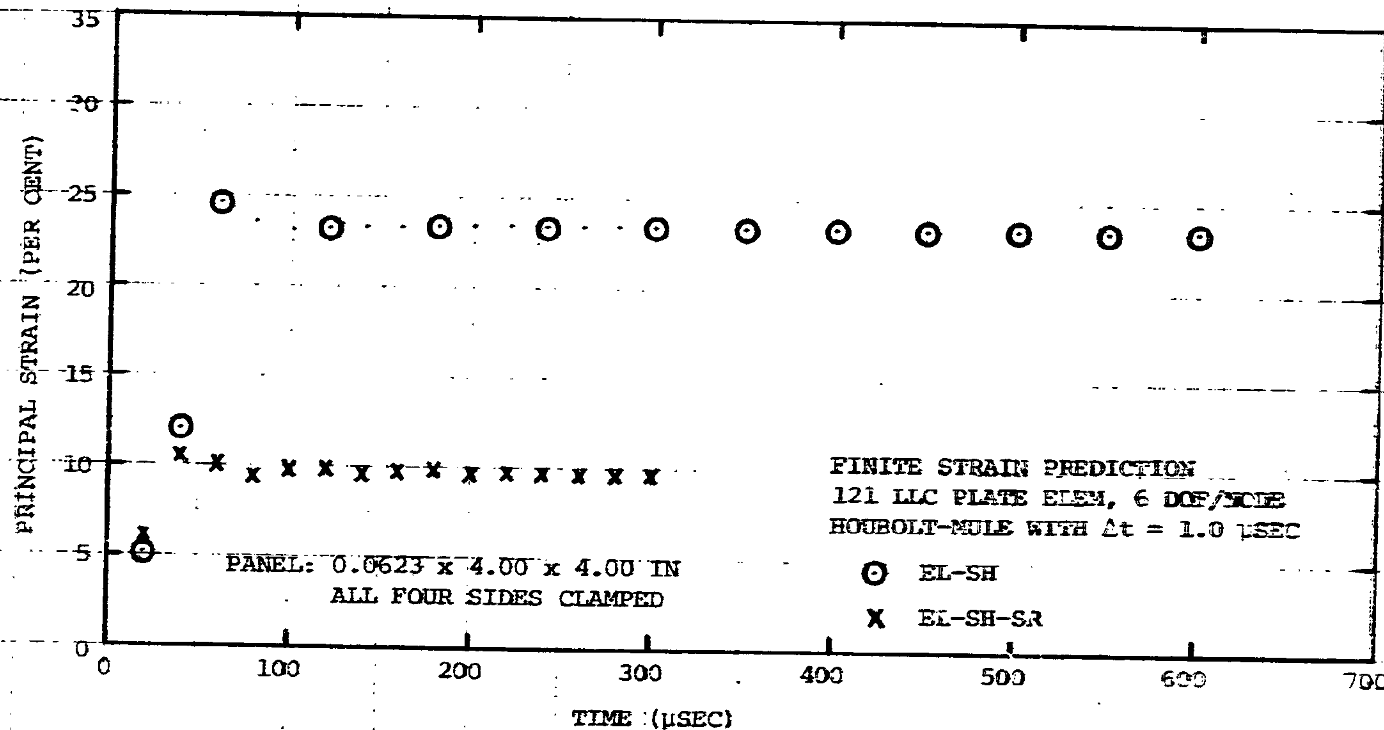

(b) Predicted Upper-Surface Transient Principal Strain at Station (x,y) = (0.333, 0.111 in)
-- Center of Element 3

FIG. 30 CONTINUED (CP-2, FINITE STRAIN PREDICTION)

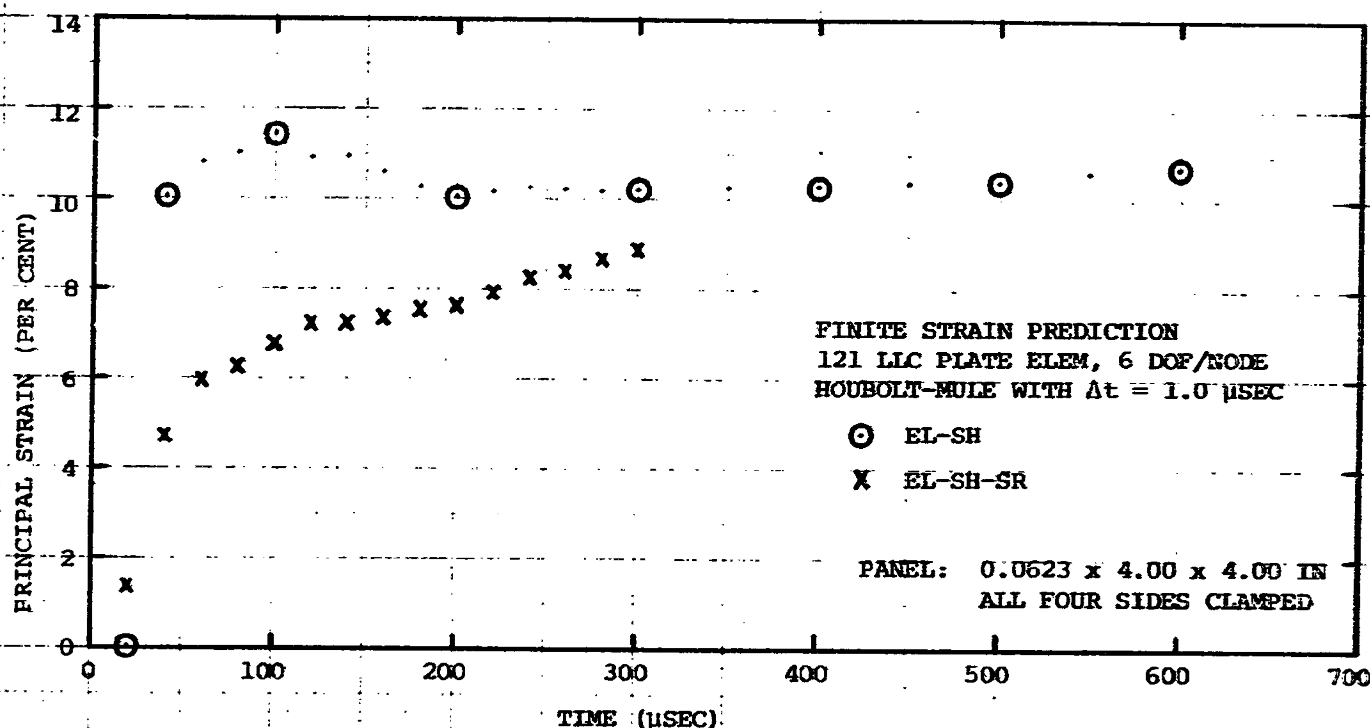

(c) Predicted Upper-Surface Principal Strain at Station (x,y) = (1.298, .111 in) — Center of Element 6

FIG. 30 CONTINUED (CP-2, FINITE STRAIN PREDICTION)

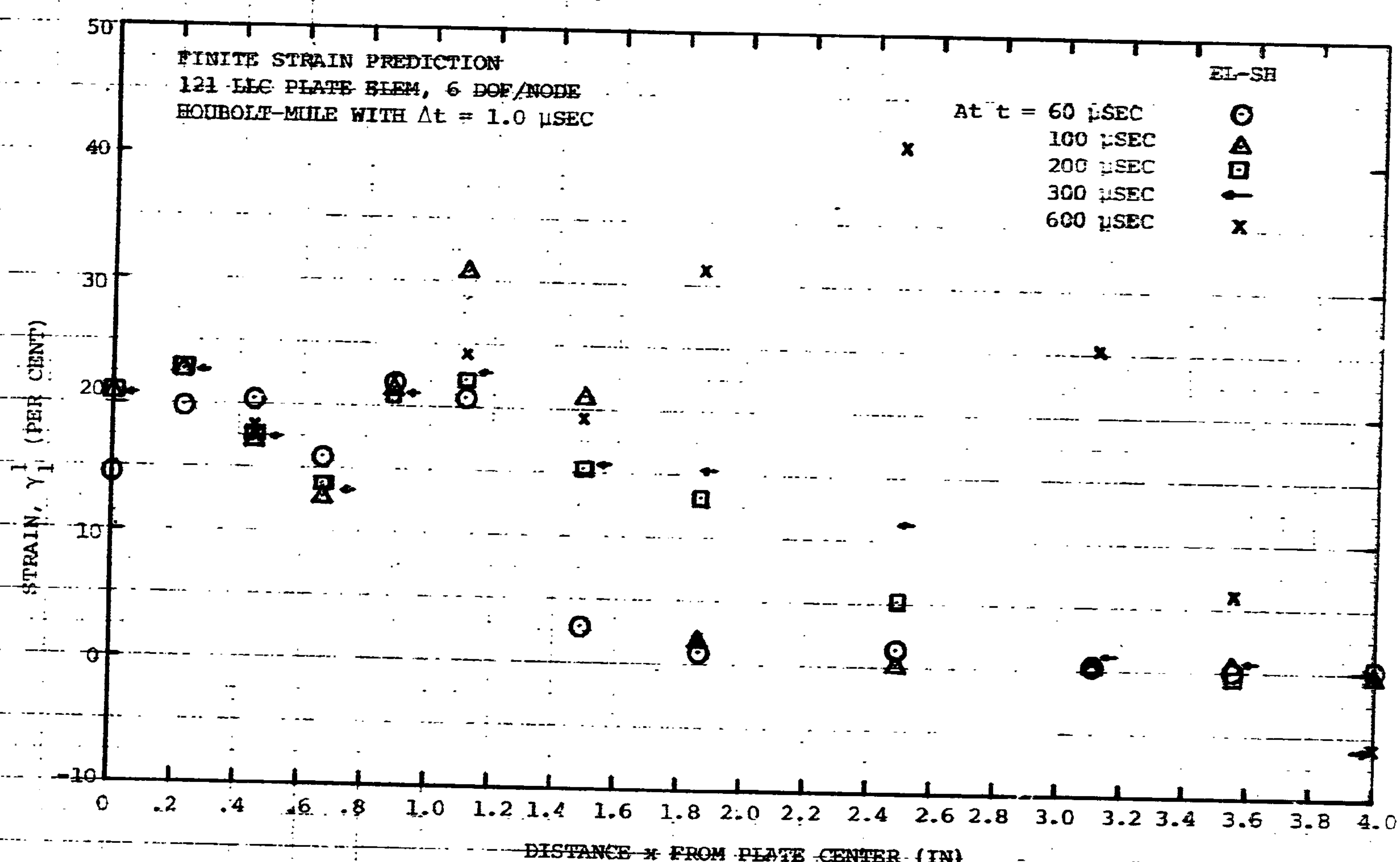

(d) EL-SH PREDICTED UPPER-SURFACE STRAIN γ_1^1 VS. x ALONG y = 0 for Various Time Instants

FIG. 30 CONTINUED (CP-2, FINITE STRAIN PREDICTION)

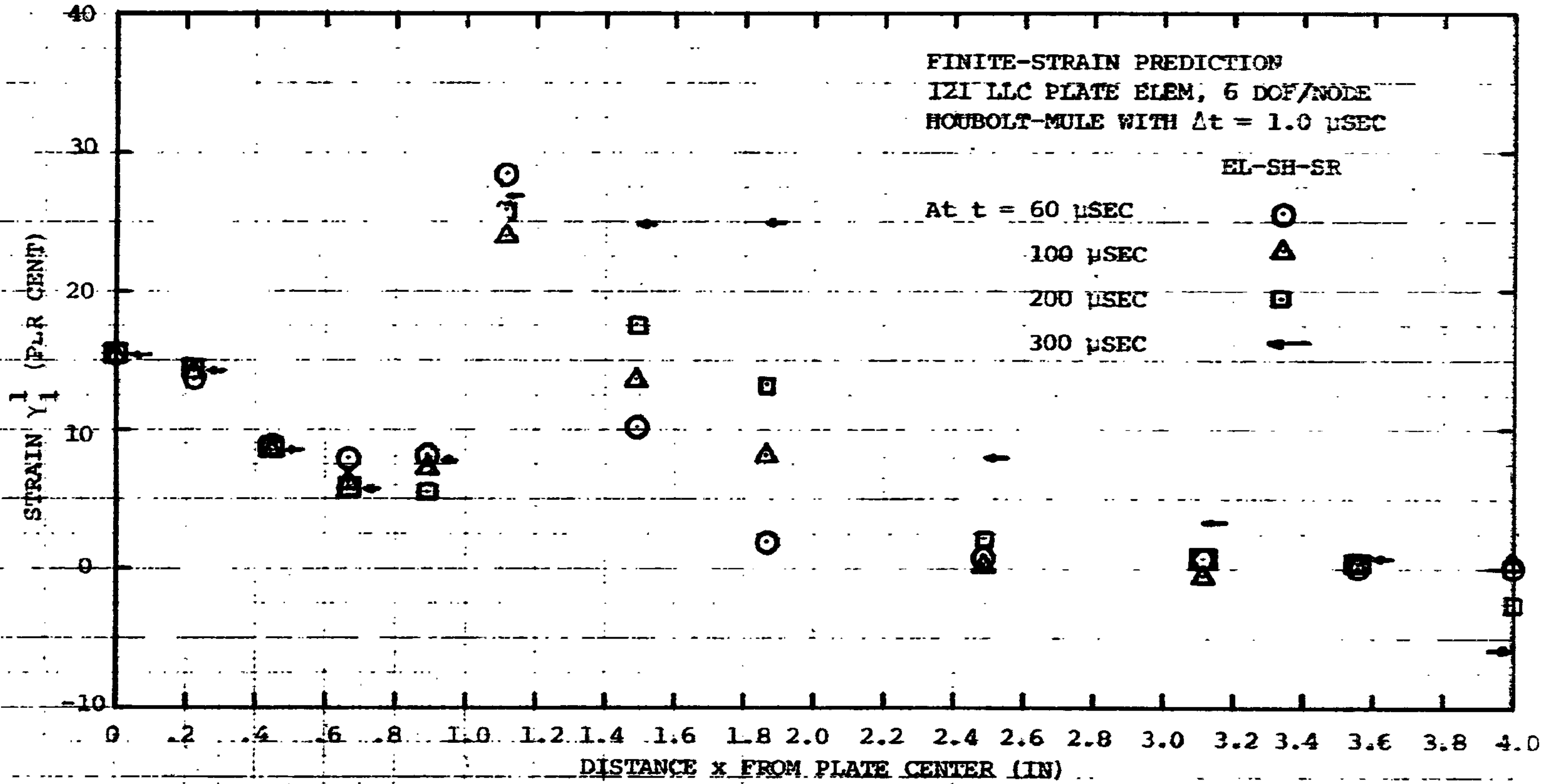

(e) EL-SH-SR PREDICTED UPPER-SURFACE STRAIN VS. x ALONG y = 0 FOR VARIOUS TIME INSTANTS

FIG. 30 CONCLUDED (CP-2, FINITE STRAIN PREDICTION)

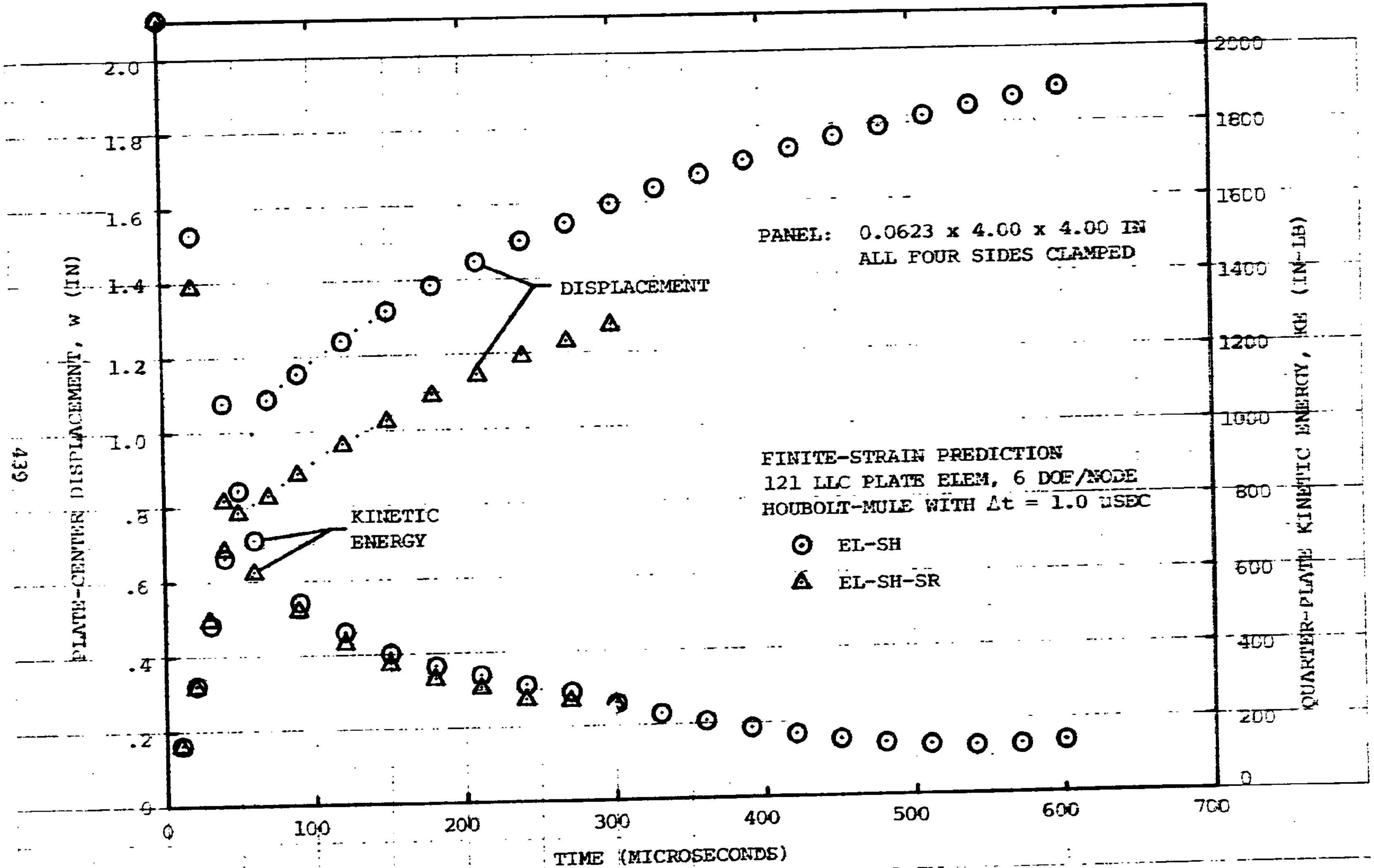

FIG. 31 FINITE-STRAIN PREDICTION OF THE PLATE-CENTER TRANSIENT DISPLACEMENT w and QUARTER-PLATE KINETIC ENERGY FOR EXPLOSIVELY-IMPULSED 6061-T651 THIN ALUMINUM INITIALLY-FLAT PANEL CP-2

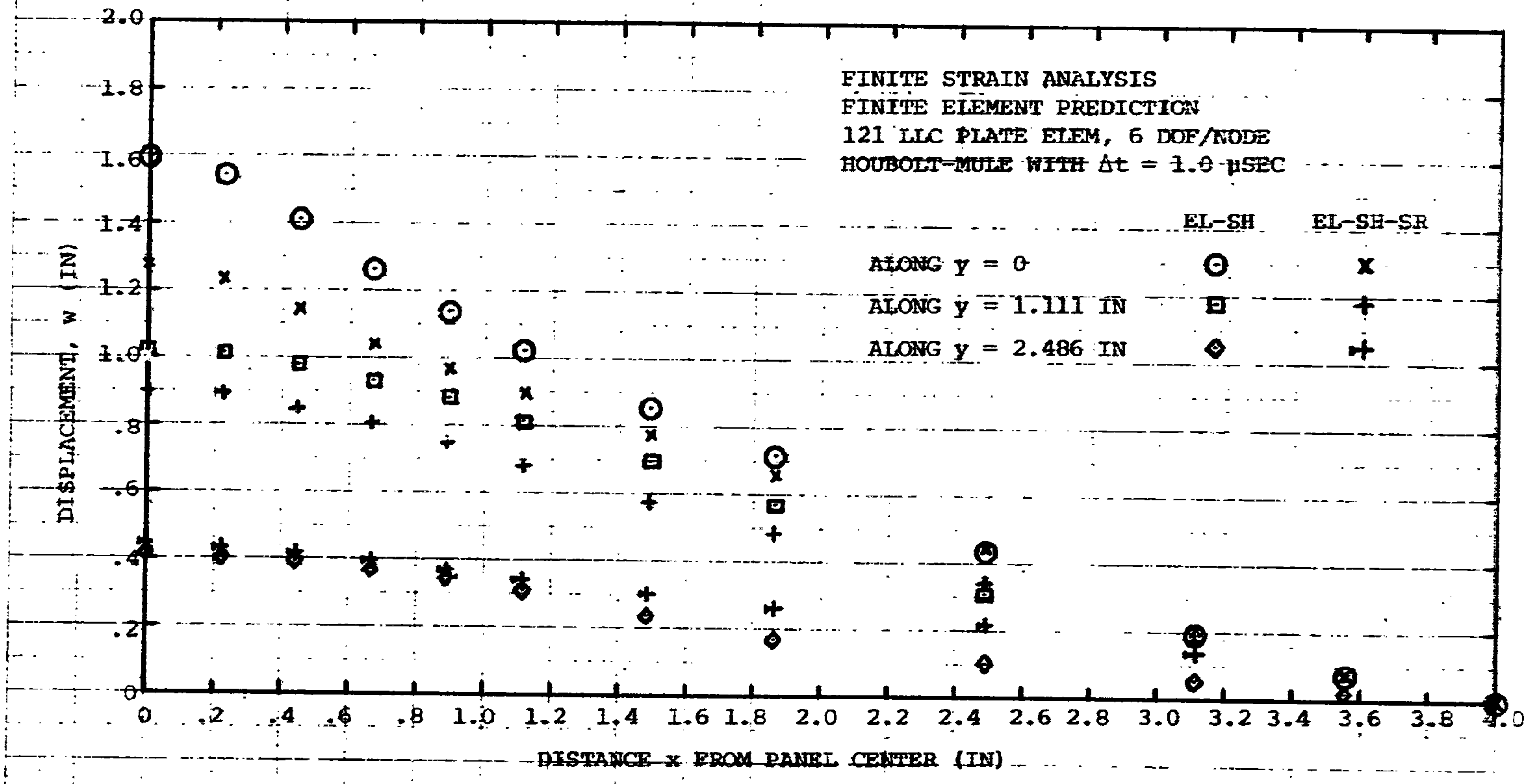

(a) Predicted EL-SH and EL-SH-SR Deflection Profiles at 300 μsec

FIG. 32 FINITE-STRAIN-PREDICTED AND MEASURED w-DISPLACEMENT PROFILES OF EXPLOSIVELY-IMPULSED 6061-T651 ALUMINUM SQUARE PANEL CP-2 WITH ALL SIDES IDEALLY CLAMPED

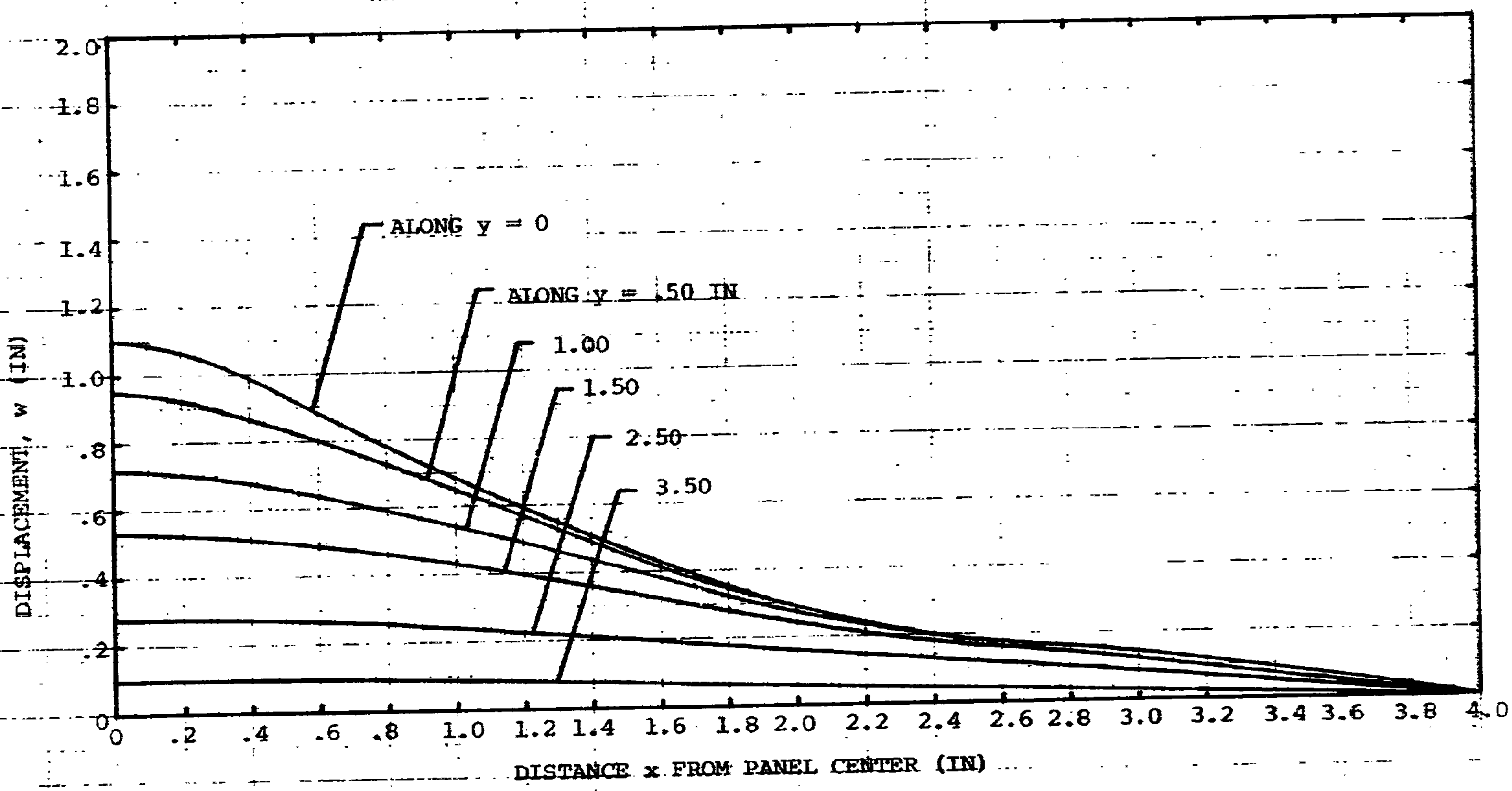

(b) Experimental Permanent Deformation Profiles

FIG. 32 CONTINUED (PANEL CP-2, FINITE STRAIN, EL-SH, EL-SH-SR, EXPT)

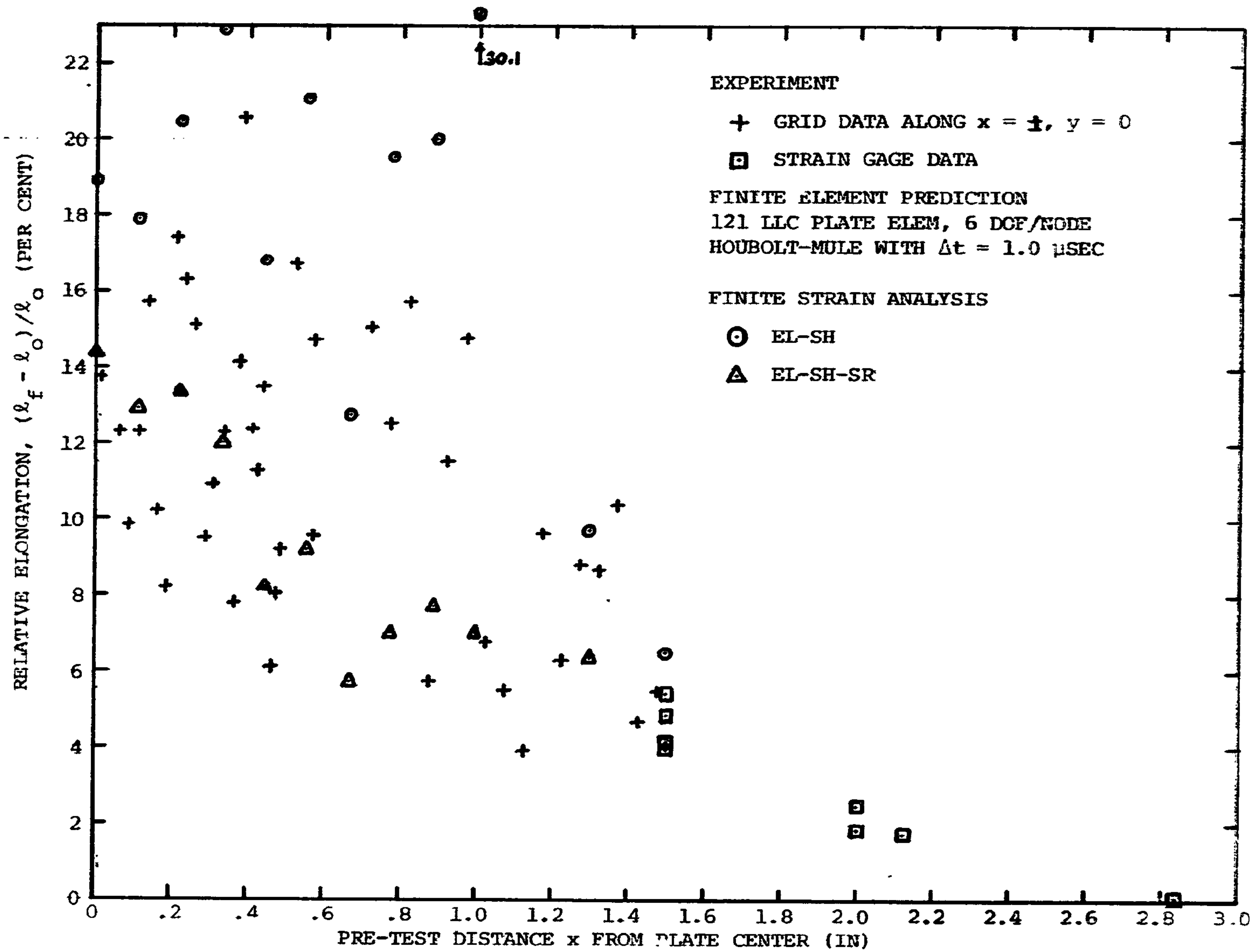

(c) Upper-Surface Permanent Relative Elongation

FIG. 32 CONCLUDED (CP-2, FINITE STRAIN PREDICTION, EXPT)

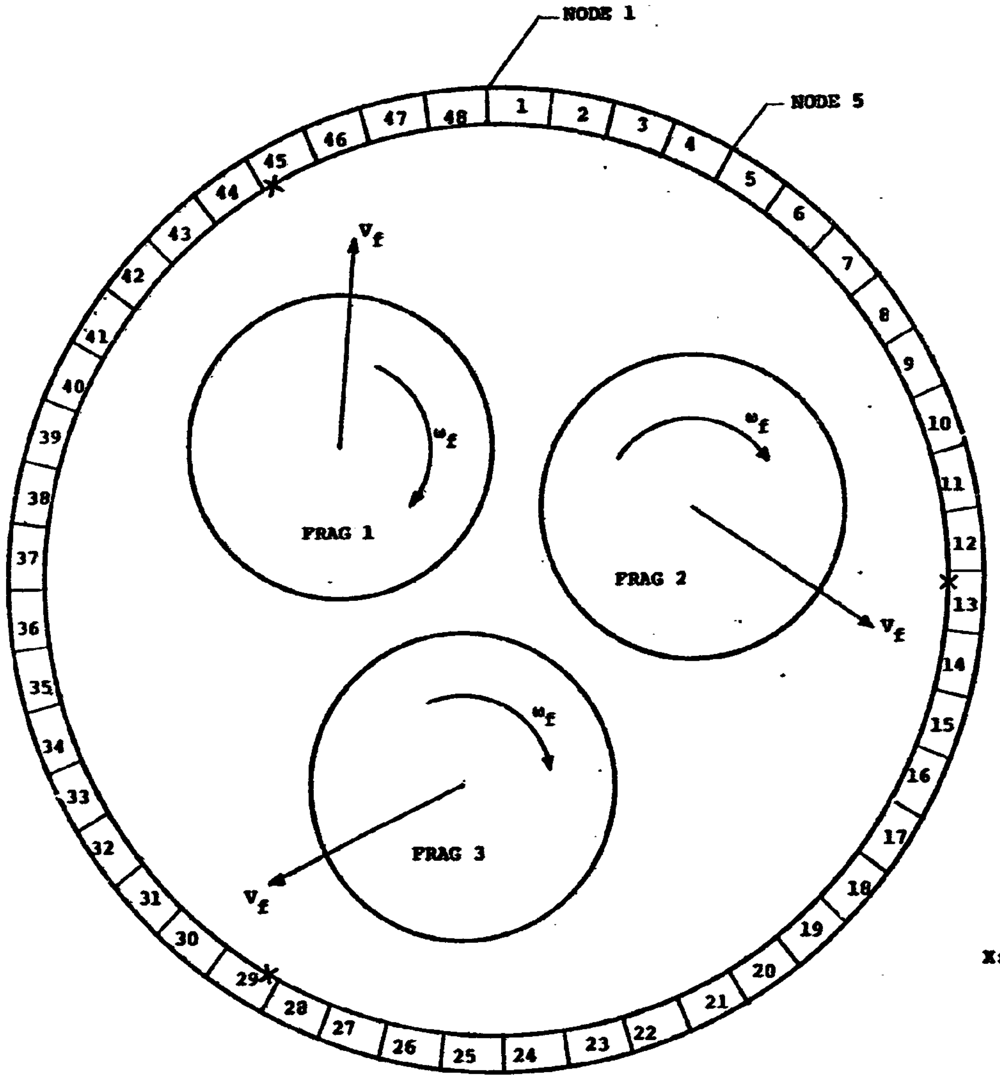

4130 STEEL RING
- INNER RADIUS = 7.50 IN
- THICKNESS = 0.625 IN
- AXIAL LENGTH = 1.50 IN

FINITE-ELEMENT ANALYSIS
- 48 EQUAL ELEMS (FULL RING)
- 4 DOF/NODE
- EL-SH-SR

FRAGMENTS: 3 EQUAL CIRCULAR AT 120-DEG. SPACING

FOR EACH FRAGMENT
- RADIUS = 2.555 IN
- MASS = 0.009395 (LB-SEC^2)/IN
- MASS MOM. INER. = 0.0666 IN-LB-SEC^2
- TRANSL. VEL., V_f = 5816.7 IN/SEC
- ROT. VEL., ω_f = 2079.6 RAD/SEC
- INITIAL KINETIC ENERGY
  - TRANSLATIONAL = 158,922 IN-LB
  - ROTATIONAL = 144,018 IN-LB
  - TOTAL = 302,940 IN-LB

X: POINT OF INITIAL IMPACT

FIG. 33 GEOMETRIC, TEST, AND MODELING DATA FOR THE 4130 STEEL CONTAINMENT RING SUBJECTED TO TRI-HUB T58 ROTOR BURST IN NAPTC TEST 201

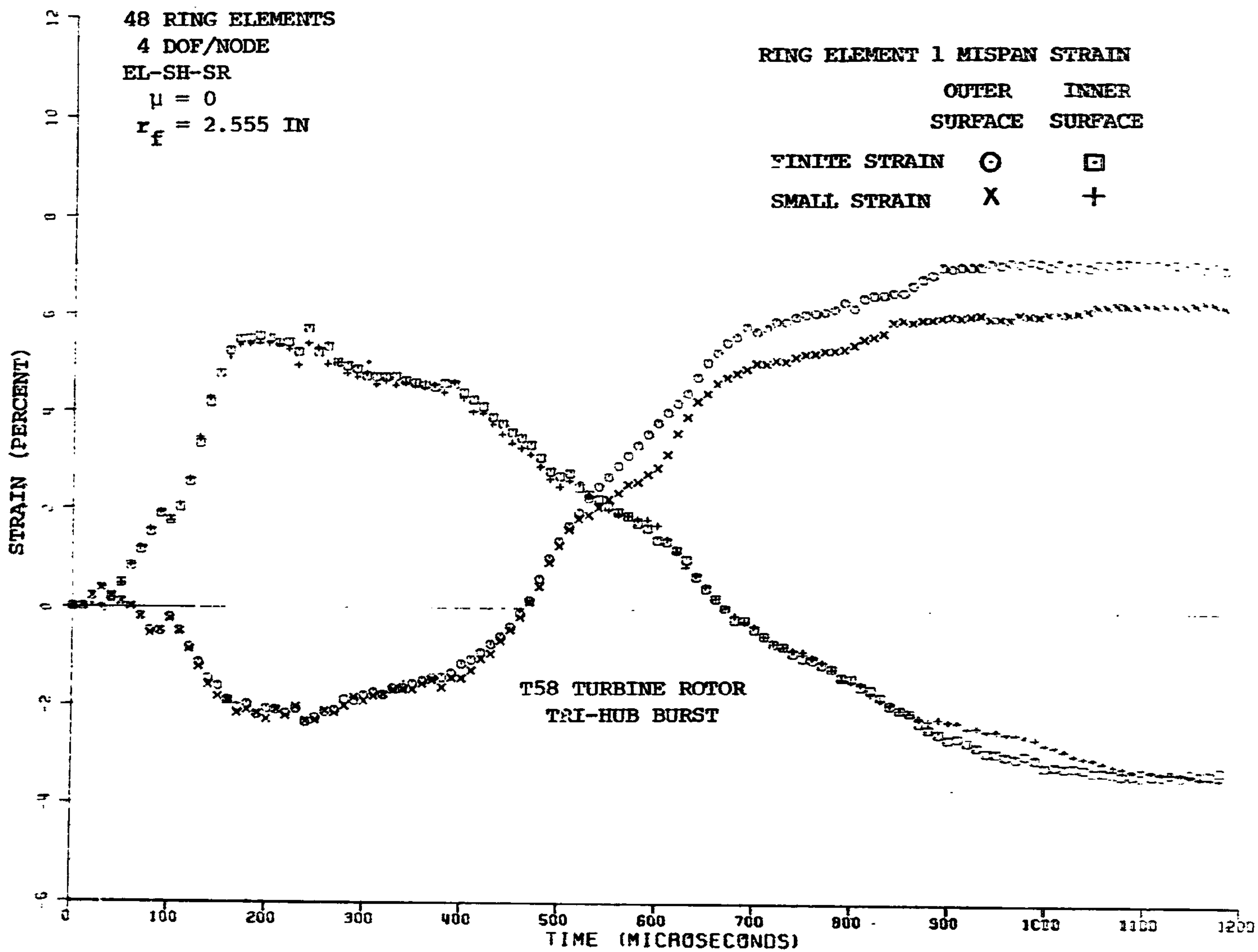

(a) Element 1 Midspan Strain

FIG. 34 COMPARISON OF FINITE-STRAIN VS. SMALL-STRAIN PREDICTIONS FOR THE INNER-SURFACE AND OUTER-SURFACE CIRCUMFERENTIAL STRAINS OF THE NAPTC TEST 201 STEEL CONTAINMENT RING

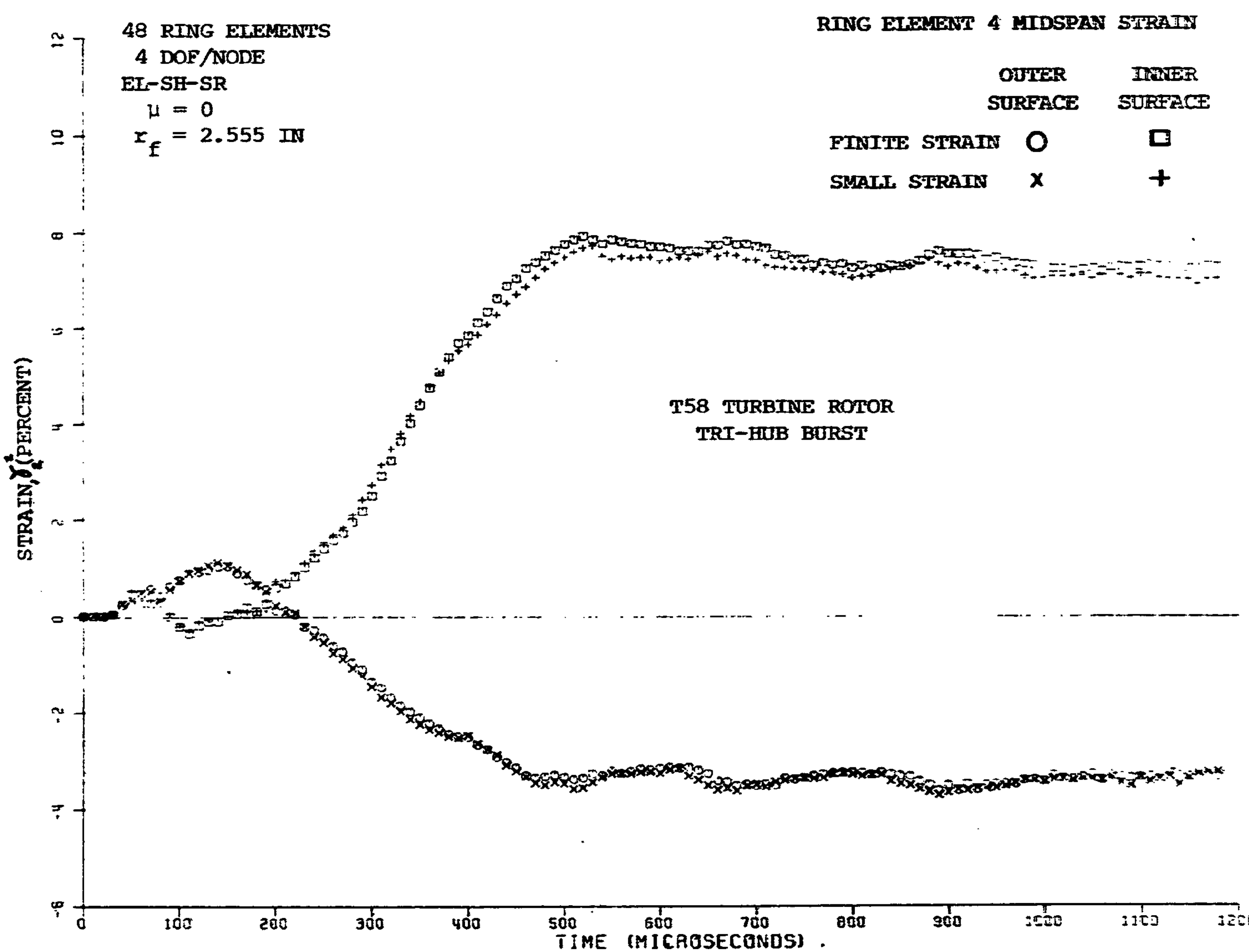

(b) Element 4 Midspan Strain

FIG. 34 CONTINUED (NAPTC TEST 201 RING, FINITE STRAIN, SMALL STRAIN)

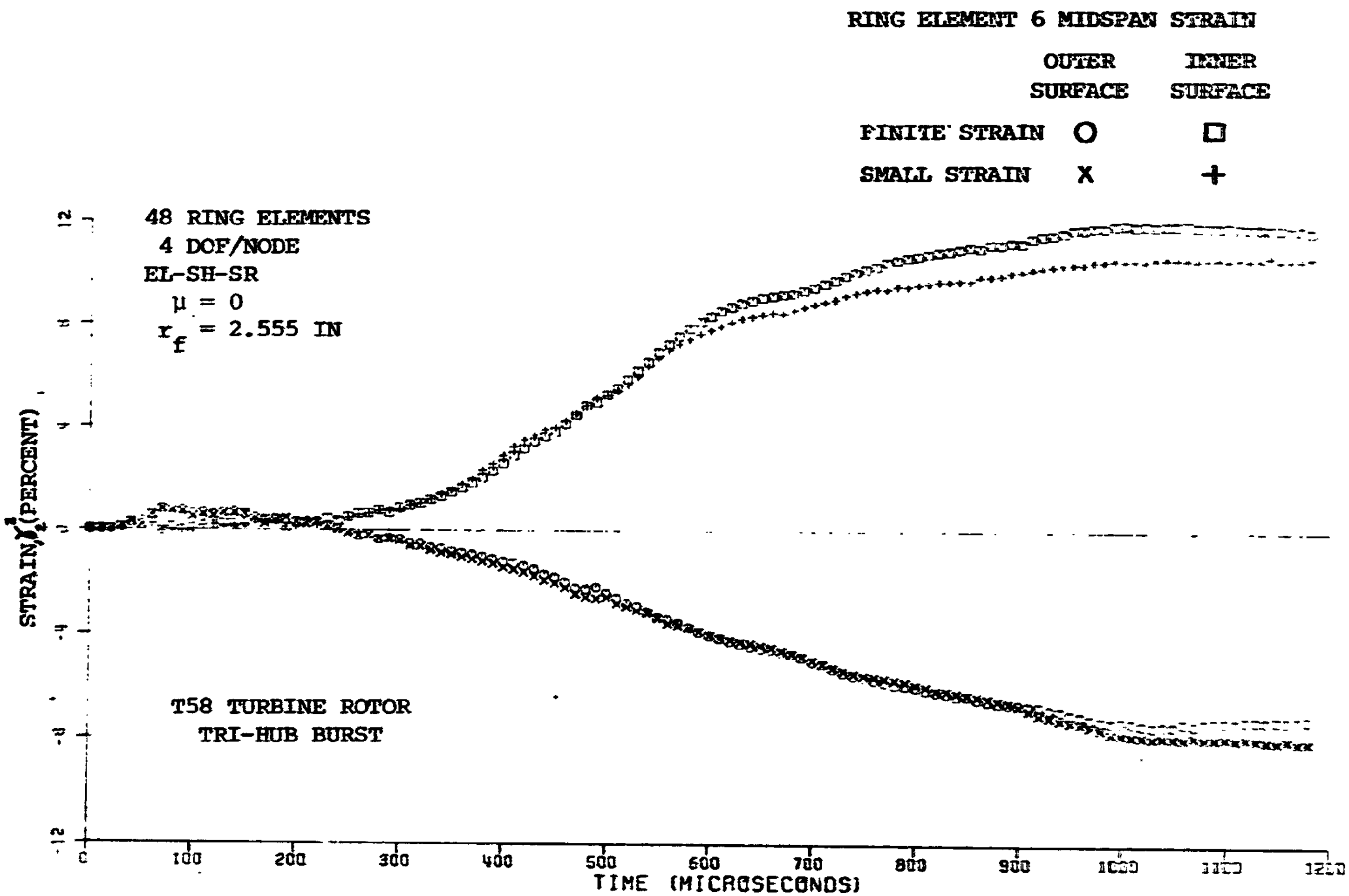

(c) Element 6 Midspan Strain

FIG. 34 CONTINUED (NAPTC TEST 201 RING, FINITE STRAIN, SMALL STRAIN)

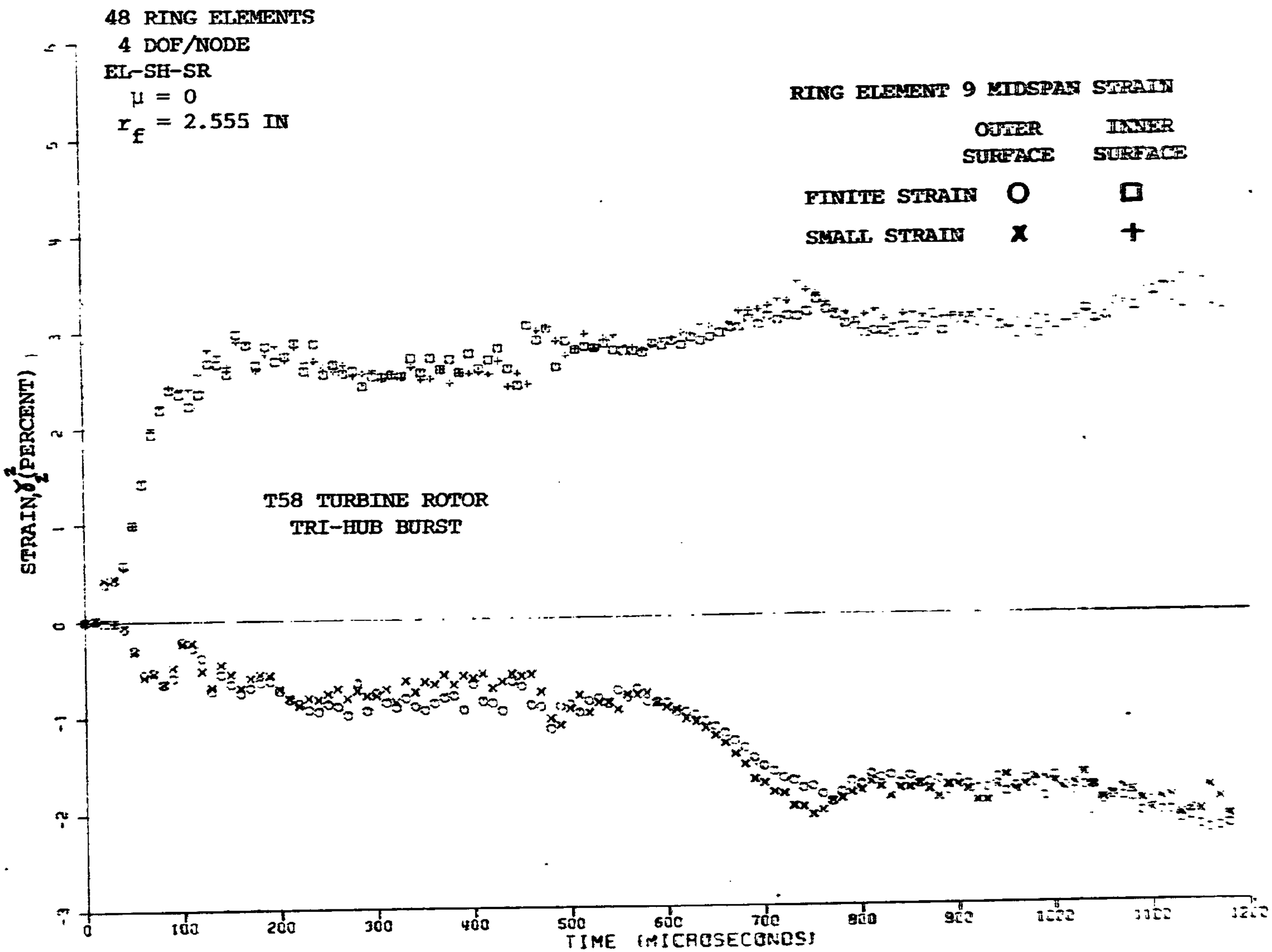

(d) Element 9 Midspan Strain

FIG. 34 CONTINUED (NAPTC TEST 201 RING, FINITE STRAIN, SMALL STRAIN)

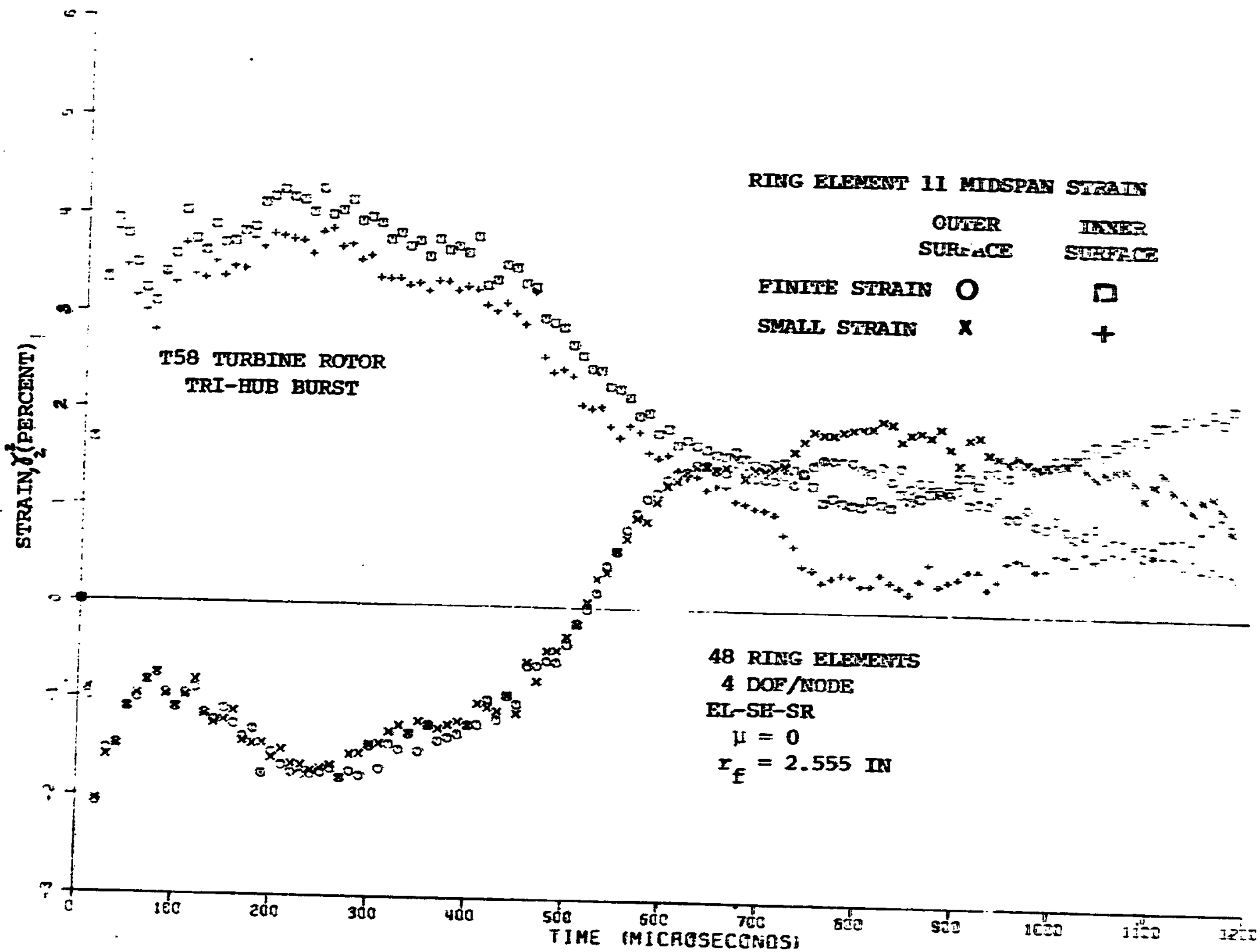

(e) Element 11 Midspan Strain

FIG. 34 CONTINUED (NAPTC TEST 201 RING, FINITE STRAIN, SMALL STRAIN)

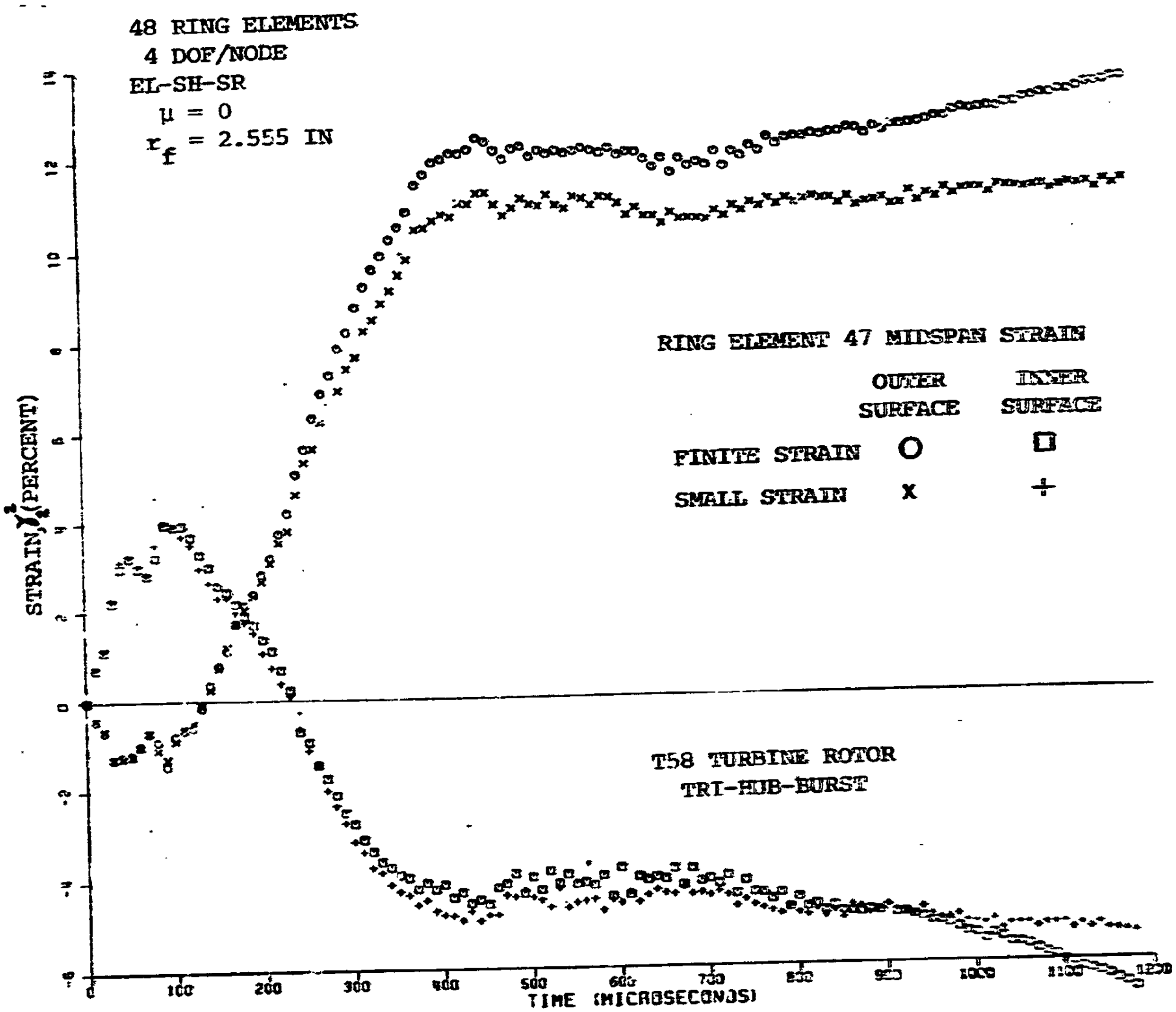

(f) Element 47 Midspan Strain

FIG. 34 CONCLUDED (NAPTC TEST 201 RING, FINITE STRAIN, SMALL STRAIN)

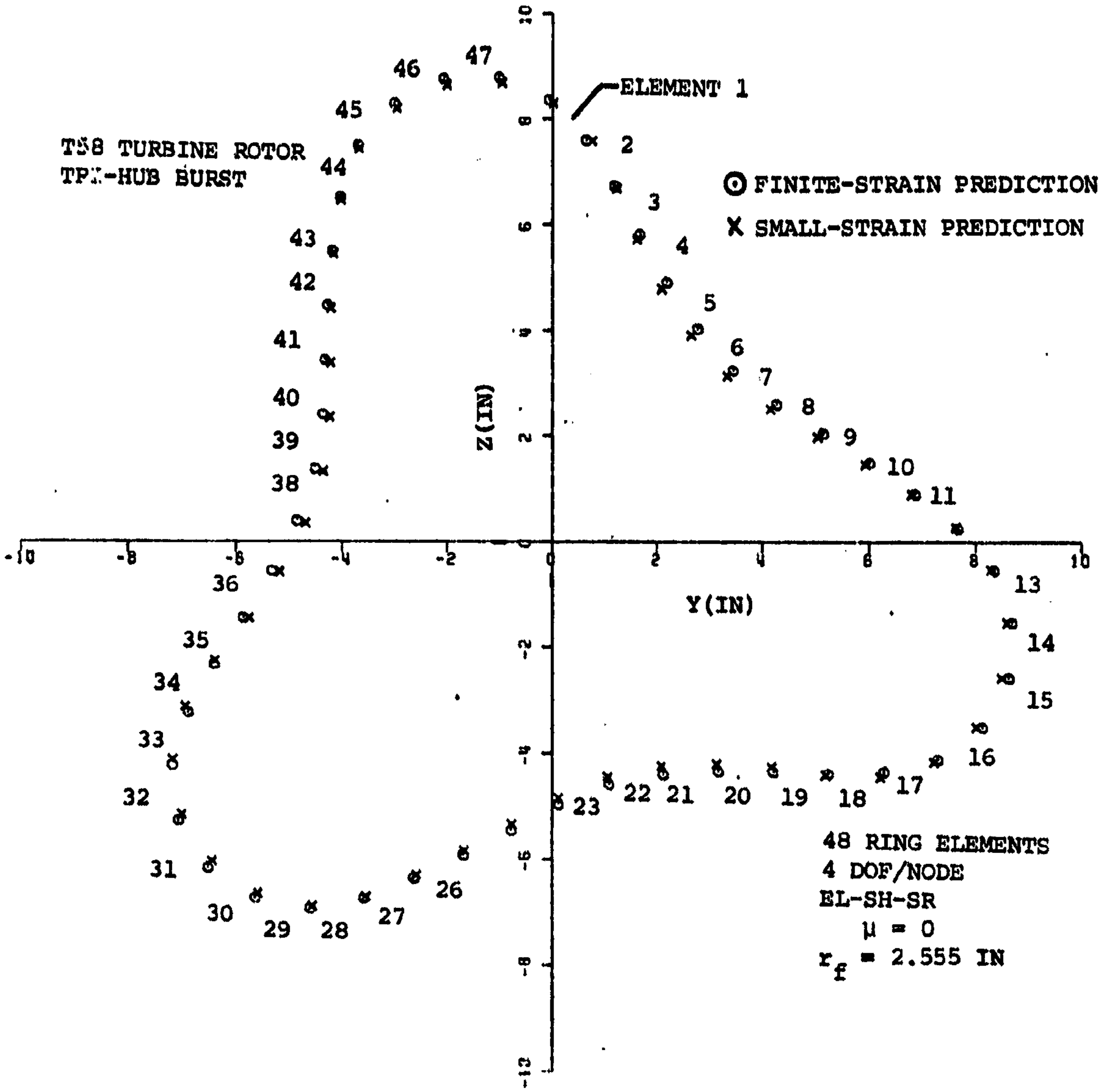

(a) Deformed Configuration at TAII = 1180 μsec

FIG. 35 COMPARISON OF FINITE-STRAIN VS. SMALL-STRAIN PREDICTIONS FOR THE DEFORMED CONFIGURATION AND FOR THE INNER-SURFACE AND OUTER-SURFACE CIRCUMFERENTIAL DISTRIBUTIONS OF CIRCUMFERENTIAL STRAIN AT TAII = 1180 μSEC FOR THE NAPTC TEST 201 STEEL CONTAINMENT RING

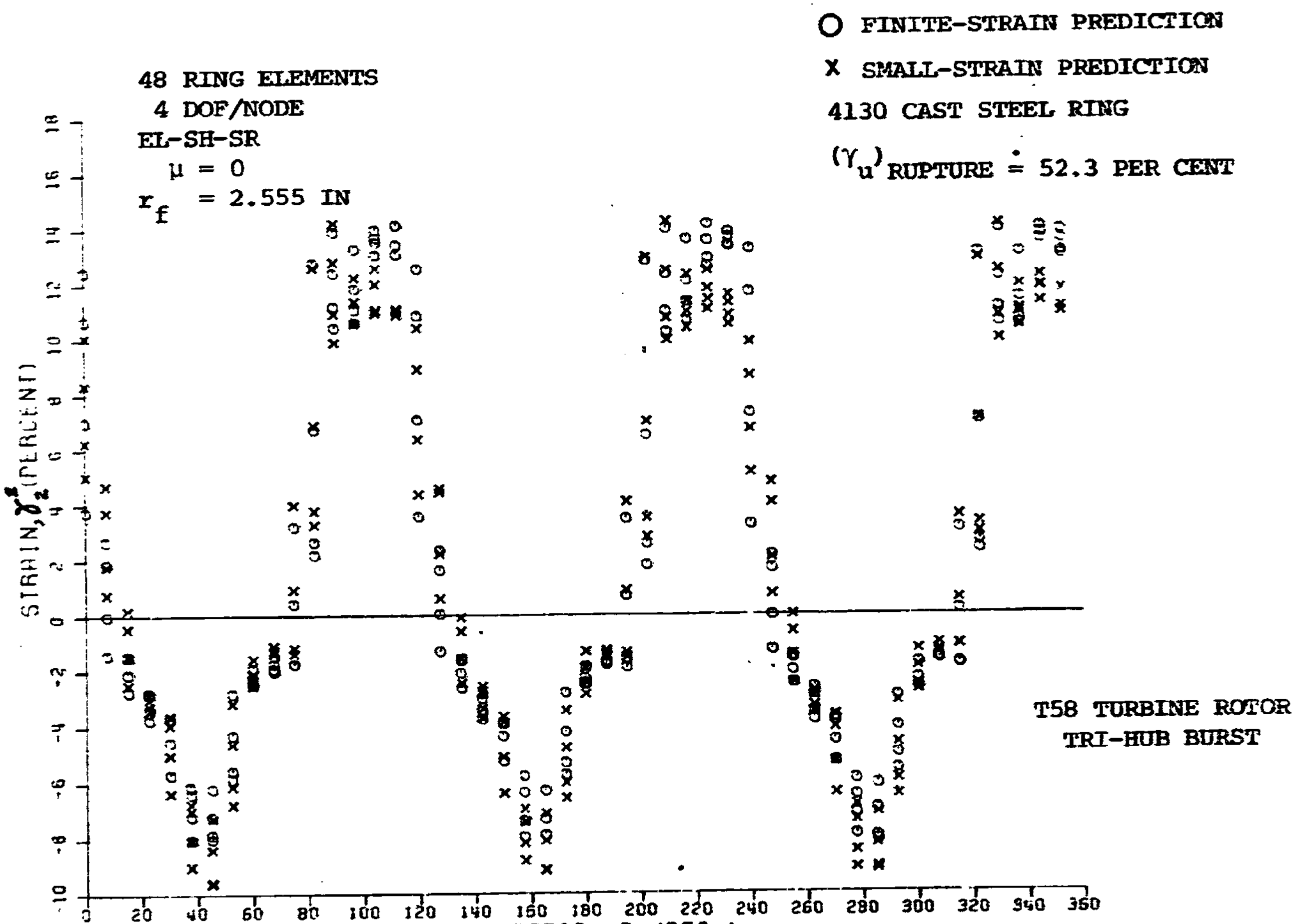

(b) Circumferential Distribution of Outer-Surface Strain at TAII = 1180 μsec

FIG. 35 CONTINUED (NAPTC TEST 201 RING, FINITE STRAIN VS. SMALL STRAIN AT TAII = 1180 μSEC)

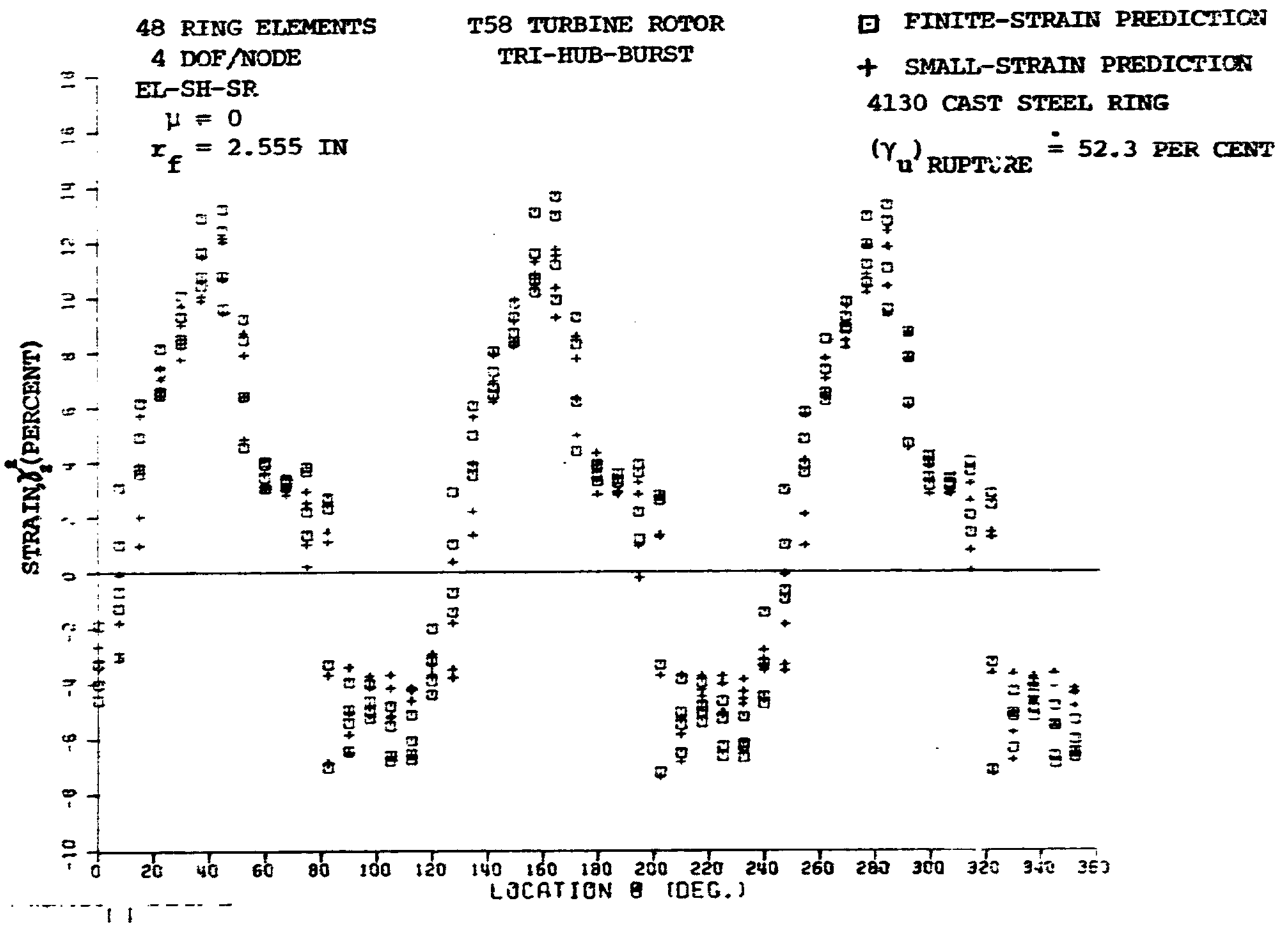

(c) Circumferential Distribution of Inner-Surface Strain at TAII = 1180 μsec

FIG. 35 CONCLUDED (NAPTC TEST 201 RING, FINITE STRAIN VS. SMALL STRAIN AT TAII = 1180 μSEC)

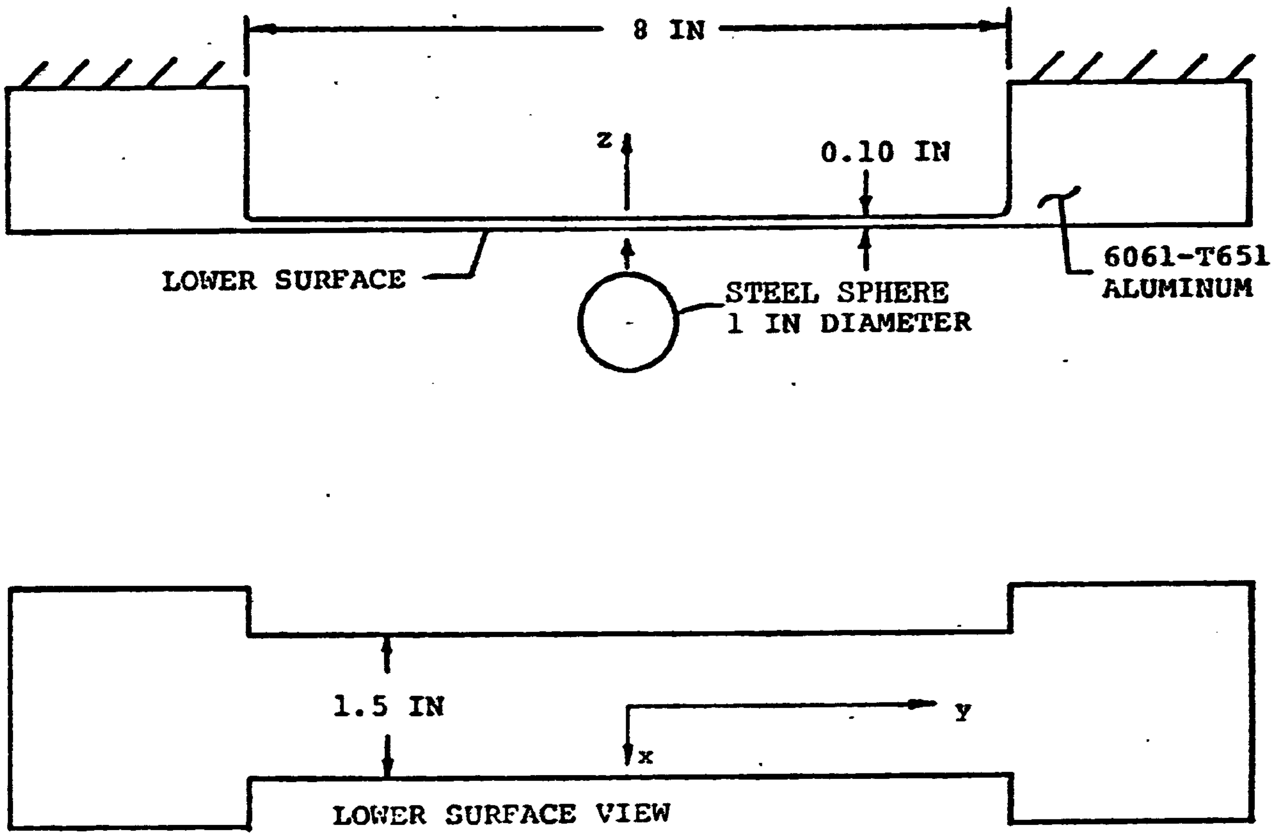

FIG. 36 SCHEMATIC OF A 6061-T651 ALUMINUM NARROW PLATE MODEL SUBJECTED TO MIDSPAN PERPENDICULAR IMPACT BY AN ONE-INCH-DIAMETER SOLID STEEL SPHERE

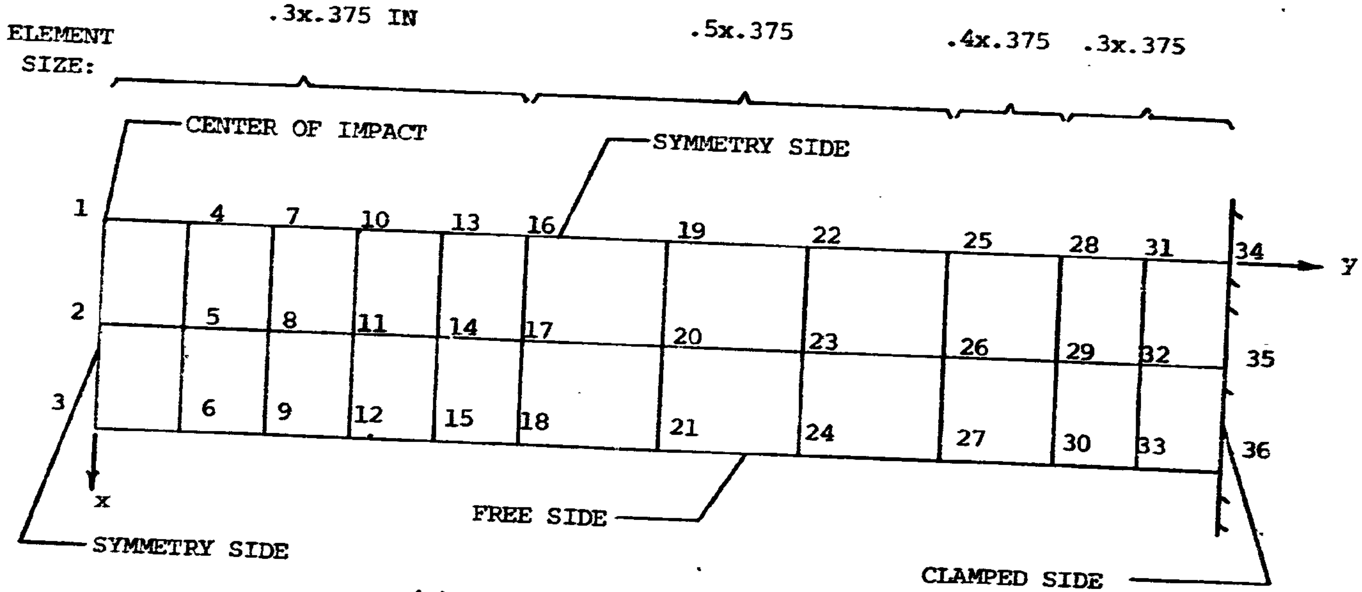

(a) Coarse Mesh Model Node Numbers

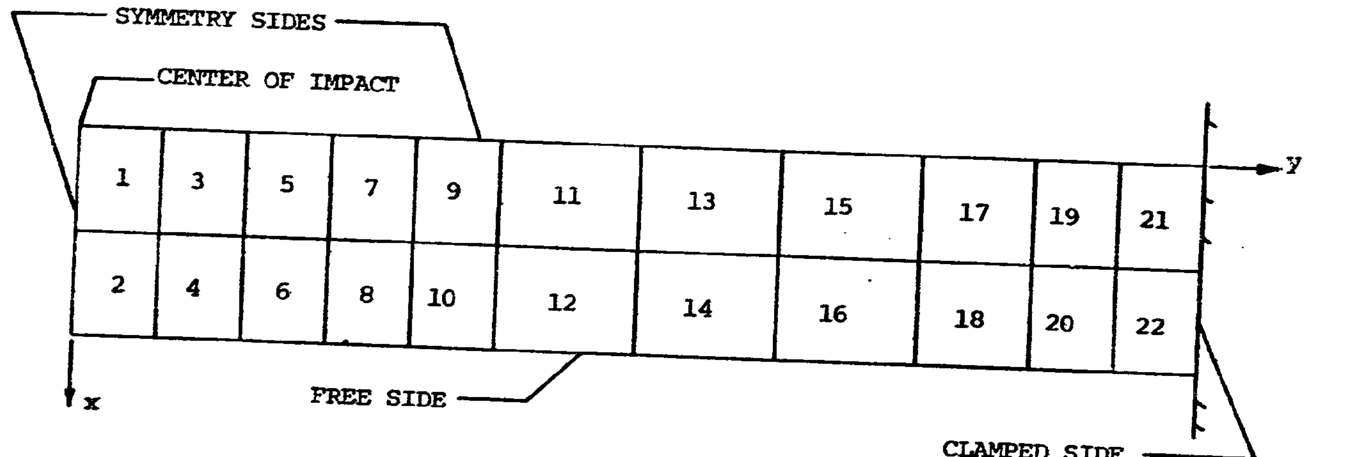

(b) Coarse Mesh Model Element Numbers

FIG. 37 PLATE ELEMENT MESH SELECTIONS USED TO MODEL THE QUARTER PLATE OF STEEL-SPHERE-IMPACTED 6061-T651 ALUMINUM NARROW-PLATE SPECIMEN CB-18

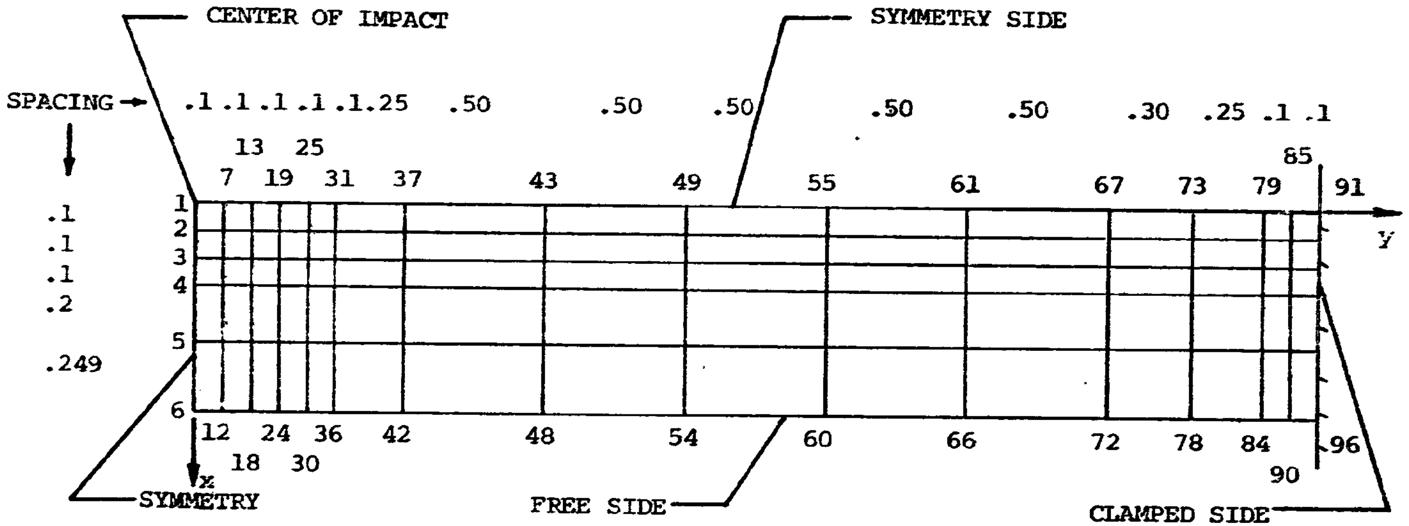

(c) Refined Mesh Model Node Numbers

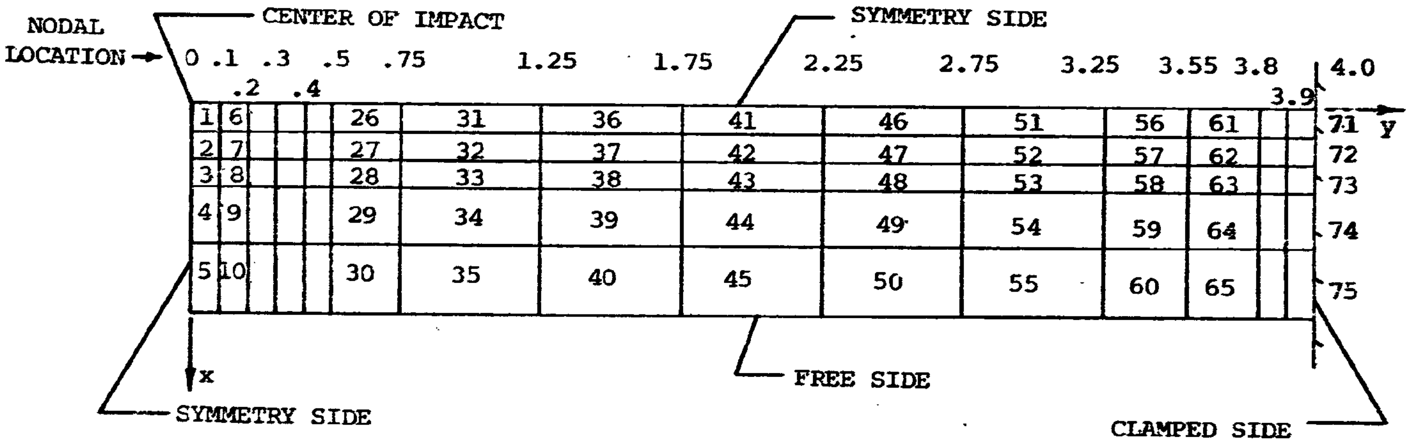

(d) Refined Mesh Model Element Numbers

FIG. 37 CONCLUDED (CB-18 PLATE ELEMENT MODEL)

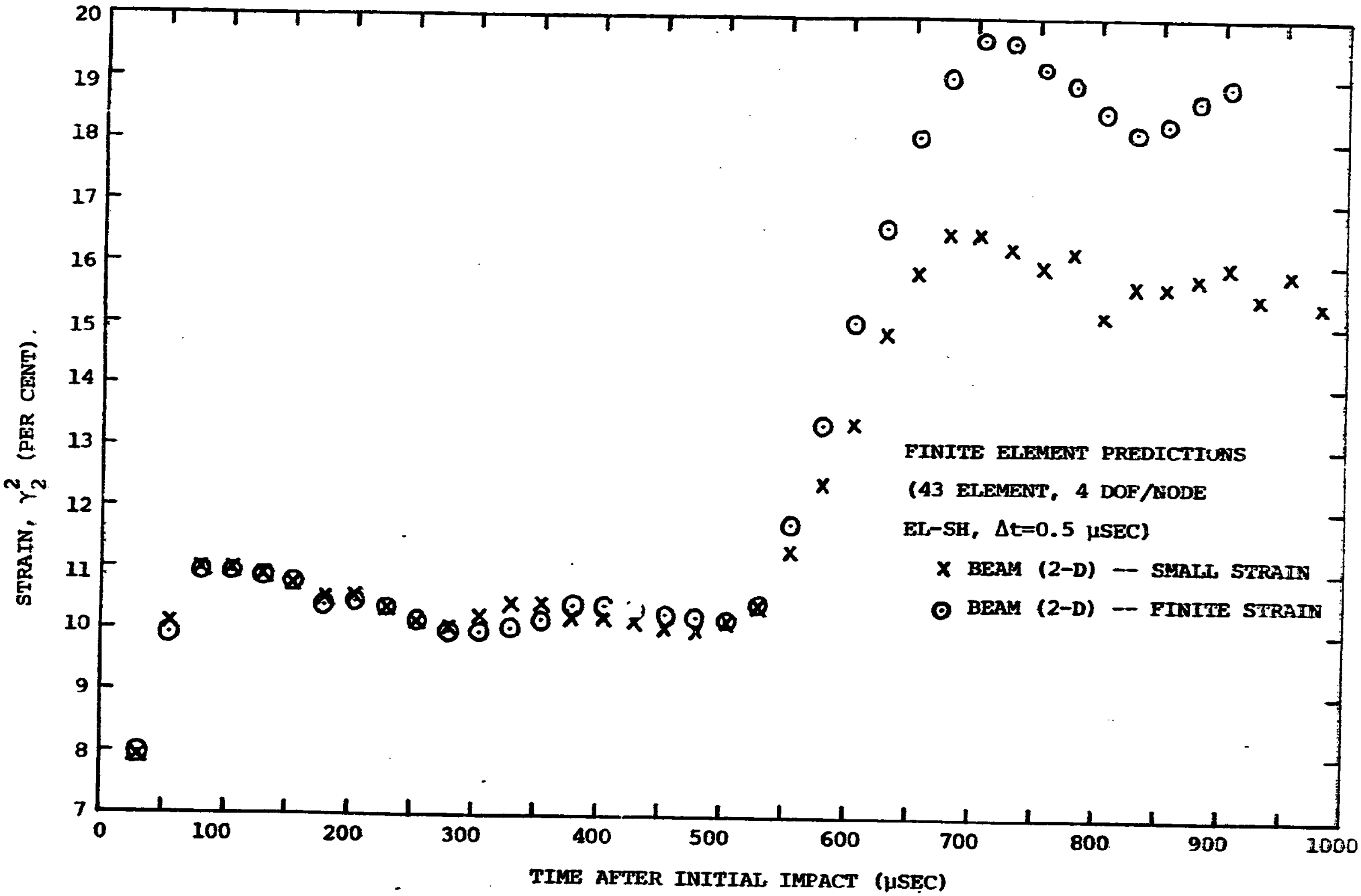

(a) Station y = 0, Upper Surface

FIG. 38 MEASUREMENTS AND/OR PREDICTIONS OF TRANSIENT LONGITUDINAL GREEN (LAGRANGIAN) STRAIN ON THE SURFACE FOR VARIOUS SPANWISE STATIONS OF STEEL-SPHERE-IMPACTED 6061-T651 ALUMINUM NARROW-PLATE SPECIMEN CB-18

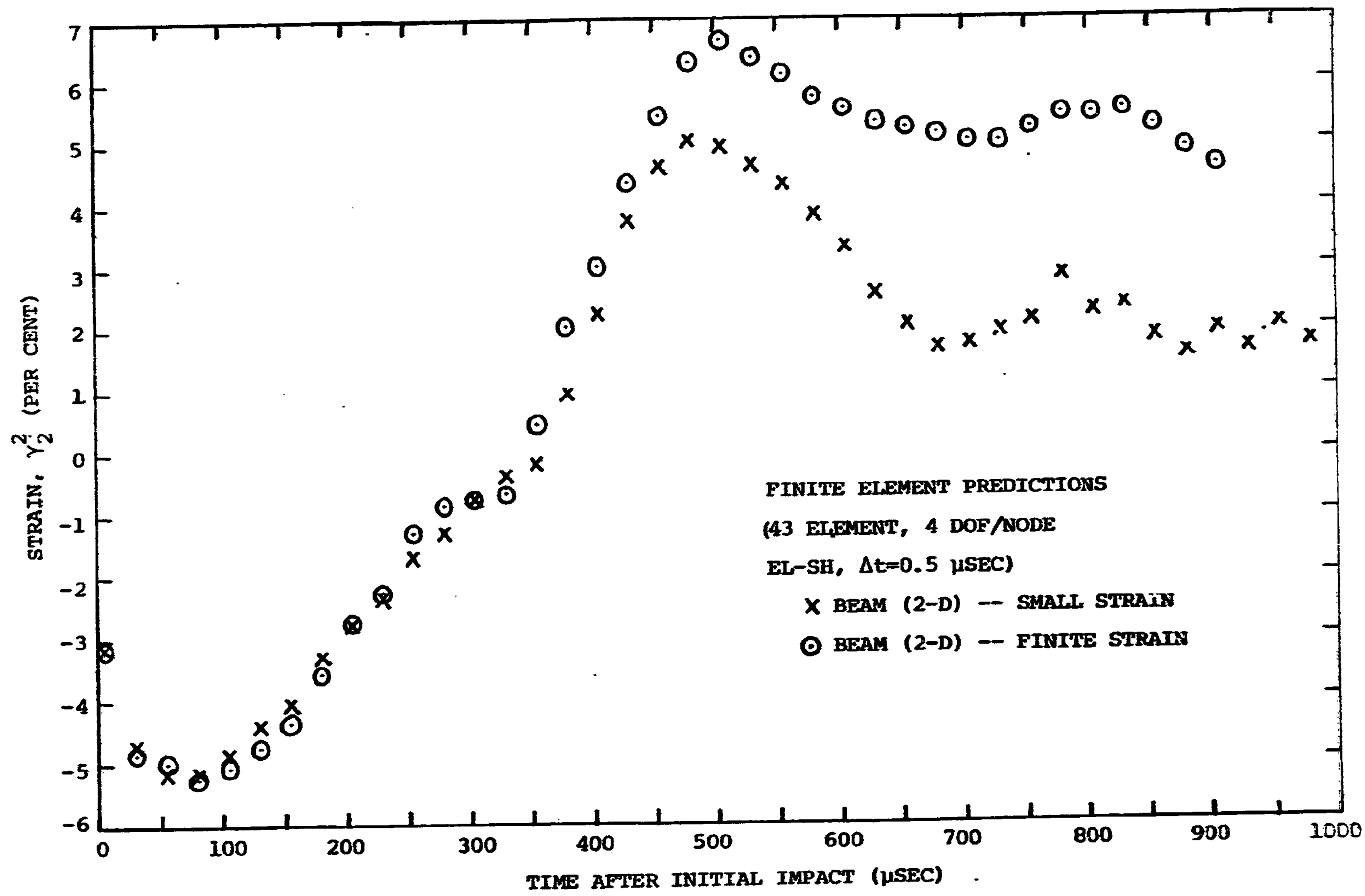

(b) Station y = 0, Lower Surface

FIG. 38 CONTINUED (CB-18)

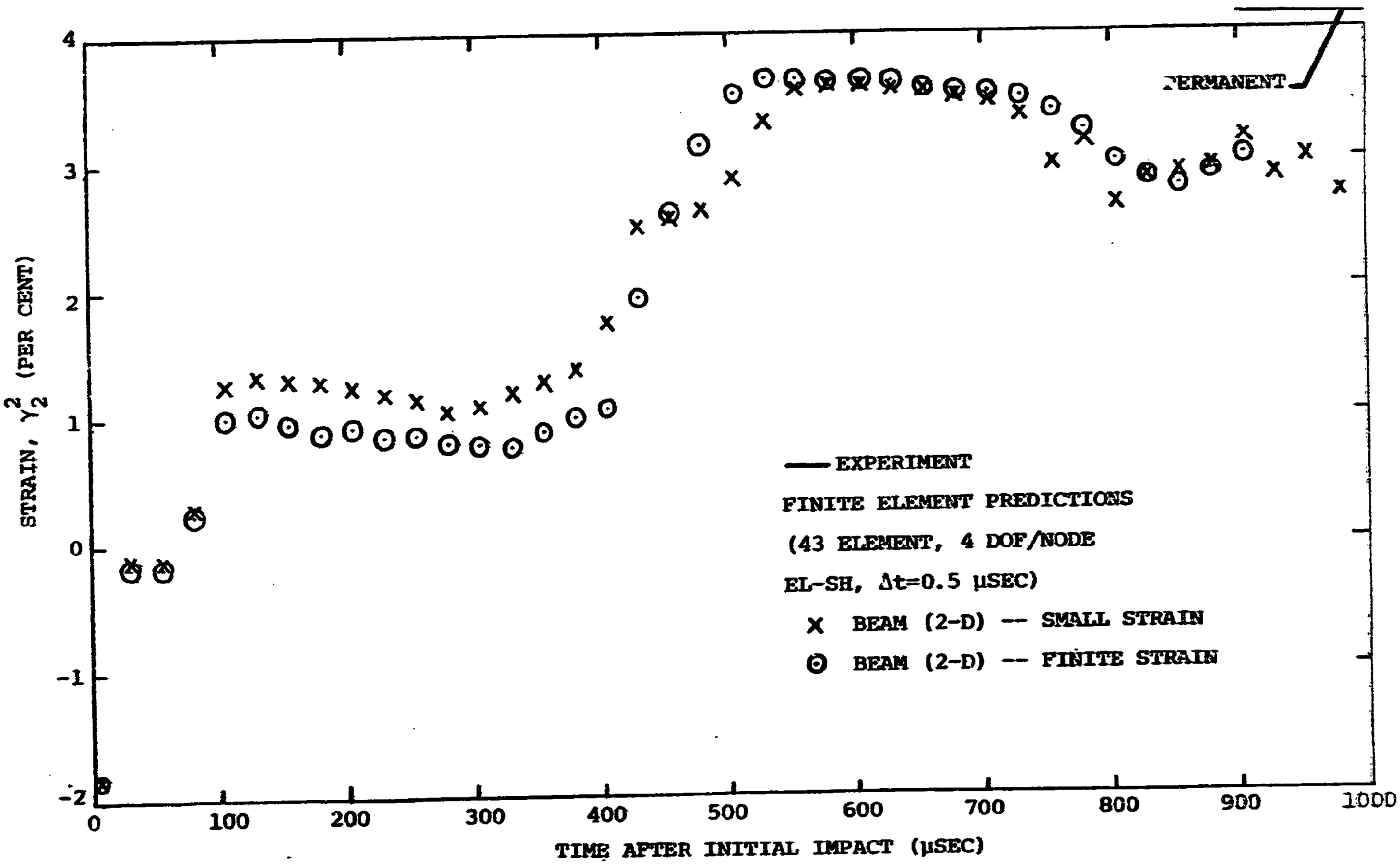

(c) Station y = 0.3 in, Upper Surface

FIG. 38 CONTINUED (CB-18)

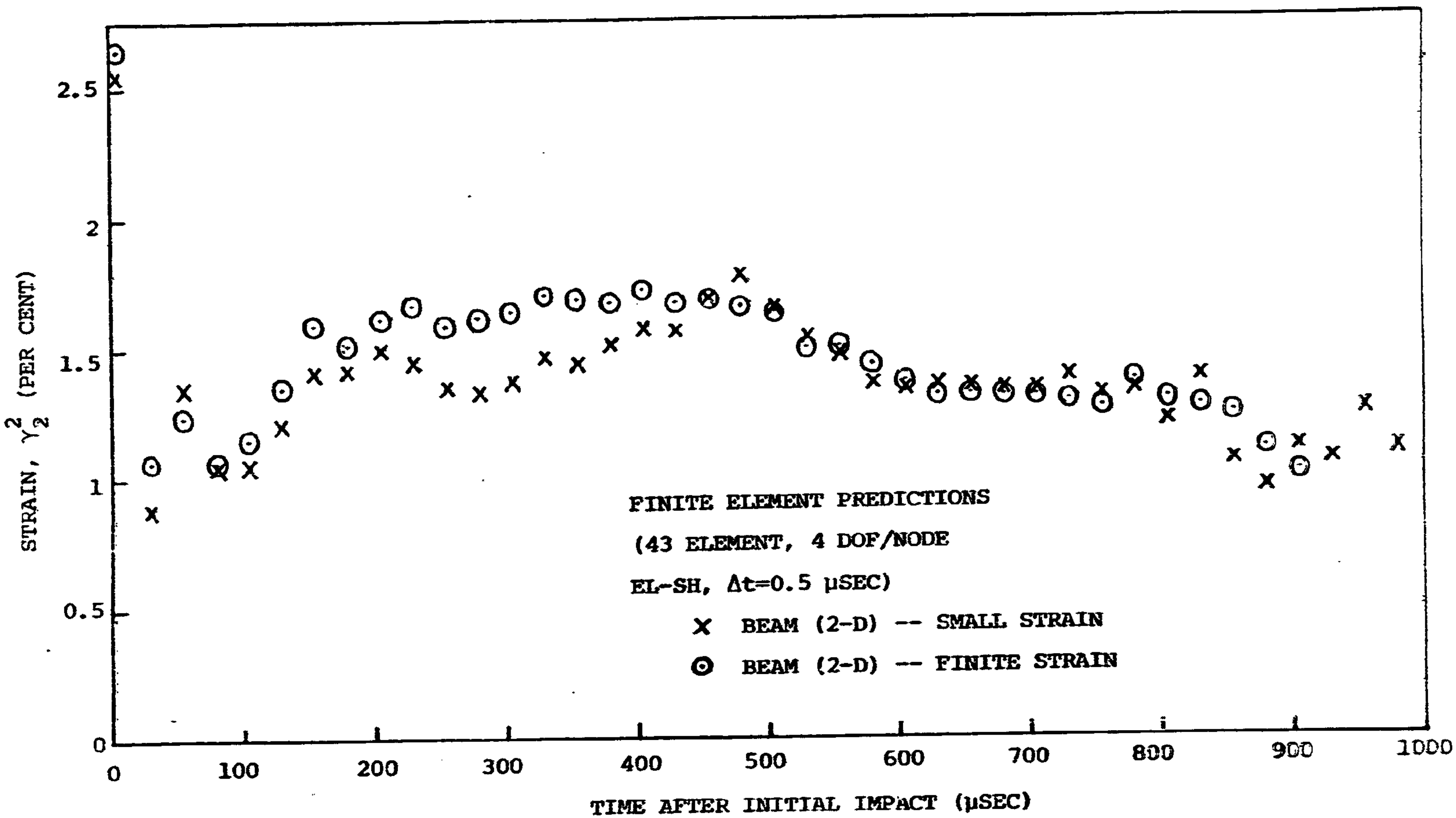

(d) Station y = 0.3 in, Lower Surface

FIG. 38 CONTINUED (CB-18)

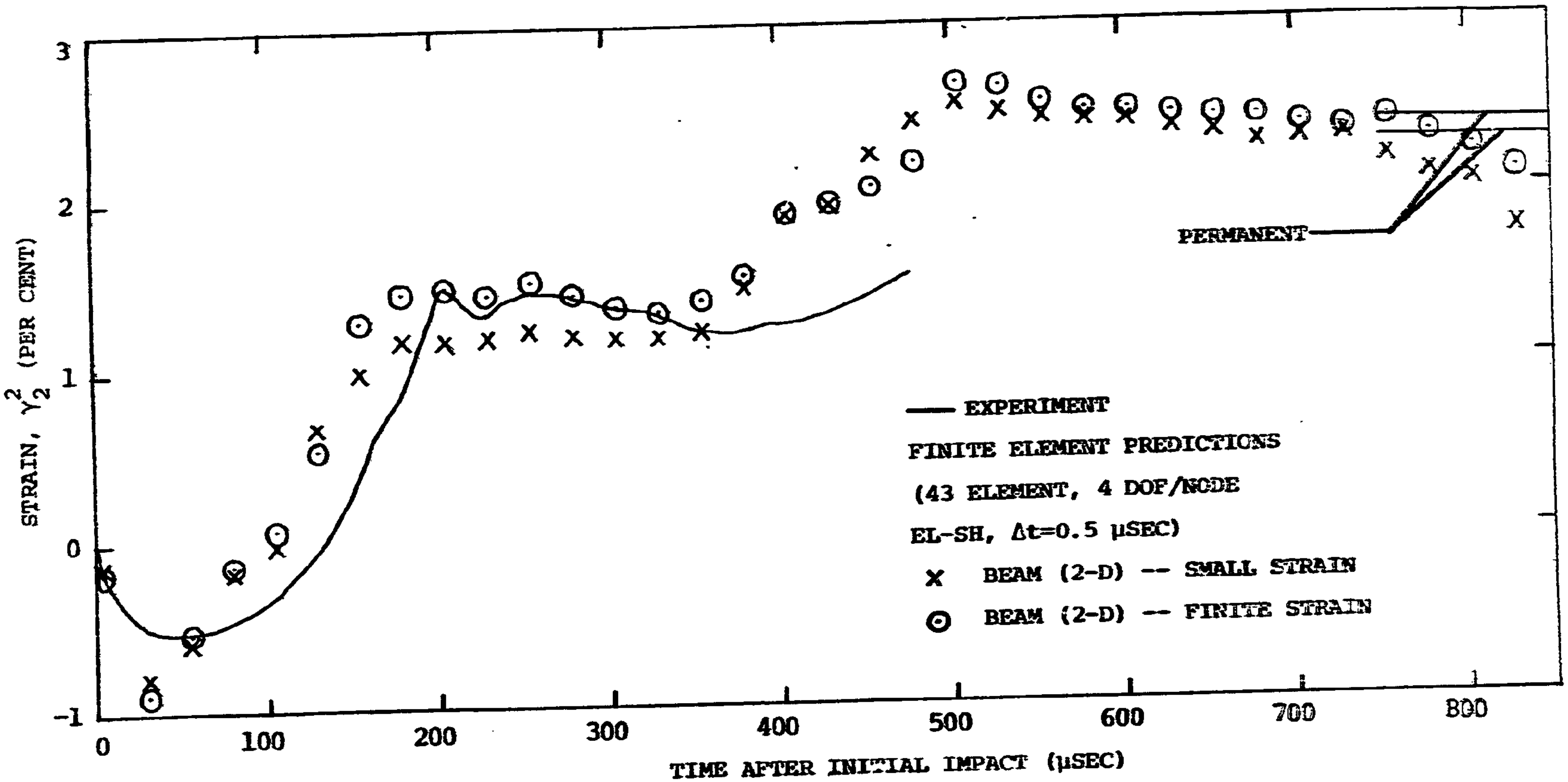

(e) Station y = 0.6 in, Upper Surface

FIG. 38 CONTINUED (CB-18)

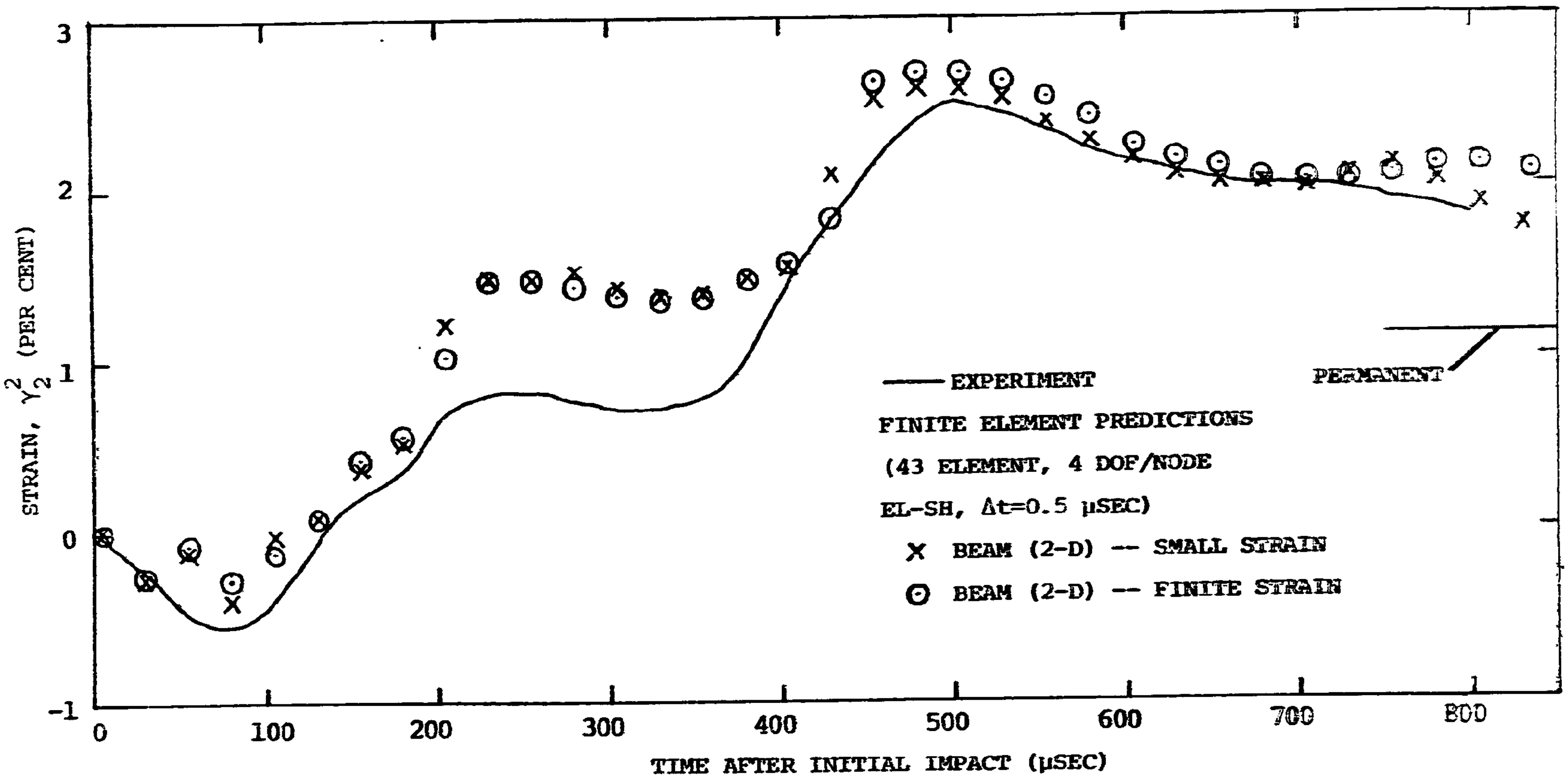

(f) Station y = 1.20 in, Upper Surface

FIG. 38 CONTINUED (CB-18)

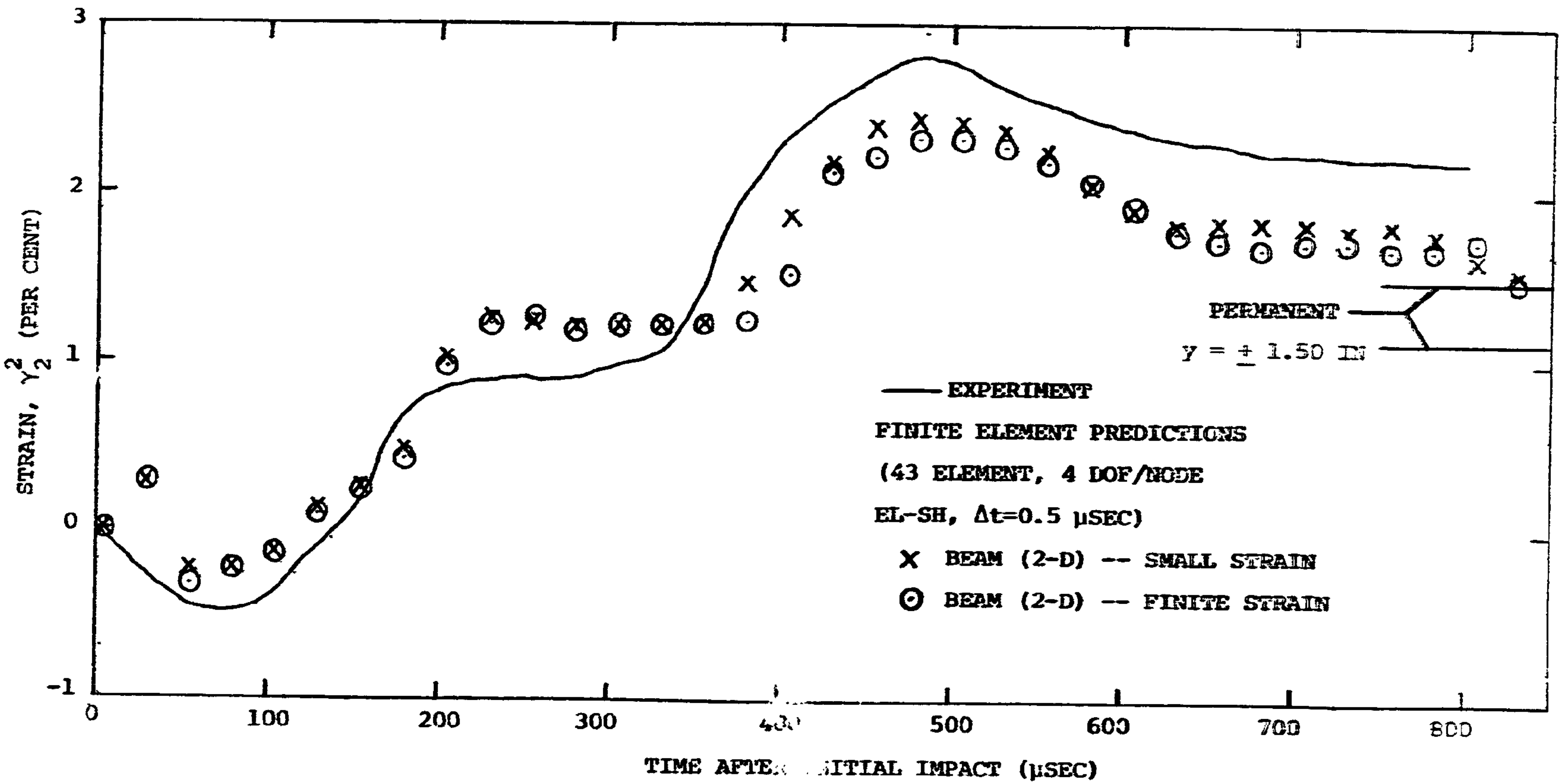

(g) Station y = .50 in, Upper Surface

FIG. 38 CONTINUED (CB-18)

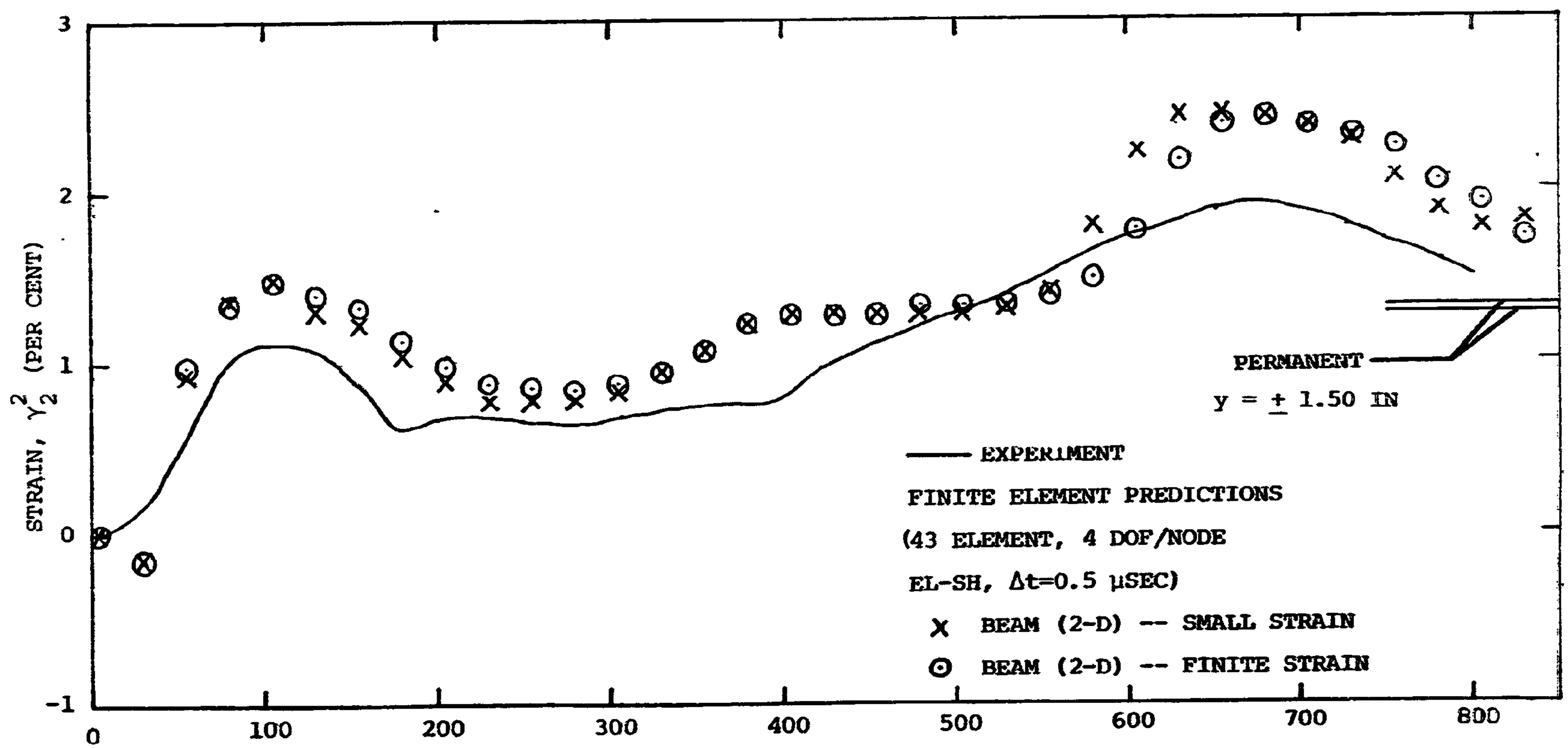

(h) Station y = 1.50 in, Lower Surface

FIG. 38 CONTINUED (CB-18)

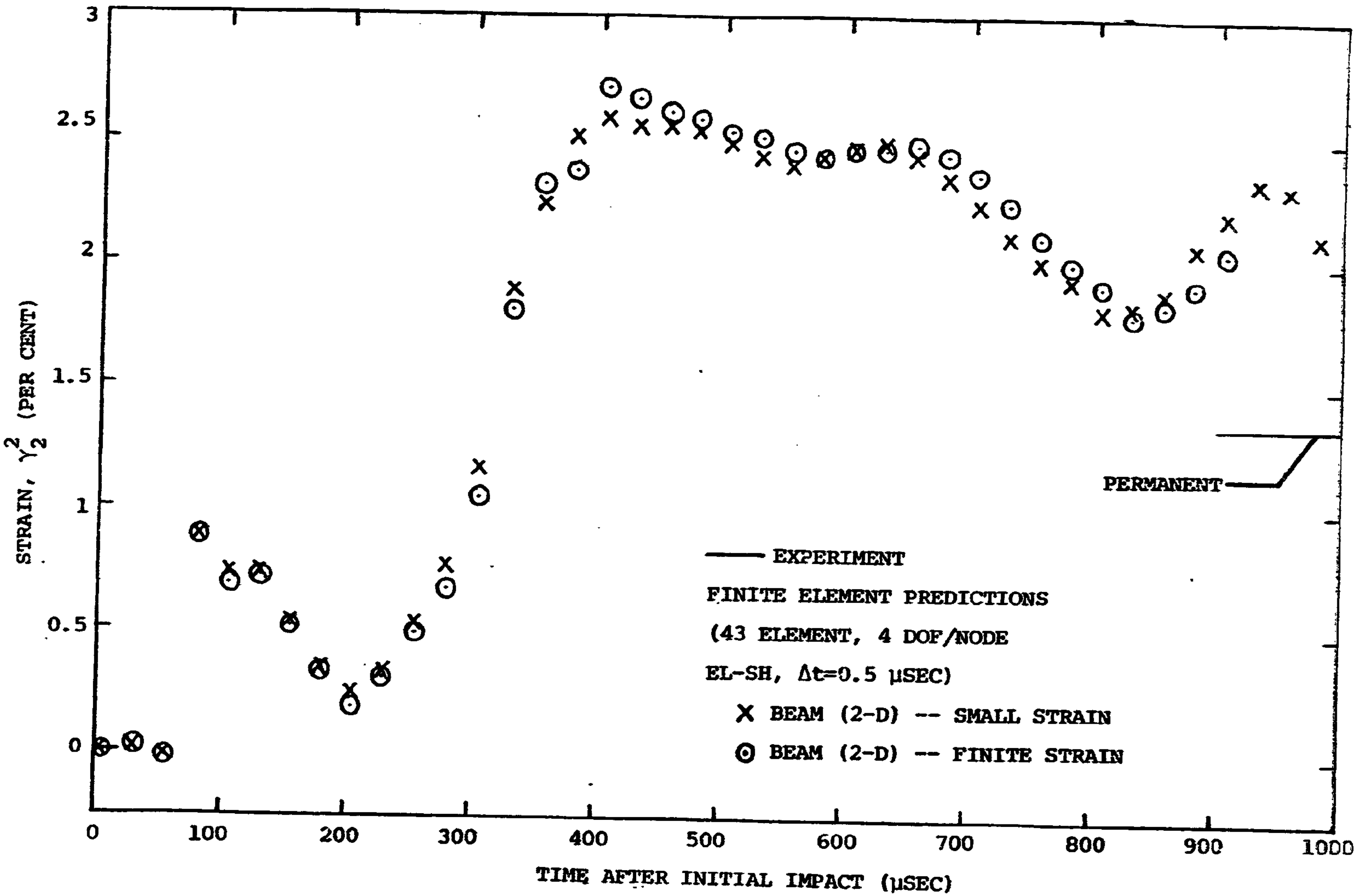

(i) Station y = 3.00 in, Upper Surface

FIG. 38 CONTINUED (CB-18)

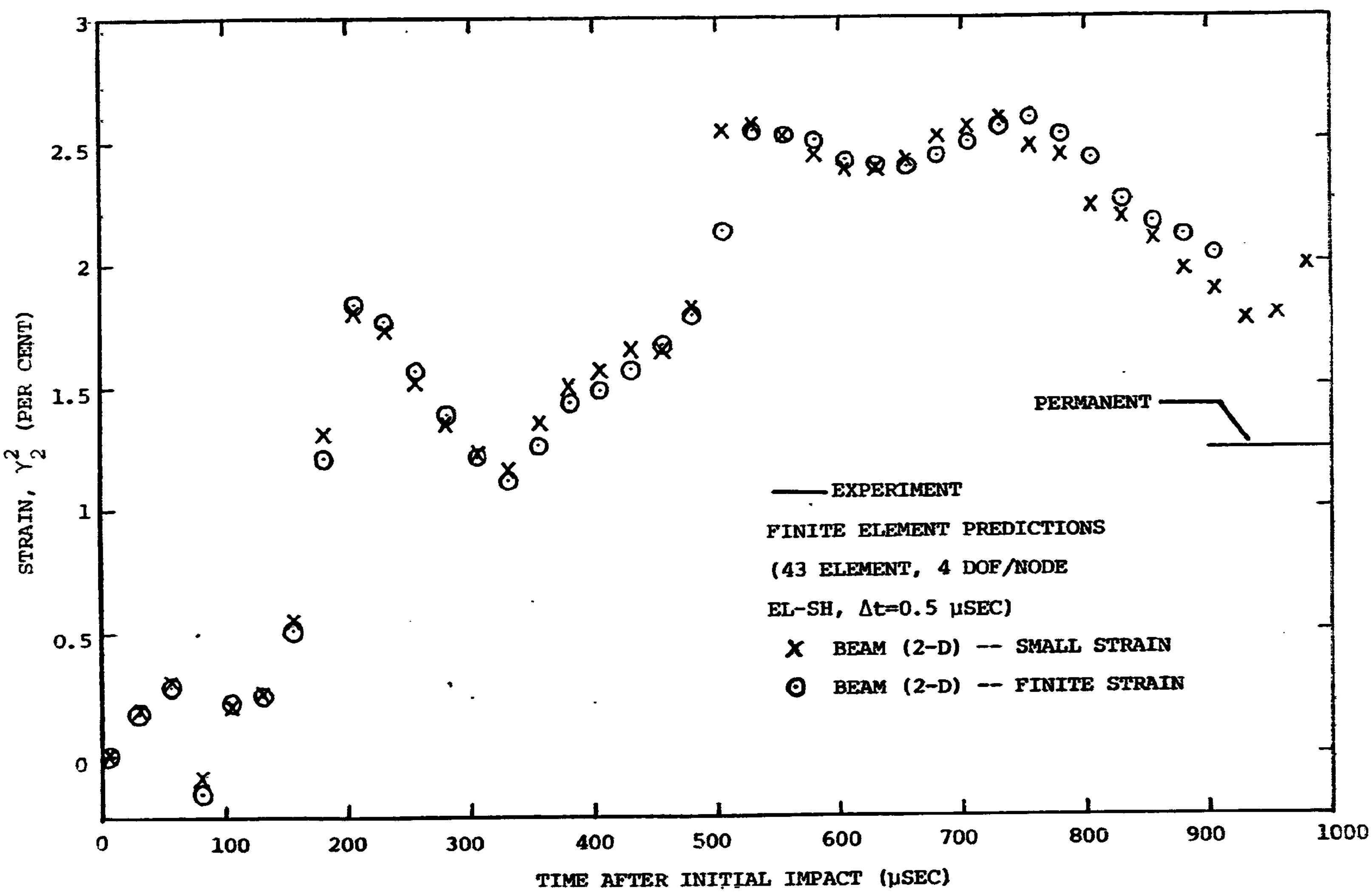

(j) Station y = 3.00 in, Lower Surface

FIG. 38 CONTINUED (CB-18)

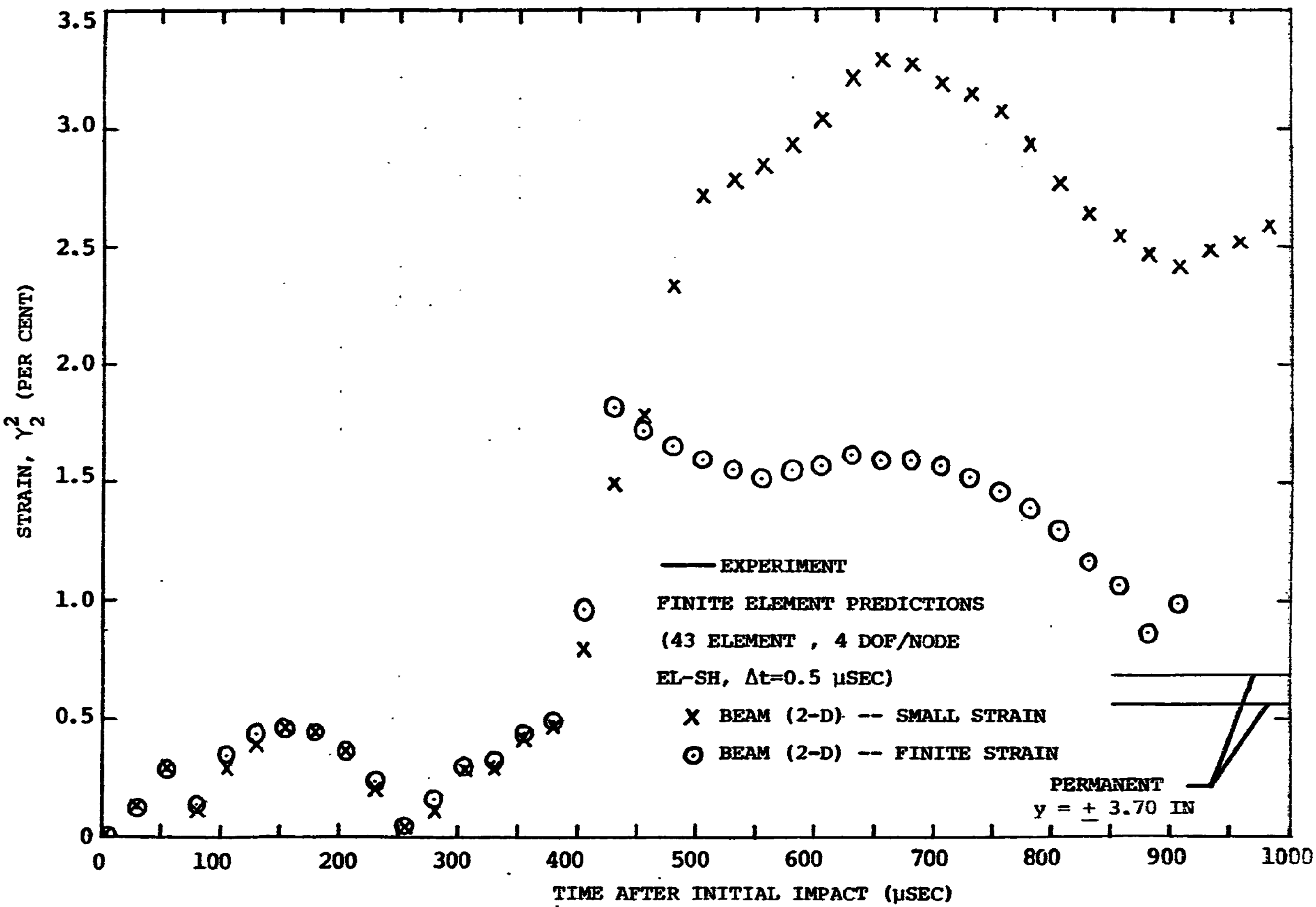

(k) Station y = 3.70 in, Upper Surface

FIG. 38 CONTINUED (CB-18)

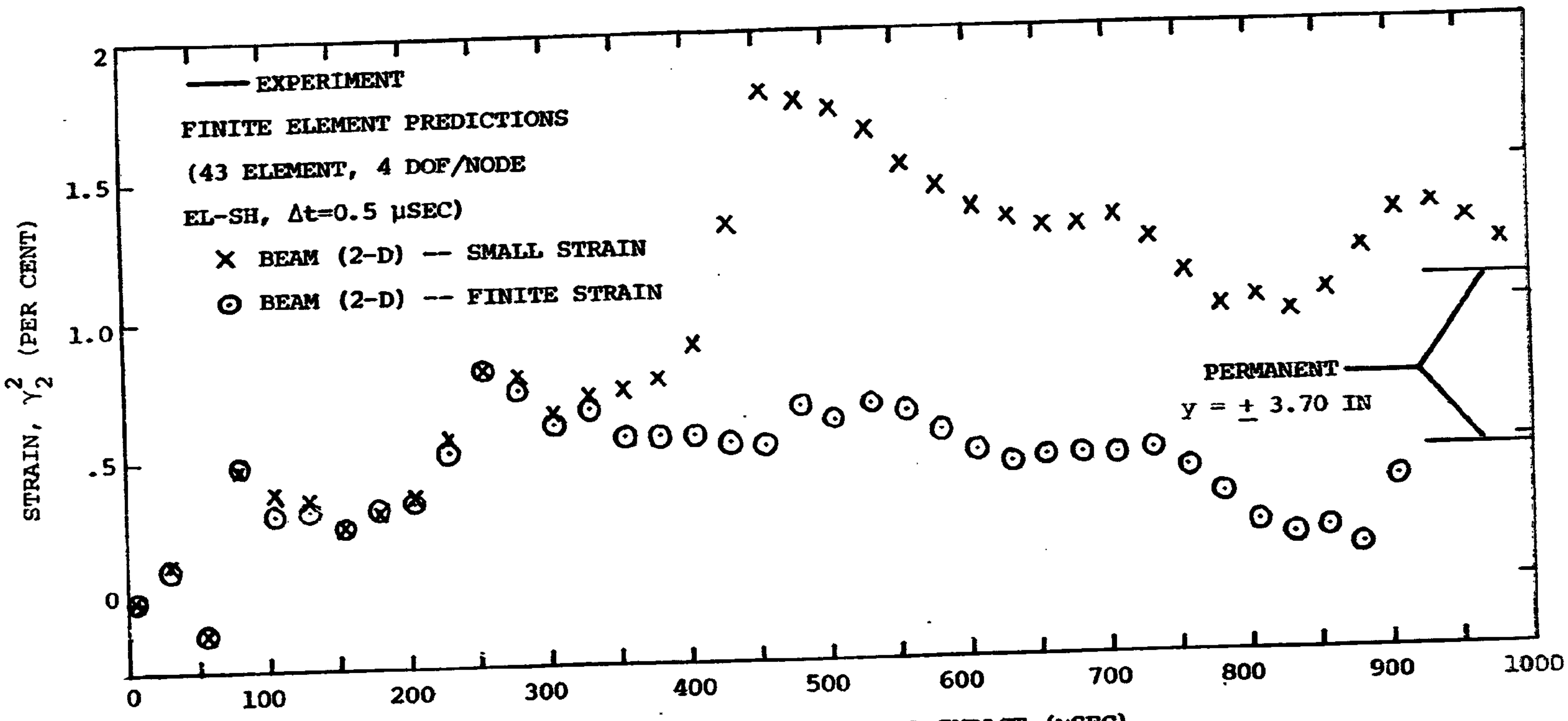

(ℓ) Station y = 3.70 in, Lower Surface

FIG. 38 CONTINUED (CB-18)

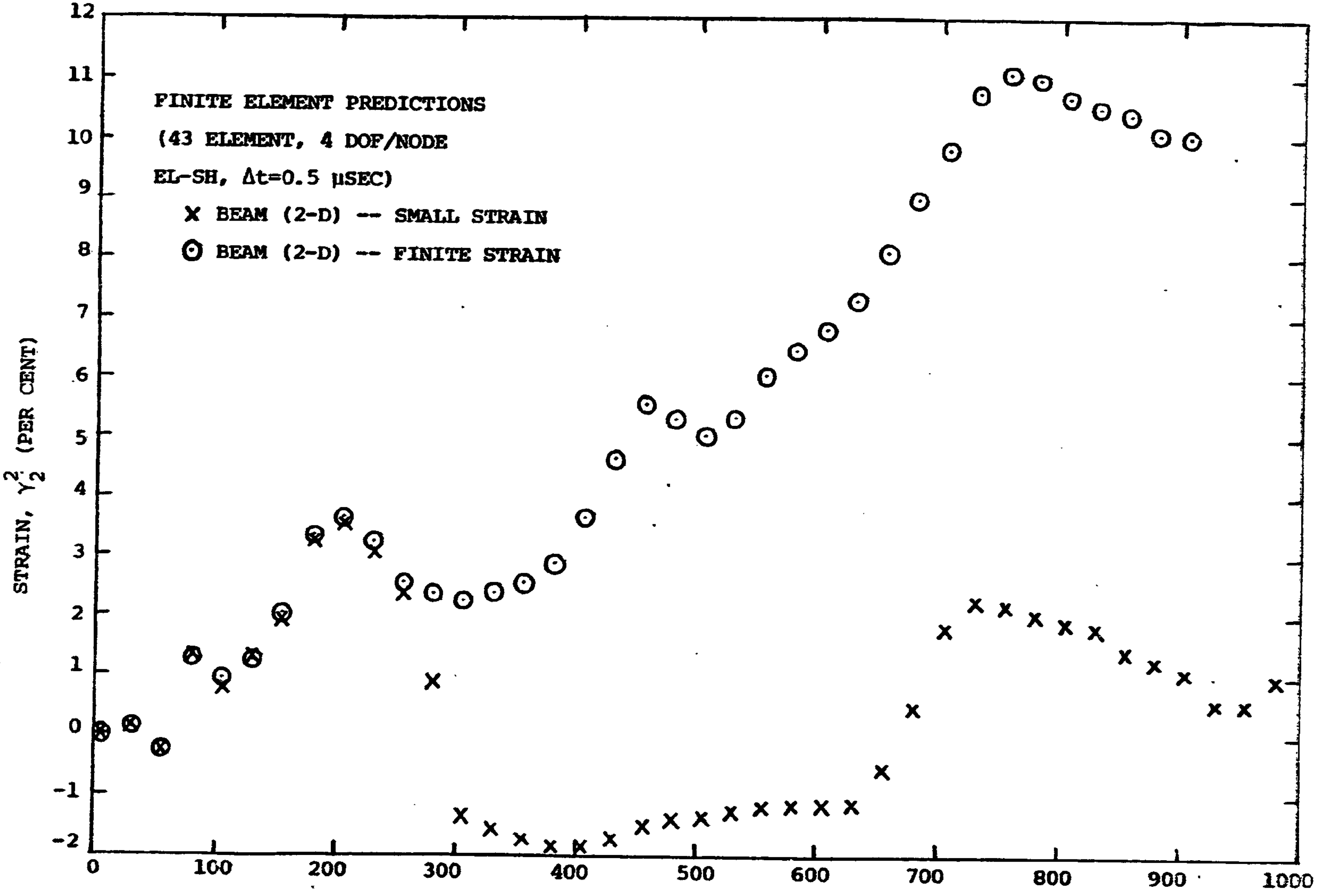

(m) Station y = 4.00 in, Upper Surface

FIG. 38 CONTINUED (CB-18)

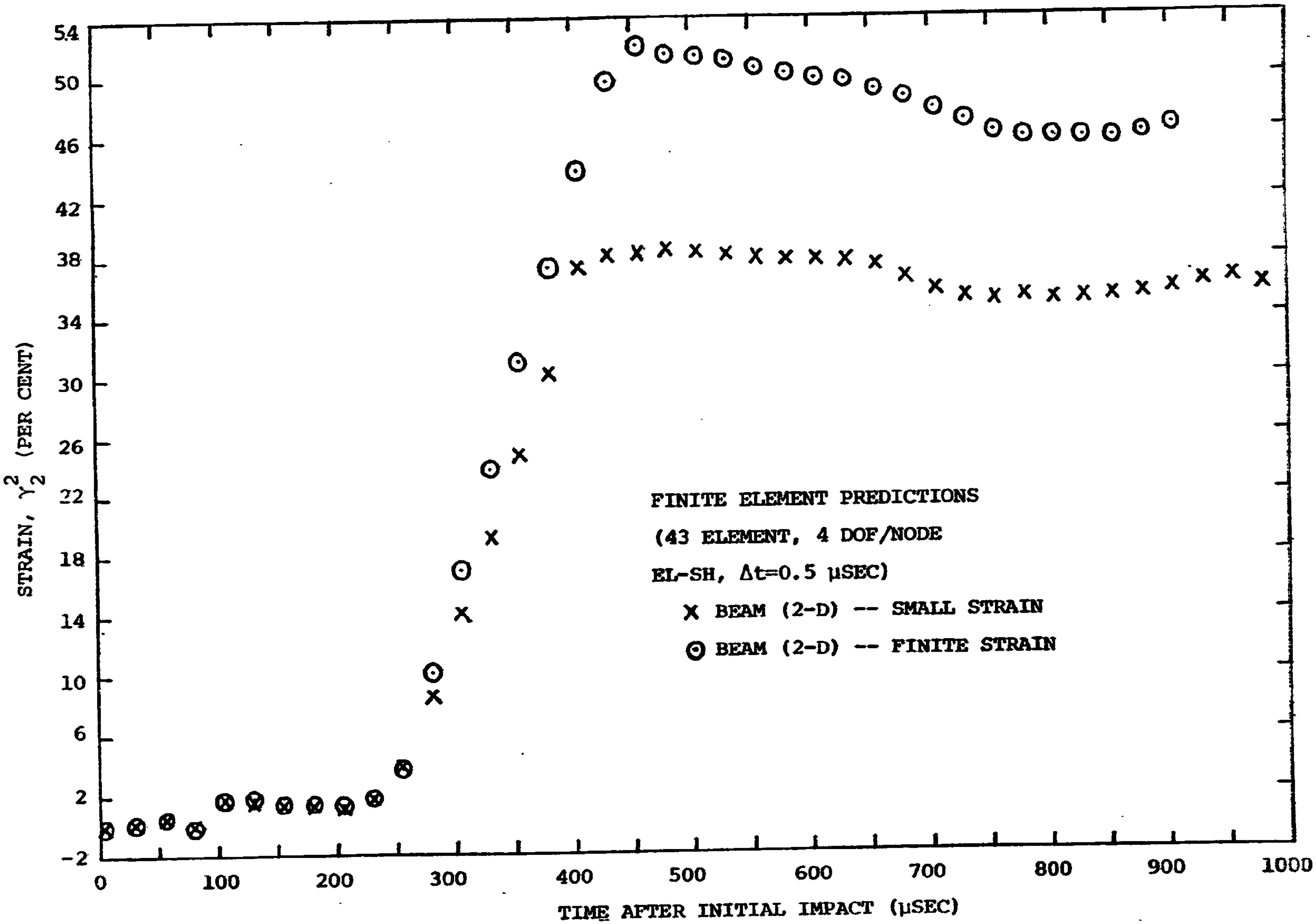

(n) Station y = 4.00 in, Lower Surface

FIG. 38 CONCLUDED (CB-18)

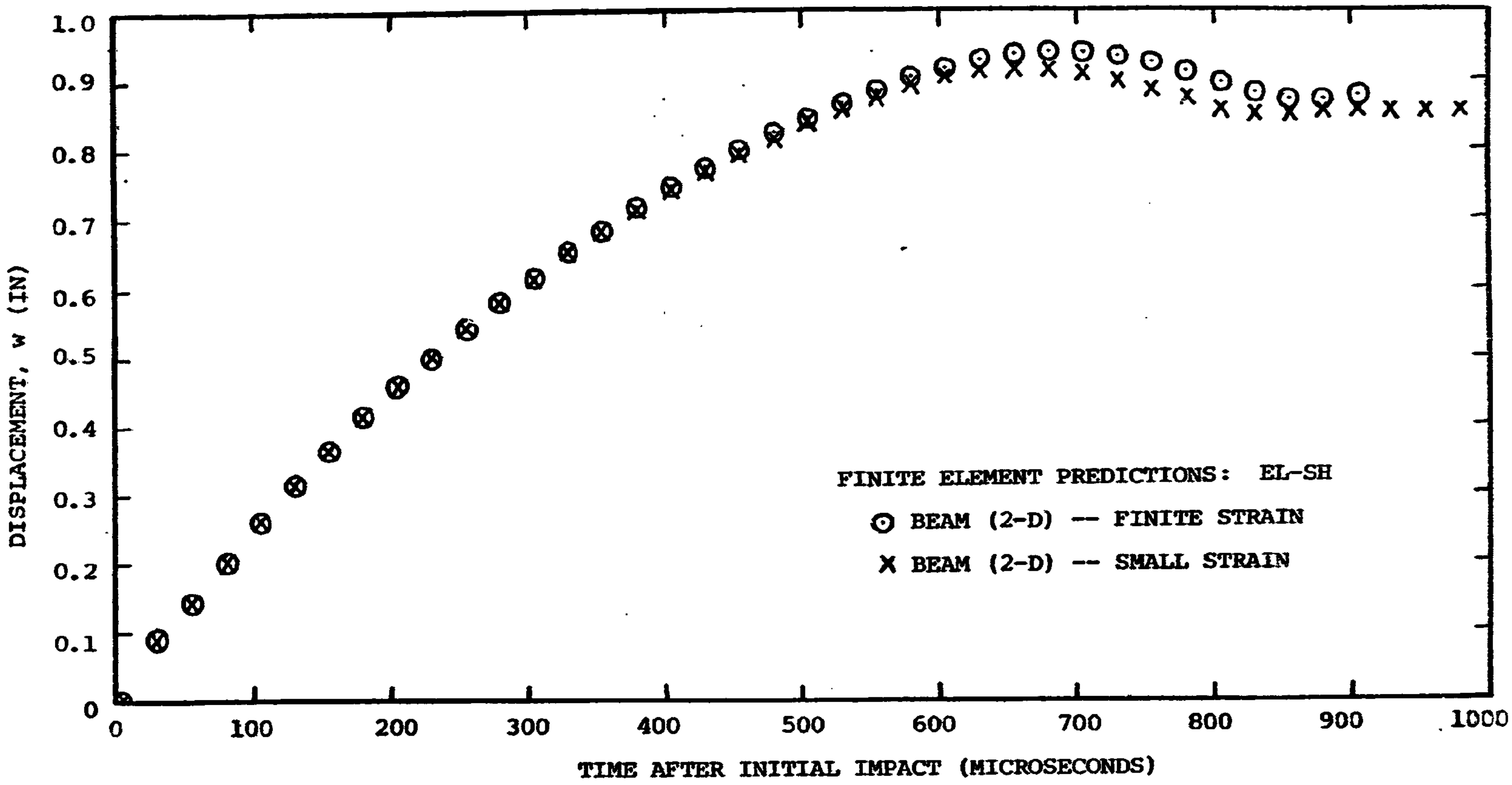

FIG. 39 PREDICTED TRANSIENT DEFLECTION AT THE MIDSPAN STATION (y=0) OF STEEL-SPHERE-IMPACTED 6061-T651 ALUMINUM NARROW-PLATE SPECIMEN CB-18

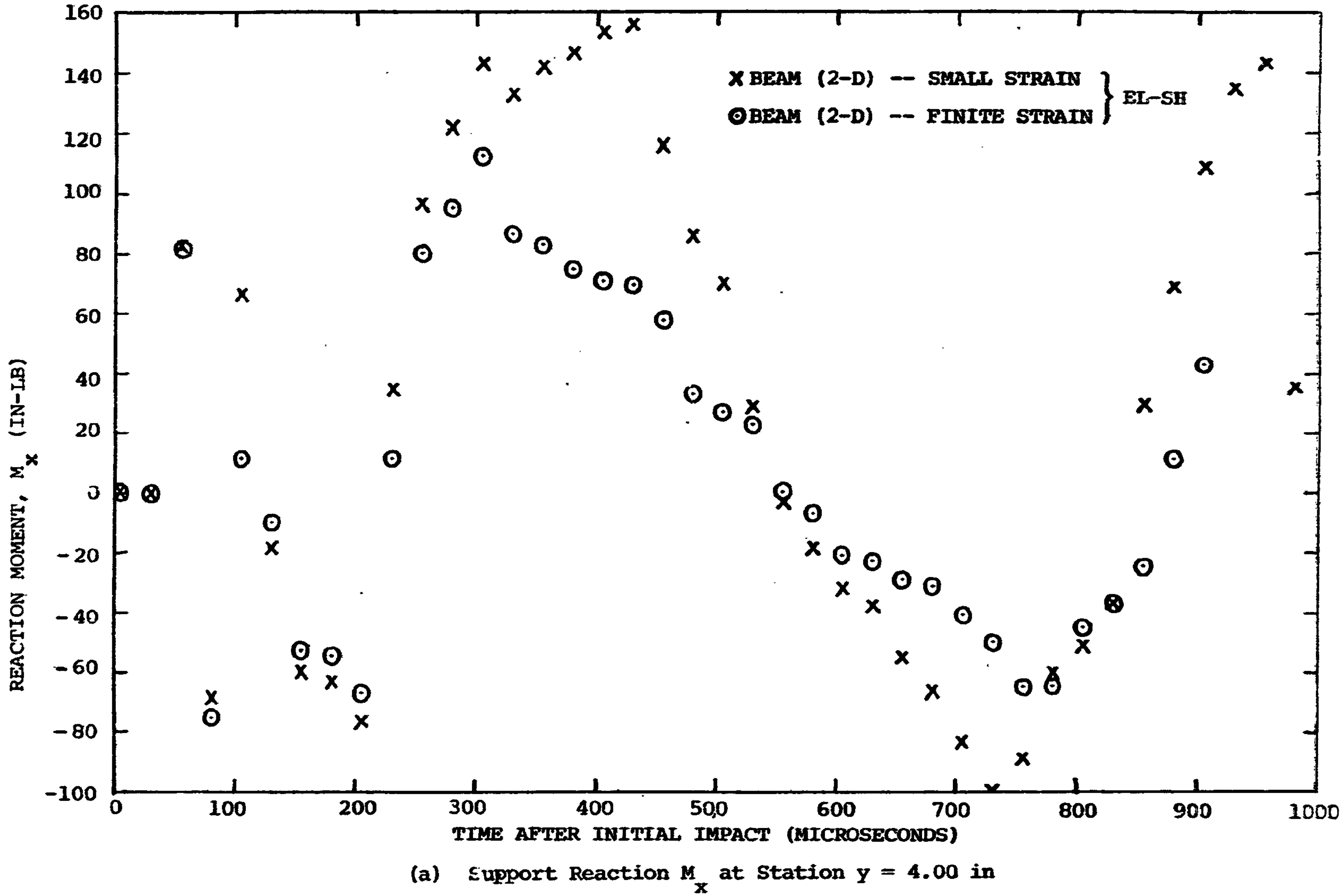

(a) Support Reaction M_x at Station y = 4.00 in

FIG. 40 FINITE ELEMENT PREDICTIONS OF SUPPORT REACTIONS OF STEEL-SPHERE-IMPACTED NARROW PLATE CB-18

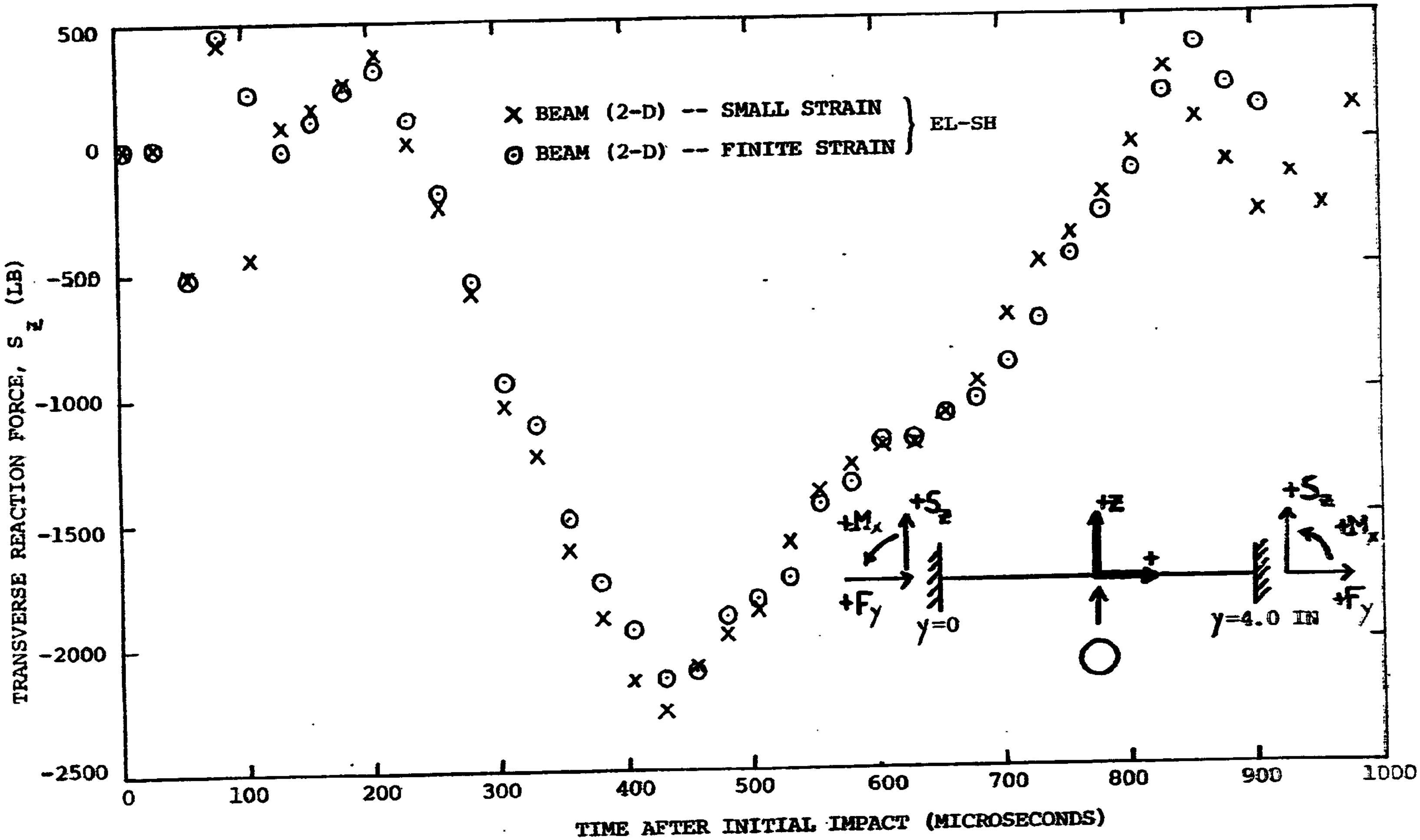

(b) Support Reaction S_z at Station $y=4.00$ in

FIG. 40 CONTINUED (CB-18)

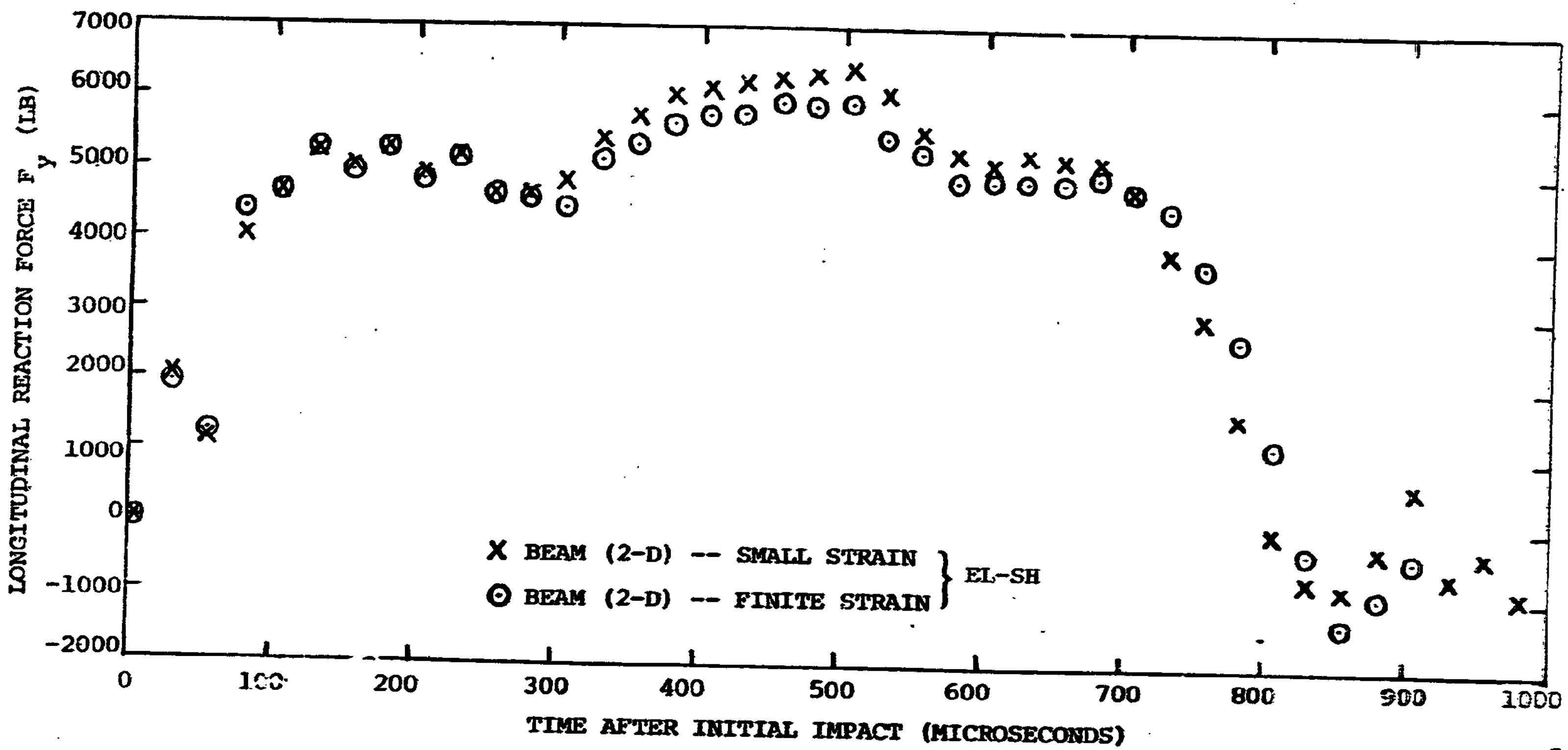

(c) Support Reaction F_y at Station y = 4.00 in

FIG. 40 CONCLUDED (CB-18)

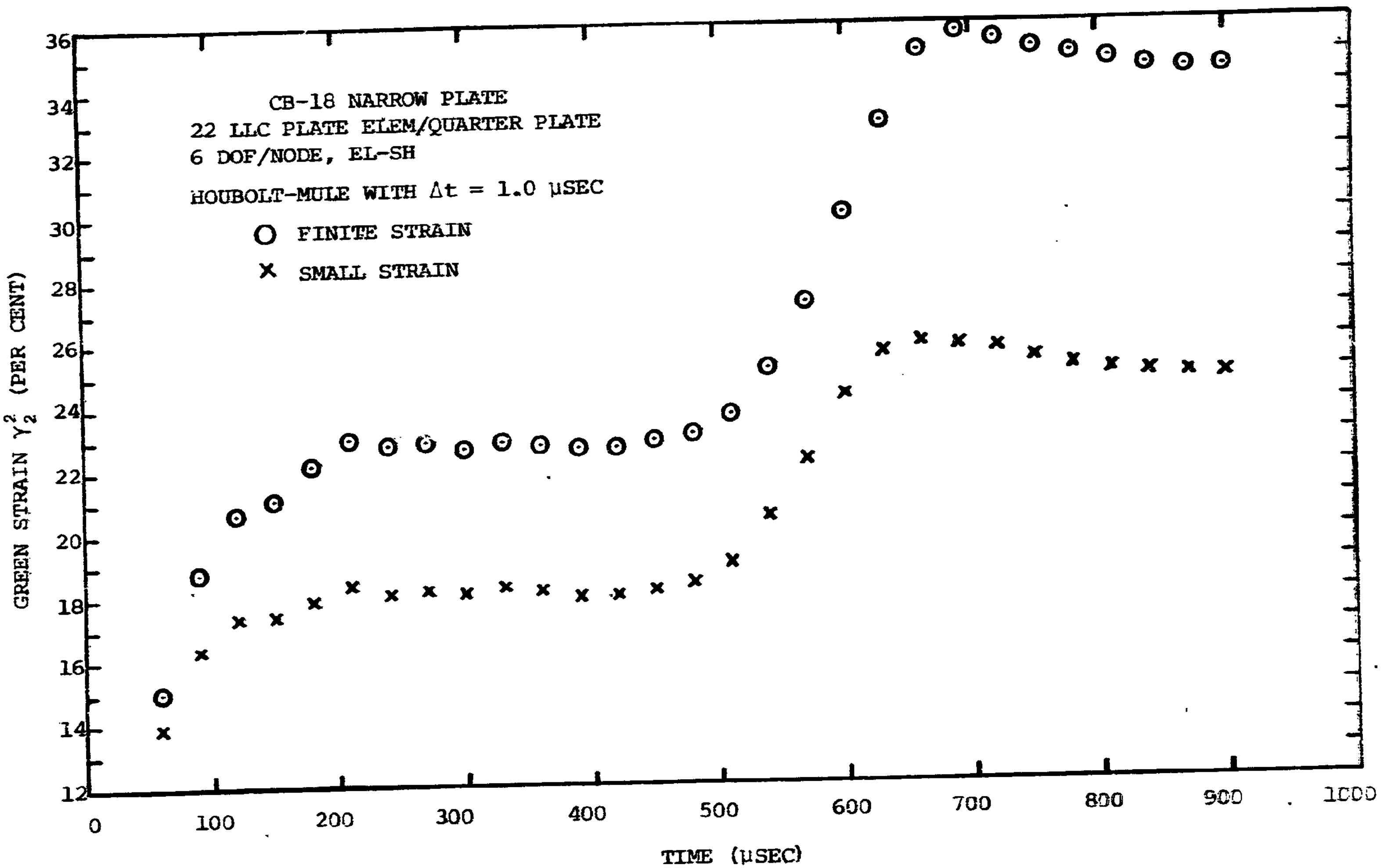

(a) Plate-Center Station (x,y)=(0,0), Upper (Non-Impacted) Surface

FIG.41 MEASUREMENTS AND/OR PREDICTIONS OF TRANSIENT LONGITUDINAL GREEN (LAGRANGIAN) STRAIN ON THE SURFACE FOR VARIOUS SPANWISE STATIONS OF STEEL-SPHERE-IMPACTED 6061-T651 ALUMINUM NARROW-PLATE SPECIMEN CB-18

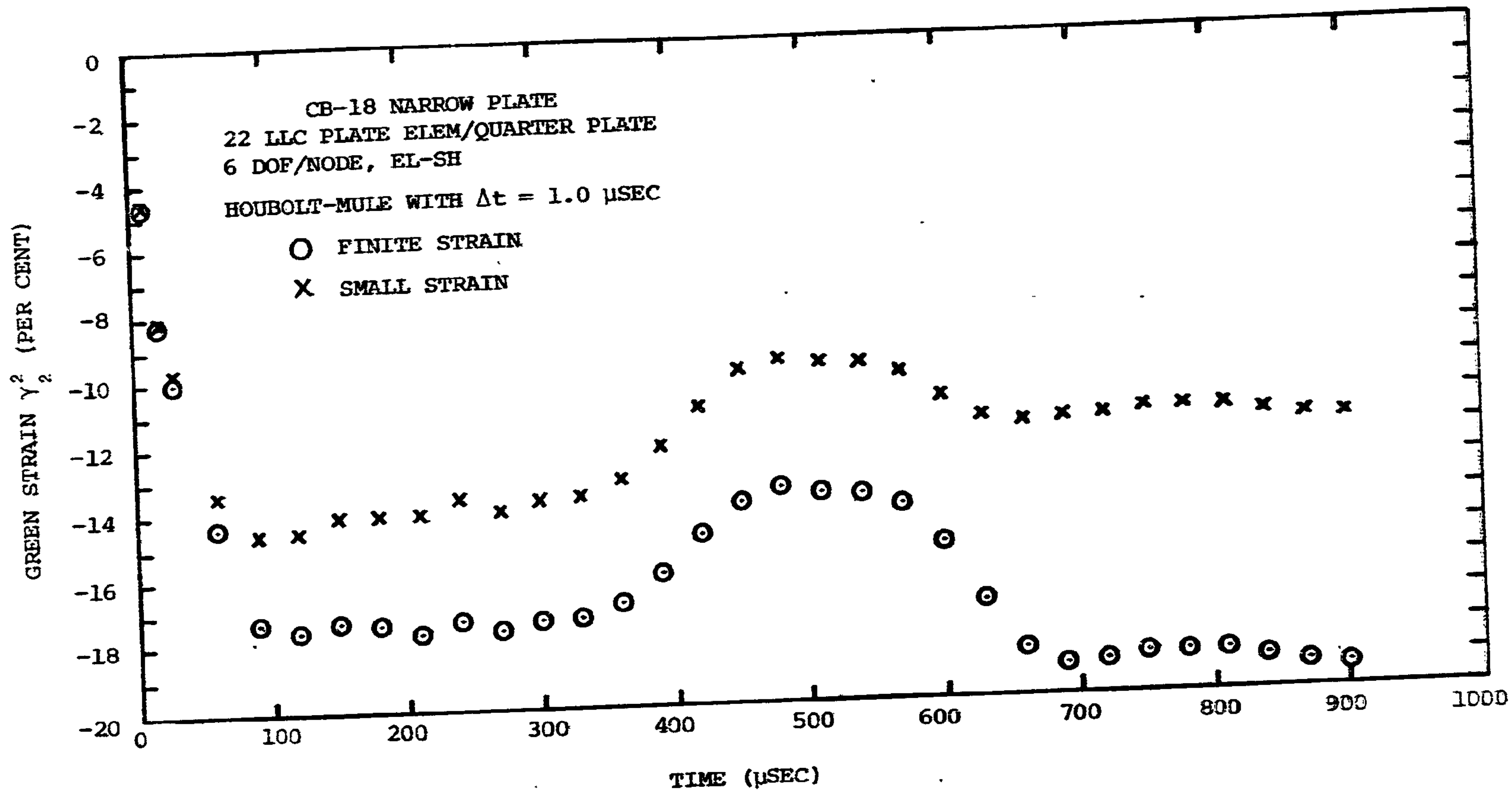

(b) Plate-Center Station $(x,y)=(0,0)$, Lower (Impacted) Surface

FIG.41 CONTINUED (FINITE STRAIN, SMALL STRAIN, CB-18)

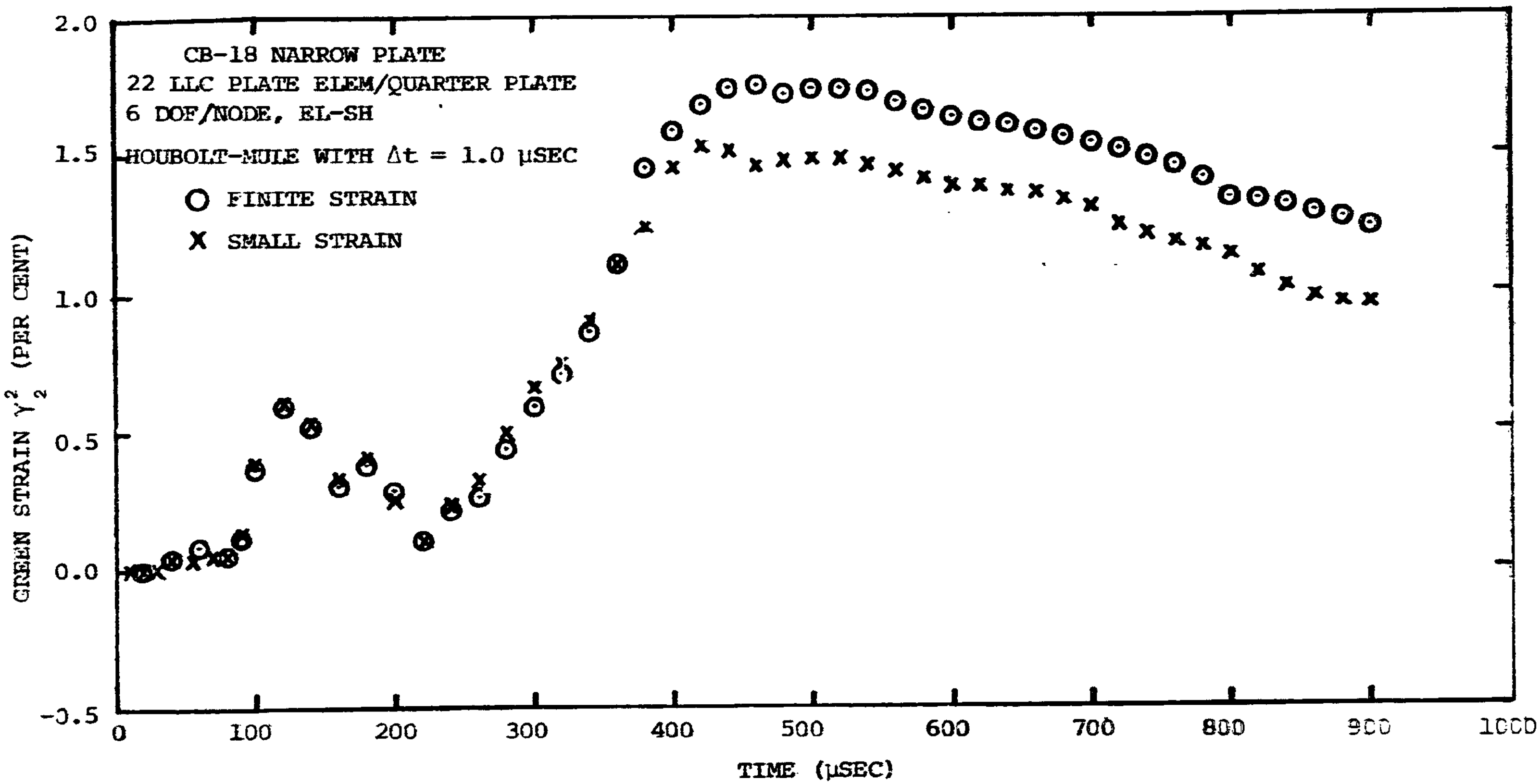

(c) Station (x,y)=(0,3.4in), Upper (Non-Impacted) Surface

FIG. 41 CONTINUED (FINITE STRAIN, SMALL STRAIN, CB-18)

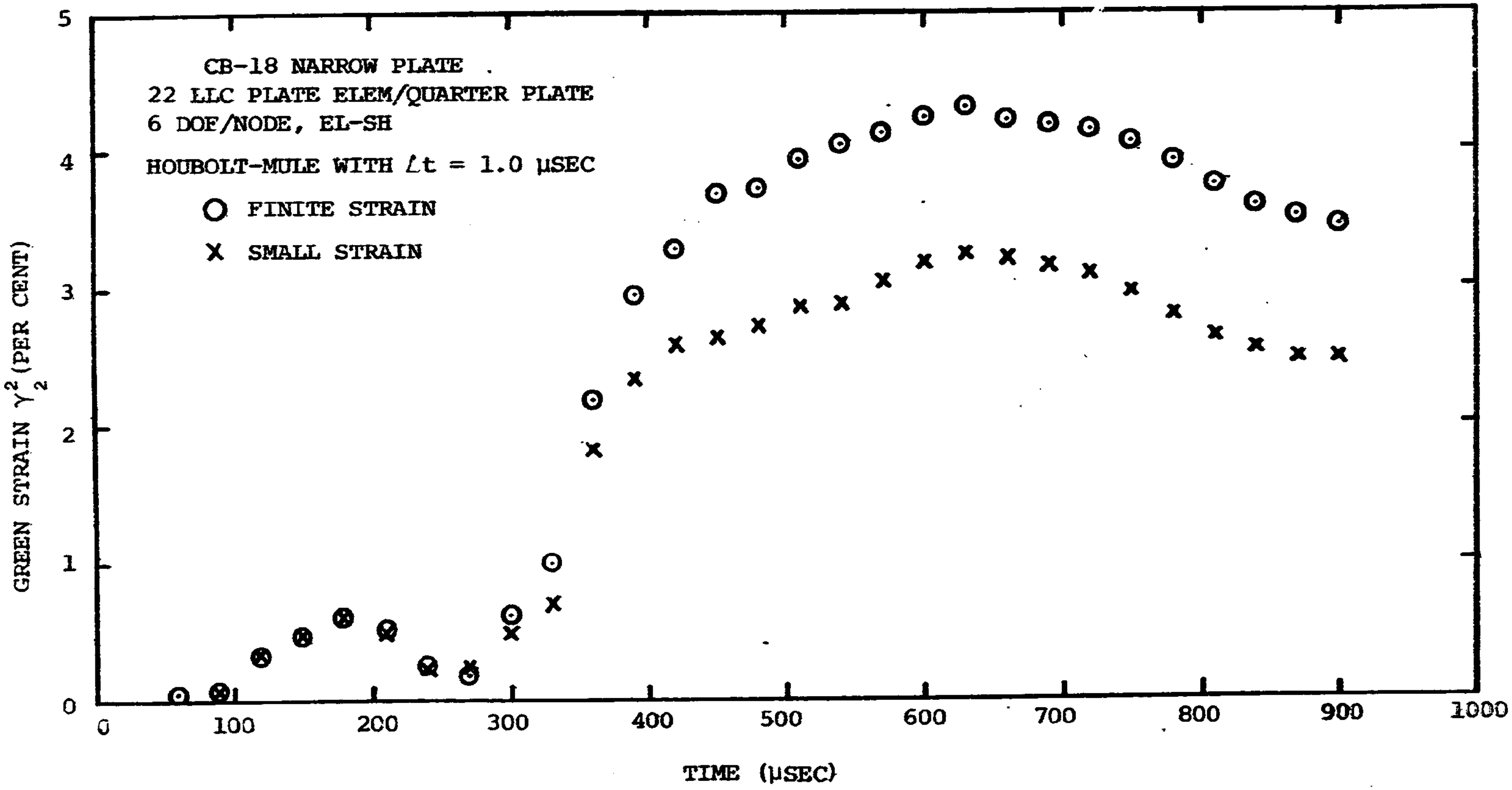

(d) Station (x,y)=(0,3.7in), Upper (Non-Impacted) Surface

FIG.41 CONTINUED (FINITE STRAIN, SMALL STRAIN, EXPT., CB-18)

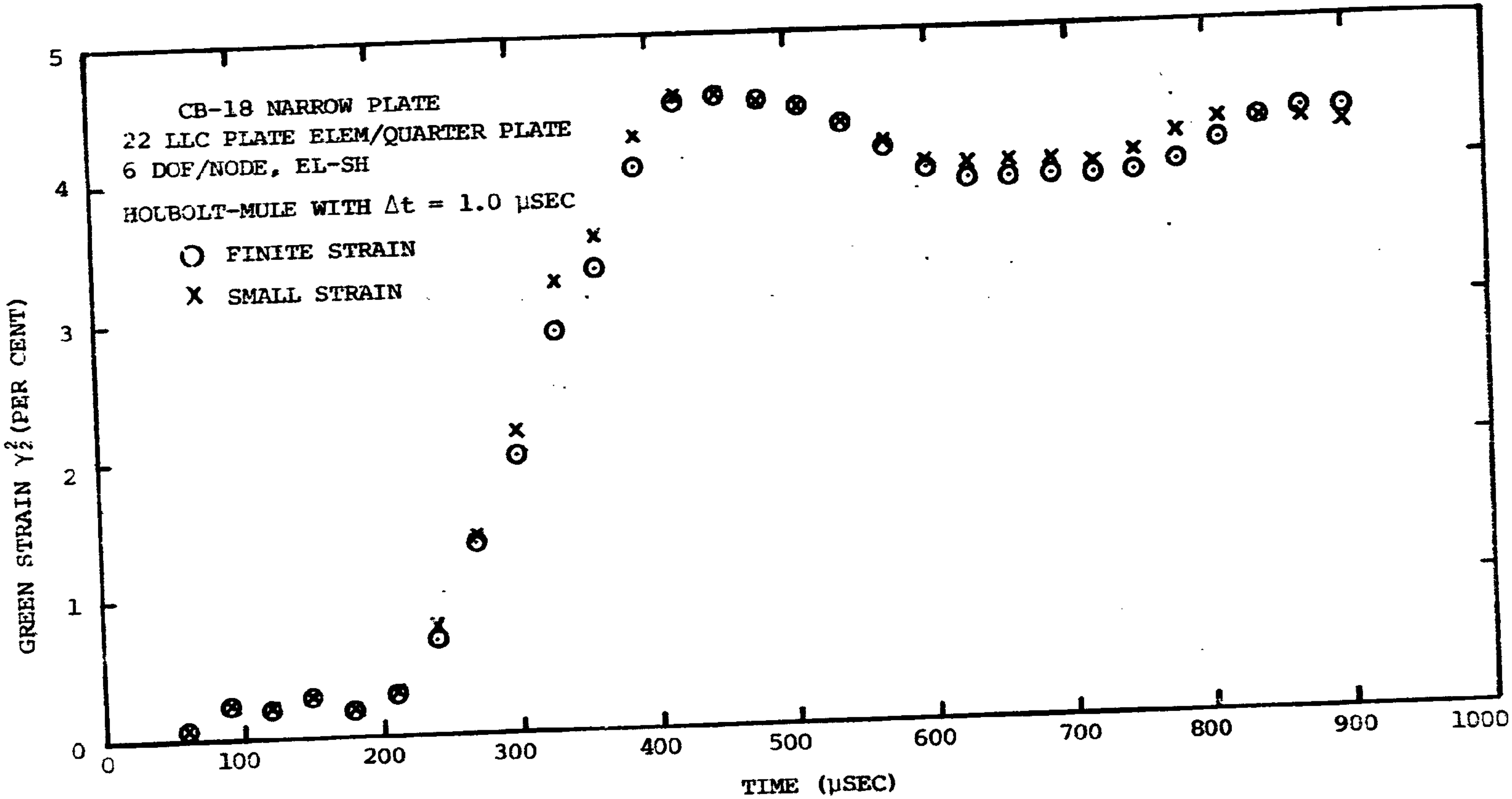

(e) Station (x,y)=(0,3.70in), Lower (Impacted) Surface

FIG. 41 CONTINUED (FINITE STRAIN, SMALL STRAIN, EXPT., CB-18)

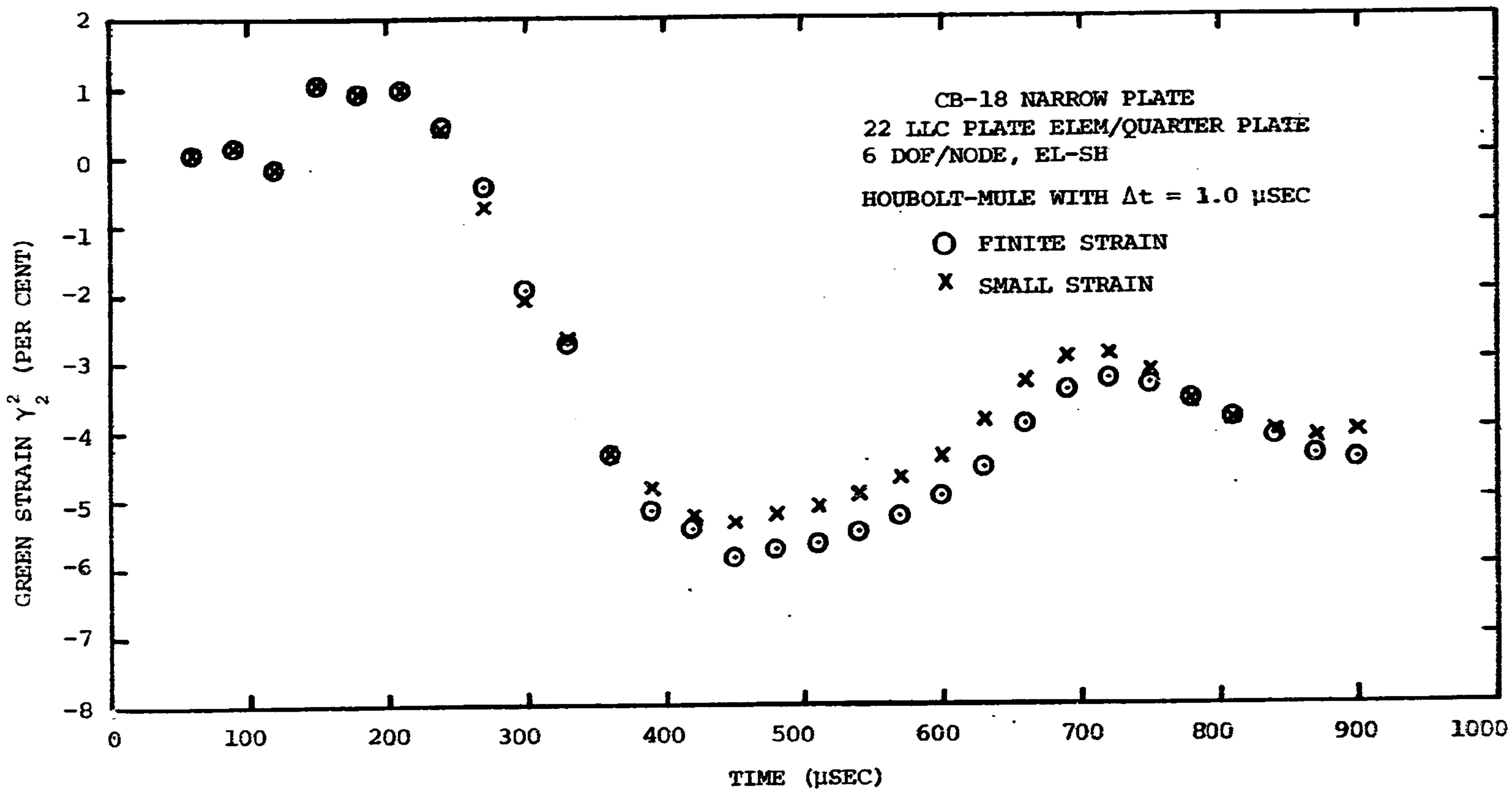

(f) Clamped End Station (x,y)=(0,4.00in), Upper (Non-Impacted) Surface

FIG. 41 CONTINUED (FINITE STRAIN, SMALL STRAIN, CB-18)

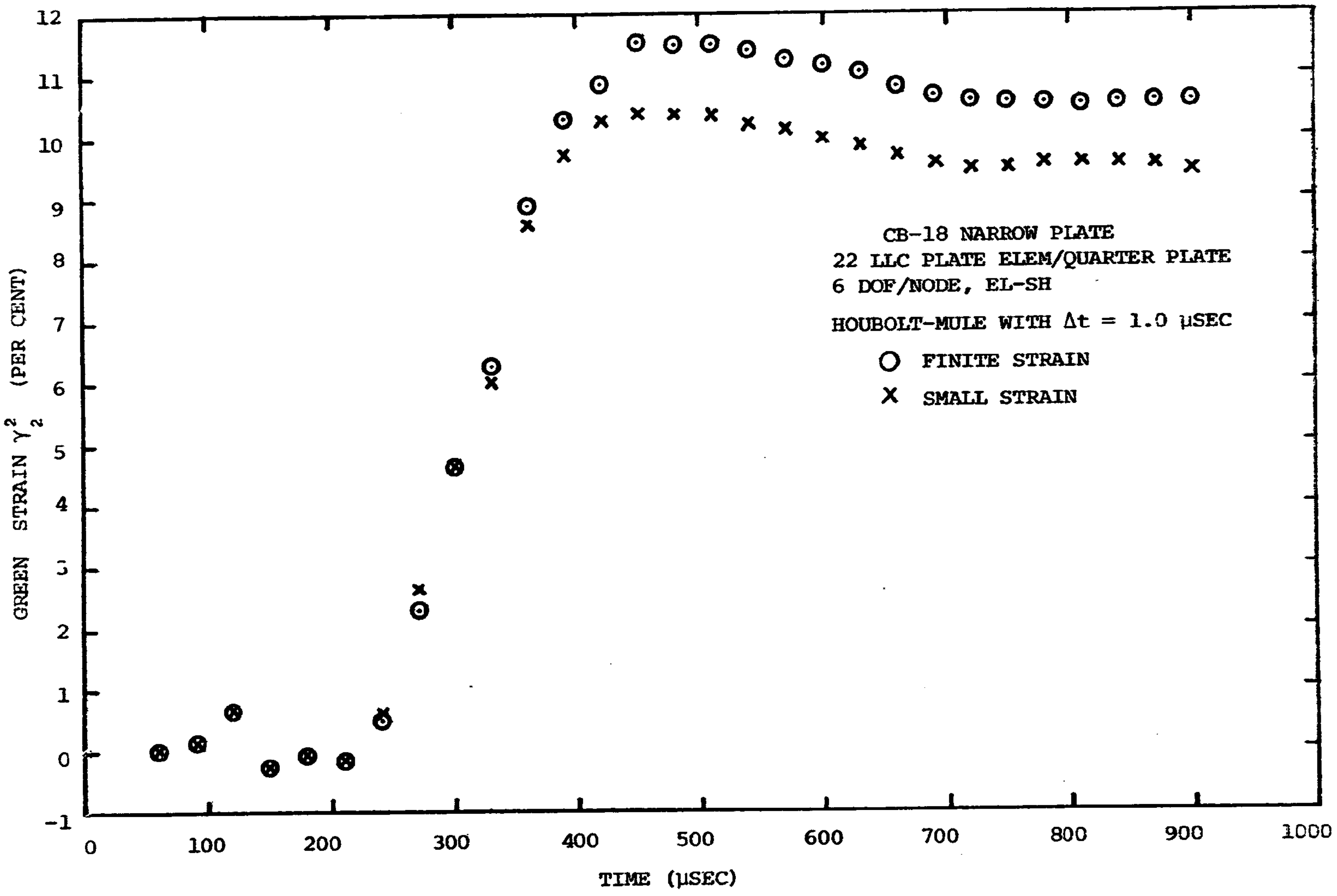

(g) Clamped-End Station (x,y)=(0,4.00in), Lower (Impacted) Surface

FIG. 41 CONCLUDED (FINITE STRAIN, SMALL STRAIN, CB-18)

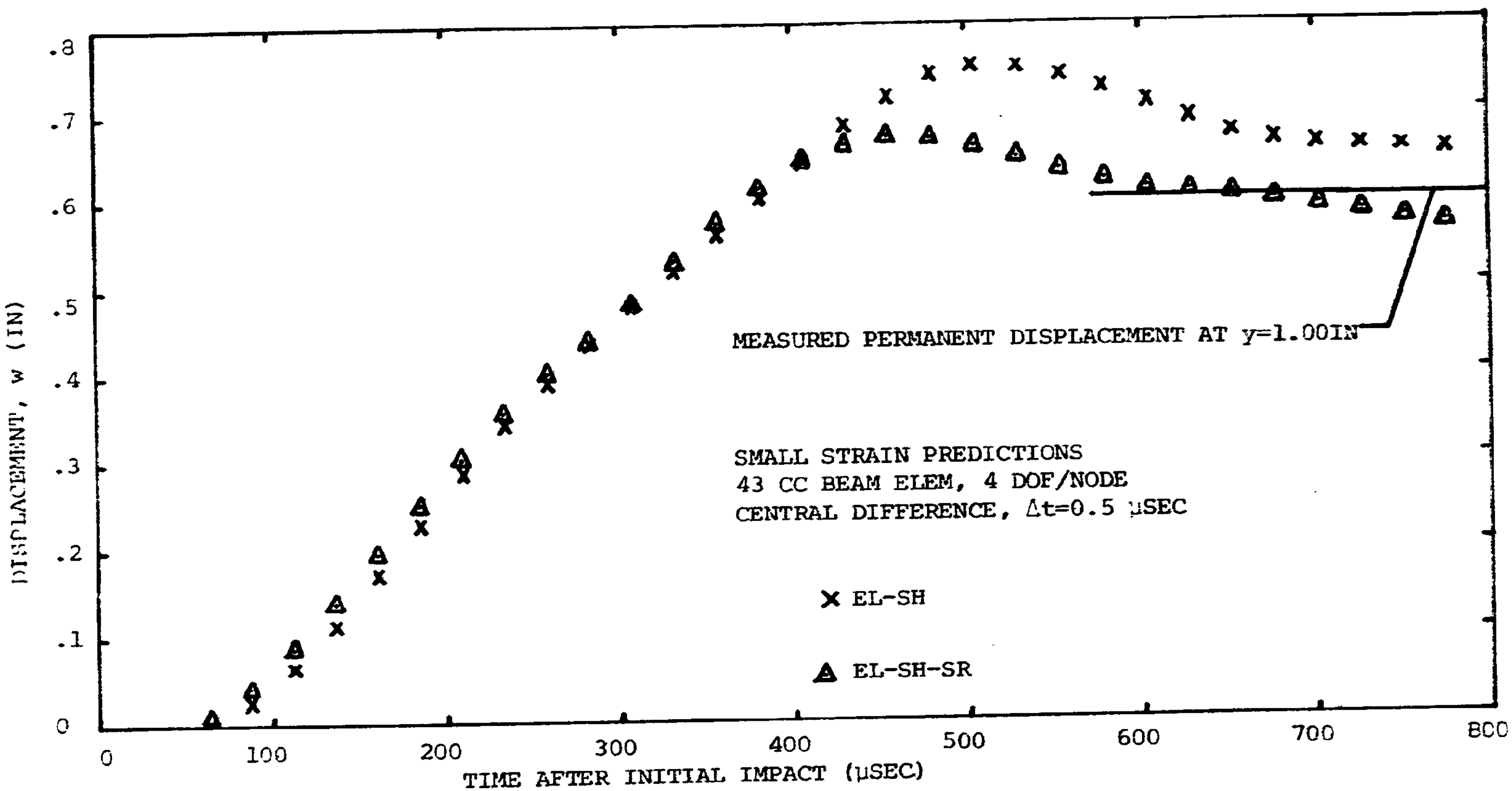

(a) Beam Element Model, EL-SH, EL-SH-SR, Station y=1.00in

FIG. 42 COMPARISON OF PREDICTIONS AND MEASUREMENTS OF THE w-DISPLACEMENT AT VARIOUS SPANWISE STATIONS OF STEEL-SPHERE-IMPACTED 6061-T651 ALUMINUM NARROW-PLATE SPECIMEN CB-18

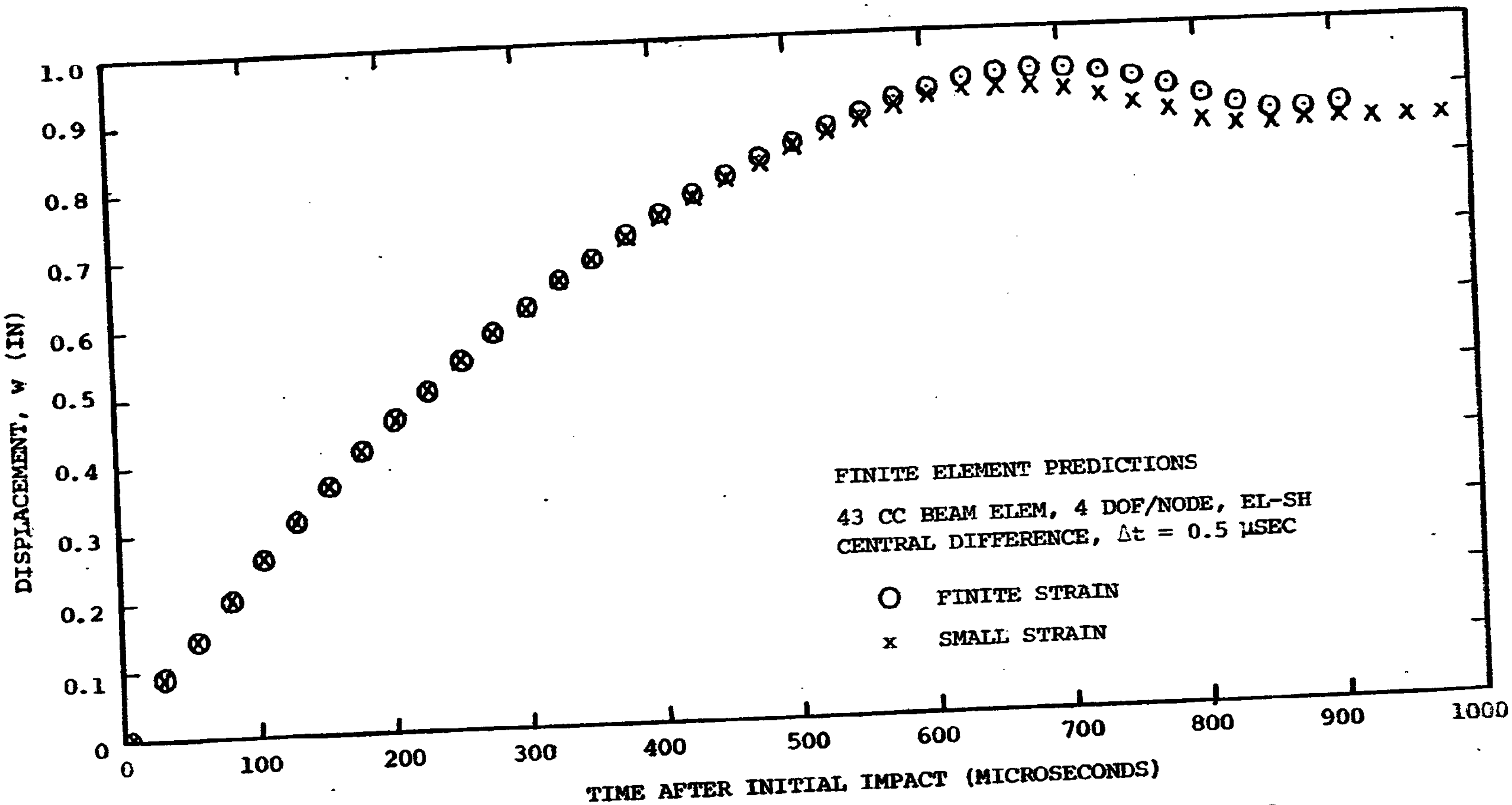

(b) Beam Element Model, EL-SH, Transient w-Displacement at y = 0

FIG. 42 CONTINUED (CB-18, w-DISPLACEMENT, FINITE STRAIN, SMALL STRAIN, EL-SH)

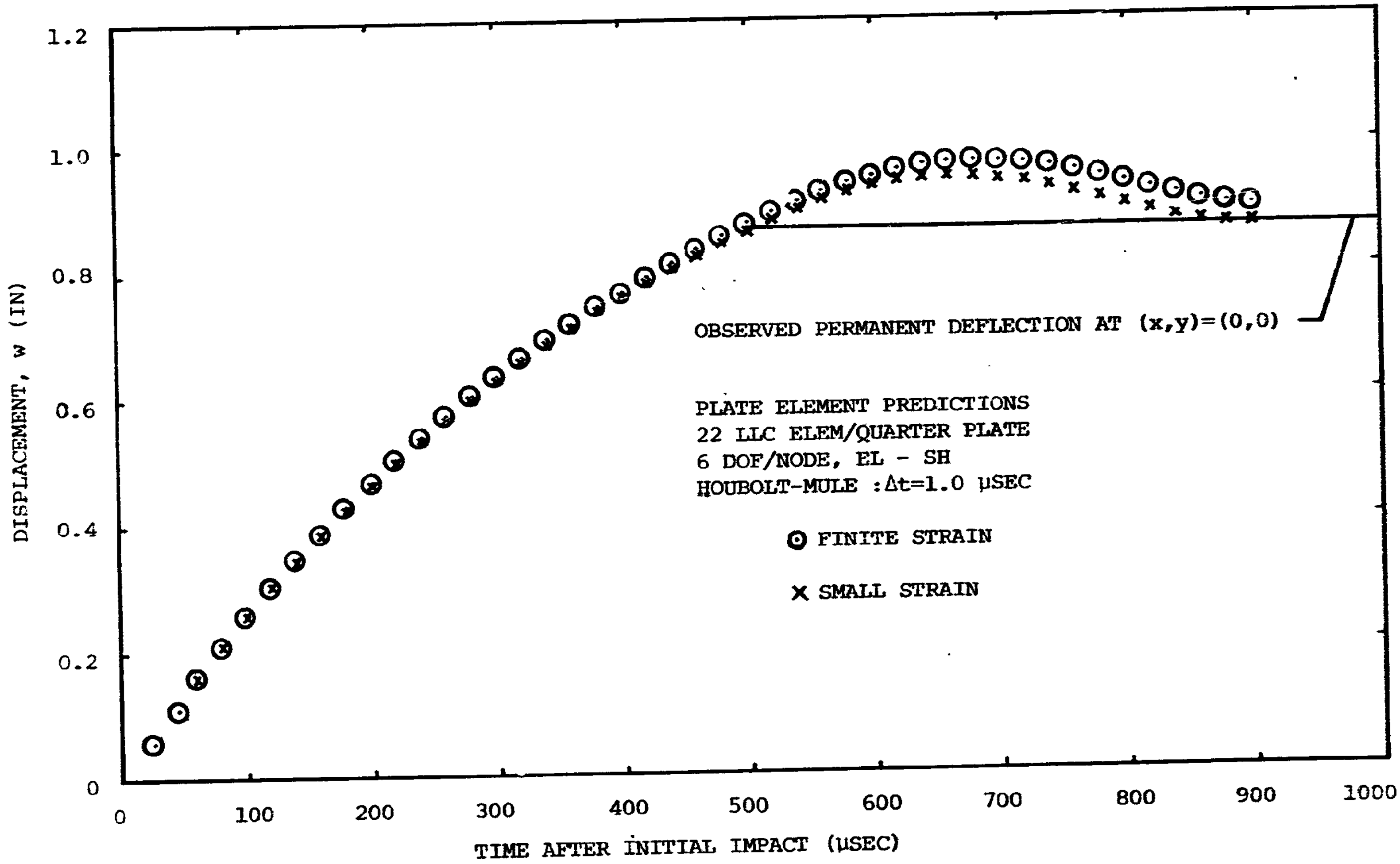

(c) Plate Element Model, EL-SH, Transient w-Displacement at (x,y)=(0,0)

FIG. 42 CONTINUED (CB-18,w-DISPLACEMENT, FINITE STRAIN, SMALL STRAIN, EL-SH, EXPT.)

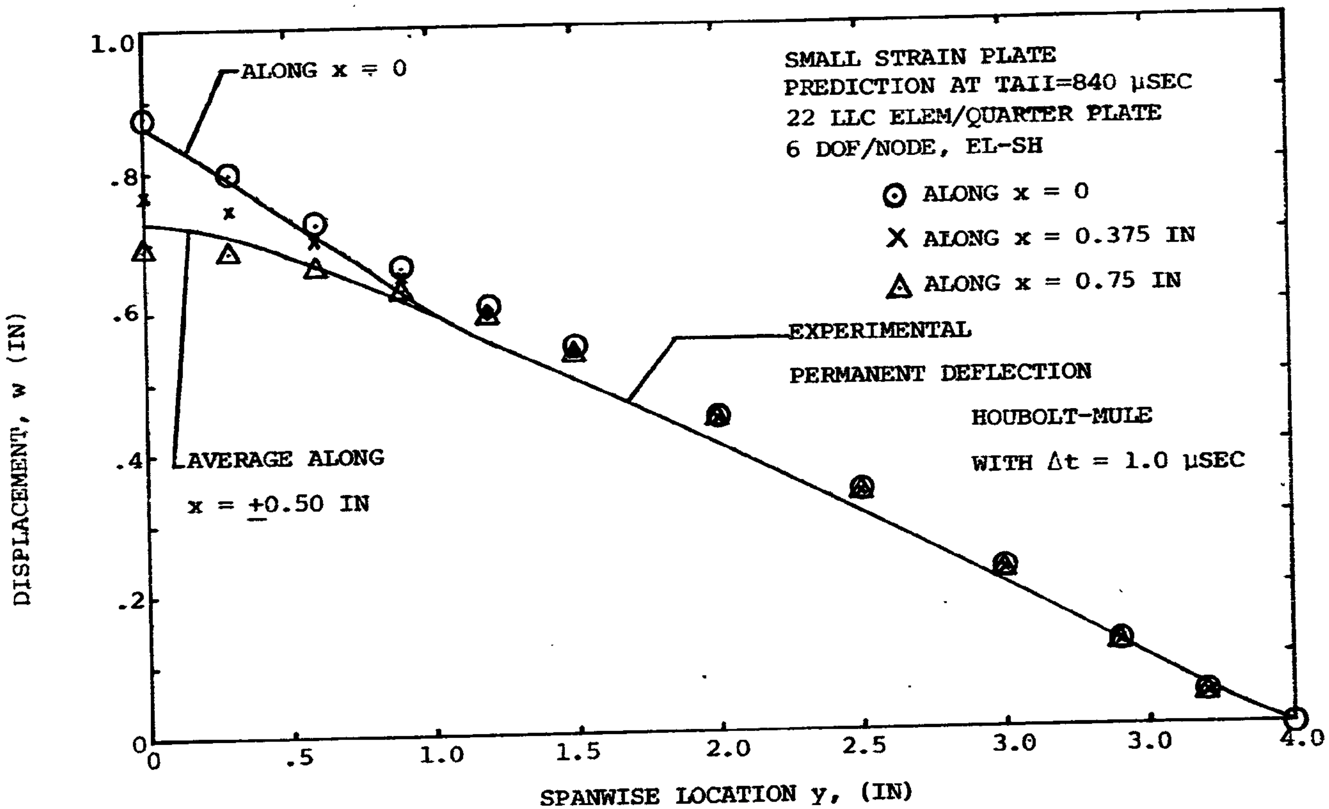

(d) Plate Element Model, EL-SH, w-Displacement at TAII=840 μSEC

FIG. 42 CONTINUED (CB-18, w-DISPLACEMENT, SMALL-STRAIN PREDICTION, EXPT.)

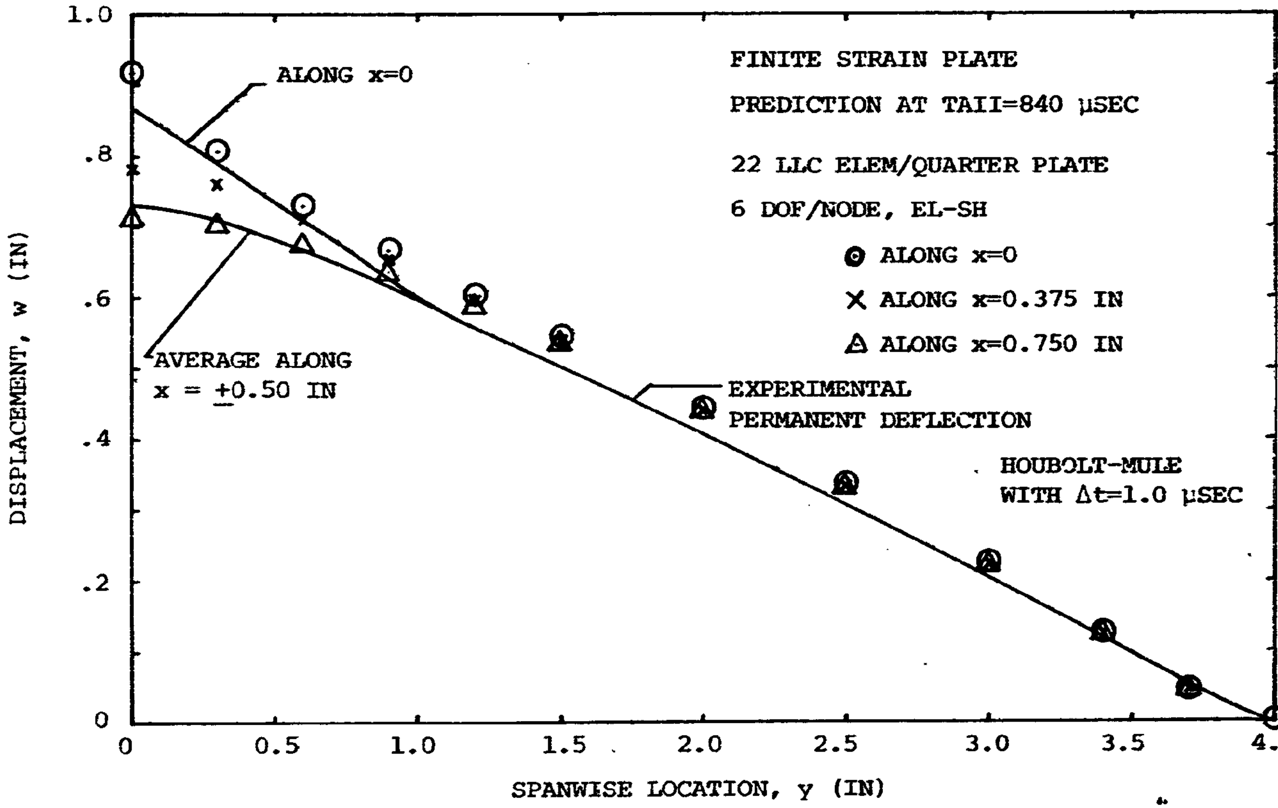

(e) Plate Element Model, EL-SH, w-Displacement at TAII=840 μSEC

FIG. 42 CONTINUED (CB-18, w-DISPLACEMENT, FINITE-STRAIN PREDICTION, EXPT.)

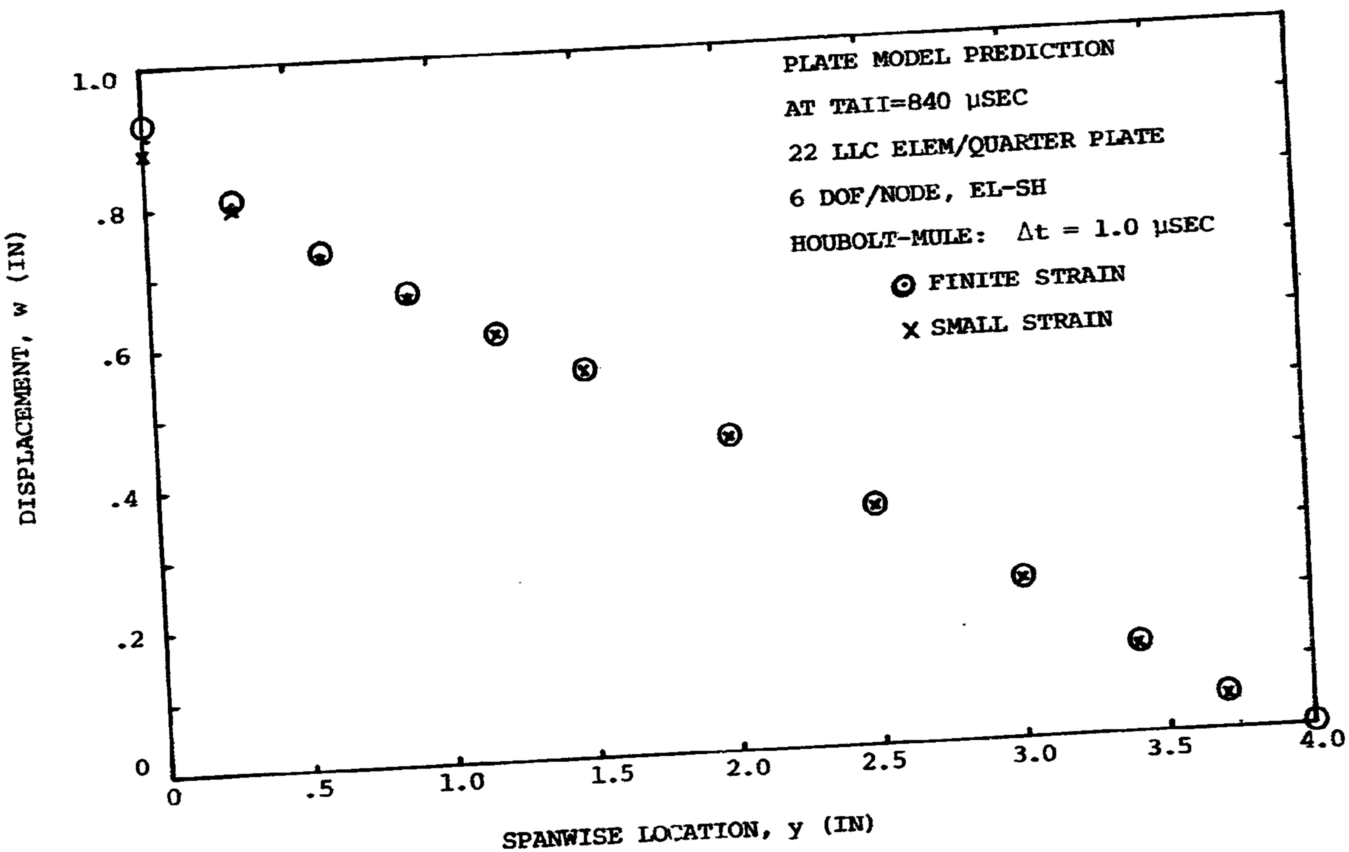

(f) Plate Element Model, EL-SH, w-Displacement along x=0 at 840 µsec

FIG. 42 CONCLUDED (CB-18, w-DISPLACEMENT, FINITE STRAIN, SMALL STRAIN, EL-SH)

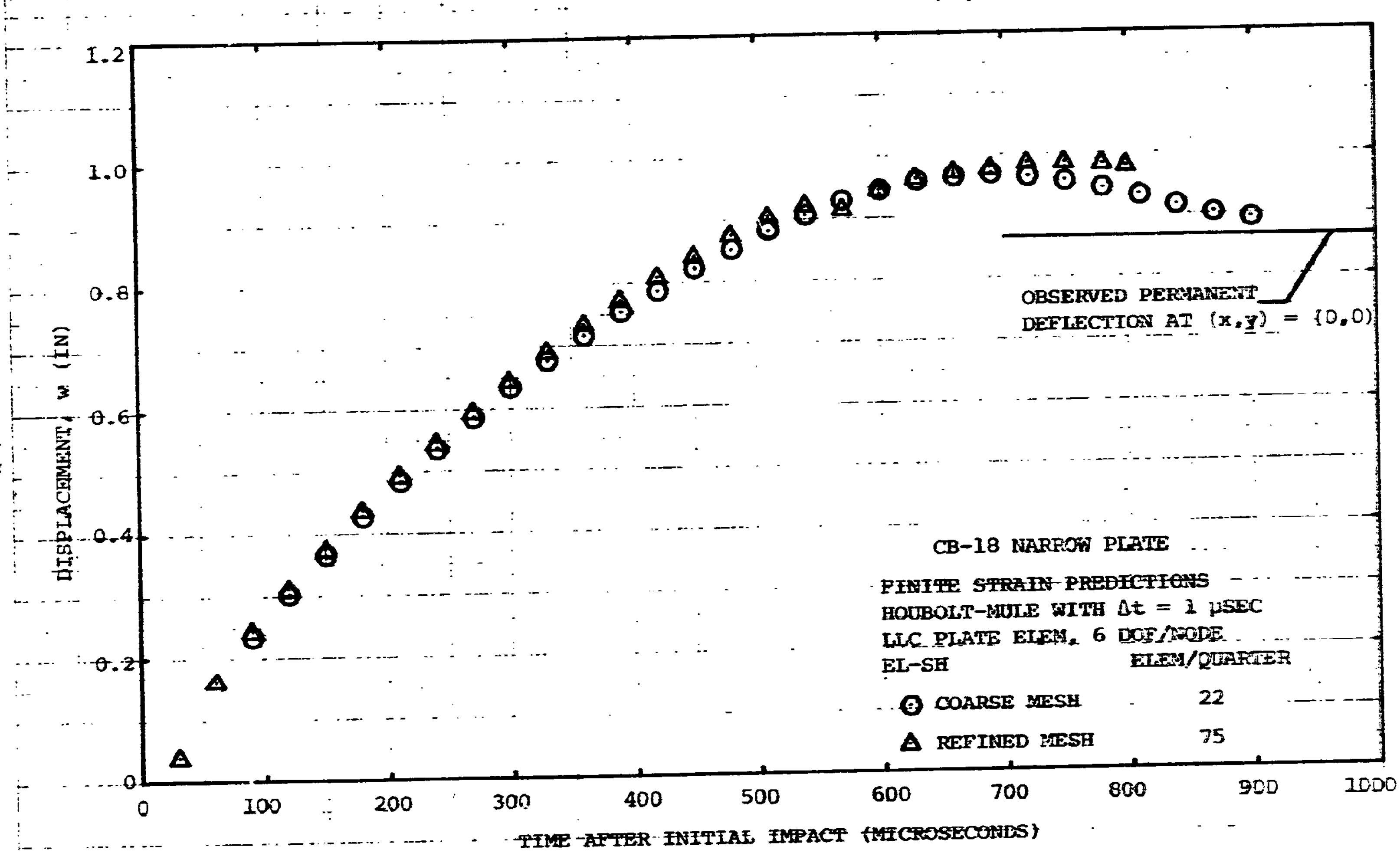

FIG. 43 COARSE-MESH VS. REFINED-MESH PLATE-ELEMENT FINITE-STRAIN PREDICTIONS OF THE TRANSIENT PLATE-CENTER DISPLACEMENT w OF STEEL-SPHERE-IMPACTED 6061-T651 ALUMINUM NARROW-PLATE SPECIMEN CB-18

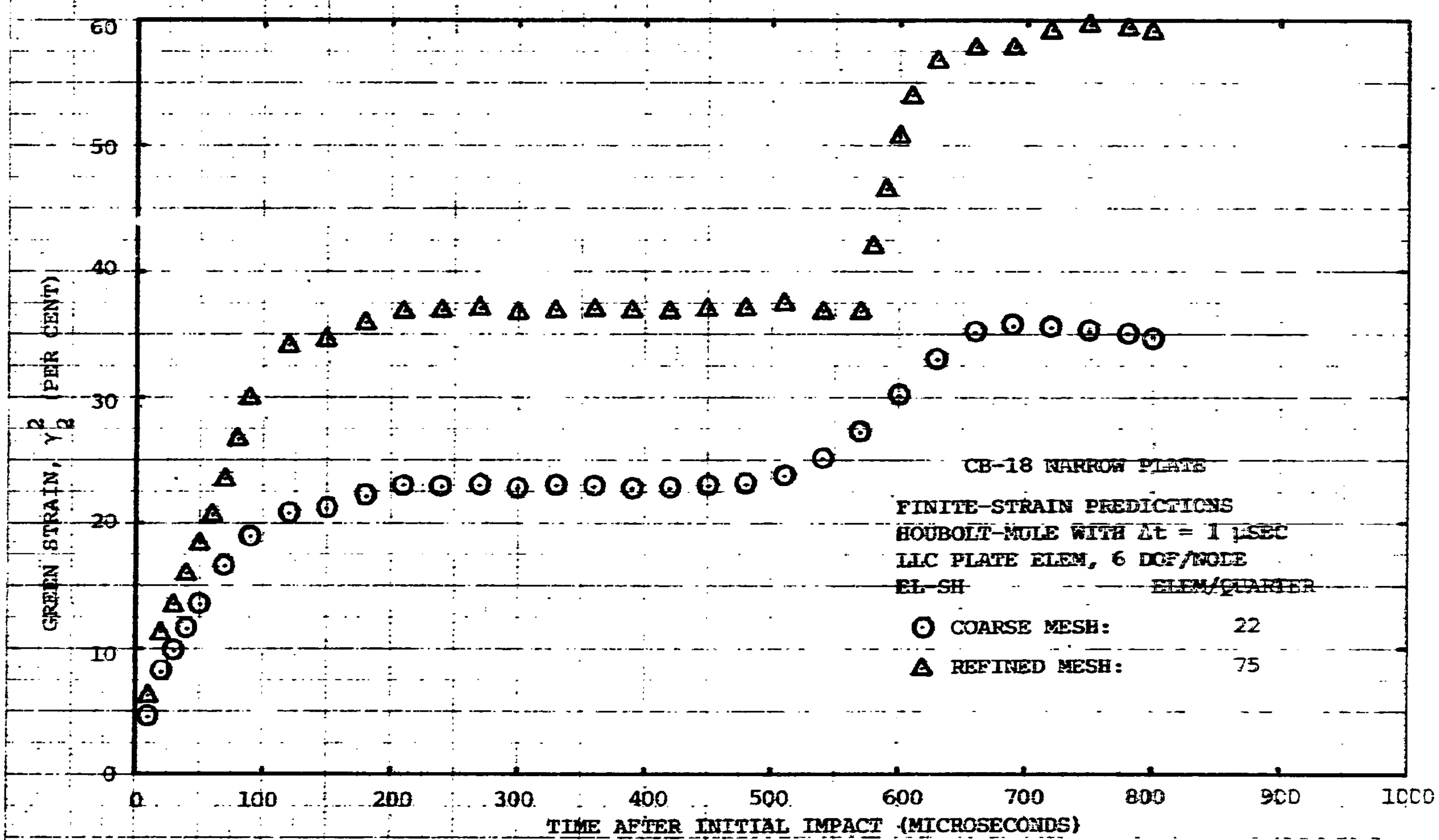

(a) Plate-Center Station (x,y) = (0,0), Upper (Non-Impacted) Surface

FIG. 44 COARSE-MESH VS. REFINED-MESH PLATE-ELEMENT FINITE-STRAIN PREDICTIONS OF TRANSIENT LONGITUDINAL GREEN (LAGRANGIAN) STRAIN ON THE SURFACE FOR VARIOUS SPANWISE STATIONS OF STEEL-SPHERE-IMPACTED 6061-T651 ALUMINUM NARROW-PLATE SPECIMEN CB-18

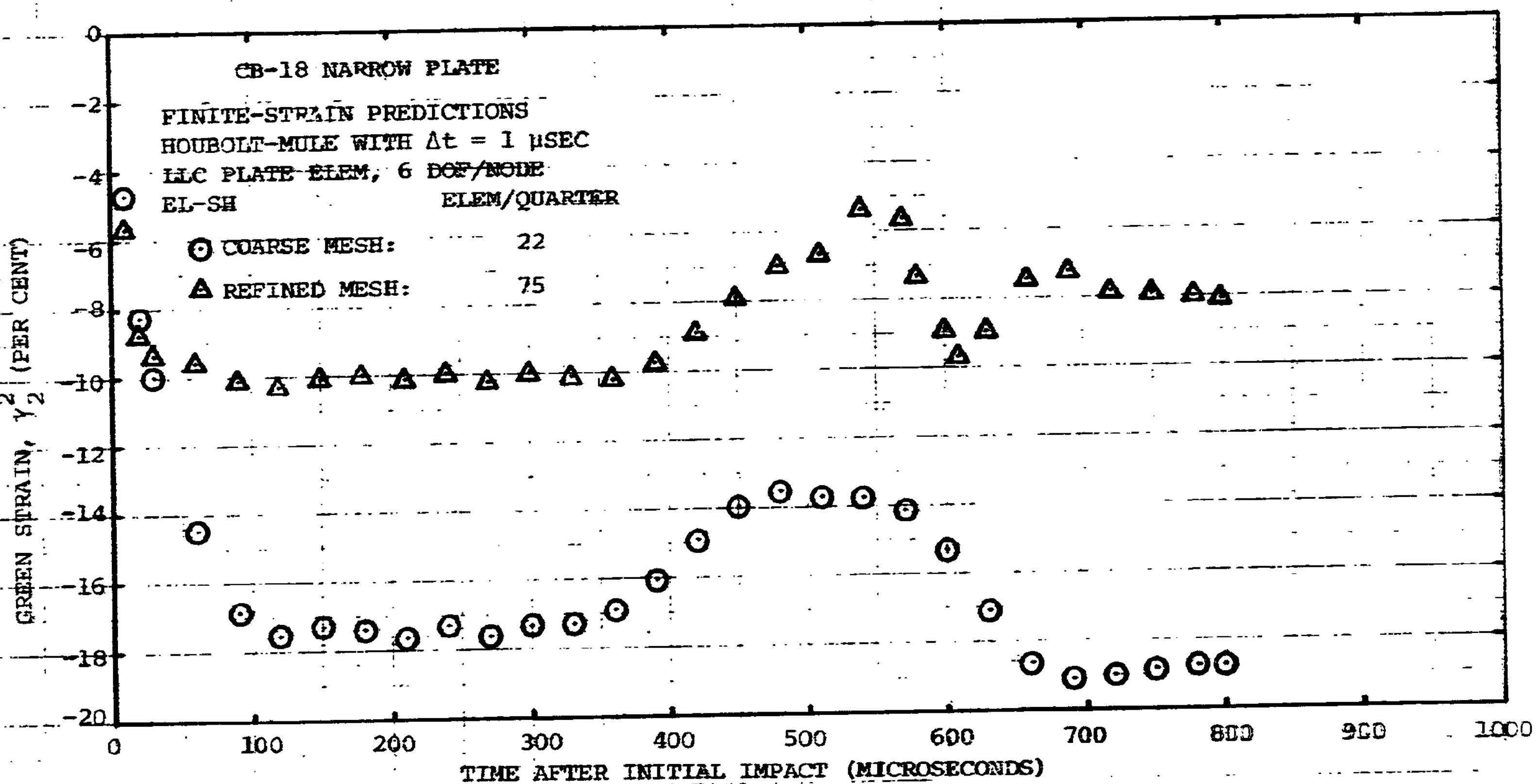

(b) Plate-Center Station (x,y) = (0,0), Lower (Impacted) Surface

FIG. 44 CONTINUED (COARSE MESH, REFINED MESH, FINITE STRAIN, CB-18)

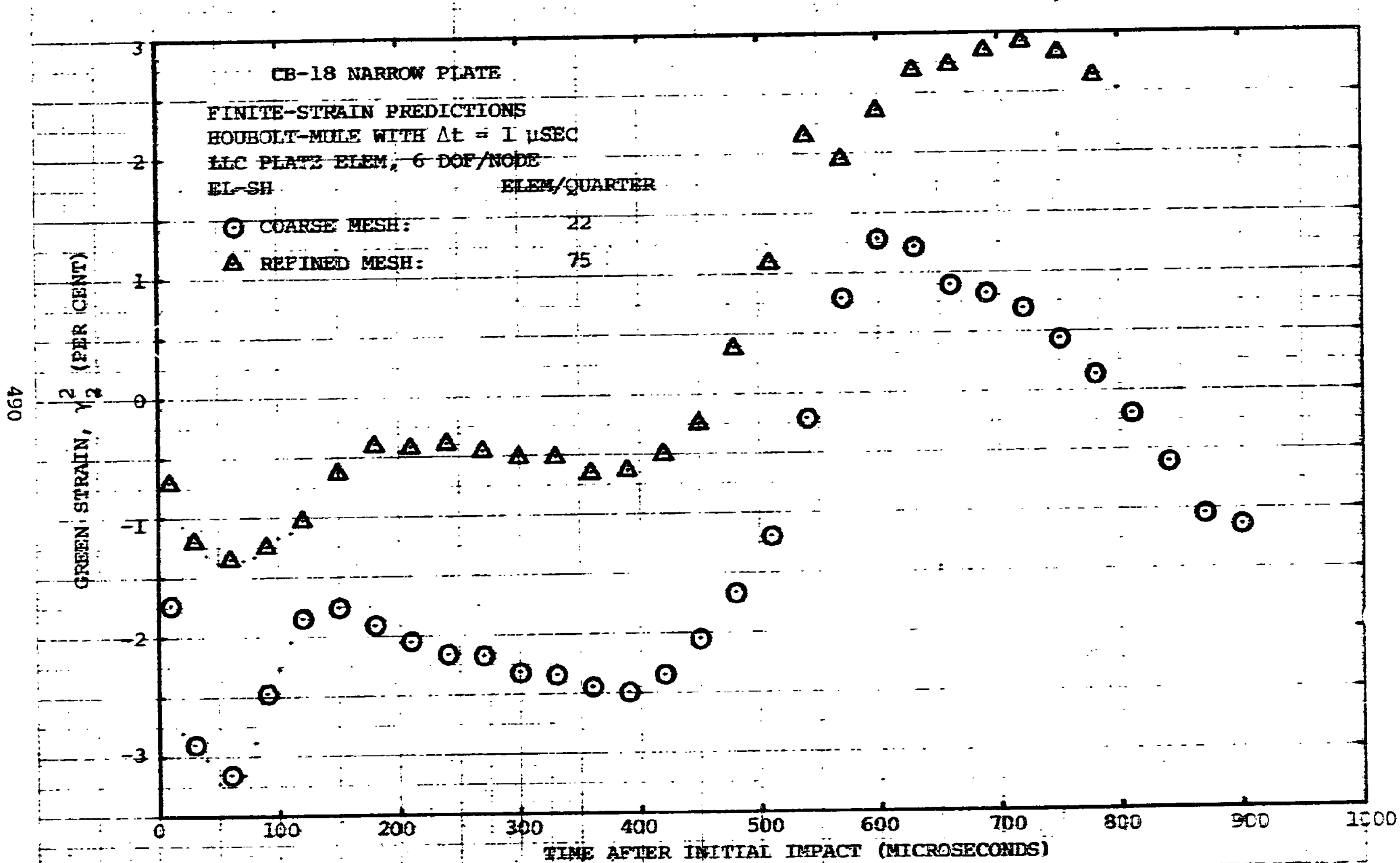

(c) Station (x,y) = (0, 0.30 in), Upper (Non-Impacted) Surface

FIG. 44 CONTINUED (COARSE MESH, REFINED MESH, FINITE STRAIN, CB-18)

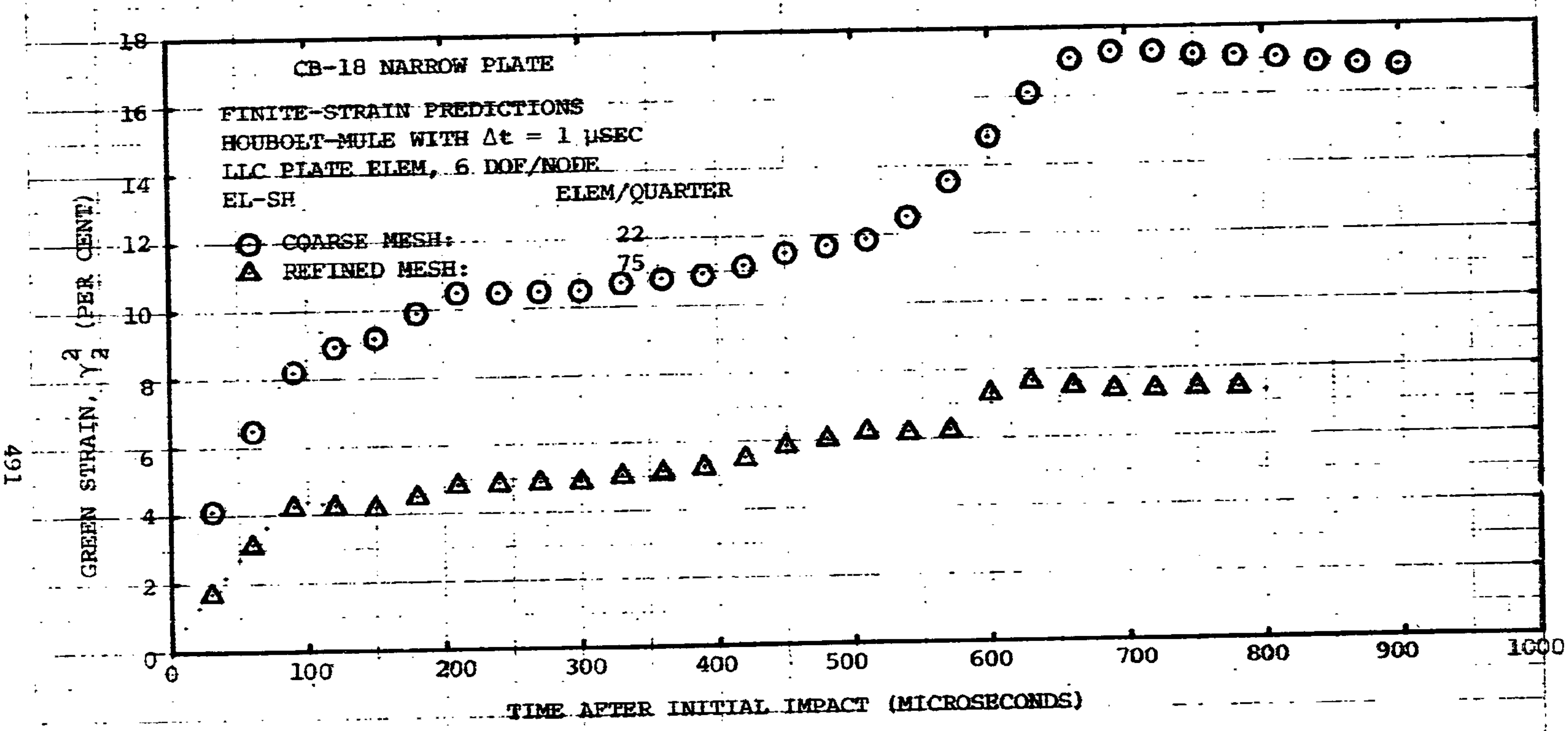

(d) Station (x,y) = (0, 0.30 in), Lower (Impacted) Surface

FIG. 44 CONTINUED (COARSE MESH, REFINED MESH, FINITE STRAIN, CB-18)

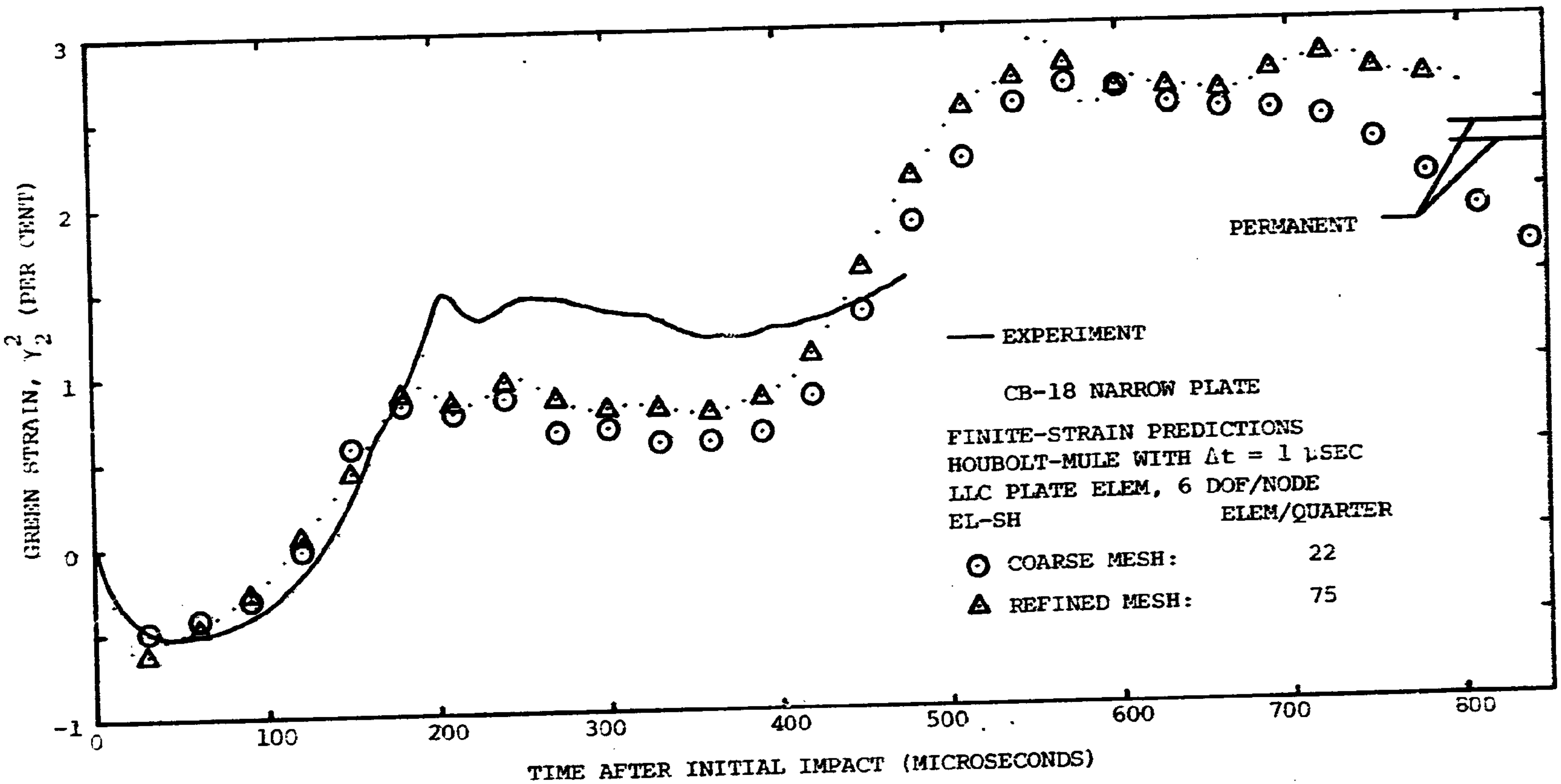

(e) Station (x,y) = (0, 0.60 in), Upper (Non-Impacted) Surface

FIG. 44 CONTINUED (COARSE MESH, REFINED MESH, FINITE STRAIN, CB-18)

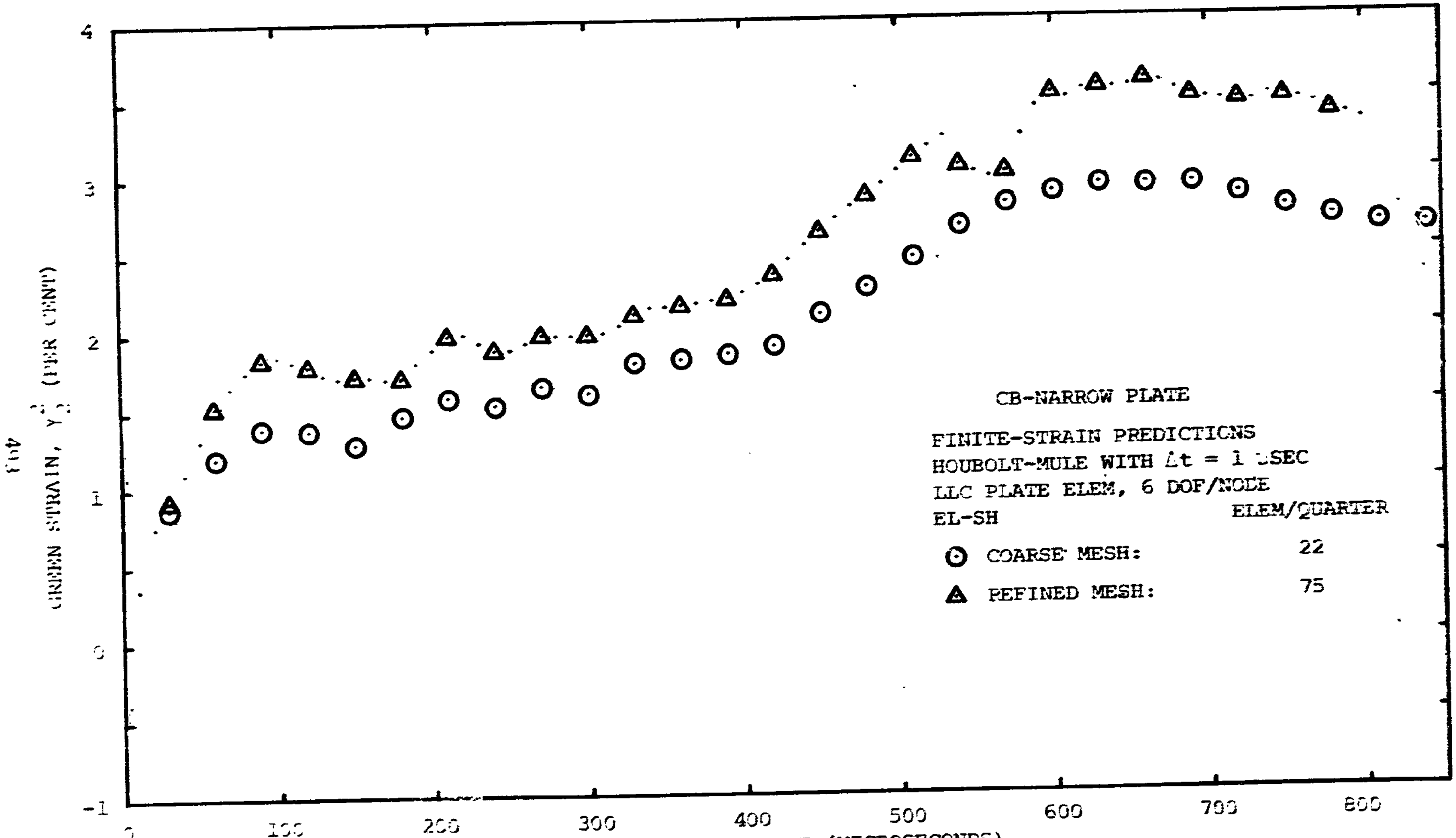

(f) Station (x,y) = (0, 0.60 in), Lower (Impacted) Surface

FIG. 44 CONTINUED (COARSE MESH, REFINED MESH, FINITE STRAIN, CB-18)

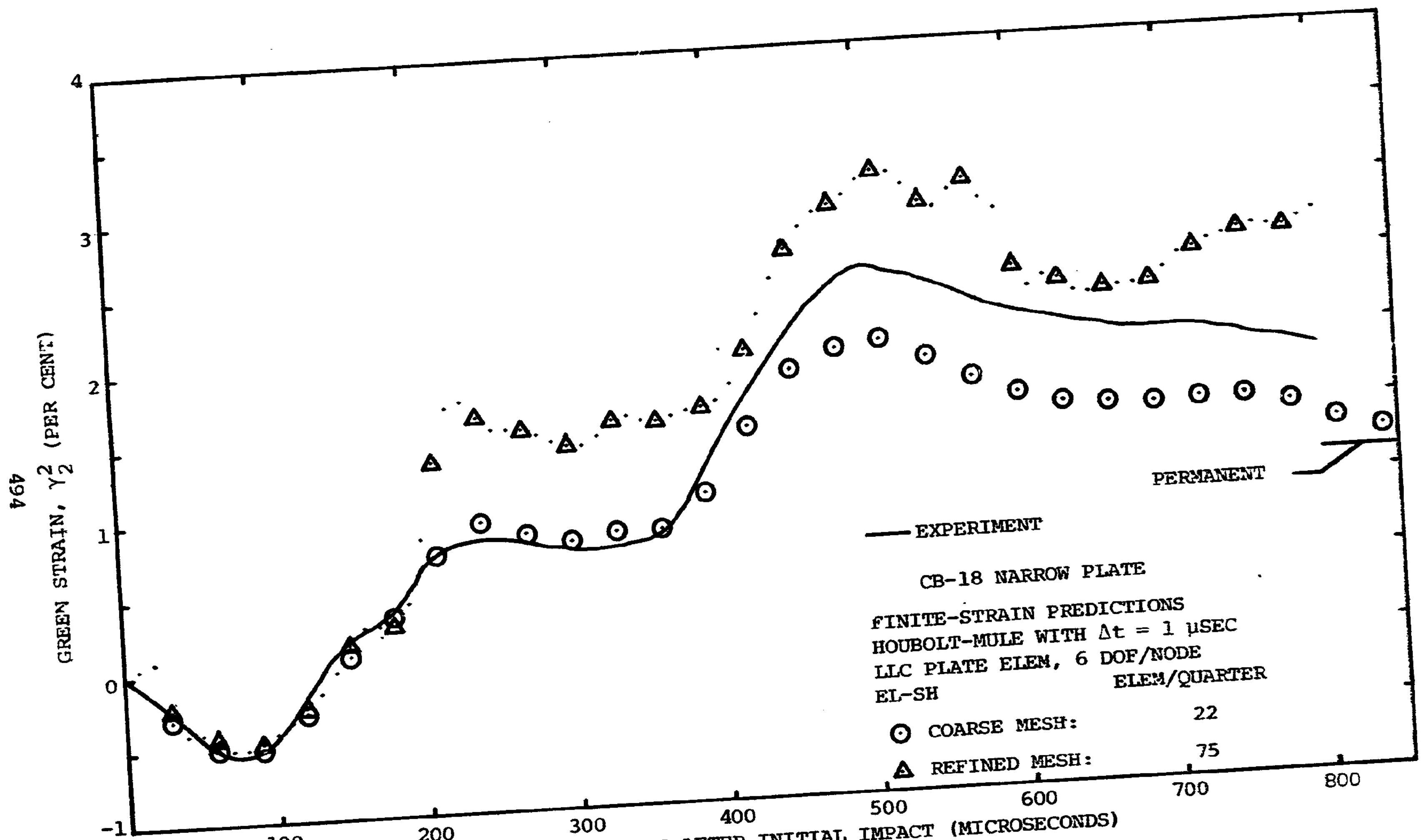

(g) Station (x,y) = (0, 1.20 in), Upper (Non-Impacted) Surface

FIG. 44 CONTINUED (COARSE MESH, REFINED MESH, FINITE STRAIN, CB-18)

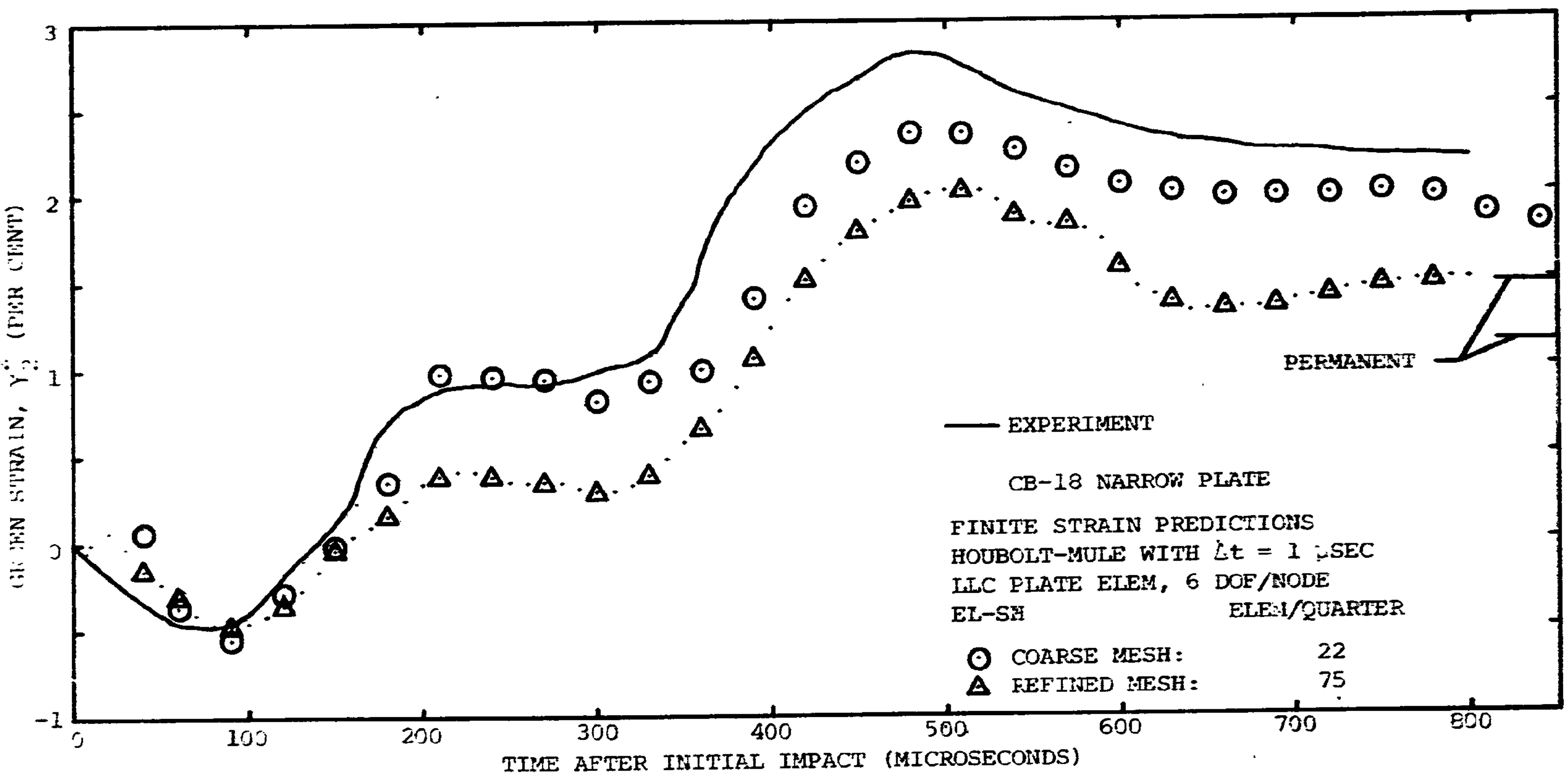

(h) Station (x,y) = (0, 1.50 in), Upper (Non-Impacted) Surface

FIG. 44 CONTINUED (COARSE MESH, REFINED MESH, FINITE STRAIN, CB-18)

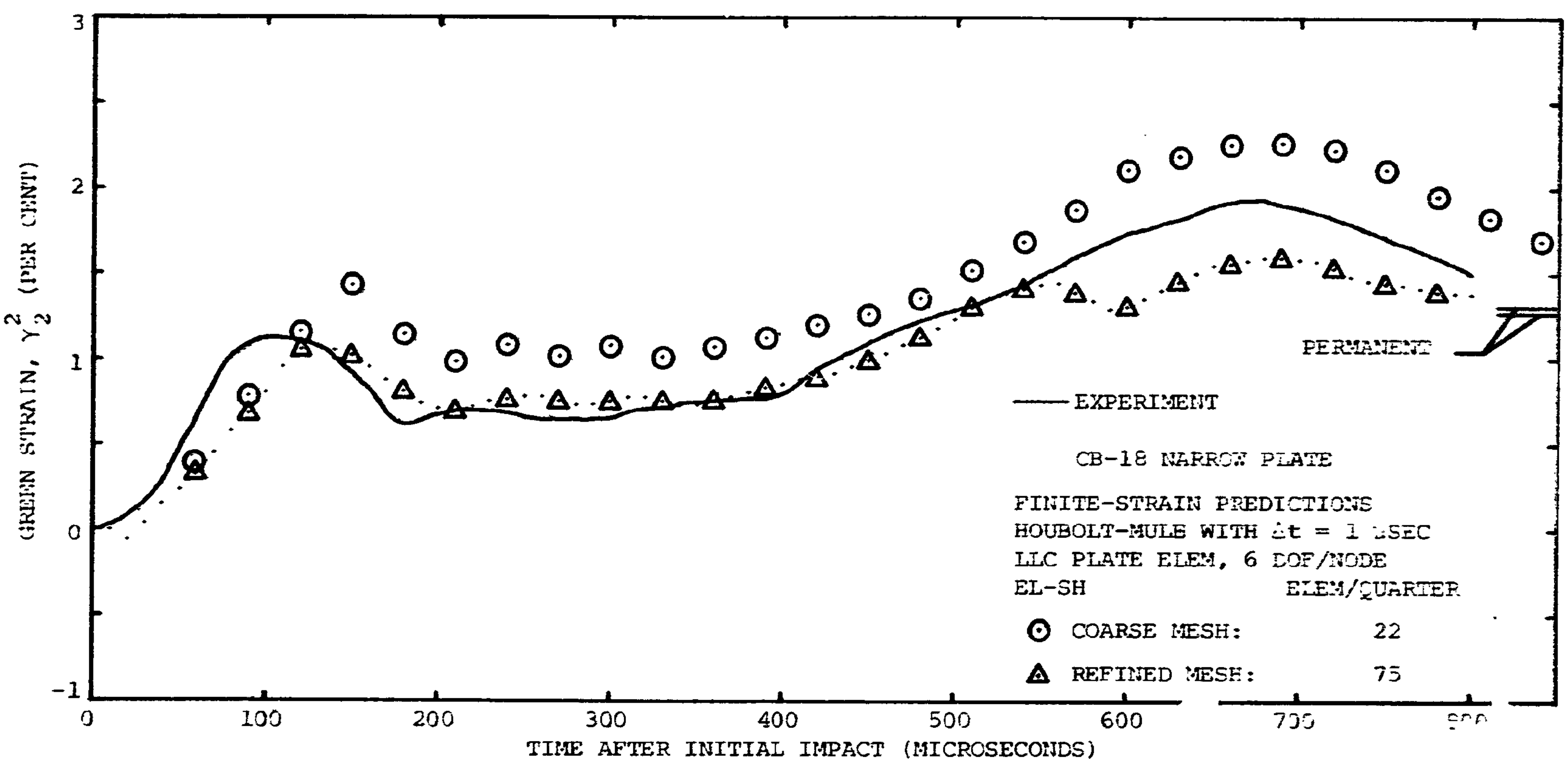

(i) Station (x,y) = (0, 1.50 in), Lower (Impacted) Surface

FIG. 44 CONTINUED (COARSE MESH, REFINED MESH, FINITE STRAIN, CB-18)

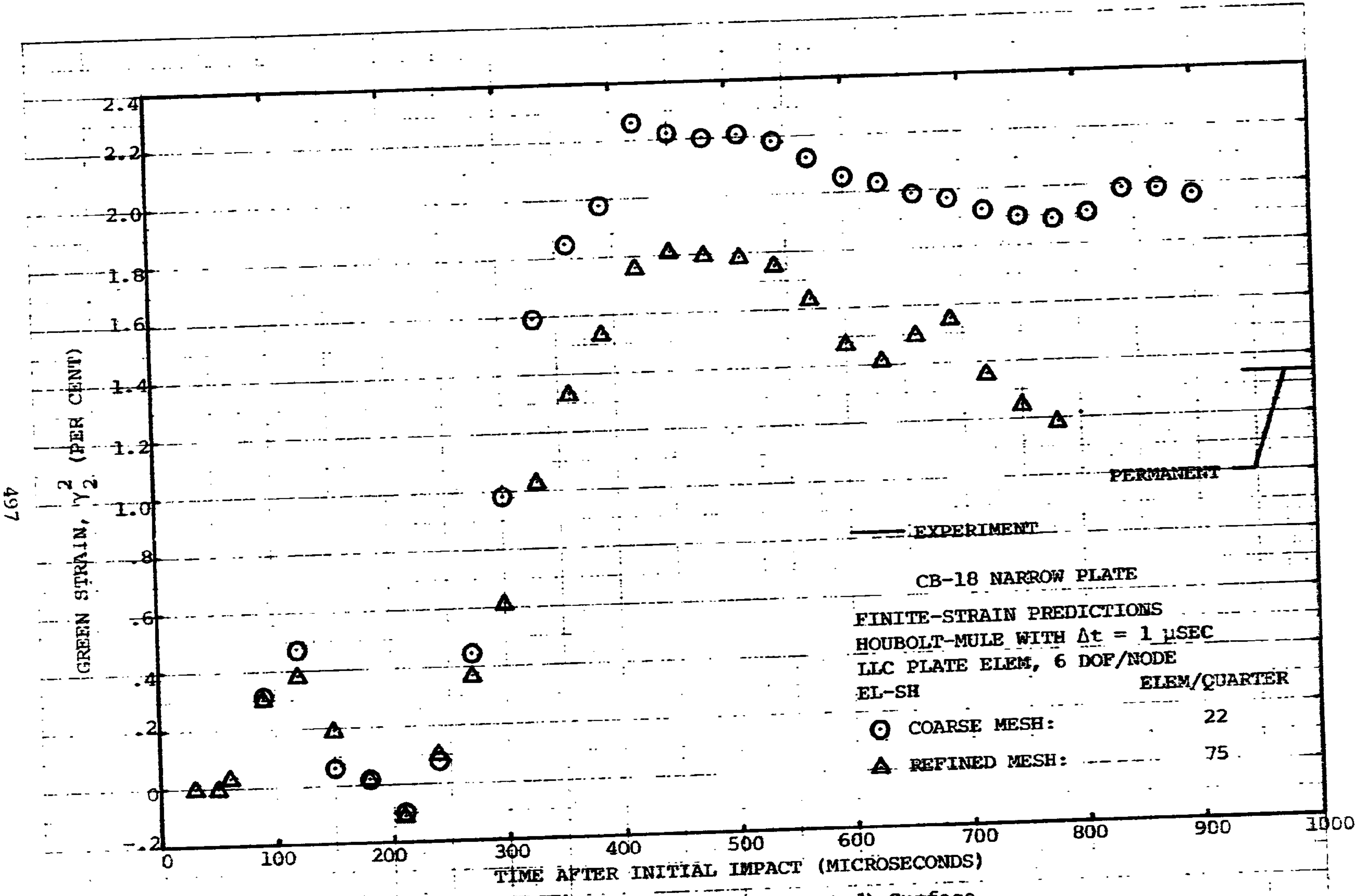

(j) Station (x,y) = (0, 3.00 in), Upper (Non-Impacted) Surface

FIG. 44 CONTINUED (COARSE MESH, REFINED MESH, FINITE STRAIN, CB-18)

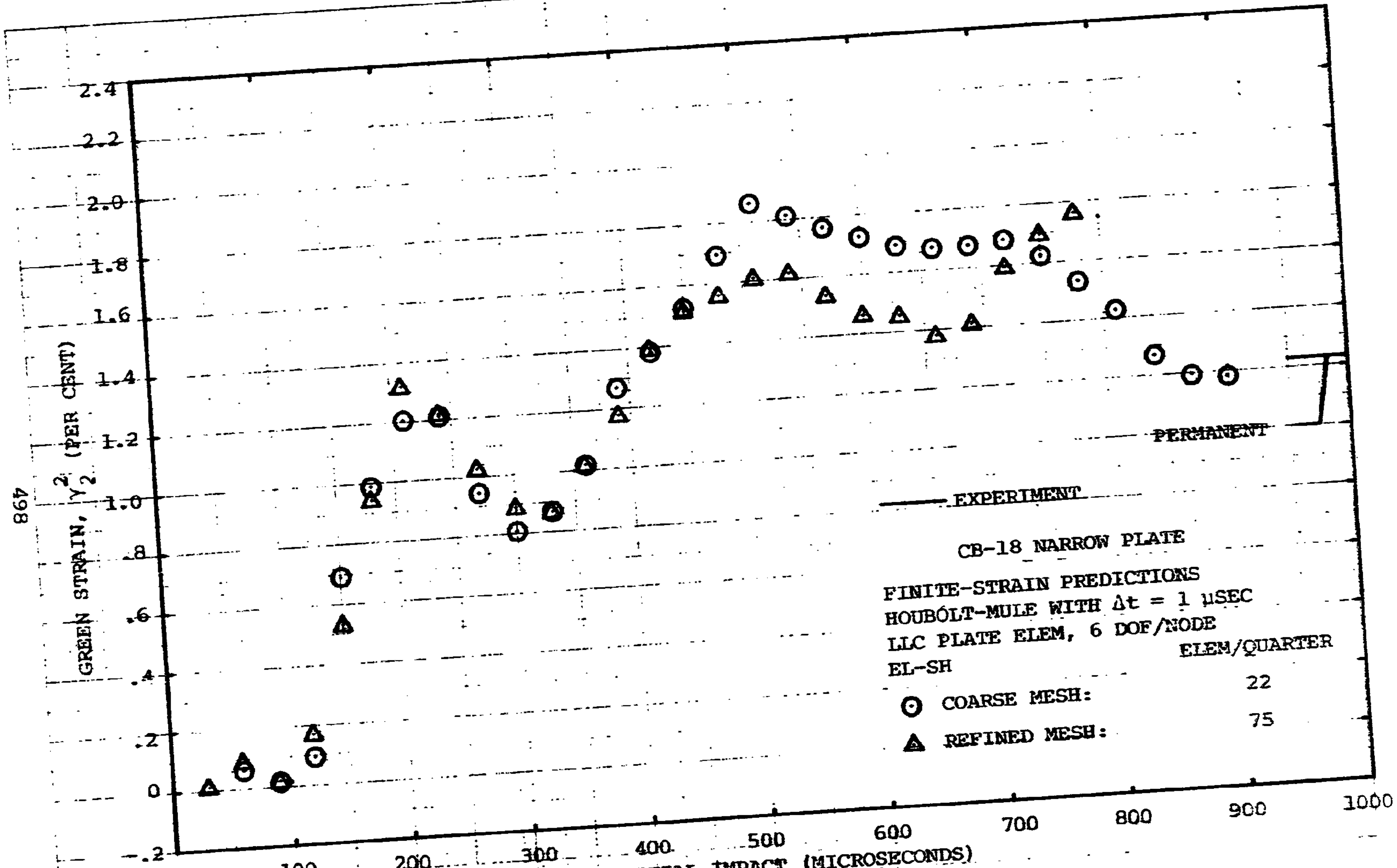

(k) Station (x,y) = (0, 3.00 in), Lower (Impacted) Surface

FIG. 44 CONTINUED (COARSE MESH, REFINED MESH, FINITE STRAIN, CB-18)

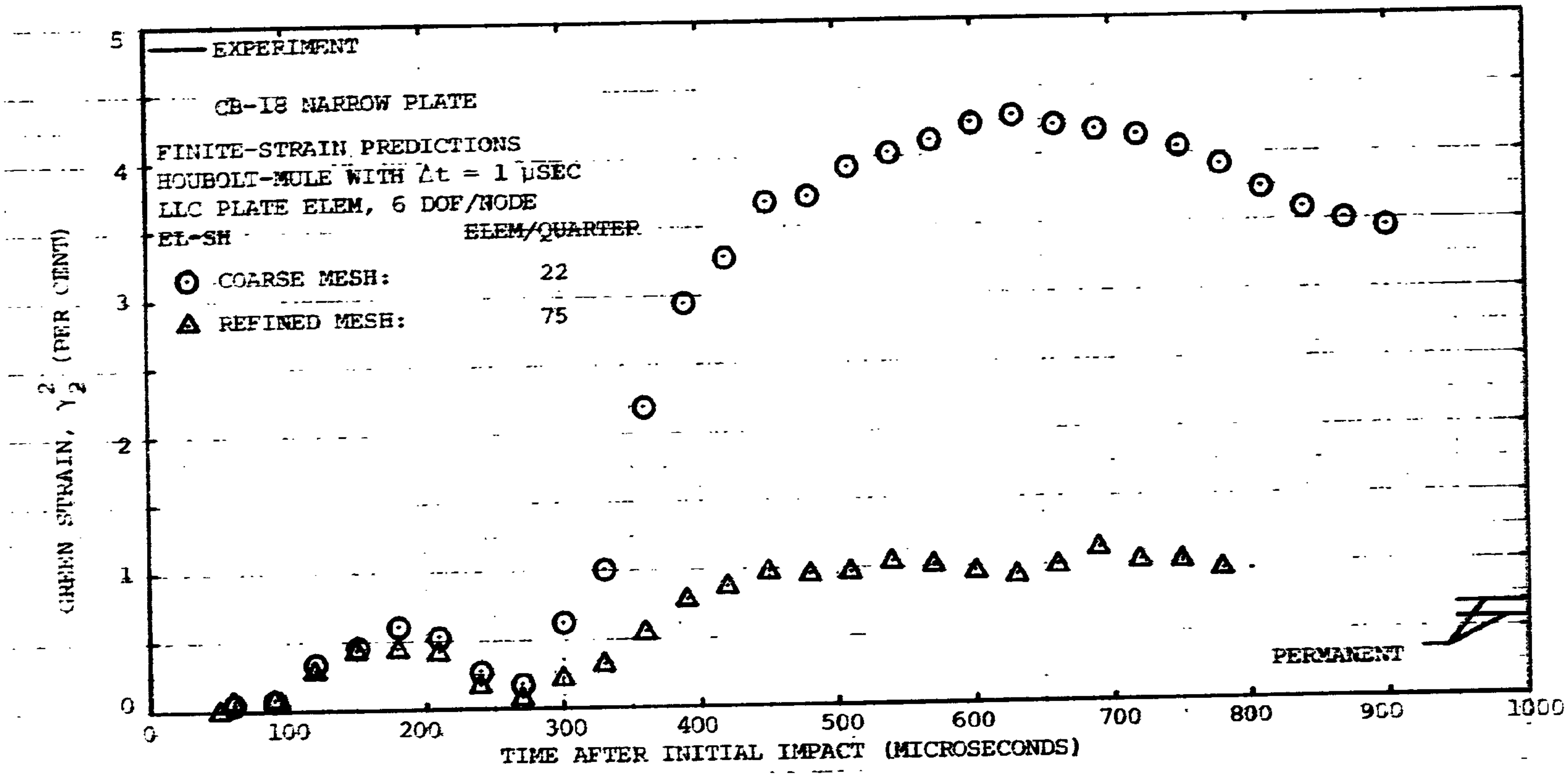

(ℓ) Station (x,y) = (0, 3.70 in) Upper (Non-Impacted) Surface

FIG. 44 ~~CONTINUED (COARSE MESH, REFINED MESH~~, FINITE STRAIN, CB-18)

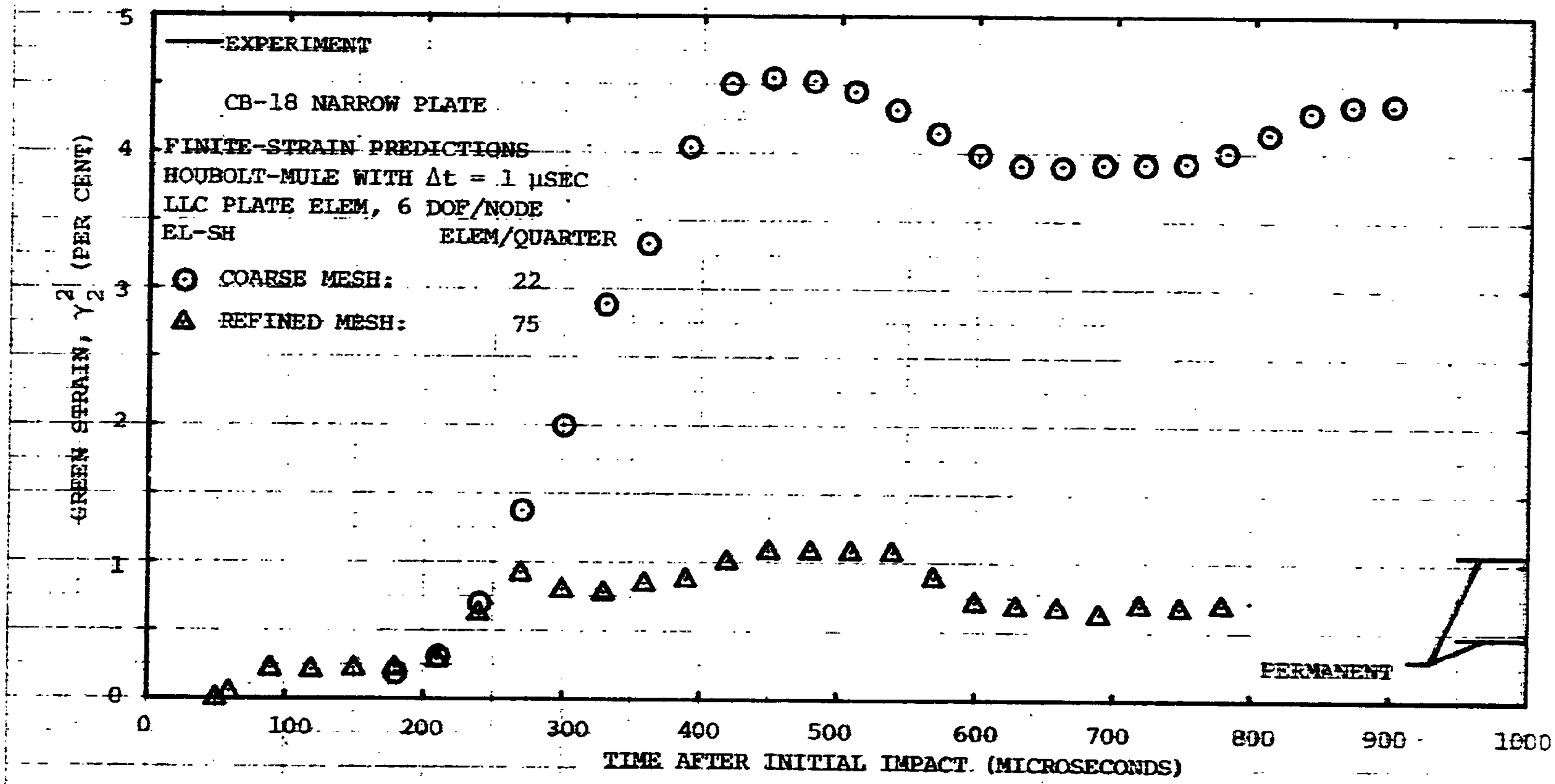

(m) Station (x,y) = (0, 3.70 in), Lower (Impacted) Surface

FIG. 44 CONTINUED (COARSE MESH, REFINED MESH, FINITE STRAIN, CB-18)

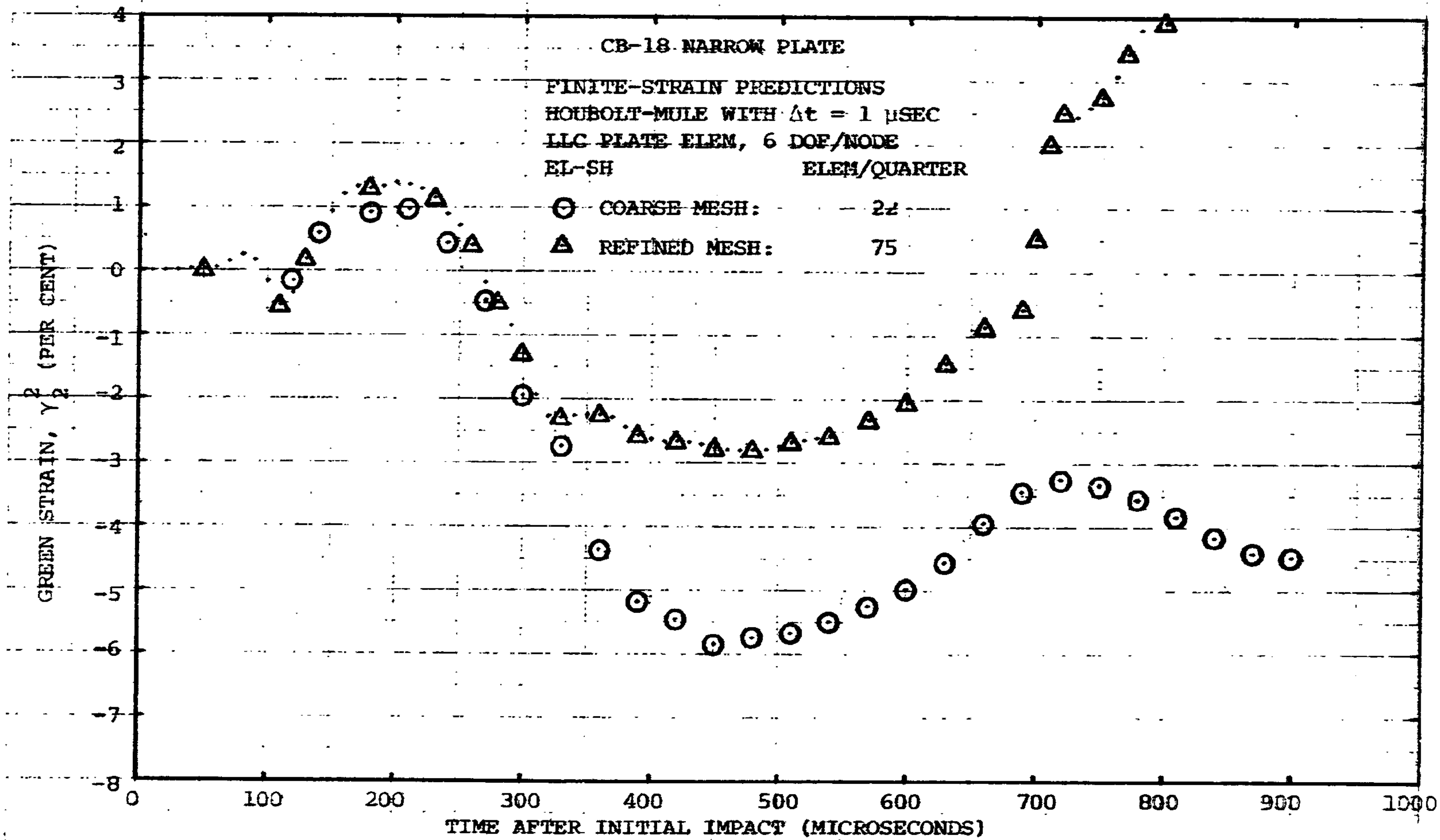

(n) Clamped-End Station (x,y) = (0, 4.00 in), Upper (Non-Impacted) Surface

FIG. 44 CONTINUED (COARSE MESH, REFINED MESH, FINITE STRAIN, CB-18)

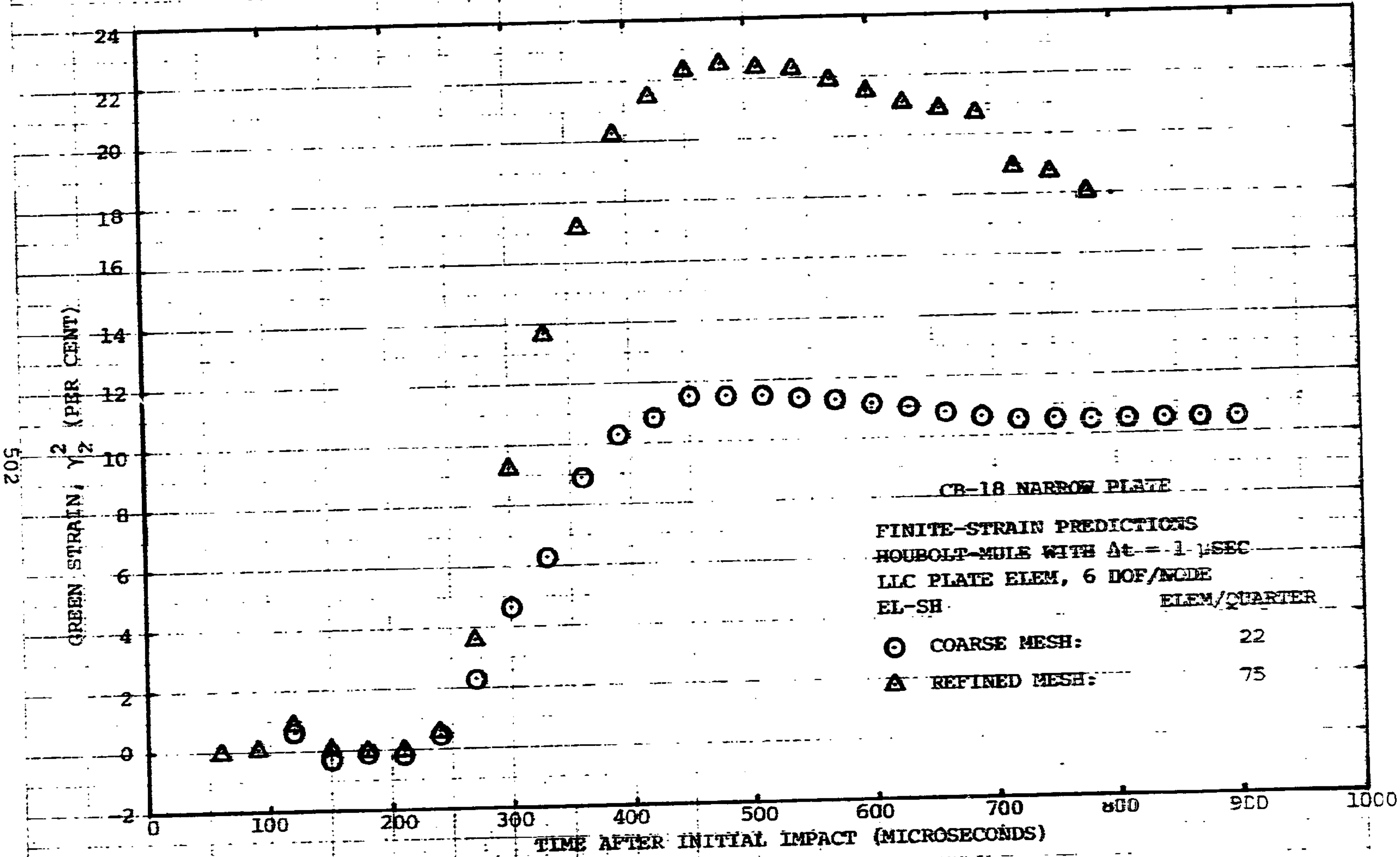

(c) Clamped-End Station (x,y) = (0, 4.00 in), Lower (Impacted) Surface

FIG. 44 CONCLUDED (COARSE MESH, REFINED MESH, FINITE STRAIN, CB-18)

APPENDIX A

DEFINITION OF THE FINITE ELEMENTS USED IN THE TEXT

A.1 Variable-Thickness Arbitrarily-Curved Beam Finite Elements

Consider an initially-undeformed, arbitrarily-curved, variable-thickness, single-layer beam or ring subjected to prescribed transient externally-applied surface loads and to only D'Alembert body forces (inertia loads). Let it be assumed that the ring consists of ductile metal and that a large-deflection, elastic-plastic transient response will be produced. For analysis the structure will be represented by a compatibly-joined assemblage of N finite elements, one of which is depicted in Fig. A.1 where its geometry and nomenclature are shown and where the deformation plane is η, ζ^o; the coordinate η along and ζ^o normal to the centroidal reference axis of the beam are employed as the reference coordinates for this curved beam element.

It is useful and convenient to use the following geometry to describe this typical curved beam element and to approximate the actual given complete beam or ring by a finite number of these "typical elements". Note first that a global Y,Z Cartesian reference axis system as well as a local y,z Cartesian reference axis system are defined; for the latter, the +y axis passes through the ends (that is, nodes i and i+1) of the element and makes an angle $+\alpha$ (for this ith element) with the +Y axis. The slope, ϕ, of the reference circumferential axis η, which is the angle between the tangent vector $\bar{a}$ to η and the y-axis of the local-reference Cartesian frame may be approximated by a second degree polynomial in η, as follows [17]:

$$\phi(\eta) = b_o + b_1 \eta + b_2 \eta^2 \tag{A.1}$$

where the constants b_o, b_1, and b_2 can be determined from the geometry of the curved beam element as described next. Assume that the change in element slope ϕ between nodes i and i+1 is small such that

$$\cos(\phi_{i+1} - \phi_i) \doteq 1 \tag{A.2a}$$

and

$$\sin(\phi_{i+1} - \phi_i) \doteq \phi_{i+1} - \phi_i \tag{A.2b}$$

This restricts the slope change within an element to $\lesssim 15$ degrees. The arc length, η_i, of element i is approximated to be the same as the length of a circular arc passing through the nodal points at the slopes ϕ_i and ϕ_{i+1}, hence, η_i is given by

$$\eta_i = \frac{L_i(\phi_{i+1} - \phi_i)}{2\sin\left(\frac{\phi_{i+1} - \phi_i}{2}\right)} \tag{A.3a}$$

where L_i is the length of the chord joining nodes i and i+1, and is given by

$$L_i = \left[(Z_{i+1} - Z_i)^2 + (Y_{i+1} - Y_i)^2\right]^{\frac{1}{2}} \tag{A.3b}$$

The three constants in Eq. A.1 are then determined from the relations

$$\begin{aligned} \phi(o) &= \phi_i \\ \phi(\eta_i) &= \phi_{i+1} \\ \int_0^{\eta_i} \sin\phi(\eta)\, d\eta &\doteq \int_0^{\eta_i} \phi(\eta)\, d\eta = 0 \end{aligned} \tag{A.4}$$

From Eq. A.4, the constants in Eq. A.1 are found to be

$$\begin{aligned} b_o &= \phi_i \\ b_1 &= -2(\phi_{i+1} - \phi_i)/\eta_i \\ b_2 &= 3(\phi_{i+1} + \phi_i)/(\eta_i)^2 \end{aligned} \tag{A.5}$$

Accordingly, the radius of curvature, R, of the centroidal axis may be expressed as $R = -(\partial\phi/\partial\eta)^{-1} = -(b_1+2b_2\eta)^{-1}$, and the coordinates $Y(\eta)$ and $Z(\eta)$ of the centroidal axis are given by

$$Y(\eta) = Y_i + \int_0^{\eta} \cos[\phi(\eta) + \alpha]\, d\eta \tag{A.6a}$$

and

$$Z(\eta) = Z_i + \int_0^{\eta} \sin[\phi(\eta) + \alpha]\, d\eta \tag{A.6b}$$

whoro

$$\alpha = \tan^{-1}\left(\frac{Z_{i+1} - Z_i}{Y_{i+1} - Y_i}\right) \tag{A.6c}$$

The thickness variation $h(\eta)$ along the element is approximated as being linear in η between nodes i and i+1 listed, respectively, at $\eta=0$ and $\eta=\eta_i$:

$$h(\eta) = h_i\left(1 - \frac{\eta}{\eta_i}\right) + h_{i+1}\,\frac{\eta}{\eta_i} \tag{A.7}$$

This completes the needed description of the geometry of the curved beam element.

The displacement field $\tilde{v}$, $\tilde{w}$ of the beam, was derived in Subsection 4.2, and was shown to be valid for arbitrarily large strains and rotations. The displacements $\tilde{v}$ and $\tilde{w}$ anywhere in the beam are specified by the displacements $v(\eta)$ and $w(\eta)$ at the centroidal axis ($\zeta^\circ=0$) of the beam, and the associated displacement gradients χ and ψ, respectively, as:+

$$\begin{aligned}\tilde{v}(\eta,\zeta) &= v(\eta) - \frac{\zeta^\circ}{\left[1 + 2\,\overset{\circ}{\gamma}{}_z^2(\eta)\right]}\,\psi(\eta)\\ \tilde{w}(\eta,\zeta) &= w(\eta) + \zeta^\circ\,\frac{\left[1 + \chi(\eta)\right]}{\left[1 + 2\,\overset{\circ}{\gamma}{}_z^2(\eta)\right]} - \zeta^\circ\end{aligned} \tag{A.8}$$

where

$$\begin{aligned}\psi(\eta) &= \frac{\partial w}{\partial \eta}(\eta) - \frac{v}{R}(\eta)\\ \chi(\eta) &= \frac{\partial v}{\partial \eta}(\eta) + \frac{w}{R}(\eta)\end{aligned} \tag{A.8a}$$

+Recall that ζ° denotes the ζ-direction location of a particle in the initial undeformed state.

A cubic-cubic polynomial interpolation function with the inclusion of rigid-body modes represented explicitly in terms of the angle ϕ, is chosen for the assumed displacement field v, w as follows:

$$\begin{Bmatrix} v \\ w \end{Bmatrix} = \begin{bmatrix} \cos\phi & \sin\phi & -(Z-Z_i)\cos(\phi+\alpha)+(Y-Y_i)\sin(\phi+\alpha) & \eta & 0 & 0 & \eta^2 & \eta^3 \\ -\sin\phi & \cos\phi & (Z-Z_i)\sin(\phi+\alpha)+(Y-Y_i)\cos(\phi+\alpha) & 0 & \eta^2 & \eta^3 & 0 & 0 \end{bmatrix} \begin{Bmatrix} \beta_1 \\ \beta_2 \\ \vdots \\ \beta_8 \end{Bmatrix} \tag{A.9a}$$

or in more compact matrix form, Eq. A.9 becomes

$$\{\underset{\sim}{u}\} \equiv \begin{Bmatrix} v \\ w \end{Bmatrix} = \begin{bmatrix} G_v(\eta) \\ \hdashline G_w(\eta) \end{bmatrix} \{\beta\} \equiv \begin{bmatrix} U(\eta) \end{bmatrix} \{\beta\} \tag{A.9b}$$

The generalized displacements {q} are selected so that there are four degrees of freedom v, w, ψ, χ at each node of the element:

$$\{q\} = \lfloor v_i \;\; w_i \;\; \psi_i \;\; \chi_i \;\; v_{i+1} \;\; w_{i+1} \;\; \psi_{i+1} \;\; \chi_{i+1} \rfloor^T = [A]\{\beta\} \tag{A.10}$$

where

$$[A] = \begin{bmatrix} \cos\phi_i & \sin\phi_i & 0 & 0 & 0 & 0 & 0 & 0 \\ -\sin\phi_i & \cos\phi_i & 0 & 0 & 0 & 0 & 0 & 0 \\ 0 & 0 & 1 & 0 & 0 & 0 & 0 & 0 \\ 0 & 0 & 0 & 1 & 0 & 0 & 0 & 0 \\ \cos\phi_{i+1} & \sin\phi_{i+1} & A_{53} & \eta_i & 0 & 0 & \eta_i^2 & \eta_i^3 \\ -\sin\phi_{i+1} & \cos\phi_{i+1} & A_{63} & 0 & \eta_i^2 & \eta_i^3 & 0 & 0 \\ 0 & 0 & 1 & \eta_i(\phi')_{\eta_i} & 2\eta_i & 3\eta_i^2 & \eta_i^2(\phi')_{\eta_i} & \eta_i^3(\phi')_{\eta_i} \\ 0 & 0 & 0 & 1 & -\eta_i^2(\phi')_{\eta_i} & -\eta_i^3(\phi')_{\eta_i} & 2\eta_i & 3\eta_i^2 \end{bmatrix} \tag{A.10a}$$

and

$$A_{53} = \left(Y_{i+1} - Y_i\right) \sin\left(\phi_{i+1} + \alpha\right) - \left(Z_{i+1} - Z_i\right) \cos\left(\phi_{i+1} + \alpha\right)$$
$$A_{63} = \left(Y_{i+1} - Y_i\right) \cos\left(\phi_{i+1} + \alpha\right) + \left(Z_{i+1} - Z_i\right) \sin\left(\phi_{i+1} + \alpha\right) \tag{A.10b}$$

Corresponding to the assumed displacement field Eq. A.9 (and recalling that $\frac{1}{R} = -\frac{\partial\phi}{\partial\eta}$), one finds the following expressions for the displacement gradients χ and ψ:

$$\chi = \lfloor G_\chi \rfloor \{\beta\}$$
$$\psi = \lfloor G_\psi \rfloor \{\beta\} \tag{A.11a}$$

where

$$\lfloor G_\chi \rfloor = \lfloor 0 \quad 0 \quad 0 \quad 1 \quad \left(-\eta^2 \frac{\partial\phi}{\partial\eta}\right) \quad \left(-\eta^3 \frac{\partial\phi}{\partial\eta}\right) \quad 2\eta \quad 3\eta^2 \rfloor$$
$$\lfloor G_\psi \rfloor = \lfloor 0 \quad 0 \quad 1 \quad \left(\eta \frac{\partial\phi}{\partial\eta}\right) \quad 2\eta \quad 3\eta^2 \quad \left(\eta^2 \frac{\partial\phi}{\partial\eta}\right) \quad \left(\eta^3 \frac{\partial\phi}{\partial\eta}\right) \rfloor \tag{A.11b}$$

The following strain-displacement relations (type F) were derived in Subsection 4.2, and are valid for arbitrarily large strains and rotations:

$$\gamma_2^2 = \overset{\circ}{\gamma}{}_2^2 + \frac{\zeta^\circ}{\left(1 + 2\overset{\circ}{\gamma}{}_2^2\right)} K \tag{A.12}$$

$$\gamma_3^3 = \frac{1}{2}\left[\frac{1}{\left(1 + 2\overset{\circ}{\gamma}{}_2^2\right)} - 1\right] \tag{A.13}$$

$$\gamma_1^1 = \gamma_2^1 = \gamma_1^2 = \gamma_3^1 = \gamma_1^3 = \gamma_3^2 = \gamma_2^3 = 0 \tag{A.14}$$

where superscript "o" refers to quantities evaluated at $\zeta^\circ=0$. The membrane strain $\overset{\circ}{\gamma}{}_2^2$ is defined in terms of the displacement gradients χ and ψ as follows:

$$\overset{\circ}{\gamma}{}_2^2 = \chi + \frac{1}{2}\chi^2 + \frac{1}{2}\psi^2 \tag{A.15}$$

where

$$\begin{aligned}\psi &= \lfloor G_\psi \rfloor \{\beta\} = \lfloor G_\psi \rfloor [A]^{-1}\{q\} = \lfloor D_2 \rfloor \{q\} \\ \chi &= \lfloor G_\chi \rfloor \{\beta\} = \lfloor G_\chi \rfloor [A]^{-1}\{q\} = \lfloor D_1 \rfloor \{q\}\end{aligned} \tag{A.16}$$

Employing Eqs. A.11 and A.10, the membrane strain $\overset{\circ}{\gamma}{}_2^2$ becomes:

$$\begin{aligned}\overset{\circ}{\gamma}{}_2^2 = \lfloor D_1 \rfloor \{q\} &+ \frac{1}{2}\lfloor q \rfloor \{D_2\} \lfloor D_2 \rfloor \{q\} \\ &+ \frac{1}{2}\lfloor q \rfloor \{D_1\} \lfloor D_1 \rfloor \{q\}\end{aligned} \tag{A.17}$$

The "curvature" κ appearing in Eq. A.12, is defined in terms of the displacement gradients χ and ψ as:

$$\kappa = \left(-\frac{\partial \psi}{\partial \eta}\right)(1+\chi) + \psi \frac{\partial \chi}{\partial \eta} \tag{A.18}$$

The derivatives $\frac{\partial\psi}{\partial\eta}$ and $\frac{\partial\chi}{\partial\eta}$ of the displacement gradients χ and ψ can be expressed as:

$$-\frac{\partial \psi}{\partial \eta} = -\frac{\partial^2 w}{\partial \eta^2} + \frac{1}{R}\frac{\partial v}{\partial \eta} + v\frac{\partial}{\partial \eta}\left(\frac{1}{R}\right) = -\frac{\partial^2 w}{\partial \eta^2} - \frac{\partial v}{\partial \eta}\frac{\partial \phi}{\partial \eta} - v\frac{\partial^2 \phi}{\partial \eta^2} \tag{A.19}$$

or

$$-\frac{\partial \psi}{\partial \eta} \equiv \lfloor G_{-\psi,\eta} \rfloor \{\beta\} = \lfloor G_{-\psi,\eta} \rfloor [A]^{-1}\{q\} = \lfloor D_3 \rfloor \{q\} \tag{A.20}$$

where

$$\begin{aligned}\lfloor G_{-\psi,\eta} \rfloor = \Big\lfloor\, 0 \quad 0 \quad 0 \quad \left(-\frac{\partial\phi}{\partial\eta} - \eta\frac{\partial^2\phi}{\partial\eta^2}\right) \quad -2 \quad -6\eta \\ \left(-2\frac{\partial\phi}{\partial\eta} - \eta\frac{\partial^2\phi}{\partial\eta^2}\right)\eta \quad \left(-3\frac{\partial\phi}{\partial\eta} - \eta\frac{\partial^2\phi}{\partial\eta^2}\right)\eta^2 \,\Big\rfloor\end{aligned} \tag{A.21}$$

$$\frac{\partial \chi}{\partial \eta} = \frac{\partial^2 v}{\partial \eta^2} + \frac{1}{R}\frac{\partial w}{\partial \eta} + w\frac{\partial}{\partial \eta}\left(\frac{1}{R}\right) = \frac{\partial^2 v}{\partial \eta^2} - \frac{\partial w}{\partial \eta}\frac{\partial \phi}{\partial \eta} - w\frac{\partial^2 \phi}{\partial \eta^2} \tag{A.22}$$

or

$$\frac{\partial \chi}{\partial \eta} \equiv \lfloor G_{\chi,\eta} \rfloor \{\beta\} = \lfloor G_{\chi,\eta} \rfloor [A]^{-1} \{q\} = \lfloor D_4 \rfloor \{q\} \tag{A.23}$$

where

$$\lfloor G_{\chi,\eta} \rfloor = \Big\lfloor\; 0 \quad 0 \quad 0 \quad 0 \quad \left(-2\frac{\partial \phi}{\partial \eta} - \eta\frac{\partial^2 \phi}{\partial \eta^2}\right)\eta \quad \left(-3\frac{\partial \phi}{\partial \eta} - \eta\frac{\partial^2 \phi}{\partial \eta^2}\right)\eta^2 \quad 2 \quad 6\eta \;\Big\rfloor \tag{A.24}$$

Therefore, the "curvature" κ can be expressed as

$$\kappa = \left(1 + \lfloor q \rfloor \{D_1\}\right) \lfloor D_3 \rfloor \{q\} + \lfloor q \rfloor \{D_2\} \lfloor D_4 \rfloor \{q\} \tag{A.25}$$

A.2 Plate Finite Elements

The geometry and nomenclature of a typical rectangular plate element are shown in Fig. A2. The element has constant thickness, h, and spanwise dimensions a and b in the x and y directions, respectively, with the origin of the element xyz coordinate system located at element node number 1. The midsurface displacements u, v, and w are approximated within each element by assuming a bilinear interpolation for the inplane displacements u and v, and a bicubic Hermetian interpolation for the transverse displacement, w. The interpolations written in terms of element x,y,z coordinates are

$$u(x,y) = \beta_1 + x\beta_2 + y\beta_3 + xy\beta_4 \equiv \lfloor G_u \rfloor \{\beta\} \tag{A.26}$$

$$v(x,y) = \beta_5 + x\beta_6 + y\beta_7 + xy\beta_8 \equiv \lfloor G_v \rfloor \{\beta\} \tag{A.27}$$

$$\begin{aligned} w(x,y) = {} & \beta_9 + x\beta_{10} + y\beta_{11} + xy\beta_{12} + x^2\beta_{13} + y^2\beta_{14} \\ & + x^2y\beta_{15} + xy^2\beta_{16} + x^2y^2\beta_{17} + x^3\beta_{18} + y^3\beta_{19} \\ & + x^3y\beta_{20} + xy^3\beta_{21} + x^3y^2\beta_{22} + x^2y^3\beta_{23} + x^3y^3\beta_{24} \\ \equiv {} & \lfloor G_w \rfloor \{\beta\} \end{aligned} \tag{A.28}$$

where β_1, β_2 ... β_{24} are unknowr parameters which will be related to the generalized nodal displacements q_1, q_2, ... q_{24}.

In order to obtain a set of generalized nodal displacements $\{q\}$ which can be related to the 24 β_i's, the generalized nodal displacements chosen are the parameters u, v, w, $w_{,x} \equiv \frac{\partial w}{\partial x}$, $w_{,y} \equiv \frac{\partial w}{\partial y}$, and $w_{,xy} \equiv \frac{\partial^2 w}{\partial x \partial y}$ at each of the four corner nodes of the element. The nodal displacement vector, $\{q\}$, for the element is thus

$$\begin{aligned} \{q\}^T = \lfloor q \rfloor = \lfloor\, & u_1\ v_1\ w_1\ \left(\frac{\partial w}{\partial x}\right)_1 \left(\frac{\partial w}{\partial y}\right)_1 \left(\frac{\partial^2 w}{\partial x \partial y}\right)_1 \\ & u_2\ v_2\ w_2\ \left(\frac{\partial w}{\partial x}\right)_2 \left(\frac{\partial w}{\partial y}\right)_2 \left(\frac{\partial^2 w}{\partial x \partial y}\right)_2\ u_3\ v_3\ w_3 \left(\frac{\partial w}{\partial x}\right)_3 \left(\frac{\partial w}{\partial y}\right)_3 \left(\frac{\partial^2 w}{\partial x \partial y}\right)_3 \\ & u_4\ v_4\ w_4\ \left(\frac{\partial w}{\partial x}\right)_4 \left(\frac{\partial w}{\partial y}\right)_4 \left(\frac{\partial^2 w}{\partial x \partial y}\right)_4 \,\rfloor \end{aligned} \tag{A.29}$$

By evaluating Eqs. A.26, A.27, and A.28, and

$$\frac{\partial w}{\partial x} = \lfloor G_{w,x} \rfloor \{\beta\} \tag{A.30}$$

$$\frac{\partial w}{\partial y} = \lfloor G_{w,y} \rfloor \{\beta\} \tag{A.31}$$

$$\frac{\partial^2 w}{\partial x \partial y} = \lfloor G_{w,xy} \rfloor \{\beta\} \tag{A.32}$$

(obtained by differentiating Eqs. A.28) at the nodes, a unique (invertible) relation between {q} and {β} is obtained:

$$\{q\} = [B]\{\beta\} \tag{A.33}$$

The 24 β_i's can be related to the 2‹ q_i's by inversion of Eq. A.33 so that

$$\{\beta\} = [B]^{-1}\{q\} \tag{A.34}$$

and the displacement interpolation (Eq. A.28) can be written in terms of nodal generalized displacements, {q}.

Therefore, one can write:

$$u = \lfloor G_u \rfloor \{\beta\} = \lfloor G_u \rfloor [B]^{-1}\{q\} \tag{A.35}$$

$$v = \lfloor G_v \rfloor \{\beta\} = \lfloor G_v \rfloor [B]^{-1}\{q\} \tag{A.36}$$

$$w = \lfloor G_w \rfloor \{\beta\} = \lfloor G_w \rfloor [B]^{-1}\{q\} \tag{A.37}$$

$$\frac{\partial w}{\partial x} = \lfloor G_{w,x} \rfloor \{\beta\} = \lfloor G_{w,x} \rfloor [B]^{-1}\{q\} \tag{A.38}$$

$$\frac{\partial w}{\partial y} = \lfloor G_{w,y} \rfloor \{\beta\} = \lfloor G_{w,y} \rfloor [B]^{-1}\{q\} \tag{A.39}$$

$$\frac{\partial^2 w}{\partial x \partial y} = \lfloor G_{w,xy} \rfloor \{\beta\} = \lfloor G_{w,xy} \rfloor [B]^{-1}\{q\} \tag{A.40}$$

The following strain-displacement relations which are valid for arbitrarily large displacements and strains were derived in Section 5 (Eqs. 5.115-5.126)[+]:

$$\gamma_{\alpha\beta} = \overset{o}{\gamma}_{\alpha\beta} + \frac{\zeta^o}{A} \kappa_{\alpha\beta} \equiv \overset{o}{\gamma}_{\alpha\beta} + \frac{z}{A} \kappa_{\alpha\beta} \tag{A.41}$$

$$\gamma_{33} = \frac{1}{2}\left(\frac{1}{A} - 1\right) \tag{A.42}$$

$$A = \left(1 + 2\overset{o}{\gamma}_{11}\right)\left(1 + 2\overset{o}{\gamma}_{22}\right) - \left(2\overset{o}{\gamma}_{12}\right)^2 \tag{A.43}$$

Here, the $\overset{o}{\gamma}_{\alpha\beta}$ are the (membrane) strains at the middle surface. They are defined as follows in terms of the displacement gradients:

$$\overset{o}{\gamma}_{11} = \frac{\partial u}{\partial x} + \frac{1}{2}\left(\frac{\partial u}{\partial x}\right)^2 + \frac{1}{2}\left(\frac{\partial v}{\partial x}\right)^2 + \frac{1}{2}\left(\frac{\partial w}{\partial x}\right)^2 \tag{A.44}$$

$$\overset{o}{\gamma}_{22} = \frac{\partial v}{\partial y} + \frac{1}{2}\left(\frac{\partial u}{\partial y}\right)^2 + \frac{1}{2}\left(\frac{\partial v}{\partial y}\right)^2 + \frac{1}{2}\left(\frac{\partial w}{\partial y}\right)^2 \tag{A.45}$$

$$2\overset{o}{\gamma}_{12} = 2\overset{o}{\gamma}_{21} = \frac{\partial u}{\partial y}\left(1 + \frac{\partial u}{\partial x}\right) + \frac{\partial v}{\partial x}\left(1 + \frac{\partial v}{\partial y}\right) + \frac{\partial w}{\partial x}\frac{\partial w}{\partial y} \tag{A.46}$$

Also, in Eq. A.41 the changes of curvature κ_{11} and κ_{22} in the x and y directions, and the "torsion" κ_{12} are expressed as follows in terms of the displacement gradients:

$$\kappa_{11} = \alpha\left(-\frac{\partial^2 w}{\partial x^2}\right) + \beta\left(-\frac{\partial^2 u}{\partial x^2}\right) + \eta\left(-\frac{\partial^2 v}{\partial x^2}\right) \tag{A.47}$$

$$\kappa_{22} = \alpha\left(-\frac{\partial^2 w}{\partial y^2}\right) + \beta\left(-\frac{\partial^2 u}{\partial y^2}\right) + \eta\left(-\frac{\partial^2 v}{\partial y^2}\right) \tag{A.48}$$

$$\kappa_{12} = \alpha\left(-\frac{\partial^2 w}{\partial x \partial y}\right) + \beta\left(-\frac{\partial^2 u}{\partial x \partial y}\right) + \eta\left(-\frac{\partial^2 v}{\partial x \partial y}\right) \tag{A.49}$$

[+]Note that $z \equiv \zeta^o$ = initial undeformed z-direction location of a particle.

where

$$\alpha = 1 + \frac{\partial u}{\partial x} + \frac{\partial v}{\partial y} \tag{A.50}$$

$$\beta = -\frac{\partial w}{\partial x}\left(1+\frac{\partial v}{\partial y}\right) + \frac{\partial w}{\partial y}\,\frac{\partial v}{\partial x} \tag{A.51}$$

$$\eta = -\frac{\partial w}{\partial y}\left(1+\frac{\partial u}{\partial x}\right) + \frac{\partial w}{\partial x}\,\frac{\partial u}{\partial y} \tag{A.52}$$

Since the strains are defined in terms of the displacement gradients, the following derivatives are derived by differentiation of the displacement expressions A.26-A.28 in order to compute $\gamma_{\alpha\beta}$:

$$\frac{\partial u}{\partial x} = \beta_2 + y\,\beta_4 \equiv \lfloor G_{u,x} \rfloor \{\beta\} = \lfloor G_{u,x} \rfloor [B]^{-1} \{q\} \tag{A.53}$$

$$\frac{\partial u}{\partial y} = \lfloor G_{u,y} \rfloor \{\beta\} = \lfloor G_{u,y} \rfloor [B]^{-1} \{q\} \tag{A.54}$$

$$\frac{\partial v}{\partial x} = \lfloor G_{v,x} \rfloor \{\beta\} = \lfloor G_{v,x} \rfloor [B]^{-1} \{q\} \tag{A.55}$$

$$\frac{\partial v}{\partial y} = \lfloor G_{v,y} \rfloor \{\beta\} = \lfloor G_{v,y} \rfloor [B]^{-1} \{q\} \tag{A.56}$$

$$\frac{\partial^2 w}{\partial x^2} = \lfloor G_{w,xx} \rfloor \{\beta\} = \lfloor G_{w,xx} \rfloor [B]^{-1} \{q\} \tag{A.57}$$

$$\frac{\partial^2 w}{\partial y^2} = \lfloor G_{w,yy} \rfloor \{\beta\} = \lfloor G_{w,yy} \rfloor [B]^{-1} \{q\} \tag{A.58}$$

$$\frac{\partial^2 u}{\partial x \partial y} = \lfloor G_{u,xy} \rfloor \{\beta\} = \lfloor G_{u,xy} \rfloor [B]^{-1} \{q\} \tag{A.59}$$

$$\frac{\partial^2 v}{\partial x \partial y} = \lfloor G_{v,xy} \rfloor \{\beta\} = \lfloor G_{v,xy} \rfloor [B]^{-1} \{q\} \tag{A.60}$$

$$\frac{\partial^2 u}{\partial x^2} = \frac{\partial^2 u}{\partial y^2} = \frac{\partial^2 v}{\partial x^2} = \frac{\partial^2 v}{\partial y^2} = 0 \tag{A.61}$$

Since a bilinear polynomial assumption is used for the in-plane lateral displacements u and v, the second derivatives $\frac{\partial^2 u}{\partial x^2}$, $\frac{\partial^2 u}{\partial y^2}$, $\frac{\partial^2 v}{\partial x^2}$, and $\frac{\partial^2 v}{\partial y^2}$ are necessarily equal to zero. Therefore, the bending expressions κ_{11} and κ_{22}, become

$$K_{11} = \alpha \left(- \frac{\partial^2 w}{\partial x^2} \right) \tag{A.62}$$

$$K_{22} = \alpha \left(- \frac{\partial^2 w}{\partial y^2} \right) \tag{A.63}$$

The mixed derivatives $\frac{\partial^2 u}{\partial x \partial y}$ and $\frac{\partial^2 v}{\partial x \partial y}$ of the in-plane lateral displacements, are equal to constants for this assumed-bilinear-displacement rectangular finite element. However, they are neglected as well for the computation of the "torsion" κ_{12}. The strain-displacement relations become

$$\gamma_{11} = \overset{o}{\gamma}_{11} + \frac{z}{A} \alpha \left(- \frac{\partial^2 w}{\partial x^2} \right) \tag{A.64}$$

$$\gamma_{22} = \overset{o}{\gamma}_{22} + \frac{z}{A} \alpha \left(- \frac{\partial^2 w}{\partial y^2} \right) \tag{A.65}$$

$$\gamma_{12} = \overset{o}{\gamma}_{12} + \frac{z}{A} \alpha \left(- \frac{\partial^2 w}{\partial x \partial y} \right) \tag{A.66}$$

The membrane strains $\overset{o}{\gamma}_{11}$, $\overset{o}{\gamma}_{22}$, and $\overset{o}{\gamma}_{12}$ are defined as in Eqs. A.44-A.46 and are valid for arbitrarily large strains and rotations. The expressions A and α are defined by Eqs. A.43 and A.50, respectively. Since the second derivatives of u and v are neglected in these strain-displacement relations, the bending expressions κ_{11}, κ_{22}, and κ_{12} are not valid for arbitrarily large rotations. However, these strain-displacement relations A.64-A.66 are useful for situations where finite membrane strains may occur, and where large rotations are associated with small curvatures. The error associated with this approximation in the analysis of large deformation of beams, has been investigated in References 28 and 212. In effect, studies conducted in Ref. 28 revealed that the second derivatives of the in-plane displacements u and v have a comparatively small influence in the predicted strains for severely loaded* aluminum alloy beams clamped at both ends. Also, observe that the factor A in Eqs. A.64-A.66 includes the effects of finite membrane strains in the reference surface as well as change-of-thickness effects due to finite membrane strains.

*Both by explosive loading and rigid-fragment impact.

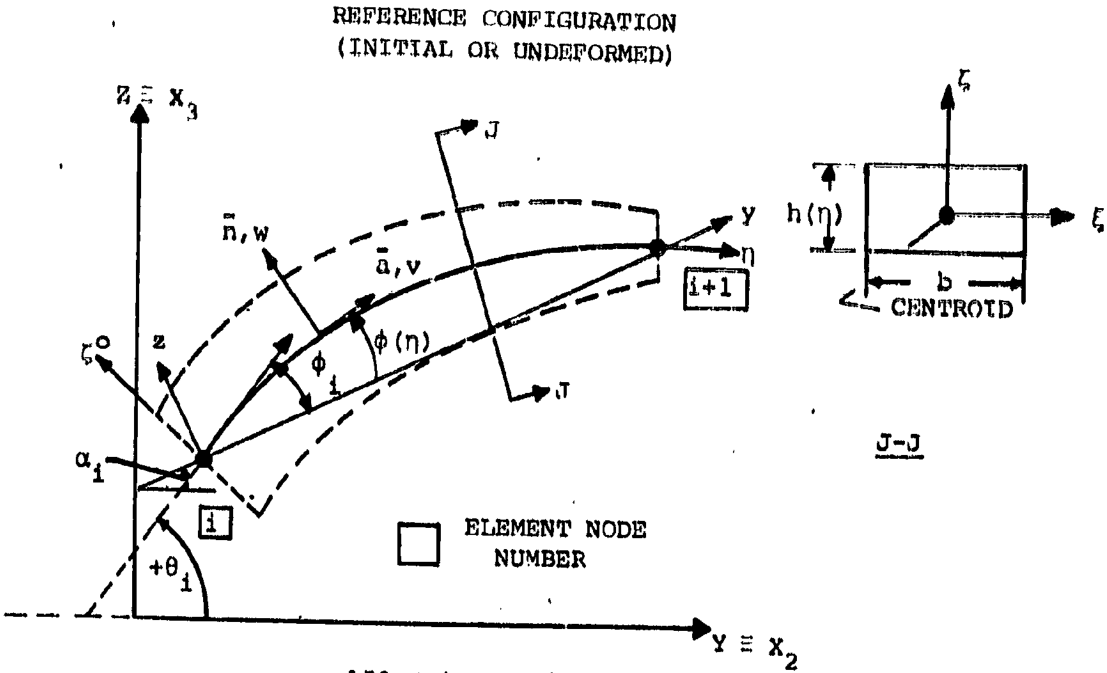

$$-15° \leq \phi_{i+1} - \phi_i \leq 0$$

$$-180° < \phi_i \leq 180°$$

$$\phi(\eta) = b_o + b_1\,\eta + b_2\,\eta^2$$

$$R(\eta) = -(\partial\phi/\partial\eta)^{-1}$$

$$h(\eta) = h_i\,\left(1 - \frac{\eta}{\eta_i}\right) + h_{i+1}\,\frac{\eta}{\eta_i}$$

NODE i: $\eta = 0$

NODE i+1: $\eta = \eta_i$

LOCAL SYSTEM

$\xi,\ \eta,\ \zeta$	-	COORDINATES
v, w, ψ, χ	-	DISPLACEMENTS
$q_1, q_2, \ldots q_8$	-	ELEMENT GENERALIZED DISPLACEMENTS

$$q_1\ q_2\ q_3\ q_4 = v_i\ w_i\ \psi_i\ \chi_i$$

$$\psi = \frac{\partial w}{\partial \eta} - \frac{v}{R} \qquad \chi = \frac{\partial v}{\partial \eta} + \frac{w}{R}$$

CARTESIAN REFERENCE

Y,Z	.-	GLOBAL COORDINATES
y,z	-	LOCAL COORDINATES

FIG. A.1 NOMENCLATURE FOR GEOMETRY, COORDINATES, AND DISPLACEMENTS OF A CURVED-BEAM FINITE ELEMENT

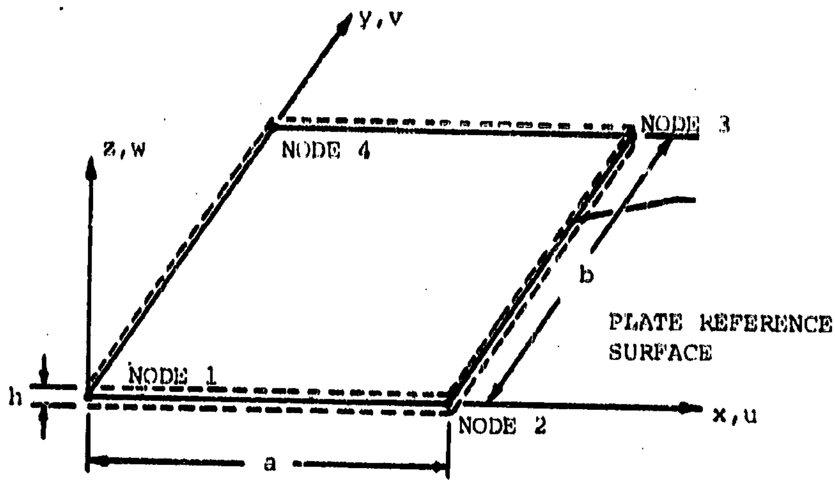

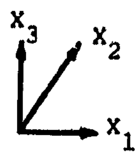

X_1, X_2, X_3 - Global Rectangular Cartesian Coordinate System

x, y, z - Local (element) Coordinate System

h - Total Element Thickness

a, b - Element Spanwise Dimension in the x and y Directions

u, v, w

$$w_{,x} = \frac{\partial w}{\partial x}$$

$$w_{,y} = \frac{\partial w}{\partial y}$$

$$w_{,xy} = \frac{\partial^2 w}{\partial x \partial y}$$

Generalized Nodal Displacements

FIG. A.2 GEOMETRY AND NOMENCLATURE FOR A UNIFORM-THICKNESS RECTANGULAR PLATE ELEMENT

APPENDIX B

FINITE ELEMENT FORMULATION AND IMPLEMENTATION FOR A HIGHER ORDER PLATE FINITE ELEMENT (48 DOF)

B.1 Selection of the Assumed Displacement Field

The strain-displacement relations for large strains and rotations of plates involve second order derivatives of all three displacement components (vertical displacement w and in-plane displacements u and v). This implies that, in order to obtain a finite value for the strain energy from the strain energy expression, at least the first order derivatives of the displacements u, v, and w should be continuous everywhere (e.g. across finite element boundaries). Otherwise, the elements would be incompatible.

The requirement that the slope of the three displacement components to be continuous across the element boundaries (continuity inside the finite elements is ensured by selection of continuous polynomials as interpolation functions), plus the requirements of including constant strain and rigid body modes lead to bicubic (in x and y) polynomial displacement interpolation field for each of u, v, and w. This finite element with a bicubic in u, v, and w is a rectangular element consisting of 4 nodes, with 12 degrees of freedom (DOF) per node and hence a total of 48 DOF for the element.

The degrees of freedom at the nodes are u, $\frac{\partial u}{\partial x}$, $\frac{\partial u}{\partial y}$, $\frac{\partial^2 u}{\partial x \partial y}$, v, $\frac{\partial v}{\partial x}$, $\frac{\partial v}{\partial y}$, $\frac{\partial^2 v}{\partial x \partial y}$ and w, $\frac{\partial w}{\partial x}$, $\frac{\partial w}{\partial y}$, $\frac{\partial^2 w}{\partial x \partial y}$. It is easily shown that the derivatives of the displacements with respect to x and y are continuous across the element boundaries. Furthermore, even the cross derivatives $\frac{\partial^2 u}{\partial x \partial y}$, $\frac{\partial^2 v}{\partial x \partial y}$, and $\frac{\partial^2 w}{\partial x \partial y}$ are all continuous. The remarkable thing is that this extra degree of continuity (not required in the variational principle to obtain a finite energy) does not seem to follow from the usual arguments. (The functions $\frac{\partial^2 u}{\partial x \partial y}$, $\frac{\partial^2 v}{\partial x \partial y}$ and $\frac{\partial^2 w}{\partial x \partial y}$ are quadratic along each edge, and only the values of $\frac{\partial^2 u}{\partial x \partial y}$, $\frac{\partial^2 v}{\partial x \partial y}$, and $\frac{\partial^2 w}{\partial x \partial y}$ at the two endpoints are automatically held in common).

The 48 DOF Hermite bicubic, bicubic, bicubic, element is formulated as a rectangle, but by subparametric transformation [Ref. 213, page 89] can be transformed into a general quadrilateral with straight sides but arbitrary angles.

The PLATE and CIVM-PLATE programs [31] use rectangular finite elements with a total of 24 DOF; the assumed-displacement interpolation field is bicubic in w and bilinear in u and v. This lower order element presents slope continuity ($\frac{\partial w}{\partial x}$, $\frac{\partial w}{\partial y}$ and $\frac{\partial^2 w}{\partial x \partial y}$) across the element boundaries only for the vertical displacement w, but not for the in-plane displacements u and v. Also, since the assumed-displacement interpolation field is only bilinear for the in-plane displacements u and v, the terms that involve the second derivatives of these displacements (present in the large strain and rotation strain-displacement equations), cannot be computed in an analysis that would make use of this finite element. It is clear that this 24 DOF element is accurate only for problems where the vertical displacement w is much more important than the in-plane displacements u and v.

It is also clear that in a general large strain and rotation program, the three displacement components deserve to share equal importance in the assumed-displacement field. Also, [Ref. 213, page 215] the condition number* for cubics is only slightly worse than for linear elements, so that the roundoff errors for a given element size (h) are comparable. The discretization error, however, is an order of magnitude smaller for cubics. Therefore, at the cross over point where roundoff prohibits any further improvement coming from a decrease in h, the cubic element is much more accurate. This applies especially to the computation of strains, where differentiation (or differencing) of displacements introduces an extra factor h^{-1} (h^{-2} for bending) into the numerical error.

One can express the displacement field u, v, w inside an element by Hermitian polynomials (Φ) that interpolate in terms of the generalized displacement degrees of freedom at the nodes (q's). Hence, one may write

*This is the ratio of the maximum eigenvalue to the minimum eigenvalue of the mathematical model of the linear structural system.

$$u = \underset{1\times16}{\lfloor \Phi \rfloor} \underset{16\times1}{\{ q_u \}} \qquad v = \underset{1\times16}{\lfloor \Phi \rfloor} \underset{16\times1}{\{ q_v \}} \qquad w = \underset{1\times16}{\lfloor \Phi \rfloor} \underset{16\times1}{\{ q_w \}} \tag{B.1}$$

Similarly, the derivatives may be written as

$$\frac{\partial u}{\partial x} = \underset{1\times16}{\left\lfloor \frac{\partial \Phi}{\partial x} \right\rfloor} \underset{16\times1}{\{ q_u \}} \;,\; \frac{\partial^2 u}{\partial x^2} = \underset{1\times16}{\left\lfloor \frac{\partial^2 \Phi}{\partial x^2} \right\rfloor} \underset{16\times1}{\{ q_u \}} \;,\; etc. \tag{B.2}$$

Therefore, one has to store matrices ($\lfloor \Phi \rfloor$, $\left\lfloor \frac{\partial \Phi}{\partial x} \right\rfloor$, etc.) that involve <u>only 16 terms</u> per element instead of 48 because exactly the same interpolation polynomials are needed for each of the three displacement components u, v, and w. This is a very attractive feature of the large strain formulation when a bicubic displacement field is used for all three displacement components.

B.2 Finite Element Formulation and Solution Procedure

As noted in Section 6, the finite element formulation and solution procedure used herein is based upon the Principle of Virtual Work including D'Alembert inertia forces; further the <u>unconventional</u> form of the equations of motion (see Eqs. 6.55 and 6.69) are utilized rather than the conventional form (Eq. 6.68) given in Subsection 6.2.3.

In the process of a finite element dynamic solution, the mass matrix is needed. Mass matrices may be formed in various ways: (a) "consistent" or non-diagonal and (b) "lumped" or diagonal. Diagonal mass matrices can be formed using an intuitive physical approach (e.g. by "placing masses" at the displacement DOF) or by using a scheme to diagonalize the consistent mass matrix according to selected rules. The consistent mass matrix is obtained from the expression for the kinetic energy through volume integration of the interpolation functions.

Both the mass and stiffness do <u>not</u> change during the transient solution and are <u>not</u> a function of the strain or stress at a given time or location.

These matrices have dimensions of 48 x 48 (2304 entries) for the 48 DOF finite element to be used in the numerical analysis. Taking into account symmetry about the diagonal, there is a total of possibly [(48 x 48 - 48)/2 + (48)] = 1176 different entries for each of these matrices.

Because of the three fold symmetry in the interpolation polynomials between the displacement components u, v, and w (the same Hermitian interpolation polynomials are required for each displacement component), the number of different entries is reduced dramatically. The exact integration of the element consistent mass matrix [m] (Eq. 6.38) has revealed only 33 different entries (out of a possible 1176). The exact integration of the element linear stiffness matrix [k] (Eq. 6.63) has revealed only 123 different entries (out of a possible 1176).

Next, note that the consistent externally-applied prescribed loads vector {f} for each element arises from (a) the non-inertial body forces f^i and involves an integration over the <u>reference volume</u> V_{o_n} of the element and (b) the applied surface tractions $\underset{\sim}{T}^i$ involving an integral over the <u>reference surface area</u> A_{o_n}, as indicated by Eq. 6.41.

The remaining terms in Eq. 6.37 for the unconventional formulation pertain to δU (Eq. 6.18-6.19) the variation of the work of the internal stresses S^{ij}. From Eq. 6.37 it is seen that the element-level contributions from δU to the equations of motion consist of {p} and [h] {q}. Also note that the evaluation of {p} and of [h] involves an integration of the stresses S^{ij} and strain-variation quantities over the reference volume of the element V_{o_n}. When applied to plate or shell analysis, these integrations are performed conveniently in terms of stress resultants:

$$L^{\alpha\beta}(\xi^1,\xi^2,t) = \int S^{\alpha\beta}(\xi^1,\xi^2,\zeta^0,t)\, d\zeta^0 \tag{B.3a}$$

$$M^{\alpha\beta}(\xi^1,\xi^2,t) = \int S^{\alpha\beta}(\xi^1,\xi^2,\zeta^0,t)\,\zeta^0\, d\zeta^0 \tag{B.3b}$$

where ζ^{o} is the Lagrangian or material thickness coordinate. Since $S^{\alpha\beta}$ changes with time, numerical integration through the thickness is used to evaluate $L^{\alpha\beta}$, $M^{\alpha\beta}$; also to complete the volume integration, numerical integration is performed over the x,y or the ξ^1,ξ^2 region of the element. It is worth pointing out at this stage, that another attractive feature of the 48 DOF element is that it requires the same number of integration points[+] as the lower order (and hence lower accuracy) element which has 24 DOF. The reason for this is that the highest order polynomial in the 24 DOF element (namely the complete bicubic in w) has exactly the same order as the polynomials in the 48 DOF element (complete bicubics in u, v and w)

Instead of proceeding in a routine fashion, taking the variation and computing the resultant terms in a straightforward way, the terms are grouped together so as to minimize the number of operations and storage in the computation of the work of the internal forces. Also, the use of Hermitian interpolation polynomials and the threefold symmetry of the 48 DOF element also helps to reduce significantly the amount of storage and computation.

In this vector formulation, one can express the internal force arising from the linear stiffness and the geometric and material nonlinearities simply as a column vector $\underset{48\times1}{\{I(t)\}}$ defined by

$$\underset{48\times1}{\{I(t)\}} = \underset{48\times1}{\{p(t)\}} + \underset{48\times48}{[h(t)]}\underset{48\times1}{\{q(t)\}} \tag{B.4}$$

Note that $\underset{48\times1}{\{I(t)\}}$ consists of 3 column vectors $\underset{16\times1}{\{I_u(t)\}}$, $\underset{16\times1}{\{I_v(t)\}}$, and $\underset{16\times1}{\{I_w(t)\}}$ that correspond to the displacement components u, v, and w, respectively. Further the same 16x1 interpolation matrix is used for each of the submatrices $\{I_u\}$, $\{I_v\}$, and $\{I_w\}$. Applying Eqs. 5.115-5.126 and B.1 to Eq. 6.19, one obtains:

$$\underset{16\times1}{\{I_u(t)\}} = \iint\left(\underset{16\times1}{\left\{\frac{\partial\Phi}{\partial x}(x,y)\right\}}H_{u_x}(x,y,t) + \underset{16\times1}{\left\{\frac{\partial\Phi}{\partial y}(x,y)\right\}}H_{u_y}(x,y,t) + \underset{16\times1}{\{F(x,y,t)\}}\,\beta(x,y,t)\right)dx\,dy \tag{B.5a}$$

[+]That is, at least 3 by 3 or 9 x,y Gaussian stations, and 4 depthwise Gaussian stations at each of these 9 Gaussian stations; hence, there would be a total of 36 stations per element.

$$\underset{16\times1}{\{I_v(t)\}} = \iint\left(\underset{16\times1}{\left\{\frac{\partial\Phi}{\partial x}(x,y)\right\}} H_{v_x}(x,y,t) + \underset{16\times1}{\left\{\frac{\partial\Phi}{\partial y}(x,y)\right\}} H_{v_y}(x,y,t) + \underset{16\times1}{\{F(x,y,t)\}}\,\eta(x,y,t)\right)dx\,dy \tag{B.5b}$$

$$\underset{16\times1}{\{I_w(t)\}} = \iint\left(\underset{16\times1}{\left\{\frac{\partial\Phi}{\partial x}(x,y)\right\}} H_{w_x}(x,y,t) + \underset{16\times1}{\left\{\frac{\partial\Phi}{\partial y}\right\}} H_{w_y}(x,y,t) + \underset{16\times1}{\{F(x,y,t)\}}\,\alpha(x,y,t)\right)dx\,dy \tag{B.5c}$$

where

$$\{F(x,y,t)\} = \frac{1}{A(x,y,t)}\left(\left\{-\frac{\partial^2\Phi}{\partial x^2}\right\}M^{11}(x,y,t) + \left\{-\frac{\partial^2\Phi}{\partial y^2}\right\}M^{22}(x,y,t) + \left\{-2\frac{\partial^2\Phi}{\partial x\partial y}\right\}M^{12}(x,y,t)\right) \tag{B.5d}$$

$$H_{u_x}(x,y,t) = H_{11}(x,y,t)\left(1+\frac{\partial u}{\partial x}(x,y,t)\right) + H_{12}(x,y,t)\frac{\partial u}{\partial y} + J_w(x,y,t) - J_v(x,y,t)\frac{\partial w}{\partial y}(x,y,t) \tag{B.5e}$$

$$H_{u_y}(x,y,t) = H_{12}\left(1+\frac{\partial u}{\partial x}\right) + H_{22}\frac{\partial u}{\partial y} + J_v\frac{\partial w}{\partial x} \tag{B.5f}$$

$$H_{v_x}(x,y,t) = H_{12}\left(1+\frac{\partial v}{\partial y}\right) + H_{11}\frac{\partial v}{\partial x} + J_u\frac{\partial w}{\partial y} \tag{B.5g}$$

$$H_{v_y}(x,y,t) = H_{22}\left(1+\frac{\partial v}{\partial y}\right) + H_{12}\frac{\partial v}{\partial x} + J_w - J_u\frac{\partial w}{\partial x} \tag{B.5h}$$

$$H_{w_x}(x,y,t) = H_{11}\frac{\partial w}{\partial x} + H_{12}\frac{\partial w}{\partial y} - J_u\left(1+\frac{\partial v}{\partial y}\right) + J_v\frac{\partial u}{\partial y} \tag{B.5i}$$

$$H_{w_y}(x,y,t) = H_{22}\frac{\partial w}{\partial y} + H_{12}\frac{\partial w}{\partial x} - J_v\left(1+\frac{\partial u}{\partial x}\right) + J_u\frac{\partial v}{\partial x} \tag{B.5j}$$

$$J_u(x,y,t) = \frac{1}{A(x,y,t)}\left[\left(-\frac{\partial^2 u}{\partial x^2}\right)M^{11} + \left(-\frac{\partial^2 u}{\partial y^2}\right)M^{22} + \left(-2\frac{\partial^2 u}{\partial x \partial y}\right)M^{12}\right] \tag{B.5k}$$

$$J_v(x,y,t) = \frac{1}{A}\left[\left(-\frac{\partial^2 v}{\partial x^2}\right)M^{11} + \left(-\frac{\partial^2 v}{\partial y^2}\right)M^{22} + \left(-2\frac{\partial^2 v}{\partial x \partial y}\right)M^{12}\right] \tag{B.5ℓ}$$

$$J_w(x,y,t) = \frac{1}{A}\left[\left(-\frac{\partial^2 w}{\partial x^2}\right)M^{11} + \left(-\frac{\partial^2 w}{\partial y^2}\right)M^{22} + \left(-2\frac{\partial^2 w}{\partial x \partial y}\right)M^{12}\right] \tag{B.5m}$$

$$H_{\alpha\beta} = L^{\alpha\beta} - \mathcal{G}\left(\delta_{\alpha\beta} + 2\gamma^{\circ}_{\alpha\beta}\right) \tag{B.5n}$$

$$\mathcal{G} = \frac{2}{(A)^2}\left[M^{11}\mathcal{K}_{11} + M^{22}\mathcal{K}_{22} + M^{12}(2\mathcal{K}_{12})\right] \tag{B.5o}$$

$$L^{\alpha\beta} = \int S^{\alpha\beta} d\zeta^{\circ}\ ;\ M^{\alpha\beta} = \int S^{\alpha\beta}\zeta^{\circ} d\zeta^{\circ}\ ;\ I^{\alpha\beta} = \int S^{\alpha\beta}(\zeta^{\circ})^2\, d\zeta^{\circ} \tag{B.5p}$$

$$A(x,y,t) = \left(1 + 2\gamma^{\circ}_{11}(x,y,t)\right)\left(1 + 2\gamma^{\circ}_{22}(x,y,t)\right) - \left(2\gamma^{\circ}_{12}(x,y,t)\right)^2 \tag{B.5q}$$

and α, β, η, $\kappa_{\alpha\beta}$, and $\gamma^{o}_{\alpha\beta}$ have been defined in the strain-displacement relations: Eqs. 5.115 5.126.

For the transient response solution, it is recommended that one employ the vector form of the equations of motion as described by Eqs. 6.89, 6.90, and 6.91. These equations may be solved by using an appropriate timewise finite-difference (or finite-element) operator such as the Houbolt, the Park, etc. -- in conjunction with (a) extrapolation of the nonlinear internal-loads terms without iteration or (b) by iterating to convergence (if possible) within a given time step Δt by, for example, the BFGS method [204] or a quasi-Newton method [215].

APPENDIX C

ASSESSMENT OF STRESS-STRAIN PROPERTIES FROM UNIAXIAL-TEST MEASUREMENTS OF INITIALLY-ISOTROPIC MATERIAL

As indicated in Subsection 2.8, the axial relative elongation E_u of a uniaxial test specimen is defined as (Eq. 2.401):

$$E_u \equiv \frac{\text{change in gage length}}{\text{original gage length}} = \frac{\ell-\ell_o}{\ell_o} \tag{C.1}$$

E_u is also called the engineering or nominal strain, and it is a quantity or measurement which extensometers or strain gages can provide. One can compute the logarithmic strain ε_u^* of a uniaxial test specimen in terms of E_u as (Eqs. 2.407 and 2.410):

$$\epsilon_u^* \equiv \ln(1+E_u) \equiv \ln\left(\frac{\ell}{\ell_o}\right) \tag{C.2}$$

The engineering stress σ_E of a uniaxial test specimen is defined as (Eq. 2.443):

$$\sigma_E = \frac{P}{A_o} \tag{C.3}$$

where P is the force transmitted across the cross-sectional area of the uniaxial specimen (the applied load) and A_o is the original cross-sectional area of the specimen. The engineering stress σ_E is also called the nominal or 1st Piola-Kirchhoff stress.

One can compute the Kirchhoff stress τ_u of a uniaxial test specimen in terms of σ_E and E_u as (Eq. 2.432):

$$\tau_u = \sigma_E(1+E_u) = \frac{P}{A_o}(1+E_u) \tag{C.4}$$

Observe that the Kirchhoff stress τ_u can be very easily obtained from experimental measurements of: the <u>original</u> cross-sectional area A_o, the applied load P, and the axial relative elongation E_u (obtained from strain gages or extensometers). These quantities (P, A_o, and E_u) are the quantities that have been and are most often measured in experiments. Many authors have referred to the Kirchhoff stress τ_u as the "true" stress, since the Kirchhoff stress τ_u is defined as (Eqs. 2.425, 2.427, and 2.432)

$$\tau_u = \frac{P}{A_o}\left(1 + E_u\right) = \frac{\rho_o}{\rho}\,\frac{P}{A} \equiv \frac{\rho_o}{\rho}\,\sigma_T \tag{C.5}$$

where $\sigma_T \equiv \frac{P}{A}$ is the "true" or Cauchy stress (Eq. 2.427), ρ_o (ρ) is the original (present) mass density, and mass conservation given by $\rho_o A_o \ell_o = \rho A \ell$ has been used. Hence, if there were no change in the mass density (that is, $\rho = \rho_o$), the Cauchy stress would be equal to the Kirchhoff stress. It is important to note that what many authors plot as an <u>approximate</u> "true" stress (under the assumption $\rho \simeq \rho_o$) is really the <u>exact</u> measurement of the Kirchhoff stress.

For example, in Eq. 8.3 of Nadai's "Theory of Flow and Fracture of Solids" [115], the stress measure used is the Kirchhoff stress (although not so stated) and, therefore, the stress measure labeled as "true stress" in the graphs pertaining to experiments in Nadai's book is really the Kirchhoff stress.

Similarly, G.I. Taylor used the Kirchhoff stress. For example, in Ref. 114, it is not clearly stated what stress measure is used. However, one can deduce what is the stress measure used by G.I. Taylor from the following paragraph (page 308, Ref. 114):

> "The condition for fracture by instability owing to the formation of a local "neck" is
>
> $$\frac{\ell}{T}\frac{dT}{d\ell} < 1 \quad \text{or} \quad \frac{d(\ln T)}{d\left(\ln \frac{\ell}{\ell_o}\right)} < 1 \text{"} \tag{C.6}$$

where T is the stress, ℓ_o is the original length of the specimen, and ℓ is the present length of the specimen. The condition for "necking" is:

$$\frac{d\sigma_E}{dE_u} < 0 \quad \text{or} \quad \frac{d\sigma_E}{d\ell} < 0 \tag{C.7}$$

Since the engineering stress σ_E is related to the Kirchhoff stress τ_u by

$$\sigma_E = \frac{\tau_u}{(1+E_u)} = \tau_u \frac{\ell_o}{\ell} \tag{C.8}$$

then

$$\frac{d\sigma_E}{d\ell} < 0 \tag{C.9}$$

is equivalent to

$$\frac{d\left(\tau_u \frac{\ell_o}{\ell}\right)}{d\ell} < 0 \tag{C.10}$$

or

$$\frac{\ell_o}{\ell}\frac{d\tau_u}{d\ell} + \tau_u \ell_o \frac{d\left(\frac{1}{\ell}\right)}{d\ell} < 0 \tag{C.11}$$

$$\frac{1}{\ell}\frac{d\tau_u}{d\ell} - \frac{\tau_u}{\ell^2} < 0 \tag{C.12}$$

or

$$\frac{d\tau_u}{d\ell} < \frac{\tau_u}{\ell} \tag{C.13}$$

Therefore, one obtains the following inequalities in terms of the Kirchhoff stress:

$$\frac{\ell}{\tau_u}\frac{d\tau_u}{d\ell} < 1 \quad \text{or} \quad \frac{d(\ln \tau_u)}{d\left(\ln \frac{\ell}{\ell_o}\right)} < 1 \tag{C.14}$$

These inequalities are exactly the same as Taylor's inequalities if one sets

$$T = \tau_u \tag{C.15}$$

The stress measure T used by G.I. Taylor is the Kirchhoff stress. Obviously, the stress measure T cannot be the true stress σ_T because

$$\frac{d\sigma_E}{d\ell} = \frac{d\left(\sigma_T \frac{\ell_o}{\ell} \frac{\rho_o}{\rho}\right)}{d\ell} < 0 \qquad \text{(C.16)}$$

and only if the density is constant,

$$\frac{d(1/\rho)}{d\ell} = 0 \qquad \text{(C.17)}$$

will the true stress σ_T be equal to T :

$$\rho = \rho_o \longrightarrow T = \sigma_T = \tau_u \qquad \text{(C.18)}$$

Also observe that J.F. Bell (page 543, Chapter IV of Ref. 216) is incorrect when he states that "Taylor found that results from simple tension and compression tests on polycrystalline copper coincided when nominal or Piola-Kirchhoff stress T (referred to original area) was plotted against logarithmic or "natural" strain (true strain)". Because, as just shown, T is the Kirchhoff stress τ_u (and to a good approximation is the true stress σ_T); T is not the nominal stress σ_E in Taylor's classic work (Ref. 114).

In preparing the uniaxial static tensile test data in Kirchhoff stress τ_{u_o}[+] versus logarithmic strain (ϵ_u^*) form, the data in the strain region where necking occurs (that is, beyond the peak in engineering stress $\sigma_E = P/A_o$) should be modified appropriately to "correct for necking", because after necking occurs a multiaxial state of stress is developed. Various schemes for making such corrections have been developed. See, for example, the procedure and correction factor proposed by Bridgman [217] based upon extensive experimental work. For more information on necking, see the book by Lubahn and Felgar [218]. Recent work on computer simulations of tension tests of ductile metals is reported by Norris et al. [219] and by Saje [220]. An excellent recent survey article on this subject was prepared by Hutchinson [221].

[+] Subscript "o" refers to static conditions.

One approach to approximate the uniaxial behavior beyond the incipient necking condition (peak in σ_E) is to assume a straight-line fit between that point and the rupture condition. After necking occurs, it is hopeless to try to measure the relative elongation E_u with extensometers or strain gages, since the precise location of the necking station is not known beforehand for uniform specimens, and because of the non-uniform state of strain in the neck region. However, the cross-sectional area A_f of the specimen at the rupture station can be measured after rupture. Hence, one can estimate the true stress $(\sigma_T)_f$ at rupture (ignoring any elastic recovery, assuming a uniform stress through the cross-sectional area A_f, and ignoring the multiaxial stress conditions) from the knowledge of the load P_f at rupture and the cross-sectional area A_f: $(\sigma_T)_F = P_f/A_f$. In order to compute the logarithmic strain after necking occurs, from a knowledge of the cross sectional area, it is necessary to assume incompressibility, since,

$$\epsilon_u^* \equiv \ln(1+E_u) = \ln\left(\frac{\rho_o}{\rho}\frac{A_o}{A}\right) \tag{C.19}$$

and for incompressibility $(\rho_o \simeq \rho)$:

$$\epsilon_u^* = \ln\frac{A_o}{A} \tag{C.20}$$

Hence, one can <u>estimate</u> the logarithmic strain $(\epsilon_u^*)_f$ at rupture (since at the associated large plastic strains, the ductile material may be regarded as behaving in an incompressible fashion) by

$$\boxed{(\epsilon_u^*)_f \doteq \ln\frac{A_o}{A_f}} \tag{C.21}$$

Similarly, one can estimate the Kirchhoff stress $(\tau_{u_o})_f$ at rupture, assuming incompressibility by

$$\tau_{u_o} = \frac{\rho_o}{\rho}\sigma_T \;;\; (\tau_{u_o})_f \doteq (\sigma_T)_f \text{ for } \rho_o \doteq \rho$$

$$\therefore \quad \boxed{(\tau_{u_o})_f \doteq \frac{P_f}{A_f}} \tag{C.22}$$

Finally, the "corrected" value to be used for $(\tau_{u_o})_f$ is called $(\tau_{u_o})_{fc}$ and may be computed, for example, by using Bridgman's [217] correction factor by (see Eq. 5.8 of [218]):

$$\left(\tau_{u_o}\right)_{fc} = \frac{P_f / A_f}{\left(1 + 2\frac{R}{a}\right) \ln\left(1 + \frac{1}{2}\frac{a}{R}\right)} \tag{C.23}$$

where

a = radius of the (assumed to be circular) rupture cross section

R = lateral final radius of curvature of the tensile test specimen at the rupture station.

Bridgman [217] presents data plots (from extensive experiments) from which one can determine the ratio a/R from a knowledge of A_o/A_f. Other correction alternatives may be found in Refs. 218-221.

As noted in Subsection 3.3.4, the static uniaxial stress-strain data expressed in τ_{u_o} versus ε_u^* form (including the data points at incipient necking and at the rupture condition as just described) can be fitted in a piecewise-linear fashion for use in the mechanical-sublayer material model. Further, data from uniaxial stress-strain tests at various strain-rate levels may be obtained and analyzed to deduce the approximate rate constants d and p (or $^s d$ and $^s p$) indicated in Eq. 3.64 (or Eq. 3.43).